THE UNIVERSITY OF
SYDNEY

Forest, fire and monsoon: A palaeo-environmental assessment of the ecological threshold dynamics of South-east Asia's dry forests

Author:
Rebecca Jenner HAMILTON

Supervisor:
Dr. Dan PENNY

A thesis submitted in fulfilment of the requirements for the degree of Doctor of Philosophy

in the

School of Geosciences
Faculty of Science

June, 2016

Statement of Originality

This is to certify that to the best of my knowledge, the content of this thesis is my own work. This thesis has not been submitted for any degree or other purposes.

I certify that the intellectual content of this thesis is the product of my own work and that all the assistance received in preparing this thesis and sources have been acknowledged.

Signature: 

Name: Rebecca Jenner HAMILTON

Date: 30/6/16

Abstract

Projections that the frequency and intensity of extremes in the Asian monsoon will rise in coming decades are being made with increasing confidence. There is concern that these events may drive south-east Asian dry tropical forest — an extensive ecoregion affected by this climate system — across critical thresholds, triggering ecological regime shifts. This could have serious implications both in terms of the loss of biodiversity from what is considered an area of global ecological significance, and for the goods and services that the associated ecosystems provide to a highly populous part of the world. There is little currently known about the nature and intensity of drivers needed to instigate ecosystem reorganisation within this ecoregion. However, research from seasonally dry tropical forests elsewhere, particularly the neo- and Afro-tropics, indicates that Asian dry forests may be susceptible to reorganisation to savanna under changing (reduced) precipitation regimes, increased seasonality of rainfall, or through introduction of fire into these ecosystems. This project uses a high-resolution, multi-proxy analysis of two sediment cores extracted from Cambodian volcanic crater lakes - situated at the heart of the south-east Asian dry forest ecoregion - to assess the response of these forests to drier climates and periods of heightened fire activity.

Reconstruction of the site climate using geochemical proxies of lake shallowing and deepening indicates a stepwise weakening of the summer monsoon from c. 4700 to 450 cal. yrs BP, after which it appears to strengthen. This trend is punctuated by nine dry events identified at c. 4250, 3300, 2650, 2250, 1915, 1755, 1550, 570 and 350 cal. yrs BP, with a particularly dry period evident between c. 1900 to 1500 cal. yrs BP.

Charcoal records produced from both lake sites demonstrate that fire has been a persistent feature of south-east Asian dry forests since at least the mid Holocene. Peaks in local and regional fire activity commonly coincide with reconstructed dry periods, though high levels of local burning are evident at one of the lake sites between c. 4700 and 3700 cal. yrs BP - a time that appears to be characterised by a relatively strong summer monsoon.

A reconstruction of the ecological history of the lake sites over c. 4700 years shows the maintenance of forest in response to gradual monsoon weakening, relatively abrupt dry events and periods of high fire activity. This indicates ecological resilience to slow and fast climatic forcing, and to the introduction of fire into the forests. Vegetation response recorded in the palaeorecord shows the gradual transition from more closed to open forest types during periods of a weak summer monsoon and/or in response to high fire activity. This finding suggests that the unique mosaics of open- and closed-units that characterise south-east Asia's dry forests may be important for promoting the overall resilience of associated ecosystems, and highlight the

value of maintaining landscape connectivity and practices that encourage forest heterogeneity (including traditional swidden agriculture) across the region.

More broadly, the resilience of the dry forests of tropical Asia to reduced precipitation and heightened fire activity highlights the limitations of generalist biome-scale models. This emphasises the importance of long-term, intra-biome level research for predicting future ecological response to drivers of change.

Acknowledgements

This research is funded by the Australian Research Council (DP1094367; LE100100141) and the Australian Nuclear Science and Technology Organisation (ALNGRA11075; ALNGRA15509).

I would like to express my deepest gratitude for my supervisor, Dr. Dan Penny, who first sparked my interest in palaeoenvironments and who has, in the years since, unwearyingly guided me though my graduate education. Without his passion and enthusiasm for this project, particularly in the face of chronology woes, this thesis would not have been possible.

My thanks are also owed to the following people for the considerable time that they have given to this project, both in the field and laboratory. Dr. Andy Maxwell generously shared with me his vast knowledge of Cambodia's dry forest ecology and associated pollen taxonomy, greatly aiding with the palynological component of this work. Dr. Janelle Stevenson also assisted with pollen and spore identification, and, along with Prof. Simon Haberle, allowed me access to the ANU Australasian Pollen and Spore collection. The technical expertise of Tom Savage, Dr. Quan Hau, Dr. Alison Blyth and Jonathon Chee Ming Lai greatly helped with solving the chronology issues encountered in this project. Mr. Chap Yuthy, Mr. Khem Rongden, Mr. Saeng Channa, Roshni Sharma, Georgia Williams, Mischa Vickas and the people of Seda, Yeak Loam and Ka Laeng communes all made invaluable contributions in the field.

I am indebted to my parents, John and Barbara, for the many hours that they have devoted to both the creation of this document and provision of continued emotional support. Thanks are also due to my office mates, particularly Elyssa and Tegan, for the many laughs along the way.

Finally, my greatest thanks go to my partner, Robert, for his tireless support, his timely sense of humour, and for keeping things in perspective.

Contents

List of Figures

List of Tables

List of Abbreviations

ANSTO	**A**ustralian **N**uclear **S**cience and **T**echnology **O**rganisation
ASL	**A**bove **S**ea **L**evel
BP	**B**efore **P**resent
BRE	**B**asaltic **R**ed **E**arth forests
CIDF	**C**entral **I**ndochina **D**ry **F**orest Ecoregion
DDF	**D**eciduous **D**ipterocarp **F**orest
EAM	**E**ast **A**sian **M**onsoon
EASM	**E**ast **A**sia **S**ummer **M**onsoon
EAWM	**E**ast **A**sian **W**inter **M**onsoon (NorthEast Winter Monsoon)
ENSO	**E**l-**N**iño **S**outhern **O**scillation
IOD	**I**ndian **O**cean **D**ipole
ISM	**I**ndian **S**ummer **M**onsoon (South Asian Monsoon)
ITCZ	**I**nter-**T**ropical **C**onvergence **Z**one
LGM	**L**ast **G**lacial **M**aximum
LIA	**L**ittle **I**ce **A**ge
LMF	**L**ower **M**ontane **F**orest
MAP	**M**ean **A**nnual **P**recipitation
MDF	**M**ixed **D**eciduous **F**orest
MODIS	**M**oderate **R**esolution **I**maging **S**pectroradiometer
MWP	**M**edieval **W**arm **P**eriod
NWP	**N**orthwest **P**acific
PF	**P**ine **F**orest
RF	**R**iparian **F**orest
RVP	**R**atanakiri **V**olcanic **P**rovince
SASDTF	**S**outh-east **A**sian **S**easonally **D**ry **T**ropical **F**orest ecoregion
SDTF	**S**easonally **D**ry **T**ropical and subtropical broadleaf **F**orest
SEDF	**S**emi-**E**vergreen **D**ry **F**orest
SeF	**Se**condary seasonally dry **F**orests
SIDEF	**S**outheastern **I**ndochina **D**ry **E**vergreen **F**orest ecoregion
SST	**S**ea **S**urface **T**emperature
SwF	**Sw**amp **F**orest
TGSS	**T**ropical and subtropical **G**rassland, **S**avanna and **S**hrubland
WNP	**W**estern **N**orth **P**acific
WNPSM	**W**estern **N**orth **P**acific **S**ummer **M**onsoon
WWF	**W**orld **W**ildlife **F**und
XRF	**X**-**R**ay **F**luorescence

1 Introduction

1.1 Ecological thresholds and climate change

Predictions that the frequency and intensity of climatic extremes will rise in coming decades are being made with increasing confidence (Christensen et al. 2013, IPCC 2013). There is concern that as a consequence, ecosystems may be driven across critical thresholds, triggering ecological regime shifts (Scheffer et al. 2001). Given that human disturbances, including suppression of natural system dynamics and reduction of biological diversity, are acting to alter (typically reduce) the capacity of receiving systems to cope with external drivers, understanding the impact of these events on ecosystems is of paramount concern for ecologists and conservation managers (Dawson et al. 2011). This is particularly the case when the ecosystems in question have been afforded high conservation priority due to their rarity, representativeness (Olson and Dinerstein 2002) or ability to produce especially valuable ecological goods and services for humankind (Naidoo et al. 2008, Perrings et al. 2010). Improving our ability to make predictions about the current and likely future resilience of these ecosystems (i.e. their capacity to resist change without undergoing a fundamental state shift (Holling 1973)) to drivers such as climatic forcing and internal disturbances is therefore of critical social and scientific relevance (Flessa and Jackson 2005).

Despite this recognised research need, little is currently known about how ecosystems are expected to respond to extreme climatic events (Andersen et al. 2009, Jentsch et al. 2011, Smith 2011). This is arguably due to the focus of most pre-21st century research on slow vs. abrupt drivers of change (e.g. gradual, linear warming) (Andersen et al. 2009). Additionally, those studies that have been conducted largely demonstrate that different ecosystems and ecosystem components respond in different ways to climatic extremes. For instance, in some cases, non-linear climatic forcing acts as a key agent driving ecological change (Shuman et al. 2009, Royer et al. 2011, Ammann et al. 2013), while in others, ecological regime shifts have not occurred in response to abrupt driver shifts due to internal stabilising processes (i.e. ecological resilience) (Larcher et al. 2010, Arnone III et al. 2011, Jentsch et al. 2011, Craine et al. 2012, Lloret et al. 2012, Sundstrom et al. 2012, Huntingford et al. 2013). These studies demonstrate the scalar challenges associated with attempting to formulate a general theory of ecological resilience across systems (Kerkhoff and Enquist 2007). As such, the need to better understand the relative influence of key drivers of change across different systems through time appears to be necessary for the development of informed predictions of future ecological response that can then be used to develop appropriate adaptive management strategies for different ecosystems. Pivotal to such research is improving knowledge of the critical thresholds and feedback processes operating within an ecosystem regime (analogous to a

stability basin) (Williams et al. 2011), and of the reorganisation factors and perturbations (internal and external) that can erode or build ecosystem resilience, serving to alter the morphology of the basin itself (Walker 2012).

One way that several researchers have attempted to approach the scalar issues associated with the varied driver-response interactions across ecosystems is to develop biome-level models of resilience for different global habitat-types. This works under the assumption that, because ecosystems occupying a similar habitat-type persist under similar climatic, and often topographic conditions, they are phenologically, and often physiognomically similar, and thus may respond in comparable ways to different drivers of change (Dinerstein et al. 1995). This research appears to provide a useful starting point for drawing out key processes acting to contribute to, or erode the resilience of different biomes (Hong et al. 2005, Loarie et al. 2009, Thompson et al. 2009, Staver et al. 2011a, Campos et al. 2013, Benito-Garzón et al. 2014, Stewart et al. 2014). However, testing the applicability of these generalisations to ecosystems within particular habitat types still appears to be in its infancy.

1.2 Threshold behaviour of seasonally dry tropical forests

Tropical forest biomes host exceptional global biodiversity, play a key function in regulating global feedbacks (Lewis 2006, Bonan 2008) — including carbon sequestration (Pan et al. 2011) — and, through their flows of direct and indirect ecosystem services, are critically important to sustaining human wellbeing (Millennium Ecosystem Assessment 2005, Sunderland et al. 2015). The impact of habitat-wide ecological reorganisation of these systems could, therefore, have far-reaching global consequences (Malhi 2012). This is particularly pertinent given that tropical forests (taken as an integrated system) have, in recent years, moved past the range of natural variability determined for the past half a million years (Lewis 2006). This demonstrates the urgent need for research on the resilience of these systems to future climatic forcing (Zuidema et al. 2013). While there has been some progress in this area within moist tropical forests (Maslin 2004, Mayle et al. 2007, Bhagwat et al. 2012, Brando et al. 2014, Cole et al. 2015), the interactions between climatic drivers and ecological dynamics are poorly understood for the seasonally dry tropical forest biome (Miles et al. 2006, Sunderland et al. 2015).

Research within the tropical and subtropical seasonally dry forest and savanna biomes in the Neotropics (Sternberg 2001, Brando et al. 2014), Afrotropics (Foley et al. 2003, Sankaran et al. 2005, Bucini and Hanan 2007, Good and Caylor 2011, Staver et al. 2011b), northern Australia (Williams et al. 1996) and globally (excluding Asia) (Hirota et al. 2011, Staver et al. 2011a) supports the existence of dry forest and savanna as alternative stable states, whereby a set of perturbations will determine the persistence of one ecosystem type over another. Key drivers of change that can instigate ecological regime shifts within this system appear to be rainfall quantity and seasonality (i.e. the length of the dry season) coupled with what (Bond 2008) has

termed top-down (fire-regime and herbivory) and bottom-up (water availability and nutrient) feedbacks. Predicted increases in climatic extremes for these systems (IPCC 2013), and their increasing exposure to a variety of anthropogenic threats (Miles et al. 2006) means that tropical dry forests may be particularly vulnerable to future change. As such, regionally-specific, resilience-focussed research within this biome, particularly with respect to disturbance, climate change and biodiversity, has been identified as a key research priority (Miles et al. 2006, Sunderland et al. 2015).

1.3 Threshold dynamics of south-east Asian seasonally dry tropical forests

South-east Asian seasonally dry tropical forests (SASDTF) represent one of the three largest, continuous tracts of tropical and subtropical dry forest across the globe (Olson and Dinerstein 2002, Maxwell and Cox 2011). Because of their extent, representativeness and biodiversity, they are recognised as a critical/endangered global 200 ecoregion (Olson et al. 2001), and form a major part of Indo-Malay biodiversity hotspot that has been prioritised as a global conservation region requiring urgent action (Myers et al. 2000). Despite this, the role of identified internal and external drivers of ecosystem change in these forests has not yet been tested, with dry-forest specific research in Asia virtually non-existent (Sunderland et al. 2015). Given that climatic factors are expected to be an important driver of state shifts with tropical dry forests, and that the Asian monsoon (which influences SASDTF) is predicted to undergo the largest shifts in rainfall and circulation change of all global monsoon areas (Christensen et al. 2013), this ecoregion may be especially vulnerable to future 21st century climatic change. This has been recognised within the IPCC AR5 (IPCC 2014), where research priorities have been established for understanding the ecological threshold dynamics of monsoon forests, with particular regard to thermal tolerance and acclimation.

1.4 A palaeoecological approach to ecosystem resilience analysis

One of the impediments to understanding broad-scale ecological threshold behaviour in the context of a changing global climate, is the lack of a data set that is of sufficient temporal length to be relevant to forest species and community dynamics (i.e. decades to centuries) (Gardner et al. 2009, Zuidema et al. 2013). Retrospective observation of past ecosystem change through the palaeorecord can provide a useful means of overcoming this temporal constraint (e.g. Virah-Sawmy et al. (2009), Bhagwat et al. (2012)). The increasing number of high-resolution Holocene palaeoclimatic and palaeoecological records for different parts of the tropics means that this technique

is especially useful for broad-scale resilience assessments. Using this approach, reconstructed ecological changes can be compared with known forcing events of various amplitudes and durations, providing a means of predicting future ecological response under a range of forcing scenarios. This has been identified as a key research need for predicting dry forest responses to disturbance regimes and future climate change (Sunderland et al. 2015), particularly given the theoretical propensity of this biome to stable state shifts.

Fortunately, there is an increasing repository of high-resolution climatic datasets from monsoon Asia that provide information on the amplitudes and durations of past precipitation regimes. These are predominantly derived from stable isotope records of monsoon rainfall derived from cave speleothems (Yuan et al. 2004, Dykoski et al. 2005, Wang et al. 2005, Berkelhammer et al. 2010, Sinha et al. 2011a)) and tree-ring reconstructions (Buckley et al. 2007, Sano et al. 2009, Buckley et al. 2010, Cook et al. 2010, D'Arrigo et al. 2011). Results of these reconstructions indicate that, throughout the Holocene, the monsoon has undergone a number of abrupt, millennial-scale shifts superimposed by lower-amplitude, multi-decadal fluctuations in precipitation. Ecological proxy data for the ecoregion, however, are scarce. Those that do exist provide some information about the long-term dynamics of tropical dry forests (Bishop et al. 1996, Kealhofer 1996, Kealhofer and Penny 1998, Maloney 1999, Penny 1999, Maxwell 2001, Penny 2001, Penny and Kealhofer 2005, Wohlfarth et al. 2012, Chawchai et al. 2013). However, these studies are limited in their application to assessing dry forest resilience because they are regionally constrained (restricted to several sites in northern Thailand and one site in north-east Cambodia (Maxwell 2001)) and are typically conducted at a low temporal resolution (i.e. the time interval spacing between reconstructed ecosystems exceeds estimated rates of total turnover for tropical forests (Phillips and Gentry 1994)). Additionally, palaeoecological data are often interpreted in the absence of complimentary driver-records, making it difficult to assess forest response to key drivers of change that have been identified for this biome (the exception to this is the Chawchai et al. (2013) and Wohlfarth et al. (2012) studies that use sedimentological and geochemical data alongside ecological data to infer qualitative precipitation change). As such, regionally disparate, high-resolution palaeoecological data that can be compared with complimentary land-use and climate records (as well as the pre-existing studies) are required in order to predict the future persistence of these forests in the face of global change.

1.5 Research objectives

Recognising the limited amount of work that has been done on the resilience of seemingly vulnerable yet ecologically significant south-east Asian seasonally dry tropical forests, the primary aim of this project is to reconstruct a high-resolution record of the response of representative ecosystems to Asian monsoon forcing over millennia. It is hoped that this can be used to better predict the likely response of these forests to projected climate change of similar amplitudes and magnitudes in coming decades.

Specifically, this project will:

- reconstruct ecological change and fire regime history by interrogating sediment-based ecological proxies from two, regionally disjunct crater lake sites in the core region of the Indo-Malay Biodiversity Hotspot. This will facilitate an assessment of dry forest threshold behaviour over millennia, and determine the role of fire in affecting ecosystem change over the same time period.
- develop a mid- to late-Holocene climate record using core geochemistry and complimentary plant microfossil data. This will be one of the first robust, high-resolution Holocene monsoon records produced for mainland south-east Asia, and will provide an in-situ climate record to which reconstructed ecological change and burn history can be compared.
- use these records in concert with pre-existing palaeoenvironmental data from ecosystems that support south-east Asian seasonally dry tropical forest in order to develop an holistic model for the threshold behaviour of these forests. More broadly, this will facilitate assessment of the regional applicability of biome-scale resilience models developed for seasonally dry tropical forests worldwide.

1.6 Study design rationale and thesis structure

The project aims will be realised by applying high-resolution, multi-proxy techniques to sediment cores extracted from volcanic crater lakes in Ratanakiri province, north-east Cambodia. The location of these lakes with respect to the distribution of seasonally dry forest within mainland south-east Asia is shown on Figure 1.1. Specifically, long cores extracted from crater lakes termed Yeak Loam and Yeak Mai are the focus for assessing long-term palaeoenvironmental change. Surface cores extracted from four crater lakes — Yeak Oam, Yeak Loam, Yeak Mai and Boeng Lumkut — are targeted for assessment of the contemporary microfossil signal to which the long-term records are compared. Yeak Kara sediments have been formerly assessed for palaeoenvironmental change in Maxwell (1999), Maxwell (2001) and Maxwell (2004), and are thus not analysed in this project. These studies do, however, provide a useful point of comparison for the subject work, and the location of this lake site is mapped on Figure 1.1 for context.

The study sites are located in the heart of south-east Asian seasonally dry tropical forest (Figure 1.1), preserve relevant ecological, climatic and land-use proxies (Maxwell 1999), are spatially offset, are known to have a relatively high sedimentation rate (Maxwell 2001), support heterogeneous forest units that have undergone varied degrees of disturbance, and have closed catchments. Combined, these characteristics facilitate a temporally high-resolution comparison of the ecological-climate-fire dynamics of a relatively dense (Yeak Loam) and a relatively open dry forest unit (Yeak Mai) across space and time. This provides ideal conditions for determining the relative

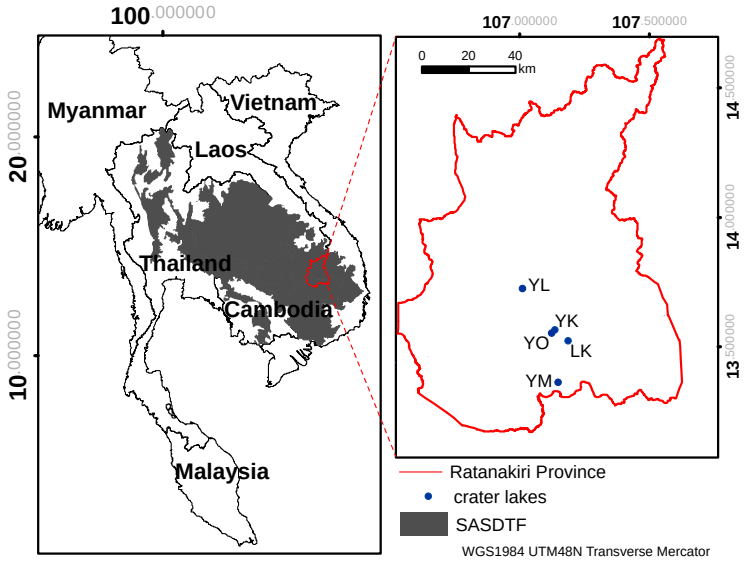

FIGURE 1.1: Map of continental southeast Asia showing location of crater lakes studied for this project in Ratanakiri Province, Cambodia. YL = Yeak Loam, YO = Yeak Oam, YK = Yeak Kara, LK = Boeng Lumkut and YM = Yeak Mai. The shaded region shows the extent of SASDTF

role of extrinsic vs. intrinsic drivers in affecting change, identified as a critical research need in the study of ecosystem threshold dynamics (Williams et al. 2011).

Chapter 2 provides an overview of the mechanisms thought to control the resilience of seasonally dry tropical forests. It argues that climate (particularly precipitation and rainfall seasonality) and fire appear to be important drivers of change (or stability) within this biome at a global scale, but that this has not been well tested within the seasonally dry tropical forest of south-east Asia. Chapter 3 describes the biotic and abiotic characteristics influencing the south-east Asian dry forest ecoregion, with a focus on the characteristics of the north-east Cambodian crater lake sites that are the subject of this study. Because there is little information on the extant conditions of the largely unstudied crater lake sites, some novel soil data collected as part of the subject study is integrated into this chapter (vs. the subsequent methods and results chapters that are focussed on the palaeoenvironmental reconstructions) for the sake of readability and clarity.

Chapter 4 presents the research techniques applied to sediment cores extracted from three of the crater lake sites to determine the chronology (necessary to provide an interpretive framework for the data), sedimentology and geochemistry (useful as climate and land-use proxies) of the records. The results of these methods are presented in the second half the chapter. Chapter 5 outlines the methods and results used to reconstruct 1) the contemporary plant microfossil record for Yeak Loam, Yeak Mai, Yeak Oam and Boeng Lumkut (each representing a different forest unit) and 2) the floristic and fire-regime history of the two lake sites selected for detailed palynological analysis (Yeak Mai and Yeak Loam). Chapter 6 integrates the

results from the previous two chapters in order to provide an interpretation of the climatic, fire regime and ecological histories of the lake sites over the past *c.* 5,000 years. These interpretations are used to discuss the threshold dynamics of south-east Asian dry forests in the face of climatic and land-use drivers since to mid-Holocene. Chapter 7 synthesises the project findings and concludes the thesis.

2 Threshold dynamics of seasonally dry tropical forests

2.1 Chapter overview

This chapter explores the threshold dynamics of seasonally dry tropical forests in order to define key drivers of change within this biome. The chapter is split into two main sections: 2.2 deals with the distribution and defining characteristics of tropical and subtropical seasonally dry tropical forests at a global scale and 2.3 reviews what is currently known about drivers of change and resilience within these systems. This is followed by a reflection on how these may relate to the under-researched south-east Asian seasonally dry tropical forests (SASDTF) that are the subject of this research.

2.2 Characteristics of the tropical and subtropical dry broadleaf forest biome

2.2.1 Global distribution of SDTF

Tropical and subtropical dry broadleaf forest — henceforth seasonally dry tropical forest or SDTF — is one of the fourteen terrestrial habitat types, or biomes, identified by the WWF global ecosystem assessment (Olson et al. 2001). Miles et al. (2006) estimate that the global extent (pre-2006) of tropical dry forest is approximately 1 048 700 km^2. They have calculated that, of this, more than half exists in South America, with the remainder split between North and Central America, Africa and Eurasia, and approximately 3.8% in Australasia and South-east Asia. These regions encompass four biogeographic realms — the Neotropics (with a small percentage extending northwards into the Neartic region), the Afrotropics, Australasia, and the Indo-Malay realm, the latter of which supports the SASDTF that is the focus of this study (Olson et al. 2001). The location of SDTF tracts within their respective biogeographic realms in shown, as mapped by (Olson et al. 2001), on Figure 2.1.

2.2.2 Defining SDTF

Mooney et al. (1995) note the heterogeneity of the SDTF both within and between biogeographic realms, suggesting that little unifies them aside from the distinct seasonality of rainfall that they are subject to. Werneck et al. (2011) — drawing on Murphy and Lugo (1986), Mooney et al. (1995) and

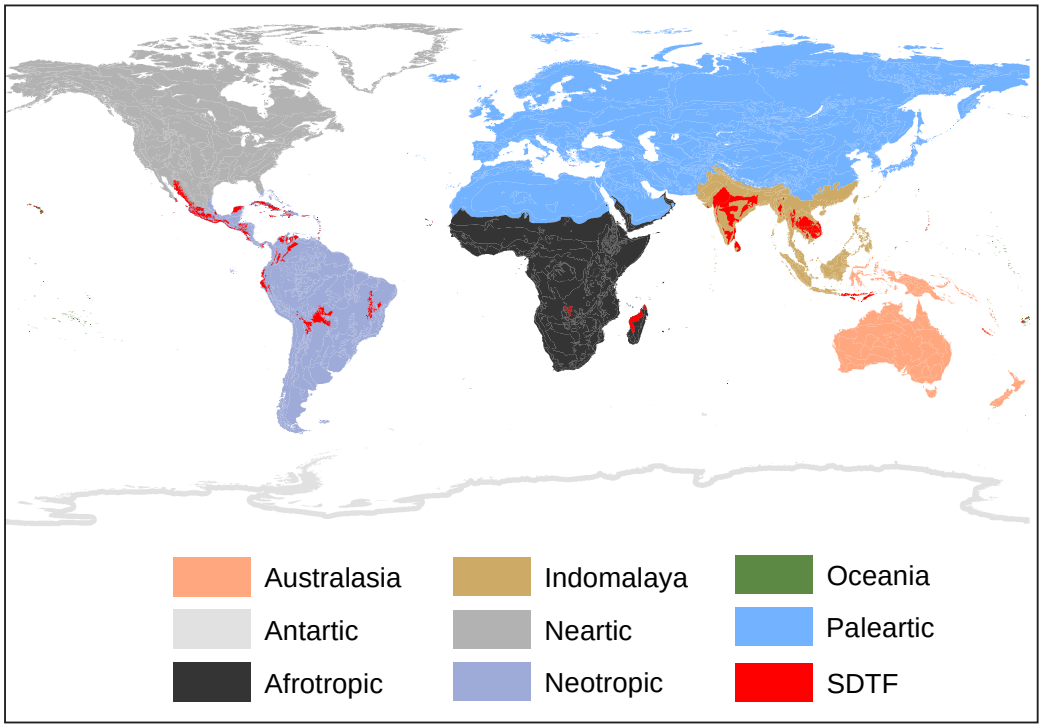

FIGURE 2.1: Global distribution of the tropical and subtropical dry broadleaf forest biome in the context of biogeographic realms (Olson et al. 2001).

Pennington et al. (2006) — offer a more constrained definition, suggesting that SDTF can be broadly defined as semi-deciduous forest that occurs in tropical (and subtropical) zones, and is subject to pronounced seasonal rainfall (minimum 5 months of annual drought) and a mean annual precipitation (MAP) of $<1\,600$ mm. While this definition may be characteristic of most Neotropical SDTF, there appear to be some forested ecosystems within this biome that defy some of these parameters. For example, several tropical dry forest units within south-east Asia persist with a MAP of up to 2 300 mm (Rundel and Boonpragob 1995) and others can be near-totally deciduous in the dry season (Ruangpanit 1995). To further complicate matters, there tends to be indistinct boundaries between dry forest and other vegetation types that often occur as patches within dry forest units and vice versa. In particular, SDTF ecosystems are often intermosaicked with tropical and subtropical grassland, savanna and shrubland (TGSS) ecosystems (Menaut et al. 1995, Sampaio 1995, Prance 2006).

Recognising the patchiness of SDTF units, Miles et al. (2006) used an encompassing SDTF classification to develop commonly-cited, global extent and distribution maps of SDTF (using MODIS Vegetation Continuous Fields modelling within WWF biome maps). Under this approach, ecosystems were classified as SDTF if they: 1) occurred in either SDTF or TGSS biomes as defined by (Olson et al. 2001); and 2) had greater than 40% canopy cover — considered the lower limit for forest ecosystems. This definition has been adopted, with caution, for the purpose of this review. It is, however, notable to point out that the amount of Neotropical dry forest classified under this

system is probably overestimated as tracts of shrubland are often included as forest (Sánchez -Azofeifa and Portillo-Quintero 2011). This is potentially also the case for the Afrotropics, where dry forest units commonly merge with tropical woodland ecosystems (Menaut et al. 1995).

A high level of floristic endemism is a key characteristic of SDTF that results in large discrepancies in genera and families between (and within) biogeographic realms. Nevertheless, there are several broad-scale ecological traits that are common to most representative SDTF and may play a key role in contributing to their resilience to external perturbations. Primarily, the plant phenology reflects adaptations to a long dry season, including (often) dry season leaf loss, and restricted timing of seed germination and seedling establishment (Quesada et al. 2009). These adaptations, according to Pulla et al. (2015), may mean that SDTF structure and biodiversity is resilient to the low- to moderate- level disturbances that are characteristics of these systems, including variable climate and herbivory. Consequently, representative forests may be more "pre-adapted" to cope with anthropogenic disturbance such as fragmentation, land degradation and modified fire regimes than their moist forest counterparts. Very generally, these adaptations include energy investment into soil seed banks and root stocks, and resprouting capacity post-disturbance. These characteristics, termed "internal ecological memory" (see Pulla et al. 2015 and references therein) mean that rapid SDTF forest succession can occur following moderately severe disturbance. Consequently, SDTF structural and species-richness attributes can be restored within decades (Pulla et al. 2015, Derroire et al. 2016). "External ecological memory" within SDTF ecosystems, whereby succession results from propagules from surrounding SDTF, is another important feature contributing to ecosystem resilience, particularly where disturbance is severe enough to erase internal ecological memory (Pulla et al. 2015).

It is, however, notable to point out that recovery of SDTF in terms of "old-growth" species composition tends to occur at a slow rate thereby indicating that "recovery" (i.e. engineering resilience) is unlikely to occur over short- to medium- timescales (Derroire et al. 2016). Additionally, as many SDTF species respond strongly to environmental cues, major changes in the annual or interannual timing of disturbance within associated ecosystems may have important implications for forest resilience, particularly if reproduction is reliant on animal pollination (Quesada et al. 2009). However, research on the role of pollination following environmental change is still in its infancy (Quesada et al. 2009). In spite of this, the aforementioned findings broadly indicate that SDTF resilience is by-and-large dependent on the magnitude, spatial scale and persistence of the disturbance as well as the specific functional traits of local SDTF species that contribute to ecological memory.

2.2.3 Review of SDTF in major biogeographic realms

The distribution and key structural characteristic of Neotropical, Afrotropical and Indo-Malay dry forests is presented below to provide a context for the synthesis of threshold behaviour in dry forests, presented in the second part of this chapter. This is important due to the bias in SDTF research in

the Neotropics and, to a lesser extent, the Afrotropics. For example, nearly all of the research articles in a recent book on the ecology and conservation of SDTF (Dirzo et al. 2011) focussed on the Neotropics. Similarly, no papers specifically focussed on south-east Asian ecosystems were included in a special issue on tropical savanna and seasonally dry forests published by the Journal of Biogeography in 2006 (volume 33). As such, most of what we presume to know about this biome comes from regions outside Indo-Malaya, providing an initial point of comparison for examination of SASDTF resilience.

Neotropical SDTF

Neotropical SDTF occurs in Meso- and South-America in a series of distinct ecoregions as shown on Figure 2.2. These range from somewhat continuous forest tracts in Bolivia, Paraguay, and Argentina extending northwards in Brazil (e.g. Chiquitano dry forests Figure 2.2 map reference K) to patches of dry forest in a mosaicked woodland/savanna/shrubland landscape (e.g. Mexican dry Forest (mapped as SDTF) and Cerrado and Caatinga (mapped as TGSS and Deserts and Xeric Shrubland biomes within central and east Brazil, respectively).

Low elevation (typically less that 800 m ASL, but occasionally reaching 2 000 m ASL), distinct rainfall seasonality and a precipitation-to-evaporation deficit are common to the majority of Neotropical dry forests. The dry season across representative ecoregions ranges from 4 to 8 months, and mean annual precipitation typically lies below 1 600 mm/year. Rainfall quantity and seasonality is often determined by geomorphic controls on patterns of ocean and atmospheric circulation. For instance, Mexican Dry Forests and Ecuadorian, Tumbes-Piura and Marañon Dry Forests (Figure 2.2 map references A and I respectively) have formed in the lowlands on the lee side of the continental mass in an orographic rain shadow. Dry forest in the semi-arid Caatinga lowlands is restricted to small areas of higher elevations, which permit the formation of more humid conditions in an otherwise arid climate (Sampaio 1995). Annual temperature variability across Neotropical SDTF is minor (Murphy and Lugo 1995).

Core dry forest units within the northern Neotropics are believed to have developed and persisted in isolation since the Last Glacial Maximum (LGM). It is hypothesised that these disjunct patches then expanded south and east in South America throughout the Holocene to their current distribution, resulting in unique biogeographic histories for different ecoregions (Caetano and Naciri 2011, Linares-Palomino et al. 2011, Werneck et al. 2011). This has caused a diverse floristic assemblage between different dry forest units (Caetano and Naciri 2011, Werneck et al. 2011). Linares-Palomino et al. (2011) have broadly categorised Neotropical SDTF ecoregions into four groups based on their floristic similarities. They include 1) Central American (including insular Central American), Colombian and Venezuelan SDTF (map references A to H on Figure 2.2); 2) Equadorian, Tumbes-Piura and Marañon Dry Forests (map reference I on Figure 2.2); 3) Bolivian Montane Dry Forests (map reference J on Figure 2.2) and isolated patches in the Chaco, and; 4) Chiquitano Dry Forests, Atlantic Dry Forests (map

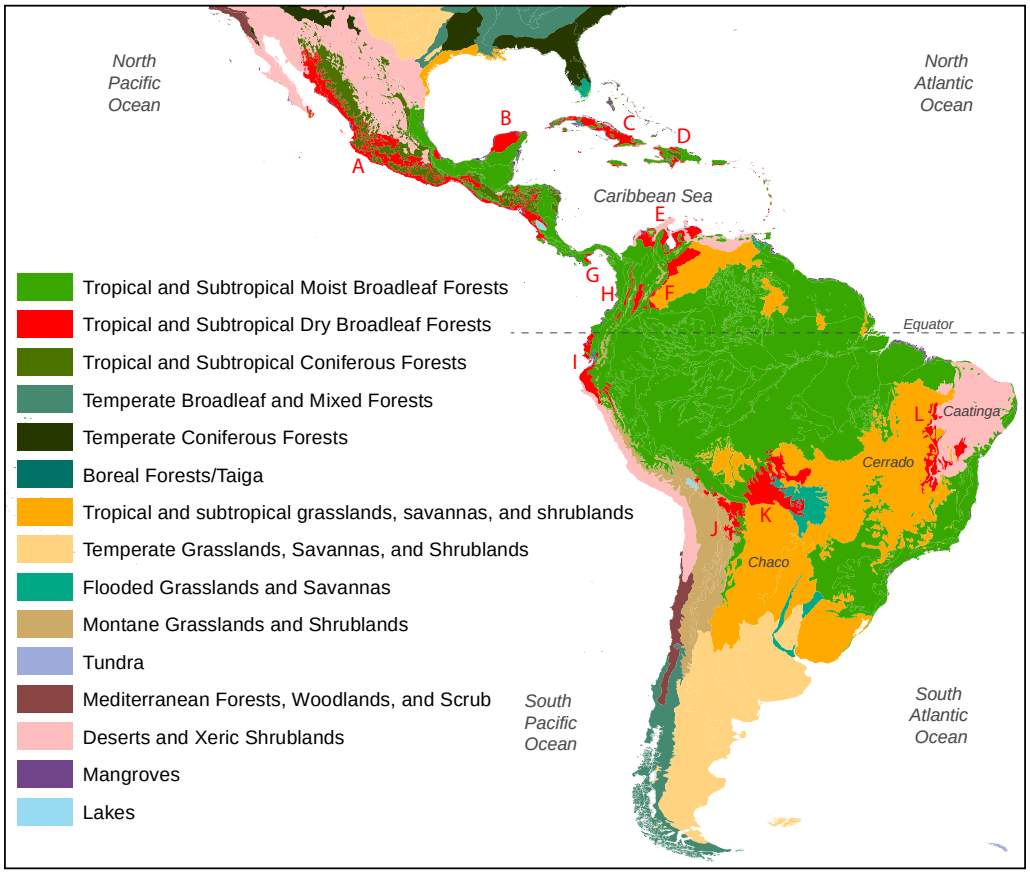

FIGURE 2.2: Distribution of Neotropical and Neartic tropical and subtropical dry broadleaf forests alongside adjacent habitat types (Olson et al. 2001). A. South Mexican and Central American Dry forests; B. Yucatàn Dry Forests; C. Cuban Dry Forests; D. Hispaniolan Dry Forests; E. Sinú Valley, Maracaibo and Lara-Falcon Dry Forests; F. Apure-Villavicencio Dry Forests; G. Panamanian Dry Forests; H. Cauca & Patia Valley Dry Forests; I. Equadorian, Tumbes-Piura and Marañon Dry Forests; J. Bolivian Montane Dry Forests; K. Chiquitano Dry Forests; L. Atlantic Dry Forests.

references K and L on Figure 2.2) and patches of dry forest in the Cerrado and Caatinga.

Despite the diversity in floristic composition of different Neotropical SDTF ecoregions, some broad generalisations can be made with respect to their vegetative makeup that may contribute to overarching resilience characteristics of these systems at a biogeographic realm scale. Compositionally, common genera within Neotropical dry forests are also present in moist and wet forest (Gentry, 1995). A review of Neotropical SDTF plant diversity, endemism and biogeography conducted by Linares-Palomino et al. (2011) shows that, of the fifty-five most widespread plant species in Neotropical SDTF, 45% are ecologically versatile (occuring across different forest biomes), and approximately 15% are dry forest specialists. Woody taxa within SDTF ecoregions is predominantly made up of genera from

the Fabaceae (Mimosoideae) family (Gentry 1995, Linares-Palomino et al. 2011). Other important SDTF arborescent families include Cannabaceae (*Celtis spp.*), Capparidaceae, Euphorbiaceae, Flacoutiaceae, Malvaceae (*Luehea spp.*), Meliaceae (*Trichilia spp.*) Rubiaceae, Rutaceae (*Zanthoxylum spp.*), and Sapindaceae (Gentry 1995, Linares-Palomino et al. 2011). Bignoniceae is the dominant liana family within Neotropical SDTF (Gentry 1995).

The prevalence of forest generalist genera within Neotropical dry forest may be controlled by 1) pollination and seed dispersion characteristics of dominant taxa, 2) possession of functional traits that allow for tolerance of a broad range of environmental conditions, and 3) habitat controls that influence plant distribution at a species-level. Two-thirds of Neotropical SDTF woody taxa are pollinated by specialists including insects or birds, and seed dispersal tends to predominantly occur via wind dispersal (Bullock, 1995). Both of these traits are important within moist and dry tropical forest, but tend to be more important in the latter (Gentry, 1995). Both Bignoniaceae and Leguminosae characteristically have conspicuous flowers that are dependent on insect and mammal pollinators, and possess wind-dispersed seeds (Gentry, 1995). Several dominant *Acacia* species within Neotropical SDTF are particularly tolerant to water stress and variable light levels during the seedling stage (Venier, 2013), which may also contribute to their presence in both moist and dry sites, but dominance in the latter (where other, more sensitive species may not survive). Within families, shubby (vs. scandent or arborescent) species — better adapted to moisture limited conditions — tend to be favoured within dry forest settings (Gentry, 1995). Other plant adaptations to moisture limitation within dry vs. moist forest systems in the Neotropics include denser wood and investment into deep root biomass (Holbrook et al. 1995).

Variation in plant structure depending on moisture availability likely contributes to the large degree of variability in the overarching structure of Neotropical SDTF. Across the biogeographic realm, canopy height can range from 2 to 40 m and structure from 2 to 4 stories (Murphy and Lugo 1995). The majority of Central and South American dry forest grows in alkaline, fertile soils, with density and height positively correlated with soil quality (Meir and Pennington 2011, Werneck et al. 2011). Some low, open formations can grow in exposed, acidic and nutrient poor soils (Murphy and Lugo 1995).

Most of the SDTF in Central and South America has been disturbed or cleared for agriculture, mostly for cattle grazing and cropping (Sampaio 1995, Sanchez-Azofeifa et al. 2005). Much of this clearance is been instigated (and sometimes maintained) with slash-and-burn (swidden) agriculture (García-Oliva and Jaramillo 2011), introducing fire to ecosystems that are thought to have "naturally" precluded fire (Murphy and Lugo 1995). This type of farming, sometimes referred to as "slash-and-burn" cultivation, involves: 1) using fire to clear land; 2) cultivating crops on that land, and; 3) subsequently abandoning the land to fallow (Sovu et al. 2009). According to a study undertaken by Guariguata and Ostertag (2001), the capacity of Neotropical forest to regenerate via secondary forest succession

following swidden farming is relatively good if there is a localised propagule source (i.e. good external ecological memory) and the level of disturbance prior to abandonment has not been severe (i.e. retention of internal ecological memory).

Afrotropical dry forest

Aside from a small core of dry forest in Zambia (Figure 2.3 reference A) and the dry forest communities of Madagascar (Figure 2.3 reference B), SDTF in the Afrotropics almost always occurs as fragmented patches within the TGSS ecoregions to the north (Sudanian TGSS) and south (Zambezian TGSS) of the continent (Olson et al. 2001, Miles et al. 2006, Linder et al. 2012). These are separated from the equatorial moist tropical forests by a relatively narrow belt of humid savanna (Menaut et al. 1995, Olson et al. 2001).

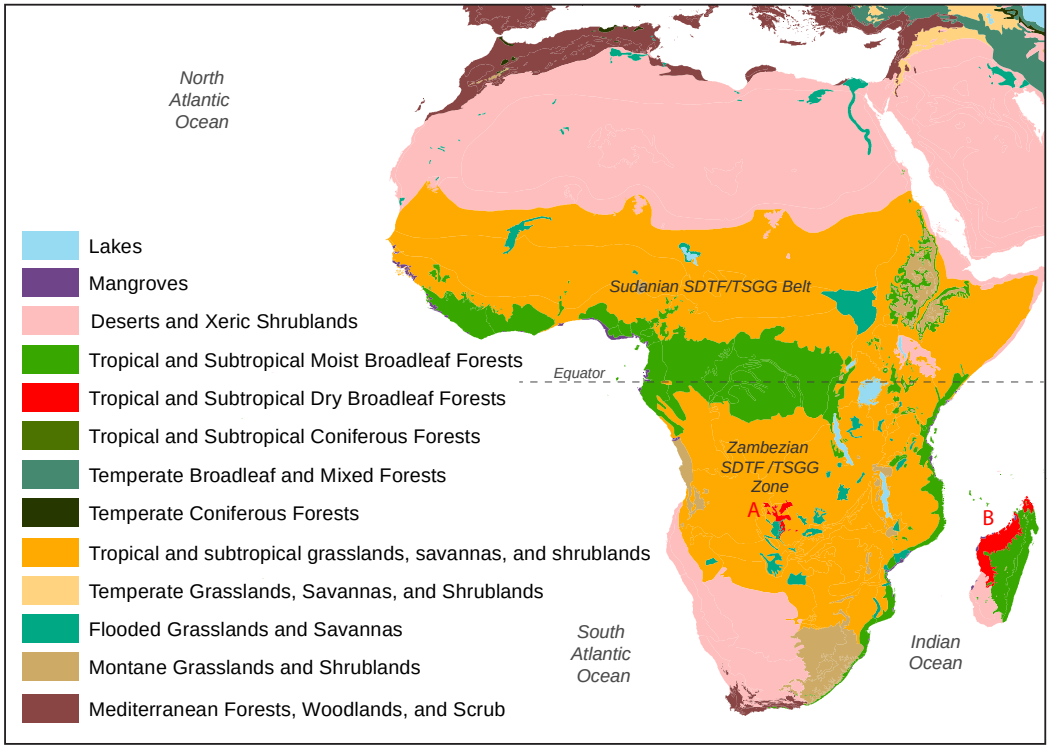

FIGURE 2.3: Distribution of Afrotropical tropical and subtropical dry broadleaf forests alongside adjacent habitat types (Olson et al. 2001). A. Zambezian Chryptosepalum Dry Forests; B. Madagascar Dry Forests. Most Afrotropical tropical dry forest units are scattered within Sudanian and Zambezian TGSS.

As with Neotropical SDTF, rainfall seasonality (4 to 8 month dry spell) and a low precipitation to evaporation ratio (0.4 to 0.6) characterise African dry forests (Menaut et al. 1995). The variance in annual rainfall is driven by the African monsoon. MAP across Afrotropical SDTF ranges from 800 to 1 000 mm (Menaut et al. 1995). While this is slightly higher for the Sudanese

region than for its southern hemisphere counterpart, the former tends to be lower in elevation (approximately 200 m ASL vs. up to 1 000 m ASL) and subjected to dry deserts winds. Thus northern forests are typically drier and more open than the denser dry forest patches interspersed with Zambezian TGSS (Menaut et al. 1995). However, within these generalisations, Afrotropical SDTF is very diverse, ranging from open woodlands comprising deciduous trees growing above a grassy understorey, to more-closed, species-rich, semi-deciduous forest communities (Swaine 1992, Timberlake et al. 2010). Structurally, most semi-deciduous forests have a canopy height of up to 25 m and a dense understorey of lianas and shrubs (Menaut et al. 1995). Though Afrotropical SDTF grows in a range of soil-types, many of the denser, semi-deciduous types are associated with lateritic formations (Menaut et al. 1995).

The floristic assemblage of Afrotropical SDTF is varied. Broadly, however, it can be categorised into northern and southern hemisphere ecoregions. The former typically comprises *Afraegle* (Rutaceae)-dominated deciduous/semi-deciduous forest with a diverse understorey (Menaut et al. 1995). Relict patches of dry evergreen forest within this region are often characterised by the presence of *Gilletiodendron/Guibourtia* (Fabaceae) species (Menaut et al. 1995). Southern SDTF formations are more species rich and phenologically complex than their northern counterparts (Menaut et al. 1995), but tend to be overarchingly dominated by semi-deciduous *Entandrophragma* (Meliaceae), broad-leaved canopy species. Three relict evergreen dry forest types that occur sporadically within the Zambezian forest comprise *Parinari-Syzygium* (Chrysobalanaceae-Myrtaceae) forest, *Marquesia* (Dipterocarpaceae) forest and *Cryptosepalum* (Fabaceae) forest (Menaut et al. 1995). These formations, particularly Chrysobalanaceae-Myrtaceae units, are fire intolerant (Chidumayo and Marunda 2010).

Indo-Malay SDTF

SDTF forest in the Indo-Malay realm occurs in three distinct zones Figure 2.4. Indian dry forests and ecoregions therein occupy much of central and eastern India as well as eastern Sri Lanka (Figure 2.4 map reference E through K). Small islands vegetated with SDTF occur in southern insular south-east Asia, including parts of Indonesia and Timor-Leste (Figure 2.4 map reference L). SASDTF, which is the subject of this research, extends east from Myanmar, through Thailand, into Laos, Cambodia and part of central and southern Vietnam (Figure 2.4 map reference A and B). Relatively small tracts of dry forest also extend into central Myanmar (Figure 2.4 map reference C).

SDTF units in India and Myanmar are relatively fragmented, whereas SASDTF tends to form a relatively contiguous biogeographic unit (Miles et al. 2006), even though it is currently subject to high levels of clearance for small- and large-scale agriculture and cash crops (Hor et al. 2014). These dry forest regions are broadly encircled by tropical and subtropical moist forest ecoregions (Olson et al. 2001) where rainfall seasonality is not significant (e.g. in equatorial zones or where elevation increases). The exception to this is

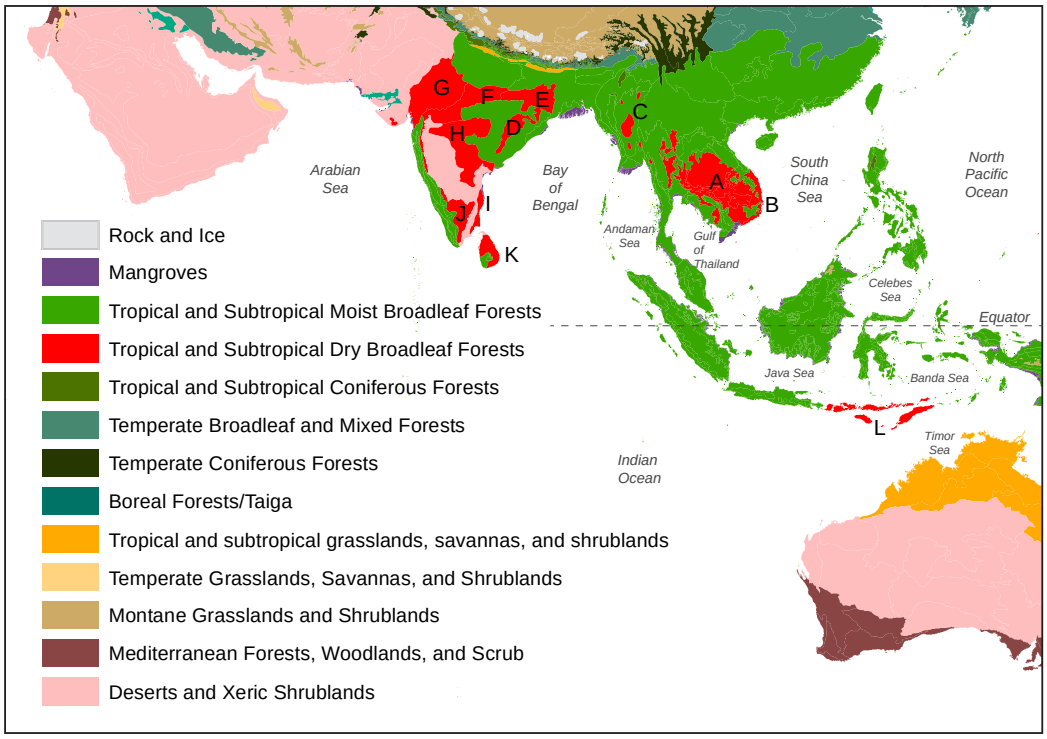

FIGURE 2.4: Distribution of Indomalayan tropical and subtropical dry broadleaf forests alongside adjacent habitat types (Olson et al. 2001). A. SASDTF (Southeastern Indochina dry evergreen forests [SIDEF] and Central Indochina Dry Forests [CIDF]); B. Southern Vietnam lowland Dry Forests; C. Irrawaddy Dry Forests; D. Northern Dry Deciduous Forests; E. Chhota-Nagpur Dry Deciduous Forests; F. Narmada Valley Dry Deciduous Forests; G. Khathiar-Gir Deciduous Forests; H. Central Decaan Plateau Dry Deciduous Forests; I. East Deccan Dry-Evergreen Forests; J. South Deccan Plateau Dry Deciduous Forests; K. Sri Lanka Dry-Zone Dry Evergreen Forests; L. Lesser Sundas Deciduous Forests, Sumba Deciduous Forests and Timor and Water Deciduous Forests.

the linear desert ecosystem on the west boundary of east-Indian Chhota-Nagpur Dry Forests (Figure 2.4 map reference E), formed from the presence of a major orographic rain shadow. Seasonality within the Indo-Malay SDTF is driven by the Indian and/or East Asian sectors of the Asian monsoon, resulting in a 4 to 8 month dry season (Wikramanayake et al. 2002). MAP received by these forests is diverse, ranging from 1 000 to 1 900 mm, though exceptions occur at either end of the scale (Wikramanayake et al. 2002, Oo and Koike 2015).

The structure and floristics of Indo-Malay dry forests are heterogeneous between the three major dry forest zones described for the biogeographic realm. For example, despite their superficial similarities, the floristic composition of SASDTF was found to be more affiliated with adjacent moist

forest than to that of the dry forests of India (Dexter et al. 2015). This suggests that, as with Neotropical dry forest ecoregions, vegetation within the different zones is likely to have persisted in isolation over a long period of time in spite of their common mid-Eocene dispersal route (Morley 2002).

As well as the variability noted across Indo-Malay dry forest zones, there is a high degree of intra-ecoregional variability in dry forest structure and composition. However, unlike neo- and Afro-tropical forest mosaics where dry forest is commonly interspersed with savanna, many Indo-Malay forests, especially SASDTF, manifest as a mosaic of dense and more open dry forest units. Here, "natural" open grassland communities are generally limited to seasonally inundated herbaceous wetlands and isolated patches of savanna on uplands where MAP is low (<500 mm) (Stott 1990).

SASDTF mosaics are dominated by three forest unit-types. Deciduous dipterocarp forest (DDF) has a low but varied canopy height of 10 to 30 m, with a cover of 53 to 77% (Neal 1967), making it the most open of the dry forest units. Deciduous species from the Dipterocarpaceae family dominate the canopy and mid-storey (Ruangpanit 1995). The understorey is generally minimal, allowing for a grassy ground cover to develop. Variants on this forest type can be found within most Indo-Malayan SDTF ecoregions, particularly in less fertile soils where MAP is relatively low (Stott 1990, Ruangpanit 1995). Unlike Neotropical dry forests, fire is an important part of DDF (in some cases being fundamental to its persistence (Stott 1984, 1988). The presence of a grassy ground cover and propensity of DDF to burn, has lead Dexter et al. (2015) to propose that this unit should be classified as savanna, despite long-term acknowledgment of its essential "forest" character by several authors who have worked extensively in the region (see Stott 1984, Stott 1986, 1990 and references therein). All dominant Dipterocarpaceae tree species within DDF have morphological (thick bark, resprouting root crowns) adaptations to fire (Rundel and Boonpragob, 1995). Germination timing (at the start of the wet season) and wind dispersion of fruits from dominant DDF aborescent species may also facilitate forest succession post-fire events (Rundel and Boonpragob, 1995).

Mixed deciduous forest (MDF) has three layers with a partially deciduous, diverse canopy reaching 30 m (Rundel and Boonpragob 1995). The forest understorey (5 to 10 m) comprises a diverse range of trees, shrubs and bamboos (Ruangpanit 1995, Rundel and Boonpragob 1995). Semi-evergreen dry forest (SEDF) is a closed formation with up to four layers of evergreen and deciduous species (Ruangpanit 1995). Lower versions of SEDF occur within the East Deccan dry-evergreen forest and Sri Lanka dry-zone dry evergreen forest ecoregions (Figure 2.4 map references I and K).

A more detailed description of the structure and ecology of SASDTF units is presented in the context of the study site in chapter 3.

2.3 Projected threshold behaviour of seasonally dry forests

Contemporary theory regarding the threshold behaviour of SDTF ecosystems is closely coupled with concepts of ecological resilience, first posited

by Holling (1973) and updated in, amongst others, Walker et al. (2004). Holling's conceptual model suggests that ecosystem resilience — that is the capacity of a system to absorb change without dramatically altering in structure or function — has limits that, when breached, can result in the rapid reconfiguration of the system to a new, fundamentally different "stable" state. This rapid reconfiguration is contemporarily referred to as a catastrophic or an ecological regime shift, and can be irreversible (or very difficult to reverse) due to positive feedbacks (Scheffer et al. 2001, Scheffer and Carpenter 2003).

It has long been noted that tropical savanna (taken here to represent ecosystems with a prevalence of C4 grasses and less than 40% tree cover (Ratnam et al. 2011) and dry forest, which occupy a similar climatic zone, are intimately linked. Small differences in topography, edaphic conditions, climate, or human modification can determine whether one state occurs over the other (Murphy and Bowman 2012). As such, these two biome types are thought to persist as alternative stable states, whereby relatively small changes to internal or external drivers can push either system across a tipping point, triggering a rapid reorganisation of ecosystem expression (Sternberg 2001, Foley et al. 2003, Hirota et al. 2011, Staver et al. 2011a, b). The projected resilience, or capacity of SDTF ecosystems to cope with future climatic extremes without undergoing a fundamental state shift (Holling 1973) — most likely to the savanna state — can thus be inferred through consideration of their inherent biogeographic and evolutionary characteristics within the context of current and projected future drivers of ecological change within these systems.

This section examines some of the key abiotic parameters that appear to drive change in SDTF. These are considered in the context of biotic characteristics of SDTF, such as ecological memory and plant functional traits, which may contribute to SDTF resilience in the face of these drivers.

Noting that, in nearly all circumstances, SASDTF has been neglected from relevant resilience research, it will then assess how the identified drivers of ecological change in SDTF interact in SASDTF contemporarily and historically. This will be used to infer how sensitive these systems should be to future change.

2.3.1 Climatic drivers

SDTF – Precipitation

Maass and Burgos (2011) assert that water is the primary factor in determining the structure and function of SDTF. This has been well-demonstrated in a recent global study undertaken by Hirota et al. (2011), who present evidence for the strong coupling between annual precipitation and the existence of forest and savanna as alternative attractors. In this study, these biomes were distinguished on the basis of satellite (MODIS) analysis of tree cover in the tropics and subtropics of Africa, the Americas and Australia. A non-linear threshold response was noted between these biomes with areas with canopy cover at approximately 50 to 60% found to be extremely rare

at a global scale (Figure 2.5), indicating the absence of an intermediate for-

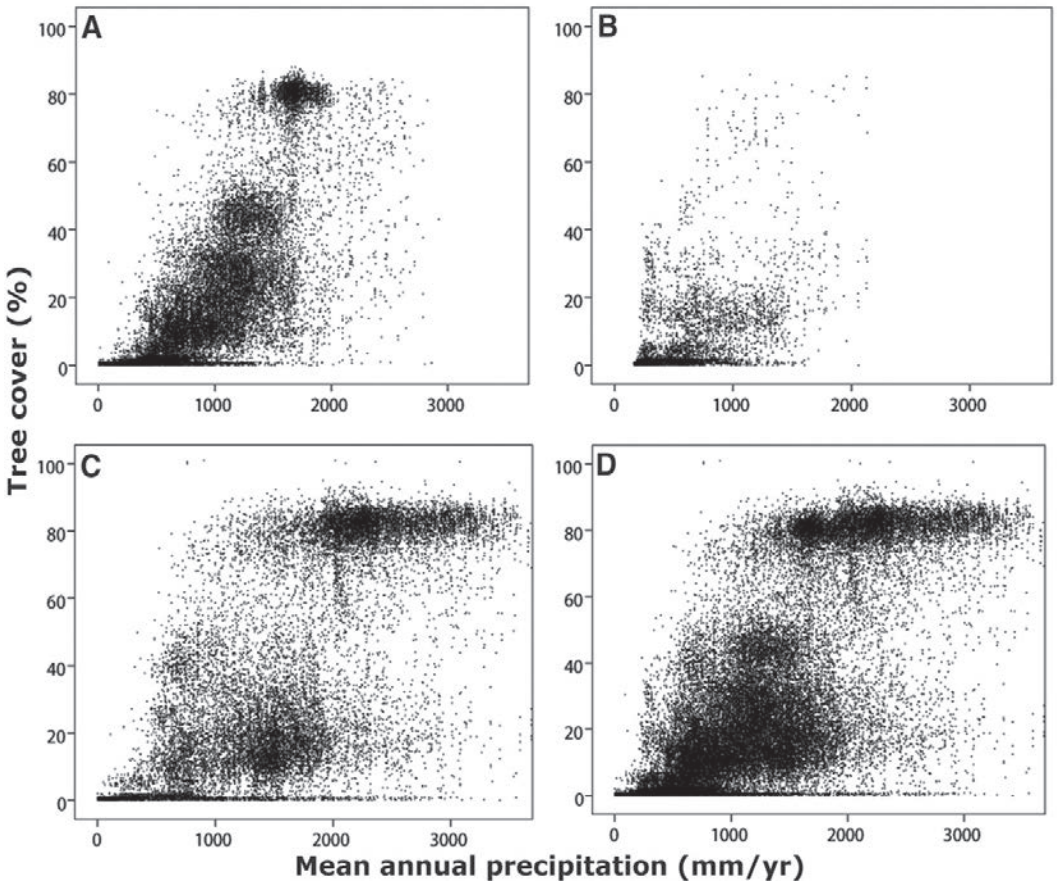

FIGURE 2.5: Figure reproduced from Hirota et al. (2011) showing tree cover (untransformed) in 1 km^2 grid cells as a function of the mean annual precipitation for (A) Africa, (B) Australia, (C) South America, and (D) intercontinental data sets (between 35°S and 15°N). Image used with permission from AAAS (licence number 3852280176217).

est/savanna hybrid in the natural environment. MAP and tree cover (and thus biome-state) were found to be intimately linked; that is, forest was found to persist where precipitation exceeds 2 500 mm/year, and savanna MAP ranged from 750 to 2 500 mm/year. Bistable areas (i.e. where annual precipitation could support either ecosystem state) lie within the range of 1 000 to 2 500 mm/year (Staver et al. 2011a). This bistable zone represents the current climate for nearly all SDTF ecoregions, though it is notable that some tracts of persistent forest do occur with MAP less than 1 000 mm. For instance, the Irrawaddy Dry Forests of central Myanmar receive an average annual rainfall of 600 mm year (Oo and Koike 2015).

Several Afrotropical studies (Sankaran et al. 2005, Bucini and Hanan 2007) also demonstrate that the persistence of woody cover in savanna (i.e. patches of dry forest or woodland) can be constrained by MAP. In Sankaran et al. (2005), woody cover was found to increase linearly with rising precipitation up to 650 mm/year. Above this threshold MAP is considered sufficient for canopy closure and fire becomes the dominant control on cover. Bucini and

Hanan (2007) found a positive relationship between tree cover and MAP, but noted a dependency on soil texture.

The role of increased precipitation on the development of the structure of SDTF has also been observed in Australia (Banfai and Bowman 2006) and the Neotropics with regard to an increased basal growth area (Murphy and Lugo 1995) and primary productivity (Jaramillo et al. 2011) and, in the case of decreased rainfall, reduced biomass (Coe et al. 2013) . A similar phenomenon has been observed in African and Australian TGSS ecosystems, where tree basal area typically increases with rising MAP (Scholes et al. 2002, Lehmann et al. 2014). This trend is, however, is not always clear for Neotropical savanna (Lehmann et al. 2014).

This body of research is of consequence for understanding the tree cover and precipitation threshold dynamics of both SDTF and TGSS. It suggests that when critical precipitation thresholds are breached, ecological reconfiguration between savanna and forest is likely to occur as a rapid response. Reconfiguration between open and dense communities within either forest or savanna, however, may be more likely to occur as a gradual change. It is, however, important to note that there are ranges of MAP that can support either forest or savanna, indicating the importance of other abiotic and biotic controls on persistence of one state over the other.

SDTF – Seasonality

As seasonality is one of the key features of dry forest biomes, dominant tree species within representative ecoregions typically have a range of physiological and phenological adaptations to drought (Meir and Pennington 2011). However, critical thresholds regarding the strength of seasonality (referring to the duration of the dry season (Staver et al. 2011a)) tolerated by SDTF do exist. This is explored by Staver et al. (2011a) who found that in Australia, South America and Africa, where annual drought exceeds seven months, savanna will persist. However, there is evidence that most biomes display a degree of resilience to multi-year droughts, indicating that intensity and duration of persistently strong seasonality may be a requirement for this state-change (Campos et al. 2013). Where seasonality is less than seven months, it is considered bistable for either TGSS or SDTF ecosystems, where either can persist (Staver et al. 2011a). These threshold interactions are strongly linked to the role of fire in these biomes, as discussed in section 2.3.2 below.

Seasonality strength also appears to play a role in determining the internal structure of SDTF. For instance, in Neotropical ecosystems, tree growth and canopy height appears to have an inverse relationship with dry season length (Murphy and Lugo 1995). As such, regions with milder seasonality (i.e. shorter dry season) are likely to support denser forest types, although these interactions also appear strongly linked to the edaphic characteristic of forest units, particularly with regard to soil water retention capacity.

SDTF – Temperature

There is little evidence to suggest that rising temperature on its own will significantly impact upon the structure or function of either dry forest or savanna, with most species seemingly well-adapted to hot conditions. However, rising temperatures are likely to exacerbate conditions related to plant water stress by increasing evapotranspiration (Pulla et al. 2015). Additionally, drought, coupled with high temperatures may decrease relative humidity, drying biomass fuel and encouraging fire. The velocity of temperature change predicted from dry broadleaved forest at (0.42 km/year) is the third highest for forested biomes, (exceeded by mangroves and taiga), largely due to their persistence in lowland regions (Loarie et al. 2009). This may have implications for the resilience of localised patches of SDTF.

SASDTF

The dry forest units within mainland south-east Asia are subjected to a MAP of <2 000 mm/year and a seasonality of less than seven months, placing the ecoregion into a bistable zone as defined by Hirota et al. (2011) and Staver et al. (2011a) (i.e., within a climatic zone that can support either forest or savanna). The drier forest units, including DDF and some MDF units, have an open canopy as low as 53% (Neal 1967), which, according to Hirota et al. (2011), is rare at a global scale (see Figure 2.5). As such, if the climate-seasonality-forest cover feedbacks used to predict the stability of SDTF apply to SASDTF, representative forests may, in their current state, be sensitive to crossing a critical threshold to savanna if subjected to drivers such as declining annual precipitation, droughts, habitat fragmentation or selective tree felling (serving to further thin the canopy). This, however, has not been quantified.

Holocene reconstructions of past precipitation, including periods of drought (Dykoski et al. 2005, Wang et al. 2005, Sinha et al. 2007, Sano et al. 2009, Buckley et al. 2010, Cook et al. 2010, Sinha et al. 2011a, b) demonstrate lower rainfall associated with a stepwise weakening of the summer monsoon over the SASDTF region between 5 and 4.5 ka, and approximately 3.5 ka, typically following periods of reduced insolation. Additionally, the presence of prolonged droughts (up to 30 years) occurred in the mid-14th and 15th centuries across India (Borgaonkar et al. 2010, Sinha et al. 2011a), Vietnam (Buckley et al. 2010), and Thailand (Buckley et al. 2007), associated with volcanism (Anchukaitis et al. 2010), ocean-atmosphere dynamics (Cook et al. 2010) and, to a lesser extent, solar minima (Shi et al. 2016). When compared to contemporary precipitation and seasonality conditions for SDTF, these past climates should, at times, favour the persistence of savanna over forest given the theoretical propensity of SDTF to transition to grassland communities under periods of reduced precipitation and prolonged water stress. This is particularly so if, during these periods, MAP was to decline, and seasonality was to increase to levels that breach the "bistable" thresholds set out by Hirota et al. (2011) and Staver et al. (2011a). Given the apparent "unstable" canopy cover of more open SASDTF units such as DDF and some MDF (as set out in Hirota et al. (2011)), these forest

units may be particularly sensitive to a regime shift to savanna under these changed conditions.

Though localised, the few palaeo-ecological studies that do elucidate SASDTF vegetation change in response to these past climate events (Bishop et al. 1996, Kealhofer 1996, Kealhofer and Penny 1998, Maloney 1999, Penny 1999, Maxwell 2001, Penny 2001, Penny and Kealhofer 2005, Wohlfarth et al. 2012, Chawchai et al. 2013), indicate that forest has persisted throughout the Holocene. The only major ecological regime shift in response to climatic forcing that can be observed in these records is the transition from pine-oak forest to tropical dry broadleaf forests at the termination of the Younger Dryas Chronozone (*c.* 12000 to 10000 cal. yrs BP), when the climate shifted abruptly toward more humid conditions (Penny 2001). What is interesting to note from these records, is the increasing variability in the composition of the ecological records over recent millennia. Such"flickering" within ecological records is often taken as sign that a critical threshold is being approached (Scheffer et al. 2009, Scheffer et al. 2012, Wang et al. 2012).

There is some evidence that a wetter climate may facilitate shifts in dry forests of similar composition to SASDTF to denser types. For instance, the so-called Medieval Warm Period (MWP), characterised by a relatively warm, humid climate (modelled in the Asian monsoon region as occurring between *c.* 901 and 1200 AD (Shi et al. 2016)), appears to have caused the non-persistent transition of a Central Deccan Plateau (India) open mixed deciduous forest into a dense mixed forest (Quamar and Chauhan 2014).

These studies suggest that the moisture requirements of SASDTF may be different from their global counterparts and/or indicate that factors external to climate, including phenological adaptations of particular species to lowered MAP, may play important roles in reinforcing forest feedbacks. This point has been emphasised by Rundel and Boonpragob (1995) who observe that south-east Asian dry forests exhibit different ecological structures and processes to their Neotropical counterparts, particularly with regard to the surprising current vegetation-rainfall relationships (e.g. deciduous forest persisting in areas of higher precipitation, and semi-evergreen assemblages present in region with relatively little annual rainfall). However, as the plant microfossil records from the SASDTF region are spatially limited, are typically conducted at a low temporal resolution, and don't tend to be compared with external climatic records (rather being used as an indication of climate themselves), the precise impact of climatic variability upon receiving dry forest ecosystems (particularly if state-shifts are not persistent) remains ambiguous.

Another complicating factor that needs to be considered when examining SASDTF response to climatic forcing is the sub-regional discrepancies that are apparent in Holocene records of Asian monsoon shifts, particularly in recent millennia and at shorter time scales (decadal to centennial) (Sinha et al. 2011a, Wan et al. 2011, Cook et al. 2013). This suggests that location-specific records are necessary in order to draw links between climate events and the attendant ecosystem, particularly given the apparent increasing ecological variance noted in the late Holocene palaeorecord (Penny 2001, Maxwell and Liu 2002). Given that most SASDTF forests lie at the intersection of two monsoon systems (the Indian Summer Monsoon and East Asian

Monsoon) (Wang and LinHo 2002, Wang et al. 2003), the complexities associated with local monsoon disparities are likely to be amplified. Currently, long-term records of climate change from this confluence zone (external to inferences made about climate from ecosystem change (e.g. Kealhofer and Penny 1998, Maxwell 2001, Penny 2001) are few (and thus highly localised) (Wohlfarth et al. 2012, Chawchai et al. 2013) or only capture the late Holocene (Buckley et al. 2007, Sano et al. 2009, Buckley et al. 2010).

2.3.2 Fire

SDTF

Most burning within the SDTF is considered to be of anthropogenic origin rather than a natural phenomenon (Hoffmann et al. 2009, Sánchez-Azofeifa and Portillo-Quintero 2011). The increased frequency and area of burning is generally considered one of the greatest threats to the survival of dry forests in the Neotropics, (Sánchez-Azofeifa and Portillo-Quintero 2011), Afrotropics (Staver et al. 2011b), Australia (Banfai and Bowman 2006) and worldwide (Miles et al. 2006). This is considered to be of particular concern given that the occurrence of fire is predicted to grow alongside rising populations, increasing temperatures and greater probability of climatic extremes including drought (Lewis 2006).

Interactions between the presence of fire and the persistence of tropical and subtropical forest in Africa, South America and Australia (where satellite analysis of tree cover was again used as a proxy for biome-type), has been tested by Staver et al. (2011a). These authors found that, where bistable climatic conditions occur with regards to seasonality and MAP (discussed in section 2.3.1), fire appears to be a key driver determining whether the landscape will support savanna or forest (>55% canopy cover) — the former coexisting with fire, and the latter persisting in areas that have not been recently burnt. In theory, the development of a forest canopy precludes the spread of fire by inhibiting the establishment of a dry, grassy ground cover. When canopy cover falls below approximately 40%, relative ground humidity drops and a grassy understorey develops. Combined, these factors tend to introduce moderate to high intensity fire into the forest, serving to further open the canopy. This causes a positive feedback cascade, reinforcing the development of open, grassland ecosystems (Staver et al. 2011a). This feedback has been confirmed in several savanna ecosystems persisting in bistable forest/savanna climatic zones within the Afrotropics (Menaut et al. 1995, Staver et al. 2011b) and in the Neotropics under climate conditions that would favour the development of forest (Ballesteros et al. 2014). Conversely, fire exclusion can permit the reestablishment of woodland or forest within bistable climate zones in the Afrotropics (Mitchard et al. 2009), and Neotropics (Moreira 2000).

Coupling of fire with other drivers of SDTF resilience, particularly seasonality and fragmentation, is particularly detrimental to the persistence

of forest over grassland communities. Brando et al. (2014) show that extreme drought coupled with forest fragmentation and anthropogenic ignition sources have resulted in significant tree mortality and forest degradation over southeast Amazonia (noting that these forest are typically moist vs. dry).

While fire is clearly an important driver of forest to savanna ecological regime shifts within many climatically bistable SDTF/TGSS zones, there are some cases where dry forest and fire can co-exist. Typically, this integration is regionally specific, being contingent on the features of the burn as well as the adaptation characteristics of the effected ecosystem. Fire resistant or fire-tolerant adaptations exist in some SDTF species in certain African (Swaine 1992), Australian (Russell-Smith et al. 1997, Andersen et al. 2005) and Indian (Kodandapani et al. 2008, Mondal and Sukumar 2015) dry forests. These adaptations result in relatively low large-tree mortality when burns are low to medium intensity (Meir and Pennington 2011, Pulla et al. 2015). Equally important to the concurrence of SDTF and fire, is the timing, intensity and recurrence interval of the burn regime. Low intensity fires usually occur where there is little build-up of ignitable ground materials, and are thus more characteristic of the early (vs. late) part of the dry season (Pulla et al. 2015). Additionally, the recurrence of fires needs to be less than the time needed for key tree species to reach a threshold at which they accumulated sufficient bark to avoid fire induced stem death (Hoffmann et al. 2012). The rate at which these thresholds are reached depends on the resource base of the site (in terms of nutrients, moisture, competition etc.), and are generally attained more quickly where environmental productivity is higher (Hoffmann et al. 2012).

SASDTF

While forest cover (>50%) typically precludes fire spread in SDTF globally, it is a current, and probably a deterministic characteristic of the SASDTF (Stott 1990, Kealhofer 1998, Maxwell 2004). This is particularly the case for DDF (Stott et al. 1990) and secondary forest units formed as a direct consequence of swidden agriculture (Heinimann et al. 2007). Evidence suggests that SASDTF has long been subject to anthropogenic fire, predominantly for slash-and-burn farming (Wharton 1966, Stott 1988, Stott et al. 1990).

The role of fire in determining the resilience of SASDTF and units within has not been well quantified (Mertz et al. 2009). In some cases, it is speculated that intense burns drive forested SASDTF units into more open, savanna states (Ruangpanit 1995). More likely, however (given the lack of true savanna in the region (Stott 1990)), is the proposition that the introduction of fire into denser SASDTF units such as SEDF — thought to naturally preclude fire — will cause the transition of these forests into more open forest types (e.g. DDF or open MDF) (Stott 1976, 1984, 1988). This process has been empirically quantified by a study undertaken between 1989 to 2000 in Thai SASDTF, whereby fire (generally associated with drought) was found to have transformed 15% of denser SEDF forest-types into degraded forest or open DDF (Johnson and Dearden 2009). However, these results by-and-large conflict with those of Baker and Bunyavejchewin (2009) and Baker et

al. (2008) who assessed the response of DDF, MDF, and SEDF to 1982 to 1983 and 1997 to 1998 El Niño Southern Oscillation (ENSO) induced fire. These studies found no evidence of heightened sensitivity to fire in SEDF units. Similarly, long-term reconstructions of fire and ecosystems in Thai DDF (Kealhofer and Penny 1998, Penny 2001) and Cambodian mosiacked SEDF/MDF (Maxwell 2001, 2004) did not demonstrate any deterministic relationship between fire and forest unit-type.

Fire incidence in SASDTF is common and does not appear to play a large role in controlling the persistence of forest or grassland communities as alternative stable states. The limited research that has been conducted in representative ecosystems suggests that it may be deterministic in catalysing forest-to-forest transitions, particularly SEDF to DDF or open MDF units. This relationship appears complex and is still unclear. Key SASDTF DDF taxa do display adaptations to fire suggesting that dry forest species survival may relate to unique plant functional traits (Rundel and Boonpragob 1995). Literature from Indian SDTF, where research on dry forest-fire interaction has been more extensive, supports this idea. For instance, it has been demonstrated that tree species that sprout from root buds as opposed to root crowns have a lower probability of mortality following low intensity (ground fire) burning in Indian SDTF (Saha and Howe, 2003). Conversely, the ratio of root sprouters to root crown sprouters rapidly declines following fire exclusion (Saha and Howe, 2003). Root sprouters considered in this study that are common to SASDTF include *Terminalia tomentosa* (Heyne ex. Roth) and *Diospyros montana* (Roxb.). However, it is notable to point out that dominant Diperocarpaceae taxa within SASDTF (absent from the Saha and Howe (2003) study area) resprout from root crowns (Rundel and Boonpragob 1995). Additionally, little association between functional groups and mortality resulting from the fire were noted in Thai SASDTF studies Baker et al. (2008).

Very high intensity fires resulting from large fuel build up (generally from fire suppression in preceding years), can destroy sub-surface seed banks and tissues of sprouting species, thereby erasing internal ecological memory. This may reduce the recovery potential of SDTF, encouraging the spread of more open formations within SASDTF (Wanthongchai and Goldammer, 2011).

2.3.3 Edaphic conditions

SDTF

Soil characteristics, particularly with respect to fertility and texture, appear to play a role in the persistence of SDTF over savanna (and vice versa) under bistable climatic conditions. The role of soil nutrient status in determining ecosystem state has been tested by Lehmann et al. (2011) who showed that in mesic areas of Africa, South America and Australia, low soil fertility precluded the rapid establishment of a woody cover, encouraging the growth of a grassy ground cover. It thus was an important interaction in the persistence of savanna. By mediating precipitation input storage, moisture

outflows via evapotranspiration, and ground percolation, soil water retention capacity (typically determined by soil depth and texture), appears to be important for the persistence of SDTF under moisture limiting conditions (Bucini and Hanan 2007). For example, soil texture was found to be weakly predictive of tree cover within Africa, South America and Australia (though overridden by the role of MAP, seasonality and fire (Staver et al. 2011a)). The relationship between soil and forest cover was more strongly established for the same continents by Murphy and Bowman (2012), who determined that soil texture was the best predictor of forest cover throughout the 6 driest consecutive months.

Soil characteristics also appear to control the distribution of internal SDTF units. Murphy and Lugo (1995), Pennington et al. (2006) and Meir and Pennington (2011) note the influence of soil on the composition, and structure of Neotropical dry forests, noting that low evergreen sclerophyllous assemblages typically grow in infertile soils, whereas taller deciduous communities are associated with higher fertility soils. In Asia and Africa, woody cover in SDTF and TGSS ecoregions is modified by edaphic conditions, with a transition from dense evergreen dry forest to more open woodland / deciduous forest types corresponding with a decrease in soil moisture content (Bucini and Hanan 2007, Toriyama et al. 2007, Ohnuki et al. 2008, Tanaka et al. 2008, Ruiz et al. 2010, Toriyama et al. 2011, Jakovac et al. 2015).

SASDTF

Though typically growing in nutrient poor conditions relative to their Neotropical counterparts (Saeki et al. 1959), soil texture, slope and aspect appear to play a contributing role in determining the local open vs. closed characteristics and the internal forest structure of SASDTD mosaics (Maxwell 2001, Ohnuki et al. 2008, Toriyama et al. 2011).

While moderate to high fertility soils favour the growth of SEDF (Rollet 1962, Maxwell 1999), research indicates that this forest unit can persist in less fertile soils across the ecoregion, provided that their depth and textural characteristics are such that water can be retained throughout the dry season (Saeki et al. 1959, Toriyama et al. 2007, Ohnuki et al. 2008, Toriyama et al. 2011). Conversely, deciduous dry forests (MDF and especially DDF) can grow in shallow, sandier soils with a low water retention capacity (Toriyama et al. 2007, Toriyama et al. 2011). However, it is important to note that in their study of Indian deciduous dry forests, (Ruiz et al. 2010) point out that a degree of soil moisture at the end of the dry season is required even for the most xeric forests, given that leaf flushing can precede monsoon rains by several weeks.

Given the role of soils, and particularly soil moisture retention in determining the distribution of SASDTF units, it is speculated that edaphic conditions, particularly when interacting with changing patterns of precipitation or seasonality, may play an important function in determining the persistence and internal composition of SASDTF.

2.3.4 Land conversion and forest fragmentation

SDTF

A high degree of structural degradation is reported for SDTF globally (Miles et al. 2006), particularly for forest tracts that grow in topographic, edaphic and seasonally optimal conditions for agriculture, including a large proportion of Neotropical SDTF (Sànchez-Azofeifa and Portillo-Quintero 2011). Quantification of the extent and degree of fragmentation is limited for this biome given that these systems often represent the first frontier of agricultural development and are usually afforded low conservation priority relative to their moist counterparts (Sànchez-Azofeifa and Portillo-Quintero 2011). This is of concern to the future management of SDTF, as land conversion, fragmentation and degradation are considered to be key drivers of change in these systems (Miles et al. 2006). Fragmentation can impact on the resilience of these systems with respect to 1) remnant tracts of fragmented forest, and 2) the regeneration capacity of moderately and highly degraded forests. These are discussed below.

Fragmentation of SDTF occurs from processes such as local land use conversion, resource extraction and alteration of natural disturbance regimes (particularly with regard to fire) (Pulla et al. 2015). One of the most significant impacts of fragmentation on remaining SDTF patches is the alteration of local and regional climatic patterns (Sternberg 2001). In Amazonia, for example, widespread conversion of forest to pasture and crop land has resulted in higher albedo, reduced evapotranspiration and ground humidity (Coe et al. 2013), increased seasonality (Costa and Pires 2010), and decreased precipitation (Knox et al. 2011) at forest/cleared land boundaries. In the long term, these processes serve to reduce overall forest carbon stocks (Chaplin-Kramer et al. 2015).

Changes in localised microclimates in Neotropical SDTF due to forest degradation have been shown to have important implications on plant functioning, including reduced leaf life span and changed timing of flowering (Quesada et al. 2011). This latter phenomenon has been shown to have important implications for pollinators that are dependent on sequential flowering, hence potentially reducing reproductive output and genetic diversity in the long run (Quesada et al. 2009, 2011).

Fragmentation, therefore, may play an important role in both 1) encouraging a forest to savanna state shift (particularly when forest ecosystems have lowered internal resilience due to reduced ecosystem functioning and/or are already approaching a precipitation or seasonality threshold), and 2) reinforcing this state change, especially at the forest fringe (Sternberg 2001, Mayle and Beerling 2004).

High-level degradation (i.e. near-complete clearance) is thought to have long-term impacts on the future ecological expression of land previously colonised with SDTF, even if left to regenerate. This is largely due to the fact that processes associated with intense clearance will not permit regrowth of secondary forest. These include depletion and alteration of soil nutrient pools (García-Oliva and Jaramillo 2011), reduction in soil moisture content via compaction, increased runoff and soil erosion, reduction of biodiversity

(Maass 1995) and alternation of forest/soil moisture feedbacks (Coe et al. 2013). Combined, it has been speculated that these factors should favour the persistence of open formations (grassland or shrubland) (Maass 1995, Menaut et al. 1995). However, a number of studies reviewed in Pulla et al. (2015) regarding the recovery potential of SDTF following a range of often persistent disturbances of various types and magnitudes (including swidden agriculture, pastoral land conversion, logging and natural disasters) indicate that such drivers are commonly insufficient to cause a fundamental state shift to savanna (or any other habitat types). The authors use this body of work to emphasise the role of reinforcing parameters (e.g. climate, edaphic conditions and ecological memory – noteably the capacity of early succession SDTF species to resprout) in maintaining the resilience of these systems. Given this, it is also important to note that the ecological characteristics of extant tracts of SDTF may, in themselves, be representing of past disturbances e.g. (Mayle et al. 2007).

SASDTF

SASDTF units growing in soils suitable for agriculture (typically secondary semi-evergreen and some mixed deciduous types) have long been subjected to traditional swidden farming practices that are, in turn, inherently linked to the fire dynamics of the forests (Heinimann et al. 2007). The capacity of land disturbed by this practice to regenerate depends on factors such as fallow length, intensity and frequency of disturbances such as fire, site conditions (including long-term impact on soil compaction and quality), ecological memory and presence of wildlife (Heinimann et al. 2007, Teegalapalli et al. 2009).

Until recently, disturbance associated with traditional short-cultivation, long-fallow cycle slash and burn techniques have seemingly been able to coexist with SASDTF dry forest succession (Boyd and McGrath 2001, Maxwell 2001, 2004, Heinimann et al. 2007). This is potentially due to the fact that disturbance associated with traditional techniques was mild to moderate in intensity, frequency and patch-size, allowing secondary forest regeneration post-abandonment to draw on both internal and external memory. While the impact of disturbance on plant functional traits has not been well quantified in SASDTF, work within Indian SDTF that host some similar species to SASDTF may shed some light on species- and community-level plant functional traits that contribute to ecological resilience to disturbance.

In general, disturbance regimes (in association with climate) play an important role in shaping diverse physiognomic forest structures (canopy cover and height) across an ecoregion (Sapkota et al. 2009, Ramesh et al. 2010). Additionally, post-disturbance succession has been shown to result in the procession from clumped to uniform population distributions (Sapkota et al. 2009). Clumping of key species within Thai SEDF has also been observed after what is postulated by to represent a large-scale, severe disturbance event, though this is attributed to edaphic and topographic habitat specialisation (Bunyavejchewin et al. 2003).

Sapkota et al. (2009) demonstrate that mild to moderate level disturbance can increase species regeneration (vs. undisturbed or heavily disturbed sites), and is, in fact, considered important for supporting key SDTF species (*Shorea robusta* (Roth)). However, it is important to note that this does not apply to all forest species (notably *Haldina cordifolia* ((Roxb.) Ridsdale) and *Terminalia tomentosa* (Sapkota et al. 2009). Plant traits, including seed size, have been found to be important for determining regeneration following mild to moderate disturbance, with large seeded species more likely to regenerate following low level disturbance (Khurana et al. 2006). Some large seeded species discussed in this study that co-occur in SASDTF include *Terminalia tormentosa*, *T. chebula* (Retz.), *Bauhina racemosa* (Lam.) and *Diospyros montana*. The observation that *T. tormentosa* is likely to regenerate following low level disturbance is intriguing given the the observed low regeneration potential of this tree across a disturbance gradient as discussed in Sapkota et al. (2009). Given that this species has the largest seed size of all the species discussed in Khurana et al. (2006), it is possible that *T. tomentosa* regeneration following perturbation may be restricted to very mild events. These findings indicate that pulses of low to moderate level disturbance events appear to be an an important driver of spatio-temporal variability in forest structure and composition. This may contribute to the unit heterogeneity observed across SASDTF, encouraging beta-diversity, and allowing for the development of a diverse source of external ecological memory. Consequently, low-level disturbance events may contribute to overall SASDTF resilience.

Anthropogenic disturbance in SASDTF has, in many cases, intensified in severity and periodicity due to increased population and competition with other commercial land uses (Heinimann et al. 2007). These include forest conversion for monoculture plantations and selective logging for high value timber species (McKenny et al. 2004, Li et al. 2014, You et al. 2015). Again, a series of studies in Indian SDTF may elucidate the impact of high intensity, high frequency disturbance on SASDTF. Khurana et al. (2006) demonstrate that following extreme perturbations, small-seeded species are likely to be more abundant in the regeneration phase, presumably due to reliance on external memory at these sites (i.e. recruitment from wind dispersion). Some of these species that co-occur in SASDTF include *Haldina cordifolia* (somewhat contradicting the above-described findings of Sapkota et al. (2009)), *Phyllanthus emblica*, *Bombax ceiba* (Linn.) and *Holoptelea integrifolia* ((Roxb.) Planch.) If disturbance is severe and extensive enough such that ecological memory can not be relied upon for regeneration, even if they are abandoned in the long term, persistent secondary savanna formation may form in place of secondary forest (Goldammer 2002). Consequently, the role of disturbance in contributing to, or reducing ecological resilience of SASDTF needs to be considered in the context of the spatial scale, severity, and frequency of the event/s.

2.3.5 Herbivory

SDTF

High densities of large mammals, particularly ungulate browsers, are considered to be major drivers of vegetation change in forests world-wide (Harrison 2011, Nuttle et al. 2014). However, the role of both bottom-up and top-down impact of herbivores on SDTF succession is a major research gap (Quesada et al. 2009). The ecological impacts of continental scale extinction of mega-herbivores and large mammals between 50 000 to 10 000 years BP therefore provides a useful testing ground for determining the role of megafauna in determining the resilience of receiving ecosystems. A review of this process, attempted by Johnson (2009) and Gill (2014), indicates that impacts are two-fold. First, large-scale herbivory may have suppressed fire in the ecosystem by reducing ground litter and fuel loads. It is notable to point out that fire may also have been enhanced post mega-fauna decline, at least temporarily, due to biomass build up (Robinson 2005, Rule et al. 2012, Zimov et al. 2012). Second, browsing is speculated to have maintained more open, mosaicked forest / woodland / grassland communities (noting that most studies focus on Europe). While this point is contested, similar patterns can be found in contemporary Afrotropical studies examining the role of extant mega-herbivores on grassland communities. For instance, Lehmann et al. (2011) argue that Afrotropical savanna persists where climatic and fire regime conditions alone should predict forest/woodlands. This is speculated to be due to the role of large mammals in crushing and grazing woody vegetation, precluding the establishment of a canopy cover. Similar results were obtained in Asner et al. (2009).

In addition to impacts associated with fire limitation and savanna maintenance, large mammals also appear to play an important role in pollen and seed dispersal in SDTF (Janzen 1988, Murphy and Lugo 1995, Teegalapalli et al. 2009, Stoner and Timm 2011). This is often overlooked due to the relatively large number of wind-dispersed species in these ecosystems, especially when compared to tropical moist forests (Teegalapalli et al. 2009, Pulla et al. 2015). However, Pulla et al. (2015) identify that SDTF may be particularly susceptible to loss of pollinators (compared to their moist forest counterparts), indicating the potential importance of considering changing patterns of herbivory when examining the resilience of associated ecoregions.

SASDTF

Prior to 1970, the relatively continuous SASDTF habitats, particularly DDF units, were important for supporting a wide range of large ungulates, including elephants (Wikramanayaka et al. 2014 a, b). However, the proliferation of gun-use for bush meat in Cambodia (including the mandated commercial hunting implemented by the Khmer Rouge regime), in combination with the emergence of wildlife trading, lead to the extirpation of many of these large mammals from the region by the mid-1990s (though a degree of recovery is evident in some areas since this period) (Loucks et

al. 2009, Maxwell and Cox 2011). The impact of the recent, significant reduction of large herbivores on SASDTF resilience has not been assessed, but, based on SDTF research, may act to close some of the more open forest units in the short term, encourage the spread of higher-intensity fire, particularly within DDF units, and impact pollen and seed dispersal. This latter point may be particularly consequential for fragmented units that require a stock of external ecological memory for recovery (Teegalapalli et al. 2009).

2.3.6 Biogeography

SDTF

While typically overlooked as a control on ecological dynamics in broad-scale habitat analysis, biogeography may be an important factor in shaping the resilience of SDTF and TGSS. This has been emphasised in a recent study undertaken by Dexter et al. (2015), who determined that the floristics of dry forest ecoregions within the different biogeographic realms were more closely related to their adjoining habitat types (e.g. TGSS or tropical and subtropical moist broadleaved forest) than to each other, bringing into question cross-continental generalisations of common habitat-type ecological traits. Such factors may play an important role in the inter-continental differences observed in SDTF distribution. For instance Murphy and Bowman (2012) noted that the abundance of Neotropical forest in climate zones that would rarely support forest in Australia or Africa.

Similar observations stem from the study of grassland biomes. For instance, Knapp et al. (2004) demonstrate that, while fire dynamics play a similar part in shaping the floristics of temperate savanna inter-continentally, vegetation response across a rainfall gradient is geographically dependent. Similarly, Lehmann et al. (2014) determined that although common environmental drivers (fire and climate) shape African, South American and Australian savannas in superficially similar ways, the relative impact of these drivers on ecosystem function is contingent on the evolutionary and environmental history of the region being studied. This has led the authors to dismiss the use of a single global model to predict the ecological dynamics of savanna, and caution that biogeographic legacies may result in very different adaptive trajectories under future climate change.

SASDTF

In their review of global savannas, Lehmann et al. (2009) ask "where are savannas of the seasonal tropics of Asia?" (p511) pointing out the absence of this biome type within a region with all the preconditions to support the formation of savanna / a savanna-forest mosaic. This is further explored in an analysis of intercontinental variability in the relationship between water availability and forest-cover conducted by Murphy and Bowman (2012). Results of this study indicate that if the 1) South-American, 2) African, and 3) Australia models of climate-tree cover dynamics were applied to mainland southeast Asia, the area occupied by SASDTF should be a forest-savanna mosaic (1), or solely support open communities (2 & 3).

The presence of a more-or-less continuous dry forest mosaic where global models predict less or no forest, suggests that either SASDTF as a whole, or units within, may either be better adapted to low moisture availability, or sitting at a critical threshold whereby small reductions in available water will trigger a state shift to a non-forested state.

2.4 Chapter synthesis

Studies of neo- and Afro-tropical SDTF dynamics indicate that these habitat-types are susceptible to rapid state shifts to TGSS. Precipitation, rainfall seasonality and fire have been identified as the major drivers of change within these biomes, although factors such as soil characteristics, herbivory and disturbance appear important. The impact of these drivers in instigating ecological regime shifts to savanna does, however, depend on the plant functional traits within SDTF ecoregions, which can play an important role in increasing or reducing ecosystem resilience, generally through control on internal and/or external ecological memory.

When drivers of SDTF change are applied to the under-researched dry forests of south-east Asia, representative ecosystems, particularly DDF units, appear to be sitting close to an ecological threshold with regards to canopy cover, seasonality and fire. The combination of predicted increases in the inter-annual variability of monsoon precipitation (i.e. periods of prolonged drought and prolonged deluge) (Christensen et al. 2013) and increased levels of anthropogenic disturbance within the forests (particularly actions serving to reduce canopy cover or cause further fragmentation), may increase the likelihood of ecological reorganisation of these systems to a savanna state. On the other hand, the overall rise in MAP and the prolonged wet season predicted for the Asian monsoons (Christensen et al. 2013), may bolster resilience, or even drive the more open dry forest-types into a denser forest assemblage, though there is little information detailing the parameters of these transitions. Nevertheless, the persistence of continuous forest where most climate-fire models predict savanna or savanna-forest mosaics, suggest that commonly overlooked biogeographic factors, including the evolution of a unique flora with distinct ecological traits may play an important role in the resilience of SASDTF. Additionally, the heterogenous, mosaicked formation that has formed as a result of many years of human perturbation (generally low-intensity fire for swidden farming) may be important for bolstering external ecological memory within these forests. As such, a biome-scale model of resilience may not be sufficient for predicting the future response of these forests to intrinsic and extrinsic forcing, highlighting the need for ecoregion- to ecosystem-specific analysis of the threshold dynamics of these systems.

3 Contemporary site conditions

3.1 Introduction

This chapter outlines the regional- to local-scale biophysical characteristics of five volcanic crater lake sites in Cambodia that are subject of this study. At a regional level, focus is placed upon factors thought to contribute to the resilience of the dry forests that grow across much of mainland south-east Asia's lowlands (including the lake catchment zones) as discussed in Chapter 2. As such, these descriptions use a biogeographic approach at an ecoregional scale (i.e. zones representing distinct biotas within SDTF) (Olson et al. 2001) where relevant. Local scale descriptions typically focus on the biophysical site properties captured within the bounds of the five crater-lake catchments. A description of the geographic and ecoregional setting of the lake sites is first provided in order to spatially orientate the reader. This is followed by an explanation of the monsoonal climate that influences the sites, including a brief synthesis of the mechanisms driving Holocene shifts in this system. The geological, geomorphological and pedological makeup of the study area is discussed, before an overview of the local and ecoregional site ecology and land use history concludes the chapter.

Due to the limited amount of recorded data about the sites, particularly at the local scale, a mixed-methods approach to characterising extant site conditions is adopted for several sections of this chapter. Catchment-scale descriptions are generally based on a desktop review of relevant literature and coarse-scale mapping data that has been ground-truthed at a local scale through geo-referenced site walkovers conducted in July 2012 and April 2013. Some catchment soil samples were collected from the field and analysed at the University of Sydney School of Geosciences laboratories throughout these field seasons. This was deemed important as edaphic conditions are thought influence the distribution of south-Asian seasonally dry forest (SASDTF) mosaic-types (Toriyama et al. 2007, Toriyama et al. 2011) and appear to have a control on the structure of dry forest and savanna elsewhere (Williams et al. 1996, Sankaran et al. 2005) — see Chapter 2 for details. Methods used to characterise these soils are presented in Appendix A, and results are incorporated into relevant site pedology descriptions for the sake of clarity.

3.2 Geographic and ecoregional setting

3.2.1 Physical setting

The lake sites are located within the Ratanakiri Province of north-east Cambodia. This province borders Vietnam and Laos to the east and north respectively, is located approximately 600 km north-east of Phnom Penh, and covers an area of approximately 12 500 km^2 (Fox et al. 2009).

Two river systems — the Tonlé San (Sesan River) (north) and the Tonlé Srepôk (Srepok River) (south) — flow west across Ratanakiri to the Mekong River. Between these rivers, the central portion of Ratanakiri is characterised by a 1 200 km^2 basaltic plateau, part of the Ratanakiri Volcanic Province (RVP) that sits at 300 to 500 m ASL (figure 3.2 inset B). The Annamite Ranges of Laos and Vietnam are located to the north and north-east of the Tonlé San, while lowland plains extend to the south and south-east of the RVP (figure 3.2 inset A and B).

Pliocene to Pleistocene volcanic craters within the RVP form the catchments of the five lakes that are the subject of this study. Yeak Loam, the most northern of the lakes, is located approximately 3 km east of the provincial capital of Ban Lung. Adjacent lakes Yeak Oam and Yeak Kara, and Boeng Lumkut, are located approximately 24 km and 29 km south-east of Yeak Loam (respectively) in the Lumphat District. Yeak Mai, located towards the south of the province in the Lumphat Wildlife Sanctuary, sits 45 km south-east of Yeak Loam. The geographic locations of the lake sites are outlined in Table 3.1 and shown on Figure 3.1.

The bathymetry of the lake sites was studied using a CEESTAR single beam sonar with a high-frequency transducer, the results of which are outlined in Sharma (2014) and summarised on Table 3.1.

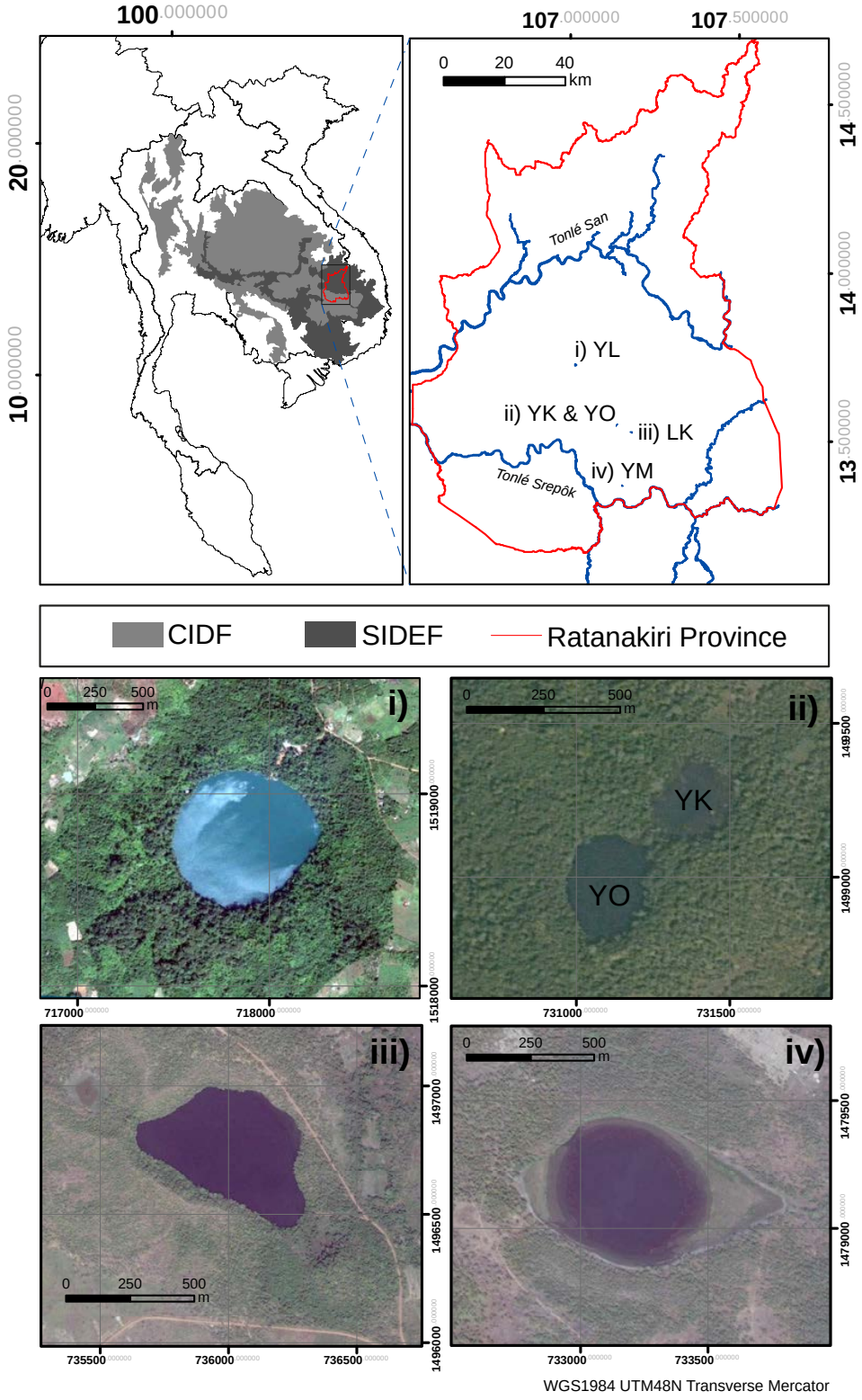

FIGURE 3.1: The geographic and ecoregional setting of the crater lake sites within Ratanakiri Province, Cambodia. YL = Yeak Loam; YK & YO = Yeak Kara & Yeak Oam; LK = Boeng Lumkut; YM = Yeak Mai. Ecoregional, hydrological and satellite data sourced from Olson et al (2001), JICA (2002c), and GoogleEarth (2015), respectively. Satellite data georeferenced to lake edge points collected in the field in ArcGIS 10.3

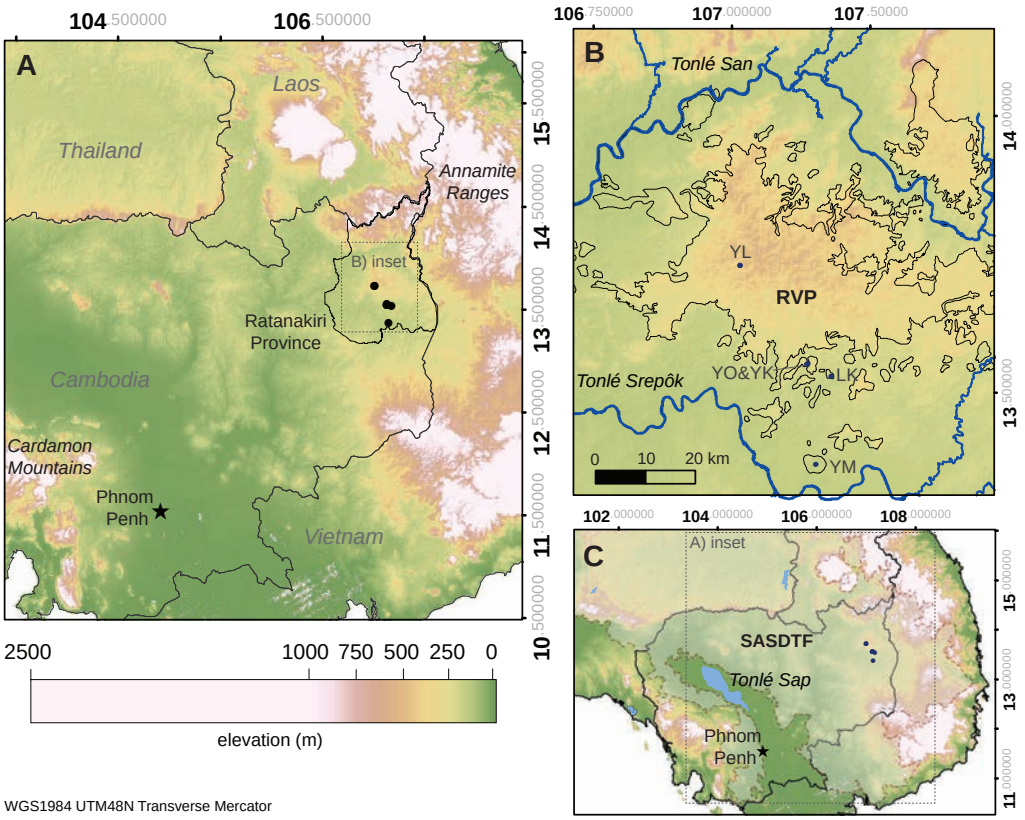

FIGURE 3.2: The location of Ratanakiri Province (A), the lake sites & Ratanakiri Volcanic Province (RVP) (B), and the South-east Asian Seasonally Dry Forest Ecoregion (SASDTF) (shaded area) (C) within the context of the regional elevation. Relief data sourced from ODC (2016a)

TABLE 3.1: Summary of lake metrics derived from the bathymetric and lake edge surveys. Data source: Sharma (2014).

lake site	location (WGS84, UTM 48N)	location (commune, district)	max. depth (m) (11/12)	modal depth (m) (11/12)	basin morphology	perimeter (m) (1/5/2014)	average radius (m) (1/5/2014)	surface area (m^2) (1/5/2014)	approx. volume (Gl)
Boeng Lumkut	736476, 1496429	Seda, Lumphat	68	67.93	Asymmetrical: very steeply sloping from south-west margin and more-gently graded from the north-east margin.	1 932	307	296 092	20.11
Yeak Loam	718273, 1518408	Yeak Loam, Ban Lung	51	49	Steep at sides, gently sloping towards middle.	2 300	366	420 835	20.62
Yeak Oam	731263, 1498626	Seda, Lumphat	45	43.77	Asymmetrical: gently sloping from the north margin.	935	149	69 747	3.05
Yeak Mai	733376, 1478850	Ka Laeng, Lumphat	6	5.5	Shallow, lenticular basin (obscured by macrophytes at lake margins).	1 571	250	196 350	1.07
Yeak Kara	731575, 1498896	Seda, Lumphat	2	0.8	Shallow, lenticular basin (obscured by macrophytes).	836	133	55 572	0.44

These data are based on bathymetric values taken in December 2011 in the early part of the dry season. As the sonar surveys did not capture the shallow littoral portion of the lake basins, and the resolution of JICA hydrological data available for the site is low (50K) (JICA, 2002c), the surface metrics of the lakes were estimated from the May 2014 satellite images of the sites in Google Earth (end of dry season). These are presented in Table 3.1. Boeng Lumkut, Yeak Loam and Yeak Oam are deep (max depth = 68 m, 51 m, and 45 m, respectively). Yeak Mai and Yeak Kara are approximately 6 m and 2 m at their deepest point. The largest lake by both surface area and volume is Yeak Loam (approx. 420 835 m^2, 20.6 Gl), followed by Boeng Lumkut (approx. 296 092 m^2, 20.1Gl). Yeak Mai has the third largest surface area (approx. 196 350 m^2) and a volume of approx. 1.07 Gl). Yeak Oam and Yeak Kara, which are separated by a 60 m wide catchment wall, have surface areas and volumes of approximately 69 747 m^2 and 55 572 m^2, and 3.05 Gl and 0.44 Gl, respectively.

Yeak Kara and Yeak Mai have shallow, lenticular basins, though the eastern bank of Yeak Mai is more gently graded than the western bank, resulting in the formation of a marshland on the eastern side of the lake in the dry season (Figure 3.1 inset iv). Yeak Loam is round with a relatively symmetrical, steep sided and flat-bottomed catchment. The Boeng Lumkut basin is very steep along the south-west margin — presumably a continuation of an outcropping basaltic escarpment above the lake edge. The elliptical lake bottom of Yeak Oam is asymmetrical, with the northern margin being more gently graded that the other lake walls.

3.2.2 Ecoregional setting

Ratanakiri sits within the Indo-Malayan biogeographic realm as described in Chapter 2 (Olson and Dinerstein 2002) and includes two WWF-recognised terrestrial ecoregions. These are the critically endangered Southeastern Indochina Dry Evergreen Forests (SIDEF [IM0210], 124 300 km^2), and the vulnerable Central Indochina Dry Forests (CIDF [IM0202] — 320 122 km^2) (Olson and Dinerstein 2002, Wikramanayake et al. 2002) (Figure 3.1). The former makes up the northern portion of the province (including Yeak Loam), while the latter extends along the southern boundary. Yeak Kara, Yeak Oam and Boeng Lumkut are located along the boundary of these ecoregions, and Yeak Mai sits within CIDF. These two ecoregions are commonly grouped into the south-east Asian seasonally dry forest ecoregion (SASDTF) (introduced in Chapter 2), out of recognition that much of the conservation value is related to large home ranges of many key species, encompassing diverse habitat requirements that shift seasonally (Tordoff et al. 2005). Among the salient characteristics of the SASDTF is the very broad range in vegetation structure, ranging from open dry deciduous forest to closed semi-evergreen forest patches (Neal 1967) to seasonal herbaceous wetlands. These units form a mosaic across SASDTF, and their characteristics are discussed in Section 3.7.

3.3 Climate

3.3.1 Ecoregional climate

As with all SDTF, SASDTF units are characterised by a distinct seasonality of annual rainfall (Miles et al. 2006), typically on the order of 4.5 to 6 months (Morice et al. 2012). This annual rainfall variance is attributable to the seasonal reversal of atmospheric patterns driven by the Indian and south-Asian monsoon systems, the mechanisms of which are detailed below in section 3.3.2. The interaction of rainfall and temperature in the region results in three recognised seasons — rainy from late-May to October (monsoon season), cool and dry (winter season) from November to February, and hot and dry from March to early May (transition season) (Maxwell 1999, Saha 2010).

Mean monthly climatic data for the Ratanakiri province between the period 1900 and 2012 has been sourced from the World Bank Group Climate Change Knowledge Portal (2016) based on research undertaken by the University of East Anglia Climate Research group (Morice et al. 2012). These data indicate that the long-term climate falls within the tropical savanna zone of Koppen's climate classification system (Aw) (Table 3.2). Mean annual precipitation (MAP) for the region over this period is approximately 1 840 mm, with the wet season falling between May / June and October / November. As with the broader ecoregion, annual precipitation is seasonal, with only 10% of the MAP falling between December and April. Being less than seven months long, this degree of seasonality is considered mild in the context of forest/savanna resilience work (Staver et al. 2011a). The mean daily temperature of the region varies from approximately 22 °C (January) to 27 °C (June).

Across the SASDTF ecoregion, MAP for the area occupied by CIDF is lower (1 000 to 1 500 mm/year) and the seasonality slightly stronger (5 to 7 month dry season) than that of the region occupied by SIDEF (MAP is 1 200 to 2 000 mm/year; dry season is 3 to 6 months long) (Wikramanayaka et al. 2014a, b). These discrepancies are generally linked to topographic features (Clift et al. 2010). The contemporary climate characteristics of both ecoregions, including that of the forests surrounding the crater lake sites, place the system into a bi-stable ecological zone whereby either dry forest or savanna can theoretically persist (Hirota et al. 2011, Staver et al. 2011a, Staver 2012).

3.3.2 Asian monsoon mechanisms

The study area is situated at the intersection of the Indian Summer Monsoon (ISM) (otherwise known as the South Asian Monsoon) and the East Asian Monsoon (EAM) (Wang et al. 2003), the latter of which is sometimes subdivided into the East Asian Summer Monsoon (EASM) and Western North Pacific Summer Monsoon (WNPSM) (Wang and LinHo 2002) (Figure 3.3). The lake sites are thus affected by both the ISM and EAM. Annual

TABLE 3.2: Mean monthly rainfall and temperature for Ratanakiri between 1900 and 2012. Data sourced from the Climatic Research Unit (CRU) at the University of East Anglia.

	Rainfall (mm)	Temperature (°C)
Jan	14.2	21.96
Feb	15.4	23.46
Mar	38.5	23.05
Apr	76.3	26.53
May	188	26.51
Jun	248.6	26.94
Jul	273.6	26.35
Aug	280.3	26.47
Sep	309.9	25.6
Oct	252.2	24.95
Nov	109	23.82
Dec	33.9	22.38
Mean Monthly	153.325	24.835
Annual Total	1839.9	

fluctuations in these systems (that, due to their coupled interactions are often discussed together as the Asian Monsoon) are driven by atmospheric responses to the land-ocean configuration of south and mainland southeast Asia (Wang et al. 2003, Saha 2010). Specifically, the seasonal temperature discrepancies between the Indian and Pacific Oceans and continental Asia set up a north-to-south thermal contrast coming into the boreal summer, establishing a circumcontinental cyclonic circulation (Wang and LinHo 2002, Clift and Plumb 2008). Eventually, this triggers a planetary-scale monsoonal rain band extending across the Arabian Sea, the Bay of Bengal, and the South China Sea and reaching the subtropical western North Pacific (WNP) (Figure 3.3). Within this process, topographic discrepancies in the Eurasian landmass lead to the formation of different monsoon cycles over India and East Asia (Saha 2010).

The ISM represents the north branch of the seasonal migration of the Inter-Tropical Convergence Zone (ITCZ), migrating northwards from the boreal winter (5 °N) to boreal summer (20 °N) (Gadgil 2003). This movement is triggered by a significant north-to-south gradient caused from the formation of a low pressure zone over the Tibetan Plateau, and a high pressure cell over the cool Southern Indian Ocean (Gadgil 2003, Fleitmann et al. 2007a), resulting in deep convective, cross-equatorial winds between the south and north Indian Ocean (Clift and Plumb 2008). Additionally, a flow of south-westerlies north of the equator (5 °N to 20 °N) transports moisture that is released over the continent as monsoon precipitation from the Arabian Sea across to the eastern Philippine Sea. Combined, these wind flows set up southwest summer monsoon rains over the study area. As the

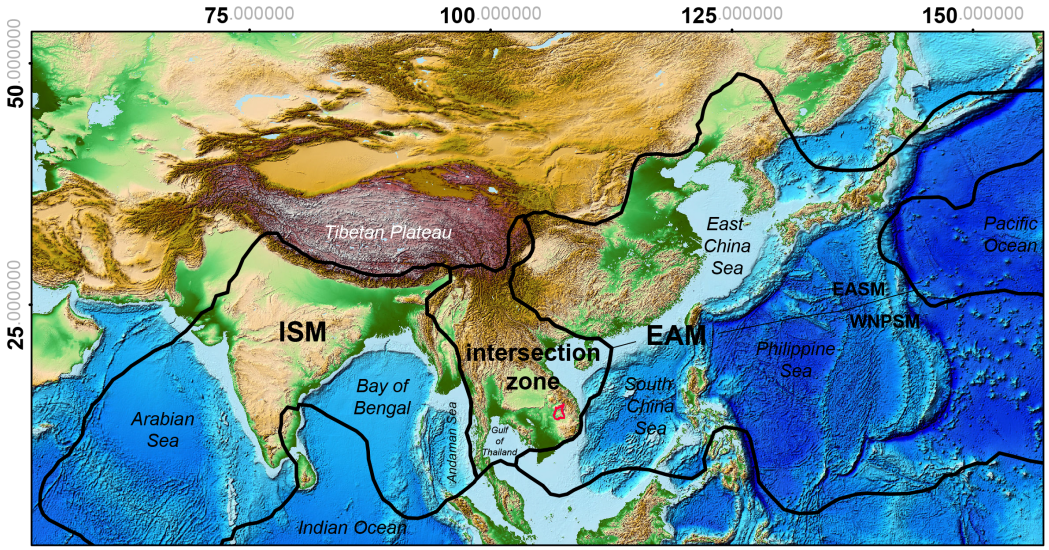

FIGURE 3.3: Map showing the extent of the Asian monsoon (ISM & EAM) in the context of the study area (red polygon) after Wang and LinHo (2002). Global relief map data sourced from Amante and Eakins (2009).

ITCZ moves south in the boreal winter, northeasterlies and easterlies derived from Siberia and the north Pacific (EASM) take over (Maxwell 1999).

Forcing of the EASM is slightly more complicated due to the more complex ocean-continent arrangement in this region. This monsoon is generated from both north-south thermal gradients (between Australia and warm western north Pacific) and an east-west contrast between continental Asia and the Pacific. Strong southerlies (110 °E to 140 °E), transport moisture to east Asia (the southeast summer monsoon) (Wang and LinHo 2002). The onset then gradually progresses northward and north-westward from the Asian marginal seas and the subtropical western north Pacific Ocean toward inland areas following the advance of the ITCZ (Fleitmann et al. 2003, Gadgil 2003). A reverse pressure gradient set up in the boreal winter sets up east Asian (north-east) winter Monsoon (EAWM) as the ITCZ retreats south (Fleitmann et al. 2007a). The EAWM is especially strong over East Asia and mainland south-east Asia due to the significant thermal discrepancies between the cool Asian landmass and the warm North Pacific Ocean (Wang and LinHo 2002).

The onset of the monsoon within the vicinity of the study area typically occurs in mid to late May, peaks in August to September and ends in late October at the onset of the dry season (Wang and LinHo 2002). A bimodal distribution of peak rainfall can be observed across much of low-latitude mainland south-east Asia in response to the northwards and southwards migration of the ITCZ. This causes a two to three week dry spell in July (Maxwell 1999).

Though typically tracking to the north or the west of the monsoon intersection zone, tropical storms can contribute to a significant proportion of the annual precipitation received at the study sites, these are detailed in Saha

(2010), and summarised below. To the west of the study area, western disturbances, occurring in the winter season from November, travel west to east, drawing moisture from the Bay of Bengal, producing thunder storms and squally conditions across the Indian subcontinent. At the same time, surges in low-level east to north-easterly trade winds converging into the low pressure equatorial trough formed over the South China Sea can produce westward flowing waves that, when arriving at the Bay of Bengal, can develop into cyclones (Saha 2010). In the transition season, cyclones form over the Arabian Sea and east Indian Ocean track northwards, impacting the north-west sector of continental south-east Asia (Saha 2010).

3.3.3 Drivers of Holocene monsoon change

The long term drivers of monsoon intensity include what Wang et al. (2003) have dubbed 'external factors' (solar intensity and associated glacial-boundary conditions) working in concert with internal influences associated with the coupled atmosphere-ocean-land systems. These include El-Niño Southern Oscillation (ENSO) cycles and more localised monsoon-oceanic interactions.

At centennial to millennial timescales, solar isolation-driven ocean-land temperature gradients have been the predominant cause of ISM and EAM precipitation change in the Holocene (Wang et al. 2001, Fleitmann et al. 2003, Wang et al. 2005, Clift and Plumb 2008). Solar insolation in the precession band was at a maximum between approximately 10.5 and 9.5 ka BP, resulting in the warming of continental Asia and subsequent shifting of the mean latitudinal position of the ITCZ northwards (Fleitmann et al. 2007a). Though this resulted in a strong ISM, the intensity of the monsoon is argued to have been moderated by global glacial boundary conditions (Fleitmann et al. 2007a). Records from the EASM monsoon also indicate high levels of precipitation between approximately 10.5 and 7 ka BP (Dykoski et al. 2005, Wang et al. 2005).

From approximately 7.8 ka BP to the present, the mean position of the ITCZ position migrated gradually south (Fleitmann et al. 2007a), and is thought to have caused the decline in ISM and EASM precipitation up to approximately 1.5 ka BP (Dykoski et al. 2005, Wang et al. 2005, Fleitmann et al. 2007a). Superimposed upon this overall trend in declining precipitation, are short-lived, abrupt, high and low precipitation events (Gupta et al. 2003), including notable 10 to 50 year dry periods (Wang et al. 2005). These rapid changes have been linked to ice-rafting Bond events in the North Atlantic and fluctuations in solar activity (Wang et al. 2005).

Notable anti-correlations observed across spatially disparate late Holocene ISM monsoon records have been attributed to shifting of the mean seasonal cycle of the monsoon in response to decreasing solar insolation (Fleitmann et al. 2007a, Sinha et al. 2011a). Berkelhammer et al. (2010) note the decoupling of monsoon precipitation records with solar insolation at the on-set of the MWP, occurring within the study region at *c.* 850 AD (Cook et al. 2013). While the reason for this shift is unclear, it is potentially associated with changing ENSO and Indian Ocean Dipole (IOD) processes (Berkelhammer

et al. 2010). However, Gupta et al. (2003) do link Holocene monsoon change (as reconstructed from an Arabian Sea *Globigerina bulloides* series) to North Atlantic cycling in response to solar forcing. Since the Little Ice Age (LIA) (*c.* 1350 to 1880 AD) — a relatively cool period (Cook et al. 2013) — warming (including anomalously warm conditions from 1990) is apparent in instrumental and proxy records of temperature change across both the ISM and EASM regions (Cook et al. 2013). Superimposed onto this warming trend are periods of multi-decadal droughts (Buckley et al. 2010). These are thought to be driven by a complex interaction of ENSO cycles driven by Pacific and Indian Ocean SST anomalies (Chakravorty et al. 2016) and large volcanic eruptions (which increase the probability of El-Niño events (Emile-Geay et al. 2008, Anchukaitis et al. 2010)), as well as chaotic oscillations in ISM monsoon precipitation (Berkelhammer et al. 2010, Borgaonkar et al. 2010, Sinha et al. 2011b). For instance, ENSO interaction with the Asian monsoon was weakened over in India (Kumar et al. 1999) simultaneous to its increased strength over Thailand (Buckley et al. 2007) in *c.* 1980, related to the cooling of the eastern Indian Ocean and a westward shift in north-west Pacific (NWP) circulation (Chakravorty et al. 2016). Thus, since the 1980s, Indian Ocean SST and Tropical Pacific Ocean SST have played a key (though not the sole) role in monsoon forcing over India and the ISM/EAM convergence zone respectively.

3.4 Tectonic and biogeographic setting

Geologically, mainland south-east Asia forms part of the Sundaland block, located at the convergence of the Indian-Australian, Philippine and Eurasian Plates (Metcalfe 2011). This plate is characterised by the several eastern Gondwanan terranes (principally located along the Indian-Australian Gondwana margin in the Early Proterozoic) that broke apart and subsequently reamassed throughout the Late Palaeozoic/Early Mesozoic to Cenozoic. These terranes are bound by a complex series of accreted island arcs, ophiolites, and fold belts, developed through episodes of arc magmatism and the opening and closure of backarc basins (Khin et al. 2014).

Cambodia forms part of the Indochina terrace (Indochina East Malay block) that is made up of a Palaeoproterozoic to Mesoproterozoic, granulite-facies metamorphic basement (Kontum massif) (Lan et al. 2003, Metcalfe 2013). This terrane is bounded to the west by the Loei Fold Belt and the Chanthaburi and Sukhothai Terranes, to the north by the Simao-Subterrane, the Song Da Suture and Terrane, and the South China Terrane (Metcalfe 2011, Khin et al. 2014). The eastern boundary is not clearly delineated, but roughly coincides with the eastern margin of Sundaland in the South China Sea (Metcalfe 2013). The Indochina terrane, alongside the North China, South China and Tarim blocks, rifted from Gondwana in the Devonian (the first of three phases), opening the Palaeo-Tethys Sea (Metcalfe 2013). In the early Carboniferous (Visean), the South China and Indochina blocks were situated along the Song Ma Suture at equatorial to low northern latitudes, with a warm water, equatorial-type biota that no longer displayed much affinity with Gondwana (Metcalfe 2011). By the early Permian, the North- and South- China, West Sumatra, West Burma and Indochina blocks

— then amalgamated into Cathaysialand (Metcalfe 2011) — supported a unique (Cathaysian-type) flora, reflecting climatic conditions of modern moist tropical forests (Sun 2006). This floral distribution has, in contemporary times, expanded to the Argoland/ South West Borneo and Sibumasu (Metcalfe 2011).

The Indochina block commenced collision with the Asian continent in the late Permian/early Triassic, resulting in the closing of the Palaeo-Tethys (Workman 1977, Sutherland et al. 2015). From approximately 200 Ma, the Indochina terrane persisted as relatively stable, continental crust (Sutherland et al. 2015).

Throughout the Eocene (55 to 45 Ma), the India-Eurasia collision instigated the rotation of southeast China and southeast Asia, resulting in the opening of the Gulf of Thailand and formation of extensional structures (graben and strike-slip faults) in Indochina (Sutherland et al. 2015). In mainland south-east Asia, this resulted in: 1) uplift and doming, triggering erosion of Mesozoic sequences (Sutherland et al. 2015), and; 2) extensional thinning of the lithosphere. Together, these processes elicited asthenospheric melting and upwelling of late Cenozoic basalts (alkaline and tholeiitic series) along faults, extruded from the late Oligocene/early Miocene to the Holocene (Federov and Koloskov 2005).

Around the same time, Dipterocarpaceae genera (*Shorea* and *Hopea*) were common alongside grass taxa, suggesting the expansion of open, seasonal forest across the region, replacing closed rainforests (Morley 2002). These floras are thought to have been dispersed to south-east Asia through Myanmar from Africa via the Indian subcontinent by the mid-Eocene when India and south-east Asia lay at similar latitudes. However, alternative hypotheses of a Malaysian origin exist (e.g. Shukla et al. (2012)). The Miocene and Early Pliocene saw warmer and wetter climates across south-east Asia when the vegetation began to take its modern form — including the dispersal and establishment of Dipterocarpaceae as a dominant family in the Asian tropics and subtropics (Aston 1988, Morley 2002) and the presence of both seasonal and everwet tropical forests (Morley and Flenley 1987).

Glaciation during the mid-Pleistocene resulted in a significant drop in sea level, causing the interconnection of what is now mainland southeast Asia with Sumatra, Java and Borneo, cross-cut by several large rivers (Heaney 1991). Throughout this period, it is hypothesised that cooler, drier conditions interacting with topography led to the formation of a strip of low rainfall extending through the centre of the Sunda Shelf, promoting the transition of moist forest to a savanna or seasonal forest in this zone (Heaney 1991, Bird et al. 2005).

3.5 Geological setting

3.5.1 Regional geology

Quaternary basalts associated with Cenozoic rifting in south-east Asia occur within north-east Cambodia and central Vietnam as approximately 10 000 km^2

plateau deposits (Sutherland et al. 2015). These either extrude into, or overlie Mesozoic red beds (Jurassic red terraces) — non-marine sandstones and clays deposited across the region in a foreland rift throughout the Late-Jurassic-Early Cretaceous (Vysotsky et al. 1994, Racey 2009, Racey and Goodall 2009). Detailed reviews of the stratigraphy and lithology of the Mesozoic red beds is presented in Racey et al. (1996) and Racey and Goodall (2009), and an overview of the geological units in Cambodia is outlined in Vysotsky et al. (1994).

3.5.2 Local geology

In Ratanakiri (and extending into adjacent regions in Vietnam and Laos), Quaternary basalts occur as 80 m thick, 1 500 km^2 deposits that were formed in two distinct events. The first (pre-0.7 Ma) was produced as fissural, Hawaiian-type flow infilling topographic lows, while the second (post-0.7 Ma) transpired from a more strombolian flow-type, causing the generation of craters and rhyolitic tuff deposits (La Combe 1969, Sutherland et al. 2015). The caldera of these craters form the catchment boundaries of the five lake-site that are the subject of this study (Bourdier 1995, Riebe 1999). The regional geology of Ratanakiri, including the basaltic province, is shown on Figure 3.4.

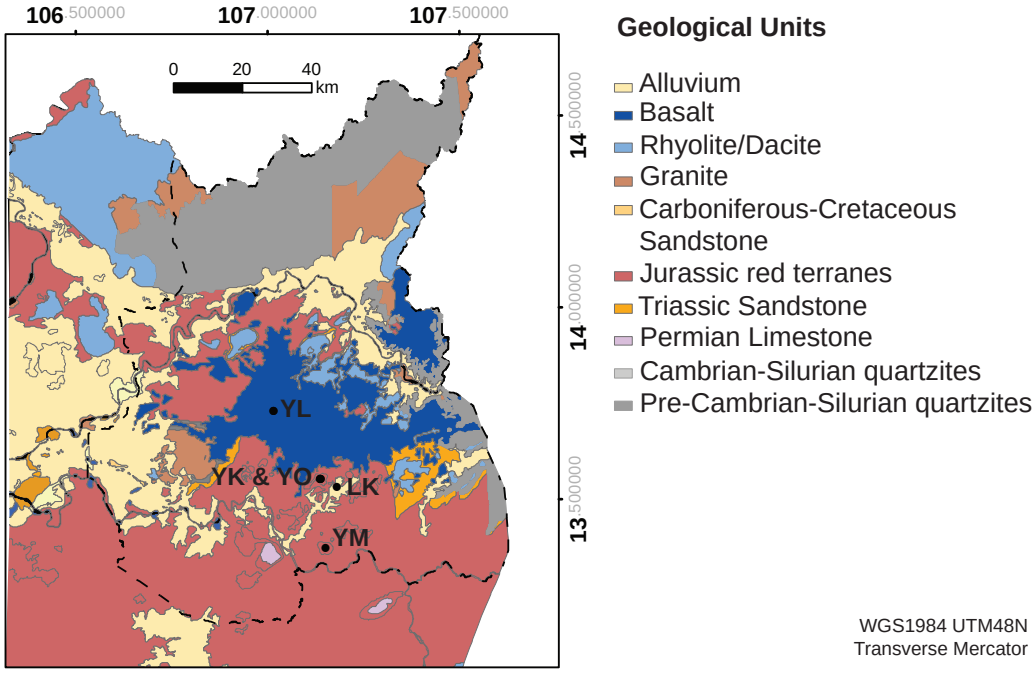

FIGURE 3.4: Geological map of Ratanakiri (boundary represented by dotted line) showing the regional extent of the basaltic plataeu extruded into and overlying sandstone and red terraces. Yeak Loam (YL), Yeak Kara (YK), Yeak Oam (YO), Boeng Lumkut (LK) and Yeak Mai (YM). Data sourced from ODC (2016b).

At the lake catchment scale, coarse-scale (50K) geological maps were produced for the sites in ArcGIS version 10.3 using pre-existing (JICA 2002a) spatial data available for the region (Figure 3.5). These show that the lake catchments are formed from basalt extruded into sandstone. Yeak Loam sits at the heart of an extensive basalt plateau (Figure 3.4 for regional extent), while the other lakes form from more localised basalts that have been extruded into the Jurassic red terranes (shown as sandstone on local-scale maps).

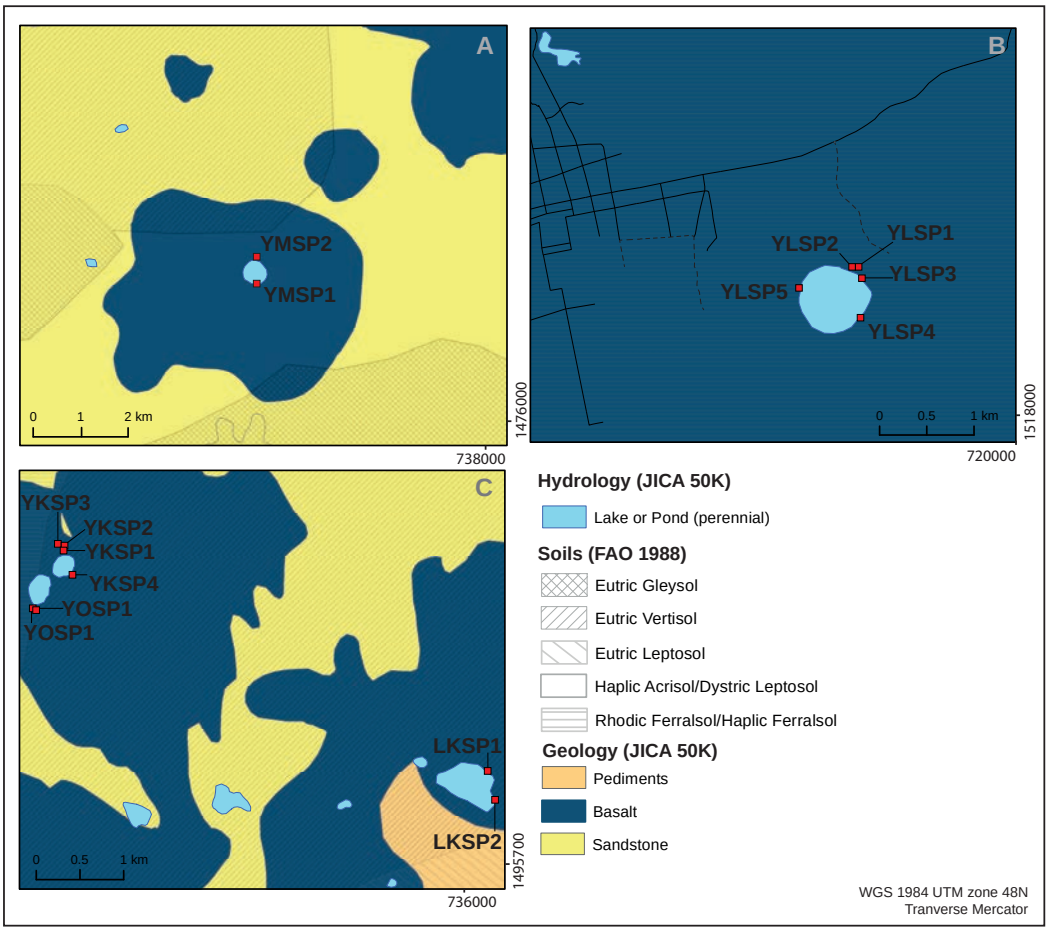

FIGURE 3.5: Geology and soil maps for A) Yeak Mai, B) Yeak Loam, and C) Yeak Oam, Yeak Kara and Boeng Lumkut lake sites. Geology and soils data (50K) from JICA (2002a) and MRC (2002) respectively. Red squares show the location of the soil samples taken from the lake catchments

Site walkovers undertaken in 2012 and 2013 indicate that local catchment geology comprises tuffs at Yeak Oam and Yeak Kara (Figure 3.6 A and B) and flow and/or vesicular basalts at all sites (Figure 3.6 C to G). The marked distinction in the morphology of the northern (Figure 3.6 G) and southern (Figure 3.6 H) sides of the Yeak Mai crater — the former being steep with basalt outcrops and black soils, and the latter being gently graded with no outcrops and pale soils — may indicate a lithological change across the site (basalt and sandstone, or basalt and alluvium). The geology above the

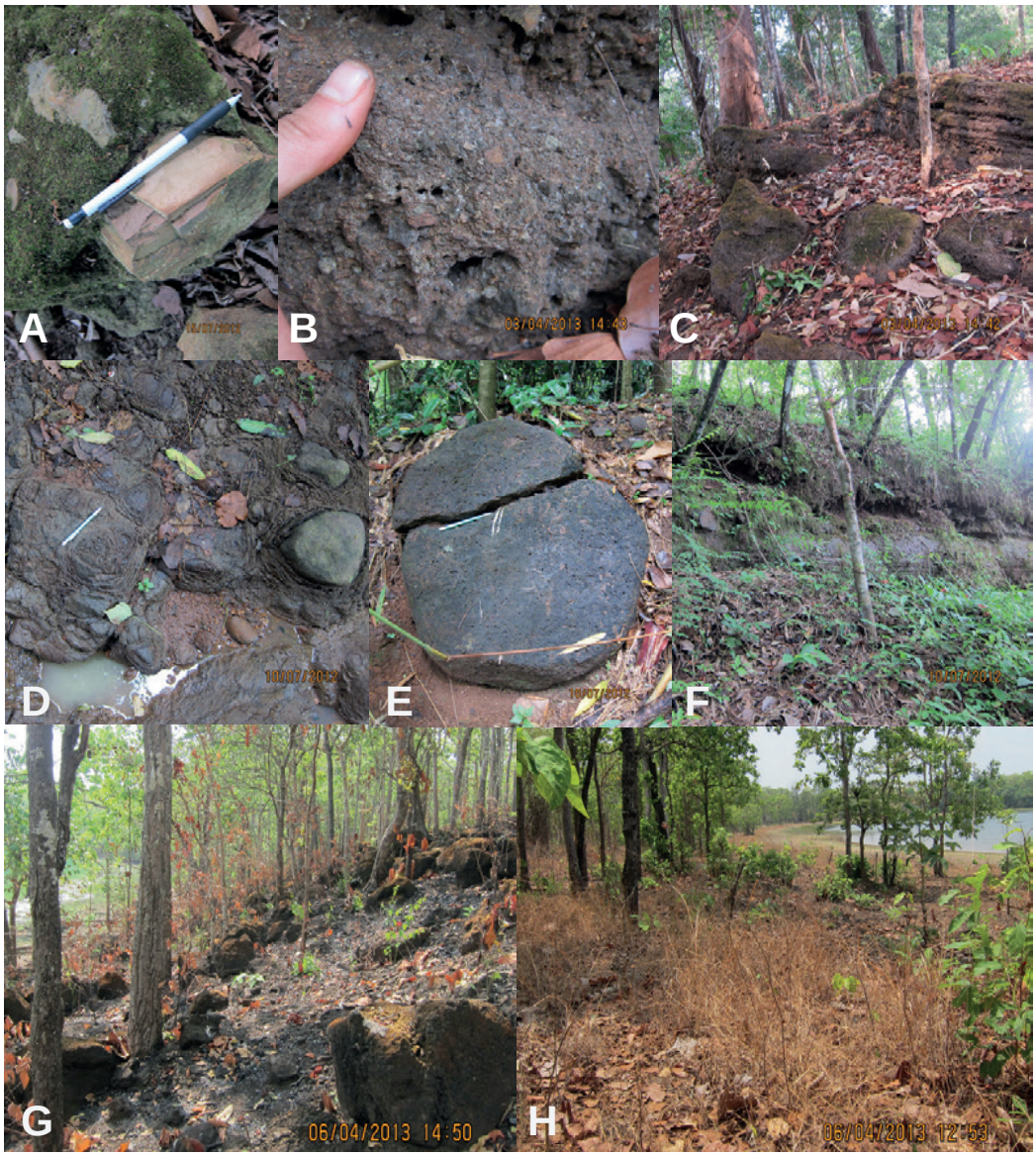

FIGURE 3.6: Photographs of outcropping bedrock at the crater lake sites. A) & B) tuffs outcropping at Yeak Kara/Yeak Oam; C) flow basalt at Yeak Oam; D) flow basalt at Yeak Loam; E) vesicular basalt at Yeak Loam; F) basalt escarpment along south-west boundary of Boeng Lumkut; G) vesicular basalt outcropping along the southern Yeak Mai lake edge; H) gently graded northern slope of Yeak Mai with no outcropping geology.

basaltic escarpment on the south-west boundary of Boeng Lumkut (Figure 3.6 F) is mapped as pediments (Figure 3.5).

3.6 Soils

3.6.1 Regional soils

Soils supporting tropical forests are typically characterised by intensive weathering and leaching, enrichment of oxides and hydroxides of Fe and Al, low organic matter accumulation and moderate acidity (Osman 2013). Basalts, which are made up of easily-weathered mafic minerals, typically break down into fine-textured (clay) soils (Osman 2013). Soils overlying Vietnamese flood basalts (derived from the first-event basalts in Ratanakiri) are commonly lateritic bauxites (Schirrmeister and Störr 1999). These represent an end-stage weathering product developed from further breakdown of montmorillonitic-kaolinitic, red (Fe-rich) soils (noting the broad-spectrum of products that can result from mineral transformation in tropical weathering of basalts) (Osman 2013). Soils overlying basalts in Cambodia have been described as either comprising deep, massive, reddish-brown, pluvial clay loams interspersed with basalt fragments that gradually transition into weathered basalt, or as concentrated iron oxides and lateritic hardpans that sharply overlie heavily weathered bedrock (Takaya 1967, Dararath et al. 2011). Laterites are common within tropical and subtropical zones (Osman 2013), and, within the Vietnamese basaltic provinces, are characterised by: 1) the enrichment of Al- and Fe-oxides (usually goethite or hematite) accompanied by a loss of K, Mg, Si and especially Ca and Na, and; 2) formation of kaolinite and gibbsite with a relatively high trace element content (Motuzova and Thi Hong Van 1999).

A survey of the physical and geochemical properties of basaltic soils in Cambodia was undertaken by Saeki et al. (1959). In general, this study found that, country-wide, basaltic soils tend to be deep (average of 15 to 18 m deep), clayey and acidic with a moisture holding capacity sufficient to maintain moisture at depth even in severe drought (even if surficial layers become very dry). Soils that were surveyed to the east of the Mekong (though not including those in Ratanakiri), were found to be generally less fertile than those surveyed to the west of the river channel. Results of this survey are summarised in Table 3.3.

Soils developed from the Mesozoic red terranes have been recorded as comprising fine, micaceous sands or pink quartz and iron-rich (weathered) sand overlying sandstone, or sandstone and shale. Clays within this geological setting are typically kaolinitic (Takaya 1967). In general, sandstone derived soils in Cambodia are nutrient poor with a limited water holding capacity (Saeki et al. 1959).

3.6.2 Local soils

The mapped site soils (MRC 2002) based off FAO (1988), are shown alongside local site geology (JICA 2002a) on Figure 3.5. At this scale (50K), Yeak Loam soils are mapped as Ferralsols derived from the underlying plateau basalts. These represent deeply weathered, red soils with low-activity clays and a high content of sesquioxides (FAO 1988, Osman 2013). This soil type

TABLE 3.3: A summary of the properties of Cambodian basaltic soils after Saeki et al. (1959).

Sampling zone	Generalised	West of the Mekong	East of the Mekong	Select top-soils	Select subsoils
Number of samples	20	7	13	4	5
Gravel (%)	17.3	27.3	7.4	4.3	2
Clay (%)	57.5	57.6	57.4	61.6	59
Soil Texture	Clay	Clay	Clay	Clay	Clay
pH (H_2O)	5.4	5.9	5.1	5	5.4
pH (KCl)	5	5.7	4.7	4.7	5.1
N (%)	0.18	0.22	0.17	0.23	0.07
C/N	8.3	7.7	8.6	7	7.6
Humus (%)	2.61	2.86	2.45	2.79	0.91
C.E.C (meq.)	31.54	33.3	30.59	34.22	23.05
Exc. CaO (meq.)	7.24	11.6	4.85	12.19	5.37
Available CaO (%)	0.032	0.05	0.023	0.044	0.016
Available P_2O_5 (%)	0.011	0.029	0.001	0.007	0.004
Available K_2O (%)	0.013	0.027	0.006	0.011	0.005

is considered typical for the humid tropics. Soils within the immediate vicinity of Yeak Mai are mapped as Haplic Acrisols/Dystic Leptosols and Eutric Vertisols. Eutric Vertisols also form the dominant soil types in the region between, and including, Yeak Oam and Yeak Kara (though the west catchment soils of Yeak Oam are classified as Ferralsols). This classification refers to soils that are fertile, non-acidic, deeply and widely cracking due to a high proportion of swelling clays (FAO 1988). Though most Vertisols occur in the semi-arid tropics, they can occur in wet tropical zones (Osman 2013). Acrisols are characteristic of tropical and subtropical regions, comprising soils with higher clay content in the subsoil vs. topsoils due to the formation of an argic horizon (white clay) from mineral migration. Leptosols comprise immature, infertile soils that form over rocks (FAO 1988). The Gleysols that are mapped in patches around Yeak Mai are weathered soils that turn a gleyish (grey/blue) colour from being saturated for an extended period of time (Osman 2013).

Due to the coarse-scale nature of the mapped data, soil samples were collected from the lake catchments to: 1) characterise the relationship (if any) between local edaphic conditions and forest structure, and; 2) determine the physical and geochemical properties of local soils to aid in lake sediment fingerprinting. In total, 15 soil profiles were described across the five lake sites, with sample locations shown on Figure 3.5. These were selectively analysed for a range of physical properties at the School of Geosciences laboratories at the University of Sydney. Methods used to describe the soils are outlined in Appendix A. A summary of results of the soil physical and geochemical properties are presented on Table 3.4 (Yeak Loam), Table 3.5 (Yeak Oam), Table 3.6 (Yeak Mai), Table 3.7 (Yeak Kara) and Table 3.8 (Boeng Lumkut). Photographs of representative soil profiles for each site are shown on Figure 3.7.

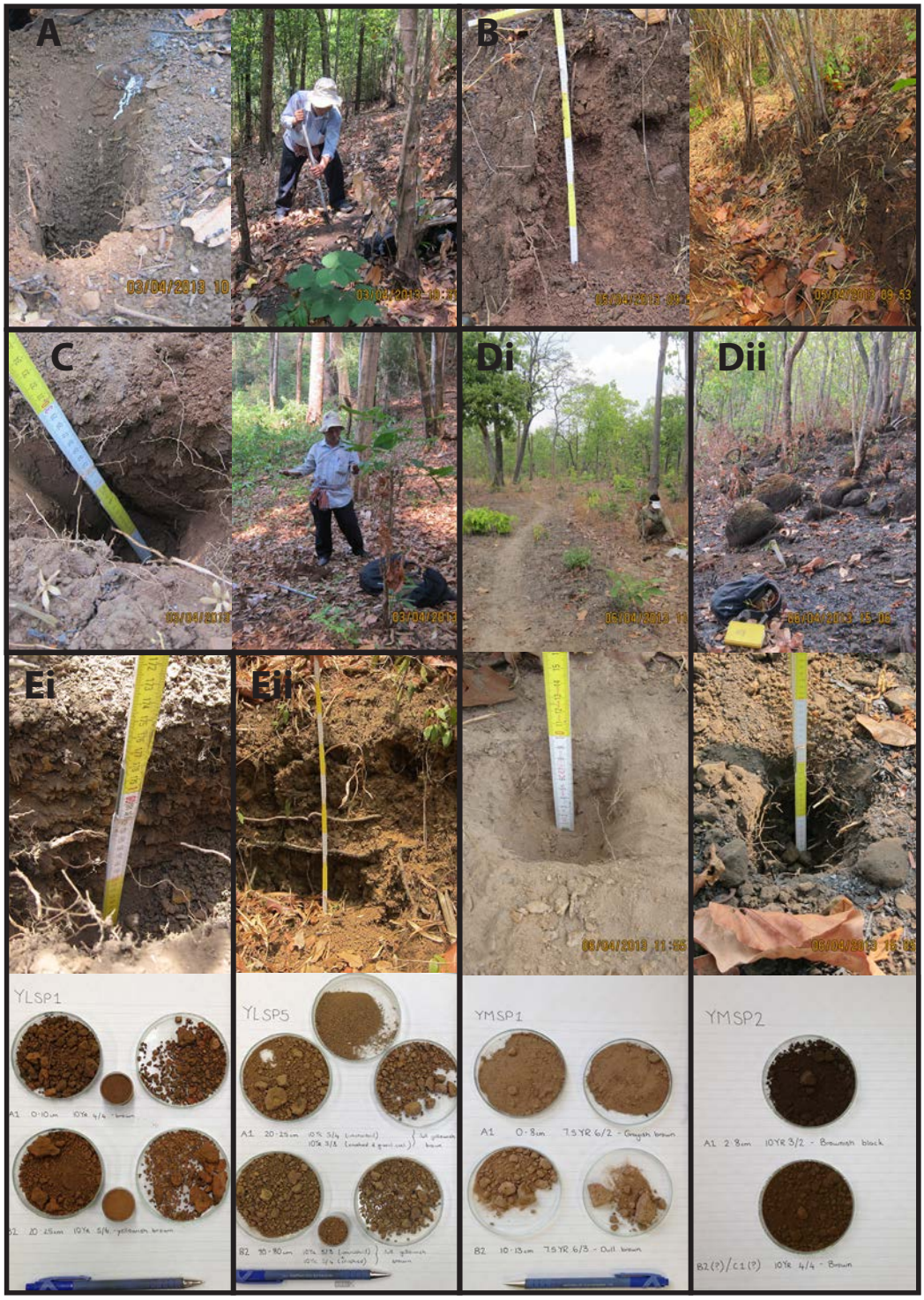

FIGURE 3.7: Photographs of select soil profiles taken from the crater lake catchments. A) Yeak Kara (YKSP3); B) Boeng Lumkut (LKSP2); C) Yeak Oam (YOSP1); D) Yeak Mai i)YMSP1 & ii) YMSP2; and E) Yeak Loam i) YLSP1 7 ii) YLSP5.

TABLE 3.4: Physical and chemical properties of the Yeak Loam catchment soil samples. Sample location is shown on Figure 3.5.

	Soil Profile 1: 0-25cm		Soil Profile 2: 0-45cm		Soil Profile 3: 0-60cm		Soil Profile 4: 0-90cm			Soil Profile 5: 0-80cm	
Sample ID	YLSP1-A1	YLSP1-B2	YLSP2-A1	YLSP2-B2	YLSP3-A1	YLSP3-B2	YLSP4-A1	YLSP4-B2i	YLSP4-B2ii	YLSP5-A1	YLSP5-B2
Sample Date	2/04/13	2/04/13	2/04/13	2/04/13	2/04/13	2/04/13	2/04/13	2/04/13	2/04/13	2/04/13	2/04/13
Sample Type	pit	pit	pit	pit	exposed path gully	exposed path gully	exposed path cut	exposed path cut	exposed path cut	exposed path cut	exposed path cut
Soil Horizon	A1	B2	A1	B2	A1	B2	A1	B2	B2	A1	B2
Total Depth (cm)	0-20	20 -25+	0-10	10-40+	0-25	25-80+	0-40	40-90+	40-90+	0-25	25-80+
Sample depth (cm)	0-10	20-25	5-10	40-45	0-25	25-80+	10-20	40-50	80-90	20-25	70-80
Field Colour (Hue / Value / Chroma)	brown (7.5YR 4/4)	brown (10YR 4/4)	dark reddish grey (7.5YR3/1)	brownish black (2.5Y3/2)	brown (7.5YR 4/4)	brown (10YR 4/4)	brown (7.5YR4/4)	brown (7.5YR4/6)	brown (7.5YR4/6)	brown (7.5YR4/4)	brown (10YR4/4)
Field moisture condition	dry	dry	moist	wet	dry	dry	dry	dry	dry	dry	dry
Depth to water table (cm)	n/a	n/a	38	38	n/a	n/a	n/a	n/a	n/a	n/a	n/a
Pore water content (%)	10.31	13.5	35.8	35.2	n/a	n/a	n/a	n/a	n/a	3.84	7.6
Dry Colour (Hue / Value / Chroma)	brown (10YR 4/4)	yellowish brown (10YR 5/6)	n/a	n/a	n/a	n/a	n/a	n/a	n/a	dull yellowish brown (10YR5/3)	dull yellowish brown (10YR5/3)

Continued...

	Soil Profile 1: 0-25cm		Soil Profile 2: 0-45cm		Soil Profile 3: 0-60cm		Soil Profile 4: 0-90cm			Soil Profile 5: 0-80cm	
Sample ID	YLSP1-A1	YLSP1-B2	YLSP2-A1	YLSP2-B2	YLSP3-A1	YLSP3-B2	YLSP4-A1	YLSP4-B2i	YLSP4-B2ii	YLSP5-A1	YLSP5-B2
>2mm wt. % (dry); description	35-45; angular-subangular gravel.	60-70; angular-subangular gravel.	0	0	n/a	n/a	n/a	n/a	n/a	45-55; subrounded-subangular, lithic gravel	40-50; subrounded-subangular, lithic gravel
Sand (%) (<2mm)	16.76	8.25	38.20	38.48	n/a	n/a	n/a	n/a	n/a	37.63	33.02
Silt (%) (<2mm)	43.59	33.52	56.12	58.38	n/a	n/a	n/a	n/a	n/a	35.26	35.05
Clay (%) (<2mm)	39.65	58.24	5.68	3.14	n/a	n/a	n/a	n/a	n/a	27.11	31.93
USDA classification (<2mm)	silty clay / silty clay loam	clay	silt loam	silt loam	n/a	n/a	n/a	n/a	n/a	loam/clay loam	clay loam
Dry Bulk Density (g/cc)	1.23	1.49	1.17	1.38	1.49	1.45	1.45	1.39	1.39	1.51	1.59
TOC (%)	9.00	5.00	n/a	n/a	n/a	n/a	n/a	n/a	n/a	4.70	3.80
χlf	0.05	0.02	0.01	0.01	0.01	0.01	0.00	0.01	0.01	0.01	0.01
χfd%	6.90	5.36	1.85	1.59	4.76	4.94	1.01	8.50	8.50	5.29	5.12
pH	4.9	5.3	5.2	6.9	n/a	n/a	n/a	n/a	n/a	5.1	5.3
Available P (ppm)	4.146	2.772	n/a	n/a	n/a	n/a	n/a	n/a	n/a	1.896	2.221
Ammonia (ppm)	2.340	1.800	n/a	n/a	n/a	n/a	n/a	n/a	n/a	0.879	1.150
Nitrate/nitrite (ppm)	0.026	-0.024	n/a	n/a	n/a	n/a	n/a	n/a	n/a	-0.021	-0.023

TABLE 3.5: Physical and chemical properties of the Yeak Oam catchment soil samples. Sample location is shown on Figure 3.5.

	Soil Profile 1		Soil Profile 2			
Sample ID	YOSP1-A1	YOSP1-A2	YOSP1-B2	YOSP2-A1	YOSP2-A2	YOSP2-B2
Sample Date	3/04/13	3/04/13	3/04/13	3/04/13	3/04/13	3/04/13
Sample Type	pit	pit	pit	pit	pit	pit
Soil Horizon	A1	A2	B2	A1	A2	B2
Total Depth (cm)	0-10	10-25	25-30	0-5	5-10	10-20+
Sample depth (cm)	5-10	15-20	25-30	0-5	5-10	10-20
Field Colour (Hue / Value / Chroma)	very dark brown (7.5YR2/3)	dark brown (7.5YR3/4)	dark reddish brown (5YR3/3)	very dark brown (7.5YR2/3)	dark brown (7.5YR3/4)	dark reddish brown (5YR3/3)
Field moisture condition	slightly moist	dry	dry	dry	dry	dry
>2mm wt. % (dry); description	n/a	n/a	n/a	35-45, subangular-subrounded gravel	30-40, subangular-subrounded gravel	n/a
Dry Bulk Density (g/cc)	n/a	n/a	n/a	1.50	1.56	1.57
χlf	n/a	n/a	n/a	7.16	7.28	7.26
χfd%	n/a	n/a	n/a	0.31	0.32	0.33

TABLE 3.6: Physical and chemical properties of the Yeak Mai catchment soil samples. Sample location is shown on Figure 3.5.

	Soil Profile 1		Soil Profile 2	
Sample ID	YMSP1-A1	YMSP1-B2	YMSP2-A1	YMSP2-C1
Sample Date	6/04/13	6/04/13	6/04/13	6/04/13
Sample Type	pit	pit	pit	pit
Soil Horizon	A1	B2	A1	C1
Total Depth (cm)	0-8	10-13+	0-10	10-20+
Sample depth (cm)	0-8	10-13	2-8	15-20
Field Colour (Hue/Value/Chroma)	dull brown (7.5YR5/4)	dull orange (7.5YR6/4) with orange (7.5YR 6/8) mottles	brownish black (10YR3/2)	brown (7.5YR4/3)
Field moisture condition	dry	dry	dry	dry
Depth to water table (cm)	n/a	n/a	n/a	n/a
Pore water content (%)	1.0	1.4	5.5	6.8
Dry Colour (Hue/Value/Chroma)	pale brown (10YR6/3)	light yellowish brown (10YR6/4)	very dark greyish brown (10YR3/2)	dark brown (10YR 3/3)
>2mm wt. % (dry); description	30-40; subangular-subrounded gravel	30-40; subangular-subrounded gravel	60-70; subangular-angular basalitc gravel & cobbles	60-70; subangular-angular basalitc gravel & cobbles
Sand (%) (<2mm)	76.28	72.21	46.78	47.50
Silt (%) (<2mm)	22.41	25.91	40.08	34.60
Clay (%) (<2mm)	1.31	1.88	13.14	17.90
USDA classification (<2mm)	loamy sand	loamy sand	loam	loam
Dry Bulk Density (g/cc)	1.35	1.35	1.46	1.67
TOC (%)	1.00	0.30	2.00	0.70
χlf	0.0023	0.00069	0.2	0.18
χfd%	3.49	3.68	5.25	5.49
pH	5.2	5.3	6.6	6.4
Available P (ppm)	6.061	3.097	66.259	85.255
Ammonia (ppm)	0.310	0.385	1.360	0.618
Nitrate/nitrite (ppm)	-0.024	0.062	0.177	0.041

TABLE 3.7: Physical and chemical properties of the Yeak Kara catchment soil samples. Sample location is shown on Figure 3.5.

	Soil Profile 1: 0-20 cm	Soil Profile 2: 0-25 cm		Soil Profile 3: 0-20 cm		Soil Profile 4: 0-15 cm	
Sample ID	YKSP1-O	YKSP2-A1	YKSP2-B2	YKSP3-A1	YKSP3-B2	YKSP4-A1	YKSP4-B2
Sample Date	3/04/15	3/04/15	3/04/15	3/04/15	3/04/15	3/04/15	3/04/15
Sample Type	pit	pit	pit	pit	pit	pit	pit
Soil Horizon	O (swamp)	A1	B2 (?)	A1	B2	A1	B2
Total Depth (cm)	0-20	0-20	20-25+	0-10	10-20+	0-10	10-15+
Sample depth (cm)	0-10	0-20	20-25	0-10	10-20	0-5	10-15
Field Colour (Hue/Value/Chroma)	brownish black (10YR 2/1)	brown (7.5YR 4/4)	dark brown (7.5YR3/3)	brownish black (10YR 2/3)	brownish black (10YR 2/3)	dark brown (10YR3/3)	dark brown (7.5YR3/4)
Field moisture condition	wet	slightly moist	slightly moist	dry	dry	dry	dry
Depth to water table (cm)	5cm	n/a	n/a	n/a	n/a	n/a	n/a
Pore water content (%)	n/a	n/a	n/a	11.8	20.12	n/a	n/a
Dry Colour (Hue/Value/Chroma)	dark brown (10YR3/3)	brownish black (7.5YR3/2)	n/a	brownish black (10YR 2/3) (burnt)	brownish black (10YR 3/2)		
>2mm wt. % (dry); description	n/a	n/a	n/a	25-35; subrounded-subangular lithic gravel	25-35; subrounded-subangular lithic gravel	n/a	n/a
Sand (%) (<2mm)	n/a	n/a	n/a	38.75	29.79	n/a	n/a
Silt (%) (<2mm)	n/a	n/a	n/a	39.46	39.92	n/a	n/a
Clay (%) (<2mm)	n/a	n/a	n/a	21.79	30.29	n/a	n/a
USDA classification (<2mm)	n/a	n/a	n/a	loam	clay loam	n/a	n/a
TOC (%)	n/a	n/a	n/a	10	7	n/a	n/a
pH	n/a	n/a	n/a	5.1	5.1	n/a	n/a

TABLE 3.8: Physical and chemical properties of the Boeng Lumkut catchment soil samples. Sample location is shown on Figure 3.5.

	Soil Profile 1: 0-25 cm		Soil Profile 2: 0-55 cm		
Sample ID	LKSP1-A1	LKSP1-B2	LKSP2-A1	LKSP2-B2	LKSP2-C1
Sample Date	5/04/13	5/04/13	5/04/13	5/04/13	5/04/13
Sample Type	lake high-water-mark cut	lake high-water-mark cut	gully exposure	gully exposure	gully exposure
Horizon	A1	B2	A1	B2	C1
Total Depth (cm)	0-3	3-25+	0-15	15-27	27-55+
Sample depth (cm)	0-3	11-16	0-10	25-30	n/a
Field Colour (Hue / Value / Chroma)	dull reddish brown (5YR4/4)	dark reddish brown (5YR4/4)	dull reddish brown (5YR4/4)	dark reddish brown (5YR3/4)	
Field moisture condition	dry	dry	dry	dry	dry
Depth to water table (cm)	n/a	n/a	n/a	n/a	n/a
Pore water content (%)	n/a	n/a	20.2	2.1	n/a
Dry Colour (Hue / Value / Chroma)	n/a	n/a	brown(7.5YR4/3)	brown(7.5YR4/4)	n/a
>2mm wt. % (dry); description	n/a	n/a	50-55; subangular-subrounded lithic gravel	20-25; subangular-subrounded lithic gravel	75-80; subangular-angular, basalt gravel, cobbles and boulders.
Sand (%) (<2mm)	40.953597	33.906659	30.107179	23.127703	n/a
Silt (%) (<2mm)	47.559617	53.328595	54.542141	60.723151	n/a
Clay (%) (<2mm)	11.5	12.76474	15.350679	16.149141	n/a
USDA classification (<2mm)	loam	silt loam	silt loam	silt loam	n/a
TOC (%)	n/a	n/a	7.00	5.00	n/a
pH	n/a	n/a	5.00	5.10	n/a
Available P (ppm)	n/a	n/a	25.786	4.824	n/a
Ammonia (ppm)	n/a	n/a	1.860	0.865	n/a
Nitrate/nitrite (ppm)	n/a	n/a	0.763	-0.021	n/a

The characteristics of the residual basaltic soils characterised at the lake sites are broadly consistent with descriptions outlined by Saeki et al. (1959). However, soil properties did vary across the sites, with the Yeak Mai soils found to be especially different.

The catchment soils broadly represent silt loams and clay loams, with the lightest texture classified as a loamy sand (YMSP1), and the heaviest a clay (YLSP1 subsoil) (Soil Survey Staff 2010). The total depth of the catchment soil profiles was difficult to determine due to the tough, dry nature of surfaces, which were sampled at the very end of the dry season (April 2013). However, top soils were typically thin (ranging from 3 cm [YMSP1] to 40 cm [YLSP4]), and the presence of outcropping bedrock at most sites suggests that the total depth is probably limited (vs. the basaltic soils described by Saeki et al. (1959)). Despite this, the profiles sampled at Yeak Loam (aside from the YMSP2 gleyic profile), Yeak Kara and Lumkut (LKSP1) showed a textural contrast between the A1 and B2 horizons, indicating a degree of pedalogical development. The basaltic Yeak Mai soils (represented by YMSP2) appear immature compared to those of the other lake sites based on: 1) the thinness of the profile; 2) lack of development of a subsoil; 3) relatively high dry bulk density values (1.5 to 1.7 g/cc); 4) low organic content (0.7 to 2%), and; 5) a comparatively neutral pH (6.4 to 6.6) that may be more representative of the basic parent material than of tropical forest soils (typical pH = 4.0 to 6.0) (Juo and Franzleubbers 2003). As such, these have cautiously been classified as Leptosolic (FAO, 1988). The pale and light-yellowish brown loamy sand profile taken from the (presumed) non-basaltic soils on the northern side of Yeak Mai appears unlike the residual basaltic soil samples taken from either Yeak Mai or the other lake sites, though this sample was too shallow to classify.

The estimated pore water content of the soil samples extracted from pits (vs. exposed cut faces) and away from the influence of a ground water table (i.e. YLSP2) is reasonably high for sampled clay and clay loam subsoils (YLSP1-B2 = 14%; YKSP3 = 20%) despite being taken at the end of the dry season. This indicates the capacity of these soils to retain water throughout a persistent dry spell. The loamy sand and loam soils taken from Yeak Mai (both lithologies) have a lower water retention capacity (1 to 7%).

The χlf SI of Yeak Loam and Yeak Mai SP1 (non-basaltic soils) is low (<0.053 SI), reflecting magnetic susceptibility values typical of topsoils, paramagnetic materials or sedimentary rocks (Dearing 1999a). Slightly higher values (0.18 to 0.2 SI) are recorded for YMSP2 (basaltic soils), and values trending towards those reflective of homogenous basic rocks were measured from Yeak Oam samples (7.15 to 7.25 SI) (Dearing 1999a). χfd%, which reflects the presence of super-paramagnetic grains in the samples, is decoupled from χlf, with high values returned for representative residual basaltic samples from Yeak Loam and Yeak Mai (4.5 to 8%), low values for non-basaltic soils from Yeak Mai (3.5 to 4%), and very low values for Yeak Oam basaltic soils (0.31 to 0.33%). This may relate to grain size, with higher χfd% values for samples with a greater abundance of clay and a lesser abundance of sand (noting that textural data was not measured for Yeak Oam samples).

The pH of the residual basaltic soils from lake catchments other than Yeak Mai, and excluding the gleyic soils extracted from YLSP2, indicates that

soils are strongly acidic, ranging from 4.9 to 5.3, with subsoils typically slightly less acidic than the topsoils. Available phosphorous is low (<10ppm) (Juo and Franzleubbers 2003) with the exception of LKSP2 topsoils and YMSP2 soils. This may reflect the presence of Al and Fe ions (abundant where pH <5.5) that fix phosphorous. Ammonia, nitrate and total organic content are low for all soils tested. The very low, or negative values for nitrate indicate that nitrification may be limited due to soil acidity (pH <5.5) (Juo and Franzleubbers 2003). However, as nitrate fluctuates with rainfall — being highest at the start of the rainy season (Juo and Franzleubbers 2003) — these dry season values may not reflect annual soil nitrate content.

3.7 Forest ecology

3.7.1 South-east Asia seasonally dry forest types

Prior to extensive clearance of the landscape from the 1960s, SASDTF extended eastward from west Vietnam into the lowlands of northern and eastern Cambodia and southern Laos, across northern-eastern Thailand and into central Myanmar, representing one of the largest continuous tracts of dry tropical dry forest globally (Maxwell and Cox 2011) (range shown on Figure 3.1). Aside from a few occurrences as high as 1000 m ASL, these forests typically occur within lowlands (50 to 800 m) (Ruangpanit 1995). As such, mountain ranges commonly bound this ecoregion (see Figure 3.2 map C). SASDTF habitats are important for supporting a broad range of vertebrates within the region, including (amongst others), kouprey and Eld's deer (critically endangered), gaur, banteng, wild water buffalo, khting-vor, serow, Javan rhinoceros and Asian elephants (Wikramanayaka et al. 2014a, b).

As discussed in Chapter 2, a mosaic of dry forest units in the absence of large tracts of savanna is a defining characteristic of SASDTF, which is especially the case for the Southeastern Indochina Dry Evergreen Forests (SIDEF) sub-units that occur within the northern portion of the study area (location delimited on Figure 3.1). Here, patches of distinctly different forest can occur within hundreds of meters of each other (Bunyavejchewin et al. 2011), contributing to the high beta-diversity of the area (Apgaua et al. 2014). The distribution of these units can, at a highly simplified level, be predicted by available moisture (MAP and soil water retention) and elevation, but is also a likely product of disturbance (see Chapter 2 for details). Semi-evergreen dry forest (SEDF) characteristically occurs at higher latitudes (approximately 700 to 1 000 m) with a MAP of 1 200 to 2 000 mm (Bunyavejchewin et al. 2011), or at lower latitudes in soils with better water retention and / or a higher MAP (Maxwell 1999, Ohnuki et al. 2008). Dry Dipterocarp forest (DDF) and mixed deciduous forest (MDF) occupy areas with elevations <700 m ASL, the former persisting in areas with a lower moisture availability (MAP = 1 000 to 1 500 mm) (Rundel and Boonpragob 1995) and the latter in moister regions (MAP = 1 400 to 1 800 mm). However, these generalisations do not always hold true (Ruangpanit 1995).

The limited work that has been conducted on the vegetation structure of SASDTF in Cambodia (in particular, Theilade et al. (2011) Tani et al. (2007) Rollet (1972) and Rollet (1962) — the latter two of which have been reviewed in English by Maxwell (1999)) as well as more generalised descriptions of SASDTF which is generally focused on Thai dry forests (Williams 1965, Stott 1976, 1984, 1986, 1988b, a, 1990, Stott et al. 1990, Ruangpanit 1995, Gardner et al. 2000, Bunyavejchewin et al. 2011, McShea et al. 2011) are drawn upon to provide an ecological overview of SASDTF. As nomenclature used to characterise SASDTF forest units varies between authors and the regions in which they work, the following section adopts the generalised classification for the ecoregion used by Bunyavejchewin et al. (2011), with additional units represented within north-east Cambodia following Maxwell (1999) (drawing on Rollet (1962)). Vegetation that is characteristic of each forest type has been compiled into Appendix B based on pre-existing research and basic, qualitative site walkovers that were conducted throughout July 2012 and April 2013 field seasons. On-site plant identification was aided with the help of A. Maxwell (independent academic) and S. Channa (Department of Environment, Banlung).

Dry deciduous forest

Dry deciduous forest make up the core forest units within the CIDF ecoregion (location delimited on Figure 3.1). Leaf shedding by canopy dominants throughout the dry season is the defining characteristic of this forest type. This process makes these forests prone to low intensity annual burning by lowering relative humidity and drying the fine fuels in the understorey (grasses and leaf litter) (Bunyavejchewin et al. 2011). As such, many dominant tree species within this formation have developed fire adaptations such as thick corky bark and root crowns that re-sprout post disturbance (Wikramanayaka et al. 2014a). In Cambodia, the presence of *Xylia xylocarpa* (Benth./Roxb.) is taken to be an indicator of dry deciduous forest (Tani et al. 2007).

Distinctions in the vegetation composition of dry deciduous forest means that it is typically sub-divided into two types — Deciduous Dipterocarp Forest (DDF) and mixed deciduous forest (MDF). The distinguishing features of each are detailed below.

Deciduous dipterocarp forest (DDF) is structurally the most open of the SASDTF forest units (Bunyavejchewin 1983), but does support a range of canopy coverage, from from semi-dense to a more "open savanna" forest (Stott 1984, 1988b, 1990). This variability is commonly linked to microclimatic, edaphic, topographic and fire-legacy conditions (Maxwell 1999). Canopy height is usually limited to 20 m, but can be as low at 10 m in xeric conditions and up to 30 to 35 m in especially favourable conditions (Bunyavejchewin et al. 2011). The distribution of DDF units is often associated with thin, acidic, shallow, sandy (freely draining), often lateritic and nutrient deficient soils (Stott 1990, Bunyavejchewin et al. 2011). In Thailand (where this forest type has been most described), these are associated with outcropping sandstones from the Mesozoic red-bed terranes (e.g. Khorat

Plateau associations), old alluvium and steep granitic slopes (Stott 1976). The typical MAP for DDF is 1 000 to 1 500 mm, occurring alongside a relatively prolonged (five to six month) dry season.

Indicator species within DDF plots surveyed in both Cambodian and northern Thailand include four Dipterocarpaceae species (*Dipterocarpus obtusifolius* (Teijsm. ex Miq.) (which can occur as near-pure stands), *D. tuberculatus, Shorea obtusa* and *S. siamesis* (Tani et al. 2007, Bunyavejchewin et al. 2011)), and *Terminalia tomentosa* ((Roxb.) Wight & Arn) (Maxwell 1999). The dominance of dry Dipterocarpaceae species (up to 90% of basal area (Maxwell 1999)) in the absence of conspicuous clumps of bamboo is a defining characteristic of DDF (Tani et al. 2007, Bunyavejchewin et al. 2011). Other important canopy and mid-storey species within this unit include *Pterocarpus macrocarpus* (Kurz), *Xylia xylocarpa* (Benth./Roxb.), *Gluta usitata* ((Wall.) Ding Hou), *Aporusa villosa* (Lindl.), and *Strychnos nux-blanda* (A.W. Hill). Dwarf bamboo (*Arundinaria*), *Dillenia* sp., *Cycas siamensis* (Miq.), *Corypha lecomtei* (Becc. Ex Lecomte) and *Phoenix acaulis* (Roxb.) growing alongside grasses (wet season) are widespread ground species in DDF (Maxwell 1999, Bunyavejchewin et al. 2011). A more comprehensive list of DDF species is outlined in Appendix B.

Periodic, low-to-moderate intensity ground fires appear important for maintaining DDF by facilitating removal of leaf litter and reinforcing the low organic content of soil (Ogawa et al. 1961, Bunyavejchewin et al. 2011). These burns are, in some cases, considered to be stabilising by preventing the establishment of more-dense forest type (Stott 1984, 1988b, a). The deciduous Dipterocarpaceae indicator species within this unit are especially well adapted, physiognomically, physiologically and phenologically, to fire (Stott 1984). The peak period for fires in DDF typically corresponds with the first half of the dry season, between late December and early March, correlating with peak accumulation of leaf litter and sufficient drying of understorey grasses (Stott et al. 1990). Hottest burns typically occur mid-season (Stott et al. 1990). Other edaphic features, particularly the soil water retention characteristics, appear important in internal structural variations within DDF forest-types, but this is not well-studied (Bunyavejchewin et al. 2011).

Mixed deciduous forest (MDF) is typically taller (25 to 30 m) and denser than DDF, and grows in deeper, less acidic (pH 5 to 6), slightly more fertile (clay loam) soil types (Ruangpanit 1995, Bunyavejchewin et al. 2011). Common canopy species in MDF include *Lagerstroemia* spp., *Pterocarpus macrocarpus* (Kurz), *Xylia xylocarpa* (Benth./Roxb.), *Bombax insigne* (Wall.), *Afzelia xylocarpa* ((Kurz.) Craib), *Anogeissus acuminata* (Wall.), *Dalbergia* spp., *Haldina cordifolia* ((Roxb.) Ridsdale) and *Terminalia* spp. (Ruangpanit 1995, Tani et al. 2007, Bunyavejchewin et al. 2011). *Irvingia malayana* (Oliv. ex A.W. Benn.), *Syzygium cumini* ((L.) Skeels.) and *Phyllanthus emblica* (L.) are common sub-canopy and understorey species (Bunyavejchewin et al. 2011). MDF ground cover is characterised by the presence of herbs and small shrubs, and where there is more light penetration, grasses growing alongside gingers (Ruangpanit 1995, Bunyavejchewin et al. 2011). Bamboos (especially deciduous bamboo) are an indicator species of this forest-type.

Dipterocarpus and *Shorea* species form a relatively minor component of these forests, though their relative proportion increases along a moisture gradient (Rundel and Boonpragob 1995). A more comprehensive list of common MDF species in outlined in Appendix B.

The interplay of edaphic and topographic conditions under specific climatic constraints appears important for unit delineation between DDF and MDF. Within MDF, floristics and structure can be quite diverse depending on soil quality (including water retention), elevation and topography. In north-east Cambodia, these forests appear to closely associate with the semi-dense dry forests described in Maxwell (1999) (drawing on Rollet (1962)), which have a preference for rocky basaltic brown earth slopes (the summits of which nearly always transition to denser SEDF). Topographic patterns of exposure and soil depth commonly cause sharp delineation of MDF and DDF at higher (>700m ASL) elevations (Rundel and Boonpragob 1995). Where elevation is less than 600 m (ASL), however, the sharp transitions that do occur are generally related to edaphic controls (Rundel and Boonpragob 1995).

Low frequency ground fire also appears to be an important ecological component of MDF (Bunyavejchewin et al. 2011). However, different fuels in MDF (vs. DDF) means that fires have the potential to be hotter and more destructive, particularly where tall bamboos facilitate spreading of the fire to the canopy (Stott et al. 1990).

Semi-evergreen dry forest

Semi-evergreen Dry Forest (SEDF) is the densest (250 to 400 stem/ha) of the forest units classified for SASDTF (McKenny et al. 2004) (though, as detailed below, some regional sub-classifications have been posited for north-east Cambodia (Rollet 1962)). Structurally, these forest have a relatively closed canopy, 30 to 40 m high, with emergents growing up to 50 to 60 m (Neal 1967). Most canopy species, and nearly all understory species are evergreen. Dominant tree species within this unit include *Dipterocarpus alatus* (Roxb.), *D. dyeri*, *D. turbinatus* (C.F.Gaertn.), *D. costatus* (C.F.Gaertn.), *Hopea odorata* (Roxb.), *H. ferrea* (Laness.), *Anisoptera* spp. that grow alongside *Irvingia malayana* (Oliv. ex Benn.), *Lagerstroemia* spp.), *Litsea vang* (Lecomte), *Dehaasia cuneata* (Blume), *Mesua ferrea* (L.), *Mangifera indica* (L.) and *Sindora cochinchinensis* (H. Baill) (Maxwell 1999, Bunyavejchewin et al. 2011).

In general, year-round canopy cover and lower annual accumulation of leaf litter means that SEDF are less susceptible to annual burning than the deciduous dry forest types. As such, it is often held that burning of SEDF can destroy the evergreen tree species, and promote a regime shift to dry deciduous forest (particularly DDF) that is thereafter reinforced by the regular presence of fire (Stott 1984, Stott et al. 1990, Johnson and Dearden 2009). However, as outlined in Chapter 2, this relationship is poorly studied (Maxwell and Cox 2011) and contested (Baker et al. 2008, Baker and Bunyavejchewin 2009).

SEDF sub-classifications — in north-east Cambodia, Maxwell (1999) (drawing on Rollet (1962)) classifies an intermediate forest type, transitionary between semi-dense dry forest (MDF) and SEDF. This subunit contains many species of the semi-dense-type MDF, but is closed with a leafy understorey without bamboo. Several SEDF species occur within the emergent layer, with the dominant SEDF Dipterocarpaceae trees gradually being replaced with *Lagerstroemia* spp. and Fabaceae taxa as the environment gets drier. Common species within this forest include *Lagerstroemia angustifolia* (Pierre ex Laness.), *Xylia xylocarpa* (Benth./Roxb.), *Pterocarpus macrocarpus* (Kurz), *Sindora cochinchinensis* H. Baill)., *Afzelia xylocarpa* ((Kurz.) Craib), and *Dalbergia bariensis* (Pierre). *Dipterocarpus intricatus* (Dyer) becomes dominant in these forests as they transition to a dry deciduous forest type. A degree of regular burning (low intensity ground fire) is apparent in this unit (Maxwell 1999).

At the other end of the spectrum, regionally-specific Basaltic red-earth forest types (BRE) are classified. These represent a variant of SEDF that grows in deep, permeable basaltic soils on uplands and plateau-tops with high water holding capacities. As such, this forest type is weakly tropophilous (Maxwell 1999). Dominant species are similar to that of SEDF, with the addition of *Aglaia gigantea* (Pierre Pellegr.), *Toona sureni* (Blume) Merr.), *Terminalia* spp., *Pterocarpus macrocarpus* (Kurz), *Afzelia xylocarpa* ((Kurz.) Craib), *Peltophorum dasyrachis* ((DC.) K. Heyne), *Adenanthera pavonina* (L.), *Lagerstroemia spp*. and *Tetrameles nudiflora* (R. Br.) as common canopy species. This forest type was once likely to have been distributed across the Ratanakiri Volcanic Province basaltic plateau in the vicinity of Yeak Loam. However, owing to the fertility of these soils, much of this forest type has been disturbed by swidden agriculture and, more recently, cleared for plantations (this is elaborated upon in Section 3.8).

Secondary dry forest

Soil conditions, microclimate and the timing and nature of past disturbances mean that secondary forests (SeF) are a common component of SASDTF. These widely-varied formations are an ecologically important, but often overlooked formation in Cambodia (Heinimann et al. 2007). The north-east Cambodian variants of SEDF secondary forest types are discussed in Maxwell (1999) (after Rollet (1962)). Here, the most extensive cause for the development of secondary forest is via swidden farming. In Ratanakiri, this practice is generally concentrated in SEDF-supporting landscapes that have more favourable soil characteristics for cropping.

Following low to moderate level disturbance, succession of SEDF usually includes a pioneer assemblage of herbs (if clearance is very frequent) and herbs and shrubs if clearance is less regular. Common pioneer trees are *Trema* spp., species from the Euphorbiaceae family, including *Macaranga* spp. and *Mallotus* spp., *Grewia tomentosa* (Juss.), *Peltophorum dasyrachis* ((DC.) K. Heyne), *Zizyphus cambodiana* (Pierre), *Colona* sp., *Memecylon edule* (Roxb.) and *Combretum quadrangulare* (Kurz). In later stages *Lagerstroemia* spp., *Cratoxylum* sp., *Vatica astrotricha* (Hance); *Dipterocarpus intricatus* (Dyer), *Shorea roxburghii* (G.Don), *Hopea* sp., *Eugenia* sp., *Sindora* sp. and *Albizzia* sp. form

secondary forest dominants, which may eventually recover to SEDF depending on disturbance events and alternation of original edaphic controls (Rollet 1962) in (Maxwell 1999).

Succession of mainland south-east Asian MDF following particularly intense fires or clearance typically results in the establishment of *Croton oblongifolius* (Roxb.), *Mallotus macrostachys* ((Miq.) Müll.Arg.), *Trema angustifolia* ((Planch.) Blume) alongside bamboos (*Gigantochloa albociliata* ((Munro) Kurz) or *Dendrocalamus strictus* ((Roxb.) Nees). A comprehensive list of species associated with secondary MDF (as well as secondary SEDF, and Basaltic Red Earth forests) is provided in Appendix B.

Secondary grasslands

In some cases, intense, or too frequent disturbance (associated with land clearance or fires) within MDF or SEDF can result in savanna as opposed to secondary forest (Rollet 1962, Maxwell 1999). This can occur following a single destructive event (Goldammer 2002), or as part of a long-term process whereby annual fire precludes regeneration of canopy species, thus gradually opening up the forest to a grassland community as mature canopy species die out (Ruangpanit 1995). The resultant grassland communities are typically dominated by *Oxytenanthera* spp. and *Imperata cylindrica* ((L.) P.Beauv.) (Goldammer 2002). These communities are fire promoting, and tend to persist over forest as long as there is annual fire preventing the establishment of shrubs (and later canopy) species (Ruangpanit 1995, Maxwell 1999).

Other SASDTF types

Other forest types that are present in the SASDTF, but not common within the immediate vicinity of the lake study sites, are pine forest, lower montane forest riparian forest, and swamp forest. A summary of the features of each is presented below, as outlined in (Ruangpanit 1995) and Bunyavejchewin et al. (2011).

Pine forest (PF) can occur across mainland south-east Asia at elevations extending from 400 to 1 500 m ASL. Lower versions of this forest are compositionally and structurally similar to DDF aside from the dominance of pine (particularly *Pinus merkusii* (Jungh. & de Vriese)). At higher elevations, these forests are structurally comparable to lower montane types (below), where *Pinus kesiya* (Royle ex Gordon) and members of the Fagaeae and Lauraceae families become compositionally important Rollet (1962) in Maxwell (1999).

Lower montane forest (LMF) occurs within south-east Asia at elevations in excess of 800 to 1 000 m ASL (Bunyavejchewin et al. 2011). While no one particular species dominates the canopy, members from the Lauraceae,

Theaceae, Magnoliaceae and Fagaceae family are important in this setting (Bunyavejchewin et al. 2011).

Riparian forest (RF) grows along stream or river lines particularly in basaltic soils, and can form a sharp contact between other forest types where the ground water table rises. These forests generally have a canopy at 20 to 30 m, and show some compositional similarities to SEDF with the addition of *Hydnocarpus anthelminticus* (Pierre ex Laness.), *Barringtonia acutangula* ((L.) Gaertn.), *Nauclea orientalis* ((L.) L.) and *Sterculia foetida* (L.) canopy species (Bunyavejchewin et al. 2011).

Swamp forest (SwF) grows in peat that has accumulated under permanently wet ground conditions. These forests can be relatively dense with a high canopy. Common canopy species include some SEDF Dipterocarpaceae alongside *Eugenia* spp., *Sterculia foetida*, *Myristica* spp., and *Ficus* spp. (Maxwell 1999). The understorey is characterised by the presence of palms (*Livistona cochinchinensis* (Merr. ex A.Chev. Syn. L.), *Licuala* spp. and Calamus sp.) Epiphytes, including *Stenochlaena palustris* ((Burm. f.) Bedd.) are common in this forest unit (Maxwell 1999).

3.7.2 Classification of local forest types

Forest units were mapped for Cambodia in the 1990s at a coarse (50K) scale by JICA (2002b), and are presented at a regional and local scale for the lake sites on figures 3.8 and 3.9. Because the region has been subjected to unprecedented levels of clearance since the time of mapping (described in section 3.8), much of what was once forest has been converted to plantation or open agricultural land. This area of land clearance (as of 2014) has been mapped by Open Development Cambodia (ODC) (2015) and is overlain (orange translucent shading) on figure 3.8. Most clearance is concentrated on the extensive basaltic plateau in central Ratanakiri where fragments of SEDF (including basaltic red-earth forests) and secondary forests grew alongside active and abandoned swidden plots in the late 1990s.

Very generally, Yeak Loam is the most developed of the crater lake sites considered in this study, with a thin lake-side buffer of SEDF the only forest retained within the vicinity of this site (figure 3.9 A). Yeak Mai, on the other hand, appears to be the least disturbed of the crater lake sites (figure 3.9 B). This site, as with Boeng Lumkut (figure 3.9 C) locally and regionally supports open forest units (DDF and MDF). The regional forest surrounding Boeng Lumkut has, however, undergone a high level of clearance in recent years (3.8). The catchment forest of Yeak Oam and Yeak Kara is SEDF (figure 3.9 C). The regional forest at these lake sites is comparably open (MDF/DDF). A detailed summary of the mapped vegetation at each lake site is described below.

The local and regional forests of Yeak Mai are mapped as predominantly undifferentiated dry deciduous forest with small pockets of MDF, woodland (less than 10% tree cover), and riparian forest that grows immediately adjacent to tributaries feeding the Tonlé Srepôk) (figure 3.9). Site walkovers

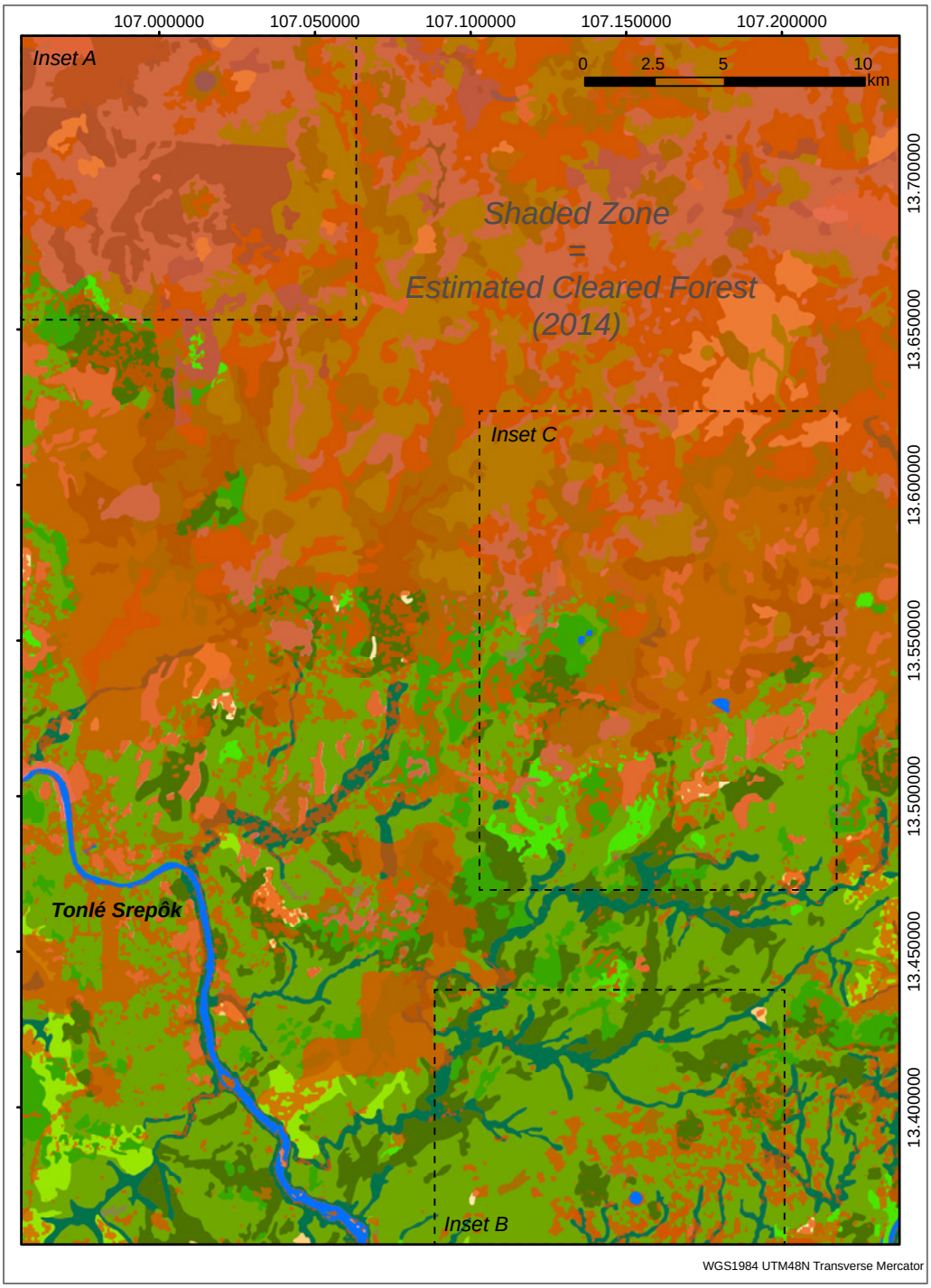

FIGURE 3.8: Regional vegetation map overlain with estimated extent of forest clearance as of 2014 (translucent orange shading). Key as per figure 3.9. Land use and forest data (50K) sourced from JICA (2002b) and ODC (2015). Insets shown on 3.9

indicated that the deciduous units in the lake catchment are dominated by *Dipterocarpus* (*obtusifolia* and/ or *tuberculatus*), *Shorea obtusa* and *S. siamesis*, suggesting that they affiliate with the DDF classification scheme (noting

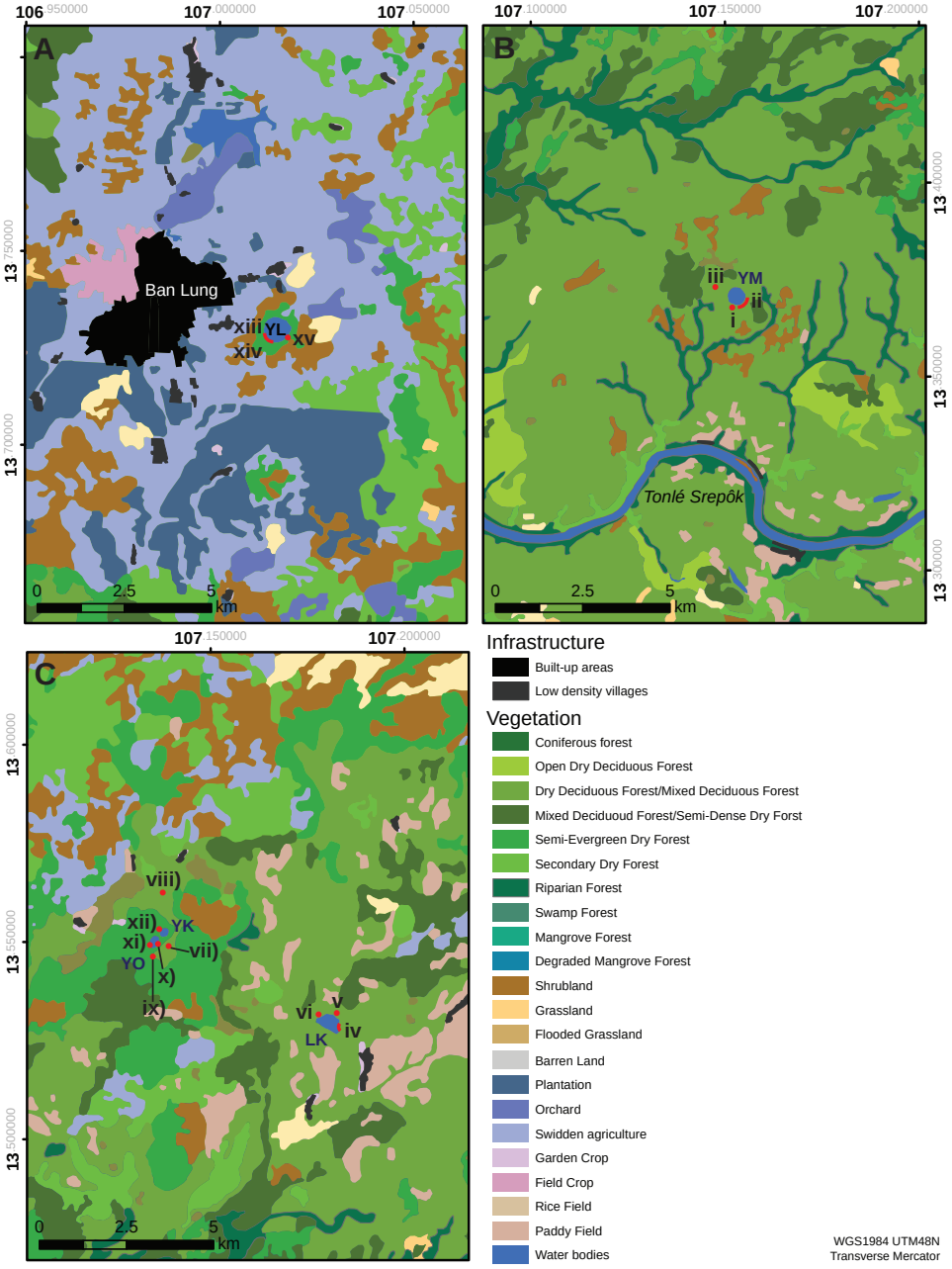

FIGURE 3.9: Local vegetation maps for A) Yeak Loam (YL); B) Yeak Mai (YM); and C) Yeak Oam (YO), Yeak Kara (YK) and Boeng Lumkut (LK). Data sourced from JICA (2002b) Roman numerals correlate with approximate location of photographs presented in figure 3.10.

that some species characteristic of MDF were observed on the moderately-graded basaltic catchment slopes (figure 3.10 photos i & ii)). The regional Yeak Mai forest — presumed to be growing in sandstone-derived soils — appears to represent both the most undisturbed and the driest of the forest-types observed across the lake sites (figure 3.10 photo iii (dry season)). Here, the open forest (approximately 50 to 55% canopy cover with a very limited mid-storey) was overwhelmingly dominated by a low (max 20 m)

Dipterocarpus/Shorea canopy growing alongside dry indicator under-storey species (e.g. *Cycas sp.*, *Acacia intsia* [(L.) Willd.]). Based on these observations, it is possible that the patches of land clearance mapped around Yeak Mai (figure 3.8) may actually represent "natural", relatively open, dry deciduous patches (especially if mapped from dry season images).

Much of the forest surrounding Boeng Lumkut has been cleared (figure 3.8). The catchment forest is mapped as comprising undifferentiated dry deciduous forest (figure 3.9). Site walkovers indicated that these predominantly represent open (50 to 60% canopy cover) DDF (figure 3.10 photo v (dry season) and photo vi (wet season)). However, several MDF indicator species (e.g. *Lagerstroemia* spp., *Bombax ceiba*) were observed in places along the western lake edge (figure 3.10 iv).

The forests that regionally surround Yeak Oam and Yeak Kara are mapped as a mosaic of undifferentiated dry deciduous forest, SEDF and MDF. A significant portion of these forests has been fragmented by active swidden agriculture and, more regionally, by widespread clearance for rubber and cashew plantations — observed during fieldwork in 2012 and 2013. The regional forest that does still persist in the vicinity of the lake sites typically comprises DDF (figure 3.10 photo viii (dry season)) mosaicked with ginger and bamboo-rich MDF in depressions (figure 3.10 photo vii) (wet season)). There is a sharp transition between deciduous forest and SEDF along the upper rim of the Yeak Oam and Yeak Kara catchments (shown on figure 3.10 photo ix), which continues down to the lake edge as a tall (30 to 40 m), dense (80 to 90% canopy cover), four storey forest (figure 3.10 photos x, xi (Yeak Oam) and photo xii (Yeak Kara).

The catchment forests of Yeak Loam occur as an approximately 500 m-wide lake buffer in an otherwise deforested region. This forest type is mapped as SEDF (figure 3.9). This classification is roughly consistent with field observations, though some canopy species are characteristic of intermediate SEDF/MDF and MDF forests (see appendix B). Structurally, the forest has a tall (20 to 35 m) canopy, with three layers and some emergents. Canopy cover is reasonably consistent throughout the wet and dry season (at approximately 70 to 90%) (see figure 3.10 photo xiii (dry season) and photos xiv and xv (wet season), consistent with SEDF.

FIGURE 3.10: Photographs of SASDTF units surrounding the lake sites. i) dry season DDF vegetation growing on YM basaltic slopes; ii) view of dry season DDF/MDF forest on the north-west YM catchment slope; iii) regional YM DDF forest resprouting at the end of the dry season; iv) Dry season LK DDF/MDF; v) resprouting LK DDF at the end of the dry season; vi) wet season DDF at LK; vii) regional YO/YK wet season MDF; viii) regional YO/YK dry season DDF; ix) transition between wet season MDF and SEDF looking towards the upper catchment rim of YO; x) & xi) wet season YO SEDF; wet season YK swampy vegetation (foreground) and SEDF (background); xiii) dry season YL SEDF; xiv) & xv) wet season YL SEDF.

3.8 Disturbances in SASDTF

As has been discussed in chapter 2, two of the key disturbances thought to control the stability of tropical dry forest or savanna, are fire and land clearance. The presence of both in SASDTF as they relate to the contemporary landscape across the ecoregion and at the crater lake sites is discussed below.

Across more rural parts of mainland south-east Asia, including Ratanakiri, the most common cause of anthropogenic fire is from swidden agriculture, which uses fire to clear forest understorey and manage land for grazing, thatching or cropping (Maxwell 2004). Traditional farming within Ratanakiri involves the burning of swidden plots during the dry season and planting at the start of the wet season. Plots are characteristically used from one to five years, after which they are left to regenerate (fallow) for five to 20 years, depending on soil quality and length of cultivation (Stott et al. 1990, Fox and Vogler 2005, Wanthongchai and Golder 2011). Old growth forests and especially spiritual sites, including many lakes, have traditionally been off-limits with regards to swidden farming and selective logging (Colm 1997, Fox and Vogler 2005).

While shifting cultivation is thought to be sustainable at low population numbers, it has been increasingly attributed to forest degradation across the SASDTF ecoregion (Colm 1997). As with most agriculture, slash-and-burn farming tends to be concentrated in regions with reasonably good soil fertility. These zones typically support SEDF, intermediate MDF/SEDF and, in some cases, denser MDF types. DDF and drier-type MDF units grow in soils too infertile for agriculture, and are normally precluded from direct slash-and-burn techniques. However, people set fires to the dry deciduous forests (alongside their denser counterparts) for the purpose of harvesting valuable timber species, construction of paths or roadways, and for herding and hunting (van Liere and McNeely 2005). Accidental burns may also occur in all forest types from flame-escape from slash-and-burn techniques or ignition from smoking or campfires (Maxwell and Cox 2011).

Large scale loss of dry forest across much of south-east Asia in recent decades has triggered attempts to exclude fire from protected areas (Stott et al. 1990, Wanthongchai and Goldammer 2011), including Virachey National Park (north of Tonlé San). This management technique, however, is often argued to be counterproductive, and even damaging to the forest in the long-term given the inherent role of regular fire in the ecoregion (especially in MDF and DDF) and that the accumulation of several years worth of ground fuels can cause high-intensity, destructive fires (Maxwell and Cox 2011). Logistically, it has proved challenging to preclude traditional land-use practices in protected areas (Stott et al. 1990).

3.8.1 Changing land-use

Prior to the 1950s, the forests of northeast Cambodia were commonly perceived as wild and inhabited by dangerous animals, hostile semi-nomadic ethnic groups, and capricious spirits (Wanthongchai and Goldammer 2011).

Efforts to "modernise" Ratanakiri were instigated from 1953 to 1959, culminating in the development of an administrative plan for the region. This included forced migration of highland villagers from forests to more concentrated communities along the Tonlé San and road ways (Bourdier 1998). Throughout this time, the recreational potential of Yeak Loam was realised, resulting in the construction of a chalet and roads on the lake shores (Colm 1997). However, the development of the province was largely disrupted by a period of conflict associated with the second Indochina war, Cambodian civil war, the establishment of the Khmer Rouge regime and unrest thereafter, extending from approximately 1967 to the 1998 (Riebe 1999). The changing socio-political environment associated with, and especially after this period, has resulted in a significant change to the traditional swidden-based management of the local forests.

Though Cambodia was not directly engaged in the Indochina War, north-east Ratanakiri was located within the vicinity of the Ho Chi Mihn trail, and thus US bombing spilt over into Ratanakiri from the late 1960s to 1973 (Maxwell and Cox 2011). This is argued to have instigated migration in the region, including retreat of the highlanders out of their villages into the lowland forests (You et al. 2015). Additionally, civil conflict between the Lon Nol administration and the Khmer Rouge as part of the Cambodian Civil War resulted in localised bombing of Ratanakiri — particularly in the vicinity of Ban Lung. This eventuated in the destruction of Yeak Loam infrastructure (Colm 1997). Throughout this period, many local villagers were relocated south to what is now the Lumphat District (Riebe 1999). Forced migration of the indigenous population of north-east Cambodia became a feature of the Khmer Rouge regime (Riebe 1999), who took control of the region between 1970 and 1979 (Riebe 1999, You et al. 2015). This initially shifted the geographic bounds of traditional swidden plots, and later this farming practice, alongside the collection of forest products, was banned (Maxwell and Cox 2011). This forced seven to eight year hiatus in swidden farming is thought to have increased the amount of canopy cover in the province (You et al. 2015). Under the "cooperation schemes" implemented by the regime, local communities were engaged in state-mandated labour, including rain-fed rice paddy cultivation, small scale corn and sugar cane cropping and commercial hunting for bush meat and wildlife trade (Fox and Vogler 2005). From 1979 to the 1980s, conflict between the Vietnamese and the Khmer Rouge left Ratanakiri province relatively cut off from the rest of the country.

As the political setting of Cambodia became more stable in the 1990s, and the country was becoming increasingly connected with international markets, land use within the region underwent significant shifts (Colm 1997, Loucks et al. 2009, Maxwell and Cox 2011, You et al. 2015). Most of this is related to the revaluation of forested land for hunting, extractable timber and alternate use, particularly with regard to development of large scale land concessions (International Organization for Migration 2009, Maxwell and Cox 2011). The increased focus on seasonal forests for commercial (including illegal) timber harvesting has resulted in the degradation and opening of the forest canopy in both in Ratanakiri and more broadly in the ecoregion (Hansen and Top 2006, Hor et al. 2014). Recognition of the impacts of

forest degradation — perceived to be related to swidden agricultural practices and logging — and attempts to increase wildlife across the region saw the designation of protected areas in the 1990s. Within Ratanakiri, these include Virachey National Park in the north of the province (declared in 1993), Lumphat Wildlife Sanctuary, including Yeak Mai (designated 1993), and Nsok Protected Forest designated 1999. The location of these is shown in figure 3.11. Management of Virachey and Lumphat protected areas only commenced in the late 1990s in collaboration with various international organisations, including WWF (Hansen and Top 2006, Kao and Iida 2006).

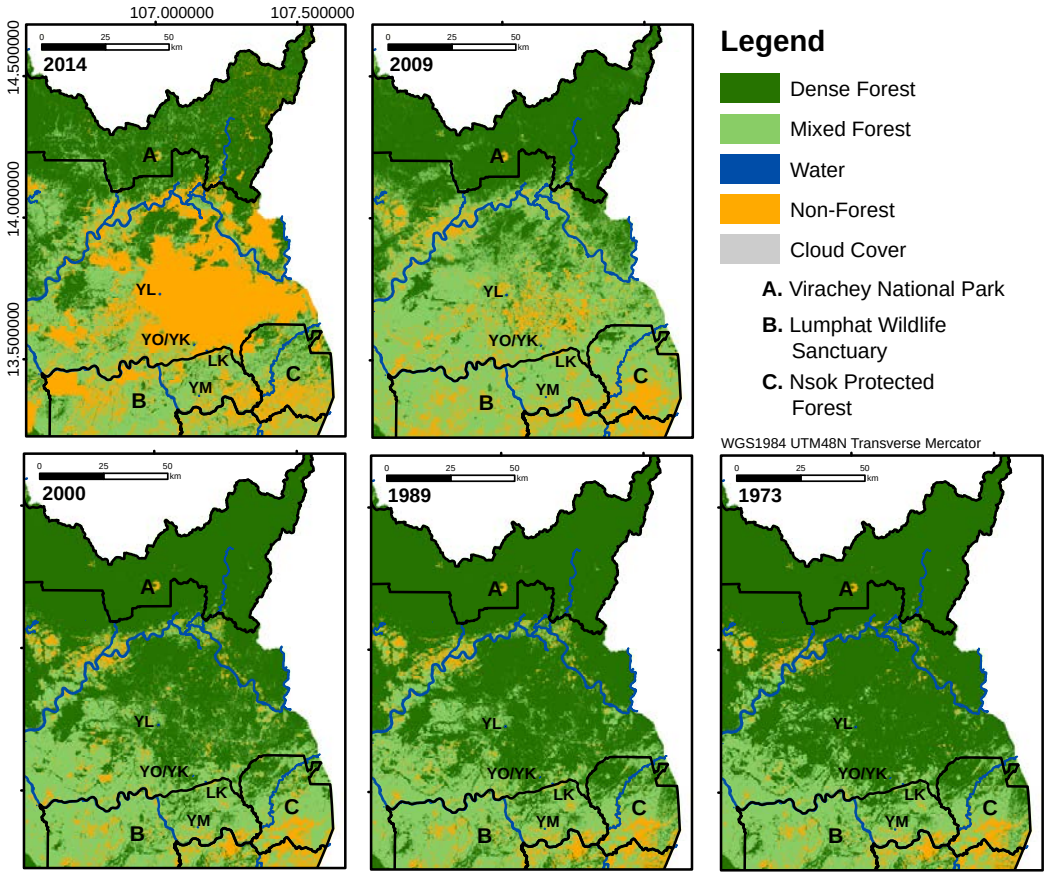

FIGURE 3.11: Comparison of forest cover across Ratanakiri Province between 1973 and 2014. Data sourced from ODC (2015).

One of the most dramatic contemporary land use changes occurring in Ratanakiri is the development of large-scale economic land concessions for the development of coffee, rubber and cashew plantations, and for other estate cash crops (e.g. cassava) (Maxwell and Cox 2011). This process has resulted in the consolidation and replacement of traditional swidden practices in the province and increased fragmentation and large-scale clearance of SASDTF units (Hor et al. 2014, Li et al. 2014, You et al. 2015). While this has been particularly concentrated in SEDF and secondary basaltic red earth forests, it is also prevalent in some deciduous dry forest units (Hor et al. 2014). The scale of these operations has led to significant degradation of the ecological intergrity of the region (McKenny et al. 2004, Hansen and

Top 2006, Sodhi et al. 2010, ODC 2015).

The extent of forest clearance in Ratanakiri through time can be observed from forest-cover maps produced from satellite images by International Organization for Migration (2009) between 1973 and 2014, replicated in Figure 3.11. Because plantations were included as "mixed forest" in this study until 2014, it is more useful to look at percentage change in dense forest cover to gauge relative timing of land conversion across the province. Most significant is the 36% drop in dense forest between 2004 and 2009. As of 2014 (which segregated plantations from mixed forest), dense forest and mixed forest represent approximately 47% and 112% of their estimated 1973 areas. Decline in dense forest is speculated to be a result of the clearance of more of the SEDF basaltic red earth forests across the central Ratanakiri volcanic province to support larger rural populations (and associated farming practices) and the development of plantations. The increase in the estimated percent of mixed forest throughout this time may be related to degradation of SEDF units (previously classified as dense forest), decreased area of swidden plots (previously classified as non-forest) or regeneration of DDF, MDF and shrubland across the region.

4 Lake core sedimentology and geochemistry

4.1 Introduction

This chapter aims to characterise physical and geochemical properties of the crater lake sediments in order to determine the type of sediment present, the mechanisms by which these sediments have accumulated, and any post-depositional modification. These data will provide a proxy record of climatic, environmental and land-use change to which palaeo-botanical and palaeo-fire records (chapter 5) can be compared.

The first section describes the techniques used for the extraction of long sediment cores from three of the Ratanakiri volcanic crater lakes described in chapter 3 — Yeak Oam, Yeak Loam, and Yeak Mai. Methods used to develop a chronology for, and characterise the stratigraphy, environmental magnetism, sedimentology and geochemistry of the sediment cores are then presented. The results of these techniques are then outlined, grouped by lake-site. This chapter then concludes by integrating the age-depth and sedimentological results for each master core to develop a model of sediment input to the lake sites. This is used to facilitate the palaeoclimatic reconstruction for the study area discussed in 6.

4.2 Methods

4.2.1 Justification for core sample selection

Yeak Mai, Yeak Loam and Yeak Oam were initially selected for sedimentological analysis based on variations in site forest type, catchment morphology and (recent) anthropogenic disturbance (see chapter 3 for details). 'Master cores' from Yeak Loam and Yeak Mai were then selected for finer-scale sedimentological and geochemical analysis. The Yeak Mai core was significantly longer than the gravity cores taken from the deeper lakes, and represented the only core within the set taken from both a shallow lake site and a relatively undisturbed dry dipterocarp forest unit catchment. The Yeak Loam master core was selected for detailed analysis based on its length, the distance from Yeak Mai (permitting a regional scale analysis), and its moderate-level of (presumably recent) anthropogenic disturbance. Analysis of a long (15 m core) from Yeak Kara (semi-evergreen dry forest catchment within regional dry deciduous forest) by Maxwell (2001, 2004) provides a valuable comparative data set to the original data presented here.

4.2.2 Core sampling

Initially, five cores were extracted from the Yeak Oam (x2), Yeak Loam (x2) and Yeak Mai (x1) lake sites that are described in chapter 3. Core sampling was undertaken over three field seasons in December 2011, July 2012, and April 2013. The techniques used for lake sediment sampling were determined by water depth, with gravity coring used to sample the deep lakes (Yeak Oam and Yeak Loam) and pushtube and percussion coring used to sample the much shallower Yeak Mai.

4.2.3 Gravity cores

Yeak Oam and Yeak Loam lake sediments were sampled using a piston gravity corer in July 2012 and December 2011 respectively. Two core samples (master and replicate) were taken from each of the lake sites approximately 2 m apart such that they could be stratigraphically compared (via visual logging and analysis of magnetic susceptbility) in order to confirm that the captured sediments represented undisturbed lake bottom samples. The coring sites were located at the deepest portion of the lakes — as determined by the results of a bathymetric survey described in Sharma (2014). Sampling locations were recorded using Trimble Nomad GPS device (latitude and longitude translated into UTM zone 48N [WGS 84]).

The coring device — comprising a corer body with steering fins and 18 kg lead weights (figure 4.1), based on the design of Kelts et al. (1986) — was clamped to 60 mm ⌀ (55 mm internal ⌀), 3 m long PVC pipe. A piston was mounted in the bottom of the PVC pipe and attached to the coring head with a 6 m long steel wire. The corer was suspended from an A-frame mounted on an aluminium deck above two inflatable boats. The corer was deployed through a moon pool in the deck between the two boats, and lowered through the water column until a weighted trigger plate, suspended 3 m below the PVC coring barrel, hit the lake floor. The coring device was then automatically released and free fell 3 m, driving the PVC tube into the sediment as the piston cable pulled taught. Following release, the apparatus was recovered using a hand-operated winch.

Core tubes were cut to one-meter sections using a pipe cutter, capped, and sealed for transportation to the School of Geosciences laboratories at the University of Sydney for analysis. The location of the Yeak Oam and Yeak Loam core sites is shown on figure 4.2.

4.2.4 Push tube and percussion coring

A long sediment core was extracted from Yeak Mai using push- and percussion-coring techniques in April 2013. As with the Yeak Oam and Yeak Loam cores, the sampling location was determined at the deepest portion of the lake and recorded using a Trimble Nomad GPS device. No replicate core was extracted from Yeak Mai due time limitations associated with percussion (vs. gravity) coring.

FIGURE 4.1: Gravity coring device.

A series of 60 mm ⌀(55 mm internal ⌀) PVC pipes (2.5 to 3 m long, each with one fluted end) were transported to the sample location on the above-described inflatable boat set-up. A piston attached to a cord was placed at the non-fluted end of the leading pipe (which was sharpened with a bevelling tool to form a make-shift cutting shoe). The piston cord was threaded through the core barrel, and the pipe was backfilled with lake water from the top to equalise the pressure within the core barrel and keep the piston at the bottom of the core pipe.

The core tube was lowered vertically (at the same rate as the piston cord) through the moon pool until 0.5 to 1 m of pipe was protruding from the water surface. The piston cord was then threaded through the next tube length (fluted end up), and the top of the first pipe was secured to the next length using three short screws (approx. 20 cm overlap between pipes). The second length was backfilled, and the pipes progressively lowered until the water/sediment interface was reached.

The piston cord was then secured to an aluminium A-frame constructed above the moon pool, and the pipes were manually pushed vertically into the sediment (connecting extra lengths as previously described) until refusal. The protruding pipe was then fitted with a percussion hammer and collar, and the pipes hammered into the sediment until refusal – figure 4.3.

The core was recovered using a hand-operated winch (attached to the A-frame), cut to 1.5m sections using a pipe cutter, and capped and taped for transportation to the geoscience laboratories at the University of Sydney for analysis. The location of the Yeak Mai core site is shown on figure 4.2.

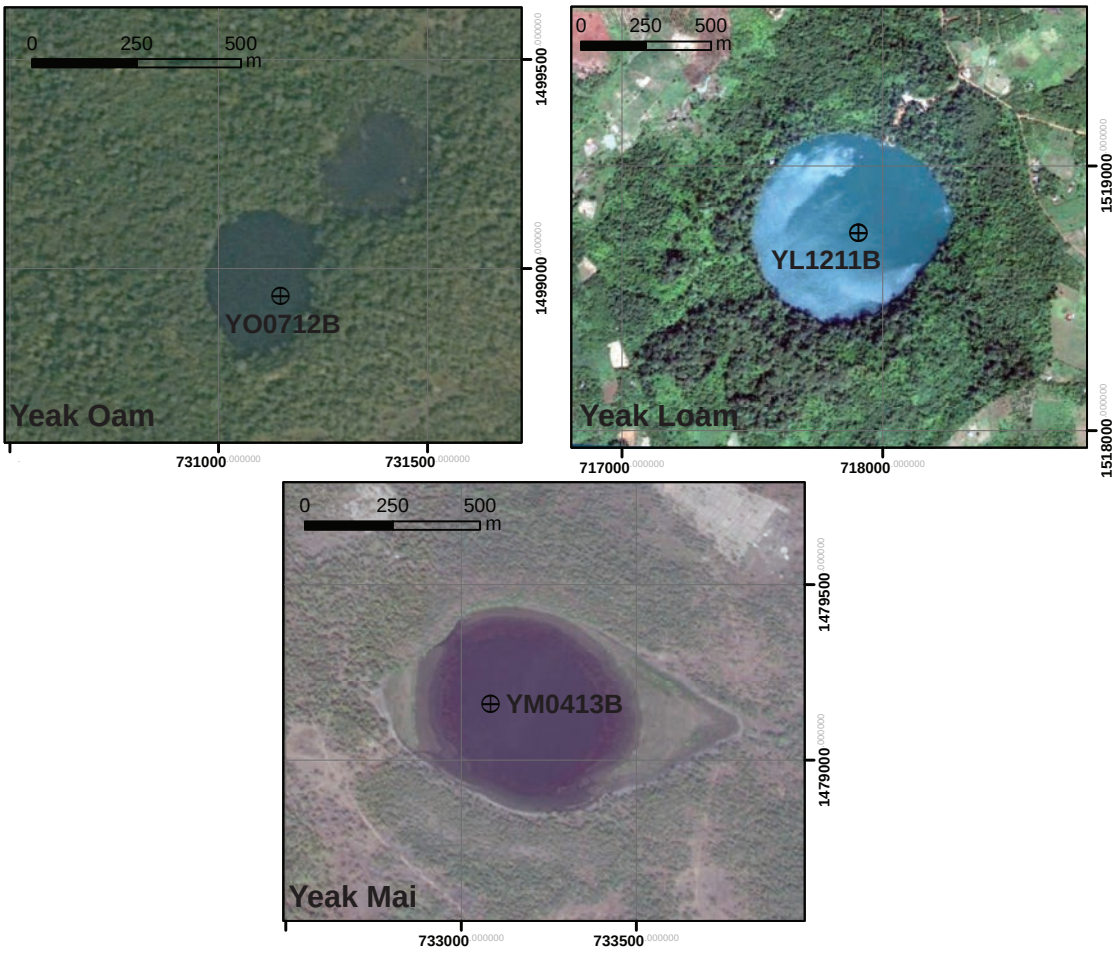

FIGURE 4.2: Approximate location of the lake core samples extracted from Yeak Oam (cores YO0712A & YO0712B), Yeak Loam (cores YL1211A & YL1211B), and Yeak Mai (YM0413B) (WGS84, UTM48N). Satellite images sourced from GoogleEarth (2015).

4.2.5 Core splitting and logging

The lake sediment cores were split at the University of Sydney. Each core section was clamped to a worker's bench and the encasing PVC pipe was cut lengthways down opposite sides of the core barrel using a circular saw. Cuts were made to a depth of approximately 2mm in order to clear the PVC pipe without significantly disturbing the core sediment. The core caps were cut in half with a hacksaw such that, upon completion, the pipe was severed into two half-cylinders, and the sediment was relatively intact. The cores were then carefully transported to a lab bench, and the sediments separated into two halves by progressively cutting the core with a paint scraper, ensuring that it was cleaned between cuts. Once in two splits, the core surface was gently scraped parallel to the assumed bedding plane to remove any sediment contamination that could have occurred during splitting, and provide a "clean" surface for photographing and logging. One split from each core was then sealed in cling film and core bags, and stored

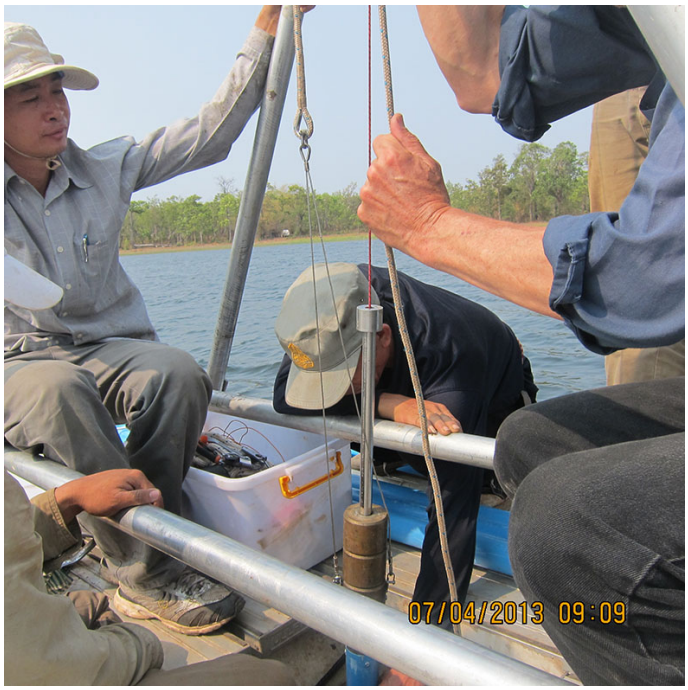

FIGURE 4.3: PVC core barrels being hammered into the sediment using percussion coring techniques.

in the laboratory refrigerator at 3 °C as an archive. The working split was then photographed. Yeak Oam and Yeak Loam master and replicate core samples were determined on the basis of their length, with the longer cores (presumed to be older at the base) favoured as master cores. These include YO0712B (replicate: YO0712C) and YL1211B (replicate: YL1211A).

Following splitting and photographing, the working splits from Yeak Mai and the Yeak Oam and Yeak Loam master and replicate cores were logged at a macro-scale in order to delimit units, cross-correlate cores (where relevant), and obtain a preliminary understanding of the sedimentary composition of each unit. All cores were logged within a week of splitting with the exception of YL1211A, which was logged 7 months after splitting. YL1211B and YM0413B — selected for palaeo-botanical analysis — were also logged at microscopic scale. This provides a non-destructive means of determining which layers to target for radiometric dating and microfossil analysis, and is important for back-validating any ecological changes observed in proxy records. Additionally, it provides a preview of environmental proxy types archived in the sediments.

Core logging methods and nomenclature follow Schnurrenberger et al. (2003). Major units, or beds, were first measured and delimited, and the texture, colour and macro-structures within each described. Colour was determined from comparison with Munsell colour charts (Munsell Colour 1994) and boundaries and thickness were assessed according parameters set out in Schnurrenberger et al. (2003). Texture was qualitatively estimated by rubbing a small sample from each bed between the fingers (though, due to the fine nature of the sediment, this was mostly determined through the microscopic component analysis described below). Macro-analysis logs were produced for YL1211A, YO0712B and YO0712C in Strater version 3.0

(Golden Software 2012) following the macro-bed description scheme outlined in Schnurrenberger et al. (2003).

Smear slide samples were taken from YM0413B and YL1211B every 10 to 30 cm, or at every new bed during the macro-logging process. Slides were constructed by taking a small (quarter thumb-nail-sized) sediment sample, thinly smearing it on a glass cover slip to dry before mounting it on a glass slide using a high refractive index mountant (Naphrax). These were examined at $\times$100 magnification and a percentage estimate of different sedimentary components made. Unusual clastic minerals were identified under an Olympus BH-2 polarizing light microscope at $\times$100 and $\times$200 magnification following MacKenzie and Adams (2007). Percentage estimates were used to describe and classify sediments using descriptors outlined in Schnurrenberger et al. (2003). All observations were compiled into a Strater log version 3.0 (Golden Software 2012) following the bed description scheme outlined in Schnurrenberger et al. (2003) (i.e. Colour, Bedding, Major Modifier, Principal Name, Minor Constituents).

4.2.6 Core chronology

Bulk sediment samples extracted from cores taken from the Yeak Loam (two samples) and Boeng Lumkut (one sample) have been previously dated by Maxwell (1999). Based on the preliminary dates obtained from this study, it is expected that the sedimentation rate across the lakes is relatively high (linear interpolation for both cores is roughly 1 mm/year). As such, it was expected that radiocarbon dating techniques were temporally appropriate for dating the Yeak Loam, Yeak Oam and Yeak Mai lake sediment cores.

Sample extraction and target material

The near absence of visible macro-organic materials (large twigs or leaves) observed in the sediment cores during logging and sampling meant that macro-charcoal (generally greater than 250 μm, but in some cases greater than 105 μm) was used as a source of datable carbon for this study. However, several small leaf/twig fragments were opportunistically selected for analysis where possible, and bulk (or undifferentiated) organic samples were used at depths where very little terrestrial carbon material could be recovered. Given the generally small mass of these samples, AMS radiocarbon dating techniques were considered the preferable method for determining the ^{14}C concentration of the samples. Sample depths were selected on the basis of: 1) the provenance of the sample materials (leaves and twigs representing a clear terrestrial signal were favoured); 2) the relative abundance of available dateable materials — particularly with regard to the charcoal samples (initially determined through analysis of smear slides, and later from the quantification of charcoal/pollen abundance during palaeo-fire analysis [see chapter 5]), and; 3) the proximity of the samples both to unit boundaries (favoured) and to other samples (avoided).

In total, 51 date samples were extracted from five cores representing three lake sites (Yeak Mai, Yeak Loam and Yeak Oam). Forty of these samples

were submitted for analysis to three different laboratories, and 38 dated using AMS ^{14}C dating techniques (details of sample types, depths and preparation techniques are listed on table 4.1). Three samples were analysed from each YO0712B, Y00712C and YL1211A (9 samples in total). Twenty-six samples were extracted from YL1211B (17 submitted for dating), and 15 from YM0413B (11 submitted for dating).

Prior to laboratory submission, the samples selected for dating were pretreated using a variety of physical and chemical techniques to isolate the target material (listed on table 4.1) in order to avoid contamination by local reservoir effects from ^{14}C in the water column that can be fixed and sequestered to the sediment by aquatic algae (Uchikawa et al. 2008). As these techniques did not always results in the successful extraction of a "clean" terrestrial source of carbon, several methods were applied for each sample type, some involving several iterations. These are outlined (grouped by methods) below. A flow chart showing the chronological ordering of these techniques as well as a summary of issues posed along the way is shown on figure 4.4.

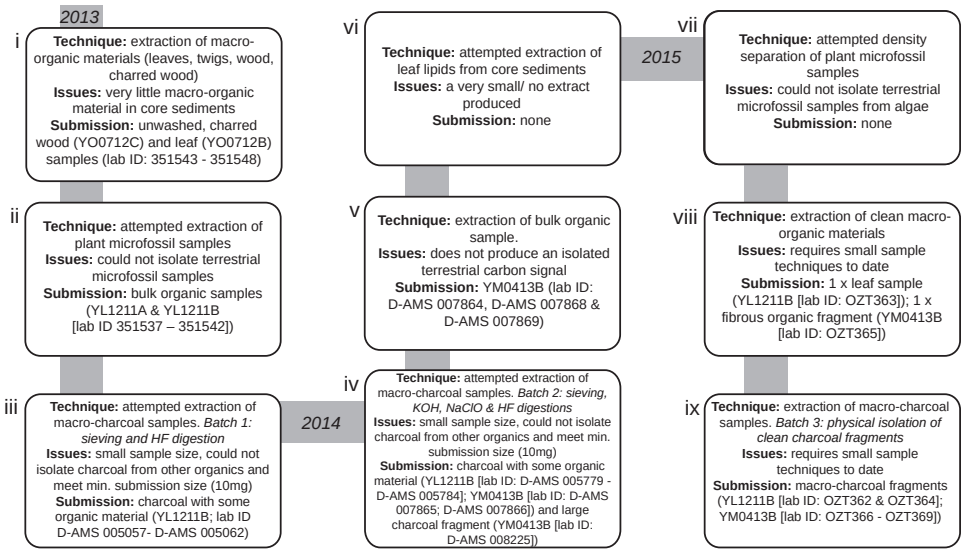

FIGURE 4.4: Progress flow diagram showing the techniques used in attempt to extract a terrestrial carbon signal from the lake core sediments.

TABLE 4.1: Depth, type and pretreatment details (pre-submission and laboratory) of samples selected for AMS radiocarbon dating from Yeak Loam, Yeak Oam and Yeak Mai sediment cores.

Core ID	Mid-sample depth (cm)	Sample thickness (cm)	Target sample material	Pre-submission treatment	Pre-submission treatment date	Actual sample material	Laboratory	Sample ID	Laboratory pre-treatment	Laboratory dating technique	Analysed for ^{14}C?
YL1211A	16.25	0.5	pollen conc.	>105 μm wet sieve; KOH (10%); NaClO (6%); HF (50%)	May-13	bulk organic	Beta	351537	acid washes	AMS radiocarbon dating	Yes
YL1211A	85.75	0.5	pollen conc.	>105 μm wet sieve; KOH (10%); NaClO (6%); HF (50%)	May-13	bulk organic	Beta	351538	acid washes	AMS radiocarbon dating	Yes
YL1211A	177.25	0.5	pollen conc.	>105 μm wet sieve; KOH (10%); NaClO (6%); HF (50%)	May-13	bulk organic	Beta	351539	acid washes	AMS radiocarbon dating	Yes
YL1211B	13	1	macro-charcoal	>105 μm wet sieve; KOH(10%); NaClO(6%); HF (50%)	Jan-14	>105 μm charcoal with some organic material	DirectAMS	D-AMS 005779	acid/ base/ acid	AMS radiocarbon dating	Yes
YL1211B	15.25	0.5	macro-charcoal	>250 μm wet sieve	Oct-13	>250 μm charcoal with some organic material	DirectAMS	D-AMS 005057	acid/ base/ acid	AMS radiocarbon dating	Yes
YL1211B	19.5	1	pollen conc.	>105 μm wet sieve; KOH (10%); NaClO (6%); HF (50%)	May-13	bulk organic	Beta	351540	acid washes	n/a	No
YL1211B	36	1	pollen conc.	HCL (10%); HF(50%); HNO_3(10%); KOH(10%); wet sieve (<105 μm); LST density separation	Feb-15	bulk organic	unsubmitted	n/a	n/a	n/a	No
YL1211B	36	1	macro charcoal	>250 μm wet sieve; freeze dry; pluck	Nov-15	>250 μm charcoal fragments - small sample	ANSTO	OZT362	acid/ base/ acid	small sample AMS radiocarbon dating	Yes
YL1211B	65.5	1	leaf lipid extract	freeze dry; DCM:MeOH (9:1); wash through silica column (hexane)	Dec-14	insignificant lipid (?) sample	unsubmitted	n/a	n/a	n/a	No
YL1211B	70.25	0.5	macro-charcoal	>250 μm wet sieve	Oct-13	>250 μm charcoal with some organic material	DirectAMS	D-AMS 005058	acid/ base/ acid	AMS radiocarbon dating	Yes

Continued...

Core ID	Mid-sample depth (cm)	Sample thickness (cm)	Target sample material	Pre-submission treatment	Pre-submission treatment date	Actual sample material	Laboratory	Sample ID	Laboratory pre-treatment	Laboratory dating technique	Analysed for ^{14}C?
YL1211B	71.5	1	macro-charcoal	>105 μm wet sieve; KOH(10%); NaClO(6%); HF (50%)	Jan-14	>105 μm charcoal with some organic material	DirectAMS	D-AMS 005780	acid/ base/ acid	AMS radiocarbon dating	Yes
YL1211B	80.75	0.5	macro-charcoal	>250 μm wet sieve	Oct-13	>250 μm charcoal with some organic material	DirectAMS	D-AMS 005059	acid/ base/ acid	AMS radiocarbon dating	Yes
YL1211B	84.5	1	macro-charcoal	>105 μm wet sieve; KOH (10%); NaClO (6%); HF (50%)	Jan-14	>105 μm charcoal with some organic material	DirectAMS	D-AMS 005781	acid/ base/ acid	AMS radiocarbon dating	Yes
YL1211B	87.75	0.5	pollen conc.	>105 μm wet sieve; KOH (10%); NaClO (6%); HF (50%)	May-13	bulk organic	Beta	351541	acid washes	AMS radiocarbon dating	Yes
YL1211B	101.5	1	pollen conc.	HCL (10%); HF(50%); HNO_3(10%); KOH(10%); wet sieve (<105 μm); LST density separation	Feb-15	bulk organic	unsubmitted	n/a	n/a	n/a	No
YL1211B	123.5	1	leaf lipid extract	freeze dry; DCM:MeOH (9:1); wash through silica column (hexane)	Dec-14	insignificant lipid (?) sample	unsubmitted	n/a	n/a	n/a	No
YL1211B	125.25	0.5	macro-charcoal	>250 μm wet sieve	Oct-13	>250 μm charcoal with some organic material	DirectAMS	D-AMS 005060	acid/ base/ acid	AMS radiocarbon dating	Yes
YL1211B	126.5	1	macro-charcoal	>105 μm wet sieve; KOH (10%); NaClO (6%); HF (50%)	Jan-14	>105 μm charcoal with some organic material	DirectAMS	D-AMS 005782	acid/ base/ acid	AMS radiocarbon dating	Yes
YL1211B	145	1	leaf fragments	>250 μm wet sieve; freeze dry; pluck	Nov-15	leaf fragments	ANSTO	OZT363	acid washes	small sample AMS radiocarbon dating	Yes
YL1211B	146.5	1	pollen conc.	HCL (10%); HF(50%); HNO_3(10%); KOH(10%); wet sieve (<105 μm); LST density separation	Feb-15	bulk organic	unsubmitted	n/a	n/a	n/a	No
YL1211B	174.75	0.5	macro-charcoal	>105 μm wet sieve; KOH (10%); NaClO (6%); HF (50%)	Jan-14	>105 μm charcoal with large leaf fragment some organic material.	DirectAMS	D-AMS 005783	acid/ base/ acid	AMS radiocarbon dating	Yes

Continued...

Core ID	Mid-sample depth (cm)	Sample thickness (cm)	Target sample material	Pre-submission treatment	Pre-submission treatment date	Actual sample material	Laboratory	Sample ID	Laboratory pre-treatment	Laboratory dating technique	Analysed for ^{14}C?
YL1211B	175.25	0.5	macro-charcoal	>250 μm wet sieve	Oct-13	>250 μm charcoal with some organic material	DirectAMS	D-AMS 005061	acid/ base/ acid	AMS radiocarbon dating	Yes
YL1211B	188.5	1	pollen conc.	HCL (10%); HF(50%); HNO_3(10%); KOH(10%); wet sieve (<105 μm); LST density separation	Feb-15	bulk organic	unsubmitted	n/a	n/a	n/a	No
YL1211B	200.5	1	leaf lipid extract	freeze dry; DCM:MeOH (9:1); wash through silica column (hexane)	Dec-14	insignificant lipid (?) sample	unsubmitted	n/a	n/a	n/a	No
YL1211B	203	1	pollen conc.	HCL (10%); HF(50%); HNO_3(10%); KOH(10%); wet sieve (<105 μm); LST density separation	Feb-15	bulk organic	unsubmitted	n/a	n/a	n/a	No
YL1211B	203	1	macro charcoal	>250 μm wet sieve; freeze dry; pluck	Nov-15	>250 μm charcoal fragments - small sample	ANSTO	OZT364	acid/ base/ acid	small sample AMS radiocarbon dating	Yes
YL1211B	206.5	1	macro-charcoal	>105 μm wet sieve; KOH (10%); NaClO (6%); HF (50%)	Jan-14	>105 μm charcoal with some organic material	DirectAMS	D-AMS 005784	acid/ base/ acid	AMS radiocarbon dating	Yes
YL1211B	208.75	0.5	macro-charcoal	>250 μm wet sieve	Oct-13	>250 μm charcoal with some organic material	DirectAMS	D-AMS 005062	acid/ base/ acid	AMS radiocarbon dating	Yes
YL1211B	209.75	0.5	pollen conc.	>105 μm wet sieve; KOH (10%); NaClO (6%); HF (50%)	May-13	bulk organic	Beta	351542	acid washes	AMS radiocarbon dating	Yes
YM0413B	46.5	1	fibrous organic fragment	>250 μm wet sieve; freeze dry; pluck	Nov-15	fibrous organic fragment	ANSTO	OZT365	acid washes	small sample AMS radiocarbon dating	Yes
YM0413B	100.5	1	pollen conc.	HCL (10%); HF(50%); HNO_3(10%); KOH(10%); wet sieve (<105 μm); LST density separation	Feb-15	bulk organic	unsubmitted	n/a	n/a	n/a	No

Continued...

Core ID	Mid-sample depth (cm)	Sample thickness (cm)	Target sample material	Pre-submission treatment	Pre-submission treatment date	Actual sample material	Laboratory	Sample ID	Laboratory pre-treatment	Laboratory dating technique	Analysed for ^{14}C?
YM0413B	141	1	macro-charcoal	>250 μm wet sieve; freeze dry; pluck	Nov-15	>250 μm charcoal fragments - small sample	ANSTO	OZT366	acid/ base/ acid	small sample AMS radiocarbon dating	Yes
YM0413B	206.5	1	bulk sediment	nil	Mar-14	bulk sediment	DirectAMS	D-AMS 007868	acid/ base/ acid	AMS radiocarbon dating	Yes
YM0413B	207.25	0.5	macro-charcoal	>250 μm wet sieve; KOH (10%); NaClO (6%); HF (50%)	Mar-14	>250 μm charcoal and organic material (small rootlets, wood fragments and unidentified organic material).	DirectAMS	D-AMS 007865	acid/ base/ acid	AMS radiocarbon dating	Yes
YM0413B	299.5	1	macro-charcoal	>250 μm wet sieve; KOH (10%); NaClO (6%); HF (50%)	Mar-14	>250 μm charcoal and organic material (small rootlets, wood fragments and unidentified organic material).	DirectAMS	D-AMS 007866	acid/ base/ acid	AMS radiocarbon dating	Yes
YM0413B	300.5	1	bulk sediment	nil	Mar-14	bulk sediment	DirectAMS	D-AMS 007869	acid/ base/ acid	AMS radiocarbon dating	Yes
YM0413B	376	1	macro-charcoal	>250 μm wet sieve; freeze dry; pluck	Nov-15	>250 μm charcoal fragments - small sample	ANSTO	OZT367	acid/ base/ acid	small sample AMS radiocarbon dating	Yes
YM0413B	447	1	macro-charcoal	>250 μm wet sieve; freeze dry; pluck	Nov-15	>250 μm charcoal fragments - small sample	ANSTO	OZT368	acid/ base/ acid	small sample AMS radiocarbon dating	Yes
YM0413B	521.5	1	pollen conc.	HCL (10%); HF(50%); HNO_3(10%); KOH(10%); wet sieve (<105 μm); LST density separation	Feb-15	bulk organic	unsubmitted	n/a	n/a	n/a	No
YM0413B	522.5	1	macro-charcoal	>250 μm wet sieve; freeze dry; pluck	Nov-15	>250 μm charcoal fragments - small sample	ANSTO	OZT369	acid/ base/ acid	small sample AMS radiocarbon dating	Yes
YM0413B	534.25	0.5	macro-charcoal	rinse	Sep-14	charcoal (1cm^2 fragment)	DirectAMS	D-AMS 008225	acid/ base/ acid		Yes

Continued...

Core ID	Mid-sample depth (cm)	Sample thickness (cm)	Target sample material	Pre-submission treatment	Pre-submission treatment date	Actual sample material	Laboratory	Sample ID	Laboratory pre-treatment	Laboratory dating technique	Analysed for ^{14}C?
YM0413B	536	1	lipid extract sample	freeze dry; DCM:MeOH (9:1); wash through silica column (hexane)	Dec-14	insignificant lipid (?) sample	unsubmitted	n/a	n/a	n/a	No
YM0413B	538.5	1	bulk sediment	nil	Mar-14	bulk sediment	DirectAMS	D-AMS 007864	acid/ base/ acid	AMS radiocarbon dating	Yes
YM0413B	539.5	1	macro-charcoal	>250 μm wet sieve; KOH(10%); NaClO(6%); HF (50%)	Mar-14	>250 μm charcoal and organic material (small rootlets, wood fragments and unidentified organic material).	DirectAMS	not assigned	acid/ base/ acid	n/a	No
YO0712B	16.75	1.5	leaf fragments	freeze dry; pluck	Jun-13	plant material with some algal material	Beta	351543	acid washes		Yes
YO0712B	62.25	0.5	leaf fragments	freeze dry; pluck	Jun-13	plant material with some algal material	Beta	351544	acid washes		Yes
YO0712B	172.75	1.5	leaf fragments	freeze dry; pluck	Jun-13	plant material with some algal material	Beta	351545	acid washes		Yes
YO0712C	20.5	1	wood & charred wood/charcoal	freeze dry; pluck	Jun-13	wood & charred wood/charcoal with trace of algae throughout	Beta	351546	acid washes		Yes
YO0712C	56.5	1	wood & charred wood/charcoal	freeze dry; pluck	Jun-13	wood & charred wood/charcoal with trace of algae throughout	Beta	351547	acid washes		Yes
YO0712C	100.5	1	wood & charred wood/charcoal	freeze dry; pluck	Jun-13	wood & charred wood/charcoal with trace of algae throughout	Beta	351548	acid washes		Yes

Pre-submission sample treatment

Macro-organic material — leaf, wood and charred wood fragments

Three points in each of the Yeak Oam sediment records (notionally from the top, middle and base of each core) were targeted for extraction of small remains of macro-organic material (i.e. leaf, wood and charred wood fragments) (n=6) (table 4.1). Three, contiguous 5 mm sediment samples (sub-samples) were taken from these targeted depths (n=18). Each sub-sample was placed into a clean plastic sample jar and frozen overnight. Following freezing, the jar lids were removed, and the samples immediately freeze-dried using a Labconco Freezone 6 at approximately -50 °C until all moisture was removed (approximately 6 hours). The dried samples were placed on clean petri dishes and analysed at 5× to 15× magnification using an Olympus SZ40 microscope. Sterilised tweezers were used to isolate macro-organic samples of probable terrestrial origin. Sample isolates were placed into individual 1.5 ml micro-vials. Contiguous samples were combined as necessary to increase sample yield (>20 mg), aiming for a maximum sample thickness of 1.5 cm. Three charred wood samples were extracted from YO0712C (20 to 21 cm [lab ID: 351546]; 55 to 56 cm [lab ID: 351547]; 100 to 101 cm [lab ID: 351548]) and three leaf fragment samples from YO0712B (16 to 17.5 cm [lab ID: 351543]; 62 to 62.5 cm [lab ID: 351544] and 172 to 173.5 cm [lab ID: 351545]). These were submitted to Beta Analytic for AMS radiocarbon dating in 2013 where they were subject to standard laboratory acid-washes in HCL prior to analysis (Beta Analytic 2016).

Leaf fragments in YL1211B at 144.5 to 145.5 cm and a fibrous plant stem sample in YM0413B at 49 to 50 cm were later extracted from their respective core sediment subsamples by wet sieving (>250 μm mesh). Each large fraction was then placed into sample jars with distilled water, and clean tweezers used to isolate the target material from the remaining sample under an Olympus SZ40 microscope at 5× to 15× magnification. Because of previous issues presumed to be associated with groundwater carbon contamination of the date samples, particular care was taken to make sure that the isolated macro-organic samples were as pure as possible. The result of this process meant that the final samples were small (<5 mg). As such, samples were submitted to ANSTO laboratories for small sample technique AMS radiocarbon analysis (YL1211B 144.5 to 145.5 cm [lab ID: OZT363]; YM0413B 46 to 47 cm [lab ID: OZT365]) in 2015. As with the Yeak Oam samples, these macro organic samples were subject to standard laboratory acid-washes in weak HCL prior to analysis.

Plant microfossil concentrates

Three points in each of Yeak Loam sediment records (notionally from the top, middle and base of each core) were initially targeted for extraction of a terrestrial pollen and spore concentrate (n=6) (table 4.1). Three, contiguous 5 mm sediment samples were taken from the targeted depths (n=18) and placed into clean 15 ml centrifuge tubes. Extraction of plant microfossils followed standard methods for physical separation via wet sieving and

removal of unsaturated of humic colloids and silicates through chemical digestions in KOH (10%) and HF (50%) (Faegri and Iversen 1989). These steps are detailed in appendix F]. Standard acetolysis techniques were replaced by room temperature digestion in weak NaClO (1.5%) for approximately 2 minutes.

Due to the small size of pollen produced by many tropical plants, it was not possible to separate specific pollen types by sieving (Brown et al. 1992), and the abundance of chemically inert algae of similar size to the pollen and spore assemblage meant that a 'pure' pollen sample could not be achieved. As a result, the samples were submitted as bulk or 'mixed' organic samples to Beta Analytic for AMS ^{14}C dating. YL1211A samples were extracted from 16 to 16.5 cm (lab ID: 351537), 85.5 to 86 cm (lab ID: 351538) and 177 to 178 cm (lab ID: 351539), and YL1211B samples from 19 to 20 cm (lab ID: 351540), 87.5 to 88 cm (lab ID: 351541), and 209.5 to 210 cm (lab ID: 351542). These samples were subject to standard laboratory acid-washes in HCL prior to analysis (Beta Analytic 2016).

In attempt to extract a "purer" plant microfossil sample for radiocarbon dating, density separation techniques outlined in Vandergoes and Prior (2003) were later applied to two YM0413B samples (100 to 101 cm and 521 to 522 cm) and five YL1211B samples (35.5 to 36.5 cm, 101 to 102 cm, 146 to 147 cm, 188 to 189 cm and 202.5 to 203.5 cm). Sample selection depths from YL1211B were based on the results of sedimentological and microfossil analysis that are presented later on in this chapter and in chapter 5. Specifically, sampling was focussed on points where the estimated absolute abundance of pollen grains and spores (per dry cubic cm) were high, and estimations of total organic matter (thought to mostly represent algae content), comparably low. Selection of samples from YM0413B (not yet processed for sedimentological and microfossil analysis at the time of extraction) was based on core position, with sediments at the top and base of the core favoured for analysis. Samples were placed into 50 ml centrifuge tubes and processed for density separation following methods outlined in appendix C. Following separation, each fraction was examined under a Zeiss microscope at $\times$100 magnification, and the relative percentages of the remaining sample constituents visually estimated. Due to the high proportion of algae still retained in the samples (see appendix C), none were submitted for radiocarbon dating.

Macro-charcoal

A total of 14 macro-charcoal extractions were attempted for YL1211B, and eight for YM0413B. Charcoal isolation techniques were performed in three iterations, which each iteration aiming to improve the total proportion of charcoal whilst still maintaining a sufficient sample size for dating. The need to alter extraction techniques between sample batches became apparent from the results of previous radiocarbon analyses, which indicated contamination of the charcoal with non-terrestrial sources of carbon. This was particularly apparent from the results returned from the Yeak Loam samples. The chronological timeframe for these batch extractions in the context

of the other attempted date sample extraction techniques is shown on figure 4.4.

Macro-charcoal extraction batch 1 (2013)

The first batch of macro-charcoal extractions was attempted on six sediment samples taken from YL1211B. The samples were wet-sieved through a 250 μm mesh. The >250 μm fraction was retained and placed into individual 50 ml centrifuge tubes. Once excess water was removed via centrifuging, the clastic component of the samples was digested by adding 4 to 5 ml of 50% HF to each tube that were then placed into a hot water bath at 60 °C for 40 minutes. Following silicate digestion, the samples were rinsed three times with DI water, and the remaining samples were transferred into microvials using a clean glass pipette. Details of the charcoal isolation methods employed for round one samples are outlined in appendix C.

The extracted samples were assessed under an Olympus SZ40 microscope at 10× to 20× magnification. They typically comprised a combination of charcoal (approximately 40 to 55%) and other organic materials such as micro-rootlets and algae. As physical isolation of charcoal fragments by plucking could not be performed without the sample volumes dropping well below the minimum 10 mg requirement of the selected laboratory (DirectAMS), the whole organic samples were submitted for radiocarbon analysis. These include D-AMS 005057 (15.0 to 15.5 cm), D-AMS 005058 (70 to 70.5 cm), D-AMS 005059 (80.5 to 81 cm), D-AMS 005060 (125 to 125.5 cm), D-AMS 005061 (175 to 175.5 cm), D-AMS 005062 (208.5 to 209 cm) (listed on table 4.1).

Macro-charcoal extraction batch 2 (2014)

The second round of charcoal isolation for radiocarbon dating was performed on a further six samples from YL1211B, and three from YM0413B. While similar to techniques applied in round one, additional chemical digestions were performed in attempt to reduce the overall proportion of non-charcoal organic material and humic colloids in the samples. These included digestion in 10% KOH and in 6% NaClO. Additionally, two macro fractions were retained during the sieving phase (>250 μm and 105 to 250 μm) so as to combine these in instances when the final sample weight was too low for submission. Details of the charcoal isolation methods employed for batch two charcoal samples are outlined in appendix C.

As with the batch one samples, the remaining sample materials were assessed under an Olympus SZ40 microscope at 5× to 15× magnification. While charcoal concentrations were slightly higher in the second batch (approx. 50 to 60%), there was still an appreciable amount of organic material present in the final sample extracts. Both size fractions from all YL1211B samples had to be combined to provide sufficient sample mass for AMS radiocarbon analysis. The batch two samples were submitted to Direct AMS laboratories, and include: D-AMS 005779 (12.5 to 13.5 cm), D-AMS 005780

(71 to 72 cm), D-AMS 005781 (84 to 85 cm) D-AMS 005782 (126 to 127 cm), D-AMS 005783 (174.5 to 175 cm), and D-AMS 005784 (206 to 207 cm).

The >250 μm fraction from YM0413B samples, (extracted from charcoal-rich layers in the core sediments observed during smear slide analysis of the core sediment) were also submitted to Direct AMS laboratories for radiocarbon analysis. These include D-AMS 007865 (207 to 207.5 cm), D-AMS 007866 (299 to 300 cm) and a sample submitted from 539 to 540 cm that was not assigned a laboratory number due its insufficient mass. This sample was replaced by a platy, 1cm^2 charcoal fragment found in core sediments at 534 to 534.4 cm that was plucked from the core sediments with clean tweezers and rinsed in DI water prior to submission (D-AMS 008225).

Macro-charcoal extraction batch 3 (2015)

The third round of charcoal isolation for radiocarbon dating was performed on two samples extracted from YL1211B and five from YM0413B. These samples were analysed at ANSTO laboratories. This facility has the capacity to analyse radiocarbon samples yielding quantities of carbon $\leq$200 μg (post processing) (Fink et al. 2004). As such, the isolation process was focused on producing as pure a charcoal sample as possible, regardless of size.

The >250 μm fraction of the selected sediment samples (chosen on the basis of down-core distribution and the presence of relatively high charcoal yields as determined from palaeo-fire analysis see chapter 5) was first isolated by wet sieving. The large fraction was then placed into a sample jar with DI water in attempt to wash away as much algae embedded in the charcoal fragments as possible. Charcoal fragments were then carefully plucked from these sample jars under an Olympus SZ40 microscope at 20$\times$ to 25$\times$ magnification with tweezers, and placed into clean sample jars. These were then submitted to ANSTO for AMS radiocarbon analysis. The YL1211B samples include OZT362 (35.5 to 36.5 cm) and OZT364 (202.5 to 203.5 cm) while the YM0413B samples comprise OZT366 (140.5 to 141.5 cm), OZT367 (375.5 to 376.5 cm), OZT368 (446.5 to 447.5 cm), and OZT369 (522 to 523 cm).

All batch one to three charcoal and charcoal and organic material samples were pre-treated at their respective laboratories with standard acid-base-acid washes in hot HCl, NaOH then HCl.

Bulk organics

Three bulk sediment samples were submitted from YM0413B at depths adjacent to charcoal & organic material samples D-AMS 007866, D-AMS 007869 and the insufficiently sized sample at 539 to 540 cm in order to provide comparison samples to assess the potential for hard water contamination within Yeak Mai sediments. These samples were submitted to Direct-AMS laboratories for AMS radiocarbon dating, and include D-AMS 007868 (206 to 207 cm), D-AMS 007869 (300 to 301 cm) and D-AMS 007864 (538 to

539 cm). The samples were subject to a standard acid-base-acid laboratory pre-treatment.

Leaf lipids

AMS radiocarbon dating of leaf lipids (plant *n*-alkanes) can eliminate problems of lake hard water contamination characteristic of bulk organic sediment samples by targeting organic material with an unequivocal terrestrial source (Uchikawa et al. 2008). Three sediment samples were selected from YL1211B (65 to 66 cm, 123 to 124 cm and 200 to 201 cm), and one towards the base of YM0413B (539 to 540 cm) for a preliminary assessment of plant lipid quantities preserved within the lake sediments.

The samples were frozen overnight and subsequently freeze dried until all moisture was removed from the sediments. Extraction of plant lipids was then attempted using sonication, the procedure of which is detailed in appendix C.

Chronological age-depth modelling

The radiocarbon ages returned from each core were calibrated in the program Calib 7.1 using the Southern Hemisphere calibration curve (Reimer et al. 2013) offset by -21 $\pm$ 6 yrs, following approaches undertaken by Hendrickson et al. (2013) and Pryce et al. (2014). A Bayesian statistics-based age-depth model was developed for YO0712B, YL1211B, and YM0413B (using the same calibration curve and offset) in the program Bacon 2.2 (Blaauw and Christen 2011) in R (R Core Team 2013).

The YM0413B dates were modelled using the following parameters: d.max (maximum depth) = 544; hiatus.depths = c(218, 289); hiatus.mean (length of hiatuses [years]) = c(2, 2); acc.mean (sediment accumulation rate in years/cm) = c (10,3,10). Very short duration hiatuses (2 years) were modelled at the boundaries of logged sedimentary unit III[1] (i.e. at 218 cm and 289 cm) in order to set different priors for the accumulation rate of the unit III (3 years/cm) as opposed to units IV, V and I (10 years/cm) (Maarten Blaauw, pers. comm. via email 16th March, 2016). Accumulation rates were estimated from linear interpolation between adjacent date samples. An assumed age of -63 cal. yrs BP (2013 AD) was set for the core top in order to derive an age-depth series for the shallowest core sediments (0 to 46 cm depth).

The three YL1211B date samples selected for age-depth modelling[2] were modelled in Bacon using the default parameters, with the exception of the accumulation rate (acc.mean), which was changed to 2 years/cm based on linear interpolation between adjacent date samples. An age depth model was only produced for core sediments extending between the lowest and highest date samples (36 to 204 cm) (see section 4.3.2 for rationale).

The YO0712B samples were also modelled using the default Bacon parameters other than the accumulation rate (acc.mean), which was changed to

[1] Details of the Yeak Mai stratigraphical units are described in the results (section 4.3.1)
[2] The selection process is discussed in the results section 4.3.2

5 years/cm based on linear interpolation between the between adjacent date samples. An assumed age of -62 cal. yrs BP) (2012 AD) was also modelled for the core top in order to extrapolate ages for the lower portion of the core (0 to 16 cm depth).

No age-depth model was produced for YL1211A and YO0712C due the apparent contamination of all of the date samples from these cores with a non-terrestrial source of carbon. This is described in the results section 4.3.

4.2.7 Core sedimentology

Environmental magnetism

Measuring changes in the magnetic susceptibility of lake cores with depth provides a means of assessing variability in the concentration of magnetic minerals within the sediments (Dearing 1999a). This can provide insight into changing rates of detrital input to the lake (e.g. Dearing 2008, Bhagwat et al. 2012) and/or delimit periods of endogenic precipitation of concentrated magnetic minerals (e.g. iron oxides) during oxic phases of lake redox cycling (e.g. Williamson et al. 1998, Tamuntuan et al. 2015). This technique, when combined with other proxies of environmental change, is therefore considered to be of value to this study as a potential climatic and/or land use indicator, particularly if it can be related to periods of lake shallowing/deepening and/or heightened erosion related to catchment run off.

Additionally, scanning of the master and replicate lake cores extracted from Yeak Loam and Yeak Oam allows for the correlation of the core profiles over space (Oldfield et al. 1983, Nowaczyk, 2001). This provides a means of assessing stratigraphic continuity between the adjacent cores, allowing for assessment of whether the master core captures representative, undisturbed lake bottom sediments.

Volumetric magnetic susceptibility

Volumetric magnetic susceptibility (κ) in SI units was measured for the master and replicate gravity cores from Yeak Loam and Yeak Oam, and for YM0413B (Yeak Mai). Both the Yeak Oam and Yeak Loam cores were processed using a Bartington MS3 magnetic susceptibility meter fitted with a MS2E sensor. Core surfaces were covered with a single layer of cling film to prevent contamination of the sensor between measurements, and measurements were taken at 5 mm intervals. Three replicate measurements were taken at each sample point to provide a mean measurement and standard deviation for each depth. Drift in ambient magnetism was determined with blank readings before and after each measurement set, and was automatically corrected using Bartsoft software. Measurements that included cracks or gaps in the core were excluded from analyses. Due to large discrepancies in the κSI measurements observed between the master and replicate Yeak Oam cores, a series of repeat measurements were taken from both of these cores at a lower sampling resolution.

Volumetric magnetic susceptibility was conducted on YM0413B at a 5 mm resolution using a Bartington MS2E sensor mounted in a Cox Analytical Systems I-TRAX XRF core scanner (details of this device are outlined in section 4.2.8). In this case, single measurements were made and no measure of precision can be made. Measurements made over core gaps or cracks (identified as peaks in mean standard error) were excluded from analysis (Löwemark et al. 2011).

Dual frequency mass specific magnetic susceptibility

Mass-specific low frequency magnetic susceptibility (χlf) shows the total concentration of ferromagnetic minerals in sediment samples corrected for mass (as opposed to κSI), while frequency-dependent susceptibility (χfd$_{\%}$) can indicate the presence and proportion of superparamagnetic minerals in core sediments (diameter <0.03 μm) (Dearing 1999a). These techniques can be useful interpreting changes in lake sediment source (Dearing et al. 1996, Dearing 1999a), and were applied to YL1211B core sediments.

Lake core sediments were subsampled as contiguous, 1 cm thick units from the archived half core splits in order to maximise sediment mass. The subsamples were placed into labelled aluminium trays, and dried at 105 °C overnight. After drying, samples were disaggregated using a mortar and pestle, and placed into pre-weighed, labelled 10 cm^3 cylindrical plastic pots designed for the Bartington MS2B Dual Frequency Magnetic Susceptibility Meter (Dearing 1999a). The sediments were very lightly compacted to remove any air gaps, and the sediment mass and, where the sample did not completely fill the pot, the volume recorded. In some cases, sample numbers were reduced by amalgamating a maximum of three adjacent samples, in attempt to obtain a minimum recommended volume of >5.7 cm^3 (Dearing 1999a) whilst maintaining a high-resolution sampling procedure. Even after amalgamation of adjacent samples, the total volume of the final sample often fell below the test volume recommendations. As such, a series of experiments were conducted on two dried and crushed lake sediment samples from Yeak Loam and Yeak Oam to assess how different sediment volumes impact χlf and χfd$_{\%}$ values from the same sample. Details of the methods and results of this test are described in appendix D.

A Bartington MS2B Dual Frequency Magnetic Susceptibility Meter was used to determine the χlf (0.46 kHz magnetic field) and χhf (mass specific high frequency magnetic susceptibility [4.6 kHz magnetic field]) of the potted samples. From these calculations, the percentage frequency dependence (χfd$_{\%}$) was auto-calculated using Barsoft software by dividing the change in susceptibility per decade frequency by the χlf measurement for the sample. Samples were run in triplicates for both frequencies, with five second sample measurements and blank (air) measurements taken at the start, end, and between χlf and χhf measurements. Blank sample measurements were made using an empty plastic cylindrical pot. The mean and standard deviation of measurements was calculated for sample replicates. A detailed outline of measurement protocols is provided in Dearing (1999a).

Analysis

Correlation of Yeak Oam and Yeak Loam master and replicate cores was attempted using combined path length sequence slotting in the Windows program CPL slot (geography.lancs.ac.uk/cemp/resources/software/cplslot). This technique can be useful for identifying matching parts of a core sedimentary sequence (Thompson et al. 2012). These methods are detailed in appendix D.

The repeat, low-resolution κSI records taken from the Yeak Oam cores were correlated (Pearson's *r*) with the original measurements in the program R (R Core Team 2013) to assess the variation in overall trend between the two data-sets, exclusive of shifts in overall κSI magnitude.

The χlf, χfd$_{\%}$ and κSI measurements taken from YL1211B were correlated (Pearson's *r*) in the program R (R Core Team 2013) in order to determine the relationship (if any) between these variables.

Moisture content, dry bulk density, loss-on-ignition and bulk mineral influx

Assessment of moisture content, dry bulk density and total-organic carbon (in concert with sediment accumulation rate determined from the age-depth modelling of core sediments) is necessary for estimation of bulk mineral influx. This variable is useful with the context of this study for determining changes in non-organic allochthonous or autochthonous sediment input to the Yeak Mai and Yeak Loam lake sites (e.g. detrital input from erosion events or precipitation of redox sensitive elements). This is necessary to account for dilution effects with respect to influx of pollen, spores and charcoal to the lake sediments.

Changes in the percentage of total organic content of core sediments (estimated from loss-on-ignition techniques), can, when considered in the context of mineral influx, be useful for interpreting changes in lake productivity, allochthonous organic inputs to the system and/or organic decomposition rates that, in turn, may relate to changing climate or catchment land use (Shuman 2003). The measurement core sediment water content and organic content is necessary for assessing the validity of using Molybdenum incoherent to coherent scattering ratios to normalise the XRF I-TRAX geochemical records obtained from Yeak Mai (YM0413B) and Yeak Loam (YL1211B) sediments. This is discussed in further detail in section 4.2.8 below.

Moisture content and dry bulk density

Core sediments were subsampled from the working splits as contiguous, 1 cm thick units, and placed into pre-weighed, labelled, aluminium trays. In some cases, particularly for YM0413B, sample numbers were reduced by amalgamating adjacent samples (where possible, units were not mixed based on the assumption that organic content and bulk density may vary between stratigraphic layers). Wet sample weight was recorded and the

samples then oven dried at 105 °C overnight (minimum 8 hours) (Håkanson and Jansson 1983). After drying, samples were reweighed and the percent moisture loss was calculated using the equation 4.1.

$$W = \frac{W_{\mathrm{W}}}{W_{\mathrm{S}}} \times 100 \tag{4.1}$$

Where: W=water content (%); W_{W}=water weight (g); W_{S}=dry sediment weight

The dry samples were then disaggregated using a mortar and pestle, and placed into pre-weighed, labelled 10 cm^3 sample pots. The sediments were very lightly compacted to remove any air gaps, and the sediment mass and volume recorded. From this, the dry bulk density of the sediment samples was calculated using the equation 4.2.

$$\rho_{\mathrm{dry}} = \frac{W_{\mathrm{S}}}{V} \times 1000 \tag{4.2}$$

Where: ρ_{dry}=dry bulk density (kg/m^3); W_{S}=dry sediment weight; V=volume (cm^3)

A series of 21 replicate moisture content samples were taken from YL1211B (working half) in September 2015 as core sediments had obviously dried out since the original sampling date (October 2013). The drier sediments were sampled at, or adjacent to, depths sampled for the second round of charcoal analysis for this core (where quantification of dry volume is required to estimate charcoal concentrations, hence necessitating recalculation of water content — see chapter 5 for details).

Total organic content

Dried and disaggregated sediment samples (recycled from dry bulk density testing) were carefully transferred into labelled, pre-weighed crucibles. The pre-ignition weight of each sample was then recorded. Organic carbon was then removed from the samples by combustion at 550 °C for 4 hours (Heiri et al. 2001). After cooling, post-ignition weight was recorded and compared with the pre-ignition weight to calculate the percentage of total organic carbon lost from each sample. Note that due to the lack of organic carbonates observed in the core sediments during smear slide analysis, igniting the samples at 950 °C to remove inorganic carbonates ($CaCO_3$) was determined unnecessary[3].

Bulk mineral influx

The mass component of core mineral sediment (kg/m^3) was estimated from percent mineral mass values (i.e. the non-organic proportion of the loss-on-ignition samples), and from the bulk density values calculated for the

[3]Subsequent to processing YM0413B for TOC analysis, rare ostracods were noted during the analysis of macro-charcoal samples from upper core sediments (190 to 120 cm depth).

core sediments. These values were used alongside the age-depth models produced for each core to approximate mineral influx ($kg/m^2/yr^{-1}$).

Grain size analysis

Core sediment samples were analysed for inter- and intra- variations in mineral grain size distribution to aid interpretation of sediment source, transportation mechanisms, and past climatic, environmental and limnological conditions. With respect to the crater lake field sites, this technique may be particularly valuable for assessing fluxes in catchment sediment supply, and hence changes in monsoon strength and/or local land use (e.g. Peng et al. 2005).

Between 0.5 and 1 g (field condition) of core sediment was placed into a 50 ml centrifuge tube, and 5 ml of 35% H_2O_2 added to each tube to oxidise the organic material present in each sample. The samples were placed into a hot water bath at 65 °C to 80 °C for 10 hours (temperature was dependent on intensity of sample reaction). This process was repeated until no ebullition was observed when 1 ml of 35% H_2O_2 was introduced to a heated sample. The samples were then washed three times with deionised water. Subsequent to rinsing, the samples were deflocculated and disaggregated into individual particles by adding 30 to 35 ml $(NaPO_3)_6$ dispersant to each tube, which were then capped and placed on a rotating mixer for 4 hours. Laser diffraction spectrometry was employed to assess the grain size distribution of each sample using a Malvern Mastersizer 2000 equipped with a Hydro G dispersion unit. Three replicate measurements were taken for each sample, with each sample sonicated for 20 seconds prior to analysis to break down any remaining aggregates. The mean and standard deviation of these replicate measurements were used as the basis for subsequent analysis.

Analysis

Grainsize data were decomposed using GRADISTAT 8.0 (Blott and Pye 2001), using the Folk and Ward (μm) method of classification (Folk and Ward 1957). Resultant mean, sorting, skewness and kurtosis data were plotted alongside relative abundance of clay, silt and sand in Strater 3.0 (Golden Software 2012). These were collectively classified in R (R Core Team 2013) using the 'rioja' package (Juggins 2012) (method: coniss, distance: Euclidean, stratigraphically constrained) in order to determine major changes in sediment texture. The different grain-size parameters were correlated (Pearson's r) both with each other and with the environmental magnetism and sediment property data (water content and bulk density) established from each core in the program R (R Core Team 2013).

4.2.8 Geochemistry

XRF I-TRAX core scanning

X-Ray fluorescence (XRF) core scanning techniques (Croudace et al. 2006) can provide a rapid and non-destructive estimation of changes in lake sediment source (Koinig et al. 2003), redox state (Thomson et al. 2006) and/or productivity (Kylander et al. 2011). They can therefore provide useful information about past land-use and/or climate. A Cox Analytical Systems I-TRAX XRF core scanner, housed at ANSTO, was used to provide down core profiles of 38 (YL1211B) and 28 (YM0413B) elements.

The core surfaces of YL1211B and YM0413B were scanned at 0.2 mm and 1 mm resolution respectively with a Mo tube set to produce a major element down-core profile for each core (20 mA current; 30 s count time; 30 kV voltage). Results for each element were obtained as peak areas that were automatically converted to counts per second (kcps), indicating the relative change in elemental concentration down core. High-resolution optical scans as well the volumetric magnetic susceptibility profile for YM0413B were also obtained during the scanning process.

Analysis

Measurements coincident with cracks, voids and core ends were deleted from the raw datasets generated for each core. These were identified by comparing the core logs and the core scan images with peaks in mean standard error (MSE) (Löwemark et al. 2011). Elements that recorded zero counts for more than 5% of samples were removed from the dataset. The remaining data were then averaged at a 1 cm interval to permit direct comparison with the other lower-resolution sedimentological datasets produced for the cores.

Pore water and organic matter are elementally light (O and C in particular). High and/or variable concentrations of these materials within lake sediments act to 'dilute' heavier element counts, reducing the accuracy of measurements targeted at characterisation of inorganic lake sediments (Löwemark et al. 2011). Normalisation of raw kcps data is thus required in order to separate fluctuations in the non-organic allogenic and endogenic fraction of the core sediment from those associated with organic or pore water content.

I-TRAX kcps data are normalised by dividing raw counts by a stable denominator, commonly Al kcps (Löwemark et al. 2011), or the ratio of Compton (incoherent) to Rayleigh (coherent) scattering (Thomson et al. 2006). The former has shown to be useful given that it is a conservative element — i.e. relatively resistant to biogenic or redox alteration and common in most lithogenic materials — and is thus considered a good proxy for flux in bulk detrital material (Löwemark et al. 2011). However, Al detection by XRF scanning using Mo tubes is unreliable (Löwemark et al. 2011). The second method assumes that incoherent to coherent scattering ratios (inc/coh) represent elementally light materials (i.e. organic matter and pore water)

given that materials with a low atomic mass produce relatively high and low levels of incoherent and coherent scattering respectively (Thomson et al. 2006, Corella et al. 2011, Kylander et al. 2011). However, when compared to organic carbon alone, this method may be limited for tropical lake sediments with high or varied quantities of organic carbon (Chawchai et al. 2016). This method of normalisation was thus tested in the context of the Yeak Loam and Yeak Mai crater lake sediment cores by correlating the inc/coh ratios obtained from XRF core scanning with loss-on-ignition (used to estimated total organic content) and water content measurements returned for each core. Correlations (Pearson's *r*) were conducted in R (R Core Team 2013). Results of this comparison indicated that inc/coh ratios were a proxy for light elements in both cores, and were thus applied as a normalising denominator for the raw kcps elemental data (this is elaborated upon the relevant results sections for each core).

Cleaned and normalised elemental data were plotted and clustered (method: coniss, distance: Euclidean; stratigraphically constrained) in R (R Core Team 2013) using the 'rioja' package (Juggins 2012) in order to determine depths at which major changes in the gross geochemical profile for each core occurred. These data were also decomposed (as a whole dataset and/ or grouped into major sedimentology units where relevant) using a Pearson's correlation matrix and principle component analysis (PCA) in Microsoft Excel with the Multibase2015 PCA add-in (Addinsoft 2016). Prior to analysis, data were transformed using a z-score (i.e. standardised by calculating the number of standard deviations each measurement is from the whole down core mean of the relevant variable). This approach was used to reveal patterns and relationships between elemental data that can otherwise be latent in such complex multi-variate datasets.

Specific elemental ratios relevant to the Yeak Mai and Yeak Loam sedimentary settings were also plotted in order to derive information on lake redox cycling (potentially relevant for palaeoclimatic reconstructions), the presence of lacustrine carbonates, and siliciclastic grainsize properties. Mn/Ti, Fe/Ti and Cu/Ti ratios were constructed for each of the cores in order to derive information about fluctuations in redox-sensitive elements (Fe and Mn), and elements prone to post-depositional mobilisation under oxic conditions (Cu) (Thomson et al. 1995, Thomson et al. 2006). Ti was used as the denominator in these ratios based on the presumption that it represents background detrital flux (Thomson et al. 2006), hence removing fluctuations associated with the erosion and deposition of allogenic Fe and Mn (that would presumably be significant in a mafic catchment settings), and leaving behind a signal of endogenic redox cycling. Mn/Fe was also plotted for YL1211B sediments as this ratio has been shown to be useful for reconstructing redox cycling associated with mixing of deep, thermally stratified lakes that are less sensitive to redox processes than shallower lakes, resulting in variable behaviour between Fe and Mn (Boyle 2001, Naeher et al. 2013). Under this approach, high Mn/Fe ratios are commonly associated with high O_2 levels in the lake bottom waters (Naeher et al. 2013). Mn/Ca ratios were plotted for the core as an indicator of lacustrine biogenic carbonate fluctuation (if any) in the sediment (Owen and Wilkinson 1983). Zr/Rb, which has been used as a proxy for siliciclastic grain size (Dypvik and Harris 2001, Chawchai et al. 2013), was also applied to the core sediments to

assess the applicability of this technique to organic-rich lake sediments and, if found to be valid, to increase the resolution of the grain size data (especially relevant for YM0413B).

4.3 Results

4.3.1 Yeak Mai (core YM0413B)

Stratigraphy

The total length of YM0413B was 543.5 cm (table 4.2). Four major beds were distinguished in the core sediments from 543.5 to 510 cm (unit I), 510 to 288.5 cm (unit II), 288.5 to 218.5 cm (unit III), and 218.5 to 0 cm (unit IV) (shown on figure 4.6). Units I, III and IV are relatively massive, and are composed of sapropel (an aquatic ooze rich in amorphous or fine organic material (Merkt et al. 1971)), sapropelic silty clay loam, and silty clay loam sapropel, respectively. Unit II displays cyclical thin to thick diffuse interbeds and interlaminations of olive-black sapropelic mud (IIa) and black sapropel (IIb) that become increasing finely-spaced with depth. Smear-slide analysis of sediments from sub-unit IIa indicates that the clastic component predominantly comprises angular siliceous glass fragments and a silt-sized (10 to 20 μm) mineral. This mineral appears micaceous, and has been tentatively classified as chlorite based on its tabular shape, green hue under plane polarized light, and weak birefringence — figure 4.5.

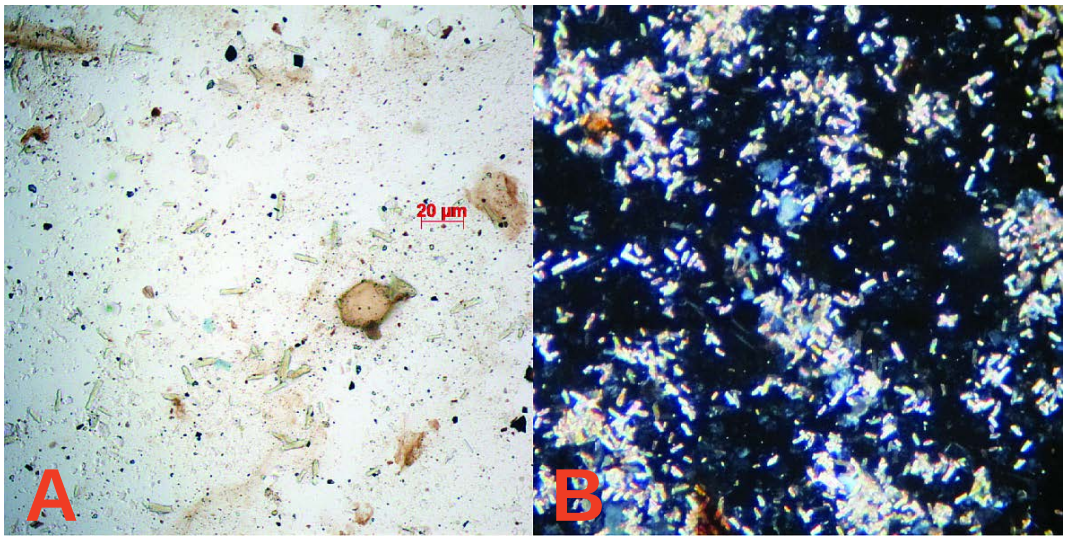

FIGURE 4.5: Tabular mineral identified in YM0413B unit IIa under normal (A) and cross-polarised (B) light.

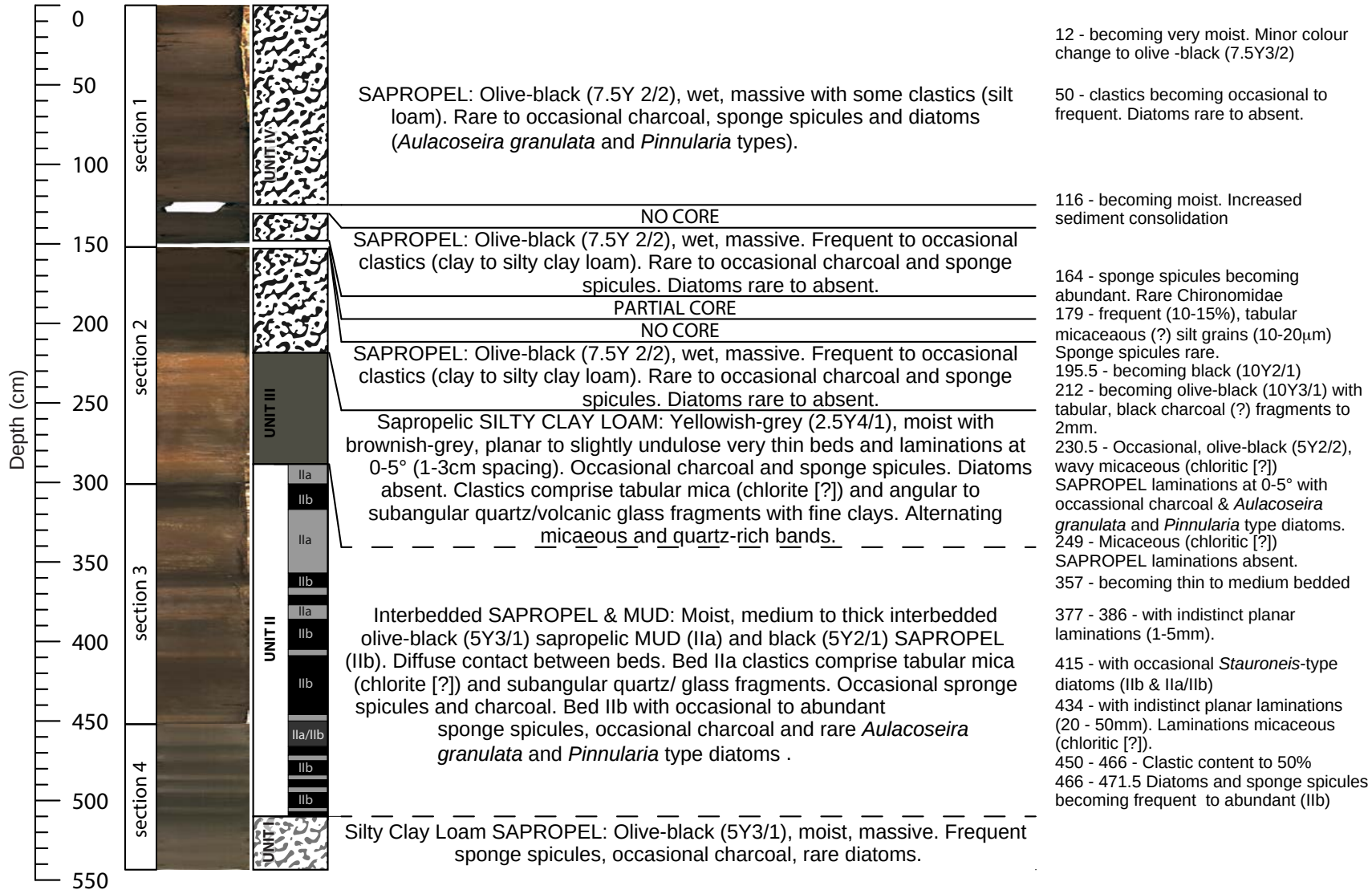

FIGURE 4.6: Photograph and log for core YM0413B.

TABLE 4.2: Details of the long cores extracted from Yeak Oam, Yeak Loam and Yeak Mai.

site	core name	type	UTM48N WGS84	length (cm)
Yeak Loam	YL1211B	gravity (master)	717908; 1518747	214
Yeak Loam	YL1211A	gravity (replicate)	717908; 1518747	181.5
Yeak Oam	YO0712B	gravity (master)	731157; 1498934	176
Yeak Oam	YO0712C	gravity (replicate)	731157; 1498934	109
Yeak Mai	YM0413B	push/percussion (master)	733062; 1479159	543.5

Reoccurring, non-clastic, non-algal core components (in order of decreasing abundance) include charcoal fragments, sponge spicules, diatoms (*Aulacoseira granulata* and *Pinnularia*-spp. [both present in unit IV from 0 to 50cm, unit IIb and unit I] and *Stauroneis* sp. [in unit IIb from 415 cm depth]), and rarely, chironomid head capsules or ligula. Though not observed during core logging, ostracods were later observed in unit IV samples from 120 cm to 190 cm depth that were processed for macro-charcoal analysis (details of associated methods are outlined in chapter 5). Biogenic sediment occurs in a lower abundance in units III and IIa than for other core units.

Chronology

The ^{14}C dates and calibrated ages (yrs BP) of samples submitted from YM0413B are presented in table 4.3. These dates show increasing age with depth with the exception of two age reversals returned from the charcoal and organic samples taken from 299 to 300 cm (D-AMS 007866) (modelled at 9533 to 9673 cal. yrs BP) and 207 to 207.5cm (D-AMS 007865) (modelled at 2785 to 2945 cal. yrs BP[4]). The age-depth model produced for YM0413B is presented on figure 4.7 (noting that model rejected the two above-described age-reversals).

Details of the results of YM0413B samples processed for plant lipid extraction and plant microfossil extraction that were not submitted for radiocarbon dating analysis are outlined in appendix C.

Bulk mineral influx, moisture content, dry bulk density & total organic content

Down-core changes in the water content, dry bulk density (ρ_{dry}) and total organic carbon (TOC) (as estimated from LOI550 percent weight loss) of YM0413B sediments, are presented on figure 4.8. The latter two of these variables were used in conjunction with the Bacon age-depth model produced for the core (discussed in section 4.3.1) to provide an estimation of down core changes in bulk mineral influx, the results of which are also included on figure 4.8.

[4]Age ranges with the highest probability at 2σ are reported in the text.

TABLE 4.3: Table of the conventional and calibrated (yrs BP) ages of ^{14}C date samples submitted from YM0413B.

Lab ID	depth (cm)	^{14}C date BP $\pm 1\ \sigma$	material	calibrated age ($2\ \sigma$) (cal. yrs BP)	probability (%)
OZT365	46-47	305 ± 25	fibrous organic fragment	298-334	31.3
				359-446	63.8
OZT366	140.5-141.5	1075 ± 35	>250 μm charcoal fragments (batch 3)	916-1001	78.3
				1009-1057	16.6
D-AMS 007868	206-207	1811 ± 28	bulk sediment	1611-1672	25.8
				1680-1981	0.3
				1691-1753	51.5
				1766-1818	17.3
D-AMS 007865	207-207.5	2789 ± 24	>250 μm charcoal with some organic material (batch 2)	2785-2945	95
D-AMS 007866	299-300	8650 ± 31	>250 μm charcoal with some organic material (batch 2)	9533-9673	95
D-AMS 007869	300-301	2050 ± 23	bulk sediment	1926-2048	95
OZT367	375.5-376.5	2570 ± 50	>250 μm charcoal fragments (batch 3)	2458-2763	94.5
OZT368	446.5-447.5	2920 ± 30	>250 μm charcoal fragments (batch 3)	2929-2939	1.4
				2941-3159	93.6
OZT369	522-523	3985 ± 30	>250 μm charcoal fragments (batch 3)	4296-4334	9.6
				4344-4523	85.3
D-AMS 008225	534-534.5	4107 ± 26	large charcoal fragment	4441-4484	8.5
				4509-4659	60.5
				4666-4708	8.1
				4756-4812	18
D-AMS 007864	538-539	5053 ± 31	bulk sediment	5662-5693	8.2
				5699-5701	0.6
				5707-5895	86.1

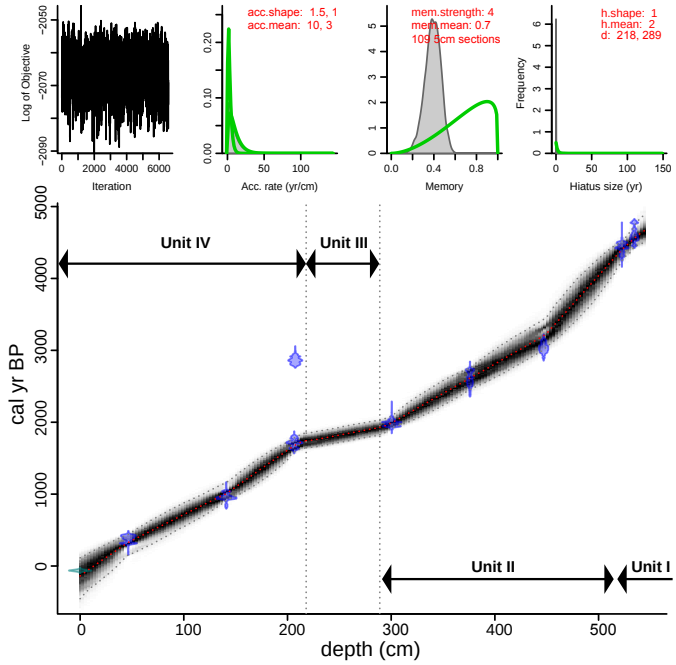

FIGURE 4.7: Bacon Age-Depth model produced from YM0413B dates. Model overlain with extent of logged sedimentary units (I to IV).

TOC and water content are strongly related (r = 0.87)[5] and are negatively correlated with dry bulk density (r = -0.53; r = -0.38 respectively). The estimated bulk mineral influx thus shows a weak positive correlation with dry bulk density values (r = 0.29), and a negative correlation with TOC (r = -0.39) and water content (r = -0.35).

Fluctuations in TOC, dry bulk density and water content appear related to the different properties of the four sedimentary units logged for this core. Unit I shows relatively constant water content (77 $\pm$ 1.3%), organic content (24 $\pm$ 2.3%) and dry bulk density (1 009 $\pm$ 20 kg/m^3) (1σ), with a mean mineral influx of 56 kg/m^2/yr^{-1}.

Fluctuations in TOC, dry bulk density and water content between 515 cm and 289 cm depth appear related to patterns of interbedding observed across unit II. These fluctuations are partially captured by the estimated influx data. However, the age-depth model is too coarse to capture any discrepancies between the accumulation rates of the interbeds (units IIa and IIb) and, as such, these are not well captured by the estimated influx values for this portion of the core. In general, unit IIa sediments are characterised by relatively low TOC (16.5 $\pm$ 1.5%) and pore water content (69 $\pm$ 2%), and high bulk density values (1090 $\pm$ 30 kg/m^3) (1σ). Unit IIb sediments display the inverse to this relationship (25.9 $\pm$ 3% TOC; 78 $\pm$ 2.6% water content; 1 000 $\pm$ 50 kg/m^3 dry bulk density (1σ)). Bulk mineral influx for unit II is estimated to be 92 kg/m^2/yr^{-1}. A significant increase in influx is estimated for unit II sediments up core of 455 cm, corresponding to an overall decline in TOC for the same sediments.

[5] All r values reported in this chapter are significant (p<0.05) unless specified in the text.

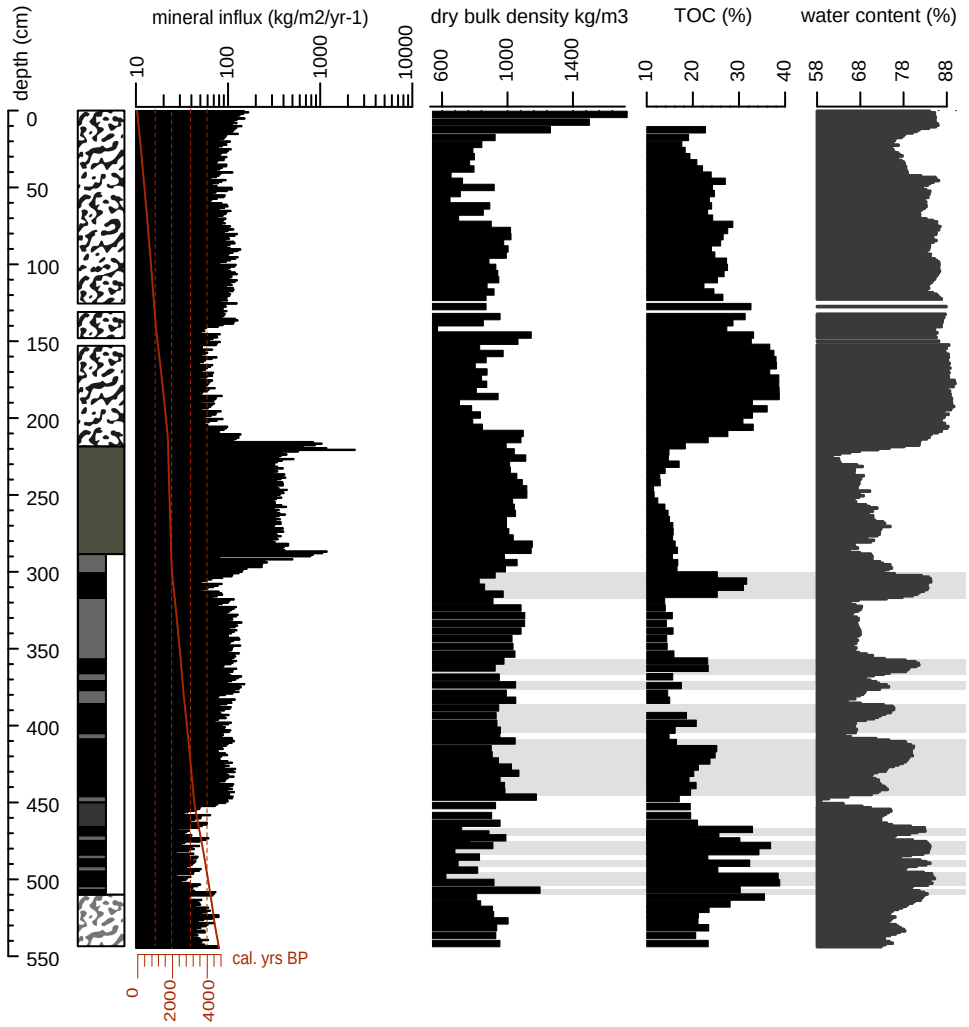

FIGURE 4.8: Plot showing estimated mineral influx (logarithmic scale), dry bulk density, moisture content and total organic content of YM0413B core sediments. Light grey bars correspond to approximate bed-widths of sedimentary unit IIb materials.

Unit III is characterised by relatively high dry bulk density ($1\,130 \pm 20$ kg/m^3), and low TOC ($14.6 \pm 0.9\%$) and sediment water content ($67.8 \pm 1.9\%$) (1σ). Exceptionally high mineral influx rates are modelled at the outer boundary of this unit ($2\,000$ kg/m^2/yr^{-1} at 219 cm depth and $1\,180$ kg/m^2/yr^{-1} at 285 cm depth). The modelled two-year hiatuses at the boundaries of unit III (218 and 289 cm) used to model accumulation rate for unit II (see section 4.3.1), may have served to overestimate influx at these depths. However, these peaks do correspond with low TOC (14 and 15%) and high dry bulk density values ($1\,150$ and $1\,200$ kg/m^3) calculated for these depths. Consequently, large peaks in influx were estimated from age-depth models that did not include any hiatuses at these depths or use any pre-prescribed accumulation rates (not shown).

Across sedimentary unit IV, TOC increases to $28 \pm 3\%$ (1σ), peaking between 160 cm and 184 cm depth. Pore water content also increases across Unit I to a relatively consistent average of 85%, before dropping between

42 cm and 15 cm to approximately 77%. Dry bulk density remains relatively low across unit I (average = 960 kg/m^3) before peaking at the core top to 1 700 kg/m^3.

Environmental magnetism

Down core fluctuations in the volumetric magnetic susceptibility of YM0413B sediments are presented on figure 4.9. The κSI behaviour of the core sediments correlates with estimated bulk mineral influx rate (r = 0.6). Major variations in κSI correspond with the four logged stratigraphic units.

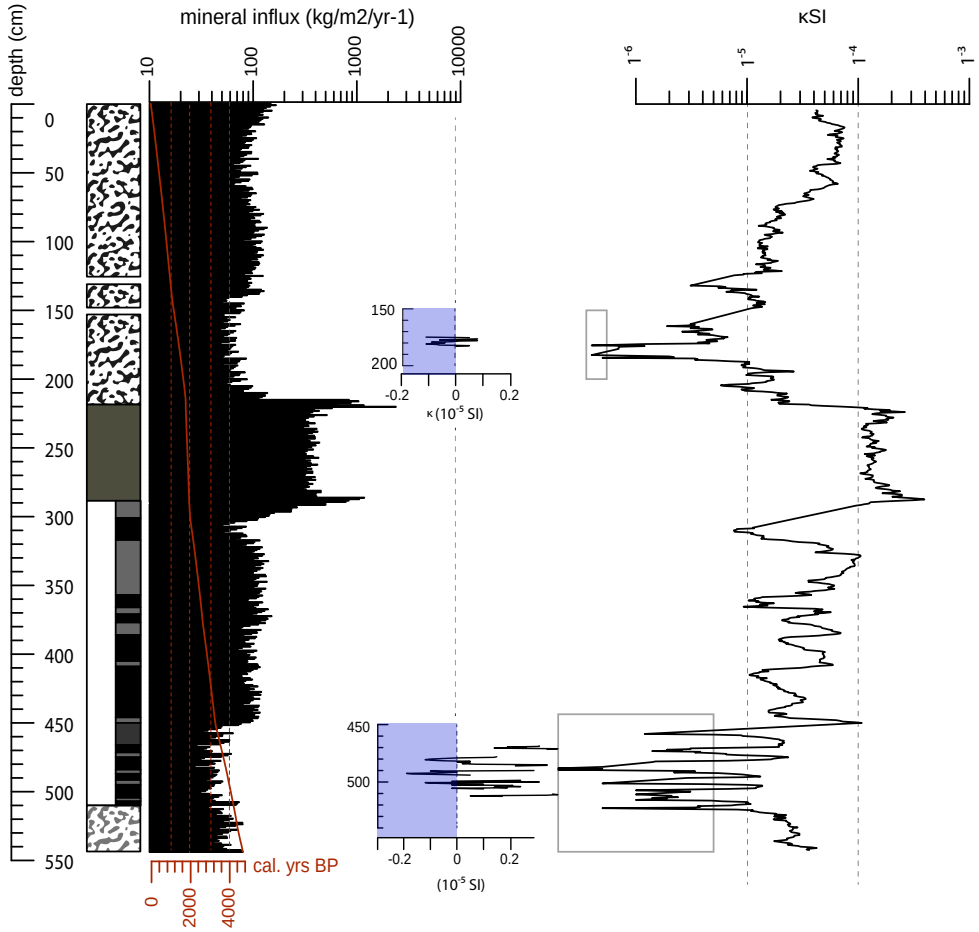

FIGURE 4.9: Down core fluxes in YM0413B volumetric magnetic susceptibility plotted alongside estimated mineral influx and core sediment units. Data are presented on a logarithmic scale.

Unit I displays κSI values consistent with paramagnetic materials (ranging from 1.7 to 4.2 $\times$ 10^{-5} SI) (Dearing 1999a). A peak in magnetic susceptibility is apparent towards very base of the core (541 cm depth).

κSI behaviour within unit II shows a clear shift from lower (mean = 7.9 $\times$ 10^{-6} SI) to higher (mean = 4.2 $\times$ 10^{-5} SI) values at approximately 450 cm. Across this boundary, however, fluctuations in magnetic susceptibility maintain a close relationship with layer stratigraphy, with susceptibility peaks corresponding with sub-unit IIa, and troughs with sub-unit IIb. Throughout the

lower half of the unit (514 to 449 cm), IIb sediments exhibit paramagnetic and occasionally diamagnetic properties (e.g. 505 to 479 cm), ranging from -1.5 $\times$ 10^{-5} to 3 $\times$ 10^{-6} SI. Across the same depth interval, IIa materials are more magnetic, though the overall magnetic properties of these sediments are still weak (approximately 1 $\times$ 10^{-5} to 2 $\times$ 10^{-5} SI). An abrupt peak in κSI (1 $\times$ 10^{-4} SI) occurs within the unit IIa layer between 446 and 449 cm depth. Up core of 446 cm, magnetic susceptibility of IIa layers peak at 5 $\times$ 10^{-5} to 1 $\times$ 10^{-4} SI, while the IIb trough-values do not fall below below 8 $\times$ 10^{-6} SI.

Unit III exhibits the highest volumetric magnetic susceptibility values for the core. This layer is bounded by large peaks in κSI that mirror peaks in estimated mineral influx data. The lower boundary occurs at approximately 287.5 cm as an abrupt positive spike, recording a core-maximum value of 4 $\times$ 10^{-4} SI. Above this layer, susceptibility values fall to approximately 1.5 $\times$ 10^{-4} SI before again peaking at 224 cm (2.7 $\times$ 10^{-4} SI).

Unit IV κSI ranges from -1.2 $\times$ 10^{-6} to 7.5 $\times$ 10^{-5} SI (mean = 2.65 $\times$ 10^{-5} SI). Sediments displaying diamagnetic behaviour occur within small core section from 187 to 170 cm. Sediments at the top of the core (67 to 0 cm) show slightly higher magnetic susceptibility than the rest of the unit (6 $\times$ 10^{-5} to 7.5 $\times$ 10^{-5}).

Grain size analysis

YM0413B was sampled for textural analysis every 2.5 cm, and the textural properties of the core sediments are shown on figure 4.10. Silt is the most common grain size down core, making up an average of 62% of the clast population of core sediments. Clay and sand make up approximately 32% and 6% of core sediments respectively. Overall there is a slightly higher proportion of clay in units I and II (mean = 35%) than in units III and IV (mean = 28%). This relationship is inverse to silt abundance, which averages at 67% across units III and IV and 57% across units II and I. The relative abundance in each grain-size fraction between samples is quite diverse, with silt ranging from 18% (205 cm) to 91% (22.5 cm), and clay from 8% (42 cm) to 82% (205 cm).

The relative proportion of silt, clay or sand within each sample appears to control the shape of their respective sediment distribution in terms of sorting, skewness and kurtosis. Higher silt percentages in each sample display a negative correlation with sorting (r = -0.47) and skewness (r = -0.39) and a positive correlation with kurtosis (r = 0.42). This relationship holds true across the four core stratigraphic units, with the exception of unit III, where silt has an insignificant positive relationship with skewness (r = 0.13) (see appendix E for unit-specific correlation matrices). In the context of the Yeak Mai sediments, silt-rich samples tend to display poorly sorted, symmetrical to fine skewed and leptokurtic distribution curves. The relationship between high silt fractions and κSI is positive across units IV (r = 0.48), I (r = 0.35) and II (r = 0.18 [insignificant]), and negative in unit III (r = -0.43) wherein κSI associates with clay (r = 0.54).

Down-core, clay abundance is positively correlated with skewness (r = 0.24) and negatively correlated with kurtosis (r = -0.49). These relationships are

consistent across all units with the exception of unit III whereby clay is negatively correlated with skewness (r = -0.39). The association between clay abundance and sorting is only significant across stratigraphic unit III (r = 0.43). Samples with high clay abundance are, in general, associated with a platykurtic, coarse-skewed distribution curve. The relationship between clay-rich samples and dry bulk density is positive across units I, II and III.

Samples with a relatively high proportion of sand are positively correlated with sorting and, with the exception of unit IV, kurtosis. In general, sand is negatively correlated with both κSI (r = -0.34) and dry bulk density (r = -0.4), and positively correlated TOC (r = 0.58).

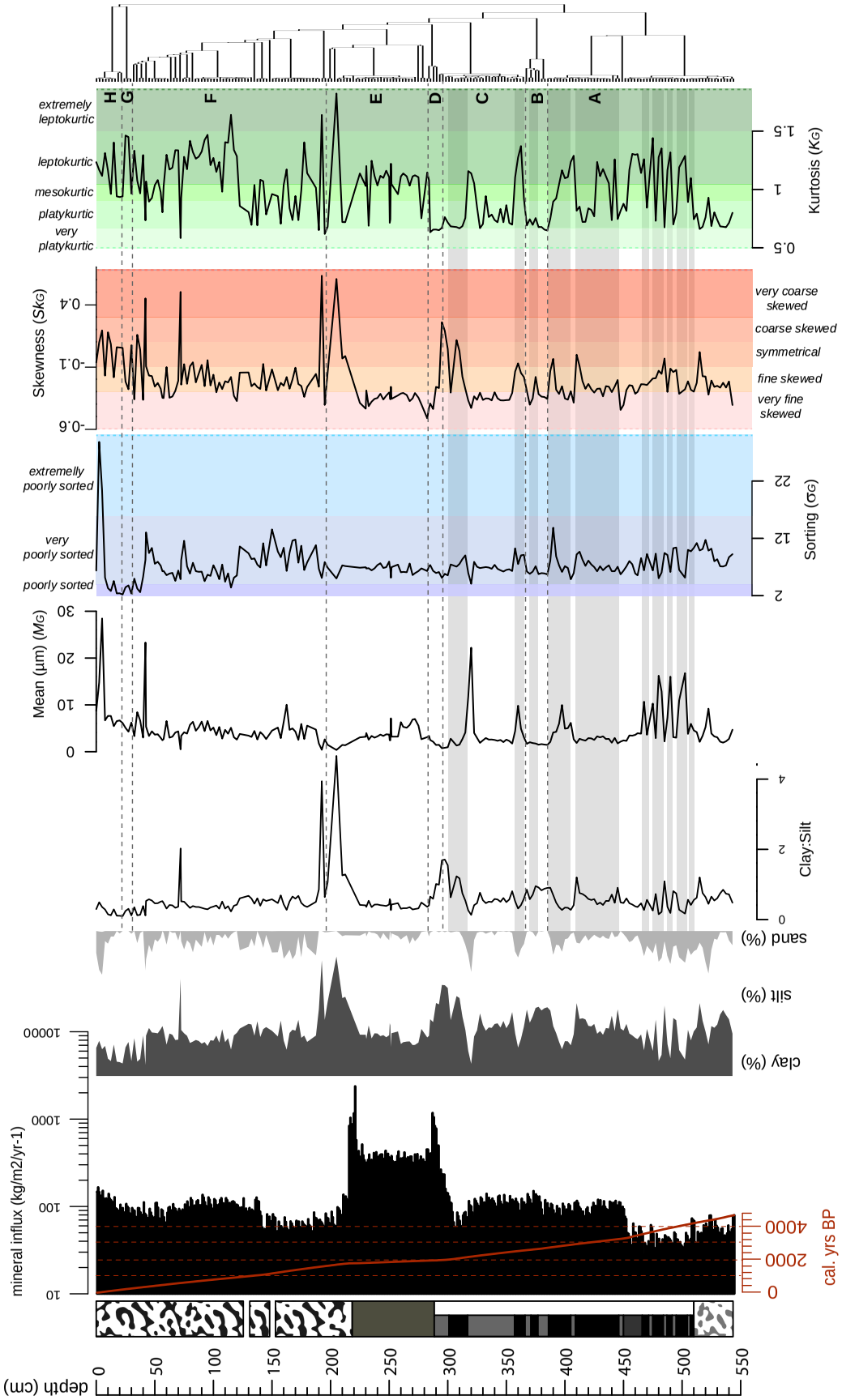

FIGURE 4.10: Textural properties of YM0413B sediments that have been classified following Folk and Ward (1957) parameters in Gradistat version 8 (Blott and Pye, 2001). Results have been grouped using a stratigraphic constrained analysis of the variables presented. Data shown relative to estimated mineral influx. Light grey bars correspond to approximate bed-widths of sedimentary unit IIb materials.

Results of stratigraphically constrained cluster analysis for the YM0413B textural data (delineated on figure 4.10) indicate changes in the record between 20 and 22.5 cm (1.16×10^5), 27.5 and 30 cm (1.19×10^5), 192.5 to 195 cm (8×10^4), 285 and 287.5 cm (8.7×10^4), 295 and 297.5 cm (9×10^4), 367.5 and 370 cm (9.7×10^4) and 382.5 and 385 cm (1.1×10^5) (dissimilarity distances are bracketed). These boundaries delineate eight clusters — A to H — shown on figure 4.10.

Clusters A to C capture basal core sediments from stratigraphic units I and II up to 295 cm depth. In general, these clusters capture high frequency, high amplitude fluctuations in grain size. This is particularly apparent in cluster A between 522.5 and 460 cm, reflecting the textural differences between stratigraphic sub-units IIa and IIb. Sediments from IIa are typically associated with peaks in clay abundance that coincide with troughs in both silt and sand abundance. Conversely, IIb sediments (shaded on figure 4.10) are defined by peaks in sand and silt abundance. Up core of 460 cm, these relationships are less well defined, likely due to the fact that sand and silt abundances are slightly decoupled. Cluster B, extending between 382.5 and 370 cm, is distinguished by a peak in clay and a near-absence of sand. A second clay peak (80%) at 295 cm is captured by the lower boundary of cluster D. A subsequent sand trough from 295 to 287 cm appears to delimit cluster D, capturing the lower boundary of logged sedimentary unit III. Above this zone, cluster E (285 to 195 cm) captures logged sediment unit III, which comprises silt rich, sand-poor sediments. The top of this cluster (205 to 195 cm) captures a large peak in clay (to 82%). Cluster F (195 cm to 30 cm) is characterised by an increased proportion of sand in the sediment sequence that varies alongside clay and silt as a series of high frequency, low amplitude fluctuations. Clusters G and H, extending from 30 cm to the core top capture an abrupt increase in the overall proportion of silt in the core sediments (on the order of 15 to 25%), with cluster G (30 to 22.5) representing a zone with negligible sand. A peak in sand abundance (30%) (and mean grain size) occurs at 5 cm depth.

Geochemistry

Normalisation

A correlation matrix showing the relationship between measured water content, total organic carbon and the inc/coh scattering ratio obtained from XRF scanning of YM0413B is presented for the whole core, and across the different units, in table 4.4. Overall, the inc/coh ratio displays a significant, strong relationship with both water content (r = 0.93) and TOC (r = 0.918). This relationship is reflected across all layers, with the exception of Unit III (288 to 218cm depth) where TOC shows a negative correlation with the inc/coh ratio (r = -0.348). This relationship is likely due to the decoupling of TOC and water content (r = -0.184) within these sediments, the latter of which appears to control the inc/coh ratio (r = 0.849). These data suggest

that that the inc/coh ratio for YM0413B sediments appears to reflect the interaction between TOC and pore water content (though more strongly controlled by the latter), and is therefore considered a suitable normalisation parameter for the XRF geochemical data.

TABLE 4.4: Pearson's correlation matrix for YM0413B showing relationship between total organic carbon (%) (TOC), water content (%) and inc/coh ratios (95% C.I.).

whole core - 0 to 543 cm

	TOC	water content	inc/coh
TOC	1	*r* = 0.872; p < 2.2e16; df = 123	*r* = 0.918; p =<2.2e-16; df = 122
water content	*r* = 0.872; p < 2.2e16; df = 123	1	*r* = 0.93; p < 2.2e-16; df = 514
inc/coh	*r* = 0.918; p =<2.2e-16; df = 122	*r* = 0.93; p < 2.2e-16; df = 514	1

unit IV - 0 to 218 cm

	TOC	water content	inc/coh
TOC	1	*r* = 0.866; p = 2.22e-16; df = 49	*r* = 0.959; p < 2.2e-16; df = 48
water content	*r* = 0.866; p = 2.22e-16; df = 49	1	*r* = 0.927; p < 22e-16; df = 2-3
inc/coh	*r* = 0.959; p < 2.2e-16; df = 48	*r* = 0.927; p < 22e-16; df = 2-3	1

unit III - 219 to 288 cm

	TOC	water content	inc/coh
TOC	1	*r* = -0.184; p = 0.478; df = 15	*r* = -0.348; p = 0.1708; df = 15
water content	*r* = -0.184; p = 0.478; df = 15	1	*r* = 0.849; p <2.2e-16; df = 68
inc/coh	*r* = -0.348; p = 0.1708; df = 15	*r* = 0.849; p <2.2e-16; df = 68	1

unit II - 289 to 510 cm

	TOC	water content	inc/coh
TOC	1	*r* = 0.876, p <2.2e-16, df = 47	*r* = 0.920; p < 2.2e-16; df = 47
water content	*r* = 0.876, p <2.2e-16, df = 47	1	*r* = 0.945, p<2.2e-16, df = 207
inc/coh	*r* = 0.920; p < 2.2e-16; df = 47	*r* = 0.945, p<2.2e-16, df = 207	1

unit I - 511 to 543 cm

	TOC	water content	inc/coh
TOC	1	*r* = 0.970, p = 6.9e-5, df = 6	*r* = 0.952, p = 0.000027, df = 6
water content	*r* = 0.970, p = 6.9e-5, df = 6	1	*r* = 0.924, p = 5.1e-14, df = 30
inc/coh	*r* = 0.952, p = 0.000027, df = 6	*r* = 0.924, p = 5.1e-14, df = 30	1

Geochemical behaviour of core sediments

Data preparation and synthesis

Elemental data comprising raw kcps counts greater than zero for at least 95% of YM0413B sample points include, in order of decreasing abundance, Fe, Ti, Ni, Zr, Sr, Rb, Mn, Zn, K, Ca, Y, Pb, Cu, Cr, S, Ba and Al. Down core changes in these elemental data, normalised to inc/coh ratios, are presented on figure 4.11. A plot of the selected elemental ratios is shown on figure 4.12.

Analysis

The stratigraphically constrained cluster analysis performed on the normalised geochemical data identifies three major sample clusters in the normalised data (see figure 4.11). Cluster A extends across the base of the core to the basal boundary of logged unit III at 288 cm depth (dissimilarity distance = 2.34×10^6). Cluster A has been divided into three sub-clusters (Ai to Aiii), the boundaries of which occur between logged sedimentary units I and II (416 cm depth; dissimilarity distance = 1.66×10^6) and within unit II at 461 cm depth (dissimilarity distance = 1.81×10^6), reflecting the logged transition between sedimentary sub-units IIIa/IIIb and IIIa. The top of cluster B occurs at 224 cm (dissimilarity distance = 3.1×10^6), just deeper than the logged upper boundary of sedimentary unit II at 218.5 cm. This cluster has been subdivided into three sub-clusters (Bi to Biii). Bi, captures sediment between 288 and 280 cm depth (dissimilarity distance = 2.15×10^6). Sub-clusters Bii and Biii are bounded at 231 cm depth (dissimilarity distance = 1.94×10^6). Cluster A extends from 224 cm to the top of the core, and is subdivided in sub-clusters Ai and Aii at 43 cm (dissimilarity distance = 1.33×10^6).

Key elemental data from the YM0413B core have been grouped according to their whole-core associations both to each other and to the other sedimentological variables outlined in this chapter.

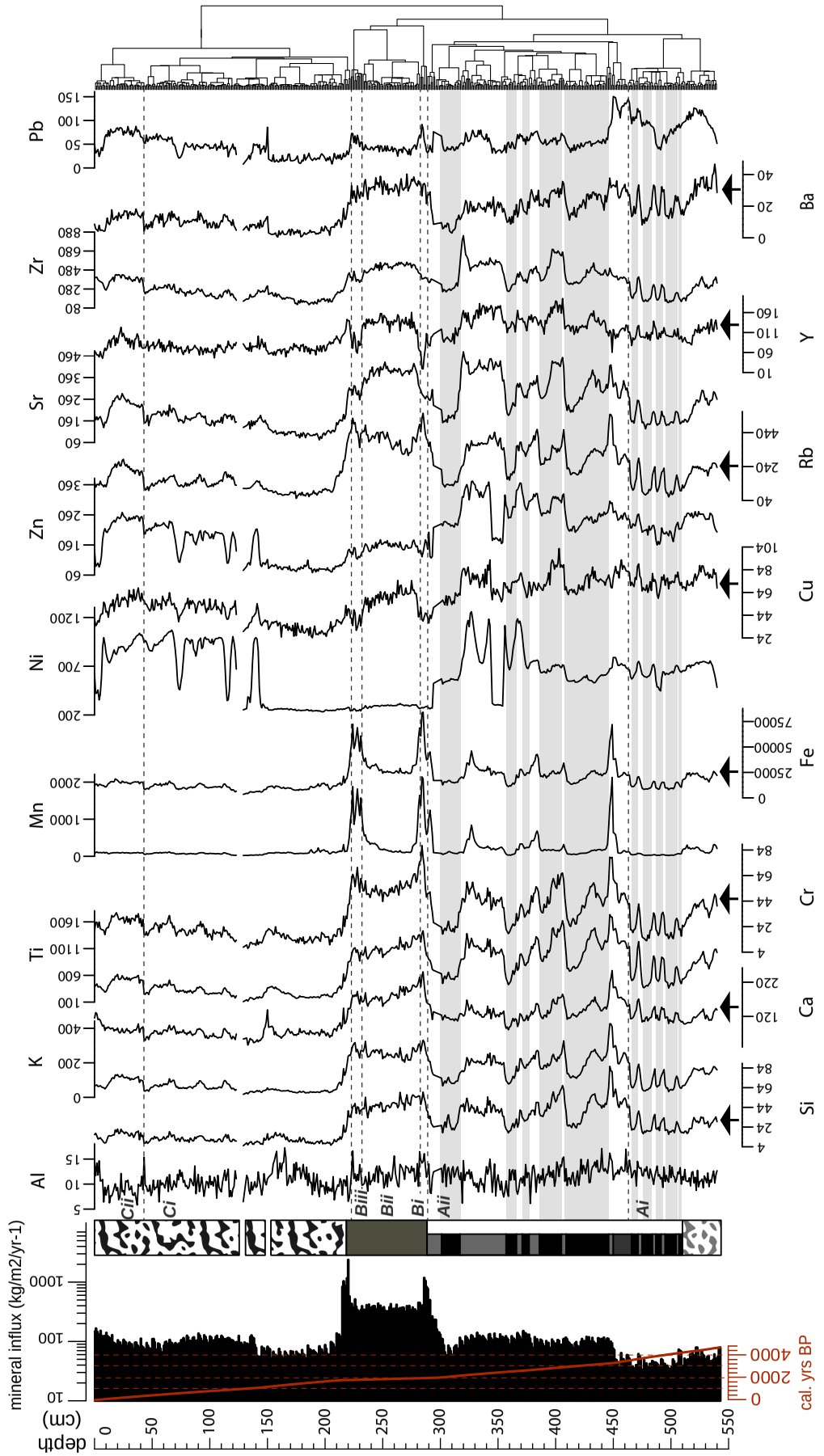

FIGURE 4.11: Plot showing YM0413B XRF geochemical data normalised to inc/coh scattering ratios.

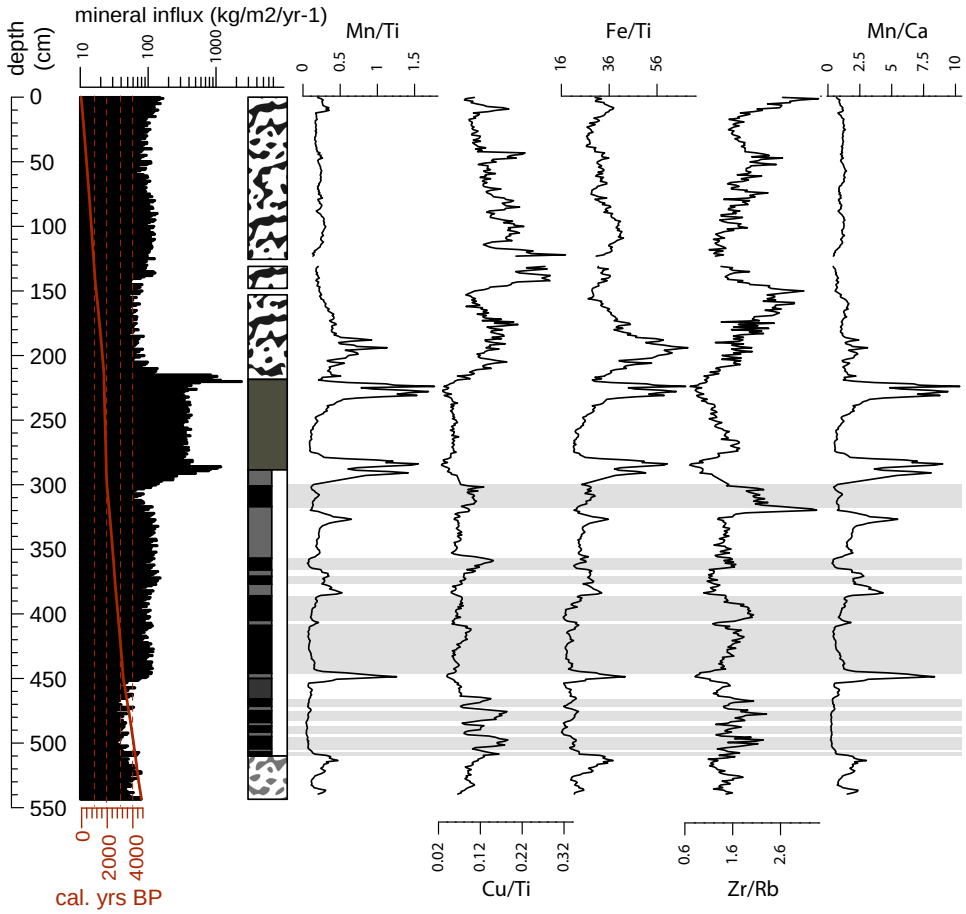

FIGURE 4.12: Plot showing downcore fluxes in selected geochemical ratios from YM0413B sediments. Grey bars used to highlight interbeds in unit II.

Si, Ti, K, Ca, Rb, Ba, Cr Sr & Zn are all strongly correlated (min. r = 0.69 [Zr and Ca]; max r = 0.97 [Ti and Si] — see figure 4.11 and appendix E for correlation matrices. Principle component (PC) 1, which accounts for 62.8% of the geochemistry data variance for the whole core, appears to be controlled by this elemental association (figure 4.13). All of these elemental data show a moderate, positive correlation with κSI (min. r = 0.51 [Ti]; max. r = 0.69 [Cr]), and a strong, negative correlation with both total organic carbon (min. r = -0.62 [Ti]; max. r = -0.86 [Sr]) and water content (min. r = -0.79 [Ca]; max. r = -0.90 [K]). This association remains fairly consistent across the core units, with the exception of Unit III which is discussed below (see figures 4.14 to 4.17 for unit-specific PCA plots and appendix E for whole-core and unit-specific correlation matrices).

High frequency fluctuations in the Si, Ti, K, Ca, Rb, Ba, Cr Sr & Zn element suite occur throughout unit I and II (cluster A), whereby peaks and troughs correspond with Units IIa and IIb respectively (figure 4.11). A decrease in the frequency of these fluctuations marks the transition from cluster Aii to Aiii at 461 cm depth. Throughout cluster A (which includes logged sedimentary units I and II), these elements are positively correlated with silt, with the exception of Rb, which is associated with clay (r = 0.3).

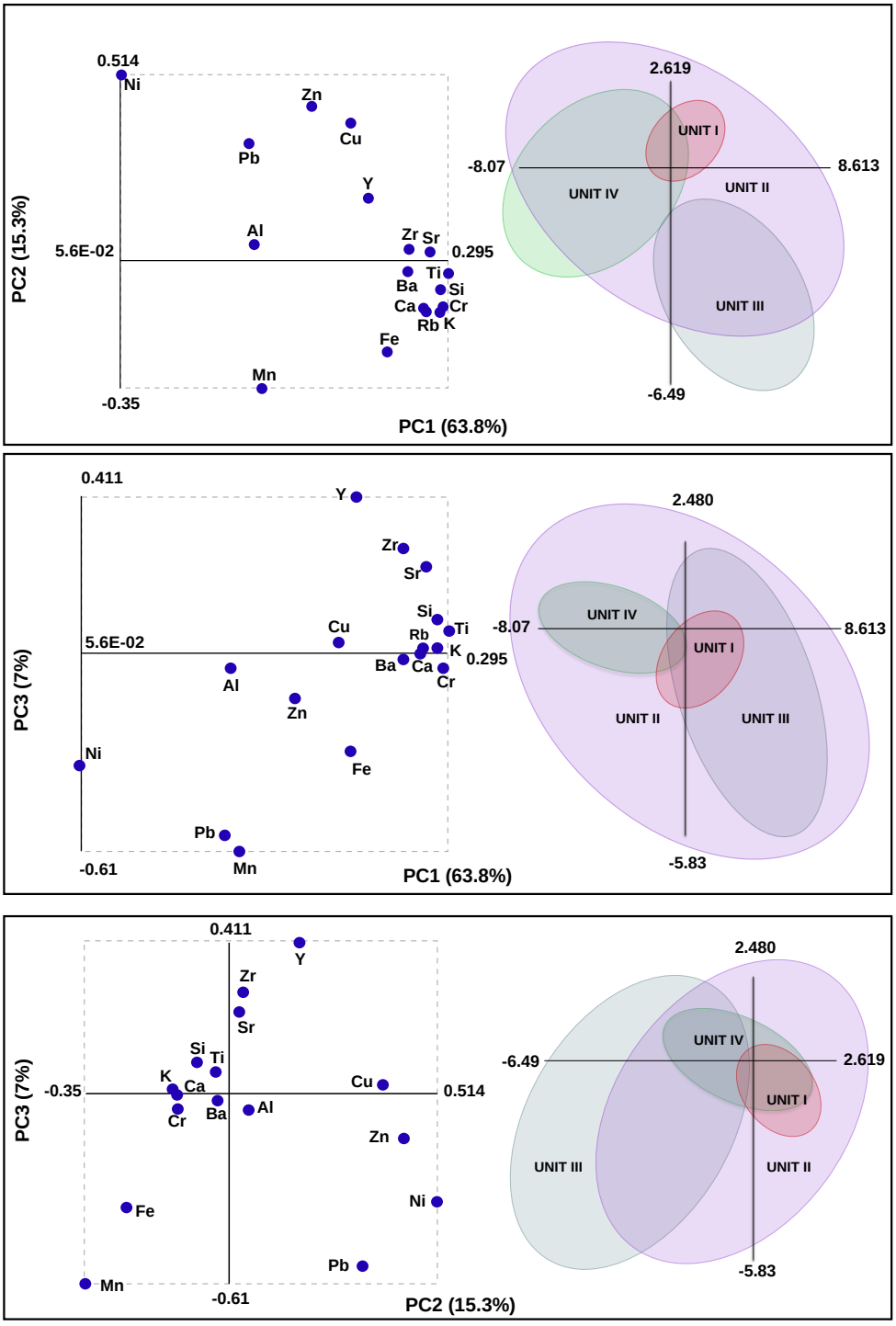

FIGURE 4.13: Whole core PCA plot for select elemental data from YM0413B.

At 288 cm, Si, Ti, K, Ca, Rb, Ba, Cr Sr & Zn abruptly peak (delimited by sub-cluster Bi), and mostly plateau across sub-units Bii and Biii towards the upper boundary of sedimentary unit III (224 cm). Throughout this unit, Si, K, Ca, Ti, Cr, and Ba are still associated, but are mostly decoupled from Sr, Rb and Zr (though K and Rb still show a strong correlation [$r = 0.81$]). Si, K, Ca, Ti, Cr and Rb remain positively correlated with κSI (although this is

low compared with the whole core), but are unrelated to TOC, and insignificantly or weakly negatively correlated with water content. Though Sr and Zr remain negatively correlated with TOC (as per the rest of the core), these data show a positive and negative correlation with water and κSI respectively across sedimentary unit III. This association reflects the behaviour of Cu, Zn and Ni in this unit and, combined, these elements control the negative variance along PC1 for sedimentary unit III (figure 4.16).

Si, Ti, K, Rb, Ba, Cr Sr & Zn re-associate across cluster C (sedimentary unit IV), dropping to values consistent with those of sedimentary unit IIa. Ca disassociates with the other elemental data described in this section (figure 4.17), and, aside from Al, is the only element within this sedimentary layer that is positively correlated with sand (r = 0.23). The delineation between clusters Ci and Cii at 42 cm is, in part, reflected by the slight overall increase in all elemental data up core, with the exception of Mn.

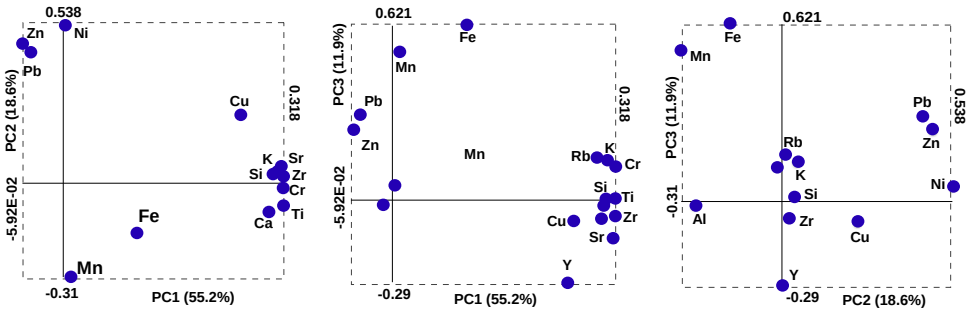

FIGURE 4.14: PCA plot for select elemental data from YM0413B sedimentary unit I.

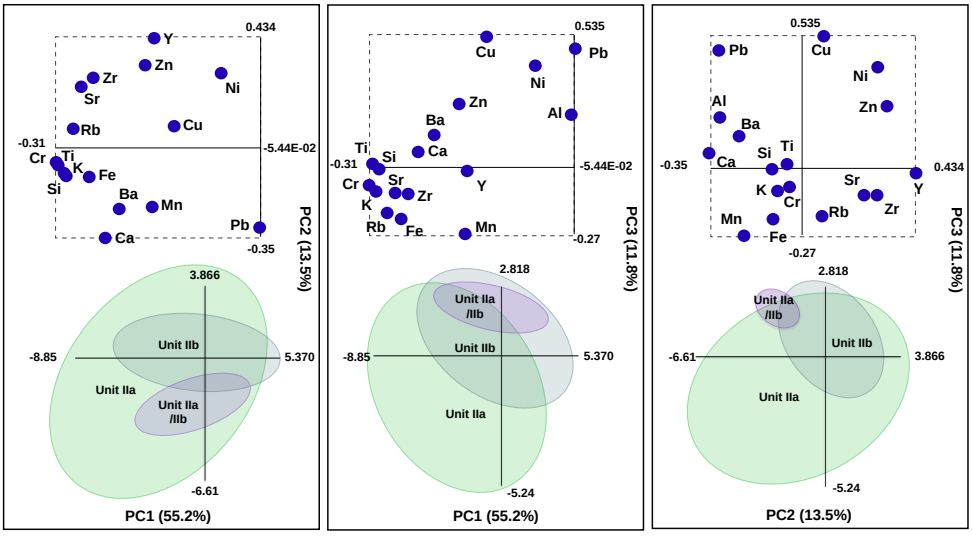

FIGURE 4.15: PCA plot for select elemental data from YM0413B sedimentary unit II.

Fe, Mn & selected elemental ratios Fe and Mn correlate with each other (r = 0.91) and κSI (r = 0.74 and r = 0.63, respectively). These elements reflect fluctuations displayed by the above-discussed Si, Ti, K, Ca, Rb, Ba, Cr Sr & Zn element suite across sub-clusters Ai (Fe only), Aii, and cluster C. Fe and

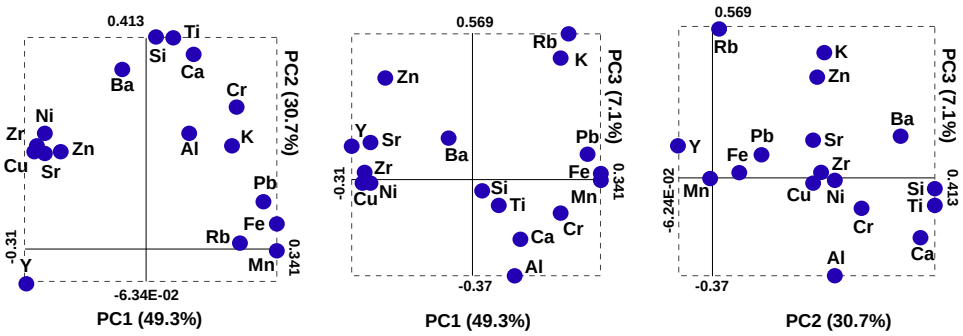

FIGURE 4.16: PCA plot for select elemental data from YM0413B sedimentary unit III.

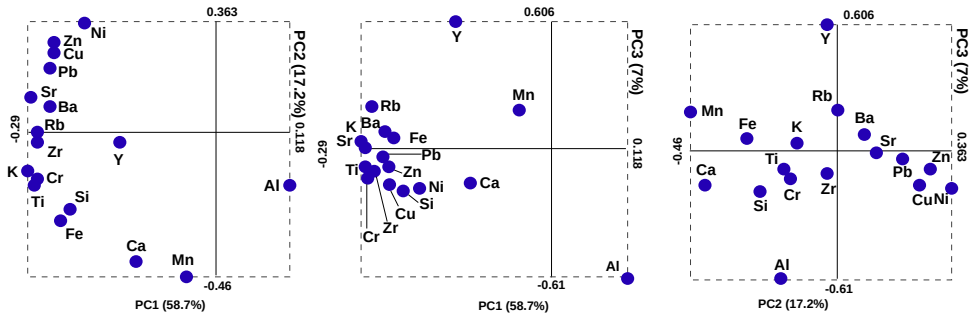

FIGURE 4.17: PCA plot for select elemental data from YM0413B sedimentary unit IV.

Mn both sharply peak at the boundaries of Unit II (sub-cluster Bi and Biii), mirroring peaks in estimated mineral influx, and drop to relatively low values between 277 to 234 cm (sub cluster Bii). Throughout sedimentary unit III (cluster B), the Fe and Mn data display a strong positive correlation with K, Cr, Rb, and especially Pb, and a negative relationship with Ni, Cu, Zn and Y — reflected by PC1 for this unit (see figure 4.16 and appendix E for unit-specific correlation matrices).

The Fe/Ti and Mn/Ti elemental ratios show a weak to moderate negative correlation with the Si, Ti, K, Ca, Rb, Ba, Cr Sr & Zn data (with the exception of K in sedimentary units II and III, and Cr in sedimentary unit II), effectively decoupling allogenic vs. endogenic sources of Fe and Mn. Fe/Ti and Mn/Ti data are strongly correlated (r = 0.8). However, while Mn/Ti data are negatively associated with the Si, Ti, K, Ca, Rb, Ba, Cr, Sr and Zr elemental suite across sedimentary units I and IV, they are positively or insignificantly correlated with these data in units II and III. The Mn/Ti and Mn/Ca datasets are strongly correlated (r = 0.92) presumably due to the tight association between Ti and Ca (r = 0.9) across the whole core (noting that correlation in sedimentary unit IV is weaker (r = 0.57)). This suggests that the source of Ca in sedimentary units I to III is mostly of detrital vs. biogenic origin, or mineral influx is driving aquatic productivity including carbonate producing organisms. Notable changes in the Fe/Ti vs. the Fe plots normalised to inc/coh ratios include the removal of the regular fluctuations in Fe/Ti elemental data across sedimentary sub units IIa and IIb, and an overall increase in variability across unit IV. In addition to the peaks

observed along the boundaries of sedimentary unit II, two high-amplitude peaks appear in the Mn/Ti and Fe/Ti record at 449cm, and between 203 and 118cm depth. Both the Fe/Ti and Mn/Ti records show a weak positive correlation with clay (r = 0.18 [Fe/Ti], r = 0.2 [Mn/Ti]).

Cu/Ti shows a weak positive correlation with Fe/Ti (r = 0.27) and weak, negative correlation with Mn/Ti (r = -0.20) across the whole core. These data tend to trough at major peaks in the Fe/Ti and Mn/Ti records.

All normalised geochemical data show an insignificant, or a negative relationship with sand — accounted for by the correlation between this variable (and mean grain size) with both total organic carbon and water content (r = 0.59, r = 0.34 respectively). This has been corrected by normalising the elemental data against the inc/coh scattering ratio and thus might not accurately reflect the relationship between the geochemistry data and grainsize. However, Zr/Rb — a proxy used for grainsize (Dypvik and Harris 2001, Chawchai et al. 2013) — does show a positive correlation with sand across the whole core (r [whole core] = 0.5).

Heavy Metals (Ni, Cu, Zn, Y and Pb) are positively correlated both with each other and, with the exception of Ni, with the Si, Ti, K, Ca, Rb, Ba, Cr Sr & Zn suite. However, Ni, Cu, Zn and Pb all show a negative or insignificant relationship with κSI, a weak negative relationship with water content and TOC, and an insignificant relationship with dry bulk density across the whole core. Ni is negatively, or insignificantly correlated with all data outside of the heavy metal elemental suite, and contributes to the greatest degree of loading for whole core PC2 (see figure 4.13 and table 4.5).

TABLE 4.5: YM0413B eigenvalues, percentages and elemental variable loading from PCA of geochemical data.

whole core	PC1	PC2	PC3
Eigenvalue	170.65	22.46	9.19
R2 (%)	80%	10%	4%
Q2 (%)	69%	35%	18%
Si	0.314289622	0.202665861	0.146476215
K	0.31977899	0.233624064	0.135193055
Ca	0.291069564	0.335297661	-0.147197782
Ti	0.33217005	0.090127132	0.015916695
Mn	0.243037408	-0.312385012	-0.872914926
Fe	0.315964503	-0.304967309	0.132490461
Zn	0.278537645	0.460491105	-0.075027984
Rb	0.276508297	-0.507414608	0.195941029
Sr	0.314382679	0.034877055	-0.097701014
Zr	0.324614619	0.031078499	0.069953335
Pb	0.294538743	-0.348576454	0.316783516

The behaviour of Cu and Y across sedimentary units I and II reflects patterns described for the Si, Ti, K, Ca, Rb, Ba, Cr Sr & Zn data above, with peaks and troughs corresponding to units IIa and IIb respectively. This is, to a degree, replicated by Zn and Ni up to 357 cm, after which these data undergo several high amplitude fluctuations before dropping to consistently

low values between 280 cm and 132 cm. The Pb record displays two major peaks at the base of the core (high points at 516 cm and 450 cm), after which it switches to behaviour more characteristic of the Cu record. Pb accounts for the maximum variance along unit II PC1 (55.2%) (figure 4.13) and, with Ni and Zn, accounts for the maximum PC2 variance for unit I (18.6%) (figure 4.14).

Cu, Zn, Y and Ni, and Pb disassociate across Unit III. The former group displays a strong negative correlation with Fe and Mn and strong positive correlation with the Zr, Rb and Sr. Pb, on the other hand, strongly correlates with Mn (r = 0.87), Fe (r = 0.89) and Rb (r =0.72). These relationships are reflected along the first principal component for unit II (49.3% variance).

The heavy metal data reassociate with each other and with Si, Ti, K, Ca, Rb, Ba, Cr Sr & Zn in Unit IV (figure 4.17)

4.3.2 Yeak Loam (cores YL1211B & YL1211A)

Stratigraphy

The master (YL1211B) and replicate (YL1211A) gravity cores extracted from Yeak Loam were 2.14 m and 1.82 m long respectively (table 4.2). Sediments therein comprise fine-grained muds and sapropel (see figures 4.19 and 4.18 for detailed logs and core images). Upon oxidation, core sediments developed fine, horizontal, planar, orange-brown laminations (presumably iron oxide) on the exposed surface. This accounts for the fabric-difference (laminated vs. massive) in the logs produced for YL1211A (logged 7-months post-splitting) vs. YL1211B (logged immediately post splitting, but noting that the photograph presented on figure 4.19 was taken during I-TRAX analysis of the core, conducted several months after it was logged).

Fine clastic materials make up the principle component (sensu Schnurrenberger et al. (2003)) of YL1211B. These include quartz (clear under plane-polarised light and displaying undulose extinction under cross polarised light) and an opaque mineral that has been tentatively classified as an iron oxide. Following microscopic analysis, core sediments were divided into two units. Unit I, extending from 214 cm to 111 cm comprises silt loam. Sediments overlying this layer have been classified as a separate layer (unit II) given that they consist of a slightly more organic silt loam material. Discreet, silty beds occur within this layer at 69 to 75 cm (sub unit IIa) and 0 to 4 cm depth (sub unit IIb). The dominant non-clastic core component observed in YL1211B comprises sapropel (approx. 15% to 20% in unit I and 20% to 25% in unit II) that occurs alongside a low abundance of charcoal fragments and sponge spicules (<5%). No diatoms, chironomid head capsules or other common microfossils (excluding pollen and spores) were noted in any of the smear slides.

YL1211A sediments, which were not subjected to smear slide analysis, are classified as a single unit (sapropelic mud/fine sapropel).

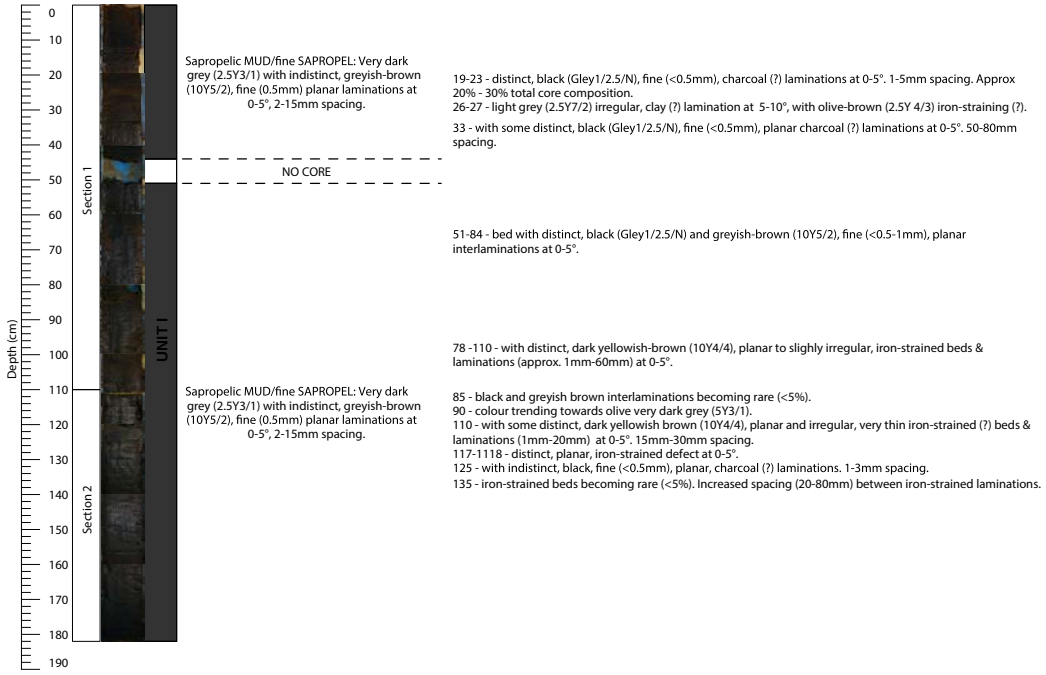

FIGURE 4.18: Photograph and log for core YL1211A.

Chronology

The conventional and calibrated (yrs BP) ages for ^{14}C date samples submitted from YL1211A and YL1211B are presented in tables 4.6 and 4.7, respectively. The distribution of the calibrated ages returned from the 16 dated YL1211B samples plotted against depth is shown on figure 4.20.

TABLE 4.6: Table of the conventional and calibrated (yrs BP) ages of ^{14}C date samples submitted from YL1211A.

Lab ID	depth (cm)	^{14}C date BP $\pm 1\ \sigma$	material	calibrated age (2 σ) (cal. yrs BP)	probability (%)
351537 (Beta)	16.0 - 16.5	2160 $\pm$ 30	bulk organic	2550	0.1
				2622 - 2627	0.4
				2707 - 2794	92.8
				2823 - 2842	1.7
351538 (Beta)	85.5 - 86	3670 $\pm$ 30	bulk organic	3832 - 3991	90.6
				4042 - 4071	4.4
351539 (Beta)	177 - 177.5	3530 $\pm$ 30	bulk organic	3727 - 3749	1
				3763 - 3793	5.1
				3821 - 3979	86.3

YL1211B

The mid core and basal bulk organic samples submitted from YL1211B core at 87.5 to 88 cm and 209.5 to 210 cm depth (green on figure 4.20) returned

TABLE 4.7: Table of the conventional and calibrated (yrs BP) ages of ^{14}C date samples submitted from YL1211B.

Lab ID	depth (cm)	^{14}C date BP $\pm 1\ \sigma$	material	calibrated age (2 σ) (cal. yrs BP)	probability (%)
D-AMS 005779	12.5 - 13.5	insufficient material	>105 μm charcoal with some organic material	n/a	n/a
D-AMS 005057	15 - 15.5	2639 ± 29	>250 μm charcoal with some organic material	2624 - 2626	0.2
				2709 - 2793	93.5
				2827 - 2841	1.2
351540 (Beta)	19 - 20	insufficient material	bulk organic	n/a	n/a
OZT362	35.5 - 36.5	3630 ± 35	>250 μm charcoal fragments - small sample	3783 - 3785	0.2
				3828 - 4001	87.9
				4034 - 4080	6.9
D-AMS 005058	70 - 70.5	3599 ± 25	>250 μm charcoal with some organic material	3730 - 3745	2.2
				3769 - 3790	3.4
				3826 - 3977	89.4
D-AMS 005780	71 - 72	3429 ± 29	>105 μm charcoal with some organic material	3569 - 3725	89.6
				3752 - 3761	1.1
				3794 - 3820	4.3
D-AMS 005059	80.5 - 81	3565 ± 27	>250 μm charcoal with some organic material	3708 - 3920	95
D-AMS 005781	84 - 85	3380 ± 34	>105 μm charcoal with some organic material	3481 - 3537	14.9
				3546 - 3654	67.2
				3656 - 3693	12.8
351541 (Beta)	87.5 - 88	3620 ± 30	bulk organic	3778 - 3787	0.8
				3827 - 3989	91.8
				4044 - 4068	2.5
D-AMS 005060	125 - 125.5	3817 ± 27	>250 μm charcoal with some organic material	4011 - 4028	1.3
				4082 - 4294	93.3
				4335 - 4337	0.2
				4342 - 4345	0.3
D-AMS 005782	126 - 127	3291 ± 30	>105 μm charcoal with some organic material	3401 - 3433	7.5
				3441 - 3576	87.4
OZT363	144.5 - 145.5	4010 ± 35	leaf fragments	4298 - 4327	2.9
				4353 - 4369	1.8
				4386 - 4539	87.4
				4541 - 4569	2.9
D-AMS 005783	174.5 - 175	2758 ± 34	>105 μm charcoal with large leaf fragment some organic material.	2758 - 2894	89.4
				2901 - 2924	5.6
D-AMS 005061	175 - 175.5	3627 ± 29	>250 μm charcoal with some organic material	2758 - 2894	89.4
				2901 - 2924	5.6
OZT364	202.5 - 203.5	4080 ± 50	>250 μm charcoal fragments - small sample	4419 - 4657	76.5
				4667 - 4707	6
				4756 - 4811	12.5
D-AMS 005784	206 - 207	2603 ± 37	>105 μm charcoal with some organic material	2497 - 2596	23.5
				2612 - 2637	7.4
				2686 - 2774	64.1
D-AMS 005062	208.5 - 209	3605 ± 30	>250 μm charcoal with some organic material	3728 - 3747	2.4
				3765 - 3792	3.6
				3823 - 3982	89
351542 (Beta)	209.5 - 210	3580 ± 30	bulk organic	3721 - 3801	23.2
				3811 - 3931	66.5
				3942 - 3968	5.2

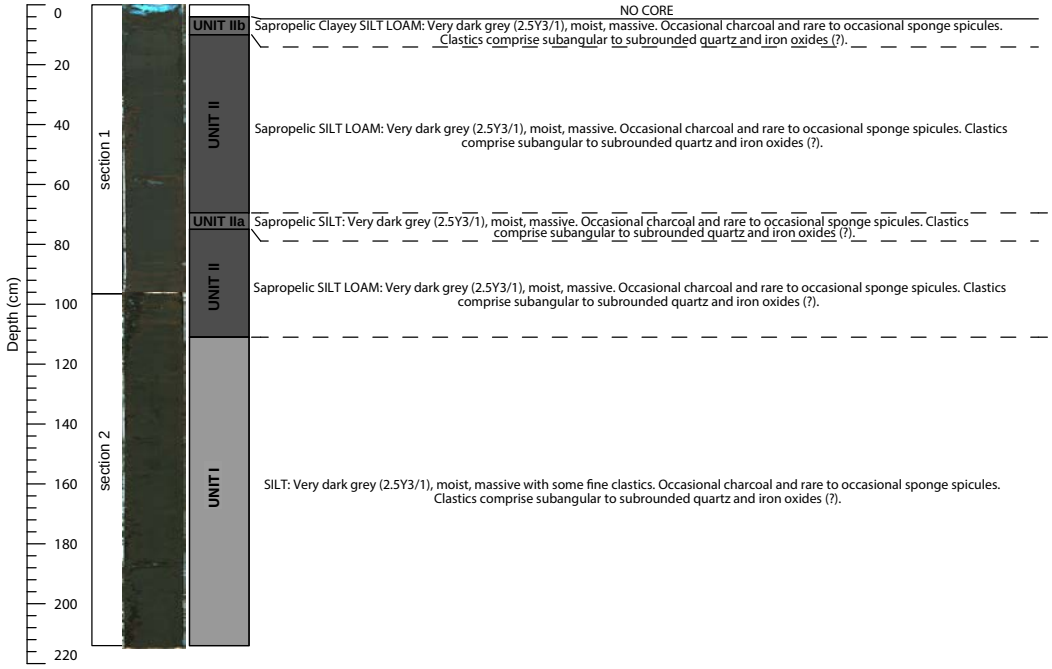

FIGURE 4.19: Photograph and log for core YL1211B.

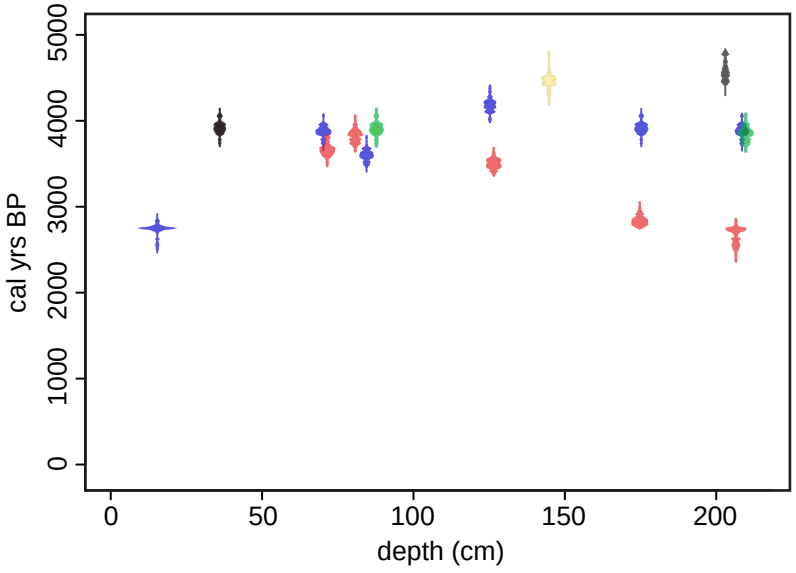

FIGURE 4.20: Bacon plot showing calibrated age probability distributions (yrs BP) of all YL1211B ^{14}C dated samples plotted against depth. Green - bulk organic samples; Blue - batch 1 charcoal and organic samples; Red - batch 2 charcoal and organic samples; Black - batch 3 small charcoal samples; Yellow - leaf fragments sample.

remarkably similar ages of 3827 to 3989 cal. yrs BP and 3811 to 3931 cal. yrs BP, respectively. The third bulk organic sample submitted for dating from 19 to 20 cm (Beta 351540) was not dated due to it being of insufficient size. A relatively consistent age across all depths was also observed from the results of the 11 batch 1 and batch 2 charcoal and organic material samples submitted for dating (respectively, blue and red on figure 4.20), noting

that the sample submitted from 12.5 to 13.5 cm (D-AMS 005779) was not dated due to its insufficient size. Samples from both batches tend to show a pattern of slightly decreasing age with depth from approximately 70 to 72 cm depth. This inflection point is dated at 3826 to 3977 (batch 1: D-AMS 005058) and 3569 to 3725 cal. yrs BP (batch 2: D-AMS 005780). The two small-sample isolated charcoal samples from 35.5 to 36.5 cm and 202.5 to 203.5 cm (black on figure 4.20), as well as the small leaf fragment sample selected from 144.5 to 145.5 cm depth (yellow on figure 4.20) show a pattern of increasing age with depth. In general, these samples returned ages older than other samples dated from this core (table 4.7).

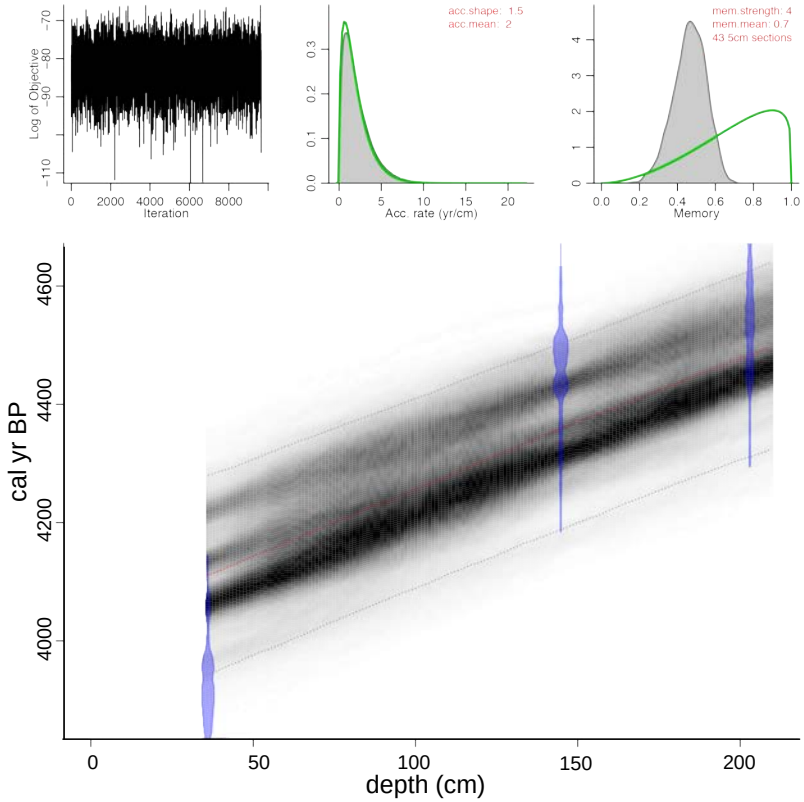

FIGURE 4.21: Bacon Age-Depth model produced from selected YL1211B dates (OZT362 to OZT364). No ages are modelled for sediments shallower than 35.5 cm depth due to age uncertainties.

The spread of the bulk organic and batch 1 and batch 2 charcoal and organic material samples (i.e. their tendency to cluster around 3000 to 4000 cal. yrs BP regardless of depth), suggests that these samples may be affected by local reservoir effects. This is speculated to be associated with sequestration of groundwater ^{14}C by aquatic algae or aquatic vegetation, which are retained in the samples and dated alongside terrestrial organic material. Given this, the small, isolated charcoal and leaf fragments (n=3), that displayed increased ageing with depth and were observed to represent a relatively "clean" terrestrial signal under microscopic analysis prior to radiocarbon analysis were selected for Bacon age modelling. The resultant model is shown in figure 4.21. The old age of the youngest samples from 35.5 to 36.5 cm (3828 to 4001 cal. yrs BP), suggests that, if this model is

accurate, it is likely that there is an hiatus in the lake sediments between 0 and 35.5 cm. The origin of this speculated break in sedimentation is uncertain, but may be associated with lake-bottom slumping. However, as no clear boundary in the sediments could be distinguished between these depths, no hiatus was used in the age model, and ages were only modelled for sediments between 36 cm and 204 cm depth.

Details of the results of the YL1211B samples processed for plant lipid extraction and plant microfossil extraction via density separation that were not submitted for radiocarbon dating are outlined in appendix C.

YL1211A

The three bulk organic sample submitted from YL1211A returned very similar ages to the YL1211B organic samples. The sample taken from towards the top of the core (16 to 16.5 cm) is dated at 2707 to 2794 cal. yrs BP. An age overlap occurs between the mid (85.5 to 86 cm at 3832 to 3991 cal. yrs BP) and basal (177 to 177.5 cm at 3821 to 3979 cal. yrs BP) core samples. Based on these results, the bulk organic samples are, (as with the bulk organic and batch 1 and 2 charcoal and organic matter samples extracted from YL1211B), expected to be contaminated by ^{14}C from the groundwater.

Bulk mineral influx, moisture content, dry bulk density & total organic content

Down-core changes in moisture content, dry bulk density and TOC (inferred from weight loss from loss on ignition at 550 °C) of YL1211B sediments are shown in figure 4.22. The latter two of these variables were used in conjunction with the age model produced for the core (discussed in section 4.3.2) to provide an estimation of down core changes in bulk mineral influx. This is estimated for core sediments extending between the shallowest (35.5 to 36.5 cm) and deepest (202.5 to 203.5 cm) dated samples (figure 4.22). Because of the relatively consistent sedimentation rate predicted by the age-depth model between the upper and lower dated points (min = 2, max = 2.4 years per cm), and minimal changes in TOC down-core, estimated influx data strongly correlate with the dry bulk density values calculated for the core (r = 0.885).

The estimated TOC for YL1211B sediments ranges from 17% (151 cm) to 24.5% (61 cm) of the sample dry mass. A 3% increase in overall core organic is observable up core of 136 cm. While the dry bulk density of the core sediments shows high frequency fluctuations between samples, ranging from 400 kg/m^3 (178 cm) and 900 kg/m^3 (43 cm), there is no observable trend in this variable with depth. The moisture water content of the sediments varies from 69% (14 cm) to 77% (146 cm depth). Drier sediments are located close to core gaps (e.g. 192 to 193 cm), and proximal to the core top and core base sediments. Thus moisture content appears to be more a product of physical core location (i.e. exposure to air) than due to any changing sedimentary properties of the core.

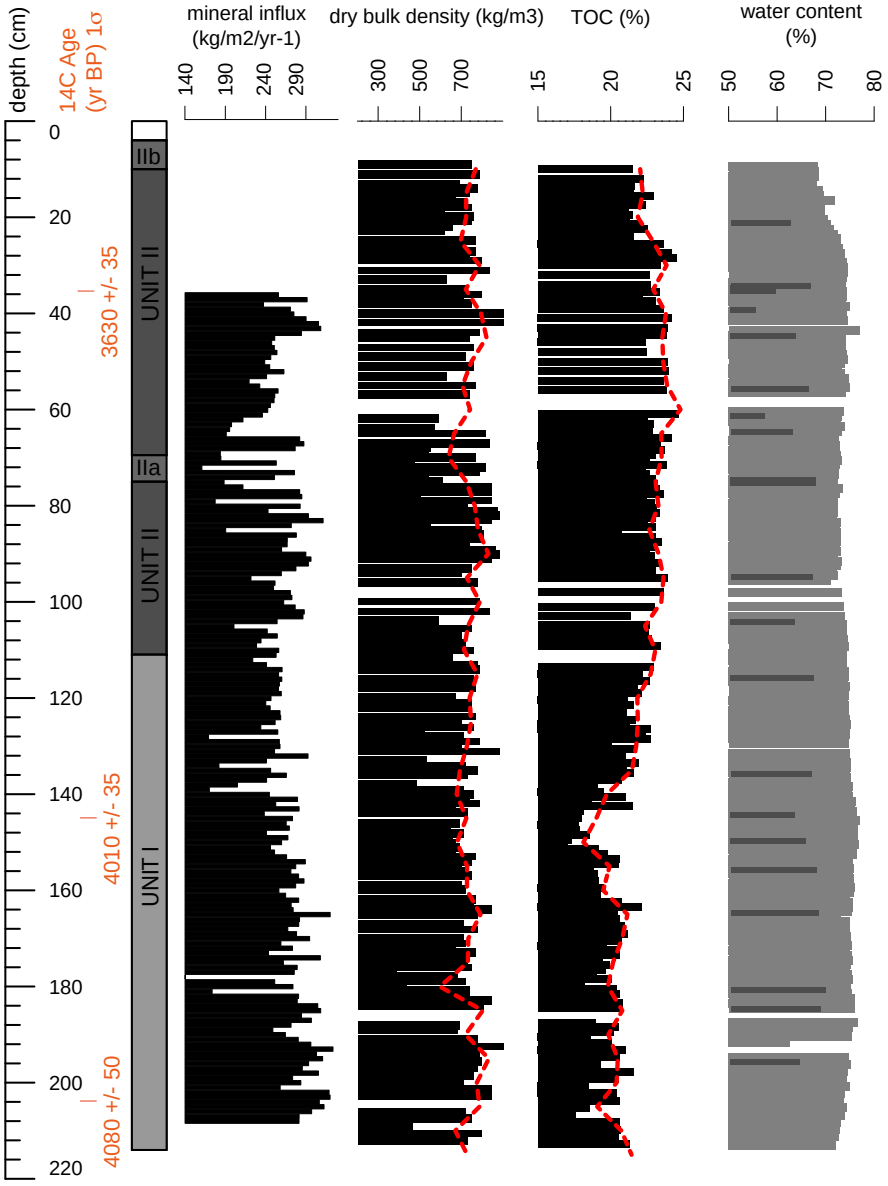

FIGURE 4.22: Down core plot showing estimated mineral influx, dry bulk density, moisture content and total organic content of YL1211B core sediments. The red overlays represent the 5 cm running mean for dry bulk density and total organic carbon calculations. Replicate moisture content measurements taken from the YL1211B master core in September 2015 are represented by dark grey-bars overlaying the moisture content graph.

Environmental magnetism

There is a major discrepancy between the mean down-core κSI values obtained from YL1211A (mean = 2.3 $\times$ 10^{-5}, n = 334) and YL1211B (mean = 9 $\times$ 10^{-5}, n= 390). This has been attributed to the time lag between splitting and analysing YL1211A for magnetic susceptibility, which permitted the sediments to dry, thereby reducing the overall proportion of water (diamagnetic) from the sediments.

A strong correlation was found between the master and replicate Yeak Loam core records in CPL slot (r = 0.89) (figure 4.23). This indicates that core sediments are probably representative of the lake centre stratigraphy, and that the YL1211B record is approximately 16 cm longer than the YL1211A record when the differential compaction and core gaps between the two samples are accounted for. Core correlation specifics are presented in appendix D.

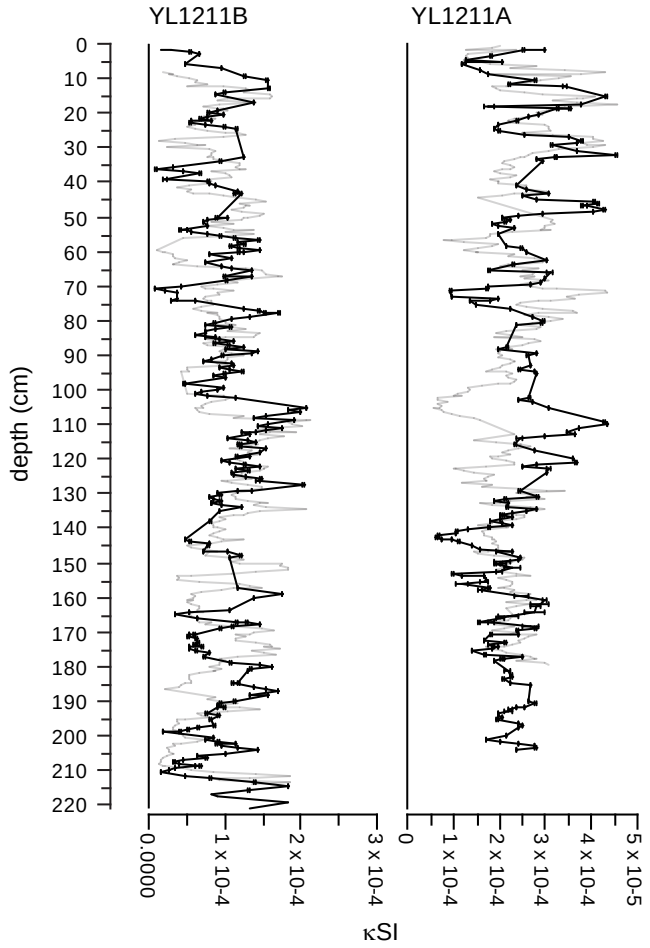

FIGURE 4.23: Graphs showing depth-corrected, correlated κSI plots for master (YL1211B) and replicate (YL1211A) Yeak Loam cores. Data are shown relative to their original depth-position (light grey line).

Magnetic properties

Discussion of the down-core magnetic behaviour will focus on the master core (YL1211B) sediments.

Volumetric magnetic susceptibility

All measurements indicate that core sediments display transitionary behaviour between homogenous diamagnetic and paramagnetic materials (Dearing 1999a). Peaks and troughs that fall outside a 1σ buffer plotted about

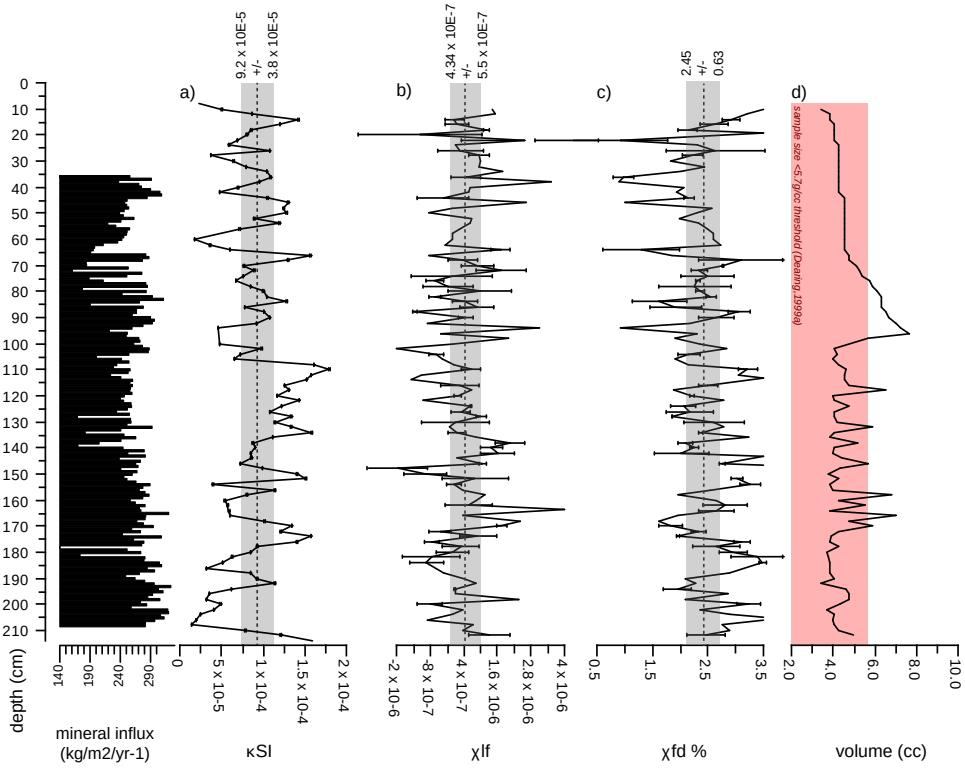

FIGURE 4.24: Down core fluxes in YM0413B volumetric (a) and mass-specific (b & c) magnetic susceptibility plotted alongside estimated mineral influx. The grey bars show a 1σ buffer zone about the mean core values (dotted lines). The red zone overlain on the volume size plot (d) shows the range of samples that fall below the minimum size recommended for mass specific magnetic susceptibility analysis (Dearing, 1999a).

the mean down-core κSI value (used in attempt to delimit any meaningful changes outside of the range of background variability) recur with relative frequency down core (figure 4.24 graph a). The dominant "zone" of higher-than-average κSI occurs between 108 and 134 cm and at the base (211 to 213 cm) of YL1211B. YL1211B κSI is negatively correlated with bulk mineral influx (r = -0.206).

Frequency dependent mass-specific magnetic susceptibility

Results of mass-specific magnetic susceptibility for YL1211B sediments are presented in figure 4.24 (graphs b and c). As with the κSI record, both χlf and χfd$_{\%}$ show high-resolution, low amplitude fluctuations down core. χfd$_{\%}$ values fall within the range of 1.5 to 3.5%, indicating that core sample is dominated by non-super-paramagnetic grains.χlf values show very weak (and occasionally negative) magnetism of the samples. These are not well correlated with corresponding κSI data (r = -0.03 [insignificant]). This may either reflect variations in dry bulk density/pore water content between the two measurement protocols, or a degree of experimental error vs. the core sediment properties, as discussed below.

The mass specific magnetic susceptibility data are approached as semiquantitative given that only 18% of the 149 samples processed were at, or above, the minimum sample volume (>5.7 g/cm^3) recommended by Dearing (1999a). Seventy-five percent of samples were less than 5 g/cm^3, 19.5% below 4 g/cm^3, and 0.6% (one sample at 185 cm) below 3 g/cm^3 (figure 4.24 plot d). These results should be treated cautiously given the linear relationship between sample volume and χlf (in the positive sign) and χfd$_{\%}$ (in the negative sign) (see appendix D for details). Sample data demonstrate that there is indeed a significant, negative correlation between χlf and χfd$_{\%}$ (r = -0.6). However, despite the fact that lower-than-adequate volume size are expected to yield lower χlf SI values (and thus correspondingly higher χfd$_{\%}$), there is no significant correlation between χlf and sample volume (r = 0.05 [insignificant]), and only a weak negative relationship between χfd$_{\%}$ and sample volume (r = -0.19). This suggests that core sedimentology is, to a degree, reflected in the mass-specific magnetic susceptibility records.

Grain size analysis

YL1112B was sampled at contiguous, 5 mm intervals between 4 and 100 cm, and every 1 cm between 100 and 212 cm depth (plus at 212.5 cm) for textural analysis. This change in sampling resolution was due to the relatively minimal change in grain size distribution with depth when initial samples were plotted. The resultant textural properties of YL1211B clastics are shown in figure 4.25. Silt is the dominant size fraction across the core sediments, making up between 50% (100 cm) to 97% (171 cm) of samples analysed. Overall, mean sand content is slightly higher in stratigraphic unit II (13.5%) than unit I (10%), though peaks in sand content occur throughout. The proportion of sand in each sample is unsurprisingly correlated with mean grain-size (r = 0.77). The proportion of clay in each sample fluctuates from 2% (171 cm) to 13% (100 cm).

The relative proportion of silt, clay or sand within each sample analysed appears to control the shape of their respective sediment distribution in terms of sorting, skewness and kurtosis. Higher silt percentages show a strong, negative correlation with sorting (r = -0.9), and a moderately strong relationship with the skewness (r = 0.39) and kurtosis (r = -0.35). In the context of the Yeak Loam sediments, silt is associated with very poorly sorted samples with symmetric to coarse skewed, mesokurtic to playkurtic distributions. The relative proportion of sand in each sample is also negatively correlated with kurtosis (r = -0.2), but is positively correlated with sorting (r = 0.48), and displays no significant relationship with sample skewness (r = 0.058). Sand is therefore associated with mesokurtic to playkurtic, poorly sorted sample distributions. The percentage of clay in sample displays a strong positive relationship with both sorting (r = 0.70) and kurtosis (r = 0.72), and a negative relationship with skewness (r = -0.62). Clay rich samples thus tend to be poorly sorted, leptokurtic and fine skewed to very fine skewed.

Stratigraphically constrained cluster analysis of down core changes in mean grain size, sorting, kurtosis and skewness identified three primary sample clusters at 136 cm (1.25×10^4) and 72 cm (7×10^3) (dissimilarity distances

bracketed). These form the boundaries of the three major clusters distinguished for the core (A,B and C) as delineated on figure 4.25. These clusters have each been further subdivided into two sub-clusters.

Cluster A extends from 213 cm to 136 cm depth. At the base of the core, there are two beds characterised by a relatively high proportion (20 to 24%) of clay from 210.5 to 208.5 cm and 204 to 196.5 cm, coincident with peaks in sorting (very poorly sorted). Above these peaks, cluster A samples are typified by relatively high-amplitude, moderately uniform, regular fluctuations in kurtosis (from extremely leptokurtic to mesokurtic) and skewness (from very fine/fine skewed to symmetrical). These shifts are apparently controlled by the regular fluctuations in the relative proportion of sand, silt, and especially clay (from 2 to 5% to 15 to 18%) every 2 to 6 cm. The subdivision of cluster A at 187 cm (dissimilarity distance = 4.8×10^3) reflects an overall increase in the proportion of sand (and corresponding decrease in clay) in subcluster Aii vs. subcluster Ai samples.

Cluster Bi samples (135 to 110 cm) display similar sorting and mean grainsize distributions to underlying sediments, presumably due to the relatively constant proportion of silt across this division. An increase in the relative proportion of sand to clay in cluster Bi samples does, however, change trends in kurtosis and skewness. In particular, the grainsize distribution of samples analysed in this zone are mesokurtic to playkurtic and symmetrical to coarse skewed.

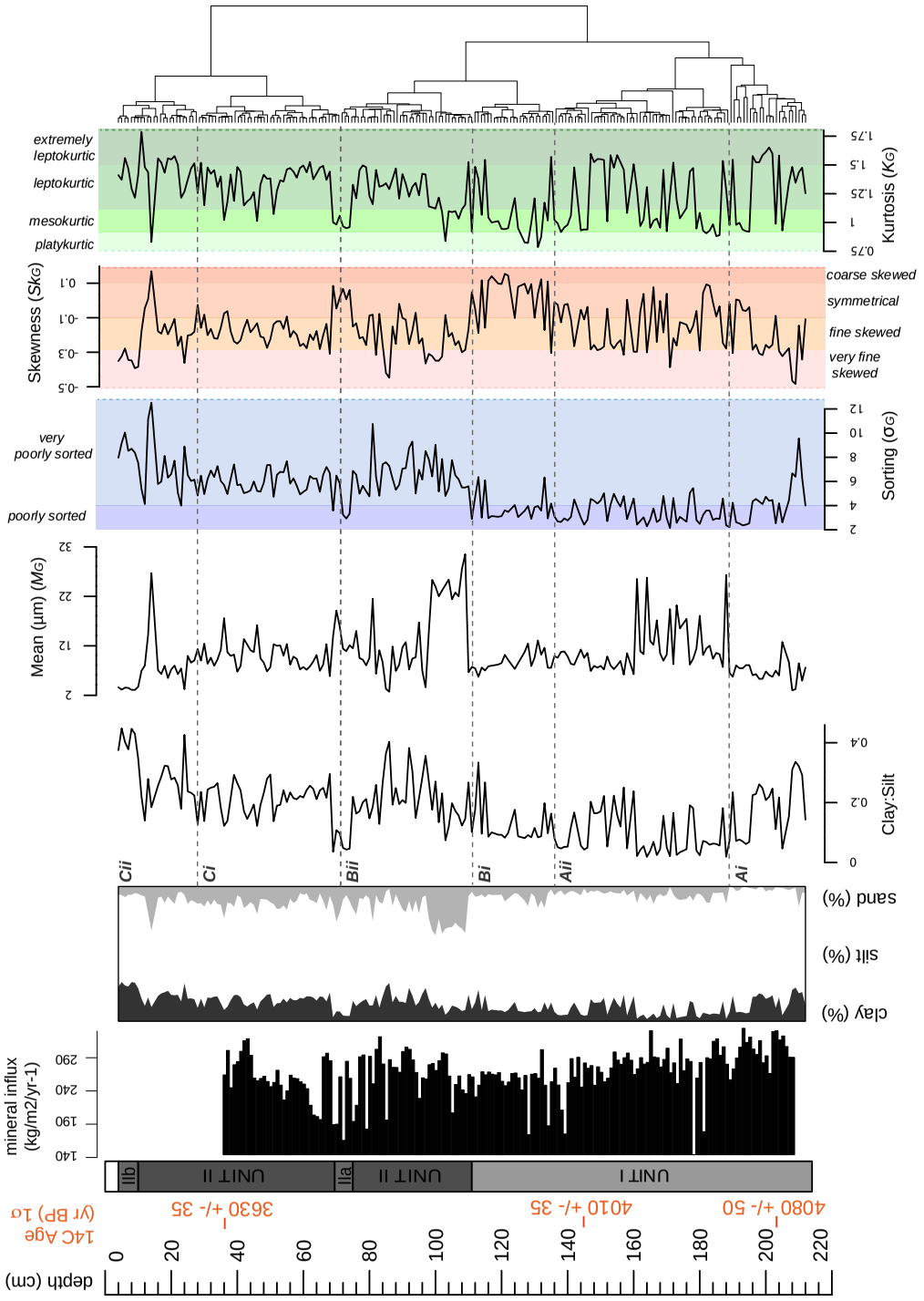

FIGURE 4.25: Textural properties of YL1211B sediments that have been classified following Folk and Ward (1957) parameters in Gradistat version 8 (Blott and Pye, 2001). Results have been grouped using a stratigraphic constrained analysis of the variables presented. Data shown relative to estimated mineral influx.

The subdivision between clusters Bi and Bii at 110 cm (dissimilarity distance = 3.3×10^3) captures the base of a band of comparatively sand-rich, very poorly sorted sediment (109.5 to 99 cm — approximately 30% sand), reflecting the boundary logged between stratigraphic units II and I.

The division between clusters B and C at 72 cm depth is defined by a temporary drop in clay abundance to approximately 3% between 74 and 69 cm. Between 69 and 24 cm, the overall amplitude of fluctuations between sand, silt and clay declines. Cluster Ci is distinguished from cluster Cii at 35 cm (dissimilarity distance = 4×10^3) by a slight increased proportion of clay- and silt-sized sediments. A sharp peak in sand abundance to 32% occurs within cluster Cii at 14 cm (32%). Sediments between 11 cm depth and the core-top sample (4 cm) are relatively clay rich (average of 27%).

Geochemistry

Normalisation

A correlation matrix showing the relationship between measured water content, TOC and the inc/coh scattering ratio obtained from XRF scanning of YL1211B is presented in table 4.8. Water content displays a significant, strong relationship with inc/coh across the whole core (r = 0.693), though this relationship is much stronger for unit I (r = 0.864) than for unit II (r = 0.345). This discrepancy likely reflects the negative relationship that exists between total organic carbon and pore water content in Unit I (r = -0.217) and the moderate positive correlation between these variables in Unit II (r = 0.527). Because both of these materials are elementally light and thereby produce high incoherent and low coherent scattering, the inc/coh ratio presumably reflects the decoupling of these variables, perhaps giving more weight to water content as it makes up a greater proportion of the core sediment mass (approximately 74%). As such, it appears to be a suitable parameter for normalising the geochemical kcps data.

Geochemical behaviour of core sediments

Data preparation and synthesis

After elemental data that recorded no kcps values for over 5% of the samples were removed, remaining data were normalised to inc/coh ratios. These include, in order of decreasing abundance for the whole core, Fe, Ti, Mn, Rb, Zr, Ni, Sr, Ca, Zn, K, Cu, Pb and Si. During I-TRAX analysis, the cores were scanned as four separate sections, or runs. Scan one encompasses sediments from 0 to 60 cm depth, scan two from 60 to 96 cm, scan three from 96 to 188 cm depth, and scan four from 188 to 213 cm depth. Following normalisation of the selected elemental data, the Ni and Cu curves were obviously offset across the different core scan sections. As such these data were assumed to reflect experimental conditions vs. the "real" core geochemistry, and were selectively removed from the data set. The remaining normalised elemental data are presented on figure 4.26. The element ratios

TABLE 4.8: Pearson's correlation matrix for YL1211B showing relationship between total organic carbon (%) (TOC), water content (%) and inc/coh ratios (95% C.I.).

whole core - 0 cm to 213 cm			
	TOC	water content	inc/coh
TOC	1	r = -0.352, p = 7.93e-6, df = 151	r = -0.462, p = 2.96e-9, df = 147
water content	r = -0.352, p = 7.93e-6, df = 151	1	r = 0.693, p < 2.2e-16, df = 191
inc/coh	r = -0.462, p = 2.96e-9, df = 147	r = 0.693, p < 2.2e-16, df = 191	1
unit I - 0 to 111 cm			
	TOC	water content	inc/coh
TOC	1	r = -0.217, p = 0.05, df = 79	r = -0.237, p = 0.03, df = 78
water content	r = -0.217, p = 0.05, df = 79	1	r = 0.346, p = 0.0004, df = 98
inc/coh	r = -0.237, p = 0.03, df = 78	r = 0.346, p = 0.0004, df = 98	1
unit II - 112 to 213cm			
	TOC	water content	inc/coh
TOC	1	r = 0.527; p = 2.017e-6; df = 70	r = 0.364; p = 0.002; df = 67
water content	r = 0.527; p = 2.017e-6; df = 70	1	r = 0.864; p < 2.2e-16; df = 91
inc/coh	r = 0.364; p = 0.002; df = 67	r = 0.864; p < 2.2e-16; df = 91	1

selected for the core are presented on figure 4.27 (excluding Cu/Ti for the above-discussed reasons).

Analysis

The stratigraphically constrained cluster analysis performed on the normalised geochemical data splits the dataset into three major clusters — A to C — the boundaries of which occur between 200 and 210 cm depth (dissimilarity distance = 5.6×10^5) and 80 and 81 cm depth (dissimilarity distance = 8×10^5). Cluster B has been further divided into four sub clusters, Bi to Biv, the upper boundaries of which occur at 172 to 173 cm depth (3.35×10^5), 145 to 146 cm (3.4×10^5), 89 to 90 cm depth (3.7×10^5), and at the cluster B/C boundary at 80 to 81 cm depth (dissimilarity distances bracketed). Cluster C has been split into three sub clusters, Ci to Ciii, which are bounded at 61 to 62 cm depth (4.3×10^5), and 22 to 23 cm depth (4.75×10^5). The boundary between sub clusters Ci and Cii coincides with the experimental core scanning boundary discussed in section 4.3.2, and thus changes in the geochemical record across this boundary are treated with caution. The cluster and sub cluster boundaries for the normalised geochemistry data are shown on figure 4.26.

Elemental data have been grouped according to their whole-core associations, both to each other, and to the other sedimentological variables outlined in this chapter. These are outlined below.

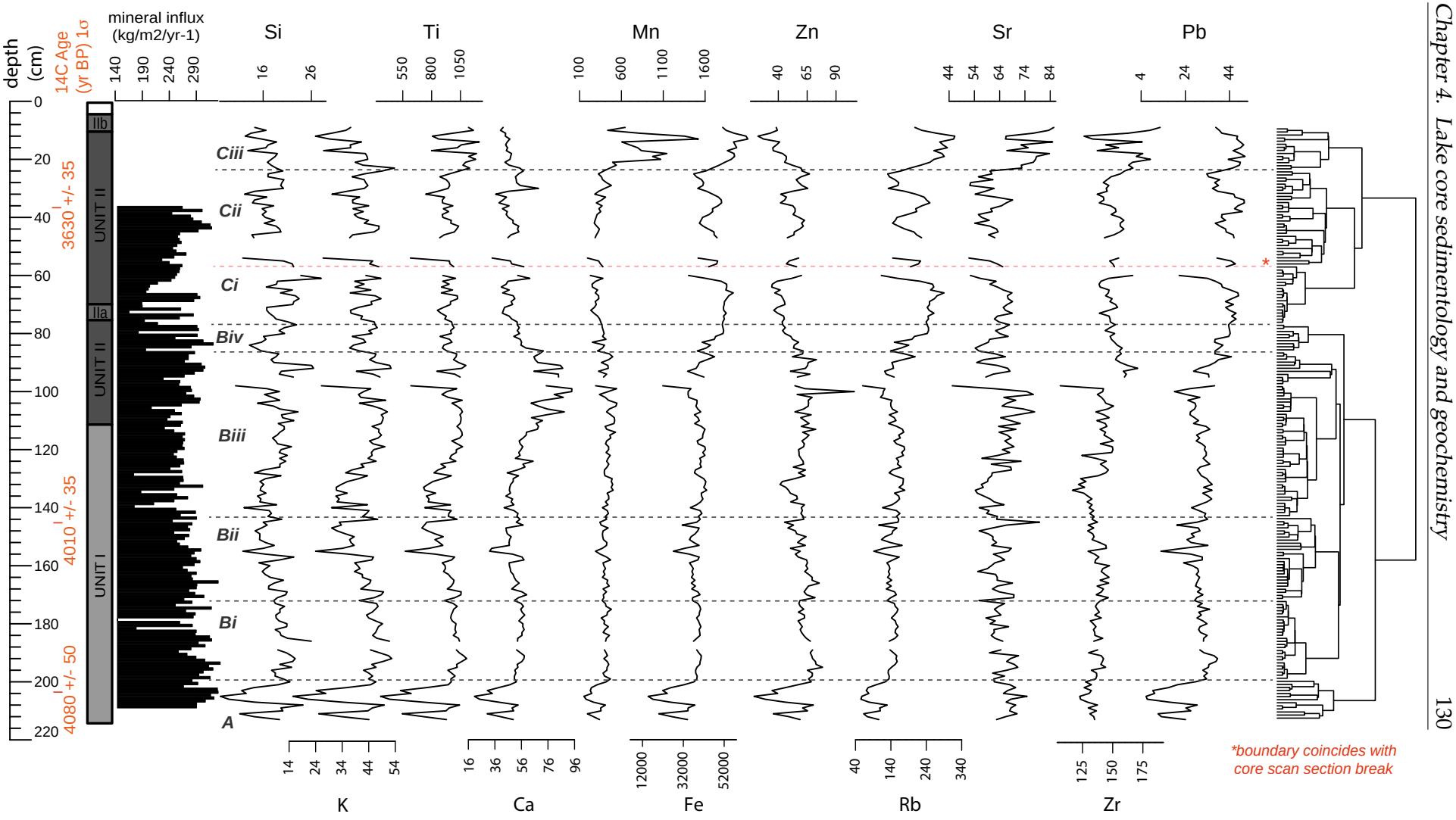

FIGURE 4.26: Plot showing YL1211B XRF geochemical data normalised to inc/coh scattering ratios.

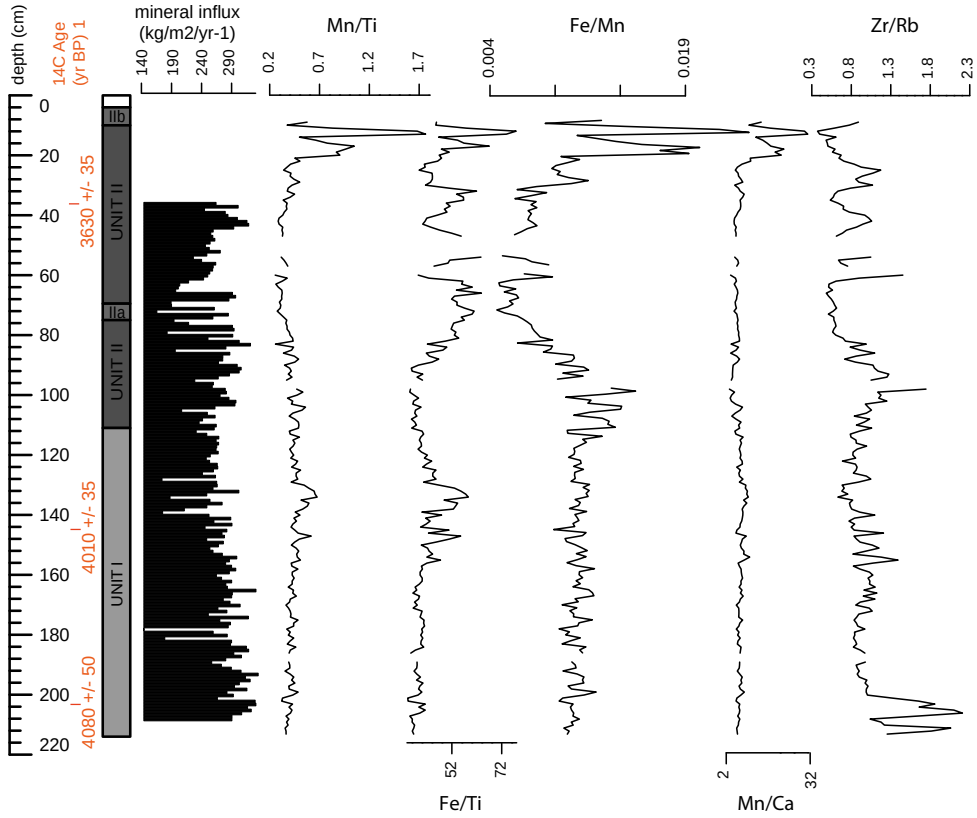

FIGURE 4.27: Plot showing downcore fluxes in selected geochemical ratios from YL1211B sediments.

Si, Ti & K, and Sr & Zr Si, K and Ti display similar behaviour with depth (r = 0.86 [Si and K]; r = 0.71 [Si and Ti]; r = 0.85 [K and Ti]). Correlation matrices are included in appendix E. This is reflected in the PCA, which shows close association of these elements with Sr and Zr along principle components (PCs) 1 and 2, that account for 79.7% and 10.5% of variance respectively (figure 4.28, table 4.9).

High amplitude fluctuations in Si, Ti and K are evident across cluster A. This pattern is reflected across all elemental data with the exception of Sr and Zr. Up core of cluster A, the Si and Ti and K data display high frequency, low amplitude fluctuations, largely reflected by Zr and Sr. A drop in the overall abundance of Si and K is apparent across sub cluster Ciii. An increase in the overall abundance of Ti, Sr and Zr is apparent in the same sub cluster, suggesting a decoupling of this element suite at approximately 22 cm.

Fe, Rb, and Pb show strong, positive correlations with each other (min. r = 0.87) and, along with Mn, contribute to the maximum negative loading along PC2 (figure 4.28, table 4.9). These elements all positively correlate with κSI (r = 0.18, r = 0.15, r = 0.16 respectively) and display insignificant, but positive associations with χlf. The same elemental data show a bimodal association with grain size, being positively correlated with clay and sand, and negatively correlated with silt (see appendix E for r values).

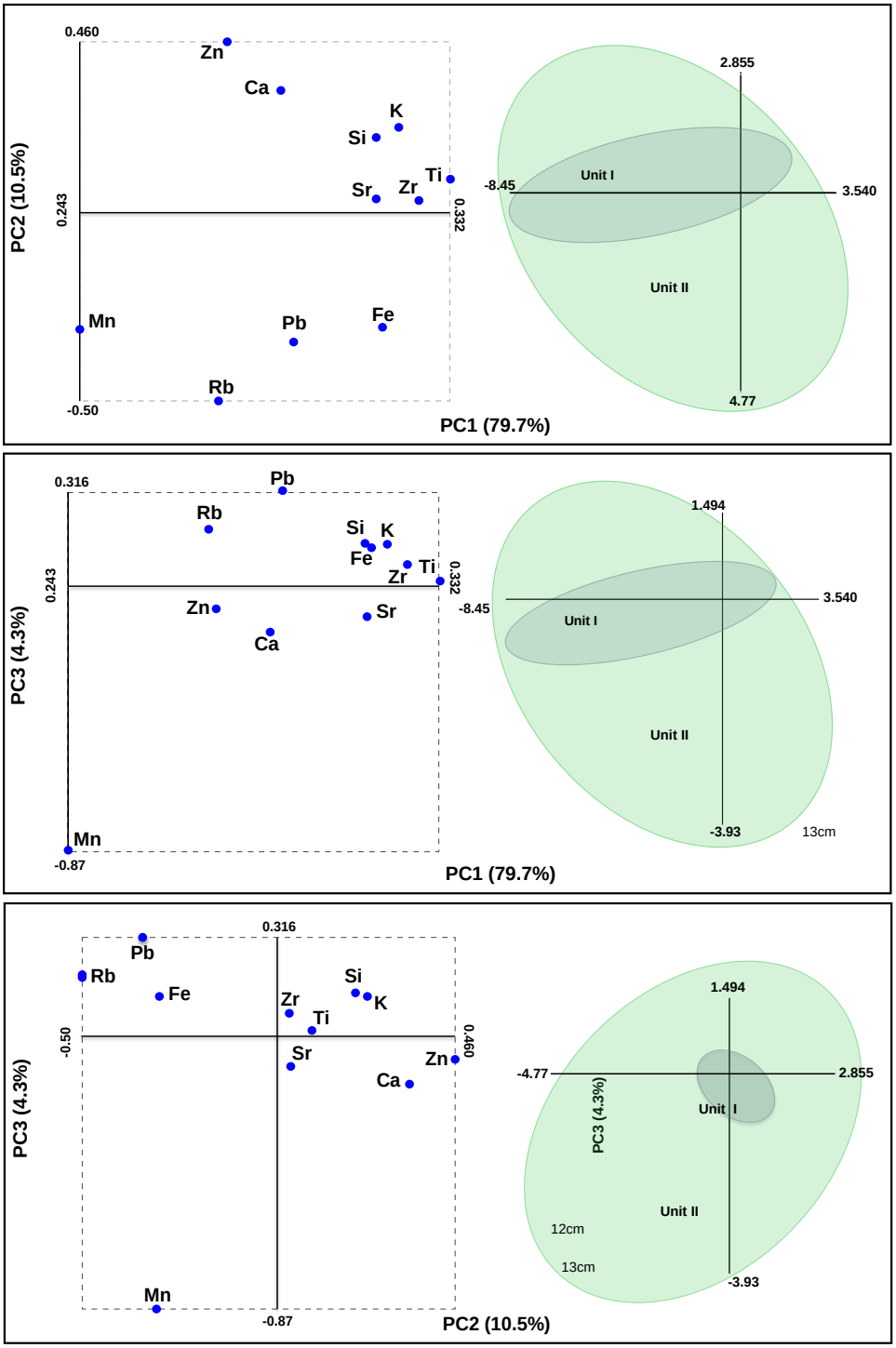

FIGURE 4.28: PCA plot for select elemental data from YL1211B.

After abruptly peaking and troughing across cluster A, the Fe, Rb and Pb data display very low amplitude fluctuations across sub cluster Bi to Biii. An upward trend in these data occurs across sub cluster Biv to a peak in cluster Ci. A second upward trend occurring alongside increased variability in these data can be observed across cluster Ciii.

Mn & selected elemental ratios Mn accounts for much of the variance in the PCA. It exhibits the largest control on PC 3 (-0.87), where it is quite isolated from the rest of the elemental data, and the second largest on PC2, where it associates with the Fe, Rb (r = 0.45) and Pb (r = 0.30) suite discussed above (table 4.9). Mn and Mn/Fe are the only variables that display a significant positive relationship with $\chi fd_{\%}$ (r = 0.17, r = 0.25).

TABLE 4.9: YL1211B eigenvalues, percentages and elemental variable loading from PCA of geochemical data.

	PC1	PC2	PC3
Eigenvalue	170.65	22.46	9.19
R2 (%)	80%	10%	4%
Q2 (%)	69%	35%	18%
Si	0.314289622	0.202665861	0.146476215
K	0.31977899	0.233624064	0.135193055
Ca	0.291069564	0.335297661	-0.147197782
Ti	0.33217005	0.090127132	0.015916695
Mn	0.243037408	-0.312385012	-0.872914926
Fe	0.315964503	-0.304967309	0.132490461
Zn	0.278537645	0.460491105	-0.075027984
Rb	0.276508297	-0.507414608	0.195941029
Sr	0.314382679	0.034877055	-0.097701014
Zr	0.324614619	0.031078499	0.069953335
Pb	0.294538743	-0.348576454	0.316783516

Relatively high, stable levels of Mn/Fe in YL1211B sediments occur between the core base and 114 cm depth. These then peak between 111 and 91 cm, and trough between 72 and 32 cm depth (figure 4.27). Two large peaks in this ratio occur within the core top sediments at 20 to 18 cm and 13 cm depth. These peaks correspond with large peaks in Mn/Ti and Fe/Ti data. Though Mn and Fe are positively correlated (r = 0.47), the Mn/Ti and Fe/Ti records, which are aimed at removing the detrital signal from the record, are negatively correlated (r = -0.31), largely reflecting the decoupling of these data sets between 95 and 35 cm depth (figure 4.27).

Ca and Zr/Rb Zr/Rb ratios, in some cases, relate to grainsize (Kylander et al. 2011, Chawchai et al. 2013). However, in the context of YL1211B sediments, there is a negative, insignificant correlation between this elemental ratio and sand (r = -0.106). Ca, on the other hand, shows a relatively strong relationship with the sand fraction of the core sediments (r = 0.46). Ca appears well correlated with the Si, Ti & K element suite from the core base to approximately 112cm depth (approximately coinciding with the boundary between logged sedimentary units I and II in mid sub cluster Biii (figure 4.26)). Up core of 112 cm, Ca peaks at approximately 104 cm depth before declining to approximately stable levels at 80 cm depth.

4.3.3 Yeak Oam (cores YO0712B & YO0712C)

Stratigraphy

The master (YO0712B) and replicate (YO0712C) gravity cores extracted from Yeak Oam were 1.75 m and 1.09 m long respectively (table 4.2). The sediments within comprise sapropel with some fine siliciclastic material (clay and silt sized). The core sediments are indistinctly horizontally laminated. A low fraction of charcoal (<5%) and irregular bands of macro organics (leaves and wood debris) were observed throughout the both cores (see figures 4.29 and 4.30 for detailed logs and core images). Two distinct beds of sediments, with grain sizes estimated from visual analysis to range from fine-sand to fine-gravel (possibly carbonates), were observed in YO0712B at 0 to 4 cm and 53 to 56 cm. These were not observed in YO0712C. A whitish-green clayey lamination at 38 cm was noted in YO0712B but not YO0712C (see figures 4.29, 4.30 and 4.31). This suggests that there may some stratigraphic differences between the two samples despite both cores preserving horizontal layering.

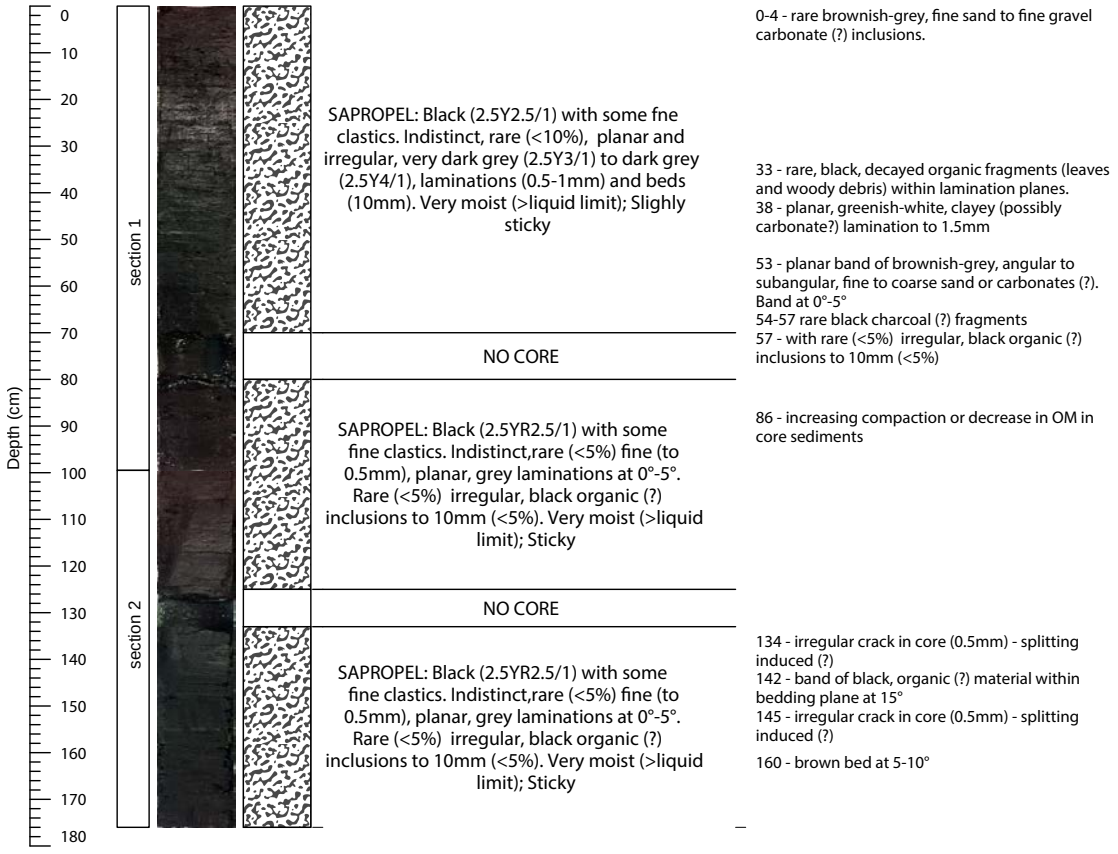

FIGURE 4.29: Photograph and log for core YO0712B.

Chronology

The conventional and calibrated (yrs BP) ages for the six ^{14}C date samples submitted from YO0712B and YO0712C are presented in table 4.10.

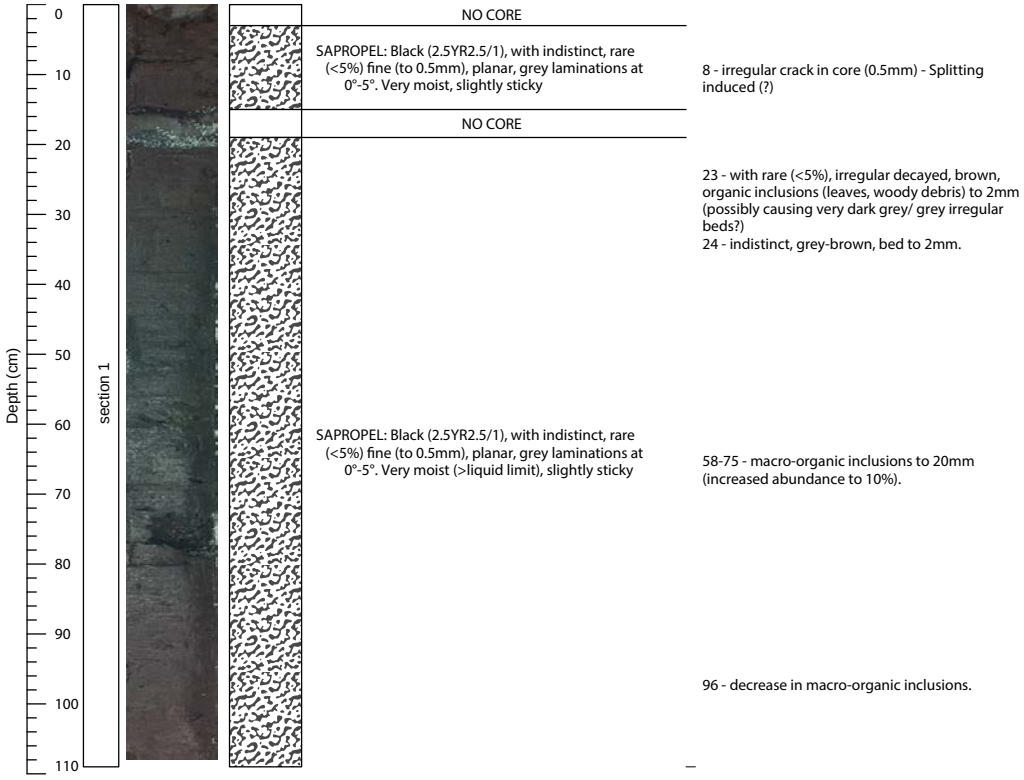

FIGURE 4.30: Photograph and log for core YO0712C.

The ages determined from leaf fragments show an expected increase in age with depth for core YO0712B. However, the ages derived from the wood & charred wood/charcoal samples from YO0712C are uniform down-core — all falling within the range of 1 719 to 1 832 yrs BP.

TABLE 4.10: Table of the conventional and calibrated (yrs BP) ages of ^{14}C date samples submitted from YO0712B and YO0712C.

Lab ID	depth (cm)	^{14}C date BP $\pm 1\sigma$	material	calibrated age (2σ) (cal. yrs BP)	probability (%)
351543 (Beta)	16.0-17.5	260 ± 30	leaf fragments with some algal material	152 - 213	23.4
				276 - 328	58.9
				378 - 391	2.1
				400 - 439	10.5
351544 (Beta)	62.0-62.5	470 ± 30	leaf fragments with some algal material	471 - 535	95
351545 (Beta)	172.0-173.5	1190 ± 30	leaf fragments with some algal material	980 - 1117	74
				1129 - 1177	20.8
351546 (Beta)	20.0-21.0	1850 ± 30	wood & charred wood/ charcoal with some algae	1792 - 1908	95
351547 (Beta)	56.0-57.0	1860 ± 30	wood & charred wood/ charcoal with some algae	1802 - 1918	95
351548 (Beta)	100.0-101.0	1830 ± 30	wood & charred wood/ charcoal with some algae	1772 - 1888	95

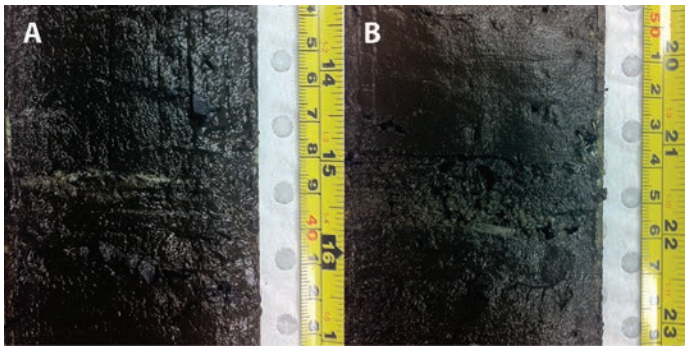

FIGURE 4.31: Photographs of distinct stratigraphic units identified in YO0712B core sediments that were absent in YO0713C, including (A) a planar, greenish-white clayey lamination (38 cm), and (B) a bed of angular and sub-angular sand and fine gravel (53 cm).

The age depth model produced for YO0712B is shown on figure 4.32 and predicts an increasing rate of lake sedimentation from the top to the base of the core. The mean accumulation rate between 0 and 17 cm is modelled at approximately 1 mm/year (noting that this uses the mean age line – a higher resolution chronology would be necessary to clarify). The sedimentation rate between 17.5 and 175 cm is predicted to be approx. 1.7 mm/year. However, as this model is currently based upon 3 dates, points of change are not well defined, and changes in accumulation rate may merely be a product of sediment compaction from coring vs. any "real" changes in the lake sediment regime.

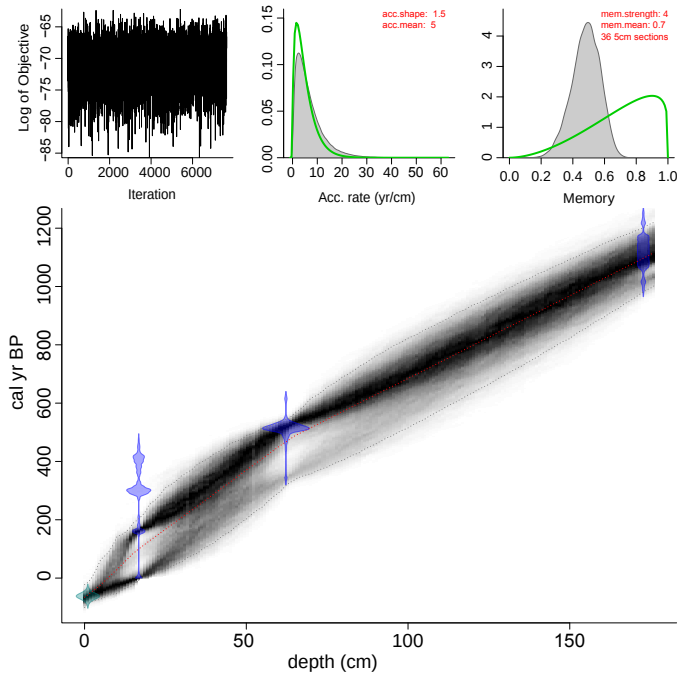

FIGURE 4.32: Bacon Age-Depth model produced from YO0712B dates.

An age-depth model was not produced for the YO0712C core. This is due to the fact that the uniformity of the ages produced for the core (*c.* 1800

to 1900 cal. yrs BP) is assumed to be related to the contamination of the date samples with a non-terrestrial source of carbon. This may be due to uptake of carbon from groundwater, as is described for the Yeak Loam sediments. This assumption is based on 1) the appreciable amount of algae observed in the wood and charred wood/charcoal samples submitted from this core and, 2) the stark comparison of these ages with those produced for YO012B. The approximate 1 500 to 2 000 year discrepancy between the "contaminated" ages returned from YO0712C vs. the Yeak Loam sediments may be linked to the amount of contaminant preserved within the different sample types submitted from the core sediments, or that the lake groundwater inflow is sourced from different reservoirs.

Environmental magnetism

Core correlation

Initial measurements of down core κSI from YO0712C (mean = 5×10^{-3}, n=184) are an order of magnitude larger than those taken from YO0712B (mean = 5×10^{-4} SI, n= 294). Retest measurements taken from YO0712B are marginally higher (mean = 7.5×10^{-4}) than initial measurements taken from the same depths (mean = 6.5×10^{-4}), while replicate measurements taken from YO0712C are, on average, 3×10^{-3} SI units lower than initial values (mean = 1×10^{-3} vs. 4×10^{-3} SI) figure 4.33. Despite these discrepancies — likely due to the difference in temperature and ambient magnetism between measurement periods in the context of diamagnetic materials — trends between initial and replicate measurements are markedly similar for both YO0712B (r = 0.85) and YO0712C (r = 0.93) (figure 4.33).

There is a reasonably strong correlation between the Yeak Oam master and replicate core κSI records (r = 0.715). CPL slot analysis indicates that both core records are approximately the same length (146 to 147 cm) when correlated (mostly correcting for the number of core gaps in the YO0712B record) (see figure 4.34 for depth corrected plots). Specifics of correlation results are presented in appendix D.

Magnetic properties

As YO0712B and YO0712C are well correlated, discussion of the magnetic behaviour of the sediments will focus on the master core, YO0712B.

Both the initial and replicate κSI measurements taken from this core indicate that core sediments display behaviour that falls into the transitionary zone between homogenous diamagnetic and paramagnetic materials (Dearing 1999a). Core sediments display high-frequency, low amplitude fluxes in κSI throughout, with no overall trend apparent down-core. There are three sections of the core where magnetic susceptibility peaks significantly above the 1σ range between 2.5 and 5 cm, 54 and 59 cm and at 103 cm depth (figure 4.35).

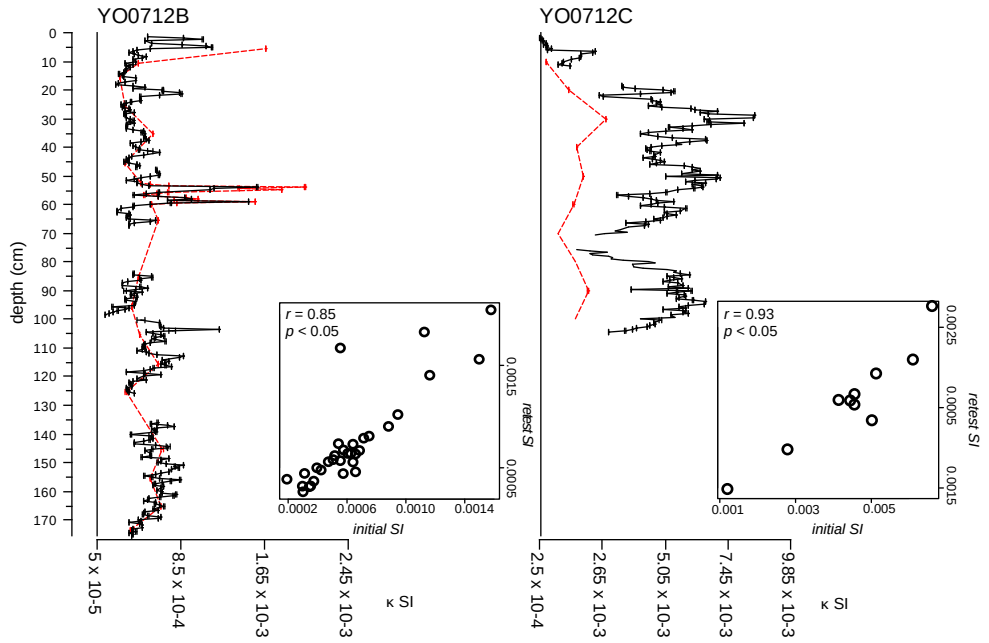

FIGURE 4.33: κSI for master (YO0712B) and replicate (YO0712C) Yeak Oam cores (black line) including lower-resolution retest measurements (red dotted line). Scatter plots show the correlation between the initial and replicate measurements.

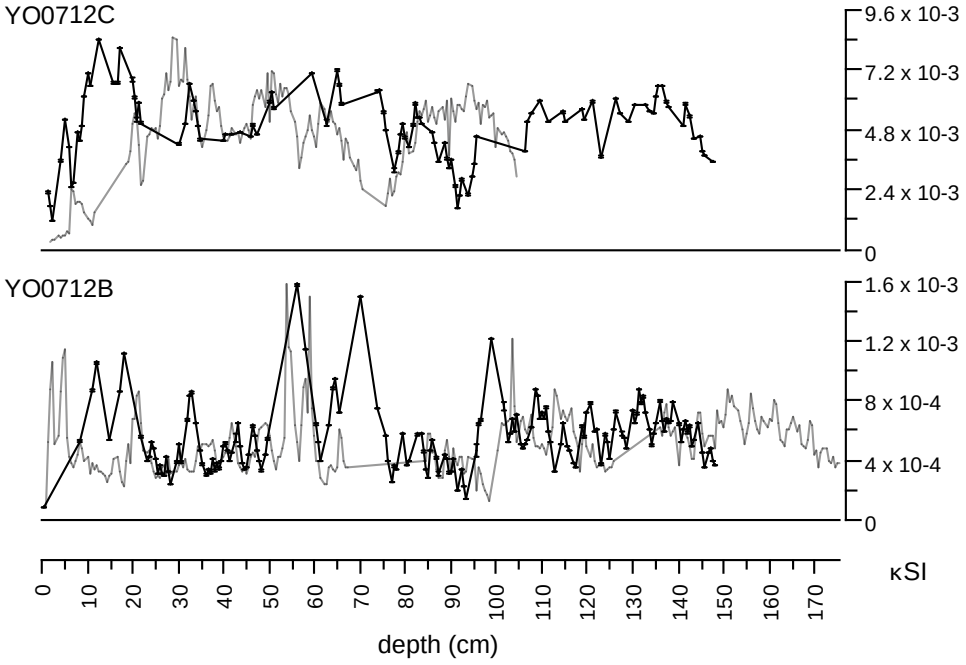

FIGURE 4.34: Graphs showing depth-corrected, correlated κSI plots for master (YO0712B) and replicate (YO0712C) Yeak Oam cores. Data are shown relative to their original depth-position (light grey line).

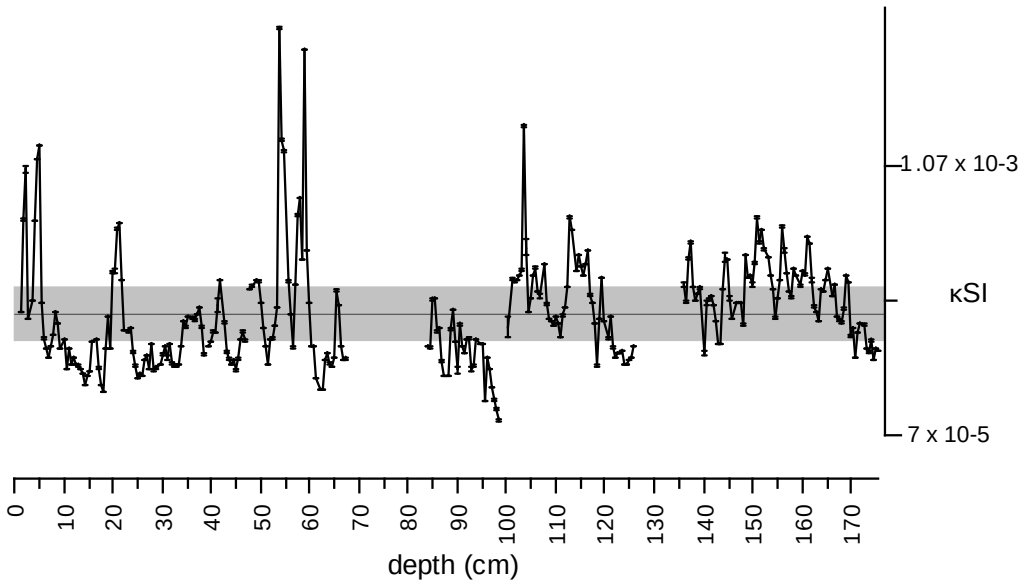

FIGURE 4.35: Down core fluxes in YO0712B volumetric magnetic susceptibility. The grey bar shows a 1σ buffer zone about the mean core value (solid grey line).

4.4 Overview: lake sediment input & deposition

4.4.1 Yeak Mai

The obvious changes in the Yeak Mai sedimentary record are the shifts between the organic (algal) rich sediment in core sedimentary units I, IIb, and IV, and more mineral-rich (organic poor), clayey silt sediment in units IIa and III. *Prima facie*, this suggests changing rates of 1) organic productivity, 2) allogenic catchment erosion, 3) endogenic chemically-mediated precipitation/dissolution of sediments, or 4) a combination of these factors.

Increased organic productivity across units I, IIb and IV seems plausible given the high relative abundance of algae in the sediments. However, it is expected that if variation in the lake sediments reflects biological productivity alone, the sedimentation rate for the organic-rich units would be higher than that of the mineral-rich units. This does not appear to be the case for Yeak Mai, with the age-depth model produced for this core indicating a high sedimentation rate across unit III. The chronological resolution across unit II is too low to determine if there is any difference in the sedimentation rate of sub unit IIa vs. IIb.

The vast rise in the mineral influx rates estimated for the core across sub units IIa and unit III (especially at the upper and lower boundaries) supports the idea of these layers representing zones of increased supply of detrital, siliciclastic material to the lake catchment via erosion of catchment soils. This idea appears to be backed by the overall increase in elemental proxies for detrital input across these units, including Ti, K and Rb (Kylander et al. 2011, Rothwell and Croudace 2015 and references therein), as well as Cr, Si and Ca. Peaks in the latter two of these elements occur in the absence of any noticeable biogenic sources. It is therefore likely that these

minerals are mainly derived from the erosion of the basaltic (and possibly sandstone) catchment, which presumably contains a relatively high proportion of Ca-plagioclase and silicon-bearing minerals. Similarly, the peaks in κSI, across units IIa and III may indicate erosion-related events (Thompson et al. 1975, Dearing 1999, Sandgren and Snowball 2001). Given the high magnetisability of the basaltic soils on the steep-sided, southern edge of Yeak Mai (presumably due to the high proportion of Fe-rich minerals within the mafic catchment soils), this interpretation makes sense. However, the high clay/low sand sediment characteristics of the major κSI and mineral influx peaks (as well as the fine overall texture of units IIa and III relative both to the rest of the core and the catchment sediments), seems incongruent with an interpretation of increased catchment erosion being the key driver of core sediment change. This is due to the typical association of runoff erosion with coarser-than-average grain sizes (e.g. Peng et al. 2005, Bhattacharyya et al. 2015).

Enrichment in fine, non-organic sediments within sapropels can occur when redox-sensitive elements (commonly Mn and Fe) precipitate under oxic conditions as endogenic oxyhydroxides (MnOx and Fe^{3+}) at the lake sediment/water interface and/or via diffusion into previously anoxic sediment (depending on the depth of the redox boundary) (Hamilton-Taylor and Davison 1995, Thomson et al. 1995, Thomson et al. 2006). Within the context of this study, these zones can be interpreted from the well-correlated peaks in Fe/Ti and Mn/Ti, noting that, because Ti appears to a reliable proxy for detrital influx to the lake, this ratio presumably decouples allogenic from endogenic sources of Fe and Mn in the lake sediments (Thomson et al. 2006, Gallego-Torres et al. 2007).

Within tropical mafic catchment settings, peaks in κSI can also indicate periods of endogenic precipitation of concentrated iron oxide during oxic phases of lake redox cycling (Williamson et al. 1998, Tamuntuan et al. 2015). Williamson et al. (1998) show that these iron oxides are derived from previously eroded ferromagnetic minerals within catchment soils that are concentrated from redox cycling. However, κSI as a redox proxy needs to be interpreted within the context of other indicators given that it is also commonly taken to represent periods of heightened surface erosion of detrital catchment materials (Dearing 2008, Bhagwat et al. 2012). Given that the volumetric susceptibility of Yeak Mai sediments positively correlates with detrital elements (all units) and the high Mn/Ti and Fe/Ti ratios in units II and III, it appears to be reflecting both erosion-related and redox cycling events, indicating that using peaks to infer either one requires corroboration with additional proxies. Coupled κSI, Fe/Ti and Mn/Ti peaks occur within YM0413B at 222 to 234 cm (*c.* 1748 to 1780 cal. yrs BP), 282 to 294 cm, (*c.* 1908 to 1949 cal. yrs BP), 328 to 330 cm (*c.* 2250 to 2268 cal. yrs. BP), 383 to 386 cm (*c.* 2701 to 2729 cal. yrs BP) and 448 to 453 cm (*c.* 3276 to 3350 cal. yrs BP) in sedimentary units III and IIa. This suggests that redox cycling of the lake may contribute to the differential sedimentary layers observed within the core. Notably, however, is a very large peak in Mn/Ti and Fe/Ti coupled with a small peak in κSI at 208 to 192 cm depth (*c.* 1680 to 1550 cal. yrs BP), occurring within sedimentary unit IV.

The combined peaks in κSI and redox sensitive elements within lacustrine

settings are commonly taken to represent oxic conditions driven by drying events (Williamson et al. 1998, Tamuntuan et al. 2015). If this is the case for the YM0413B record, sedimentary units III and IIa may be associated with weaker-than-present summer monsoon conditions. Within this setting, it is very possible that lake productivity may decline (Gasse and Van Campo 2001, Selvaraj et al. 2011, Selvaraj et al. 2012, Zhang et al. 2014). Low productivity can further facilitate oxidation of surficial lake sediments given that decomposition of lake organic matter – a process concentrated within lake sediments - consumes oxygen (Davison 1993, Hamilton-Taylor and Davison 1995). Given this, it is possible that the high proportion of fine-grained, non-organic sediment within YM0413B units III and IIa may be associated both with reduced lake productivity, and enrichment in Mn and Fe oxides. If the interpretation of deposition of unit IIa and III sediments under relatively dry, arid conditions is valid, it is conceivable that high elemental counts for the detrital elements within these units may be associated with deposition of wind-entrained sediment (Qiang et al. 2014) or from increased erosion of catchment sediments results from reduced canopy of ground cover.

4.4.2 Yeak Loam

Chronology and sedimentation

The greatest challenge posed with regard to reconstructing the sediment input to Yeak Loam is accounting for the perplexing chronology produced for the core, both with respect to 1) the homogenous ages returned from the dated samples that were rejected from the final age-depth model, and 2) the old age of the sediments predicted by the final age-depth model that was applied to the core. The rationale for rejecting the dates returned from the 14 bulk sediment and batch 1 and 2 charcoal and organic material samples from the age-depth model applied to YL1211B was introduced above, but is briefly expanded on below.

Contamination of ^{14}C date samples by an external source of carbon (i.e. carbon that is not derived from the targeted terrestrial organic matter) can result in relatively homogeneous ages and/or age reversals occurring downcore, regardless of depth, presuming that the contamination is consistent over time or the sediments are uniformly 'reset' in some way (e.g. Kilian et al. 2002). Both of these characteristics can be observed from the age-depth profiles produced for YL1211B from the bulk organic and batch 1 and batch 2 charcoal and organic material samples. Consequently, these sample materials were deemed unsuitable for producing a reliable age-depth model for the core sediments.

A common source of carbon contamination within deep, closed catchment lake settings is from groundwater inflow that can leach and entrain carbon from carbonate bedrock, soils, mineral matter and relict terrestrial organic material (Vance and Telka 1998, Uchikawa et al. 2008). This carbon can then be fixed and sequestered into the sediment by aquatic algae (Uchikawa et al. 2008). The appreciable amount of algae retained within the bulk organic

and charcoal and organic material samples submitted from YL1211B for radiocarbon analysis is presumed to be the key pathway for sample contamination with "old" groundwater ^{14}C. As such, the"clean" leaf and batch 3 charcoal samples that did not contain any algae and showed an aging-with-depth progression were considered more reliable for age-depth modelling.

It was initially expected that carbon contamination of the date samples was leading to anomalously old ages, especially for the shallower core samples, which were expected be deposited relatively recently (i.e. within the past couple of centuries). However, comparison of the ages returned from the samples that were presumed to be contaminated, with those presumed to represent a relatively "clean" terrestrial signal, indicates that the age of the contaminant carbon may, in fact, be younger than the timing of sediment deposition by several hundred to several thousand years. This poses several challenges for interpreting the core record. Firstly, it suggests that contamination of the core sediments, or at least those deeper than 36 cm, must have occurred via post depositional groundwater flow through the sediments. Given the lake depth (likely sufficient to intersect with the groundwater table) and the relatively high proportion of algae and pore water preserved within the sediments, this may be plausible if the sediments are permeable and can support interstitial biological activity in the anoxic sediment that is sequestering C, which would presumably relate to methanogenesis (Aravena et al. 1995, Nüsslein et al. 2003, Conrad et al. 2011). Second, and perhaps more problematically, is if the ages used within the age-depth model are reliable for interpreting timing of sediment deposition, one must account for the loss of approximately 4000 years-worth of sedimentation from the core top. Given that Yeak Loam has a closed catchment and is deep, it is highly improbable that changing environmental conditions (e.g. erosion of the lake-bottom sediments or lake drying) instigated either a period of sediment outflow from the lake, or a break in sediment influx to the lake. This is awkward as it means that, if the high sedimentation rate predicted by the ages returned from the "clean" samples used in age modelling for the core (maximum of 5.85 years/cm [6]) is held constant through time, a minimum of 6.2 metres-worth of sediment loss from the core top needs to be accounted for. Some possible mechanisms for this loss may be 1) slumping of the lake bottom sediments, 2) sediment disturbance associated with the localised bombing of Ratanakiri between the late 1960s and 1973 (known to have destroyed lake-side infrastructure (Colm 1997), or 3) from a sampling error.

Coring through a slip face caused by slumping of the lake bottom sediments could account for the old age of the core sediments deeper than 35.5 cm. The bathymetric survey of Yeak Loam presented in Sharma (2014) (albeit low resolution) indicates that the central portion of the lake sediment surface (from where the core was extracted) is relatively flat, and provides no evidence of slump debris. This makes it difficult to envisage subsurface landslides within the vicinity of the coring location. Sediment loss directly associated with bombing the Yeak Loam catchment is also unlikely given the depth of water column (Carpenter 1967). However, it may be possible

[6]This calculation is based on a linear interpolation between the oldest age calculated for the 202.5 to 203.5 cm sample (4811 cal. yrs BP) and youngest age calculated for the 35.5 to 36.5 cm sample (3783 cal. yrs BP)

that associated vibrational disturbance may activate lake sediment slumping. Sampling errors that may account for some sediment loss could include double-coring from the same location (YL1211A was extracted prior to sampling YL1211B). However, this is unlikely given that the cores were taken some metres away from each other, and that this still cannot account for a minimum of 6.2 metres worth of sediment loss. As it is difficult to convincingly reconcile the old age of the dates applied in the age model against any of these models of sediment loss, and no clear hiatus-boundary is observable in the stratigraphy of YL1211B or YL1211A, interpretation of the timing of changes reconstructed from the core sedimentation is approached with a degree of scepticism.

Sediment source and input

The somewhat homogenous stratigraphy of the YL1211B sediments suggests little change in sedimentary input and deposition across the time period represented by Yeak Loam sediments. The algal-rich core sediments indicate relatively high levels of lake productivity across the record, particularly between 128 cm and 26 cm depth (modelled at 4320 to <4111 cal. yrs BP). The textural records reconstructed from the core sediments indicate that the deeply weathered, silty-clay, clay loam and silt-loam basaltic catchment soils are the likely source for much of the fine-grained siliciclastic fraction of the core sediment. This appears validated by the geochemical record that indicates that Fe, an element concentrated weathered basaltic soils, is overwhelmingly the most common element in the core sediments. Fe also shows a positive association with Ti and K - elements commonly used as a detrital signal within sediment cores (Kylander et al. 2011, Rothwell and Croudace 2015 and references therein), though this relationship is weak.

As with Yeak Mai, it is expected that a proportion of Fe and Mn within the core sediments could be sourced from redox cycling of the lake waters. However, while Mn/Ti and Fe/Ti appear to act as valid proxies for post-depositional oxidation within a shallow lake setting, reconstructing redox conditions from sediments deposited in deeper, thermally stratified meromictic lakes such Yeak Loam (Sharma 2014) can be complex (Davison 1993, Boyle 2001). This is largely due to the significant proportion of dissolved elements that can be held in solution in deep waters, resulting in redox-sensitive elements exhibiting variable responses to changing oxygen concentrations in the lake waters (Boyle 2001). In particular, precipitation and (re)dissolution of Mn and Fe occur at different rates under the same conditions, with Fe typically more sensitive under oxic conditions (thus precipitating out of solution earlier than Mn), and Mn typically more sensitive under reducing conditions (thus (re)dissolving into solution earlier than Fe) (Davison 1993, Boyle 2001). This process likely accounts for the inverse relationship observed between Fe/Ti and Mn/Ti ratios between 99 and 25 cm (modelled at *c.* 4255 to <4111 cal. yrs BP). Consequently, Mn/Fe may serve as preferable proxy for estimating past O_2 concentrations of bottom waters within Yeak Loam, particularly given the short-lived nature of redox changes associated with lake turnover events (see Naeher et al. (2013)

for details). Changes in this ratio across the age-depth modelled part of the core indicate 1) somewhat stable and relatively high levels of bottom water oxygenation between 203.5 and 111 cm depth (modelled age *c.* 4485 to 4280 to cal yrs BP), 2) peak oxygen concentration between 111 and 98 cm (modelled at *c.* 4282 to 4252 cal yrs BP) followed by a gradual decline to 88 cm, and 3) relatively low bottom water oxygenation between 88 and 36 cm (modelled at *c.* 4230 to 4111 cal. yrs BP). Above 23 cm depth, the peaks in Mn/Fe that correspond with high amplitude fluctuations in Fe/Ti and Mn/Ti, are likely indicative of ephemeral cycling processes in the water column that often lead to enrichment of trace metals, especially Mn, in the surface sediments (Bryant et al. 1997, Boyle 2001).

The inferred peak in bottom water oxygenation between 98 and 111 cm depth corresponds with the sedimentary bed rich in silt and very fine sand that was originally used as a visual marker to distinguish YL1211B core sediment unit I from unit II. While it is tempting to use this relatively coarse-grained bed to infer a period of heightened catchment erosion (Peng et al. 2005, Bhattacharyya et al. 2015), counts of elements associated with detrital influx (Si, Ti and K) are relatively low across at this depth interval. This suggests limited addition of excess allogenic siliciclastic sediment to the lake at this point in the record. Ca, however (an element that is only weakly or negatively correlated with the detrital element suite) peaks in this bed. Biologically mediated precipitation of calcite or aragonite is a common source of calcium within core sediments (Brown et al. 1989, Ito 2001, Pełechaty et al. 2013). Authigenic aragonite (and occasionally calcite) have been observed within Yeak Kara sediments as 25 to 30μm (long axis) crystals that are often aggregated to form coarse silt- to sand-sized particles (Sharma 2014). While no biogenic sources of carbon were observed during smear slide analysis of YL1211B (and hence no test of inorganic carbon was conducted as part of this study), it is possible that past lake mixing events may have encouraged biological productivity via nutrient upwelling, and permitted the precipitation, deposition and preservation of relatively coarse carbonate minerals within the lacustrine sediments via draw down of the redox boundary in the water column (Nelson et al. 2009, Pełechaty et al. 2013). This interpretation is considered plausible given the relatively high levels of TOC and Mn/Fe calculated for the sediments between 98 and 111 cm, suggesting high biological productivity and high bottom water oxygenation. This is particularly the case if drying conditions (inferred from high Mn/Fe ratios (Naeher et al. 2013)) resulted in lake shallowing and subsequent concentration of dissolved ions within the lake water. It is notable to point out that while aragonite and/or calcite should have been digested in the sediment pre-treatment with H_2O_2 for grain-size analysis, this process is not especially effective for the removing carbonates from samples (Murray 2002).

4.4.3 Yeak Oam

The relatively homogeneous sediments observed in YO0712B may indicate a consistent pattern of Yeak Oam sedimentation through time. The multi-proxy analyses of Yeak Mai and Yeak Loam sediments outlined above suggest that peaks in κSI (the only sedimentological analysis conducted on

this core) may either indicate increased erosion of the mafic catchment soil and/or increased precipitation of redox sensitive elements under oxic lake bottom water conditions. Given that this is the only analysis done on this core, it is difficult to intepret the source and cycling of sediments to Yeak Oam through time.

4.5 Chapter summary

A brief synthesis of results derived from sedimentological analysis of the master lake cores extracted from Yeak Mai, Yeak Loam and Yeak Oam is included in table 4.11

TABLE 4.11: Summary table of the results from chronological and sedimentological analysis of the master cores.

	Yeak Mai (YM0413B)	Yeak Loam (YL1211B)	Yeak Oam (YO0712B)
Coring technique	Gravity	Gravity	Push & percussion
Core length (cm)	543.5	214	175
Core stratigraphy	I — 543.5 to 510 cm — sapropel; II — 510 to 288.5 cm —interbedded sapropelic mud (IIa) & sapropel (IIb); III — 288.5 to 218.5 cm — sapropelic mud; 218.5 to 0 cm — sapropel	I — 214 to 111 cm — silt; II — 111 to 0 cm — sapropelic mud	Massive sapropel
Radiocarbon date analysis	11 — 3 x bulk sediment; 4 x macro-charcoal; 3 x macro-charcoal & organic material; 1 x plant fibre	17 — 12 x macro-charcoal & organic material; 2 x macro-charcoal; 1 x leaf fragments; 2 x bulk organics	3 x leaf fragments with some algal material
Chronological modelling	Bacon v2.2; 2 x outliers excluded from age-depth model; modelled basal age = 4722 cal. yrs BP.	Bacon v2.2; only leaf fragments and macro-charcoal samples modelled – highly uncertain –reservoir effects likely; range of ages modelled = 4497 (209 cm) to 4111 (36 cm) to cal. yrs BP.	Bacon v2.2; modelled basal age = 1115 cal. yrs. BP.
Modelled down-core sedimentation rate	Approx. 1.1mm/year	Approx. 4.5mm/year (uncertain)	Approx. 1.5mm/year
Total Organic Carbon (LOI_{550})	Ranges from 14 to 31%. Higher values associated with sapropel-rich beds (I, IIb, IV).	Ranges from 17 to 25%. Values slightly higher up core of 136 cm.	Not analysed

Continued...

	Yeak Mai (YM0413B)	Yeak Loam (YL1211B)	Yeak Oam (YO0712B)
Bulk mineral influx	Higher values associated with mud-rich beds (units IIa & III). Exceptionally high values modelled at the outer boundaries of unit III.	No significant change down core.	Not analysed
Field moisture content	Ranges from approximately 65 to 85%	Ranges from approximately 69 to 77%	Not analysed
Magnetic susceptibility (κSI)	Higher values across unit II at depths shallower than 450 cm (> 1 x 10^5), and across unit III ((> 1 x 10^4). Peaks correspond with mud-rich beds.	Low amplitude, high frequency fluctuations. No significant change down core. Mean = 9.2 x 10^5.	Low amplitude, high frequency fluctuations. Mean = 4.3 x 10^4. No significant change down core though peaks occur between 54 and 59 cm depth.
Magnetic susceptibility (χfd$_{\%}$)	Not analysed	Low amplitude, high frequency fluctuations. No significant change down core. Many samples below minimum recommended volume.	Not analysed
Grain size analysis	Silt dominant fraction (17 to 92%; mean = 62%). Finer clast sizes tend to align with more mud-rich units.	Silt dominant fraction (50 to 97%). Sand peaks at 109.5 to 99 cm (30%) and 14 cm (32%).	Not analysed

Continued...

	Yeak Mai (YM0413B)	Yeak Loam (YL1211B)	Yeak Oam (YO0712B)
Geochemistry	Si, Ti, K, Ca, Rb, Ba, Cr Sr & Zn correlated and probably represent the detrital signal. Fe/Ti and Mn/Ti correlated and probably represent endogenic redox cycling. Fe/Ti & Mn/Ti peaks tend to associate with unit IIa and the boundaries of unit III. Additional peaks occur in unit IV at 195 cm depth.	Elemental associations include Si, Ti & K, and Sr & Zr (detrital signal?); Fe, Rb, and Pb; Ca and Zr/Rb. Mn/Fe may represent redox cycling in this deep lake setting.	Not analysed

5 Palaeo-vegetation and palaeo-fire analysis of the lake sediments

5.1 Introduction

This chapter describes the methods and results used to reconstruct long term vegetation and fire activity from Yeak Mai (YM0413B) and Yeak Loam (YL1211B) sediments, as well as those used to construct modern microfossil analogues from the various SASDTF units described in Chapter 3. With respect to modern pollen analogues, lake sediment surface samples were analysed from Yeak Mai, Yeak Loam, Yeak Oam and Boeng Lumkut, representing relatively continuous dry deciduous forest, localised semi-evergreen dry forest, localised semi-evergreen dry forest and regional deciduous forest, and fragmented dry deciduous forest units, respectively. These are considered in light of the species compositions of SASDTF units (reviewed in chapter 3 and listed in appendix B) in attempt to link the modern microfossil assemblages to forest type in the absence of any ecological surveying. These are used to reconstruct changes the long term vegetation records.

5.2 Methods

5.2.1 Charcoal analysis

Analysis of black carbon fragments (charcoal) that tend to be easily preserved in lacustrine sediment records can permit an approximation of historic local and regional fire regimes (Whitlock and Larsen 2001, Scott 2010). Microscopic charcoal fragments, defined for the purpose of this study as fragments <105 μm, are able to be transported in the atmosphere for long distances once entrained, potentially reflecting regional to distal fire regimes (Clark 1988, Clark and Patterson 1997, Scott and Damblon 2010). While micro-charcoal fragments can also represent local (i.e. catchment scale) fire activity if they have been broken down in the system over a long period of time, this is considered unlikely within the context of the crater lake sites given their small catchment areas. Macro-charcoal, on the other hand can represent local (>250 μm fraction) and local to sub-regional (105 to 250 μm fraction) burning (Whitlock and Millspaugh 1996, Whitlock and Larsen 2001, Stevenson and Haberle 2005), with these particle sizes being too large to be easily entrained by normal surface winds (Clark 1988). In the context of this study, analysis of micro- and macro- charcoal is useful

for examining the role of fire as a driver of ecological change in south-east Asian dry deciduous forest (Yeak Mai) and dry semi-evergreen forest (Yeak Loam) units (see chapter 3 for theoretical details).

Macro-charcoal preparation and analysis

Sampling and processing

Methods used to extract macro-charcoal from the long sediment cores extracted from Yeak Mai and Yeak Loam are based on those detailed in Stevenson and Haberle (2005), which are modified from Rhodes (1998). Analysis of macro-charcoal was conducted on the same subsamples that were analysed for microfossil analysis (i.e. at 5 cm intervals from the core top sample, and the basal core sample).

Nineteen additional samples were extracted from YM0413B at 1) major unit boundaries; 2) the centre-depth point of any of the fine beds logged in unit II that were excluded by the 5 cm interval counts (see chapter 4) for stratigraphic details), or 3) adjacent to initial sampling depths that recorded anomalously high or low charcoal fragment counts. These included samples from 12.5 to 13 cm, 130.5 to 131 cm, 217 to 217.5 cm, 218.5 to 219 cm, 220.5 to 221 cm, 221.5 to 222 cm, 230.5 to 231 cm, 307 to 307.5 cm, 362.5 to 363 cm, 368 to 368.5 cm, 372.5 to 373 cm, 407.5 to 408 cm, 447 to 447.5 cm, 468 to 468.5 cm, 472 to 473 cm, 493 to 493.5 cm, 508.5 to 509 cm, 521 to 521.5 cm and 521.5 to 522 cm.

Following analysis of the initial samples, 21 additional samples were processed from YL1211B to check the highly variable charcoal counts observed between consecutive sampling depths. Where possible, these samples were taken adjacent to those tested in the initial round of analysis. These included samples from 14.5 to 15 cm, 26.5 to 27 cm, 34 to 35 cm, 24.5 to 35 cm, 44.5 to 45 cm, 55.5 to 56 cm, 64.4 to 65 cm, 74.5 to 75 cm, 80.5 to 81 cm, 84.5 to 85 cm, 94.5 to 95 cm, 104 to 104.5 cm, 115.5 to 116 cm, 124.5 to 125 cm, 135.5 to 136 cm, 144.5 to 145 cm, 155.5 to 156 cm, 164.5 to 165 cm, 174.5 to 175 cm, 184.5 to 185 cm and 195.5 to 196 cm.

One cubic cm of sediment (field moisture condition) was taken from each of the selected sample depths using a syringe, and placed into individual, 15 ml centrifuge tubes. Approximately 8 ml of 10% KOH was first added to each before the sample tubes were placed in a hot water bath set to 80 °C for 20 minutes to break down humic acids retained in the sediments. Samples were then rinsed twice in DI water via centrifuging at 3 000 rpm for 3 minutes and decanting supernatant. Approximately 10 ml of DI water was added to each sample tube following the second rinse, and the samples were well-mixed with a vortex mixer set to a mid-speed. Once completely suspended, the samples were passed through a clean 250 μm and 105 μm sieve stack using a spray bottle filled with DI water. Each coarse fraction (>250 μm and 105 to 250 μm) was then retained in DI water in individually labelled sample jars.

Analysis

Each suspended charcoal sample was poured into a clean petri dish underlain with gridded paper, and the charcoal fragments encountered within each grid cell were counted under an Olympus SZ40 binocular microscope at 10× to 20× magnification. The charcoal was distinguished from other materials in the sample by its black colour, opaqueness, lustre, planarity and angularity (Whitlock and Larsen 2001).

Six and four samples were randomly double-sampled from the YM0413B and YL1211B core sediments respectively. These were processed and counted as per the original samples, and the standard deviation between the original and replicate count was calculated in order to estimate the experimental counting error. The mean of the standard deviations (each taken as a percent of the mean count value of the respective original and replicate samples) was then used to estimate error across the sample set for each core.

The raw count data for each fraction size were transformed into an estimation of absolute abundance of macro-charcoal fragments per dry cubic cm using water content data produced for each core (see chapter 4).

Micro-charcoal preparation and analysis

Sampling and processing

Micro-charcoal (<105 μm) is retained in samples prepared for plant microfossil analysis and can thus be enumerated from the slide samples prepared for pollen and spore analysis (Whitlock and Larsen 2001). Details of the samples prepared for extraction of plant microfossils and micro-charcoal, as well as the extraction methods are summarised in sections 5.2.2 and and appendix F.

Analysis

Micro-charcoal fragments were counted by tallying individual fragments (Finsinger et al. 2008) under a Zeiss Axioskop II at ×400 magnification. *Lycopodium clavatum* spores were simultaneously counted. Final charcoal counts were established when 10 *L. clavatum* spores were counted. In the case of the YM0413B samples, the number of charcoal fragments counted between each *Lycopodium* spore was recorded until 10 spores were counted, and the total standard deviation of these counts was calculated such that uncertainty could be estimated. Raw count data for each fraction size were then transformed into an estimation of the absolute abundance of micro-charcoal fragments per dry cubic cm using water content data presented in chapter 4.

Plotting and analysis of charcoal counts

A whole-core mean charcoal count per unit dry mass was calculated for each fraction size from each core. The charcoal count data for each sample were then recalculated as a deviation value from the relevant fraction size whole-core mean. This was attempted in order to recognise the stochastic 'background noise' of environmental charcoal, and emphasise periods where charcoal concentrations were above or below that background level. These data were then plotted alongside the volume corrected count values using the software package C2 version 1.7.6 (Juggins 2014).

The resulting sequences were depth-aligned against the mineral influx records estimated for the cores in chapter 4. This permits comparison of absolute abundance of charcoal influx to an approximate bulk mineral sedimentation rate.

Stratigraphically constrained cluster analyses of the macro-charcoal data (i.e. >250 μm and 105 to 250 μm fractions) and the micro-charcoal data were undertaken in order to identify major changes in the fire-history records. These were calculated in R (R Core Team 2013) using the 'rioja' package (Juggins 2012) (method: stratigraphically constrained, coniss, distance: Euclidean).

5.2.2 Plant microfossil analysis

Preparation and collation of reference materials

A pollen and spore reference sample collection was collated to permit morphological comparison of plant microfossils extracted from the lake sediments to known and vouchered plant species, genera or families. This was considered especially important for the purpose of this project given the lack of pollen and spore morphological data available for key SASDTF species and, in many cases, genera.

Sample selection

The reference samples assembled for this project are derived from two plant microfossil slide collections. The first of these was collected and compiled by D. Penny from The Rijksherbarium, Leiden in the Netherlands as part of a palynological study of north-east Thai dry forest communities (Penny 1998, Penny 2001). The techniques used to collect and prepare these reference slides are outlined in Penny (1998). This collection is currently held at the University of Sydney, School of Geosciences. The second reference sample set used for this project is the Australasian Pollen and Spore Atlas (APSA) microfossil slide collection, archived at the Australian National University Department of Archaeology and Natural History (though many samples are published online at http://apsa.anu.edu.au).

The process of shortlisting microfossil reference slides for the project initially involved matching species (or genera) from available, undescribed

slides with those known to form part of the SASDTF units present in Cambodia (described in chapter 3 and listed in appendix B). Due to the geographical proximity of Yeak Kara to Yeak Mai and Yeak Loam, samples matching the plant microfossils identified in Maxwell (1999) were also selected for analysis where available. After preliminary core microfossil analysis, additional reference sample slides were examined in attempt to classify recurring, unknown pollen grains extracted from the core sediments. These samples were selected on the basis of belonging to genera known to exist in Cambodia (Dy Phon 2000) with similar morphological features to that of the unknown pollen grain or spore — greatly aided through the use of Huang (1972).

Two flower (pollen) samples collected in the field in 2013 were also processed as part of the reference sample collection. These were derived from *Lagerstroema* sp. (comparable to *L. floribunda* [Jack]) –sampled from the catchment of Boeng Lumkut, and what was identified as *Tetrameles nudiflora* (R.Br.) — a major component of the pollen record compiled in Maxwell (1999) and Maxwell (2001) – sampled from the catchment of Yeak Loam (figure 5.1). These samples were placed into paper envelopes and transported to the University of Sydney School of Geosciences laboratories for analysis. The flower samples were transferred to 50 ml centrifuge tubes for pollen extraction following standard procedures (Faegri and Iversen 1989) involving sequential sieving and chemical extractions to remove humic colloids and cellulose. Resultant pollen concentrates were then mounted with glycerol solution onto glass slides for analysis alongside the other reference sample slides. A detailed outline of the procedures used to extract and mount the field reference samples is presented in appendix H.

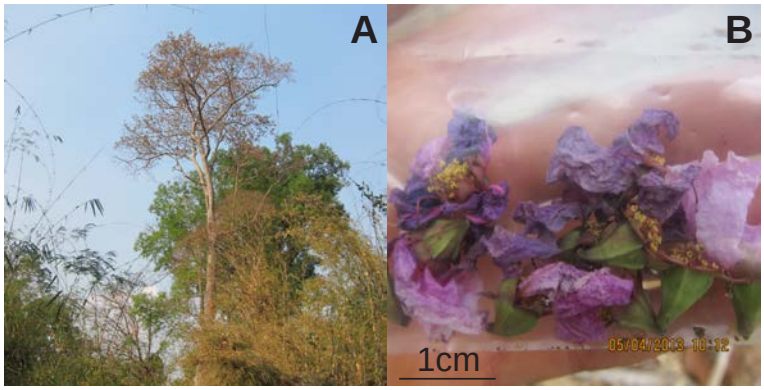

FIGURE 5.1: Photographs of microfossil reference sample specimens collected in the field, tentatively identified as A) *Tetrameles nudifolia* (R.Br.) (Yeak Loam), and B) *Lagerstroemia* sp. (Boeng Lumkut).

Sample analysis

The selected reference sample slides were photographed and described following standard terminology (Punt et al. 2007). Photographs were taken using a Zeiss Axioskop II light microscope fitted with an AxioCam HRc camera at $\times 600$ or $\times 1\,000$ magnification using plan-apochromatic oil-immersed

objectives. The images were processed and measured using Axiovision 4 software.

Preparation of modern microfossil benchmarks

Short cores were extracted from each of the five lake sites in order to capture surficial lake sediment samples. Four of these cores were sampled at the lake bottom/ water interface for plant microfossil analysis, with the aim to derive a modern pollen and spore signal from SEDF nested within a cleared region (Yeak Loam), local SEDF and regional deciduous dry forest (Yeak Oam), and fragmented and continuous dry deciduous forest units (Boeng Lumkut and Yeak Mai respectively). These samples were used to provide a modern vegetation "benchmark" to which the long-core microfossil reconstructions could be compared. Yeak Kara surficial sediments were not analysed given 1) the proximity of this site to Yeak Oam, and 2) that the pollen and spore assemblage for these sediments has previously been described (Maxwell 1999, Maxwell 2001).

Sampling

Lake surface sediments were sampled with a custom-made miniature gravity corer fitted with a screw-in, 760 mm long (⌀=30 mm), Perspex sampling tube and cutting shoe. The design of this device follows that detailed in Glew (1991) — developed to obtain an undisturbed surficial sediment sample. Minor modifications were made to this design to permit stable free fall in the deep lakes, including fins and 5 kg lead weights (figure 5.2). This device was deployed off the side of the boat, anchored above the deepest point of each lake site, approximately 1 m offset from the gravity core/ percussion core sites described in chapter 4. Following retrieval with a hand-held wench, the corer was detached from the sample tube, sealed at the base and transported vertically to the shore. Observations of the in-situ core sediments were noted through the clear tube. Short cores taken from Yeak Oam, Yeak Loam, Boeng Lumkut and Yeak Mai that were analysed for this project were termed YO0712A, YL0413A, LK0712A, and YM0413A respectively.

Following recovery, the short cores were subsampled on-site at contiguous 5 mm depth increments. Sampling was conducted using a custom-made extruder developed for the corer following principles specified in Verschuren (1993), whereby the core tube was vertically secured (with the piston at the base), and the core sediments incrementally extruded into a flat tray by pushing on the piston (from the base) with a hand-held screw (figure 5.2). In this design, the screw was calibrated such that sediment could be extruded as consistent slices at a specified interval (5 mm). The watery core-top sediments were sampled from the top of the extruder using a syringe, while deeper, more consolidated sediments (usually below 5 mm depth) were sampled with a plastic scraper that was cleaned between each subsample. Sediment subsamples were sealed in airtight sample bags and transported to the University of Sydney School of Geosciences laboratories for analysis.

FIGURE 5.2: Photographs of miniature gravity corer (L) and sediment extruding device (R).

Laboratory extraction and enumeration

The first two subsamples from the core tops of YO0712A, YL0413A, YLK0712A, and YM0413A (i.e. 0 to 1 cm depth) were combined and sampled for plant microfossil analysis. One cubic cm of sediment was measured with a syringe from each combined sample, and transferred into individual, appropriately labelled 15 ml centrifuge tubes for pollen and spore extraction. One *Lycopodium clavatum* spore tablet from batch #3862 (9,666 $\pm$ 671 spores per tablet; Department of Quaternary Geology, Lund University, Sweden) was added to each sample tube in order to facilitate calculation of absolute pollen and spore abundances (Stockmarr 1971). The samples were then processed for microfossil sampling following standard methods (Faegri and Iversen 1989). This involved sequential physical and chemical removal of unwanted components of the sediment through sieving (retaining the <105 μm fraction), a series of chemical digestions in HCL, KOH, HF, and acetolysis. Approximately 20 ul of the remaining material was mounted onto glass microscope slides in glycerol solution for microscopic analysis. A detailed outline of the procedure used for extraction of plant microfossils from core sediments is provided in appendix F.

Core plant microfossil preparation and extraction

Sample selection

The first batches of samples prepared for microfossil analysis were selected from evenly-spaced intervals down both cores. In YL1211B, samples were initially taken every 10 cm between 5 cm and 205 cm, and from 212 cm (n=21). Samples were also taken every 10 cm from YM0413B between 0 cm and 540 cm (n=55). As the sample at 90 cm from YM0413B coincided with a core gap (see chapter 4 for details), this sample was substituted for one extracted from 89 to 89.5 cm depth. Sampling resolution was doubled for both cores, starting from 10 cm in YL1112B (n=20), and 5 cm in YM0413B (n=54), with additional samples taken from YM0413B at 12.5 to 13 cm, 230.0 to 230.5 cm (discreet organic lamination), and 543 to 543.5 cm (core base) (n=3).

Laboratory extraction and enumeration

One (field moisture condition) cubic cm of sediment from selected sampling intervals, measured with a syringe, was placed with one *Lycopodium clavatum* spore tablet (batch #3862) into a 15 ml centrifuge tube for microfossil extraction. Procedures followed those described for the short core samples in section 5.2.2. A detailed method is provided in appendix H.

Enumeration and analysis of plant microfossils

Plant microfossils extracted from the surficial and core sample were identified and enumerated under a Zeiss Axioskop II light microscope fitted with an AxioCam HRc camera at $\times$400 magnification. A count target of at least 100 dryland taxa (excluding grasses) per slide was aimed for based on 1) a qualitative estimation of the pollen saturation point, and 2) counts used in other palynological studies undertaken in SASDTF (Penny 1998, Maxwell 1999, Maxwell 2001, Penny 2001). However, several samples from YM0413B and the surface core assemblages fell short of this minimum count criteria. Additionally, a dryland count minimum of 200 dryland pollen taxa was applied where the microfossil assemblage was overwhelmingly dominated by one type (as was the case for several YL1211B samples), requiring a higher dryland-type count for representativeness (Keen et al. 2014).

A pollen and spore taxonomy for the samples was developed from comparison with published reference material (Huang 1972, Tissot et al. 1994, Banks 1997, Nakagawa et al. 1998, Penny 1998, Maxwell 1999, Parnell 2003, Punt et al. 2003, Rull 2003, Singh et al. 2010, Quamar and Chauhan 2011, Demske et al. 2013, Quamar and Chauhan 2014, Schori and Furness 2014, Trivedi et al. 2014), the APSA online database (Australian National University 2016), and the reference sample set prepared for this study. Each new type of pollen grain or spore was imaged and measured using Axiovision 4 software.

Analysis of surficial sediment samples

Plant microfossil counts from lake surface sediments were standardised to relative abundances (% of total pollen and spore sum for each sample) in order to provide a basis for comparison between the different lake sites. These data were compared to each other using a clustered column graph.

Analysis of lake sediment core samples

Data synthesis and plotting

Summary plots showing relative changes in major plant functional types (grasses, dryland taxa, aquatics and pteridophytes) were first produced for each core to delimit depths at which major floristic change occurred, and provide a context for interpreting absolute abundance changes for taxa within each of these functional groups, free from the influence of bulk mineral sediment influx. Individual plant microfossil counts from YM0413B and YL1211B were converted into corrected absolute abundances (grains per dry cubic cm) using the core water content data outlined in chapter 4. Pollen and spore types comprising greater than 0.1% of the total count (raw) were plotted stratigraphically, with arboreal (woody) dryland taxa grouped into SASDTF units where possible based on classifications made in Maxwell (1999), Maxwell (2001), and the vegetation lists synthesised for this study (chapter 3 and appendix B). In the case of YM0413B, which has highly variable estimated mineral influx down core, the sum of the total relative abundance of taxa within each identified SASDTF classification was calculated and plotted in order to highlight depths at which any changes in overarching forest structure may have occurred.

All pollen and spore diagrams were produced in the software package C2 version 1.7.6 (Juggins 2014), and were plotted adjacent to the sedimentary influx and chronological models developed for each core in chapter 4. This was done to both place the vegetation records into a chronological sequence and to permit comparison in overall changes in microfossil absolute abundance with estimated bulk mineral influx.

Statistical analysis

The down core relative (functional plant groups) and absolute (taxa representing >0.1% of total raw count) abundances that were used for plotting the pollen and spore diagrams for each core were subject to Q-mode and R-mode statistical analysis in order to quantify associations both between sampling units and amongst pollen and spore types.

Analysis of cross-sample associations

The down-core microfossil sequences were each clustered (method: coniss, distance: Euclidean; stratigraphically constrained) in the program R (R Core

Team 2013) using the 'rioja' package (Juggins 2012) to determine depths at which major changes in the plant microfossil assemblage occurred.

Analysis of microfossil taxon and charcoal associations

A Pearson's correlation and PCA were used on the core plant microfossil and charcoal sequences to determine trends in co-dominance of microfossil taxa. This was undertaken in Microsoft Excel using the XLSTAT PCA add-in (Addinsoft 2016). Only relatively common pollen and spores (i.e. those contributing to greater than 0.5% of the total (raw) core count) were used for the PCA given that this test is only suited to datasets were there are few zero values (McKillup and Dyar 2010). Mineral influx data were incorporated into the Pearson's correlation to determine the relationship between changes in non-organic sedimentation rate and the pollen and spore and charcoal sequences. Data were scaled prior to all analyses using a Z-score.

5.3 Results

5.3.1 Charcoal records

YM0413B

Macro-charcoal

Macro-charcoal was extracted and counted from 128 depth intervals in core YM0413B. The mean down-core abundance was 134 and 1365 fragments per cubic cm for the >250 μm and 105 to 250 μm fraction sizes, respectively. Six additional replicate samples were taken from 180 to 180.5 cm, 200 to 200.5 cm, 245 to 245.5 cm (two replicates), 275 to 275.5 cm and 500 to 500.5 cm. The average standard deviation calculated from these replicates was approximately 21% and 24% for the >250 μm and 105 to 250 μm fraction sizes respectively. These were used to estimate experimental error across the entire down-core sample set. Downcore fluctuations in macro- and micro-charcoal for this core are presented in figure 5.3. A moderate correlation exists between the two macro-charcoal fractions (r = 0.48).

Stratigraphically constrained cluster analysis of macro-charcoal found a primary division in the data at 180.5 to 190 cm at a dissimilarity distance of 8.9×10^4. The two resultant clusters — A (543 to 190 cm) and B (180.5 to 0 cm) — were each divided into sub-clusters, as delineated on figure 5.3.

The primary sub-cluster in cluster A (dissimilarity distance = 8.2×10^4) at 218 to 218.5 cm (modelled at 1743 cal. yrs BP) coincides with the top of the logged sedimentary layer III. The second to sixth strongest subdivisions within cluster A occur between 255.5 and 260 cm, 280.5 and 285 cm, 522 and 525 cm, 520.5 and 521 cm and 320.5 and 325 cm (at dissimilarity distances of 7.8×10^4, 7.4×10^4, 6.8×10^4, 6.7×10^4 and 6.2×10^4, respectively). These divisions mark the upper boundaries of macro-charcoal sub-clusters av, aiv, ai, aii and aiii marked on figure 5.3. In general, these

subdivisions tend to reflect the fluctuations between relatively low (ai, avi) and relatively high (av, avii) charcoal counts. The exception to this occurs in sub-cluster aiii between depths of 515 and 410 cm (modelled at 4316 to 2949 cal. yrs BP), which is characterised by relatively high frequency fluctuations between above- and below- average counts. These fluctuations tend to align with the closely-spaced sedimentary interbeds present in the stratigraphic unit II (and associated fluctuations in mineral influx) and thus may reflect different levels of charcoal "dilution" by changing rates of inorganic sedimentation.

Anomalously high peaks in the >250 μm charcoal fraction occurs within the aiii subcluster at 475 to 475.5 cm (modelled at 3732 cal. yrs BP) and 495 to 495.5 cm (modelled at 4037 cal. yrs BP). These correlate with peaks in the 105 to 250 μm fraction.

Cluster av (modelled at *c.* 1851 to 1904 cal. yrs BP) displays higher than average charcoal influx despite the high sediment influx predicted for this core section.

One major subdivision occurs within cluster B at 120.5 to 124 cm (dissimilarity distance = 4.5×10^4), modelled age of *c.* 891 cal. yrs BP). This represents a shift in the 105 to 125 μm size fraction from low-amplitude count fluctuations around the core mean count values, to persistently below average counts (though variability appears to increase towards the core top).

Micro-charcoal

116 samples were analysed for micro-charcoal from YM0413B sediments. The average down core micro-charcoal abundance across the YM0413B samples was approximately 3.57×10^6 fragments per dry cubic cm. Due to the relatively low concentration of *Lycopodium* spores relative to charcoal fragments present in the slide samples, experimental error was high (mean standard deviation across the samples was approximately 1.62×10^6 – approximately 45% of the total down core mean count). The down core moisture-content corrected micro-charcoal counts showing this error plotted alongside deviation from the core mean counts are presented on figure 5.3.

Stratigraphically constrained cluster analysis of the down core micro-charcoal counts cluster the data at two major division points between 515.5 and 520 cm (dissimilarity distance = 1.28×10^8, modelled age of *c.* 4327 cal. yrs BP) and 145.5 and 150 cm (dissimilarity distance = 1.2×10^8, modelled age of *c.* 1083 cal. yrs BP). These divisions form the boundaries of the major micro-charcoal clusters — A, B and C — shown on figure 5.3.

Micro-charcoal cluster A is delimited on the basis of its high charcoal counts relative to the rest of the core. Cluster B is divided into sub-clusters at 280.5 to 285 cm, 320.5 and 321 cm, 235.5 and 240 cm and 255 and 260 cm (dissimilarity distances are 1.07×10^8, 1.01×10^8, 9.5×10^7 and 9.2×10^7, respectively). Similar to the patterns observed in the down core macro-charcoal record, fluctuations in micro-charcoal counts from the deeper portion of cluster B (i.e. between 515 and 320 cm), are frequent and align with the closely-spaced interbeds occurring across sedimentary unit II. Above

320 cm, divisions within cluster B form around above-average (subcluster bv) or below-average (subclusters bii, biv) count groupings. Subunit biii (280 to 280.5 cm, modelled at *c.* 1904 cal. yrs BP) represents a well-above average micro-charcoal peak taken from a single sample within an otherwise below-average count grouping. Cluster C reflects a shift to overall higher charcoal counts between 145 and 25.5 cm (modelled at *c.* 1073 to 167 cal. yrs BP), with a major peak present within the 105 to 105.5 cm sample (modelled at *c.* 780 cal. yrs BP).

YL1211B

Macro-charcoal

Macro-charcoal samples from 53 depth intervals were extracted and counted from YL1211B. The mean down-core abundance was 28 and 791 fragments per dry cubic cm for the >250 μm and 105 to 250 μm fraction sizes respectively. Replicate samples were taken from 75 to 75.5 cm, 135 to 135.5 cm, 150 to 150.5 cm, and 195 to 195.5 cm. The average standard deviation calculated from these replicates represented approximately 14% and 19% of the sample count value for the >250 μm and 105 to 250 μm fraction sizes respectively. These values were used to estimate count error across the entire down-core sample set. No significant correlation exists between the abundance of the two macro-charcoal fractions, or between either of the macro-charcoal fractions and mineral influx. Down core fluctuations in macro- and micro-charcoal are presented in figure 5.4.

In general, the record is noisy, displaying high-frequency fluctuations in charcoal abundance across both fractions. Stratigraphically constrained cluster analysis of macro-charcoal divides the data set between 50.5 and 55 cm (dissimilarity difference = 1.19×10^3), 55.5 cm to 60 cm (dissimilarity distance = 1.12×10^3), and 125.5 and 130 cm (dissimilarity difference = 1.0×10^3). These have been used to group the data into four cluster zones — A (212.5 to 130.5 cm), B (125.5 to 55.5 cm), C (55.5 to 55 cm) and D (55 to 10 cm [the upper most sampled depth]) — as presented in figure 5.4. Cluster zone A captures macro-charcoal data that is highly variable both between adjacent sample depths and between the two macro-sample fractions. The base of cluster B appears to be delineated from cluster C due to the presence of a series of lower-than-average counts across both fraction sizes from 125.5 to 95 cm (sub-cluster bi). Above 95 cm, the variability of the record again increases across most of sub cluster bii, and clusters C and A. Unit C captures a large peak in the 105 to 250 μm sized fraction at 55 to 55.5 cm.

Micro-charcoal

Slides from 39 depth intervals from YL1211B were analysed for micro-charcoal, and a whole core abundance of 3.56×10^6 fragments per cubic cm was calculated from these samples. The resulting record is characterised by high-frequency, but relatively low-amplitude shifts in charcoal abundance, punctuated by five peaks at 10 to 10.5 cm, 50 to 50.5 cm, 110 to 100.5 cm, 180 to 180.5 cm and 210.0 to 210.5 cm (figure 5.4). The three largest of these

peaks drive the clustering pattern of the record, which is divided at 6 points (forming 7 clusters) about these samples. These divisions occur between 180.5 and 185 cm, 175.5 and 180 cm, 110.5 and 115 cm, 105.5 and 110 cm, 50.5 and 55 cm, and 45.5 and 50 cm (dissimilarity distances of 3.78×10^{-7}, 3.95×10^{-7}, 3.18×10^{-7}, 3.37×10^{-7}, 4.35×10^{-7}, and 4.7×10^{-7}, respectively) (shown on figure 5.4). Aside from the presence of the peak occurring within the 10 to 10.5 cm sample, the upper portion of the record, extending from 50 to 5 cm (cluster G), displays lower than average micro-charcoal abundance. No significant correlation between micro-charcoal fraction and mineral influx exists.

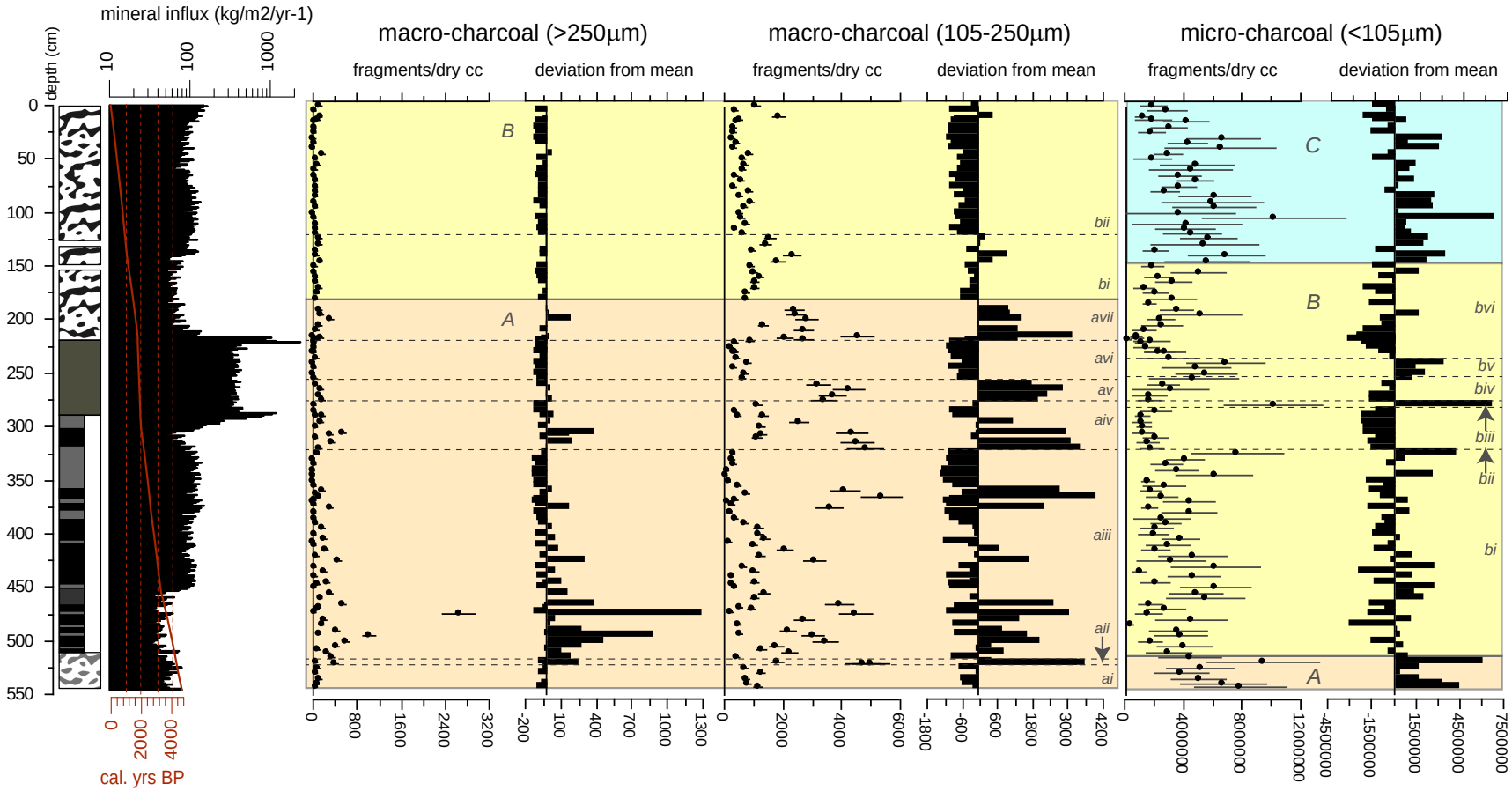

FIGURE 5.3: Down core charcoal plots for YM0413B. The macro- and micro-charcoal data are grouped into major zones based on results of the stratigraphic cluster analysis. Data are plotted next to estimated mineral influx.

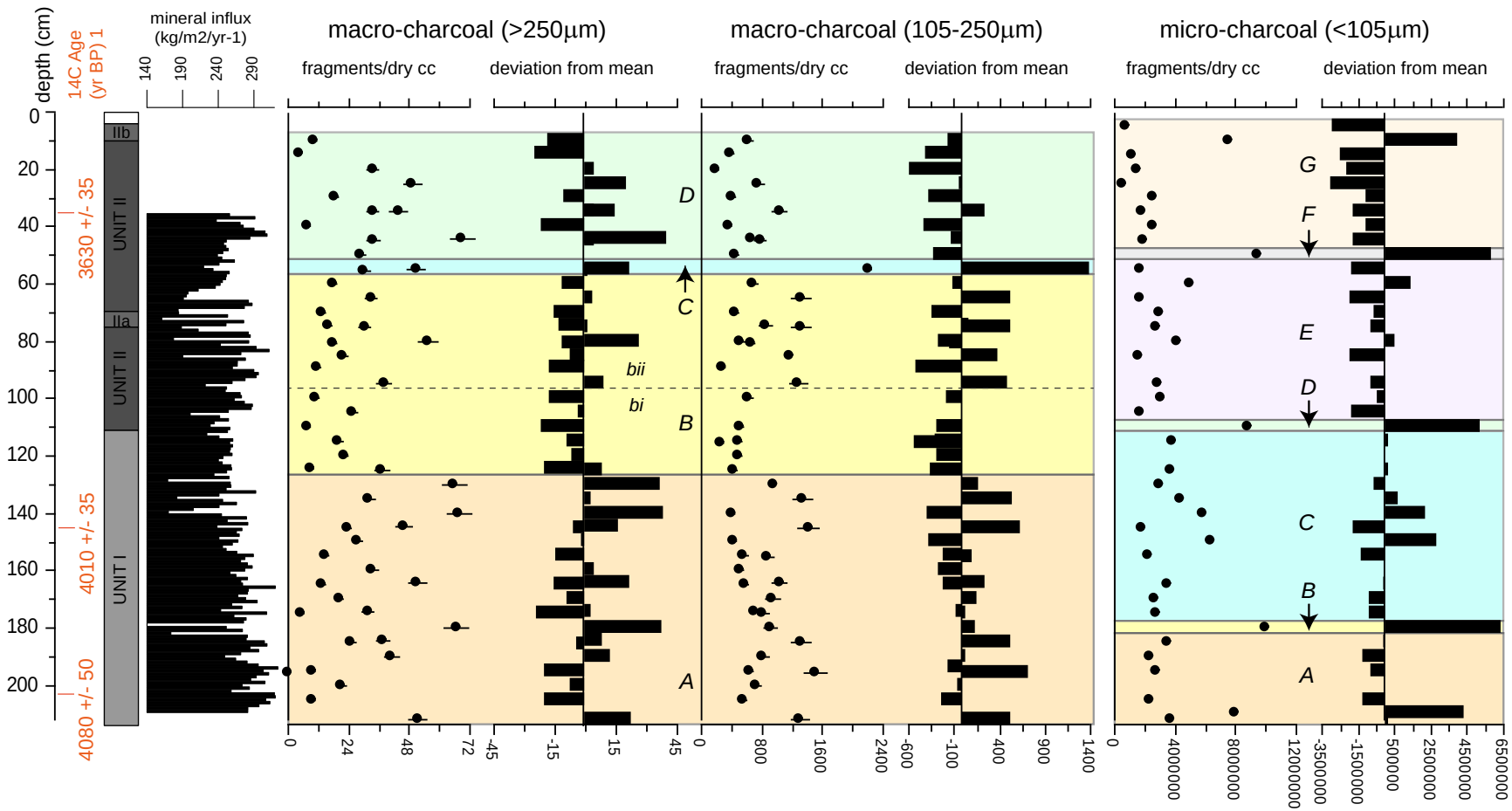

FIGURE 5.4: Down core charcoal plots for YL1211B. The macro- and micro-charcoal data are grouped into major zones based on results of the stratigraphic cluster analysis. Data are plotted next to estimated mineral influx.

5.4 Palaeo-vegetation records

5.4.1 Reference samples

A total of 76 reference samples, representing 76 species from 27 families were photographed and described for the project reference collection. Photographs and brief descriptions of these taxa are presented in appendix G.

5.4.2 Modern plant microfossil samples

The unconsolidated sediment-water interface was unmixed in the short cores (e.g. figure 5.5), suggesting that the core tops record the most recent sedimentation in the lake basin (assuming no recent re-suspension of sediment). The plant microfossils sampled from the core tops are thus likely to represent a modern signal.

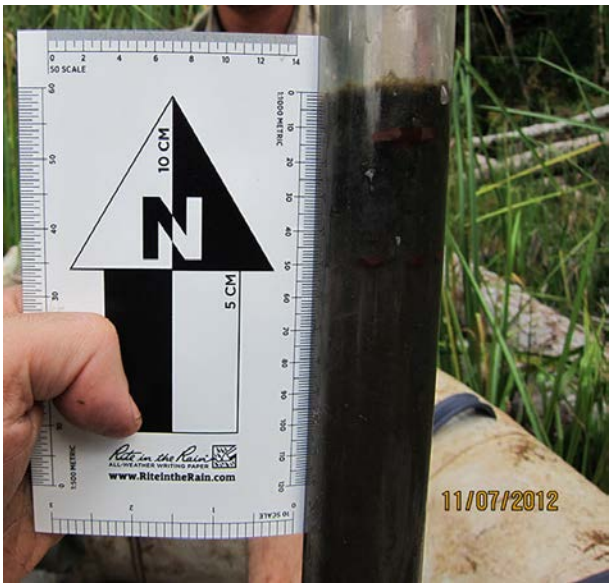

FIGURE 5.5: Photograph of short core lake surface sediments extracted from Yeak Oam (YO0712A).

A total of 342, 170, 194 and 164 pollen grains were counted from the YO0712A, YL0413A, YM0413A, and LK0712A surface samples respectively. Across the core samples, these are classified into 42 different plant microfossil "types" from 30 families (97.5% of total count). Nine "unknown" types (1 monolete spore and 8 types of pollen) that could not be identified from comparison with reference material make up the other 2.5% of the count. As with most palaeoecological studies undertaken in the tropics, particularly within the relatively under-researched dry forests of mainland south-east Asia (e.g. Maxwell 2001, Penny 2001), pollen identification was not well resolved beyond a familial or generic taxonomic level. Description of uncertainty in the classification of pollen and spore types follows Benninghoff & Kapp (1962), where cf = comparable form (less certain identification) and sf = similar form (general resemblance to reference samples).

The relative abundance of taxa comprising greater than 1% of each surface core count are plotted in figure 5.6, and listed alongside reference sources, plant functional group and SASDTF forest unit classifications, basic descriptions and photomicrograph code on table 5.1. Complimentary photomicrographs of the samples are presented in appendix H.

Given that there is some evidence for climate and particularly fire being important drivers of change between SASTF forest unit types (particularly from open to dense types under dry condition with fire, and *vice versa*) (Stott 1976, Stott 1984, Stott 1988a, b, Johnson and Dearden 2009, Quamar and Chauhan 2014), an attempt is made to draw relationships between the modern microfossil records analysed from the lake surface samples and their SEDF, DDF and MDF forest settings. However as noted in Maxwell (1999), this relationship is subtle. A description of the dominant microfossils present within the broad forest units represented by each surface sample (as well as types that are notably absent given the species composition of the represented unit – detailed in 3) is discussed below. In particular, an attempt is made to draw out some basic microfossil indicators of forest unit type that can be used to reconstruct changes in the forest structure though time, as recorded in YM0413B and YL1211B.

Dry Deciduous Forest (Yeak Mai – YM0413A & Boeng Lumkut – LK0712A)

The plant microfossil assemblage of YM0413A surface sediments is dominated by Poaceae (45%), Cyperaceae (9%) and pteridophytes (particularly *Stenochlaena* (6%) and grouped spores (4%)). Key arboreal microfossil taxa (i.e. trees and shrubs) include *Trema* (7%), *Lagerstroemia* (4%), *Syzygium* (3.5%), *Terminalia tomentosa* cf (3%) and *Schleichera oleosa /Cupaniopsis* cf (3%). Grouped Urticaceae/ Moraceae triporate (C0P3) types, *Mallotus*, and *Lithocarpus/ Castanopsis* each contribute to greater that 2% of the total assemblage. Grouped Dipterocarpaceae and *Hopea/ Shorea* types each make up approximately 1% of the total plant microfossil count. Though analysis of reference material indicates a clear distinction in the average polar and equatorial size of *Hopea* and *Shorea* pollen (on the order of approximately 6 to 8μm (see appendix G)), there was no clear bimodal distribution in the grain sizes of comparable Dipterocarpaceae pollen in the plant fossil material. As such, these types were grouped.

The dominant non-arboreal plant microfossils within the surface sediments of LK0712A include Poaceae (20%) and Cyperaceae (2.5%). The arboreal signal includes *Syzygium* (17%), *Lagerstroemia* (10%), *Terminalia tomentosa* cf (7%), *Trema* (6%), Myrtaceae type 2 (>17μm) (7%), *Anogeissus/ Memecyclon* (3.5%), Urticaceae/ Moraceae C0P3 type (2.5%), *Schleichera oleosa/ Cupaniopsis* cf (2.5%), undifferentiated Combretaceae/ Melastomataceae types (2.5%), *Celtis* (2.5%) *Dipterocarpus* other (2.5%) and *Aporusa/ Antidesma* cf (2.5%).

One challenging aspect to identifying a dry dipterocarp forest microfossil signal is the poor representation of *Dipterocarpus* species within the pollen record. This is apparent from analysis of the Yeak Mai and Boeng Lumkut surface samples, from which no *D. obtusifolius / tuberculatus* pollen grain

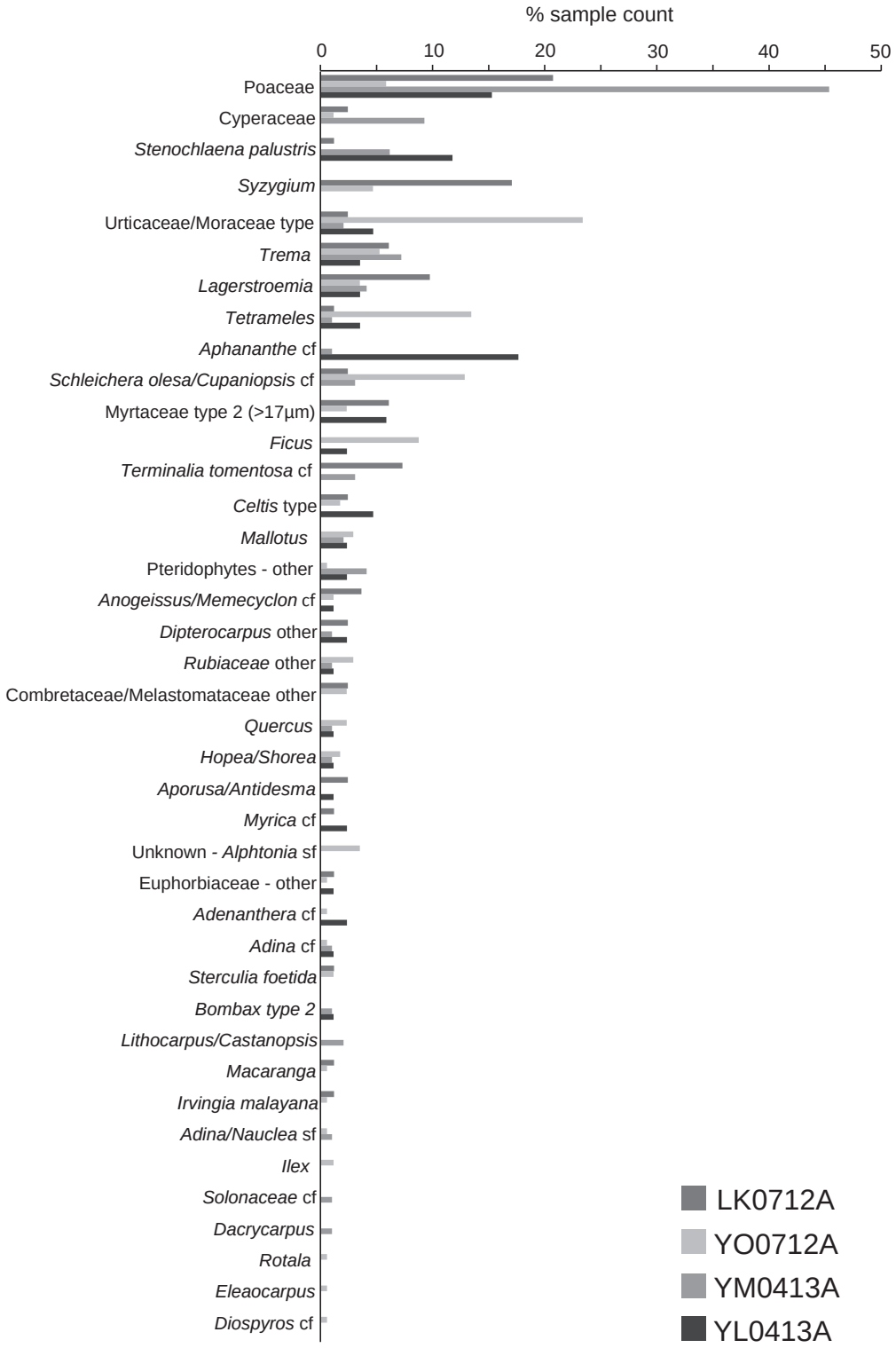

FIGURE 5.6: Plot of dominant pollen and spore types encountered in lake surface samples. Data presented as relative abundances.

were identified, despite these species being abundant in the modern catchment vegetation (especially for Boeng Lumkut). These observations are

consistent with those of Penny (1998, 2001), who analysed modern pollen rain within various Thai DDF/MDF settings, and Maxwell (1999, 2001), who analysed a surficial sample from Boeng Lumkut extracted in 1996. The presence of pollen classified as ''*Dipterocarpus* other' is apparent in the modern pollen record for both of these lakes, but is also present in comparable levels within the Yeak Loam surface sample, suggesting that this cannot be used as a deciduous dry forest indicator.

One pollen type that does occur solely within the Yeak Mai and Boeng Lumkut surface samples is *Terminalia tomentosa*, suggesting that an abundance of this species may indicate a DDF/MDF setting. This is potentially attributable to the capacity of this species to store water in its stem (Atluri et al. 2003) and to produce vast amounts of pollen that can be preserved in the microfossil record (Prasad Rao 2004). Poaceae counts are also high from the core samples taken from modern DDF/MDF settings, perhaps reflecting the grassy understorey that occurs within dry deciduous forest. However, it is important to note that grass currently occurs as part of the wetland assemblage growing around the shallow margins of Yeak Mai, which is likely to result in overrepresentation in the record.

Trema and *Mallotus*, which are relatively prevalent pollen types across dry deciduous forest, are commonly considered secondary forest indicators establishing themselves in open sites (Vazquez-Yanes 1998, Maloney 1999). High abundance may, therefore, indicate succession following disturbance. The relatively high presence of *Mallotus* within the surface microfossil record is unsurprising given that relevant species to SASDTF are typically wind pollinated (Yamasaki and Sakai 2013). Though most Ulmnaceae species found within SASDTF settings are thought to be insect pollinated, high numbers of *Trema* and *Celtis* pollen have been captured within pollen traps and surface samples taken elsewhere in the region, indicating relatively good aerial transport of these types (Corlett 2004), and potentially overrepresentation of these types within the pollen record.

Semi-Evergreen Dry Forest (Yeak Loam – YL0413A & Yeak Oam (Y0712A)

The Yeak Loam surface sample microfossil assemblage is dominated by *Aphananthe* cf (17.5%). Myrtaceae type 2 (>17μm) (6%), Urticaceae/Moraceae C0P3 type (4.5%), *Celtis* (4.5%), *Trema* (3.5%), *Lagerstroemia* (3.5%) and *Tetrameles* (3.5%). Pollen from *Mallotus, Dipterocarpus* other[1], *Ficus*, and *Adenanthera* cf are other dryland taxa that each comprise approximately 2.5% of the total Yeak Loam core top count. The non-arboreal core top plant microfossil assemblage is dominated by Poaceae (15%) and *Stenochlaena palustris* (12%). Consistent with observations made by Maxwell (1999), surprisingly few swidden or cultivated plant species are represented within the modern Yeak Loam pollen record despite the relatively thin SEDF forest buffer growing around the lake in an otherwise very disturbed setting.

The dominant arboreal pollen archived in the modern Yeak Oam sediment were Urticaceae/ Moraceae C0P3 type (23%), *Tetrameles* (13.5%), *Schleichera*

[1]This classification excludes pollen from *D.obtusifolius/ D. tuberculatus*

oleosa/ Cupaniopsis cf (13%), *Ficus* (9%), *Trema* (5%), *Syzygium* (4.5%), *Lagerstroemia* (3.5%), unknown *Alphitonia* (?) sf (3.5%), *Mallotus* (3%), grouped Rubiaceae types (3%), Myrtaceae type 2 (>17μm) (2.5%), *Quercus* (2.5%) and undifferentiated Combretaceae/ Melastomataceae types (2.5%). The non-arboreal signal is dominated by Poaceae (6%).

As with the deciduous forest pollen, it is difficult to distinguish a clear SEDF signal from the Yeak Loam, Yeak Oam and Yeak Kara (described in Maxwell (2001)) settings, with types such as *Lagerstroemia*, grouped Urticaceae/Moraceae, *Hopea/Shorea*, *Tetrameles* and Myrtaceae >17 μm apparently common to all of the assessed SASDTF settings. The presence of Lagerstroemia across all records is interesting given that this genus is commonly underrepresented in the pollen record despite being common tropical forest elements due to low pollen production (Quamar and Bera 2014). This indicates that they are an important canopy component across different SASDTF unit types. Other underrepresented tropical forest taxa within the microfossil record that have been identified in the surface samples across a drying SASDTF gradient include *Adina cordifolia*, *Shorea robusta* and, *Phyllanthus emblica* (Quamar and Bera 2014).

In general the arboreal pollen assemblages of the crater lakes with a SEDF catchment are more diverse than those reconstructed from MDF/DDF settings. Additionally, there appear to be some pollen types more common within denser forest settings. Pollen from *Ficus* and *Adenanthera* occur solely within the Yeak Loam and Yeak Oam samples, while other types occur at higher relative abundances within SEDF settings, including *Tetrameles* and *Aphananthe*. *Ficus* and *Tetrameles* pollen has previously been classified as a SEDF indicator (Maxwell 2001). *Adenanthera* and *Aphananthe* pollen, likely representing *Adenanthera pavonine* ((Teijsm. Binn.) I. C. Nielson) and *Aphananthe cuspidata* (Blume), respectively, favour dense, forest settings (Dy Phon 2000, Ayyappan and Parthasarathy 2004).

TABLE 5.1: List of pollen and spores encountered in the lake surface samples analysed from from Yeak Oam (YO0712A), Yeak Loam (YL0413A), Yeak Mai (YM0413B), and Boeng Lumkut (LK0712A), and >0.1% of the total counts from YM0413B and YL1211B lake sediment cores. Descriptions follow Punt et al. (2007). Sample numbers match those specified on table H.1. Taxonomic references also listed on table H.1 and associated photomicrographs are presented figures H.1, H.2, H.3 & H.4. ♣ - TS = tree/shrub; H = dryland herb; W/A = wetland/aquatic; P = pteridophyte, ⊕ - C = circular; R = rectangular; HL = hexalobate; SA = subangular; A = angular; L = lobate; IH = interhexagonal; Q = quatrefoil; H = hexagonal; SL = semilobate, and ♠ - O = oblate; SO = sub-oblate; OS = oblate spheroidal; S = spheroidal; PS = prolate spheroidal; SP = sub-prolate; P = prolate.

Family	Sample Name	photo code	Forest Unit	Plant functional group ♣	YO0712A (%)	YL0413A (%)	YM0413A (%)	LK0712A (%)	YM0413B (%)	YL1211B (%)	morphology	mean P axis (μm)	mean E axis (μm)	⊕ P shape	♠ E shape
Poaceae	Poaceae	p1	undiff.	H	5.8	15.3	45.4	20.7	45.4	11.3	C0P1	var.	var.	C	O-P
Cyperaceae	Cyperaceae	p2	W, MDF	W/A	1.2	0.0	9.3	2.4	6.6	1.5	inaper.	var.	var.	C	P
Cannabaceae	*Trema*	p3i,ii	SF, SEDF, MDF	TS	5.3	3.5	7.2	6.1	5.0	40.4	C0P2	13.5	16.0	C	SO
Cannabaceae	*Aphananthe* cf	p4	SEDF	TS	0.0	17.6	1.0	0.0	0.3	0.7	C0P3	18.0	20.0	C	O-S
Cannabaceae	*Celtis*	p5i,ii	SEDF, MDF	TS	1.8	4.7	0.0	2.4	0.6	0.3	C0P3	21;22	21; 23	C	S;OS
Ulmaceae/ Apocynaceae	Holoptelea/ Wrightia sf C0P4	p6	SF, MDF, SEDF/ MDF	TS	0.0	0.0	0.0	0.0	0.1	0.5	C0P4	18.0	21.0	R	SO
Ulmaceae	*Holoptelea* C0P5 cf	p7	MDF	TS	0.0	0.0	0.0	0.0	<0.1	0.1	C0P5	20.0	22.5	C	OS
Ulmaceae	*Holoptelea* C0P6 sf	p8	MDF	TS	0.0	0.0	0.0	0.0	<0.1	0.1	C0P5	22.0	23.0	C	SO
Ulmaceae	*Zelkova*	p9	LMF	TS	0.0	0.0	0.0	0.0	<0.1	0.1	C0P4	20.0	24.0	C	SO
Combretaceae	*Terminalia tomentosa* cf	p10	DDF, MDF	TS	0.0	0.0	3.1	7.3	2.9	0.4	C3P3	15.0	12.0	HL	SP
Combretaceae/ Melastomataceae	Combretaceae/ Melastomataceae undiff.	p11i-iii	undiff.	TS	2.3	0.0	0.0	2.4	0.6	0.1	C3P3	21;24;16	20;19;14	HL	PS-SP
Combretaceae/ Melastomataceae	*Anogeissus/Memecyclon*	p12	MDF, RF, SF	TS	1.2	1.2	0.0	3.7	0.7	1.1	C3P3	11.5	9.5	HL	SP
Myrtaceae	*Syzygium*	p13	MDF, RF/ SwF	TS	4.7	0.0	0.0	17.1	3.4	5.1	C3P3	8.5	11.5	SA	SO

Continued...

Family	Sample Name	photo code	Forest Unit	Plant functional group ♣	YO0712A (%)	YL0413A (%)	YM0413A (%)	LK0712A (%)	YM0413B (%)	YL1211B (%)	morphology	mean P axis (µm)	mean E axis (µm)	⊕ P shape	♠ E shape
Myrtaceae	Myrtaceae >17µm	p14	undiff.	TS	2.3	5.9	0.0	6.1	0.1	0.2	C3P3	11.0	18.5	SA	O
Urticaceae/ Moraceae	Urticaceae/ Moraceae type	p15i-iv	undiff.	TS	23.4	4.7	2.1	2.4	2.4	8.1	C0P2	13;20;13;14	14;20;13.5;14.5	C	OS-S
Moraceae	*Ficus*	p16	SEDF	TS	8.8	2.4	0.0	0.0	0.4	1.1	C0P2	10.0	16.0	C	O
Fagaceae	Lithocarpus/ Castanopsis	p17	LMF	TS	0.0	0.0	2.1	0.0	1.7	3.5	C3P3	14.0	10.5	L	O
Fagaceae	*Quercus*	p18i,18ii	LMF	TS	2.3	1.2	1.0	0.0	2.4	1.4	C3P3	23.0	21.0	C-L	PS
Betulaceae	Carpinus/ Ostrya sf	p19	LMF	TS	0.0	0.0	0.0	0.0	1.2	1.8	C0P3	14.5	18.0	C-HL	SO
Betulaceae	*Betula* sf	p20	LMF	TS	0.0	0.0	0.0	0.0	0.3	0.3	C0P3	14.0	19.0	C	O
Myricaceae	*Myrica* cf	p21	LMF, RF	TS	0.0	2.4	0.0	1.2	0.1	0.3	C0P3	18.0	21.0	C	SO
Juglandaceae	*Engelhardtia* cf	p22	LMF	TS	0.0	0.0	0.0	0.0	<0.1	<0.1	C0P3	16.0	16.5	C	OS
Dipterocarpaceae	Hopea/ Shorea type	p23i,ii	SEDF, MDF, DDF	TS	1.8	1.2	1.0	0.0	1.1	1.2	C3P0	22;20	22;21	C	S-OS
Dipterocarpaceae	Dipterocarpaceae obtusifolia/ D. tuberculatus	p24	MDF, DDF	TS	0.0	1.2	0.0	2.4	0.3	<0.1	C3P0	50.0	49.0	C	PS
Dipterocarpaceae	*Dipterocarpus* undiff grouped	p25	MDF, DDF	TS	0.0	2.4	1.0	2.4	0.9	<0.1	C3P0	25.5	30.0	C	SO
Datiscaceae	*Tetrameles*	p26i,ii	SEDF, MDF	TS	13.5	3.5	1.0	1.2	1.1	1.0	C3P3	9.5	11.5	C	PS
Datiscaceae	*Tetrameles* sf	p27i-iii	SEDF, MDF	TS	0.0	0.0	0.0	0.0	0.3	0.5	C3P3	13.0	12.0	C	PS
Primulaceae (formerly Myrisinaceae)	*Ardisia* cf	p28	SF	TS	0.0	0.0	0.0	0.0	<0.1	0.1	C3P3	15.5	12.5	IH	SP
Elaeocarpaceae	*Elaeocarpus* cf	p29	RF	TS	0.6	0.0	0.0	0.0	0.1	0.9	C3P3	8.5	9.0	C	OS
Unknown	Unk. pollen type 7	p30	?	n/a	0.0	0.0	0.0	0.0	0.2	<0.1	C3P3	5.5	5.5	C	S
Euphorbiaceae	*Mallotus*	p31	SF	TS	2.9	2.4	2.1	0.0	1.0	5.1	C3P3	18.0	19.0	C	OS
Euphorbiaceae	*Macaranga*	p32	SF	TS	0.6	0.0	0.0	1.2	0.6	0.8	C3P3	12.0	11.5	C	PS
Euphorbiaceae	*Aporusa/ Antidesma cf*	p33	DDF, SF, MDF, SF	TS	0.0	1.2	0.0	2.4	1.5	1.9	C3P0	19.0	16.0	IH	SP
Phyllanthaceae	*Phyllanthus*	p34	MDF, SF	TS	0.0	0.0	0.0	0.0	0.2	<0.1	C4P4	16.0	16.0	Q	S

Continued...

Family	Sample Name	photo code	Forest Unit	Plant functional group ♣	YO0712A (%)	YL0413A (%)	YM0413A (%)	LK0712A (%)	YM0413B (%)	YL1211B (%)	morphology	mean P axis (µm)	mean E axis (µm)	⊕ P shape	♠ E shape
Phyllanthaceae	*Glochidion*	p35	SF	TS	0.0	0.0	0.0	0.0	0.1	<0.1	C4P4	16.0	16.5	Q	OS
Lythraceae	*Lagerstroemia*	p36	MDF, SF, SEDF	TS	3.5	3.5	4.1	9.8	0.7	0.6	C3P3	20;26	24;25.5	H	SO-SP
Lythraceae	*Rotala*	p37	W	W/A	0.6	0.0	0.0	0.0	0.2	<0.1	C3P3	13.0	11.5	H	PS
Lythraceae	Lythraceae cf	p38	n/a	TS	0.0	0.0	0.0	0.0	0.1	0.2	C3P3	28.0	22.0	H	SP
Sapotaceae	Madhuca cf	p39i,ii	SF	TS	0.0	0.0	0.0	0.0	<0.1	<0.1	C3P3	24.5;23	25;21	C	OS-PS
Lauraceae	*Litsea* cf	p40	SEDF, SF	TS	0.0	1.0	0.0	0.0	<0.1	0.1	inaper.	25.0	25.0	C	S
Rubiaceae	Adina/ Nauclea type	p41i,ii	undiff.	TS	1.2	1.2	2.1	0.0	0.0	0.4	C3P3	17;11	18.5;12	SA;C	OS
Rubiaceae	*Uncaria/ Wendlandia*	p42	undiff.	H	0.0	0.0	0.0	0.0	0.2	0.3	C3P3	15.5	15.0	SA	PS
Rubiaceae	*Rubia* cf	p43	?	H	0.0	0.0	0.0	0.0	0.1	<0.1	C6P6	18.0	18.0	C	S
Rubiaceae	*Timonius* sf	p44	?	TS	0.6	0.0	0.0	0.0	<0.1	<0.1	C3P3	32.0	31.0	C	PS
Rubiaceae	Rubiaceae sf type 1	p45	?	TS	1.2	0.0	0.0	0.0	<0.1	<0.1	C3P3	19.5	19.0	C	PS
Rubiaceae	Rubiaceae other grouped	n/a	undiff.	TS/H	0.0	1.2	0.0	1.2	0.2	0.3	misc.	misc.	misc.	misc.	misc.
Sapindaceae/ Rubiaceae	Sapindaceae/ Rubiaceae t1 & t2	p46i,ii	undiff.	TS/H	0.6	0.0	0.0	0.0	0.5	0.2	C3P3	11;12.5	13.5;14.5	SA	SO
Sapindaceae	*Schleichera oleosa/ Cupaniopsis cf*	p47	SEDF, SF, MDF	TS/H	12.9	0.0	3.1	2.4	0.2	<0.1	C3P3	10.5	19.0	SA	O
Rhamnaceae	*Rhamnus/ Sageretia*	p48	?	TS	0.0	0.0	0.0	0.0	0.2	0.2	C3P3	15.0	13.0	SL	SP
Rhamnaceae/ Sapindaceae	Zizyphus/ Nephelium sf	p49	SEDF	TS	0.0	0.0	0.0	0.0	0.2	0.1	C3P3	16.5	18.0	SA	OS
Irvingiaceae	*Irvingia malayana*	p50	MDF, SF	TS	0.6	0.0	0.0	1.2	0.2	0.2	C3P0	14.0	15.5	SA	OS
Rutaceae	*Zanthoxylum* cf	p51	SEDF	TS	0.0	0.0	0.0	0.0	0.1	0.5	C3P3	17.0	14.5	C-SA	SP
Ebenaceae	*Diospyros* cf	p52	SEDF, MDF, SF	TS	0.6	0.0	0.0	0.0	0.1	<0.1	C3P3	19.0	17.5	IH	PS
Stemonuraceae/ Proteaceae	Gomphandra/ Roupala/ Helicia sf	p53	?	TS	0.0	0.0	0.0	0.0	<0.1	0.2	C0P3	13.0	17.0	SA	O
Rhamnaceae (?)	Unknown - *Alphitonia* sf (?)	p54	?	n/a	3.5	0.0	0.0	0.0	<0.1	0.2	C3P0	12.0	13.0	SA	OS
Burseraceae	*Canarium cf*	p55	SEDF	TS	0.0	0.0	0.0	0.0	<0.1	0.1	C3P3	26.5	20.0	C	SP
Meliaceae	*Toona*	p56	SEDF	TS	0.6	0.0	0.0	0.0	<0.1	0.1	C4P4	27.5	24.5	R	PS
Aquifoliaceae	*Ilex*	p57	SEDF	TS	1.2	0.0	0.0	0.0	<0.1	0.1	C3P0	19.0	18.0	C-SA	PS

Continued...

Family	Sample Name	photo code	Forest Unit	Plant functional group ♣	YO0712A (%)	YL0413A (%)	YM0413A (%)	LK0712A (%)	YM0413B (%)	YL1211B (%)	morphology	mean P axis (μm)	mean E axis (μm)	⊕ P shape	♠ E shape
Fabaceae - Mimosoideae	*Adenanthera cf*	p58	SEDF, MDF	TS	0.6	2.4	0.0	0.0	<0.1	<0.1	polyad	18.0	23.0	A	SO
Fabaceae - Mimosoideae	*Acacia/ Albizzia*	p59	RF, MDF, SF	TS	0.0	0.0	0.0	0.0	<0.1	0.2	polyad	26.0	26.0	A	S
Fabaceae - Caesalpinioideae	*Intsia*	p60	?	TS	0.0	0.0	0.0	0.0	<0.1	<0.1	C3P0	41.0	40.0	C-L	PS
Fabaceae	Legume	p61	undiff.	TS	0.0	0.0	0.0	0.0	<0.1	0.1	C3P3	23.0	13.0	C-L	P
Bombacaceae	Bombax sf type 1	p62	MDF	TS	0.0	1.2	0.0	0.0	<0.1	<0.1	C3P0	16.0	34.0	C	O
Bombacaceae	Bombax type 2	p63	MDF	TS	0.0	0.0	1.0	0.0	<0.1	<0.1	C3P0	?	50.0	SA	O
Pinaceae	*Pinus*	p64	LMF	TS	0.0	0.0	0.0	0.0	0.8	0.3	sacc.	20-37	30-56		O
Podocarpaceae	*Dacrycarpus*	p65	LMF	TS	0.0	0.0	0.0	0.0	<0.1	<0.1	sacc.	40	43		O
Podocarpaceae	Podocarpaceae	p66	LMF	TS	0.0	0.0	1.0	0.0	<0.1	<0.1	sacc.	29	22		SP
Chenopodiaceae	Chenopodiaceae sf e>10μm	p67	SF	H	0.0	0.0	0.0	0.0	0.1	<0.1	pantopor.	9.0	9.0	C	S
Chenopodiaceae	Chenopodiaceae	p68	SF	H	0.0	0.0	0.0	0.0	0.1	<0.1	pantopor.	16.0	16.0	C	S
Caryophyllaceae	Caryophyllaceae	p69	SF	H	0.0	0.0	0.0	0.0	<0.1	<0.1	pantopor.	30.0	30.0	C	S
Asteraceae	other Asteraceae grouped	p70i-v	undiff.	H	0.0	0.0	0.0	0.0	0.3	0.3	C3P3	18;19;16;16.5;16	18;20;17.5;17;17	C	OS-PS
Arecaceae	Arecaceae cf	p71	undiff.	TS	0.0	0.0	0.0	0.0	0.3	0.3	P0S1	9.0	17.9	C	O
Polygonaceae	*Persicaria* cf	p72i,ii	undiff.	H	0.0	0.0	0.0	0.0	<0.1	<0.1	inaper.	16;27	16;27	C	S
Amaranthaceae ?	Unk. - Amaranthaceae sf	p73	?	H	0.0	0.0	0.0	0.0	0.8	<0.1	inaper.	23.0	23.0	C	S
Unknown	Unk. pollen type 1	p74	?	?	0.0	0.0	0.0	0.0	0.2	<0.1	C3P3	13.0	13.5	C	OS
Unknown	Unk. pollen type 2	p75	?	?	1.2	0.0	0.0	0.0	0.1	<0.1	C2P0	8.0	8.0	R	S
Unknown	Unk. pollen type 3	p76	?	?	0.0	0.0	0.0	0.0	0.1	<0.1	P0S1	32.0	53.0		O
Euphorbiaceae (?)	Unk. pollen type 4	p77	?	?	0.0	0.0	0.0	0.0	<0.1	0.2	C3P3	16.6	11.5	IH	P
Potamogetonaceae (?)	Unk. pollen type 5	p78	?	?	0.0	0.0	0.0	0.0	<0.1	0.1	inaper.	15.0	15.0	C	S
Unknown	Unk. pollen type 6	p79	?	?	0.0	0.0	0.0	0.0	<0.1	0.1	C3P3	13.0	11	C-L	SP
Balsaminaceae	*Hydrocera trifolia*	p80	n/a	W/A	0.0	0.0	0.0	0.0	3.3	<0.1	C3P3	?	25.0	SA	?
Hydrocharitaceae	*Blyxa* cf	p81	n/a	W/A	0.0	0.0	2.4	0.0	0.7	<0.1	inaper.	23.0	29.0	C	SO
Blechnaceae	*Stenochlaena palustris*	p82	n/a	W/A	0.0	11.8	6.2	1.2	1.3	0.4	P0S1	24.0	38.0	C	O

Continued...

Family	Sample Name	photo code	Forest Unit	Plant functional group ♣	YO0712A (%)	YL0413A (%)	YM0413A (%)	LK0712A (%)	YM0413B (%)	YL1211B (%)	morphology	mean P axis (µm)	mean E axis (µm)	⊕ P shape	♠ E shape
Aspleniaceae	*Asplenium* cf	p83	n/a	P	0.0	0.0	0.0	0.0	0.1	<0.1	P0S1	27.0	44.0	C	O
Gleicheniaceae	*Gleichenia* cf	p84	n/a	P	0.0	0.0	0.0	0.0	0.1	<0.1	trilete	24	27.5	SA	SO
Nephrolepidaceae	*Nephrolepis* cf	p85	n/a	P	0.0	1.2	2.1	0.0	0.2	0.4	P0S1	20.0	33.0	C	P
Davalliaceae	Davalliaceae cf	p86	n/a	P	0.0	1.0	0.0	0.0	0.1	0.2	P0S1	21.0	34.0	C	P
Unknown	Unk. spore type 1	p87	n/a	P	0.0	0.0	0.0	0.0	<0.1	0.5	inaper.	12.5	14.0	C	OS
Pandanaceae (?)	Unk. spore type 2	p88	n/a	P	0.0	0.0	0.0	0.0	<0.1	0.3	inaper.	10.0	16.0	C	O

5.5 Description of plant microfossil record reconstructed from lake sediment cores

5.5.1 Yeak Mai palaeo-vegetation record (core YM0413B)

A plant microfossil record was produced for YM0413B from 112 samples. An average of 217 pollen grains and spores, including an average of 89 dryland pollen taxa (excluding grasses), were counted per sample depth. A total of 232 microfossil types were identified, including 69 pollen types and 16 spore types that could not be identified from comparison with available reference samples (representing <2.5% of the total microfossil count for the whole core). Identified plant microfossil taxa comprising greater than 0.1% of the total count[2] are grouped into major functional plant types and forest unit classifications, and are described alongside the surface core counts in table 5.1. Associated photomicrographs are presented in appendix H.

Cross-core plant microfossil makeup and associations

The plant microfossil assemblages from YM0413B are here described in the context of 1) summed relative abundance data (used to describe relative dominance of different microfossil taxa) and, 2) the PCA and Pearson's correlation results (used to delimit associations amongst microfossil taxa). It is notable to point out that the results of the PCA, conducted on scaled absolute abundance data, indicate a relatively high degree of inconsistency amongst the variables, with the first three principle components representing only 25.6%, 10.3% and 7% (total = 42.9%) of the variance, respectively (see figure 5.8 and table 5.2).

Dryland herbs

Poaceae is the dominant pollen type in the YM0413B samples, ranging from 7% (5 cm depth) to 72% (220 cm depth) of the total plant microfossil count for each sample. Of the plant microfossil variables, Poaceae contributes the largest degree of loading (negative) along PC3 (figure 5.8 and table 5.2). Following classifications by Maxwell (1999) (who draws on Maloney (1990)), Poaceae is split into two types based on size; >33 μm and <33 μm. This is based on the premise that the <33 μm fraction (ranging from 3% to 65% of the sample abundance) should be too small to have derived from rice agriculture, and thus is likely to reflect a somewhat "natural" site ecological setting. The two Poaceae size fractions do, however, correlate (r = 0.3), suggesting that at least some of the >33 μm type is derived from a similar environmental setting to the <33 μm fraction. Other dryland herbs that comprise between 0.1 and 0.3% of the total core count include grouped

[2] 0.1% was selected as a minimum cut off value for representing the core microfossil record so as to show a diverse assemblage of common and moderately common taxa while removing noise from taxa too rare to contribute to overall patterns of change down core.

Asteraceae types, *Uncaria/Wendlandia*[3], Chenopodiaceae types and *Rubia* cf. An unknown palynomorph comprises between 0% and 11% (185 cm) of the total sample count. This palynomorph displays a similar dodecahedral morphology, size and luminoid depressions to Amaranthaceae - *Telanthera* (Huang 1972 plate 11), though is missing micro-spines arranged along the tectum. Due to the lack of ornamentation, it is possible that this type is an alga, though no comparable morphologies were identified.

Wetland types, aquatics and pteridophytes

Prevalent wetland taxa include Cyperaceae (0% to 22% (70 cm) sample count), and *Stenochlaena palustris* (0 to 11% sample count). Subaquatic and aquatic pollen include *Hydrocera triflora* (0 to 17% sample count), *Blyxa* cf (0 to 4% sample count), and *Rotala* (0 to 1% sample count). Less common pteridophytes identified in the core sediments include *Nephrolepis* cf, *Davalliaceae* cf, *Asplenium* cf, and *Gleichenia* cf.

Wetland microfossil types — Cyperaceae and *Stenochlaena palustris* — alongside the unknown — Amaranthaceae type palynomorph (alga?), the swamp forest tree *Syzygium* and grouped Urticaceae/Moraceae, contribute to the maximum negative loading along PC2. Maximum positive loading along the same principle component is driven by the shallow water aquatics (*Blyxa* cf and *Hydrocera*) and secondary forest/ intermediate dry forest tree types *Trema* and *Celtis*. The Pearson's correlation indicates that variability in the abundance of *Blyxa* cf and *Hydrocera* is correlated throughout the record (r = 0.57).

Trees and shrubs

Pollen morphologies from trees and shrubs have been grouped into eight different classifications based on the florisitic composition of SASDTF unit-types discussed in chapter 3. Taxa comprising >0.1% of the raw count across the entire core are described in relation to these classifications below.

Semi-evergreen dry forest (SEDF) types

Key pollen taxa from this classification include (in order of whole core abundance) grouped Urticaceae/Moraceae types, *Tetrameles*, *Ficus*, *Aphananthe* cf, *Zizyphus/Nephelium* sf and *Zanthoxylum* cf. No association between the two dominant SEDF pollen types (Urticaceae/Moraceae types and *Tetrameles*) is evident from the PCA, and the no covariance is indicated in the correlation matrix (r = 0.07).

[3]Vegetation lists prepared for representative SASDTF units (see chapter 3) indicate that *Uncaria* spp. are more likely to occur as woody herbs or lianas vs. shrubs or trees, and that *Wendlandia* spp. (usually occurring as small shrubs or trees) do not appear to be common within this forest setting. Consequently, this pollen type was placed into the dryland herb classification.

Grouped mixed dry forest (MDF), intermediate mixed dry/semi-evergreen forests (Intermediate MDF & SEDF) and secondary forest (SF) types

Trema is the dominant tree/shrub species encountered in the core sediments, making up 12% of the dryland count across the entire core. Though a common pioneer tree following disturbance of SASDTF (Ruangpanit 1995), *Trema* is placed into this mixed classification as opposed to the pure secondary forest classification due to the presence of certain species (e.g. *T. velutina/tomentosa* Blume /(Roxb) Hara) in MDF and SEDF (Dy Phon 2000). However, results of the Person correlation show that *Trema* abundance has the strongest correlation with secondary forest type *Mallotus* (r = 0.59) and dry forest type *Terminalia tomentosa* cf (r = 0.45).

Other taxa included in this forest unit classification include *Aporusa/Antidesma* cf, *Anogeissus/Memecyclon* and *Celtis* comprising 4%, 2%, and 1.5% of the whole core dryland count, respectively. Less common pollen types include, in order of decreasing abundance across the whole core, *Phyllanthus*, *Schleichera oleosa/Cupaniopsis* cf, *Irvingia malayana*, *Holoptelea/Wrightia* sf C0P4 and *Diospyros* cf.

Dry deciduous forest (DDF) types: Mixed dry forest (MDF) & Dry Dipterocarp forest (DDF)

Terminalia tomentosa cf, *Dipterocarpus* other, and *Dipterocarpus obtusifolia/ D. tuberculatus* are the dominant pollen types from the MDF/DDF communities, comprising 8%, 2%, and 1% of the whole core dryland count, respectively. *Terminalia tomentosa* cf contributes to the greatest loading along PC1, strongly associating with *Poaceae* (r = 0.608) as well as *Aporusa/Antidesma* cf, *Mallotus* and lower montane forest types (*Quercus* and *Carpinus/Ostrya* sf).

SF types

Euphorbiaceae genera comprise the dominant taxa within the secondary forest classification. These include *Mallotus*, *Macaranga*, and *Glochidion*, making up 2.5%, 1.5%, and 0.2% of the whole count dryland count, respectively.

Semi-evergreen and deciduous dry forest generalists (DF generalists)

Grouped *Hopea/Shorea* and *Lagerstroemia* are DF generalist types comprising 3% and 2% of the total dryland core count respectively. The PCA indicates association of both *Lagerstroemia* and *Hopea/Shorea* types with *Dipterocarpus* and with dominant lower montane forest types (*Pinus* and *Lithocarpus/Castanopsis*) along PC1 and PC2 (figure 5.8 and table 5.2).

Swamp forest (SwF) and riparian forest (RF) types

Syzygium (9% total dryland count) and *Elaeocarpus* cf (0.3% total dryland count) pollen types have been classified as SwF/RF. The latter type has been

classified with a degree of uncertainty due to the small size of pollen grains encountered in the core (P = 8.5 $\pm$ 0.7 μm; E = 9 $\pm$ 0.4 μm) when compared with analysed reference material (P = 13.8 $\pm$ 0.8 μm; E = 14.3 $\pm$ 0.6 μm) (appendix G).

Lower montane forest (LMF) types

LMF types encountered in YM0413B include *Quercus*, *Lithocarpus/Castanopsis* type, *Carpinus/Ostrya* sf, *Pinus*, *Betula* cf, and *Myrica* cf, representing 6.5%, 5%, 4%, 2%, 0.6% and 0.4% of the whole core dryland count, respectively. *Carpinus/Ostrya* sf type is classified with a degree of uncertainty due to its relatively small size (P = 14.5 $\pm$ 1 μm; E = 18 $\pm$ 1.5 μm) and dissimilar rectangular pore when compared with the project reference collection specimens from *Carpinus betulus*, *C. orientalis* and *Ostrya carpinifolia*, which are typically larger and have round, annulate pores (appendix G).

Undifferentiated (Undiff.) types

Dominant undifferentiated tree and shrub pollen taxa include Sapindaceae / Rubiaceae type (1.2% dryland count) and Combretaceae/Melastomataceae undiff. (1.5% dryland count). The PCA indicates no clear association of either of these types with other classified tree and shrub taxa. Less common undifferentiated tree and shrub pollen types found within YM0413B sediments include Arecaceae cf, *Rhamnus/Sageretia*, Rubiaceae grouped (excluding those representing dry herbs), Lythraceae cf and Myrtaceae type 2 (>17 μm).

Unknown types

Unknown pollen types that each comprise between 0.1 and 0.2% of the total core count for YM0413B include unknown types 1, 2, 3 and 7. Descriptions and photomicrographs of these are presented in table 5.1 and appendix H, respectively.

Description of pollen and spore diagrams

Down core change in total microfossil abundance

The total absolute microfossil abundance count data calculated from YM0412B pollen and spore samples are plotted as pollen grains and spores per dry cubic cm (hereafter referred to as grains/cm^3) on figure 5.7.

The overall trend in total pollen abundance displays a negative relationship with modelled mineral influx (r = -0.46), and four major shifts are apparent. From the core base (543 cm) to approximately 455 cm, total pollen abundance displays high amplitude, high frequency fluctuations, and is overall relatively high (an average of 2.00 $\times$ 10^6 grains/cm^3, compared with an average of 7.74 $\times$ 10^4 grains/cm^3 for the entire record). The frequency and

amplitude of the fluctuations in total pollen abundance as well as overall abundance declines between 455 and 305 cm (5.94×10^4). Abundance thereafter sharply drops to the core low at 295 cm (1.00×10^4 grains/cm^3) and remains low to 220 cm before it rapidly rises to peak at 165 cm (1.89×10^5). This pattern by-and-large reflects the inverse to trends in bulk mineral influx across the same depth interval. Up core of 165 cm, there is an overall gradual decline in the total abundance of pollen and spores encountered in the samples (average abundance across this depth interval is 9.32×10^4).

Down core change in major functional types

A summary diagram of the relative abundance of the functional plant types (i.e. grass, other dryland taxa, wetland and aquatic types and pteridophytes) is plotted alongside abundance data on figure 5.7. The microfossil abundance is positively correlated with dryland taxa (excluding grasses) (r = 0.407) and pteridophytes (r = 0.339). The relative abundance of grass, on the other hand, displays a negative correlation with absolute microfossil abundance (r = - 0.457).

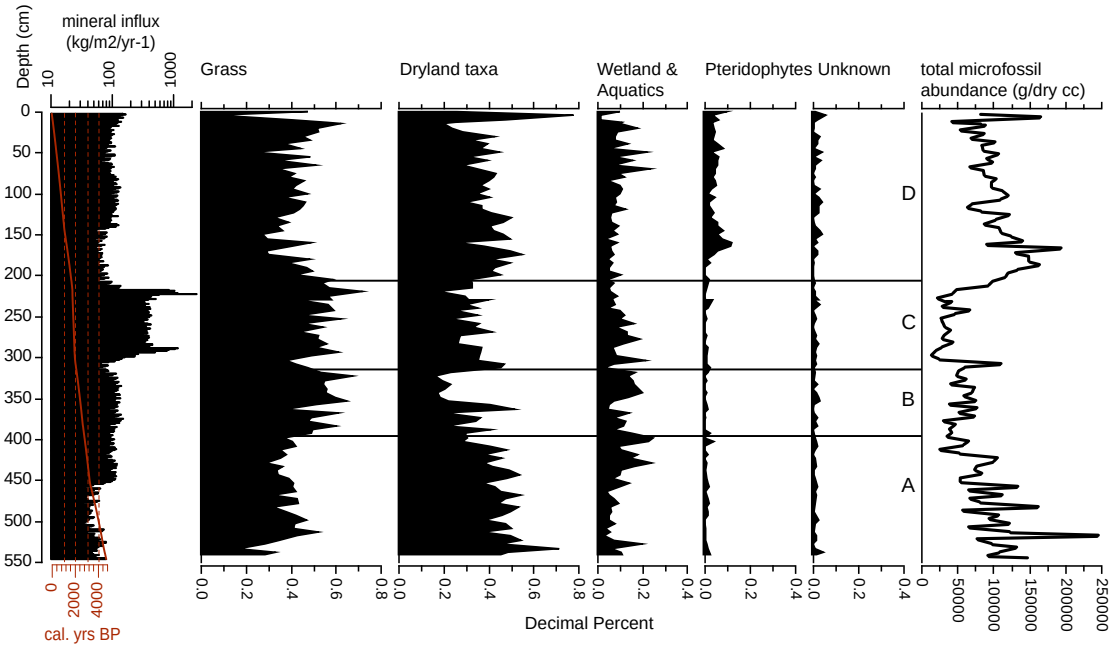

FIGURE 5.7: Summary diagram showing down core changes in relative abundance of YM0413B major plant microfossil groups. These are plotted as decimal percentages alongside the total abundance of pollen and spore counts per sample and estimated bulk mineral influx values calculated for the core.

Results of stratigraphically constrained cluster analysis for relative abundance data (delineated on figure 5.7) indicate major assemblage changes between 395.5 and 400 cm (dissimilarity distance = 11.2), 315.5 and 320 cm (dissimilarity distance = 9), and 205.5 and 210 cm (dissimilarity distance = 10.1). The primary, and most basal of these boundaries, captures a shift from an assemblage comprising a roughly equal proportion of grass and

other dryland taxa between 543.5 and 400 cm (figure 5.7 cluster A), to one dominated by grasses between 395.5 and 320 cm (figure 5.7 cluster B). A particularly large peak in grass abundance to approximately 60% occurs within cluster B between 355.5 and 325 cm, corresponding with a peak in wetland and aquatic types (approximately 15%), and a trough in the relative abundance of dryland taxa to approximately 20%. Cluster C, extending from 315.5 to 210 cm captures an initial sharp peak in the relative abundance of dryland taxa (and corresponding drop in grasses and wetland and aquatic taxa) between 315.5 and 295 cm. Between 295 and 200 cm, the relative abundance of grass is high, approximately corresponding to logged sedimentary unit II (see chapter 4), a peak in bulk mineral influx and a trough in total microfossil abundance. Across this depth interval, wetland and aquatic taxa peak at 285 cm (18% relative abundance) before gradually declining to approximately 5 to 6% relative abundance up core of 230 cm. The uppermost core cluster (D), extending from 205.5 cm to the core top sample (0 to 0.5 cm), sees the recovery of dryland taxa and grasses to levels roughly comparable to those observed in cluster A. The relative abundance of pteridophytes rises from a relatively constant average of 1.2% (543.3 and 180 cm) to 5.5% between 175.5 cm and the top of core. A major peak in the relative abundace of dryland taxa, corresponding with high total microfossil abundance, occurs at 5cm depth.

Down core change in pollen and spore abundance

Pollen and spore types representing greater than 0.1% of the total count have been grouped by major functional group and are plotted as absolute abundance down-core sequences on figures 5.9 & 5.10 (A). The trees and shrubs sequence, presented on figure 5.10, has been further grouped by the forest unit classifications described in section 5.5.1 above. The down core changes in the relative abundance of these classifications is shown on figure 5.10 (B).

Results of the stratigraphically-constrained cluster analysis grouped the absolute abundance microfossil sequence into eight major zones (boundaries shown on figures 5.9 & 5.10 (A)). Cluster boundaries and their dissimilarity distances (bracketed) occur between 520 and 515.5 cm (1.04×10^6), 510.5 and 515 cm (1.08×10^6), 480 and 475.5 cm (9.45×10^5), 305 and 300.5 cm (1.15×10^6), 215 and 210.5 cm (1.27×10^6), 135 and 130.5 cm (9.14×10^5) and 80 and 75.5 cm (9.81×10^5). Major changes in the microfossil sequence are described in the context of these clusters below.

Cluster zones 1 to 3: 543.5 to 475.5 cm (*c.* 4722 to 3746 cal. yrs BP)

The non-arboreal pollen assemblage reconstructed from the basal core sediments is characterised by a high abundance of Poaceae, *Blyxa* cf and *Hydrocera trifolia* alongside a relatively low abundance of other wetland taxa, including *Stenochlaena palustris*, *Rotala* and Cyperaceae (figure 5.10).

Cluster zones 1 through 3 coincide approximately with relative abundance cluster RAz1 (543.5 to 470.5 cm, dissimilarity distance = 6.4) reconstructed

from analysis of relative changes in the pollen contributions from the different forest unit classifications (figure 5.10 B). Cluster RA1 shows significantly high proportions of pollen types from the secondary forest and grouped mixed dry forest, intermediate mixed dry/semi-evergreen forests classifications. The absolute abundance sequence (figure 5.9) indicates that this trend is likely due to high abundance of *Mallotus*, *Trema* and *Celtis* between 543.5 and 475.5 cm. Additional changes in the absolute abundance of arboreal pollen taxa include the high abundance of *Tetrameles* across cluster 1 (543.5 to 515 cm) and high abundance of *Anogeissus / Memecyclon* across cluster 3 (510 to 475.5 cm).

Cluster zone 2 represents one sample (515 to 515.5 cm, modelled at *c.* 4327 cal. yrs BP) within cluster zones 1 to 3 that is distinguished by a major spike in Poaceae (both size fractions) alongside anomalously high abundance of some tree and shrub pollen types, including *Terminalia tomentosa* cf, *Dipterocarpus obtusifolius / D. tuberculatus*, *Mallotus*, *Trema*, *Aporusa / Antidesma* cf, *Holoptelea / Wrightia* cf. and *Aphananthe* cf.

A spike in pollen from *Mallotus*, *Trema*, *Celtis*, *Rubia* cf, *Blyxa* cf and Poaceae marks the upper boundary of cluster 3 at 475.5 cm.

Cluster zone 4: 475.5 to 300.5 cm (*c.* 3746 to 1993 cal. yrs BP)

Cluster zone 4 is most clearly distinguished from cluster zones 1 to 3 by the abrupt drop in *Mallotus*, *Trema*, *Macaranga* and *Celtis* pollen. A slight rise in the abundance of *Hopea / Shorea* and *Syzygium* pollen also distinguishes the lower portion of zone 4 (475.5 to 420 cm) from the pollen assemblage reconstructed from underlying sediments.

Up core of 450 cm (modelled at 3299 cal. yrs BP), there is a decline in overall abundance, and increased variability of most pollen and spore types across the record. This coincides with an overall increase in mineral influx and increased spacing of interbeds (IIa and IIb) within logged sedimentary unit II (see chapter 4 for core log details).

A second drop in the overall abundance of many dominant tree and shrub taxa occurs within cluster 4 at 425 cm (modelled at 3078 cal. yrs BP), including *Terminalia tomentosa* cf, *Trema*, *Aporusa / Antidesma* cf, *Hopea / Shorea*, *Lagerstroemia*, *Syzygium*, *Quercus*, *Lithocarpus / Castanopsis* and *Carpinus / Ostrya* sf. This drop does not coincide with a logged sedimentary interbed boundary or a significant change in mineral influx, but does correspond with a decline in overall microfossil abundance (see figure 5.7).

A major drop in the abundance of *Blyxa* cf and *Hydrocera* pollen occurs between 380 cm and 355 cm (modelled age 2676 to 2478 cal. yrs BP), after which abundance only partially recovers to the top of cluster 4 (300.5 cm).

A significant spike in Cyperaceae, and a moderate spike in *Blyxa* cf occurs within the upper sample from cluster 4 (300 to 300.5 cm, modelled at 1993 cal. yrs BP). This corresponds with relatively high numbers of arboreal taxa from the mixed dry forest, intermediate mixed dry/semi-evergreen forest classification (figure 5.10), driven by an increase in the absolute abundance

of *Trema*, *Aporusa* / *Antidesma* cf, *Celtis* and *Anogeissus* / *Memecyclon* pollen. A spike in *Lagerstroemia* pollen at this sample depth is also evident.

Cluster zone 5: 300.5 to 210.5 cm (*c.* 1993 to 1711 cal. yrs BP)

Cluster 5 is distinguished from the underlying record by an abrupt reduction of pollen and spore abundance. This coincides with the dramatic increase in mineral influx modelled for logged sediment unit III (288 to 217 cm, see chapter 4 for stratigraphic details), particularly at the upper and lower boundaries.

Poaceae and Cyperaceae pollen persist through zone 5 at a comparably high abundances relative to the rest of the plant microfossil record. The absolute abundance of *Blyxa* cf, and especially *Hydrocera trifolia* drops dramatically in cluster zone 5 and thereafter (to the core top), become minor components of the plant microfossil record.

Arboreal taxa from the SEDF forest classification (other than Urticaceae types) occur at very low abundances relative to the other forest classification types throughout zone 5. Taxa from the dry deciduous forest, secondary forest and dry forest generalist classifications persist across cluster 5 at relative abundances that are largely consistent with levels in overlying and underlying sediments (figure 5.10 (B)).

Cluster zones 6 to 8: 210.5 to 0 cm (*c.* 1711 cal. yrs BP to 2013 AD)

The transition from cluster zone 5 to cluster zone 6 represents an abrupt increase in the overall abundance of pollen and spore types across the record, corresponding with a decline in estimated mineral influx (figure 5.7) for the core.

Zone 6 marks the emergence of wetland types *Rotala* and *Stenochlaena palustris* (sharply peaking at 185 to 165 cm) alongside the unknown Amaranthaceae-type palynomorph (alga ?) and grouped monolete spore types as dominant components of the microfossil record. The abundance of *Rotala*, however, drops to negligible levels in cluster zone 8 between 65 cm and the core top.

The relative abundance of taxa from SEDF, swamp forest / riparian forest and lower montane forest classifications is relatively high throughout zones 6 (from 190 cm) to 8 when compared to the rest of the record, contributed to by the high absolute abundances of grouped Urticaceae / Moraceae (C0P3 types), *Tetrameles*, *Syzygium* and all lower montane forest types, as well at the emergence of *Ficus* and *Zanthoxylum* sf as novel dominants within the record (Figure 5.10). In general, this relates to the relatively low abundance of taxa from the mixed dry forest, intermediate mixed dry / semi-evergreen forest classification compared with the underlying sediments, particularly throughout cluster zones 7 and 8. In particular, the abundance of *Celtis* gradually declines to the core top, and *Phyllanthus* abundance drops to negligible levels throughout clusters 7 and 8.

The second shallowest core sample (5 to 5.5 cm, modelled at 1968 AD), shows an anomalous spike in arboreal taxa that occurs across the majority

of the dominant tree and shrub types (exceptions include *Celtis*, *Phyllanthus*, *Urticaceae / Moraceae* (C0P3 type), *Elaeocarpus* cf and *Betula* cf). A corresponding trough in Poaceae and Cyperaceae taxa is evident at this depth.

TABLE 5.2: YM0413B plant microfossil and charcoal eigenvalues, percentages and elemental variable loading from PCA.

	PC1 (26%)	PC2 (10%)	PC3 (7%)
Eigenvalue	7.17	2.88	1.96
R2 (%)	25.600	10.300	7.000
Poaceae	0.240	0.063	-0.306
Cyperaceae	0.147	-0.226	-0.219
Hydrocera trifolia	0.070	0.251	-0.127
Trema	0.201	0.350	0.015
Celtis	0.174	0.202	-0.214
Mallotus	0.268	0.135	-0.029
Macaranga	0.128	0.121	0.073
Aporusa/Antidesma cf	0.232	0.132	-0.190
Terminalia tomentosa cf	0.272	0.135	-0.137
Combretaceae/Melastomataceae undiff.	0.102	-0.077	-0.134
Syzygium	0.248	-0.246	0.047
Lithocarpus/Castanopsis	0.222	-0.141	0.284
Quercus	0.261	0.005	-0.037
Hopea/Shorea	0.215	-0.080	0.143
Dipterocarpus undiff.	0.197	-0.094	0.339
Pinus	0.244	-0.077	0.031
Urticaceae/Moraceae types	0.147	-0.262	0.048
Carpinus/Ostrya sf	0.247	0.108	0.125
Tetrameles	0.197	0.124	0.334
Lagerstroemia	0.225	-0.046	0.021
Sapindaceae/Rubiaceae types	0.155	-0.197	-0.040
Blyxa cf	0.072	0.411	-0.165
Anogeissus/Memecyclon	0.154	-0.016	0.261
Unknown - Amaranthaceae sf	0.183	-0.233	-0.070
Stenochlaena palustris	0.168	-0.265	-0.222
macro-charcoal ($\geq$ 250 μm)	0.058	0.277	0.233
250 μm > macro-charcoal $\geq$ 105 μm	0.007	0.189	0.257
micro-charcoal (<105 μm)	0.076	-0.002	-0.309

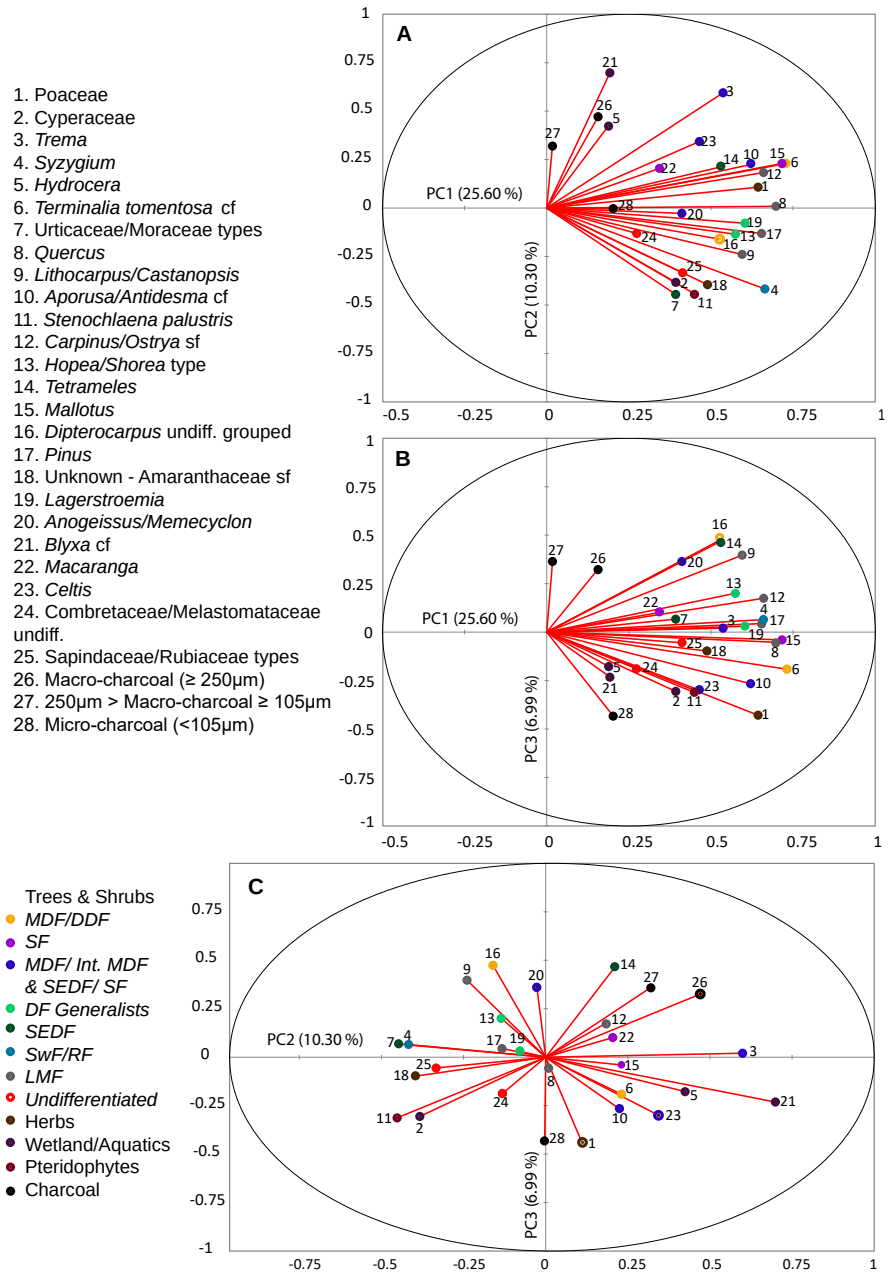

FIGURE 5.8: PCA of YM0413B microfossil (>0.5% raw count) and charcoal abundance data. Data normalised using z-scores prior to analysis. A) PC1 vs. PC2 (35.9% variance); B) PC1 vs. PC3 (32.59% variance); C) PC2 vs PC 3 (17.28% variance).

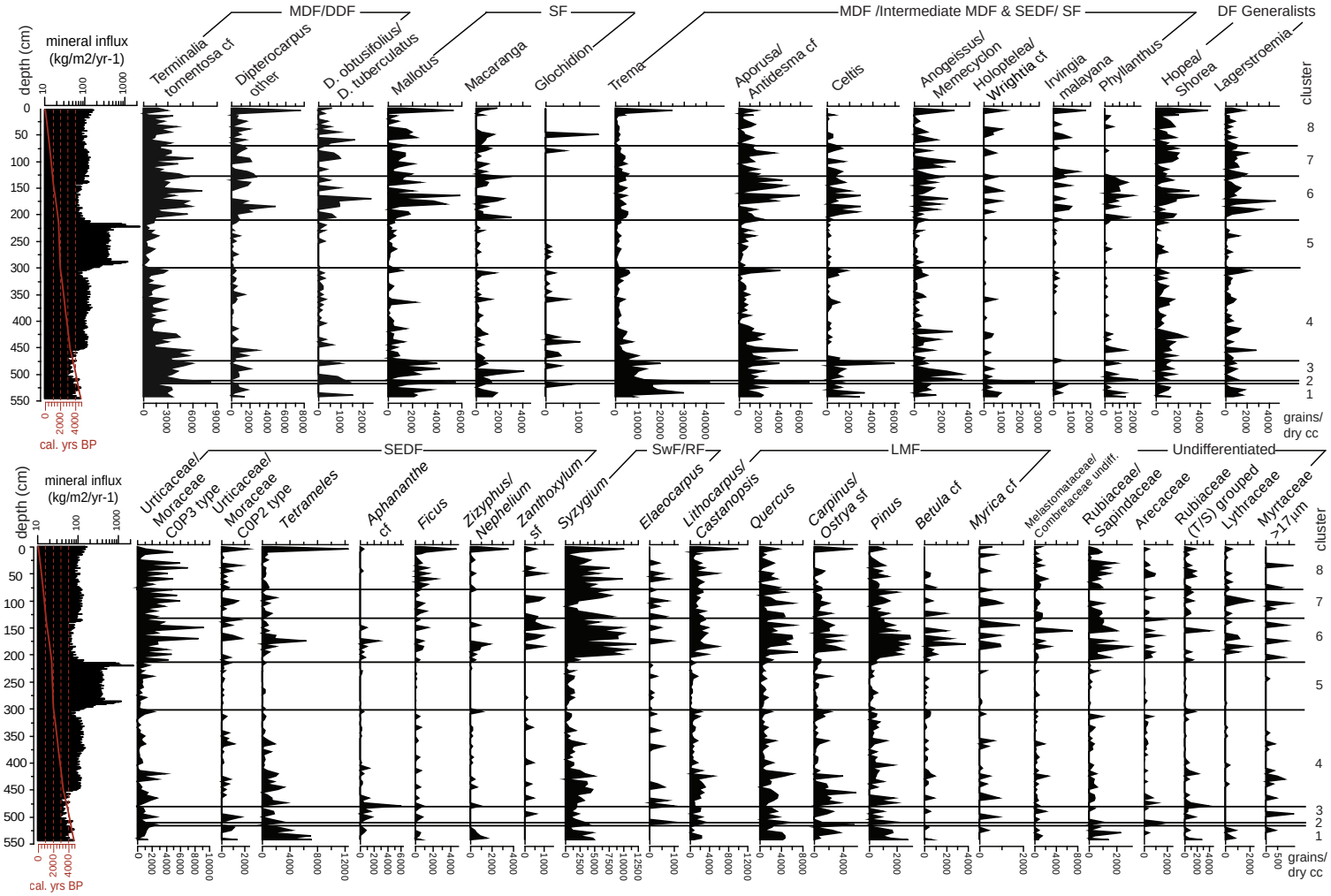

FIGURE 5.9: YM0413B pollen diagram showing absolute abundance of tree and shrub taxa that comprise greater than 0.1% of the total core count. Taxa have been grouped into forest units - MDF = Mixed Dry Forest; DDF = Dry Dipterocarp Forest; SF = Secondary Forest; SEDF = Semi-evergreen Dry Forest; DF = Dry Forest; SwF = Swamp Forest; RF = Riparian Forest; LMF = Lower Montane Forest. Note discrepancies in x-axis scaling between taxa.

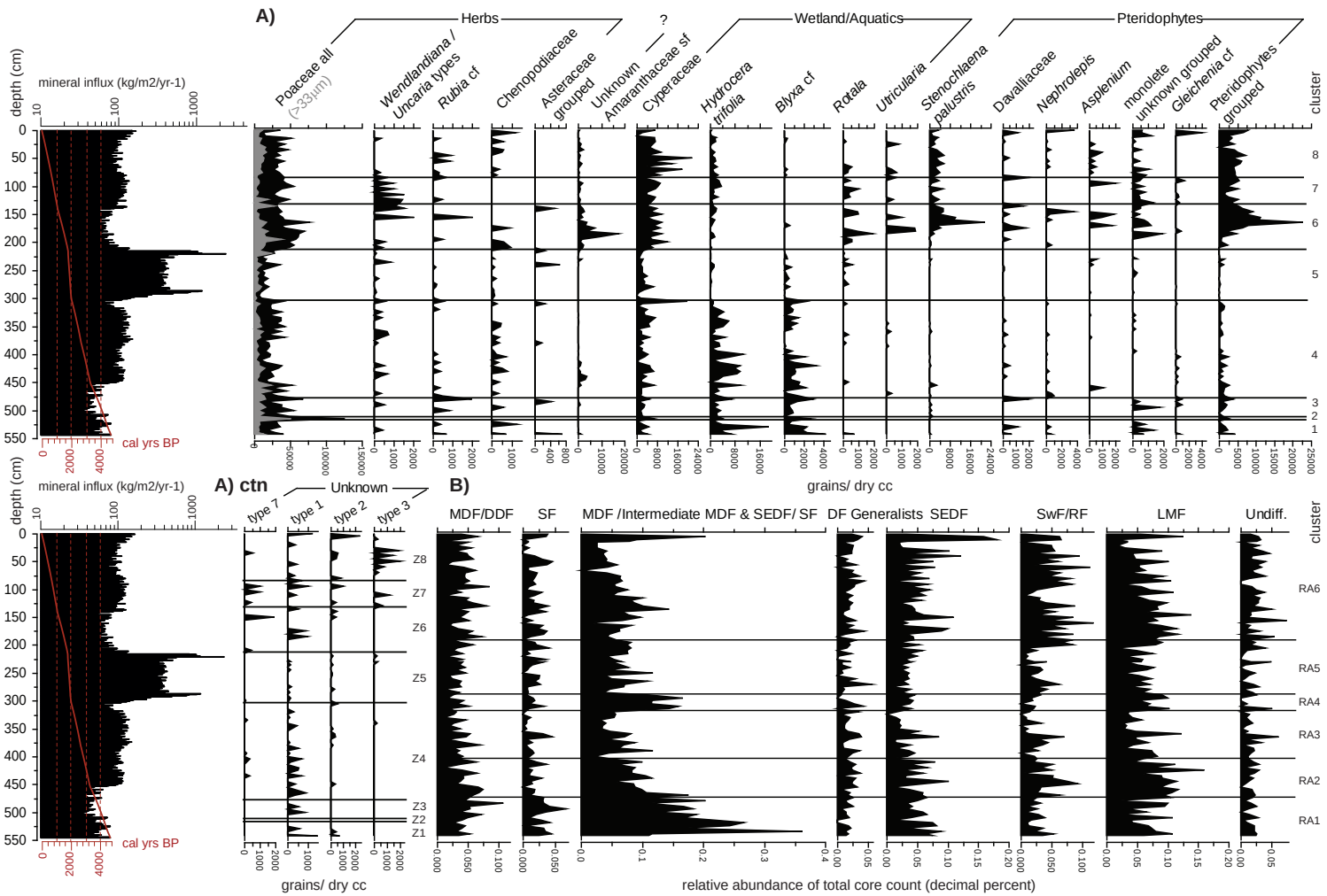

FIGURE 5.10: YM0413B pollen diagram. Top: Absolute abundance of dryland herb, wetland/aquatic, pteridophyte and unknown taxa that comprise greater than 0.1% of the total core count. Note discrepancies in x-axis scaling between taxa. Bottom: Relative abundance (total core microfossil count) of tree and shrub taxa grouped into forest units. Abbreviations as per figure 5.9.

5.5.2 Yeak Loam palaeovegetation record (core YL1211B)

A microfossil assemblage was produced for YL1211B from 42 samples. An average of 438 pollen grains and spores, including an average of 367 dryland pollen taxa (excluding grasses), were counted per depth sample. A total of 169 different plant microfossil types were identified from the whole core assemblage, including 42 pollen types and 9 spore types that could not be identified from comparison with available reference samples. As with YM0413B, the unknown types are relatively rare, comprising less than 3% of the total microfossil count for the whole core.

Cross-core plant microfossil makeup and associations

The plant microfossil makeup and association reconstructed from YL1211B sediments are described in the context of 1) summed relative abundance data (used to describe relative dominance of different microfossil taxa) and, 2) the PCA and Pearson's correlation results (used to delimit associations amongst microfossil taxa). As with the YM0413B microfossil record, a high degree of inconsistency exists amongst the YL1211B variables, with the top three principle components representing 21.7%, 13% and 10.5% (total = 45.2%) of the variance (see figure 5.12, and table 5.3).

Dryland herbs

Grouped Poaceae makes up approximately 11.5% of the total plant microfossil count for YL1211B. Seventy-three percent of this count is made up of large (>33 μm) grass pollen (i.e. 8.5% of the total core count). Grouped Asteraceae types and grouped *Uncaria / Wendlandia* types each make up approximately 0.3% of the total core count.

Wetland types, aquatics and pteridophytes

The dominant wetland plant microfossils encountered in YL1211B sediments are Cyperaceae (1.5% of the total core count) and *Stenochlaena palustris* (0.4% of the total core count). Less common pteridophytes include *Nephrolepis* cf and Davalliaceae cf. Two other palynomorphs that have tentatively been identified as spores, unknown spore (?) types 1 and 2, comprise 0.5% and 0.3% of the total core count respectively (see table 5.1 and appendix H for descriptions and photomicrographs of these types).

Trees and shrubs

Semi-evergreen dry forest (SEDF) types

Grouped Urticaceae/Moraceae pollen makes up 9% of the total core dryland count, (5% C0P2 types; 4.5% C0P3 types). *Ficus* and *Tetrameles* each make up 1.2% of the total core dryland count. Less common SEDF types

TABLE 5.3: YL1211B plant microfossil and charcoal eigenvalues, percentages and elemental variable loading from PCA.

	PC1 (22%)	PC2 (13%)	PC3 (11%)
Eigenvalue	5.413	3.249	2.608
R2 (%)	21.650	13.000	34.650
Trema	0.369	-0.207	-0.008
Poaceae	0.344	-0.203	-0.078
Urticaceae/Moraceae type	0.316	0.152	0.057
Syzygium	0.354	0.104	-0.038
Mallotus	0.318	-0.053	-0.090
Lithocarpus/Castanopsis	0.159	-0.073	0.296
Aporusa/Antidesma cf	0.191	-0.352	0.039
Carpinus/Ostrya sf	0.224	0.021	-0.284
Cyperaceae	0.182	-0.111	0.321
Quercus	0.118	0.258	0.197
Hopea/Shorea	0.173	-0.155	0.020
Ficus	0.125	0.275	0.064
Anogeissus/Memecyclon	0.220	0.079	0.244
Tetrameles	0.101	-0.179	0.263
Elaeocarpus cf	0.050	0.211	0.407
Macaranga	0.074	-0.211	-0.083
Aphananthe cf	0.101	0.401	-0.073
Lagerstroemia	0.015	0.105	0.317
Zanthoxylum cf	0.074	0.080	-0.118
Holoptelea/Wrightia sf C0P4	0.171	0.286	-0.106
Unknown spore type 2	0.208	0.342	-0.125
macro-charcoal ($\geq$ 250 μm)	-0.002	0.019	-0.233
250 μm > macro-charcoal $\geq$ 105 μm	-0.040	0.209	-0.218
micro-charcoal (<105 μm)	0.082	-0.145	-0.190

include, in order of decreasing abundance, *Aphananthe* cf, *Tetrameles* sf, *Zanthoxylum* cf, *Zizyphus / Nephelium*, *Toona*, *Litsea* cf, *Canarium* cf and *Ilex*. *Tetrameles* sf is morphologically similar to the *T. nudiflora* reference sample collected from the Yeak Loam lake catchment (see section 5.2.2), though has been classified with a degree of uncertainty as it does not exhibit the pinched colpi over the pore that was apparent in most of the *T. nudiflora* pollen grains that were analysed from both the lake catchment sample and the APSA reference collection (sample code: 208 3 1) (see appendix G for morphological details of these reference samples). The plant microfossil types classified as *Tetrameles* are, on the other hand, a similar size and shape to the *T. nudiflora* samples analysed from the APSA reference sample collection.

Aphananthe cf, which displays the greatest degree of loading (positive) along PC2, associates with *Ficus*, *Quercus*, *Holoptelea / Wrightia* sf (C0P4) and Unknown spore type 2 (figure 5.12).

Grouped mixed dry forest (MDF), intermediate mixed dry/semi-evergreen forests (Intermediate MDF & SEDF) and secondary forest (SF) types

Trema is the overwhelmingly dominant plant microfossil encountered in YL1211B, making up 48% of the dryland core count (40% of the total core count). Other pollen types falling into the intermediate dry forest and/or secondary forest classification include *Aporusa / Antidesma* cf (2% dryland count) and *Anogeissus / Memecyclon* (1.5% core dryland count). Less common taxa in this forest classification include *Celtis*, *Acacia / Albizzia*, grouped *Holoptelea* types, *Irvingia malayana*, and *Holoptelea / Wrightia* sf.

Trema contributes to the greatest degree of loading (positive) along PC1, and strongly associates with Poaceae ($r = 0.841$), as well as Urticaceae/Moraceae grouped types ($r = 0.543$), *Syzygium* ($r = 0.635$) and *Mallotus* ($r = 0.663$) (figure 5.12). Given that these variables are the top five dominant plant microfossils encountered in the core sediments, this relationship may be a product of the consistent representation of these pollen types in every core sample rather than representing any ecological association. *Aporusa / Antidesma* cf contributes to the greatest degree of negative loading along PC2, and associates with Poaceae, *Trema* and *Macaranga*.

MDF/ Dry deciduous forest (DDF) types

Terminalia tomentosa cf makes up 0.5% of the total core dryland count, and is the only taxon greater than 0.1% of the core count that falls into the MDF/DDF category.

SF types

Secondary forest types occurring within YL1211B include *Mallotus*, *Macaranga*, and *Ardisia* cf, representing 6%, 1% and 0.1% of the total dryland count, respectively.

Semi-evergreen and deciduous dry forest generalists (DF generalists)

Hopea / Shorea and *Lagerstroemia* make up 1.5% and 0.7% of the total dryland microfossil count for YL1211B, respectively.

Swamp forest (SwF) and riparian forest (RF) types

Syzygium and *Elaeocarpus* cf comprise 6% and 1% of the total dryland count respectively. *Elaeocarpus* cf contributes to the greatest degree of loading (positive) along PC3, and associates with *Lagerstroemia* ($r = 0.640$) as well as *Cyperaceae*, *Lithocarpus / Castanopsis*, *Tetrameles* and *Anogeissus / Memecyclon* types (figure 5.12).

Lower montane forest (LMF) types

Common LMF microfossil types from YL1211B include *Lithocarpus / Castanopsis* (4% total dryland count), *Carpinus / Ostrya* sf (2% total dryland count) and *Quercus* (1.5% total dryland count). Less common types within this classification include *Myrica* cf, *Pinus*, *Betula* sf and *Zelkova*.

Undifferentiated (Undiff.) types

Undifferentiated arboreal pollen types within the YL1211B microfossil assemblage include *Adina*-type, Sapindaceae/Rubiaceae type, Combretaceae / Melastomataceae undiff., Arecaceae cf, *Rhamnus / Sageretia*, Rubiaceae grouped, *Gomphandra / Roupala / Helicia* sf, Lythraceae cf, Myrtaceae >17 μm and Legume types. Each of these pollen types contribute to less than 1% of the total arboreal count for the core.

Unknown types

Unknown pollen types that each comprise between 0.1 and 0.2% of the total dryland core count for YL1211B include unknown types 4 (Euphorbiaceae?), 5 (Potamogetonaceae?), 6, 7 and unknown *Alphitonia* sf type. Descriptions and photomicrographs of these unknown pollen types are presented in appendix H.

Description of pollen and spore diagrams

Down core change in total microfossil abundance

A summary diagram of the relative abundance of major functional plant groups is plotted alongside the total microfossil abundance estimated for each core in figure 5.11. The total abundance of pollen and spores shows high-frequency, low-amplitude fluctuations down core. Abundance peaks occur at 150 and 70 cm. Up core of 70 cm, abundance is overall slightly lower than for the rest of the core. There is no correlation between microfossil abundance and mineral influx.

Down core change in major functional types

There is very limited change in the relative abundance of major functional plant groups down core. Results of stratigraphically constrained cluster analysis for the relative abundance data identifies minor changes in the assemblage between 89.5 and 95 cm (dissimilarity distance = 1.21), 25.5 and 30 cm (dissimilarity distance = 1.16) and 10.5 and 15 cm (dissimilarity distance = 1.04). The primary division, separating cluster A from cluster B at 95 cm depth (figure 5.11), appears to represent a minor shift from higher to lower relative abundance in dryland taxa (excluding grass) up core. This boundary also delineates a depth representing low abundances of grass and

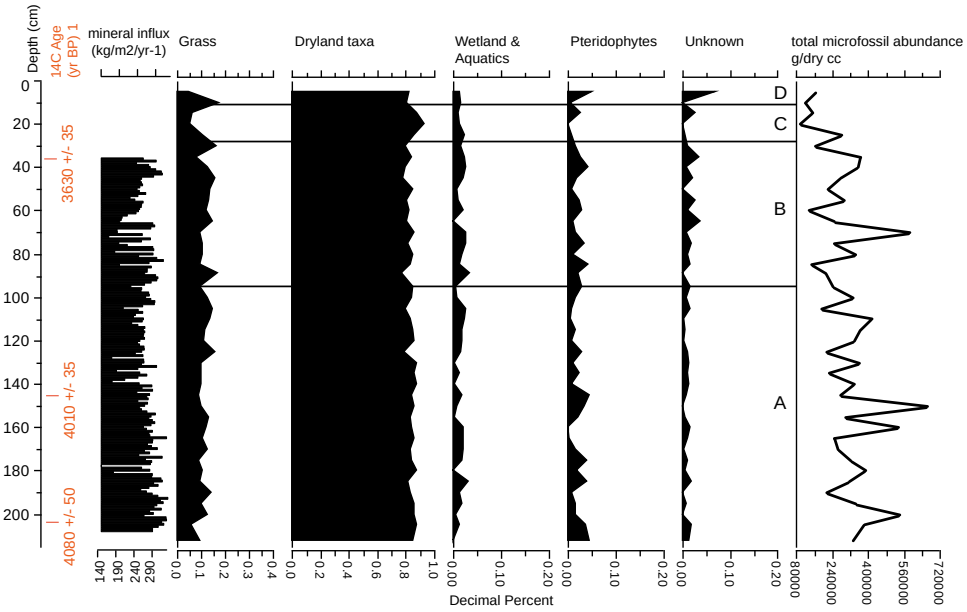

FIGURE 5.11: Summary diagram showing down core changes in relative abundance of YL1211B major plant microfossil groups. These are plotted as decimal percentages alongside estimated total abundance of pollen and spore counts per sample.

wetland/aquatic pollen. The secondary and tertiary cluster boundaries, capturing what has been termed cluster C (figure 5.11) between 25.5 and 15 cm, delimits a peak in dryland taxa. A large peak in pteridophytes and unknown taxa occurs within the uppermost part of the core (5 to 10.5 cm).

Down core change in pollen and spore abundance

Plant microfossil taxa comprising greater than 0.1% of the total core count from YL1211B are plotted stratigraphically as absolute abundances on figure 5.13 (trees and shrubs grouped into forest units) and figure 5.14 (herbs, wetland/aquatics, pteridophytes and unknown types). Results of stratigraphically-constrained cluster analysis have split the total assemblage into eight clusters (boundaries shown on figures 5.13 and 5.14). Cluster boundaries and their dissimilarity distances (bracketed) occur between 200 cm and 190.5 cm (1.15×10^{-6}), 155 cm and 150.5 cm (1.36×10^{-6}), 150 cm and 145.5 cm (1.43×10^{-6}), 75 cm and 70.5 cm (1.5×10^{-6}), 70 cm to 65.5 cm (1.68×10^{-6}), and 35 cm and 30.5 cm (1.24×10^{-6}). Major changes in the microfossil sequence are described in the context of these clusters below.

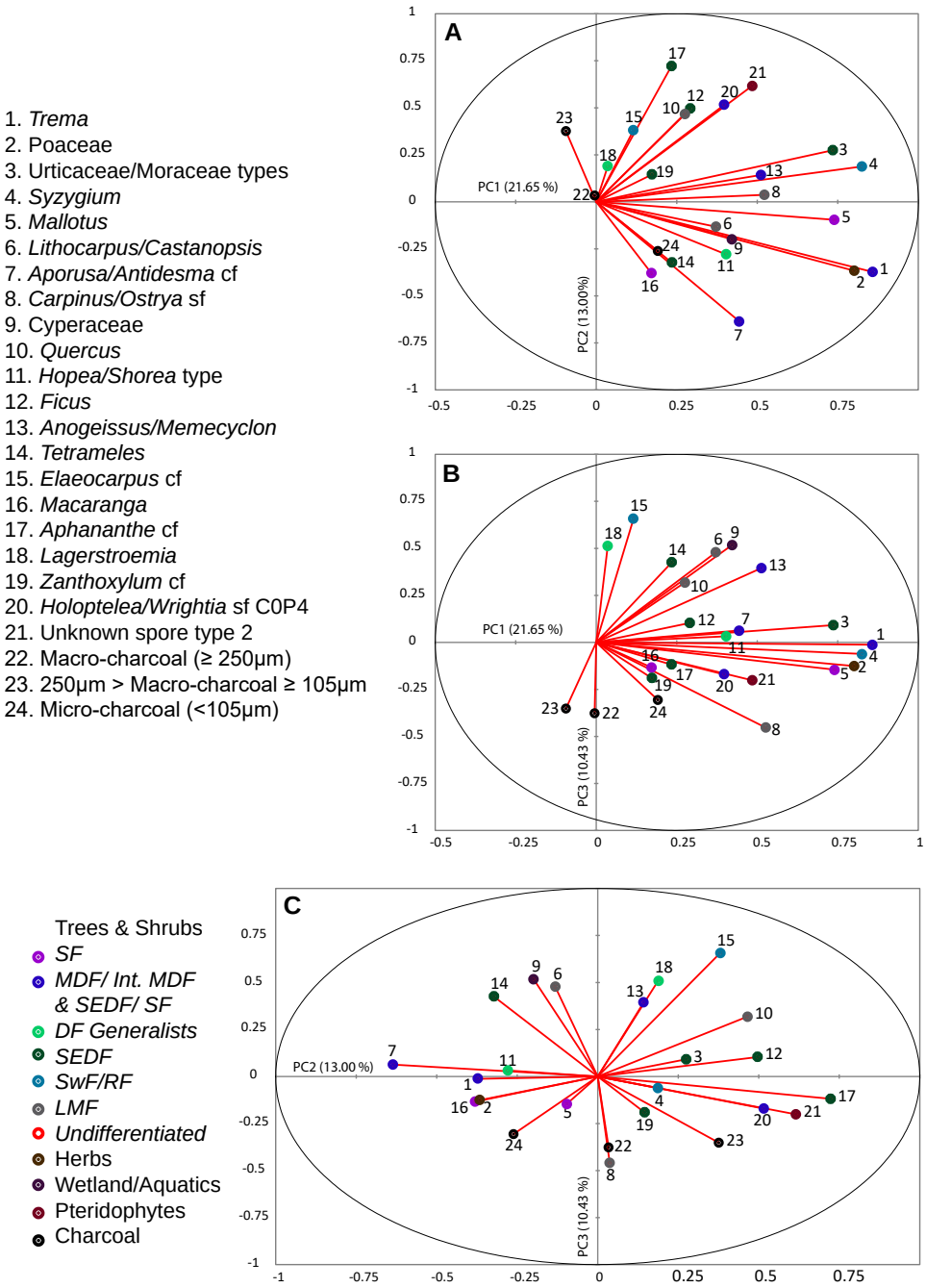

FIGURE 5.12: PCA of YL1211B microfossil (>0.5% raw count) and charcoal abundance data. Data normalised using z-scores prior to analysis. A) PC1 vs. PC2 (35.9% variance); B) PC1 vs. PC3 (32.59% variance); C) PC2 vs PC 3 (17.28% variance).

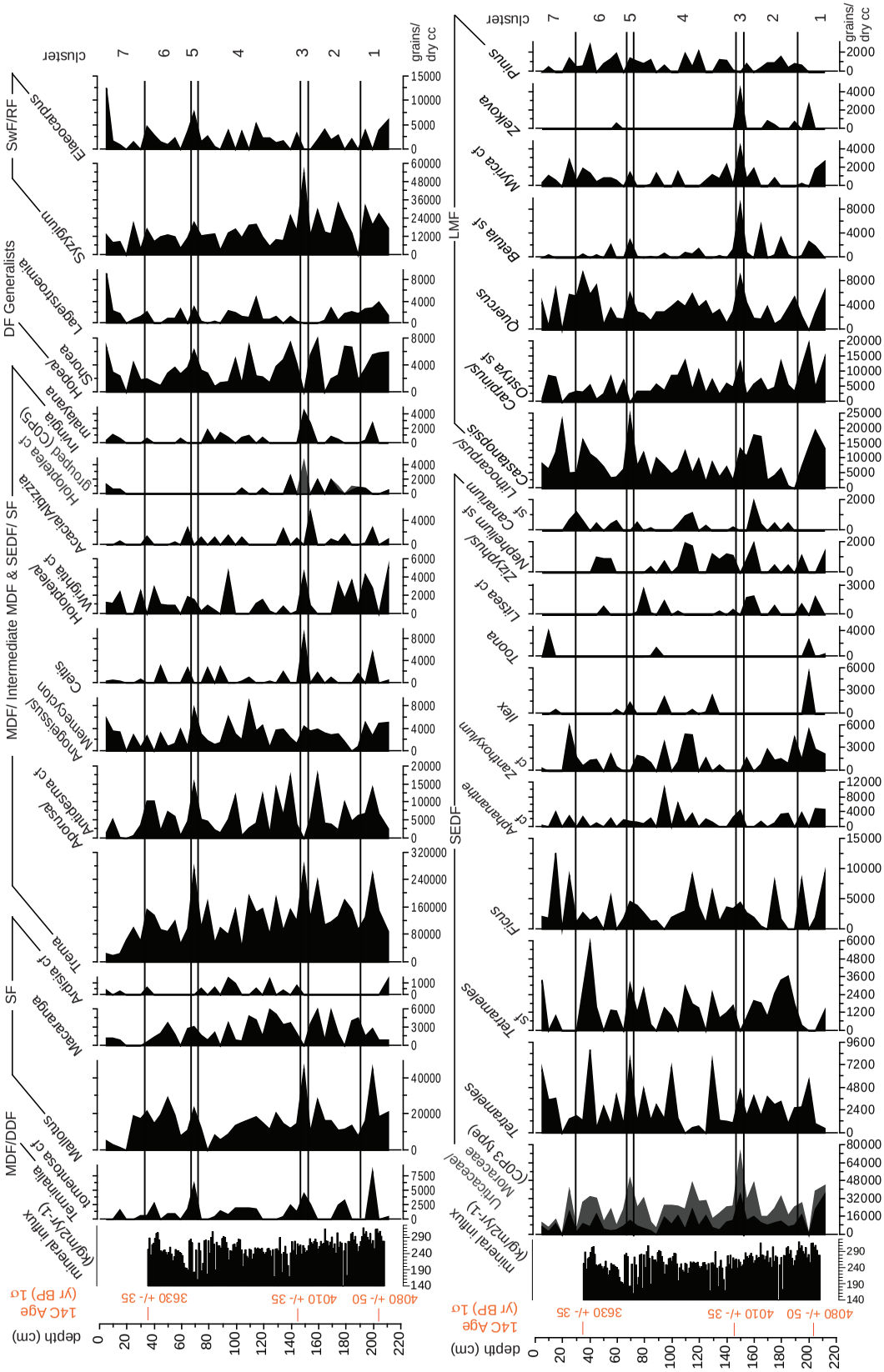

FIGURE 5.13: YL1211B pollen diagram showing absolute abundance of tree and shrub taxa that comprise greater than 0.1% of the total core count. Abbreviations as per figure 5.9. Note discrepancies in x-axis scaling between taxa.

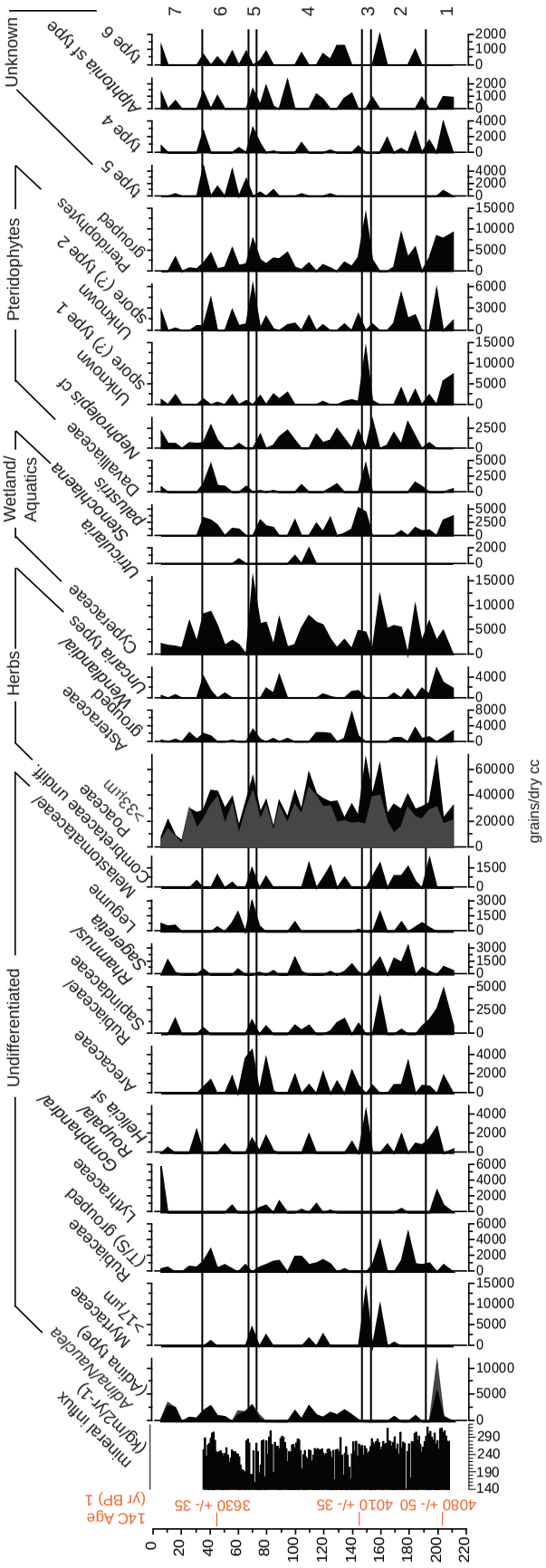

FIGURE 5.14: YL1211B pollen diagram showing the absolute abundance of dryland herb, wetland/aquatic, pteridophyte and unknown taxa that comprise greater than 0.1% of the total core count. Note discrepancies in x-axis scaling between taxa.

Cluster zone 1: 214 cm to 190.5 cm (*c* 4507 to 4457 cal. yrs BP)

Cluster zone 1 represents high abundances of *Mallotus*, *Trema*, *Holoptelea / Wrightia* cf. *Lithocarpus / Castanopsis*, *Carpinus / Ostrya* cf, *Celtis*, *Ilex*, grouped Rubiaceae / Sapindaceae types and, to a lesser extent, *Syzygium*, and *Aporusa / Antidesma* cf taxa, relative to the rest of the core. High abundances of Poaceae and grouped pteridophytes also occur within this zone.

The upper boundary of cluster 1 is characterised by a trough in most taxa that corresponds to a peak in mineral influx. Exceptions to this include Urticaceae/Moraceae (C0P3 type) *Zanthoxyllum* sf, *Quercus*, Arecaceae and Cyperaceae.

Cluster zones 2 to 6: 190.5 cm to 30.5 cm (*c* 4457 to < 4111 cal. yrs BP)

Abundance cluster zones 2 to 6 represent variable, but overall high abundances of Poaceae and Cyperaceae taxa as well as *Mallotus*, *Macaranga*, *Trema*, *Aporusa/Antidesma* cf, *Syzygium*, Urticaceae / Moraceae (C0P3 type), *Tetrameles* sf and Arecaceae types relative to the rest of the core. Two samples within this zone delimit cluster zone 3 (150 to 150.5 cm, modelled at 4371 cal. yrs BP) and cluster zone 5 (70 to 70.5 cm, modelled at 4187 cal. yrs BP).

Cluster zone 3 is marked by anomalously large spikes in unknown spore (?) type 1, *Stenochlaena palustris*, Poaceae, *Gomphandra / Roupala / Helicia* sf, Myrtaceae type 2 (>17 μm), Urticaceae / Moraceae (C0P3 type), *Syzygium*, *Myrica* cf, *Betula* sf, *Quercus*, *Irvingia malayana*, *Holoptelea* cf (C0P6 type), *Holoptelea / Wrightia* cf, *Celtis*, *Trema*, *Mallotus* and *Terminalia tomentosa* cf.

Up core of cluster 3, *Zelkova* and *Betula* sf decline to negligible levels, and there is a reduced abundance of *Syzygium*, *Trema* and *Holoptelea* cf (grouped) pollen throughout the rest of the record. *Ardisia* cf becomes a consistent part of the record within zone 4 (150 to 70.5 cm).

Cluster zone 5 corresponds with a trough in mineral influx, thus contributing to an overall increase in absolute abundance across the microfossil assemblage. In particular, there are pronounced peaks in Cyperaceae, Poaceae, unknown spore (?) type 2, Arecaceae, Legume type, *Lithocarpus / Castanopsis*, *Tetrameles*, Urticaceae / Moraceae (C0P3 type), *Elaeocarpus* cf, *Anogeissus / Memecyclon*, *Aporusa / Antidesma* cf, *Trema* and *Terminalia tomentosa* cf.

Cluster zone 7: 30.5 cm to 5 cm (*c* < 4111 cal. yrs BP)

Cluster zone 7 generally represents the increase of semi-evergreen dry forest types (*Tetrameles*, *Tetrameles* sf, *Ficus*, *Zanthoxyllum*) and lower montane forest types (*Lithocarpus / Castanopsis*, *Carpinus / Ostrya* sf, and *Quercus*). Conversely, *Stenochlaena palustris*, Davalliaceae type, Arecaceae and Myrtaceae (>17 μm type) near completely disappear from the record within cluster 7. Additionally, a significant decline in nearly all taxa from the deciduous dry forest, secondary forest and grouped mixed dry forest, intermediate mixed dry/semi-evergreen forest types as well as Poaceae and

Cyperaceae is observable. A notable second drop in most of these taxa occurs between 15 and 25 cm. A significant spike in *Lagerstroemia*, *Elaeocarpus* cf and *Tetrameles* is evident within the core top sample (5 to 5.5 cm).

5.5.3 Charcoal and plant microfossil associations

Results of the PCA and Pearson's correlation test show associations between macro- and micro- charcoal fractions and microfossil data. These are discussed in the context of each core below.

Yeak Mai (core YM0413B)

Macro-charcoal – vegetation relationships

Both macro-charcoal fractions extracted from YM0413B sediments are not significantly correlated with total microfossil abundance, but show significant, weak, positive correlations with the relative abundance of taxa in both the secondary forest (r = 0.266 [>250 μm fraction], r = 0.202 [105 to 250 μm fraction]), and the grouped mixed dry forest, intermediate dry forest and secondary forest (r = 0.204 [>250 μm fraction], r = 0.190 [105 to 250 μm fraction]) classifications. The PCA conducted on absolute charcoal and microfossil abundance data shows an association between both macro-charcoal fractions and *Blyxa*, *Hydrocera*, *Celtis* and *Trema* along PC2 (figure 5.8 and table 5.2).

Micro-charcoal – vegetation relationships

The micro-charcoal record reconstructed from YM0413B, is weakly (but significantly), correlated with the total microfossil abundance, and displays a negative correlation with mineral influx (r = -0.214). Micro-charcoal abundance also has an insignificant (r =-0.187) and significant (r = -0.327) negative correlation with the >250 μm and 105 to 250 μm macro-charcoal fraction sizes respectively.

A positive correlation exists between micro-charcoal abundance and the absolute abundance of Quercus (r = 0.246) and Blyxa (r = 0.199).

Yeak Loam (core YL1211B)

Macro-charcoal – vegetation relationships

Both macro-charcoal fractions extracted from YL1211B sediments are not significantly correlated with total microfossil abundance. The abundance of both fractions (along with micro-charcoal abundance) does, however, associate with *Carpinus / Ostrya* sf pollen along the negative axis of PC3. Both fraction show a significant (>250 μm, r = -0.452), and an insignificant (105 to 250 μm, r = -0.205) negative correlation with the relative abundance of pollen from aquatic plants.

Micro-charcoal – vegetation relationships

The YL1211B micro-charcoal record in not significantly correlated with total microfossil abundance. There is a positive correlation between micro-charcoal and the absolute abundance of Poaceae ($r = 0.364$) and *Carpinus/Ostrya* sf ($r = 0.552$), and a negative correlation between micro-charcoal and the abundance of *Elaeocarpus* cf.

5.6 Chapter summary

A brief synthesis of results derived from the palaeobotanical and charcoal analysis of the master lake cores extracted from Yeak Mai and Yeak Loam are shown within the context of the age-depth models produced for the cores (outlined in Chapter 4) in table 5.4.

TABLE 5.4: Summary of major changes in the plant microfossil and charcoal records reconstructed from YM0413B and YL1211B through time. Changes are described in the context of the age-depth models produced for each core.

Cal. yrs. BP	Yeak Mai vegetation change	Yeak Loam vegetation change	Yeak Mai fire activity	Yeak Loam fire activity
1500 to present	Increase in SEDF taxa. Drop in relative abundance of Poaceae.	No age-modelled data from YL1211B.	Stepwise drop in macro-charcoal counts to lower-than-average fire activity at c. 1500 and c. 900 cal. yrs BP.	No age-modelled data from YL1211B.
1900 to 1500	Major drop in total microfossil abundance to c. 1800 cal. yrs BP. Increase in wetland taxa. Near total decline of aquatic taxa. Increase in *Syzygium* pollen and LMF pollen from c. 1800 cal. yrs. BP. Poaceae abundance relatively high. Abundance of SEDF arboreal taxa low.	No age-modelled data from YL1211B.	High macro-and micro-charcoal counts relative to high bulk mineral influx estimated for sedimentary unit III. Anomalous peaks in micro-charcoal at 1900, and 1840 to 1790 cal. yrs BP.	No age-modelled data from YL1211B.

Continued...

Cal. yrs. BP	Yeak Mai vegetation change	Yeak Loam vegetation change	Yeak Mai fire activity	Yeak Loam fire activity
3300 to 1900	Stepwise decline in total microfossil abundance at 3300 and 3000 cal. yrs BP. Relatively high Poaceae counts from 2800 to 2100 cal. yrs BP. Drop in aquatic types at 2675 to 2480 cal. yrs BP Spike in *Trema, Aporusa/ Antidesma, Celtis* and *Lagerstroemia* abundance at. 1900 cal. yrs BP.	No age-modelled data from YL1211B.	Overall decline in macro-charcoal counts. High frequency fluctuations related to bulk mineral influx across sedimentary units IIa and IIb.	No age-modelled data from YL1211B.

Continued...

Cal. yrs. BP	Yeak Mai vegetation change	Yeak Loam vegetation change	Yeak Mai fire activity	Yeak Loam fire activity
4700 to 3300	Relatively high abundance of aquatic vs. wetland non-arboreal pollen. High relative abundance of *Trema, Mallotus* and *Celtis* pollen types (pioneer successional forest genera) to c. 3700 cal. yrs BP. Large peak in Poaceae and dry and secondary forest types at c. 4300 cal. yrs BP.	High frequency shifts in most taxa across the age-modelled part of the record. Relative abundance of plant functional groups mostly constant down core. High abundance of disturbance taxa. Decrease in Poaceae abundance from c. 4300 cal. yrs BP. Slight increase in SEDF taxa in sediments younger that c. 4100 cal. yrs BP (not age-depth modelled).	High frequency fluctuations related to bulk mineral influx across sedimentary units IIa and IIb. Anomalously large peaks in macro-charcoal at c. 4040 cal. yrs BP and 3700 cal. yrs BP. Anomalously large peaks in micro-charcoal at c. 4300 cal. yrs BP.	High frequency fluctuations in count data across the age-modelled part of the record. While no clear trend is apparent, anomalous peaks in micro-charcoal occur at c. 4440, 4280 and 4150 cal. yrs BP, with lower than average abundance in sediments between c. 4300 and 4100 cal. yrs BP. Peaks in macro-charcoal occur between c. 4320 to 4380 cal. yrs BP and c. 4100 to 4150 cal. yrs BP.

6 Interpretation of south-east Asian seasonally dry forest threshold dynamics from lake core records

6.1 Introduction

As outlined in chapter 2, the distribution of seasonally dry tropical forest (SDTF) and tropical grassland, savanna and shrubland (TGSS) as alternative stable states appears strongly tied to climatic factors (particularly mean annual precipitation (MAP) and seasonality) and the presence of fire. However, this premise has not been well tested within south-east Asian seasonally dry tropical forest (SASDTF). This chapter will seek to resolve this by interpreting key drivers of change for forest to savanna transitions and the associated vegetation responses from the lake sedimentary records presented in chapters 4 and 5.

This chapter is structured into four main sections. The first reconstructs a *c.* 4 700 year long climate record using core geochemistry, sedimentology and complimentary plant microfossil data. Secondly, a record of charcoal influx to the lake catchments is reconstructed in order to delimit past periods of high local and regional fire activity. The third section uses these climatic and fire history records in concert with records of SASDTF vegetation change derived from the Yeak Mai and Yeak Loam lake cores as well as other palaeo-ecological studies from the region to determine the threshold behaviour of SASDTF (and units within). Finally, a discussion of the regional applicability of biome-scale resilience models developed for seasonally dry tropical forests worldwide is posed.

6.2 Reconstruction of monsoon fluctuations over the past *c.* 4700 years

In order to determine the response of the site vegetation to past shifts in the Asian monsoons, it is necessary to first delimit a spatially and temporally well-constrained reconstruction of climate change for the lake sites. In the context of this research, it is of particular importance to reconstruct periods of drier-than-present conditions given that SDTF appears sensitive to shifts to savanna where mean annual precipitation declines or seasonality

increases (Hirota et al. 2011, Staver et al. 2011a). Past monsoon conditions within the vicinity of the lake sites is reconstructed by distinguishing periods of lake shallowing and, where possible, deepening via interpretation of past sedimentological and geochemical redox conditions and changing abundance of pollen and spores from aquatic and wetland vegetation. This is cross-validated by comparison with other records of ISM and EAM change.

6.2.1 Redox proxies of lake wetting and drying

Reconstructing redox conditions of the Yeak Mai and Yeak Loam lake surface sediments is thought to be a viable means for interpreting past changes in lake water level of shallow lakes (Yeak Mai) and changes in the water level or stratification of deep lakes (Yeak Loam) (Naeher et al. 2013, Tamuntuan et al. 2015). These processes have been linked to fluctuations in summer monsoon precipitation, with drier conditions associated with precipitation of redox-sensitive elements – Mn/Ti and Fe/Ti in Yeak Mai, and Mn/Fe in Yeak Loam (Naeher et al. 2013). The Yeak Mai sediments - being extracted from a shallow lake setting and representing a continuous and better dated sequence than Yeak Loam sediments – appear to be of particular value for reconstructing past periods of lake deepening/shallowing, though both records may provide insight into regional palaeomonsoon conditions for the study area.

Post-depositional oxygenation of shallow lake sapropelic sediments could be facilitated by a drop in lake water level, drawing the redox boundary down below sediment-water interface (Hayes et al. 1958, Davison 1993). The corresponding peaks observed in the Mn/Ti and Fe/Ti profiles from the Yeak Mai sedimentary record may therefore represent relatively dry periods over the past *c.* 4700 cal yrs BP. Nine of these are identified centred on *c.* 350, 570, 1550, 1755, 1915, 2250, 2650, 3300 and 4250 cal. yrs BP, numbered *i* to *ix* on figure 6.1. Note that the peak in Mn/Ti and Fe/Ti data at (*c.* 37 cal. yrs BP) is not included as a possible dry event given that it is probably representing the very common surface enrichment in trace metals observed in lake sediment cores, caused by ephemeral cycling of redox-sensitive elements in the water column (Bryant et al. 1997, Boyle 2001).

Despite uncertainties associated with the chronology of Yeak Loam sediments, the modelled timing for periods of high bottom water O_2 inferred from Mn/Fe records (thought to be indicative of drying conditions (Naeher et al. 2013)) matches well with drying event *ix* at *c.* 4250 cal. yrs BP (figure 6.1). Correlation between the Yeak Mai Mn/Ti record and the Yeak Loam Mn/Fe records, measured across the length of the Yeak Loam age-depth record (i.e. 4110 to 4485 cal. yrs. BP) is moderate to strong (r = 0.74), lending a degree of credibility to this interpretation.

Kylander et al. (2011) indicate that caution need be applied when using XRF proxy data to infer climate events due to the different thresholds of, and various roles occupied by different elements under variable conditions. Thus, the reliability of using the Yeak Mai Mn/Ti and Fe/Ti peaks as a proxy for a dry "events" is assessed in this study though cross-correlation

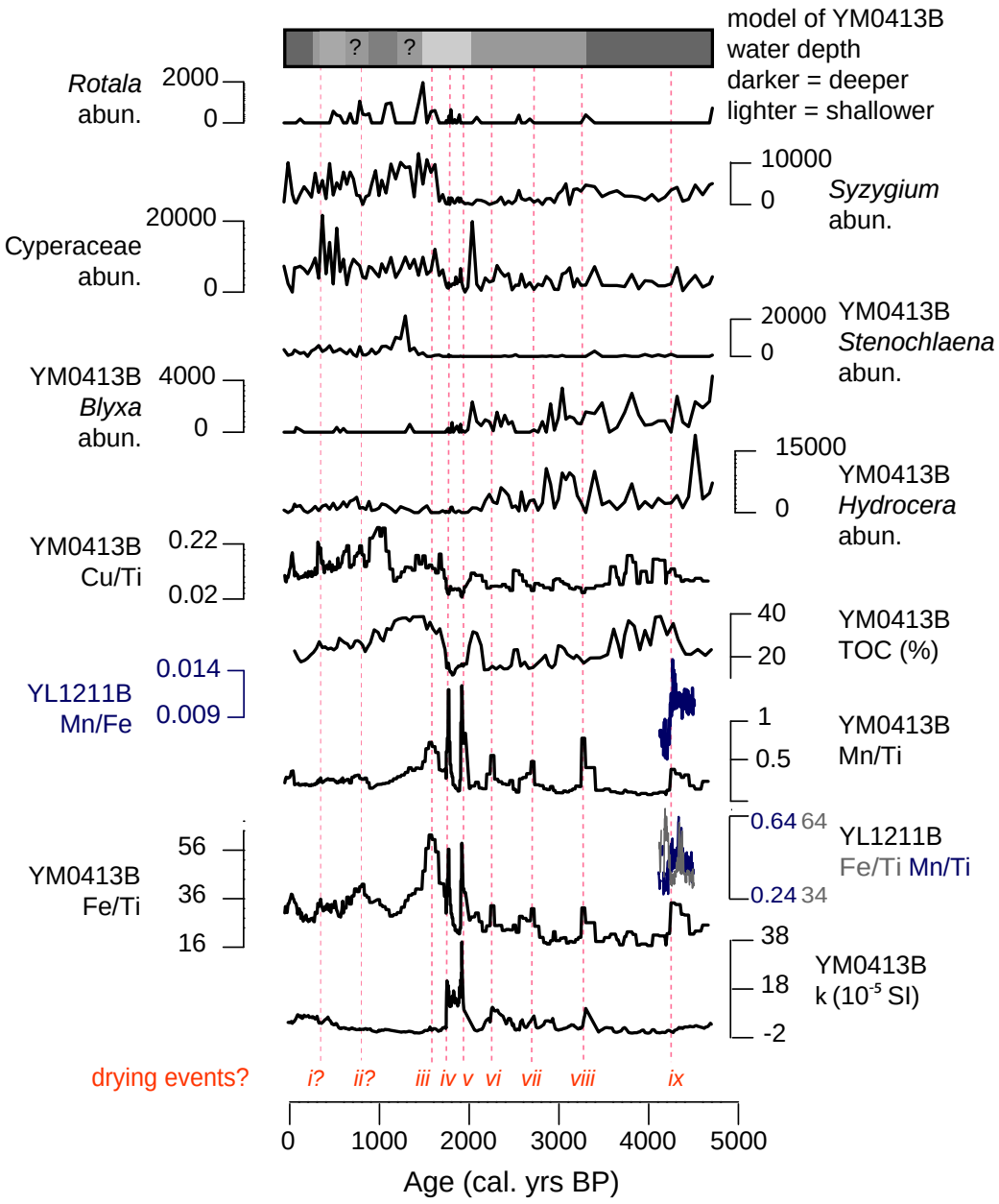

FIGURE 6.1: Plot showing selected sedimentological and palaeovegetation proxies from Yeak Mai and Yeak Loam that are used to reconstruct past climate change at the lake sites. Nine drying events have been identified (*i* to *ix*) marked on the diagram with red dotted lines. Question marks are placed beside the dry events that are classified with a higher degree of uncertainty due to limited cross-correlation between proxy records.

with other palaeoclimatic indicators. These include 1) other relevant geochemical and sedimentology parameters suggestive of drying climatic conditions from the lake cores assessed in this study, 2) changes in the abundance of pollen from wetland and especially aquatic taxa, which can be

sensitive to changing water levels in shallow lake settings, and 3) the relationship of these dry events with external palaeoclimatic records from the ISM and EASM. These associations are outlined below.

6.2.2 Other indicators of lake level fluctuations

Peaks in κSI can also be used to infer lake bottom sediment oxygenation within tropical lake settings (Tamuntuan et al. 2015), but require corroboration with other redox proxies. In Yeak Mai, five peaks in κSI associate with Mn/Ti and Fe/Ti peaks (drying events *iv* to *viii* shown on figure 6.1). The negative correlation between κSI and Mn/Ti and Fe/Ti, and simultaneous positive association between κSI and detrital elements (Si, K and Ti) suggest that κSI may switch from predominantly representing a redox proxy to predominantly representing an erosion proxy in sediments younger than *c.* 1000 cal. yrs BP. This is important in the context of constructing a climate record from the Yeak Mai sediments, as it may mean that peaks in κSI change from reflecting a weak summer monsoon (lake shallowing) to potentially representing a strong summer monsoon (high precipitation can lead to high catchment runoff erosion).

While there are no clear peaks in the Yeak Mai Cu/Ti record at the lower boundary of any of the nine identified Fe/Ti and Mn/Ti oxidation fronts from Yeak Mai (a trend that can be used to indicate post depositional oxidation of sapropels (Thomson et al. 2006)), peaks in Mn/Ti and Fe/Ti from these sediments clearly coincide with troughs in Cu/Ti between *c.* 1755 and 3300 cal. yrs BP (events *iv, v, vi, vii* and *viii* – see figure 6.1). This may suggest some degree of Cu mobilisation under oxic conditions. However, this ratio displays a moderate positive correlation with the core organic matter, suggesting a potential association between non-detrital Cu and algae that may not be directly related to sediment redox conditions.

6.2.3 Floristic indicators of lake level change

The presence and abundance of wetland and depth-sensitive aquatic plants can be useful for inferring past climatic conditions. This is particularly the case for shallow lakes where relatively small changes in rainfall can have marked effects on the local aquatic environment (Gasse and Van Campo 2001, Wohlfarth et al. 2012, Chawchai et al. 2013). *Hydrocera triflora* (L.) (Wight & Arn.), *Blyxa* and *Rotala* are the dominant aquatic or semi-aquatic taxa encountered within the Yeak Mai record, while Cyperaceae, *Syzygium* and *Stenochlaena palustris* ((Burm. f.) Bedd.) comprise the dominant wetland signal. Fluctuations in the abundance of the pollen and spores from these plants are shown in the context of the dry events identified from the geochemistry record on figure 6.1.

Hydrocera triflora is a semi-aquatic plant that is sensitive to both lake shallowing (to the extent where the lower stem is exposed) or deepening (it won't grow in water depths greater than 70 cm) (Grey-Wilson 1980). Within the Yeak Mai record, the abundance of *H. triflora* pollen declines in stepwise succession. From *c.* 4710 to 2800 cal. yrs BP, abundance is relatively

high, with significant peaks at *c.* 4520 cal. yrs BP and between *c.* 3400 and 2800 cal yrs BP. Abundance then declines to moderate levels to *c.* 2000 cal. yrs BP and negligible levels to *c.* 800 cal. yrs BP, before making a slight recovery in the upper core sediments. Inferred from this pattern is either step-wise lake shallowing or lake deepening. Given that all dry events at Yeak Mai when *H. triflora* is well represented within the record coincide with troughs in its abundance, the later decline in abundance is considered more likely to be driven by lake shallowing.

Based on a review of the geographic distribution of *Blyxa* included in Cook and Lüönd (1983), five species of this genus may grow within the vicinity of SASDTF. These include *Blyxa aubertii* (L. C. Richard), *B. japonica* ((Miq.) Maxim. ex Asch. & Gürke), *B. octandra* ((Roxb) Planch. ex Thwaites), *B. quadricostata* (Hartog) and *B. vietii* (C. D. K. Cook & Lüönd). While these species all have different tolerances with respect to water level fluctuation and nutrient loading, all favour a shallow water habitat (maximum 40 cm depth) (Cook and Lüönd 1983). The abundance of *Blyxa* pollen is high at the base of the record (*c.* 4710 cal yrs BP) and gradually declines to *c.* 1744 cal. yrs BP. This overall trend is punctuated by several peaks in abundance at modelled ages of *c.* 4710, 4317, 3813, 3481, 3036, 2907, and 2034 cal. yrs BP, suggesting shallow but fluctuating lake levels throughout this time. Drying events *iv* to *ix* correspond to troughs in the estimated abundance of *Blyxa*, suggesting that these events promoted conditions less favourable (presumably too dry) for the plant to flourish. The concurrence of drying event *vii* and especially *iv* with the near demise of *Blyxa* from the pollen record suggests that these may have been of sufficient intensity or duration to temporarily eliminate this plant from the local area. Recovery of *Blyxa* is poor subsequent to event *iv*, suggesting the establishment of an aquatic habitat unsuitable for the plant and/or out competition by another plant type/community.

Five species of *Rotala* are considered geographically more likely to occur within the vicinity of Yeak Mai, including *R. indica* ((Willdenow) Koehn), *R. cordata* (Koehne), *R. rosea* ((Poiret) C. D. K. Cook ex H. Hara), *R. rotundifolia* (Buchanan-Hamilton ex Roxburgh) Koehne, and *R. wallichii* (J. D. Hooker) Koehne (Graham et al. 2011). These typically short-lived annuals have a preference for wetland-type habitats and require seasonally fluctuating water levels, with an annual dry period required for several species (Graham et al. 2011). Climatic conditions conducive to this habitat requirement are inferred from high *Rotala* pollen abundance, which occurs within the Yeak Mai record between *c.* 1890 and 485 cal. yrs BP (noting that the apparent low abundance between 1985 and 1738 cal. yrs BP is due to high sediment influx calculated for sedimentary unit III, thereby diluting the pollen input). Peaks in the abundance of *Rotala* are also apparent immediate prior to and/or post drying events *viii, vii, v, iv, iii,* and one coincides with event *ii*, suggesting that the abundance of pollen from this plant may increase under relatively dry conditions.

In the Yeak Mai record, the abundance of Cyperaceae is relatively high between *c.* 2035 to 242 cal. yrs BP (noting that, as with *Rotala*, the apparent decline in abundance between 1985 and 1738 cal. yrs BP is due to the high sediment influx calculated for sedimentary unit III). High abundance

of sedge pollen is often interpreted as representing shallow conditions that permit the establishment of a wetland assemblage (Gasse and Van Campo 2001, Maxwell 2001, Wohlfarth et al. 2012).

The establishment of drier, wetland type flora at the lake site (presumably around the lake margin) in sediments younger than 2035 cal. yrs BP, inferred from sedge pollen abundance, is supported by the abrupt increase in *Syzygium* pollen in the core record between *c.* 1600 cal yrs. BP and 2013 AD. The morphology of this pollen type (Australian National University 2016: sample 225-18-51) is consistent with that of the extant *Syzygium* species growing at Yeak Mai at the time of fieldwork, which was identified as *S. cumini* ((L.) Skeels) (Khmer: pri:ing ba:y) (S. Channa, D. Penny and A. Maxwell pers. comm. 6th April, 2014), translated using Dy Phon (2000). This tree grows gregariously in wetland habitats, though once established it can sustain extended periods of either flood or drought (Orwa et al. 2009).

Stenochlaena palustris spores occur in moderate abundance in the Yeak Mai record from *c.* 1840 cal. yrs BP to 2013 AD, peaking at 1290 to 1180 cal. yrs BP. This fern favours moist wetland conditions, and peaks in abundance may indicate slightly increased moisture availability at the site during this period (Brown 1920, Laumonier 1997). However, this needs to be interpreted with caution given that proliferation of this fern can also be associated with forest disturbance in the everwet tropics of insular Southeast Asia (Chai 2016).

When considered together, the changing abundance of the dominant aquatic and wetland species from Yeak Mai suggests lake water depths favourable for the proliferation of sub aquatic vegetation including *Hydrocera triflora* and *Blyxa* from *c.* 4700 to 2800 cal. yrs BP. This is followed by what has been interpreted as a shallowing of the lake to *c.* 2100 cal. yrs BP due to the overall decline in *H. triflora* and *Blyxa* pollen in the record. A relatively significant dry period is interpreted to have occurred as a single or series of events between *c.* 2100 and 1400 cal. yrs BP, with a particularly dry stage between *c.* 1900 and 1500 cal. yrs BP. This is based on the progressive decline of first *H. triflora* then *Blyxa* (likely tolerant of shallower conditions) pollen from the record, followed by the subsequent increase in *Rotala* pollen. Additionally, the relatively abrupt increase in Cyperaceae in the record suggests the establishment, or encroachment of a very shallow water wetland towards the deepest portion of the lake from where the core was taken, suggesting further shallowing of the lake. This correlates with the very large peaks in Mn/Ti and Fe/Ti used to infer drying events *v, iv* and *iii*, and the inferred change in the environmental setting of the lake may explain the changes in core sedimentology observed over the same time period. Following this inferred dry period, is it expected that the lake remained in a condition suitable for the persistence of a wetland-type environment (presumably around the lake margins) up to approximately *c.* 250 cal. yrs BP, after which there is a decline in the abundance of wetland indicators, suggesting re-deepening of the lake.

6.2.4 Comparison with regional monsoon records

Within the intersection zone of the ISM and EAM where SASDTF occurs (see chapter 3 for details), several high-resolution dendrochronological records of climate have been reconstructed (Sano et al. 2009, Buckley et al. 2010), however, none are sufficiently long to cover the length of the Yeak Mai and Yeak Loam sediment records. As such, temporally well-constrained Holocene monsoon records from the EAM zone (Wang et al. 2005a, Wang et al. 2005b, Zhang et al. 2008) and ISM (Fleitmann et al. 2003, Fleitmann et al. 2007a, b, Berkelhammer et al. 2010) are used to compare the crater lake climatic records with external monsoon records of various lengths and sampling resolutions. The location of these records relative to the study lake sites is shown on figure 6.2. Additionally, the South Asian Summer Monsoon Index (SASMI), compiled from 15 tree ring chronologies from the ISM, EAM and intersection zones (Shi et al. 2014) is utilised to compare monsoon precipitation change over the last millennium with the lake proxy records. The abundance of *Tetrameles* pollen from the Yeak Kara lake sediment record (BKY2) reconstructed in Maxwell (1999) and Maxwell (2001) also appears to reflect changing monsoon summer strength in the late Holocene, and is thus also used as a potential climatic proxy from the intersection zone. A plot of these climatic records over the past *c.* 4700 years (the approximate time frame captured by the Yeak Mai sedimentary record) is shown alongside the lake core monsoon geochemistry and magnetic climate proxies in figure 6.3. The association between the lake climate records and the external monsoon records is discussed below.

Changes in the EASM reconstructed from speleothem sample DA from Dongge Cave, southern China (Wang et al. 2005a, Wang et al. 2005b), correlates relatively well with changes in the Mn/Ti (r = 0.31), and especially Fe/Ti (r = 0.56) records reconstructed over the same period from Yeak Mai, particularly given the relatively poorly constrained chronological resolution of the lake record when compared with the speleothem record (figure 6.3). In particular, Bond events 0 (LIA), 1, 2 and 3 that are identified within the Dongge record reflect the drying events *i*, *iii*, *viii* and *ix* captured in the Yeak Mai Fe/Ti and Yeak Loam Mn/Fe (event *ix* only) records. The other six drying events reconstructed from Yeak Mai can be well-matched to peaks within the Dongge Cave record, and the MWP (occurring in Asia between 1100 and 900 cal. yrs BP (Cook et al. 2013)), can be matched to a subtle trough in Mn/Ti and Fe/Ti ratios (figure 6.3). These patterns are also reflected, at relevant timescales, in the WX42B Wanxiang Cave $\delta^{18}O‰$ record (Zhang et al. 2008) and the BYK2 *Tetrameles* pollen record (where peaks in pollen correspond with drying events), though the MWP period does not appear to be as well defined in either of these studies, and the abundance of *Tetrameles* is low from *c.* 5000 to 2000 cal. yrs BP, making it difficult to cross correlate changes in the older portion of the record. The relationship between the Yeak Mai climate record with $\delta^{18}O‰$ monsoon reconstructions from the central (DAN-D (Berkelhammer et al. 2010)) and marginal (Q5 (Fleitmann et al. 2007b)) ISM zone is less well defined, noting that the resolution (DAN-D) and timeframe (DAN-D and Q5) of these records is not optimal for comparison. This suggests that the monsoon conditions within the mainland south-east Asia monsoon intersection zone are

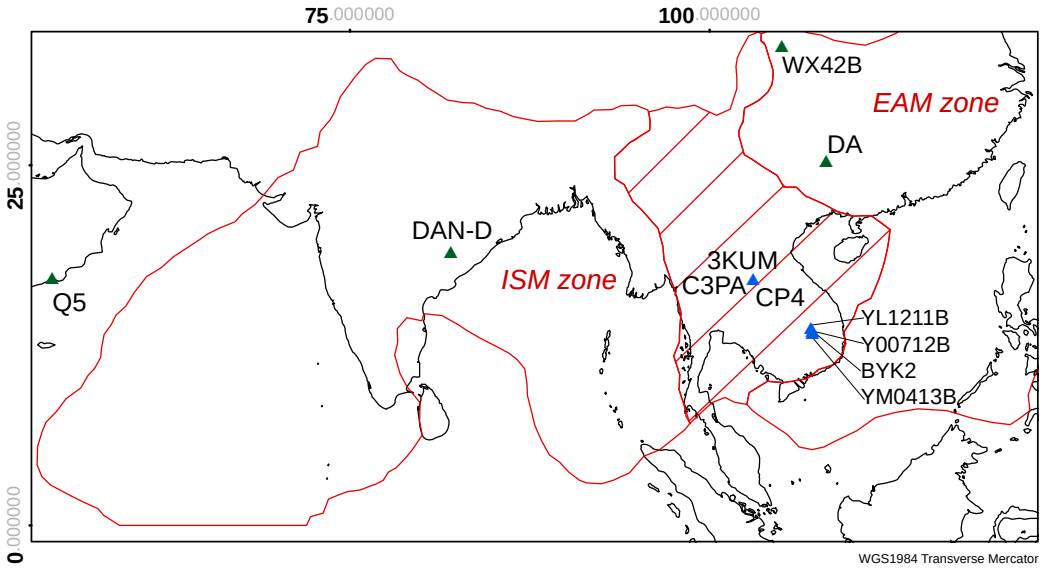

FIGURE 6.2: Location of the regional climate records used in this study for comparison with the wetting/drying proxy records reconstructed from Yeak Mai and Yeak Loam sediments. Cave speleothem records are represented by the green triangles and lake records by the blue triangles. Sites include Wanxiang Cave, China (WX42B) (Zhang et al. 2008), Dongge Cave, China (DA) (Wang et al. 2005a, b), Lake Kumphawapi, Thailand (3KUM, C3PA, CP4) (Kealhofer and Penny, 1998, Wohlfarth et al. 2012, Chawchai et al. 2013), Yeak Kara, Cambodia (BYK2) (Maxwell, 2001 & 2004), Dandak Cave, India (Berkelhammer et al. 2010) and Qunf Cave, Oman (Q5) (Fleitmann et al. 2007a, b).

significantly influenced by the EAM, particularly the EASM, particularly from the mid-Holocene to *c.* 1000 cal. yrs BP.

Over the past *c.* 1000 years, the Yeak Mai Fe/Ti record appears to decouple with the DA isotope record (r = 0.13), while the κSI record from the same time core correlates moderately with the SASMI (r = 0.54), where κSI peaks (interpreted to representing an erosion signal within this part of the core) match periods of a strengthened summer monsoon (visual representation shown on figure 6.4). If κSI is accurately reflecting periods of higher effective moisture throughout the late Holocene, it suggests that the climate mechanisms operating within the vicinity of the study site may be increasingly influenced by the ISM, driven by a complex interaction of ENSO variability, volcanic forcing and solar irradiance over this time period (Shi et al. 2014).

The association of core sedimentological and geochemical proxies for lake wetting and drying with external monsoon records, notably the EASM from *c.* 4700 to 1000 cal. yrs BP, and ISM over the last millennium demonstrates that geochemical proxies for changing post depositional (Yeak Mai) and lake water (Yeak Loam) redox conditions can be used to reconstruct climatic conditions from lake sediments, a relatively novel approach within tropical lake settings. This is significant as the resultant climate record provides one

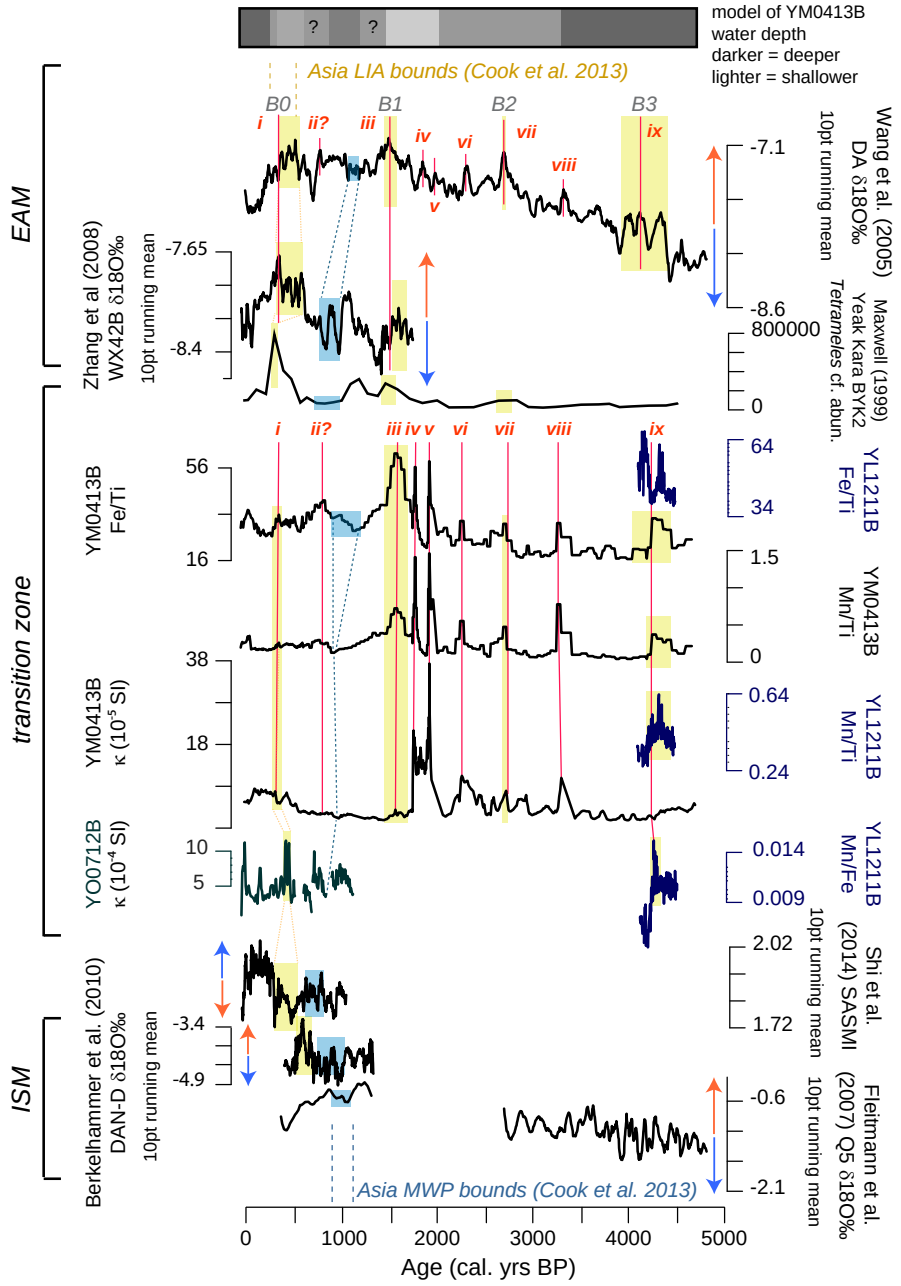

FIGURE 6.3: Comparison of the climate record reconstructed from the crater lake sediments with regional climate records from the EAM zone (DA & WX42B speleothem δ^{18}O‰ records), ISM zone (DAN-D & Q5 speleothem δ^{18}O‰ records) and the intersection zone of these monsoons (SASMI & BYK2 *Tetrameles* abundance record) over the past 5000 cal. yrs BP. Yellow bars represent Bond events 0 to 3 identified in Wang et al. (2005a), and blue bars represent the approximate timing of the MWP in the various records. Red lines represent drying events reconstructed from the Yeak Mai and Yeak Loa, geochemistry and sedimentology records.

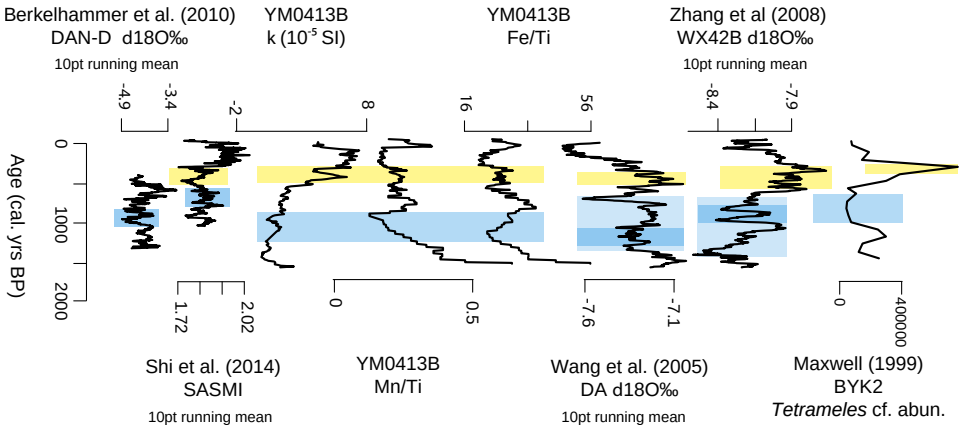

FIGURE 6.4: Comparison of the climate record reconstructed from Yeak Mai with regional climate records from the EAM zone (DA & WX42B speleothem δ^{18}O‰ records), ISM zone (DAN-D δ^{18}O‰ record) and the intersection zone of these monsoons (SASMI & BYK2 *Tetrameles* abundance record) over the past 2000 cal. yrs BP. Yellow bars represent interpreted timing of Bond event 0 (LIA), and blue bars represent the interpreted timing of the MWP.

of the first robust, multi-millennial records of monsoon change within the ISM/EAM intersection zone.

6.2.5 Synthesis: palaeoclimate model for the lake sites

A summary of climate change for the lake sites over the past 4700 years as interpreted from this multi-proxy, comparative approach is provided below.

c. 4700 to 3300 cal. yrs BP: a moderate monsoon

Throughout this period, Yeak Mai appears to have supported relatively abundant shallow-water aquatic plants including *Blyxa* and *Hydrocera triflora*. Given that the gradient of the land extending above the west, east and southern margins of the lake is low, an expansive area of land sitting above the current lake margin could flood easily if water levels were to rise, and this would likely be capable of supporting a shallow lake water aquatic community. It is thus difficult to determine from these parameters alone if the lake was shallower or deeper than present. However, the low abundance of wetland indicators (Cyperaceae and *Syzygium*) throughout the same time indicates that conditions were either not suitable for the development of an extensive wetland community around the lake margins, or that the wetland was some distance from the deepest portion of the lake from where the lake core was extracted. This supports the idea of the lake being more extensive than it is at present. This interpretation is consistent with the Dongge cave DA δ^{18}O‰ record, which indicates that the EASM was stronger than (up to *c.* 3500 cal. yrs BP), or approximately equivalent

to (*c.* 3500 to 3300 cal. yrs BP) contemporary monsoon conditions (Wang et al. 2005a, Wang et al. 2005b). Two dry events (*ix* and *viii*) occur throughout this timeframe at approximately 4250 and 3300 cal. yrs BP. The earliest of these corresponds well with Bond event 3 identified in Wang et al. (2005a) — a high magnitude, long duration event persisting in south China from *c.* 4500 to 4000 cal. yrs BP.

c. 3300 to 1900 cal. yrs BP: a weakening monsoon with dry events

Between *c.* 3300 and 1900 cal. yrs BP, the abundance of *Hydrocera triflora* and, to a lesser extent, *Blyxa* pollen declines, whilst the abundance of Cyperaceae pollen, a wetland indicator, increases. This suggests shallowing of the lake such that a relatively significant wetland region could be supported at the site, presumably at the lake periphery. This interpretation is supported by the gradual weakening of the EASM as interpreted from climate records reconstructed from Dongge Cave (Dykoski et al. 2005, Wang et al. 2005a, Wang et al. 2005b), which show a good correlation with the Yeak Mai Fe/Ti record over the same period. Two drying events, *vii* (*c.* 2700 to 2600 cal. yrs BP) and *vi* (*c.* 2250 cal. yrs BP — coinciding with Bond event 3 noted in Wang et al. (2005a)) occur throughout this time period. Given the drop in abundance of *Hydrocera triflora* and *Blyxa* pollen at event *vii*, it appears to have been relatively long and/or relatively severe. This is supported by the correlation of this event with a weak ISM event between 2900 and 2400 cal. yrs BP noted in a relatively distal foraminifera sequence reconstructed from the Arabian Sea (Gupta et al. 2003). More locally, an hiatus in the C3PA sedimentary record extracted from Lake Kumphawapi, North Thailand (figure 6.2) occurs within a similar timeframe (*c.* 2700 to 2500) (Wohlfarth et al. 2012), suggesting low effective moisture throughout this period. The near complete demise of *Hydrocera triflora* and a significant spike in Cyperaceae pollen occurring in the Yeak Mai record at *c.* 1900 cal. yrs BP indicates further expansion of wetland taxa at the site, implying further lake shallowing and dry site conditions.

c. 1900 to 1500 cal. yrs BP: a very weak monsoon

This period appears to be characterised by a very weak Asian summer monsoon, capturing three, closely spaced drying events (*v* [*c.* 1915 cal. yrs BP], *iv* [*c.* 1755 cal. yrs BP] and *iii* [*c.* 1550 cal. yrs BP]), resulting in what appears to be a phase shift in the aquatic/wetland taxa from a wetland and shallow water aquatic community to a wetland community with *Rotala*. Event *iii* (coinciding with Bond event 1 identified in Wang et al. (2005a)) captures what is a relatively abrupt increase in *Syzygium* pollen and a peak in Cyperaceae pollen. What is intriguing about the shift from event *iv* to *iii* is the relatively abrupt change in core sedimentology across this boundary from relatively mineral-rich silty sediments (unit III) to the organic rich sapropels of unit IV at *c.* 1750 cal. yrs BP. An abrupt increase in sediment organic content has been linked to a shallowing within an already shallow lake (Wohlfarth et al. 2012). The reconstruction of closely space droughts

from the Yeak Mai record correlates relatively well with the timing of a hiatus modelled for Lake Kumphawapi sediments (core C3PA) between 1900 and 1600 cal. yrs BP, which has been linked to drying of the lake under weak monsoon conditions (Wohlfarth et al. 2012). It is, however, notable to point out that an hiatus for the same lake is modelled from a different core (CP4) as occurring over a much longer time frame 6500 to 1600 cal. yrs BP (Chawchai et al. 2013).

c. 1500 cal. yrs BP to 2013 AD: a weak monsoon, strengthening from *c.* 450 cal. yrs BP

Though high frequency dry events appear to discontinue from *c.* 1550 cal. yrs BP., the persistence of wetland and *Rotala* pollen within the record at high (albeit fluctuating abundances) to *c.* 400 cal. yrs BP is suggestive of relatively shallow lake conditions throughout this time period, though it is noted that the persistence of the wetland could in fact represent an ecological state shift (Scheffer et al. 2001, Folke et al. 2004). An interpretation of low effective moisture conditions at the site throughout this period does, however, correspond well with patterns of step-wise EASM monsoon weakening observed from *c.* 7000 to 400 cal. yrs BP (Wang et al. 2005a, Wang et al. 2005b) (figure 6.3).

Small troughs in Mn/Ti and Fe/Ti that correspond with slightly lower abundances of Cyperaceae and *Syzygium* pollen and the absence of *Rotala* pollen from the Yeak Mai record at 1070 to 820 cal. yrs BP may indicate the onset of the MWP. The timing of this event corresponds well with troughs in *Tetrameles* pollen from BK2 (Maxwell 2001), a trough in the Dandak cave (DAN-D) δ^{18}O‰ record, and a peak in the SASMI (920 to 670 cal. yrs. BP). The timing of this event is slightly later than that observed into the EASM records (Wang et al. 2005a, Wang et al. 2005b, Zhang et al. 2008) (figure 6.4). This may indicate increased control of lake site climatic conditions by ISM circulation. Subsequent to the MWP, a small peak in Mn/Ti and Fe/Ti may indicate a drying event at *c.* 700 to 800 cal. yrs BP, though, aside from a corresponding peak in *Rotala* pollen, there is limited evidence for drying in the other proxy climate records.

Drying event *i*, appears to correspond with Bond event zero (LIA) modelled from the Dongge cave record. This event is reflected in the Yeak Mai record by peaks in Mn/Ti and Fe/Ti, and a trough in κSI, the timing of which places this event within the age range of *c.* 500 to 340 cal. yrs BP. This is relatively consistent with the timing of this event proposed by Shi et al. (2014) (550 to 250 cal. yrs BP) and in more distal records, including Zhang et al. (2008) (marginal EASM: 330 cal. yrs BP) and Gupta et al. (2003) (marginal ISM: 300 to 400 cal. yrs BP). The correspondence of this event to a peak in *Rotala*, Cyperaceae and *Syzygium* pollen from the Yeak Mai record supports the idea of lake shallowing throughout this period. The timing of this event also corresponds with relatively high peaks in Yeak Oam κSI (modelled from *c.* 400 to 440 cal. yrs BP), which can suggest drier conditions (Tamuntuan et al. 2015), though this needs to be interpreted cautiously in the absence of other proxy data for the site.

Subsequent to the drying event *i*, troughs in Yeak Mai Mn/Ti and Fe/Ti and the corresponding peak in κSI suggest strengthening of the monsoon. This is validated by the SASMI, EASM and ISM speleothem δ^{18}O‰ records, the decreasing abundance of *Tetrameles* pollen from BK2 (Maxwell 2001), and the decreased abundance of pollen from wetland indicators and *Rotala*. Reversal of nearly all of these trends within the upper dated parts of the relevant records (i.e. within the past century) may suggest re-instigation of weaker monsoon conditions in recent decades. This is in keeping with the EASM and ISM records.

The interpretation presented here is of a gradually weakening monsoon within the ISM and EASM intersection zone from the start of the core record (*c.* 4700 cal. yrs BP) to *c.* 450 cal. yrs BP, that is punctuated by several especially dry events, consistent with patterns apparent in the EASM isotope records. However, this model is inconsistent with the climate models developed from Lake Kumphawapi sediments (Wohlfarth et al. 2012, Chawchai et al. 2013), though dry periods noted in Wohlfarth et al. (2012) between *c.* 2700 to 2500 and *c.* 1900 to *c.* 1600 cal. yrs BP do correspond well with drying events *viii*, and *v* to *iii* reconstructed from the Yeak Mai record. The Wohlfarth et al. (2012) study indicates restrengthening of the monsoon from *c.* 3000 cal. yrs BP. The discrepancies between Wohlfarth et al's (2012) interpreted climatic conditions in mainland south-east Asia and those reconstructed for South China (Wang et al. 2005a, Zhang et al. 2008) are attributed to the positioning of the ITCZ between these zones from *c.* 3000 years BP onwards (Chawchai et al. 2013). A key foundation for the development of this argument is the interpreted monsoon strengthening at Yeak Kara at approximately the same time period as for Lake Kumphawapi (Maxwell 2001). However, in this study, Maxwell (2001) uses the abrupt increase in the abundance of *Tetrameles* pollen (interpreted within this study to be a SEDF indicator) alongside a decrease in wetland taxa to suggest increased available moisture at the site. Though the mechanisms are unclear, the distict, positive association between *Tetrameles* abundance and periods of EASM monsoon weakening in the Dongge Cave record (Wang et al. 2005a, Wang et al. 2005b) (shown on figure 6.3) brings this interpretation into question, and highlights that caution needs to be applied when using records of vegetation response to interpret climatic drivers.

6.3 Local and regional fire regime history over the past *c.* 4700 years

As has been discussed in chapter 3, fire incidence appears to be an important driver of change within SDTF ecosystems, thought to cause the reconfiguration of forest into savanna (Staver et al. 2011a). Though research indicates that SASDTF may be more resilient to burning than other types of SDTF, there are conflicting findings regarding the extent to which fire impacts the threshold dynamics of internal SASDTF units, particularly with respect to whether or not burning will drive SEDF to more open (MDF or DDF) forest types (e.g. Baker et al. 2008, Baker and Bunyavejchewin 2009, Johnson and Dearden 2009). Additionally, the interaction of fire with other

drivers of change in SDTF (e.g. prolonged drought) which may be important for causing the reconfiguration of forest to savanna (Brando et al. 2014), has not been well quantified within this ecoregion.

The fire regime history reconstructed for the Yeak Loam and Yeak Mai sites is discussed in the context of the climate records produced for the region (section 6.2) in order to delimit periods where local and regional forest might be particularly susceptible to a regime shift. Additionally, a comparison of regional burning with the fire histories reconstructed from lake cores extracted from other SASDTF sites - 3KUM from Lake Kumphawapi, Thailand (Kealhofer and Penny 1998, Penny 1998) and BKY2 from Yeak Kara, Cambodia (Maxwell 1999, Maxwell 2004)[1] — will be used to determine periods of high regional burning.

6.3.1 Local and regional fire regimes at the lake sites

Charcoal counts from Yeak Mai and Yeak Loam have been plotted as charcoal influx (fragments/cm/year) to account for the variable accumulation rate of core sedimentary layers that appears to drive much of the down core changes observed in the charcoal abundance reconstructed from Yeak Mai in particular (chapter 5). Charcoal influx is shown in the context of the nine drying events identified from the Yeak Mai Fe/Ti record and the Dongge cave DA record of EASM change (Wang et al. 2005a, Wang et al. 2005b) on figure 6.5.

6.3.2 Comparison with palaeoclimate records

Local signal

Macro-charcoal influx to Yeak Mai appears relatively high between *c.* 4400 and 3700 cal. yrs BP, suggesting heightened local fire activity — i.e. increased frequency, intensity or extensiveness of burning (Clark and Patterson 1997). The early part of this period parallels Bond event 3 modelled from the Dongge Cave EASM record (Wang et al. 2005a). However, the major peak in charcoal influx at 3700 cal. yrs BP appears to correspond with a subsequent wetter period. This peak may reflect increased transport of charcoal retained in the catchment to the lake basin via run off erosion, though this is unlikely to contribute significantly to influx given the small size of the catchment (Maxwell 2004). Alternatively, it could be associated with anthropogenic burning. Based on the high macro-charcoal levels occurring within lake sediments thought to be deposited under relatively strong monsoon conditions relative to the rest of the record, this interpretation is considered plausible not only for the peak period, but for local fire

[1] Though Maxwell (2004) presents a fire history from a core extracted from Yeak Loam (BYL6), this is not used in this discussion due to the fact that the chronology for this core is based on an interpolation from a single date (3800 cal. yrs BP) measured from a bulk sediment sample taken from the base of the core. The present study indicates that this date, which falls well within the range of bulk organic and charcoal and organic material samples dated from Yeak Loam sediments, is likely contaminated with a non-terrestrial source of carbon.

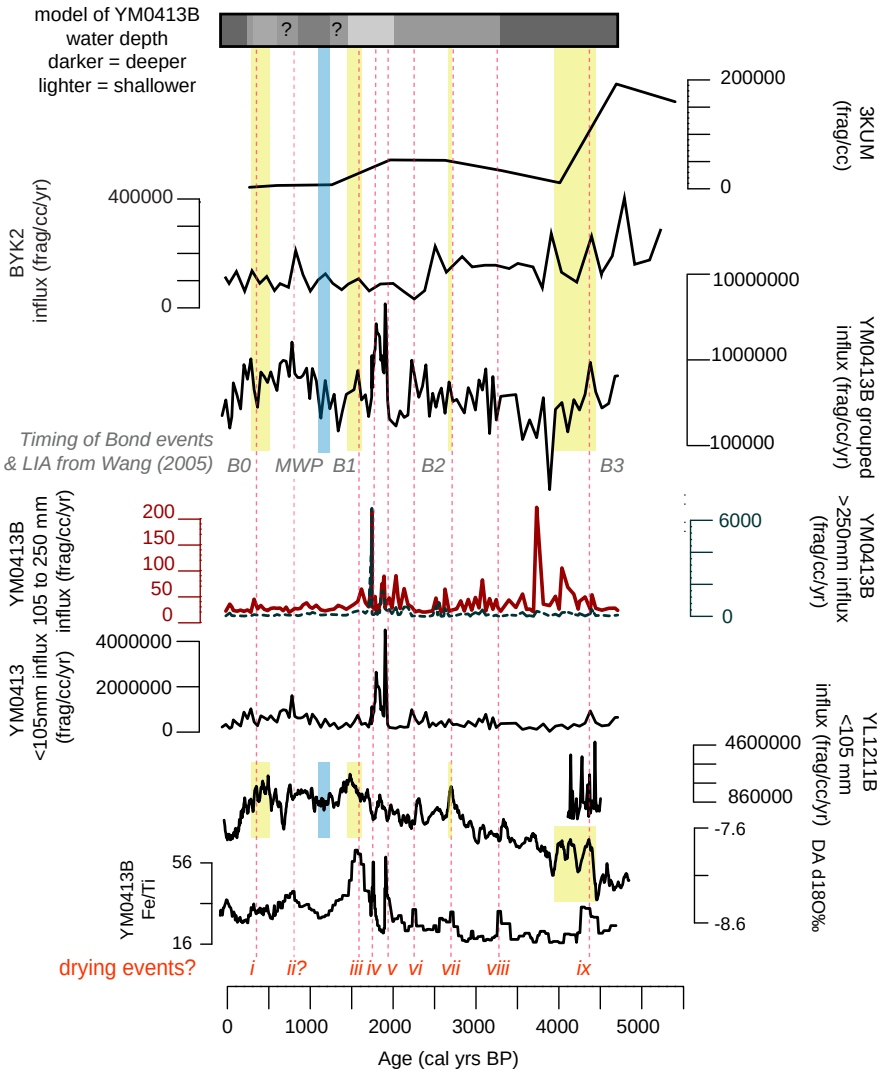

FIGURE 6.5: Diagram of estimated charcoal influx records to Yeak Mai (micro-, macro-, and combined fragments) and Yeak Loam (combined fraction), shown in the context of interpreted site climate change and charcoal influx (BKY2) and concentration (KUM3) from regional SASDTF records over the past *c.* 4700 cal. yrs BP. Yellow bars represent Bond events 0 to 3 identified in Wang et al. (2005a), and blue bars represent the approximate timing of the MWP estimated from Yeak Mai. Red lines represent drying events reconstructed from the Yeak Mai and Yeak Loam geochemistry and sedimentology records.

activity prior to *c.* 3700 cal yrs BP. Subsequent to *c.* 3700 cal. yrs BP, local fire activity at Yeak Mai is low to moderate before peaking again between *c.* 2600 and 1500 cal. yrs BP. Unlike the earlier peaks in the record, this phase of high fire activity is well timed with the high frequency dry events that occur across this time frame (*vi* to *iii*), suggesting that climate may be an important driver for fire throughout this period. The small decline in macro-charcoal input to the lake between *c.* 2500 and 2300 cal. yrs BP corresponds to a peak in micro-charcoal influx, and thus may either reflect reworking of

the larger fraction within the catchment or in the laboratory, or represent a local event that has regional expression. Fire activity is low between *c.* 1500 cal yrs BP and the core top sediments, corresponding with the major division modelled for these data from stratigraphically constrained cluster analysis (chapter 4). However, a small peak corresponds with drying event *i*. In general, high local fire activity at Yeak Mai post *c.* 3700 cal. yrs BP appears to be driven by climate, and potentially by a combination of climatic and anthropogenic factors between *c.* 3700 and 4700 cal. yrs BP.

There is evidence for an increase in local fire activity at Yeak Loam in response to drying event *ix* (figure 6.6), though the limited and questionable timeframe modelled for this core record makes it difficult to conclusively draw inferences with respect to climatic driving of fire at this site.

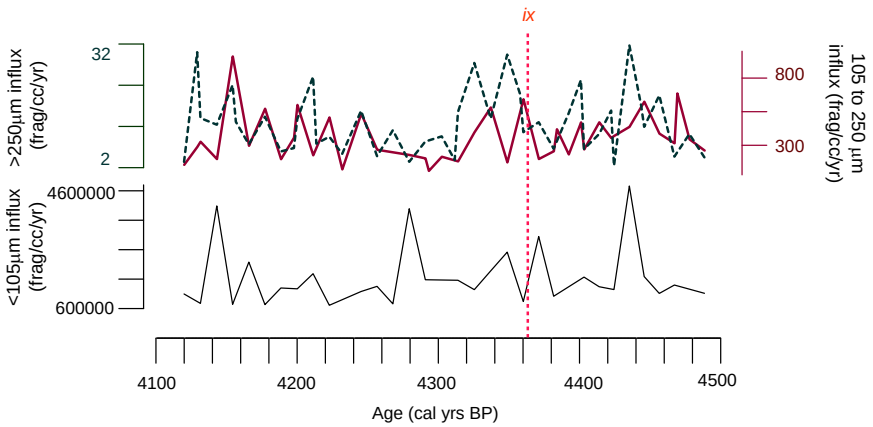

FIGURE 6.6: Macro- and micro- charcoal influx plotted from Yeak Loam, shown in the context of drying event *ix*.

Regional signal

Peaks in micro-charcoal influx to Yeak Mai that are taken to represent heightened regional fire activity, correspond with drying events *ix* and Bond event 3 (Wang et al. 2005a), *vi*, *v*, *iv*, *iii* and Bond event 1 (Wang et al. 2005a), and *ii*. A slight increase in regional fire activity occurs after dry event *viii* at *c.* 3300 cal. yrs BP, consistent with the start of the interpreted period of lake shallowing and hence reduced effective moisture at the site. A second increase in charcoal influx to Yeak Mai between *c.* 2400 and 1575 cal. yrs BP (peaking at 1905 cal. yrs BP), is also coincident with the interpretation of further lake shallowing, and the presence of high frequency dry events at the site. The small drop in fire activity between *c.* 2180 and 1985 cal. yrs BP coincides with a period of a slightly stronger EASM (Wang et al. 2005a) (figure 6.5). A small drop in micro-charcoal influx to Yeak Mai coincides with the timing of the MWP interpreted in Wang et al. (2005a). There is no clear association between increased regional fire activity and the LIA. A decline in micro-charcoal influx to Yeak Mai coincides with the inferred period of slight increased effective moisture at the site at *c.* 1500 cal. yrs BP, but this

could also be related to the implementation of regular, low intensity anthropogenic burning associated with swidden agriculture (Maxwell 2004). Overall, the regional fire record reconstructed for Yeak Mai indicates that higher regional fire activity may, to a large degree, be driven by climate.

There is no apparent correspondence between micro-charcoal influx and dry event *ix* as identified from the Yeak Loam record (figure 6.6), though, as discussed with respect to macro-charcoal influx, the limited and questionable timeframe modelled for this core record makes it difficult to conclusively draw links between climate and fire activity at Yeak Loam.

6.3.3 Comparison with other SASDTF fire records

Climate as a driver of regional fire is somewhat inconsistent with the charcoal records reconstructed from 3KUM (Kealhofer and Penny 1998, Penny 1998) and BYK2 (Maxwell 2004)[2]. These studies indicate a stepwise decline in fire activity at *c.* 3700 cal. yrs BP (both records), *c.* 2500 cal. yrs CP (BKY2), and *c.* 1200 cal. yrs BP (3KUM). However, small peaks in BYK2 charcoal influx do correspond with drying events *ix*, *iii* and *ii*, suggesting some degree of climatic influence on fire activity.

The inconsistencies between fire activity reconstructed from these studies and the current project may be due to the fact that the external records analysed charcoal samples at a lower temporal resolution (samples taken every *c.* 110 years from BK2 and every *c.* 642 years from 3KUM vs. every *c.* 40 years from Yeak Mai). Additionally, given that an increase in macro-charcoal influx to Yeak Mai sediments older than 3700 cal. yrs BP corresponds relatively well with the high charcoal influx modelled at Lake Kumphawapi and Yeak Kara over the same time period, it is possible that the charcoal records constructed from the external sites may be reflecting both the local and the regional fire signal. This interpretation is considered especially plausible for BYK2 given that all charcoal fractions greater than 100 μm^2 were included in the analysis (Maxwell 2004). In the case of 3KUM sediments, which were sieved and enumerated using comparable methods to the subject study (Penny 1998), it is possible that the charcoal deposited to the Lake Kumphawapi catchment was subject to a greater degree of reworking prior to deposition in the lake.

6.4 Dry forest threshold behaviour over millennia and the role of monsoonal dynamics and fire in affecting ecosystem change

The following section will use the drying events and interpretation of monsoon change in conjunction with identified periods of high fire activity at

[2]Raw fragment counts per cm^3 and moisture content data for core BYK2 were provided by A. Maxwell, and converted into estimated influx values. An updated Bacon age-depth model was also produced for this core using the Southern Hemisphere calibration curve (Reimer et al. 2013) offset by -21 $\pm$ 6 yrs, following Hendrickson et al. (2013) and Pryce et al. (2014).

the lake sites to discuss the resilience of SASDTF to these potential drivers of change. The pollen diagrams produced for each core in chapter 5 are reproduced for the purpose of this discussion, superimposed with dry events *i* to *ix* (red lines) and times of heightened local burning at the sites (grey bars) to show vegetation response to what are expected to be key drivers of change in these systems (figures 6.7 and 6.8 [Yeak Mai]; 6.9 and 6.10 [Yeak Loam]). Additionally, the ratio of arboreal pollen to non-arboreal pollen (AP:NAP) for each of the lake core record is presented on figure 6.11 against the same burning and climate events. This ratio should nominally capture any shifts from a higher to lower tree cover environment (Bhagwat et al. 2012). Sedges and aquatic taxa are excluded from the non-arboreal count in an attempt to reduce the influence of wetland development from the dryland signal, though it is noted that some grasses are likely to represent wetland taxa at Yeak Mai.

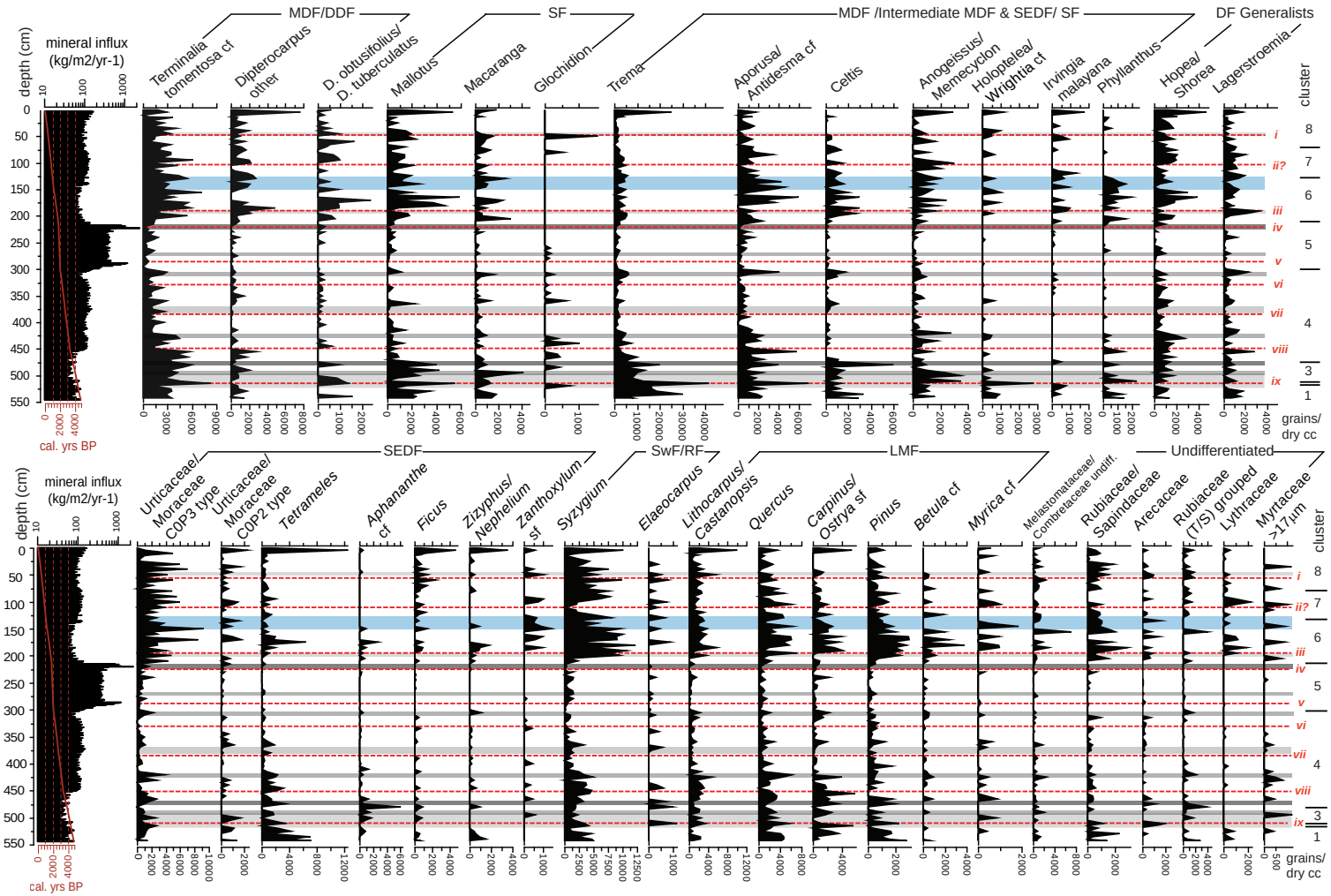

FIGURE 6.7: Reproduction of pollen and spore diagram produced from Yeak Mai that is overlain with climate events (red lines) and periods of high fire activity (grey bars) reconstructed at the Yeak Mai lake site. Blue bar represents approximate timing of the MWP. MDF = Mixed Dry Forest; DDF = Dry Dipterocarp Forest; SF = Secondary Forest; SEDF = Semi-evergreen Dry Forest; DF = Dry Forest; SwF = Swamp Forest; RF = Riparian Forest; LMF = Lower Montane Forest.

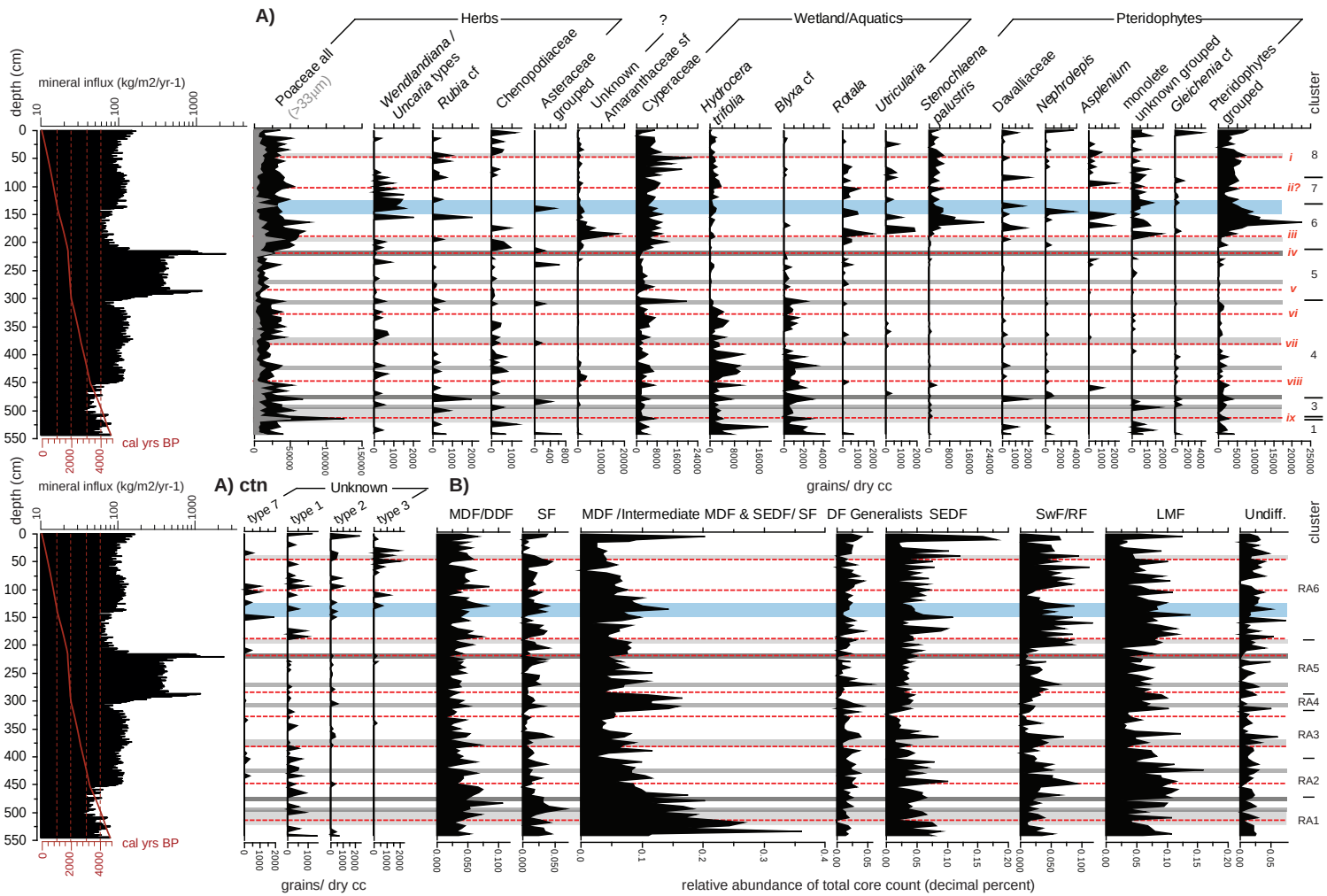

FIGURE 6.8: Reproduction of pollen and spore diagram produced from Yeak Mai that is overlain with climate events (red lines) and periods of high fire activity (grey bars) reconstructed at the Yeak Mai lake site. Blue bar represents approximate timing of the MWP. MDF = Mixed Dry Forest; DDF = Dry Dipterocarp Forest; SF = Secondary Forest; SEDF = Semi-evergreen Dry Forest; DF = Dry Forest; SwF = Swamp Forest; RF = Riparian Forest; LMF = Lower Montane Forest.

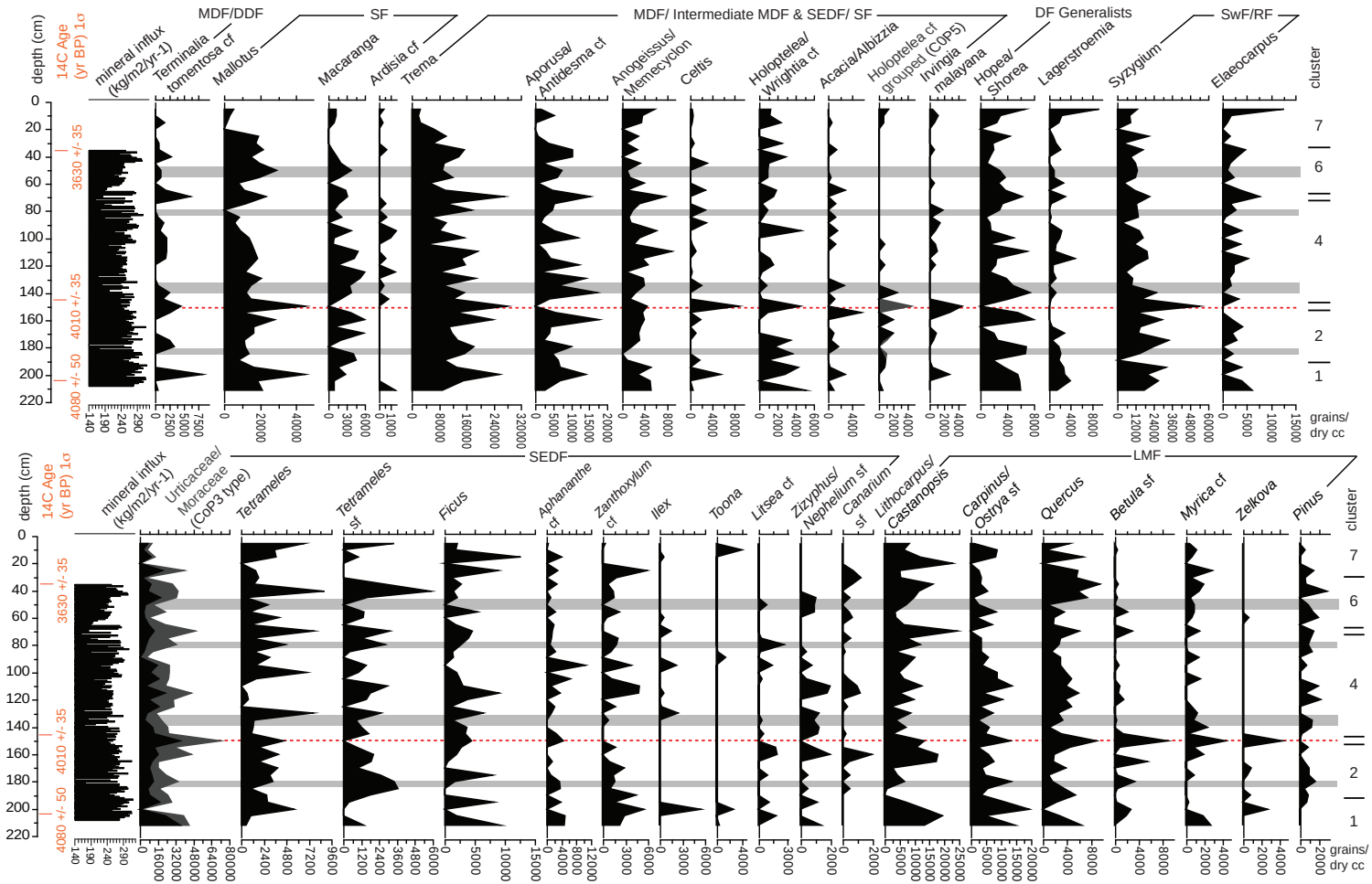

FIGURE 6.9: Reproduction of pollen and spore diagram produced from Yeak Loam that is overlain with climate event *ix* (red line) and periods of high fire activity (grey bars) reconstructed at the Yeak Loam lake site. MDF = Mixed Dry Forest; DDF = Dry Dipterocarp Forest; SF = Secondary Forest; SEDF = Semi-evergreen Dry Forest; DF = Dry Forest; SwF = Swamp Forest; RF = Riparian Forest; LMF = Lower Montane Forest.

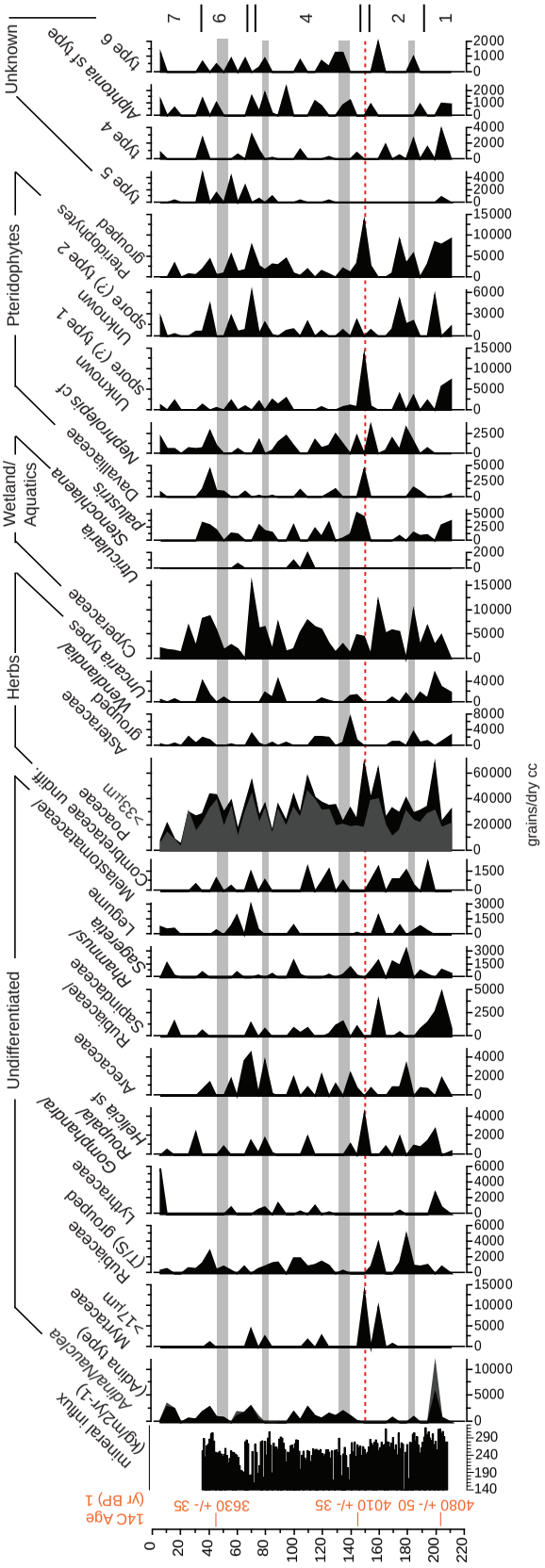

FIGURE 6.10: Reproduction of pollen and spore diagram produced from Yeak Loam that is overlain with climate event *ix* (red line) and periods of high fire activity (grey bars) reconstructed at the Yeak Loam lake site.

c. 4700 to 3300 cal. yrs BP: secondary forest pulses in response to fire & climate

This period captures changes in pollen cluster zones 1,2,3 and part of 4 as classified from cluster analysis of the absolute abundance of pollen taxa from Yeak Mai sediments (see 5 and figures 6.7 and 6.8 A). The same period captures relative abundance (RA) clusters RA1 and RA2, which represent points of change in the relative abundance of arboreal taxa from the different SASDTF dry forest units (6.8B).

Microfossil cluster 2 coincides with dry period *ix* (Bond event 3) and is centred on a period of relatively high fire activity, while the upper boundary of cluster 3 (and RA1) is well matched to a period of very high local fire activity at *c.* 3700 cal. yrs BP. This suggests that high local fire activity and dry conditions, to an extent, drive patterns of change in the vegetation record. A similar observation is apparent in the Yeak Loam record, where cluster 3 aligns with drying event *ix*, though there is no apparent relationship between peaks in local fire activity and vegetation change in this record.

Clear peaks in DDF indicators from the Yeak Mai record — *Terminalia tomentosa, Dipterocarpus obtusifolius/ tuberculatus* and Poaceae — correspond with periods of high fire activity and, in particular, drying event *ix*, suggesting the expansion of more open forest types following burning and/or decreased effective moisture. This corresponds with observations made in Maxwell (2004) that indicate the transition of regional forest around Yeak Kara from dense to more open types following heightened fire activity from *c.* 5400 cal. yrs BP (though these events are not explicitly linked to climatic factors). Interestingly, the abundance of 'other *Dipterocarpus*' taxa within the Yeak Mai record appears to decline at points of high fire activity, perhaps indicating that this pollen type should not be classified as a DDF/MDF indicator.

Within the Yeak Loam sediments, drying event *ix* coincides with peaks in vegetation that are likely representative of secondary forest types (*Mallotus*, *Trema*, *Celtis*, *Holoptelea/Wrightia* cf and *Holoptelea* cf grouped), *Terminalia tomentosa*, Poaceae, and *Syzygium* 6.9 and 6.10. This provides a degree of support for forest opening in response to drying. However, it is interesting to note the corresponding peaks in all LMF types (aside from *Pinus*) and certain SEDF types, especially species that are considered to be indicators for this forest unit - *Ficus* and *Aphananthe* cf - in response to this drying event. While it may be possible to explain a greater degree deposition of distal wind-blown LMF pollen types to the lake under arid conditions, it is difficult to reconcile why SEDF indicator types proliferate under drying conditions unless they are flowering in response to drought stress, a phenomenon that has been observed post unusually dry periods within tropical Asian forests (Corlett and Lafrankie Jr 1998).

Troughs in the AP:NAP ratio coincide with drying event *ix* in both cores, further supporting the idea of forest opening during dry periods (figure 6.11). However, there is no clear relationship between tree cover and fire activity in either record, possibly due to the high abundance of pollen from secondary forest taxa that coincide with burning peaks. Within the Yeak

Mai record, the increased abundance of *Mallotus*, *Celtis* and *Trema* following or coinciding with peaks in fire activity indicates that fire-vegetation dynamics throughout this period are characterised by secondary forest succession rather than by a transition to savanna. This finding replicates those of Maxwell (2001, 2004), which discuss the increase in secondary forest taxa in response to increased fire activity around Yeak Kara from *c.* 5400 cal. yrs BP. This suggests that rapid recovery of the forest via primary succession arboreal taxa following burning may contribute the resilience of the forests, a finding somewhat validated by a recent study on SDTF secondary forest succession (Derroire et al. 2016). It is possible that the lack of association between fire and vegetation from the Yeak Loam record is due to the poor correlations that exist between the different charcoal fraction sizes and the short timeframe covered by the core (assuming that the age-depth model produced for the core is accurate), meaning that the identified peaks in the local record are possibly insignificant.

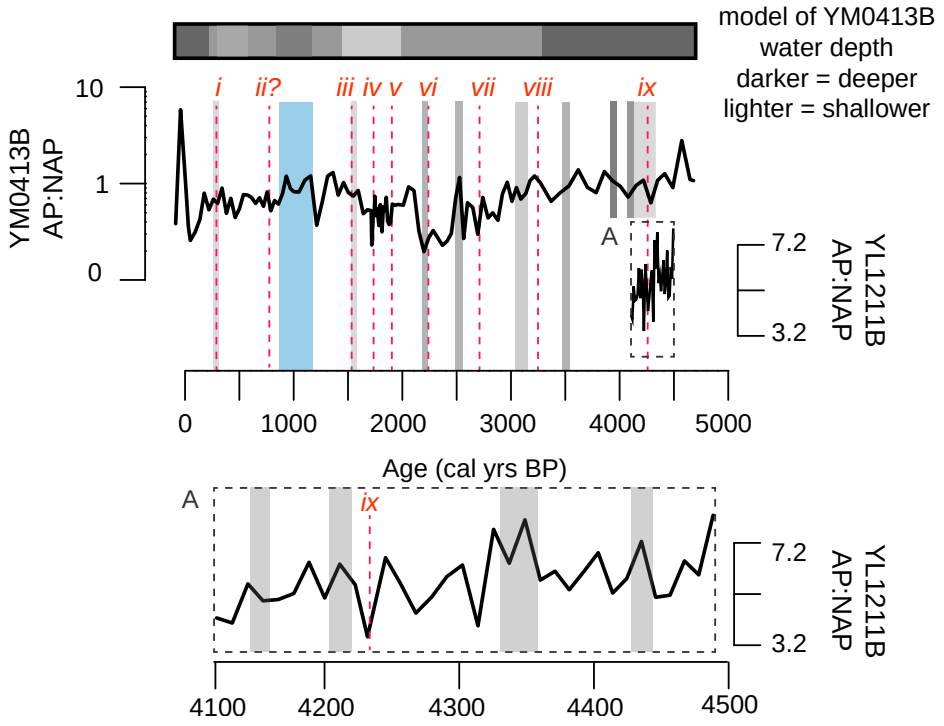

FIGURE 6.11: AP:NAP ratios plotted from Yeak Mai and Yeak Loam plant microfossil records against time. Records shown in context of climatic events reconstructed for the sites. Grey bars represent periods of high fire activity, and the blue bar represents the approximate timing of the MWP estimated from Yeak Mai. Red lines represent drying events reconstructed from the Yeak Mai and Yeak Loam geochemistry and sedimentology records.

c. 3300 to 1900 cal. yrs BP: forest opening

There is no clear evidence that decreased effective moisture at the Yeak Mai site (as interpreted from the climatic indicators), had any significant impact

upon the arboreal taxa, though the AP:NAP ratio shows a steady decline across this time zone, and displays a trough between 2400 and 2250 cal. yrs BP (figure 6.11). While this is likely associated with the expansion of grass as a wetland species, it may also imply opening of the forest. As observed in the above-described time-period, the abundance of *Trema* and *Terminalia tomentosa* increase in response to drying events *viii* ,*vii*, and *vi* and significant burning events. However, the same relationship is no longer consistently represented by *Mallotus* or *Dipterocarpus obtusifolius/ tuberculatus*.

c. 1900 to 1500 cal. yrs BP: open forest persistence & wetland expansion

This is interpreted as a period of a weak summer monsoon punctuated by several dry events (*v*, *iv* and *iii*) that all correspond to high fire activity. AP:NAP ratios are relatively low at Yeak Mai, with an especially significant trough corresponding to event *iv* and associated high local and regional fire activity. Though the very low absolute abundance of pollen and spores within the Yeak Mai record between *c.* 1900 and 1750 cal. yrs BP is likely to be most strongly reflecting the higher mineral influx predicted for sedimentary unit III, the negative correlation that exists between total plant microfossil abundance and the relative abundance of grass across this unit is notable. Given that this relationship occurs in the absence of a similar negative correlation between wetland taxa and abundance (which could then be explained solely by the expansion of a grassy wetland under shallowing conditions), lower pollen abundance may also, to a degree, be representing a reduced presence of arboreal taxa throughout this period, hinting at the expansion of a more grassy, open terrestrial ecosystem type under dry conditions. The higher abundance of DDF/MDF, SF and generalist dry forest species when compared with SEDF forest types across this zone also supports the idea of more open forest types developing during this time period. However, all common arboreal types persist through this dry, high fire activity timeframe, indicating forest resilience to these compounded forcing events.

c. 1500 cal. yrs BP to 2013 AD: gradual establishment of denser forest vegetation

From *c.* 1500 cal. yrs BP to the present, dry events and periods of high fire activity appear to be of a lower magnitude than those previously seen within the record. A lower-magnitude fire regime is apparent in the Yeak Kara record starting from *c.* 2500 cal. yrs BP (Maxwell, 2004). This is attributed to either a wetter climate, or to more constant control by humans via swidden agriculture (Maxwell 2004), both of which are possible at Yeak Mai from *c.* 1500 cal. yrs BP. At Yeak Kara, this changed fire regime relates to a shift back to SEDF. At Yeak Mai, an edaphically drier site (chapter 3), relationships between fire activity, climatic forcing and forest response across this time period are subtle, indicating that the poorer soil types at Yeak Mai may impact upon the capacity of the site to fully develop SEDF. Nevertheless, a slight increase in SEDF taxa from *c.* 1500 cal. yrs BP, and an increase in AP:NAP during the MWP may indicate the development of a denser

forest throughout this time. The much more significant spike in Yeak Mai AP:NAP at *c.* 1968 AD and corresponding drop in macro charcoal influx relates to the approximate timing of the forced migration of local villagers south and banning of traditional swidden practices in Ratanakiri, leaving local SASDTF relatively cut off from human disturbance (Riebe 1999, Fox 2002, Maxwell and Cox 2011). If this peak is associated with (a lack of) human activity, it validates the assertions of You et al. (2015) that a decline in swidden agriculture across this timeframe resulted in increased forest canopy cover across the region and, more significantly, highlights the potential capacity of the site forest (MDF/DDF) to transition into what is interpreted to be a denser formation in the absence of human disturbance. This validates findings posited by Maxwell (2004), that contemporary SASDTF, at least within north-eastern Cambodia, is an anthropogenic formation that persists due to regular fire disturbance.

6.5 Threshold behaviour of south-east Asian dry forest

6.5.1 Resilience of SASDTF in the context of global modelling of dry forest-savanna threshold dynamics

Given that precipitation (amount and seasonality) appears to be the most important control on the persistence of neotropical and Afrotropical SDTF, and that SASDTF contemporarily persists in a bistable state — able to support either SDTF or savanna (Hirota et al. 2011, Staver et al. 2011a, Staver 2012) — south-east Asian tropical dry forests should be sensitive to an ecological regime shift if precipitation were to drop, or seasonality were to increase. Within the context of Hirota et al's (2011) work, open SASDTF forest units, such as those currently supported at Yeak Mai, should be particularly sensitive to transition to savanna given that the average canopy cover of these forests is rare at a global scale, indicative of low resilience (figure 2.5). A second, major determinant of forest over savanna is a lack of fire in the system (Staver et al. 2011a, Staver 2012). While SASDTF has long been distinguished from other SDTF ecoregions due to its propensity to burn (Stott 1988a, b, 1990), what is unclear is whether high fire activity can cause a persistent state shift from more closed to more open types (Baker et al. 2008, Baker and Bunyavejchewin 2009, Johnson and Dearden 2009).

Asian monsoon records developed independently of this project and the climate record reconstructed for the lake sites as part of this research both indicate that the contemporary MAP for the region is high relative to the previous *c.* 4700 years. This suggests that past MAP, particularly between 3300 and 1500 cal. yrs BP, may have fallen below the critical threshold levels for the persistence of SDTF over savanna. Superimposed upon this, are several significant dry events, implying times of persistently low MAP, and potentially an extended dry period, which current theory would suggest would further encourage a stable state shift to savanna. Within the Yeak Mai record, identified dry events relate to periods of high regional, and often local burning, making it challenging to decouple one from the other.

However, under current theory, both should encourage a stable state shift to an open, non-forested community.

The vegetation record produced from Yeak Mai and Yeak Loam, which are of sufficient temporal resolution to capture at least one cycle of forest turnover (Phillips and Gentry 1994), indicate resilience to reduced MAP trends over millennia, periodic dry events, and periods of high fire activity — i.e. resilience to both abrupt and slow drivers of change. Subtle forest response to drying events and/or high fire activity include the transition of the site forests to more open MDF and DDF types with a high presence of secondary forest taxa. This finding may validate claims made by Dexter et al. (2015) that forests with a grassy understorey (e.g. DDF and MDF) may, ecologically, occupy the role of savanna. However, what is notable about the shifts from closed to open SASDTF units in the palaeorecord (also apparent in Maxwell (2004)), is that they tend to occur smoothly (vs. abruptly), appear to be reversible and hence do not appear to represent stable state shifts. This is perhaps best demonstrated by the major spike in arboreal vegetation within the Yeak Mai record at *c.* 1968 in response to presumed removal of anthropogenic fire from the system. This suggests that denser forest types are likely to develop (and subsequently open) when fire is removed (then reintroduced) to the system.

These findings highlight the ecologically important role of spatially and temporally variable burning for the maintenance of SASDTF as a heterogeneous, integrated system (as has also been noted in Maxwell and Cox (2011)). Localised burning is characteristic of the swidden agriculture that has been practiced in SASDTF over millennia, indicating that anthropogenic disturbance may in fact play an important role in promoting SASDTF as a heterogeneous, integrated system. This may ultimately contribute to the resilience of the ecoregion holistically, where interconnected patches of forest at different stages of succession (and hence species composition) enhance the beta diversity of the region. This presumably provides a diverse stock of external ecological memory, permitting flows of species from dry deciduous, semi-evergreen and especially secondary forest species across unit boundaries in response to variable climatic and fire forcing.

Additionally, phenological and physiological adaptations unique to the key constituent species of SASDTF may promote forest stability in the face of drivers that instigate ecological regime shifts in SDTF elsewhere. Specific taxa that, from the pollen record, appear to be key in forest resilience in the face of these drivers include several secondary forest types (notably *Trema* and *Mallotus*) (forest establishers), and dry forest types (notably *Terminalia tomentosa* and *Dipterocarpus obtusifolius/tuberculatus* (forest persisters).

Some overarching functional traits of SASDTF secondary forest genera encourage their establishment following disturbance, and later the regeneration of closed forest systems. For instance, the rapid establishment of *Trema* following disturbance appears to relate to its capacity to 1) produce viable seed banks at a relatively large distance from its source (Cheke et al. 1979), 2) profusely germinate in open canopy settings (Goodale et al. 2012), and 3) grow very rapidly (Vàzquez-Yanes 1998). The establishment of these typically short-lived species, plays an important role in re-establishing microclimatic and soil conditions suitable for the expansion of denser forest species,

thereby promoting a shift from more open- to more- closed forest communities in the absence of disturbance (Vázquez-Yanes 1998).

While secondary forest taxa exhibit traits encouraging rapid establishment following disturbance, key dry forest taxa may possess characteristics permitting persistence through periods of dry climatic conditions and/or high fire activity. For instance, several xeromorphic adaptations of *Dipterocarpus obtusifolius/tuberculatus*, including leaf shedding, tomentose leaves, terminal buds and thick bark Stott, 1984 124, likely contribute to their apparent resilience to dry periods in the microfossil record. Additionally, their high production of seedlings that are resistant to dry season fire may contribute to their resilience to burning. *Terminalia tomentosa* has been shown to have high plasticity with respect to leaf functional attributes (including relative growth and intrinsic water use efficiency), indicating high resilience to seasonality and drought relative other SDTF canopy species (Chaturvedi et al. 2011). This, in addition to this species' capacity to store large quantities of water in its stem, may contribute to its high relative abundance in the pollen record during dry periods.

6.5.2 Projected resilience of SASDTF to future climate and fire drivers: findings and future research priorities

The IPCC AR5 indicates that monsoon extremes are likely to increase over the 21st century, and that the ISM is likely to undergo the greatest degree of change of all global monsoon systems (Christensen et al. 2013). This includes an increased probability of a longer wet season, as well as an increase in mean precipitation over mainland south-east Asia, but with a greater likelihood of climatic extremes characterised by larger rainfall events and longer intervals between events (Knapp et al. 2008, Christensen et al. 2013). Understanding the impacts of these changes in Asia "is currently limited by the incompleteness and inaccessibility of biodiversity information . . . (with) major research gaps includ(ing) . . . thermal tolerances and acclimation capacities of plants and animals" (IPCC 2014 p1331).

This study indicates that SASDTF — an extensive ecoregion within Asia — should be resilient to the increased climatic extremes predicted for the Asian monsoon region (outlined in Christensen et al. (2013)), particularly to those pertaining to extended drought. However, what is not considered in this assessment, is the impact of the rapid levels of selective logging and broad area clear-felling for timber, agriculture and cash cropping that is currently occurring across much of mainland south-east Asia, including Ratanakiri (Sodhi et al. 2010). This could pose problems for the persistence of SASDTF given that it may disrupt the connectivity of the heterogeneous, mosaicked characteristic of these forests, which appears central for adaptation to changing patterns of precipitation and periods of increased or decreased fire activity. Compounding this may be the abrupt decline in forest herbivores — important for seed dispersal (Teegalapalli et al. 2009) — during the conflict period in the late 20th century. Additionally, the decline of traditional swidden practices across some parts of the region and intensification in others, which this study suggests are important for the persistence of SASDTF (also been noted by (Maxwell 2004, Maxwell and

Cox 2011)), may have important implications for the future conservation of associated forests. These may include forest fragmentation (if fire intensification no longer permits the successful establishment of secondary forest species), and the homogenisation of any remaining forest patches to a potentially denser types where fire is excluded.

Future research priorities within SASDTF may therefore be to look at the cumulative impacts of fragmentation, changing fire practices and altered herbivory on forest response. Given that these changes are relatively recent in Ratanakiri, it is expected that the instrumental record could provide valuable insights into these questions, particularly with respect to changing patterns of land clearance. Such research, combined with a temporally high-resolution palaeo-environmental reconstructions of herbivory (utilising techniques such as analysis of the coprophillic fungus *Sporomeilla* and sedimentary DNA (Shokralla et al. 2012)), land-use and forest dynamics over the past century could provide useful information pertaining to future conservation planning for these forests. With respect to climatic forcing, it may be beneficial for additional research to focus on projected drivers of change for the region that have not been well-quantified within this research, such as resilience to an elevated CO_2 climate, and response to rainfall extremes and heightened dry/wet season contrasts.

7 Conclusion

This study has applied palaeo-environmental techniques to sediment cores extracted from three Cambodian crater lakes — Yeak Mai,Yeak Loam and Yeak Oam — to investigate the threshold dynamics of south-east Asian seasonally dry tropical forest over the past 4700 years. This research is of consequence given that:

- this ecoregion has, to date, been largely neglected from resilience research;
- the associated ecosystems are of global significance, with respect both to their high biodiversity (Myers et al. 2000, Olson and Dinerstein 2002) and the goods and services that they provide to a highly populous portion of the world (Clift and Plumb 2008);
- research on tropical dry forest elsewhere indicates that SDTF should be sensitive to a stable state shift to savanna if seasonality were to increase, MAP were to decline, or fire was introduced to associated ecosystems (Hirota et al. 2011, Staver et al. 2011a); and,
- the Asian monsoon, which affects this ecoregion, is predicted to undergo the greatest degree of change of all global monsoon systems into the 21st century (Christensen et al. 2013).

The key objective of this study was therefore to use the palaeo-record to determine the response of representative SASDTF ecosystems to drivers of change that are considered to be important in tropical dry forest ecosystems, notably reduced MAP, increased seasonality, and fire. This is important for determining whether SASDTF exhibits similar pattern of resilience to SDTF elsewhere, and ultimately for making conservation decisions for these forests with respect to future climate change projections. In order to achieve this objective, it was also necessary to generate a record of past climatic and fire conditions to which the vegetation response could be compared.

The climate record produced from this study, which uses geochemical, sedimentological and aquatic/wetland plant microfossil indicators to infer periods of lake shallowing and deepening over 4700 years, provides one of the longest monsoon records from the ISM/EASM zone. This record, in particular fluctuations in the Fe/Ti ratio from the Yeak Mai sediments, shows a close association with the EASM from *c.* 4700 to 1000 cal. yrs BP (notably the Dongge Cave isotopic record (Wang et al. 2005a *c.*a)), and a strong association with the ISM (predominantly reflecting the SASMI reconstructed in Shi et al. (2014)), over the past millennium. Overall, the climate record produced in this study shows a stepwise weakening of the summer monsoon to *c.* 450 cal. yrs BP, after which it appears to strengthen. The record is punctuated by nine dry events centred on *c.* 4250 (*ix*), 3300 (*viii*), 2650 (*vii*),

2250 (*vi*), 1915 (*v*), 1755 (*iv*), 1550 (*iii*), 570(*ii?*) and 350(*i*) cal. yrs BP. Events *ix*, *vii*, *iii*, and *i* correspond well with the Bond events 3 to 0 identified within Wang et al. (2005a), and the period between 1900 and 1500 has been identified as particularly dry within the study area. One significant aspect of this finding is that it highlights the potential for using redox proxies for shallow (Mn/Ti, Fe/Ti) and deep (Mn/Fe) lakes for reconstructing high-resolution palaeoclimates in the tropics — a relatively novel approach.

Charcoal records produced from both lake sites indicate that fire has been a persistent feature of SASDTF over the length of the records (4700 cal. yrs BP to 2013 AD). In general, regional burning tends to reflect climate, with peaks in influx generally showing a good relationship with the dry events identified from the climate record. Charcoal influx from local fires at Yeak Mai suggests periods of higher fire activity at the site prior to *c.* 3700 cal. yrs BP that do not appear to be associated with climate. From *c.* 3700 cal. yrs BP onwards, however, local fire is well timed with the dry events at the site, and particularly high fire activity is evident within the dry period between *c.* 1900 and 1500 cal. yrs BP. No clear trends can be drawn from the local fire signal reconstructed from the Yeak Loam record.

Palaeo-reconstructions of forest response to drier climates and periods of high fire activity in the past indicate resilience of SASDTF to these drivers. As such, this research concludes that the tropical dry forests of south-east Asia exhibit different threshold characteristics to their neotropical and Afrotropical counterparts. However, there is subtle evidence that denser forest units (SEDF) may transition into more open forest types (DDF or MDF) with high numbers of successional species during dry periods that are characterised by high frequency and/or intensity burning. This is especially apparent in the Yeak Mai record during the 1900 to 1500 cal. yrs BP dry event. However, these shifts appear transient, with reversion to SEDF apparent under milder climatic conditions coupled with low fire activity. This indicates that these are not stable state shifts, and that the unique, forest-mosaic nature of the ecoregion, created by a combination of traditional swidden cultivation practices and topographic and edaphic controls, may play an important role in contributing to the resilience of these forests in the long term. Additionally, pioneer secondary forest types may be important for the rapid recovery of forest following disturbance. If the major spike in arboreal pollen at *c.* 1968 in the Yeak Mai record does reflect a period of increased forest density when swidden agriculture was temporarily abandoned in the region, it provides strong evidence for the role of anthropogenic fire in the persistence of SASDTF as a mosaicked ecosystem. However, a temporally and geographically higher resolution analysis of this event would need to be undertaken to confirm this assertion.

These findings are important within the context of contemporary SDTF resilience theory, as they indicate that contemporary biome-scale modelling for this habitat type is inadequate for forecasting (or hindcasting) threshold changes within representative ecoregions (Hirota et al. 2011, Staver et al. 2011a). Rather, they indicate that biogeographic factors combined with anthropogenic maintenance of the heterogeneous nature of SASDTF may be important for controlling its ecoregional resilience, as has been discussed

within several recent studies (Maxwell and Cox 2011, Murphy and Bowman 2012, Dexter et al. 2015). From a methodological perspective, this research demonstrates the value of adopting a multi-proxy palaeoenvironmental approach in order to facilitate a long term resilience assessment. This is particularly the case for forested ecosystems that operate on time cycles of decades to centuries, demanding a longer term focus than many instrumental studies permit (Gardner et al. 2009, Zuidema et al. 2013). Additionally, the discrepancy between the climate and forest dynamics that has been demonstrated by adopting a multi-proxy approach, highlights the need to decouple drivers of change from response parameters within palaeoecological records, particularly when making assumptions about climate change from vegetation response.

The IPCC AR5 identifies lack of knowledge on the "thermal tolerances and acclimation capacities of plants and animals" (IPCC 2014 p1331) as a major research gap within in tropical Asia. This study contributes to filling this gap by providing evidence that SASDTF, as a relatively connected, heterogenous forested system, is unlikely to be sensitive to the 21st century climatic conditions that are projected for the region (i.e. overall increased precipitation but with more climatic extremes). However, what is not considered in this study is the high levels of fragmentation and broad-scale clearing that are currently occurring across much mainland south-east Asia, including Ratakanakiri (Sodhi et al. 2010). This could plausibly reduce the resilience of SASDTF given that the dry forest mosaic that is so characteristic of this ecoregion appears important for allowing adaptation to change. Additionally, the recent decline of swidden practices across the region and extirpation of large herbivores from the forest by the 1990s may also have important implication for the future resilience of the forests (Loucks et al. 2009, Maxwell and Cox 2011).

As such, a key recommendation for future work within this area is to investigate how fragmentation, altered herbivory and suppressed fire regimes may impact upon the resilience of SASDTF, particularly if these process serve to significantly fragment or homogenise the ecoregion. A mixed methods approach, using land clearance data in concert with a temporally high resolution, multiproxy analysis of the palaeorecord over the past century could address this question. Additionally, more high-resolution palaeoecological analyses within other representative SASDTF ecosystems within mainland south-east Asia are necessary to determine whether the model presented here, of ecoregional resilience, is sufficient at an ecosystem-level scale.

In summary, this study has demonstrated that the key drivers of threshold change for neotropical and Afrotropical SDTF — mean annual precipitation, seasonality and fire — do not apply to comparable habitat types within south-east Asia in their current state. Rather, these forests appear resilient in the face of climatic forcing, including extended dry events and periods of a weaker-than-present summer monsoon. Additionally, they appear to rely on anthropogenic fire as an inherent part of their ecology. This indicates the need to move beyond biome-scale models of resilience models may be of limited value for conservation planning at the regional or local scale where detailed palaeo-resilience studies are lacking.

8 References

Addinsoft. 2016. PCA analysis: Excel add-in. Addinsoft, www.xlstat.com.

Amante, C., and B. W. Eakins. 2009. ETOPO1 1 Arc-Minute Global Relief Model: Procedures, Data Sources and Analysis. NOAA Technical Memorandum NESDIS NGDC-24. National Geophysical Data Center, NOAA.

Ammann, B., J. F. N. van Leeuwen, W. O. van der Knaap, H. Lischke, O. Heiri, and W. Tinner. 2013. Vegetation responses to rapid warming and to minor climatic fluctuations during the Late-Glacial Interstadial (GI-1) at Gerzensee (Switzerland). Palaeogeography, Palaeoclimatology, Palaeoecology 391:40-59.

Anchukaitis, K. J., B. M. Buckley, E. R. Cook, B. I. Cook, R. D. D'Arrigo, and C. M. Ammann. 2010. Influence of volcanic eruptions on the climate of the Asian monsoon region. Geophysical Research Letters 37:L22703.

Andersen, A. N., G. D. Cook, L. K. Corbett, M. M. Douglas, R. W. Eager, J. Russell-Smith, S. A. Setterfield, R. J. Williams, and J. C. Z. Woinarski. 2005. Fire frequency and biodiversity conservation in Australian tropical savannas: implications from the Kapalga fire experiment. Austral Ecology 30:155-167.

Andersen, T., J. Carstensen, E. Hernandez-Garcia, and C. M. Duarte. 2009. Ecological thresholds and regime shifts: approaches to identification. TRENDS in Ecology and Evolution 24:49-57.

Apgaua, D. M. G., R. M. Santos, D. G. S. Pereira, G. C. Oliveira Menino, G. G. Pires, M. A. L. Fontes, and D. Y. P. Tng. 2014. Beta-diversity in seasonally dry tropical forests (SDTF) in the Caatinga Biogeographic Domain, Brazil, and its implications for conservation. Biodiversity and Conservation 23:217-232.

Aravena, R., L. I. Wassenaar, and L. N. Plummer. 1995. Estimating 14C groundwater ages in a methanogenic aquifer. Water Resources Research 31:2307-2317.

Arnone III, J. A., R. L. Jasoni, A. J. Lucchesi, J. D. Larsen, E. A. Leger, R. A. Sherry, Y. Luo, D. S. Schimel, and P. S. J. Verburg. 2011. A climatically extreme year has large impacts on C4 species in tallgrass prairie ecosystems but only minor effects on species richness and other plant functional groups. Journal of Ecology 99:678-688.

Asner, G. P., S. R. Levick, T. Kennedy-Bowdoin, D. E. Knapp, R. Emerson, J. Jacobson, M. S. Colgan, and R. E. Martin. 2009. Large-scale impacts

of herbivores on the structural diversity of African savannas. Proc Natl Acad Sci U S A 106:4947-4952.

Aston, P. S. 1988. Dipterocarp biology as a window to the understanding of tropical forest structure. Annual Review of Ecology and Systematics 19:347-370.

Atluri, J. B., C. S. Reddi, and S. P. Venkata Ramana. 2003. Breeding and pollination systems in the Indian Almond tree Terminalia catappa Linn. Ecology, Environment and Conservation 9:331-335.

Australian National University. 2016. Australasian Pollen and Spore Atlas. Australian National University. http://apsa.anu.edu.au.

Ayyappan, N., and N. Parthasarathy. 2004. Short-term changes in tree populations in a tropical evergreen forest at Varagalaiar, Western Ghats, India. Biodiversity & Conservation 13:1843-1851.

Baker, P., J., and S. Bunyavejchewin. 2009. Fire behavior and fire effects across the forest landscape of continental Southeast Asia. Pages 311-334 in M. A. Cochrane, editor. Tropical Fire Ecology. Springer Berlin Heidelberg.

Baker, P. J., S. Bunyavejchewin, and A. P. Robinson. 2008. The impacts of large-scale, low-intensity fires on the forests of continental South-east Asia. International Journal of Wildland Fire 17:782-792.

Ballesteros, T., E. Montoya, T. Vegas-Vilarrubia, S. Giralt, M. Abbott, and V. Rull. 2014. An 8700-year record of the interplay of environmental and human drivers in the development of the southern Gran Sabana landscape, SE Venezuela. The Holocene 24:1757-1770.

Banfai, D. S., and D. M. J. S. Bowman. 2006. Forty years of lowland monsoon rainforest expansion in Kakadu National Park, Northern Australia. Biological Conservation 131:553-565.

Banks, H. 1997. The Pollen of Delonix (Leguminosae: Caesalpinioideae: Caesalpinieae). Kew Bulletin 52:417-434.

Benito-Garzón, M., P. W. Leadley, and J. F. Fernández-Manjarrés. 2014. Assessing global biome exposure to climate change through the Holocene-Anthropocene transition. Global Ecology and Biogeography 23:235-244.

Berkelhammer, M., A. Sinha, M. Mudelsee, H. Cheng, R. L. Edwards, and K. Cannariato. 2010. Persistent multidecadal power of the Indian Summer Monsoon. Earth and Planetary Science Letters 290:166-172.

Beta Analytic. 2016. Beta Analytic Standard Pretreatment Protocol. Beta Analytic, Miami, Florida.

Bhagwat, S. A., S. Nogué, and K. J. Willis. 2012. Resilience of an ancient tropical forest landscape to 7500 years of environmental change. Biological Conservation 153:108-117.

Bhattacharyya, A., K. Sandeep, S. Misra, R. Shankar, A. K. Warrier, Z. Weijian, and L. Xuefeng. 2015. Vegetational and climatic variations during the past 3100 years in southern India: evidence from pollen,

magnetic susceptibility and particle size data. Environmental Earth Sciences 74:3559-3572.

Bird, M. I., D. Taylor, and C. Hunt. 2005. Palaeoenvironments of insular Southeast Asia during the Last Glacial Period: a savanna corridor in Sundaland? Quaternary Science Reviews 24:2228-2242.

Bishop, P., J. Grindrod, and D. Penny. 1996. Holocene palaeoenvironmental reconstruction based on microfossil analysis of a lake sediment core, Nong Han Kumphawapi, Udon Thani, Northeast Thailand. Asian Perspectives: the Journal of Archaeology for Asia and the Pacific 35:209-228.

Blaauw, M., and J. A. Christen. 2011. Flexible Paleoclimate Age-Depth Models Using an Autoregressive Gamma Process. Bayesian Analysis 6:457-474.

Blott, S. J., and K. Pye. 2001. GRADISTAT: a grain size distribution and statistics package for the analysis of unconsolidated sediments. Earth Surface Processes and Landforms 26:1237-1248.

Bonan, G. B. 2008. Forests and climate change: forcings, feedbacks, and the climate benefits of forests. Science 320:1444-1449.

Bond, W. J. 2008. What Limits Trees in C_4 Grasslands and Savannas? Annual Review of Ecology, Evolution, and Systematics 39:641-659.

Borgaonkar, H. P., A. B. Sikder, S. Ram, and G. B. Pant. 2010. El Niño and related monsoon drought signals in 523-year-long ring width records of teak (Tectona grandis L.F.) trees from south India. Palaeogeography, Palaeoclimatology, Palaeoecology 285:74-84.

Bourdier, F. 1995. Knowledge and Practices of Trditional Management of Nature in a Remote Province: Report of a Research Mission on the Theme of Environment in Cambodia, Honolulu, Hawaii.

Bourdier, F. 1998. Health, women and environment in a marginal region of north-eastern Cambodia. GeoJournal 44:141-150.

Boyd, W. E., and R. J. McGrath. 2001. The geoarchaeology of the prehistoric ditched sites of the upper Mae Nam Mun Valley, NE Thailand, III: Late Holocene vegetation history. Palaeogeography Palaeoclimatoloy Palaeoecology 171:307-328.

Boyle, J. F. 2001. Inorganic geochemical methods in paleolimnology. Pages 83-142 in W. M. Last and J. P. Smol, editors. Tracking Environmental Change Using Lake Sediments Volume 2: Physical and Geochemical Methods. Kluwer Academic Publishers, Dordrecht, The Netherlands.

Brando, P. M., J. K. Balch, D. C. Nepstad, D. C. Morton, F. E. Putz, M. T. Coe, D. Silverio, M. N. Macedo, E. A. Davidson, C. C. Nobrega, A. Alencar, and B. S. Soares-Filho. 2014. Abrupt increases in Amazonian tree mortality due to drought-fire interactions. Proc Natl Acad Sci U S A 111:6347-6352.

Brown, T. A., D. E. Nelson, R. W. Mathewes, J. S. Vogel, and J. R. Southon. 1989. Radiocarbon Dating of Pollen by Accelerator Mass Spectrometry. Quaternary Research 32:205-212.

Brown, W. H. 1920. Minor Products of Phillippine Forests. Bureau of Forestry, Manila.

Bryant, C. L., J. G. Farmer, A. B. MacKenzie, A. E. Bailey-Watts, and A. Kirika. 1997. Manganese Behavior in the Sediments of Diverse Scottish Freshwater Lochs. Limnology and Oceanography 42:918-929.

Bucini, G., and N. P. Hanan. 2007. A continental-scale analysis of tree cover in African savannas. Global Ecology and Biogeography 16:593-605.

Buckley, B. M., K. J. Anchukaitis, D. Penny, R. Fletcher, E. R. Cook, M. Sano, L. C. Nam, A. Wichienkeeo, T. T. Minh, and T. M. Hong. 2010. Climate as a contributing factor in the demise of Angkor, Cambodia. Proc Natl Acad Sci U S A 107:6748-6752.

Buckley, B. M., K. Palakit, K. Duangsathaporn, P. Sanguantham, and P. Prasomsin. 2007. Decadal scale droughts over northwestern Thailand over the past 448 years: links to the tropical Pacific and Indian Ocean sectors. Climate Dynamics 29:63-71.

Bullock, S. H. 1995. Plant reproduction in neotropical dry forests. Pages 277-296 in S. H. Bullock, H. A. Mooney, and E. Medina, editors. Seasonally Dry Tropical Forests. Cambridge University Press, Cambridge.

Bunyavejchewin, S. 1983. Canopy Structure of Dry Dipterocarp Forest of Thailand. Thai Forest Bulletin 14:1-132.

Bunyavejchewin, S., P. J. Baker, and S. J. Davies. 2011. Seasonally Dry Tropical Forests in Continental Southeast Asia: Structure, Composition, and Dynamics. Pages 9-35 in W. J. McShea, S. J. Davies, and N. Bhumpakphan, editors. The Ecology and Conservation of Seasonally Dry Forests in Asia. Smithsonian Institution Scholarly Press, Washington D.C.

Bunyavejchewin, S., J. V. LaFrankie, P. J. Baker, M. Kanzaki, P. S. Ashton, and T. Yamakura. 2003. Spatial distribution patterns of the dominant canopy dipterocarp species in a seasonal dry evergreen forest in western Thailand. Forest Ecology and Management 175:87-101.

Caetano, S., and Y. Naciri. 2011. The Biogeography of Seasonally Dry Tropical Forests in South America. Pages 23-44 in R. Dirzo, H. S. Young, H. A. Mooney, and G. Ceballos, editors. Seasonally Dry Tropical Forests. Island Press, Washington, D.C.

Campos, G. E. P., M. S. Moran, A. Huete, Y. Zhang, C. Bresloff, T. E. Huxman, D. Eamus, D. D. Bosch, A. R. Buda, S. A. Gunter, T. H. Scalley, S. G. Kitchen, M. P. McClaran, W. H. McNab, D. S. Montoya, J. A. Morgan, D. P. C. Peters, E. J. Sadler, M. S. Seyfried, and P. J. Starks. 2013. Ecosystem resilience despite large-scale altered hydroclimatic conditions. Nature 494:349–352.

Carpenter, E. W. 1967. Teleseismic signals calculated for underground, underwater, and atmospheric explosions. Geophysics 32:17-32.

Chai, P. P. K. 2016. Midin (Stenochlaena palustris), the popular wild vegetable of Sarawak. Utar Agricultural Science Journal 2:18-20.

Chakravorty, S., C. Gnanaseelan, and P. A. Pillai. 2016. Combined influence of remote and local SST forcing on Indian Summer Monsoon Rainfall variability. Climate Dynamics DOI: 10.1007/s00382-016-2999-5.

Chaplin-Kramer, R., I. Ramler, R. Sharp, N. M. Haddad, J. S. Gerber, P. C. West, L. Mandle, P. Engstrom, A. Baccini, S. Sim, C. Mueller, and H. King. 2015. Degradation in carbon stocks near tropical forest edges. Nature Communications 6:10158.

Chaturvedi, R. K., A. S. Raghubanshi, and J. S. Singh. 2011. Leaf attributes and tree growth in a tropical dry forest. Journal of Vegetation Science 22:917-931.

Chawchai, S., A. Chabangborn, M. Kylander, L. Löwemark, C. M. Mörth, M. Blaauw, W. Klubseang, P. J. Reimer, S. C. Fritz, and B. Wohlfarth. 2013. Lake Kumphawapi – an archive of Holocene palaeoenvironmental and palaeoclimatic changes in northeast Thailand. Quaternary Science Reviews 68:59-75.

Chawchai, S., M. E. Kylander, A. Chabangborn, L. Löwemark, and B. Wohlfarth. 2016. Testing commonly used X-ray fluorescence core scanning-based proxies for organic-rich lake sediments and peat. Boreas:180–189.

Cheke, A. S., W. Nanakorn, and C. Yankoses. 1979. Dormancy and Dispersal of Seeds of Secondary Forest Species Under the Canopy of a Primary Tropical Rain Forest in Northern Thailand. Biotropica 11:88-95.

Chidumayo, E. N., and C. Marunda. 2010. Managing dry forests and woodlands in sub-saharan Africa: context and challenges. Pages 1-10 in E. N. Chidumayo and D. J. Gumbo, editors. The Dry Forests and Woodlands of Africa: Managing for Products and Services. Earthscan, London and Washington D.C.

Christensen, J. H., K. Krishna Kumar, E. Aldrian, S.-I. An, I. F. A. Cavalcanti, M. de Castro, W. Dong, P. Goswami, A. Hall, J. K. Kanyanga, A. Kitoh, J. Kossin, N.-C. Lau, J. Renwick, D. B. Stephenson, S.-P. Xie, and T. Zhou. 2013. Climate Phenomena and the Relevance for Future Regional Climate Change. Pages 1217-1308 in T. F. Stocker, D. Qin, G.-K. Plattner, M. Tignor, S. K. Allen, J. Boschung, A. Nauels, Y. Xia, V. Bex, and P. M. Midgley, editors. Climate Change 2013: Contribution of Working Group I to the Fifth Assessment Report of the Intergovernmental Panel on Climate Change. Cambridge University Press, Cambridge and New York.

Clark, J. S. 1988. Particle motion and the theory of charcoal analysis: Source area, transport, deposition, and sampling. Quaternary Research 30:67-80.

Clark, J. S., and W. A. I. Patterson. 1997. Background and local charcoal in sediments: scales of fire evidence in the palaeorecord. Pages 23-48 in J. S. Clark, H. Cachier, J. G. Goldammer, and B. Stocks, editors. Sediment records of biomass burning and global change. Springer Verlag, Berlin.

Clift, P. D., and R. A. Plumb. 2008. The Asian Monsoon: Causes, History and Effects. Cambridge University Press, Cambridge.

Clift, P. D., R. Tada, and H. Zheng. 2010. Monsoon evolution and tectonics-climate linkage in Asia: an introduction. Geological Society, London, Special Publications 342:1-4.

Coe, M. T., T. R. Marthews, M. H. Costa, D. R. Galbraith, N. L. Greenglass, H. M. Imbuzeiro, N. M. Levine, Y. Malhi, P. R. Moorcroft, M. N. Muza, T. L. Powell, S. R. Saleska, L. A. Solorzano, and J. Wang. 2013. Deforestation and climate feedbacks threaten the ecological integrity of south-southeastern Amazonia. Proceedings of the Royal Society B: Biological Sciences 368:20120155.

Cole, L. E. S., S. A. Bhagwat, and K. J. Willis. 2015. Long-term disturbance dynamics and resilience of tropical peat swamp forests. Journal of Ecology 103:16-30.

Colm, S. 1997. Land Rights: The Challenge for Ratanakiri's Indigenous Community. Watershed 3:1-9.

Conrad, R., M. Noll, P. Claus, M. Klose, W. R. Bastos, and A. Enrich-Prast. 2011. Stable carbon isotope discrimination and microbiology of methane formation in tropical anoxic lake sediments. Biogeosciences 8:795-814.

Cook, C. D. K., and R. Lüönd. 1983. A revision of the Genus Blyxa (Hydrocharitaceae). Aquatic Botany 15:1-52.

Cook, E. R., K. J. Anchukaitis, B. M. Buckley, R. D. D'Arrigo, G. C. Jacoby, and W. E. Wright. 2010. Asian monsoon failure and megadrought during the last millennium. Science 328:486-489.

Cook, E. R., P. J. Krusic, K. J. Anchukaitis, B. M. Buckley, T. Nakatsuka, and M. Sano. 2013. Tree-ring reconstructed summer temperature anomalies for temperate East Asia since 800 C.E. Climate Dynamics 41:2957-2972.

Corella, J. P., A. E. Amrani, J. Sigró, M. Morellón, E. Rico, and B. Valero-Garcés. 2011. Recent evolution of Lake Arreo, northern Spain: influences of land use change and climate. Journal of Paleolimnology 46:469-485.

Corlett, R. T. 2004. Flower visitors and pollination in the Oriental (Indomalayan) Region. Biological Reviews 79:497-532.

Corlett, R. T., and J. V. Lafrankie Jr. 1998. Potential impacts of climate change on tropical Asian forests through an influence on phenology. Pages 299-313 in A. Markham, editor. Potential Impacts of Climate Change on Tropical Forest Ecosystems Springer, The Netherlands.

Costa, M. H., and G. F. Pires. 2010. Effects of Amazon and Central Brazil deforestation scenarios on the duration of the dry season in the arc of deforestation. International Journal of Climatology 30:1970-1979.

Craine, J. M., J. B. Nippert, A. J. Elmore, A. M. Skibbe, S. L. Hutchinson, and N. A. Brunsell. 2012. Timing of climate variability and grassland productivity. Proc Natl Acad Sci U S A 109:3401-3405.

Croudace, I. W., A. Rindby, and R. G. Rothwell. 2006. ITRAX: description and evaluation of a new multi-function X-ray core scanner. Geological Society, London, Special Publications 267:51-63.

D'Arrigo, R., J. Palmer, C. C. Ummenhofer, N. N. Kyaw, and P. Krusic. 2011. Three centuries of Myanmar monsoon climate variability inferred from teak tree rings. Geophysical Research Letters 38:L24705.

Dararath, Y., N. Top, and V. Lic. 2011. Rubber Plantation Development in Cambodia: At What Cost? EEPSEA, Singapore.

Davison, W. 1993. Iron and manganese in lakes. Earth-Science Reviews 34:119-163.

Dawson, T. P., S. T. Jackson, J. I. House, I. C. Prentice, and G. M. Mace. 2011. Beyond predictions: biodiversity conservation in a changing climate. Science 332:53-58.

Dearing, J. 1999a. Environmental Magnetic Susceptibility: Using the Bartington MS2 System. 2nd edition. British Library Catalogue, West Yorkshire.

Dearing, J. 1999b. Holocene environmental change from magnetic proxies in lake sediments. Pages 231-278 in B. A. Maher and R. Thompson, editors. Quaternary Climates, Environments and Magnetism. Cambridge University Press, Cambridge.

Dearing, J. A. 2008. Landscape change and resilience theory: a palaeoenvironmental assessment from Yunnan, SW China. The Holocene 18:117-127.

Dearing, J. A., R. J. L. Dann, K. Hay, J. A. Lees, P. J. Loveland, B. A. Maher, and K. O'Grady. 1996. Frequency-dependent susceptibility measurements of environmental materials. Geophysical Journal International 124:228-240.

Demske, D., P. E. Tarasov, and T. Nakagawa. 2013. Atlas of pollen, spores and further non-pollen palynomorphs recorded in the glacial-interglacial late Quaternary sediments of Lake Suigetsu, central Japan. Quaternary International 290-291:164-238.

Derroire, G., P. Balvanera, C. Castellanos-Castro, G. Decocq, D. K. Kennard, E. Lebrija-Trejos, J. A. Leiva, P.-C. Odén, J. S. Powers, V. Rico-Gray, M. Tigabu, and J. R. Healey. 2016. Resilience of tropical dry forests - a meta-analysis of changes in species diversity and composition during secondary succession. Oikos:10.1111/oik.03229.

Dexter, K., B. Smart, C. Baldauf, T. R. Baker, M. P. Balinga, R. J. W. Brienen, S. Fauset, T. R. Feldpausch, L. F.-D. Silva, J. Muledi, Ilunga;, S. L.

Lewis, G. Lopez-Gonzalez, B. H. Marimon-Junior, B. S. Marimon, P. Meerts, N. Page, N. Parthasarathy, O. L. Phillips, T. C. H. Sunderland, I. Theilade, J. Weintritt, K. Affum-Baffoe, A. Araujo, L. Arroyo, S. K. Begne, E. C.-D. Neves, M. Collins, A. Cuni-Sanchez, M.-N. Djuikouo K, F. Elias, E. G. Foli, K. J. Jeffery, T. Killeen, Y. Malhi, L. Maracahipes, C. Mendoza, P. Morandi, C. O.-D. Santos, A. Parada-Gutierrez, G. Pardo, K. S. H. Peh, R. P. Salomão, M. S. Silveira, H. Miranda, J. W. F. Silk, B. Sonke, H. E. Taedoumg, M. Toledo, R. K. Umetsu, R. G. Villaroel, V. Vos, L. J. T. White, and R. T. Pennington. 2015. Floristics and biogeography of vegetation in seasonally dry tropical regions. International Forestry Review 17:10-32.

Dinerstein, E., D. M. Olson, D. J. Graham, A. L. Webster, S. A. Primm, M. P. Bookbinder, and G. Ledec. 1995. A Conservation Assessment of the Terrestrial Ecoregions of Latin America and the Caribbean, Washington D.C.

Dirzo, R., H. S. Young, H. A. Mooney, and G. Ceballos. 2011. Seasonally Dry Tropical Forests. Island Press, Washington, D.C.

Dy Phon, P. 2000. Dictionary of Plants used in Cambodia. First edition. Imprimerie Olympic, Phnom Penh.

Dypvik, H., and N. B. Harris. 2001. Geochemical facies analysis of fine-grained siliciclastics using Th/U, Zr/Rb and (Zr+Rb)/Sr ratios. Chemical Geology 181:131-146.

Emile-Geay, J., R. Seager, M. A. Cane, E. R. Cook, and G. H. Haug. 2008. Volcanoes and ENSO over the Past Millennium. Journal of Climate 21:3134-3148.

Faegri, K., and J. Iversen. 1989. Textbook of pollen analysis. 4th edition. John Wiley & Sons, Chichester.

FAO. 1988. Soil Map of the World: Revised Legend Food and Agriculture Organization of the United Nations, Rome.

Federov, P. I., and A. V. Koloskov. 2005. Cenozoic Volcanism of Southeast Asia. Petrology 13:352-380.

Fink, D., M. Hotchkis, Q. Hua, G. Jacobsen, A. M. Smith, U. Zoppi, D. Child, C. Mifsud, H. van der Gaast, A. Williams, and M. Williams. 2004. The ANTARES AMS facility at ANSTO. Nuclear Instruments and Methods in Physics Research Section B: Beam Interactions with Materials and Atoms 223-224:109-115.

Finsinger, W., W. Tinner, and F. S. Hu. 2008. Rapid and accurate estimates of microcharcoal content in pollen slides. Pages 121-124 in G. Fiorentino and D. Magri, editors. International Meeting of Antracology. Archaeopress, Oxford, Cavallino - Lecce.

Fleitmann, D., S. J. Burns, A. Mangini, M. Mudelsee, J. Kramers, I. Villa, U. Neff, A. A. Al-Subbary, A. Buettner, D. Hippler, and A. Matter. 2007a. Holocene ITCZ and Indian monsoon dynamics recorded in stalagmites from Oman and Yemen (Socotra). Quaternary Science Reviews 26:170-188.

Fleitmann, D., S. J. Burns, A. Mangini, M. Mudelsee, J. Kramers, I. Villa, U. Neff, A. A. Al-Subbary, A. Buettner, D. Hippler, and A. Matter. 2007b. Qunf Cave, Oman Stalagmite Oxygen Isotope Data. IGBP PAGES/World Data Center for Paleoclimatology Data Contribution Series # 2007-090. NOAA/NCDC Paleoclimatology Program, Boulder, CO.

Fleitmann, D., S. J. Burns, M. Mudelsee, U. Neff, J. Kramers, A. Mangini, and A. Matter. 2003. Holocene Forcing of the Indian Monsoon Recorded in a Stalagmite from Southern Oman. Science 300:1737-1739.

Flessa, K. W., and S. T. Jackson. 2005. The Geological Record of Ecological Dynamics: Understanding the Biotic Effects of Future Environmental Change. National Academy Press, Washington D.C.

Foley, J. A., M. T. Coe, M. Scheffer, and G. Wang. 2003. Regime Shifts in the Sahara and Sahel: Interactions between Ecological and Climatic Systems in Northern Africa. Ecosystems 6:524-532.

Folk, R. L., and W. C. Ward. 1957. Brazos River bar: a study in the significance of grain size parameters. Journal of Sedimentary Petrology 27:3-26.

Folke, C., S. Carpenter, B. Walker, M. Scheffer, T. Elmqvist, L. Gunderson, and C. S. Holling. 2004. Regime Shifts, Resilience, and Biodiversity in Ecosystem Management. Annual Review of Ecology, Evolution, and Systematics 35:557-581.

Fox, J. 2002. Understanding a dynamic landscape: Land use, land cover, and resource tenure in Northeastern Cambodia. Pages 113-130 in S. J. Walsh and K. A. Crews-Meyer, editors. Linking People, Place, and Policy: A GIScience Approach. Springer, New York.

Fox, J., and J. B. Vogler. 2005. Land-Use and Land Cover Change in Montane Mainland Southeast Asia. Environmental Management 36:394-403.

Fox, J., J. B. Vogler, and M. Poffenberger. 2009. Understanding Changes in Land and Forest Resource Management Systems: Ratanakiri, Cambodia. Southeast Asian Studies 47:309-329.

Gadgil, S. 2003. The Indian monsoon and its variability. Annual Review of Earth and Planetary Sciences 31:429-468.

Gallego-Torres, D., F. Martínez-Ruiz, A. Paytan, F. J. Jiménez-Espejo, and M. Ortega-Huertas. 2007. Pliocene–Holocene evolution of depositional conditions in the eastern Mediterranean: Role of anoxia vs. productivity at time of sapropel deposition. Palaeogeography, Palaeoclimatology, Palaeoecology 246:424-439.

Garcia-Oliva, F., and V. J. Jaramillo. 2011. Impact of Anthropogenic Transformation of Seasonally Dry Forest on Ecosystem Biogeochemical Processes. Pages 159-172 in R. Dirzo, H. S. Young, H. A. Mooney, and G. Ceballos, editors. Seasonally Dry Tropical Forests. Island Press, Washington, D.C.

Gardner, S., P. Sidisunthorn, and V. Anusarnsunthorn. 2000. A Field Guide to the Forest Trees of Northern Thailand. Kobfai Publishing Project, Bangkok.

Gardner, T. A., J. Barlow, R. Chazdon, R. M. Ewers, C. A. Harvey, C. A. Peres, and N. S. Sodhi. 2009. Prospects for tropical forest biodiversity in a human-modified world. Ecology Letters 12:561-582.

Gasse, F., and E. Van Campo. 2001. Late Quaternary environmental changes from a pollen and diatom record in the southern tropics (Lake Tritrivakely, Madagascar). Palaeogeography, Palaeoclimatology, Palaeoecology 167:287-308.

Gentry, A. H. 1995. Neotropical Floristics. Pages 146-194 in S. H. Bullock, H. A. Mooney, and E. Medina, editors. Seasonally Dry Tropical Forests. Cambridge University Press, Cambridge.

Gill, J. L. 2014. Ecological impacts of the late Quaternary megaherbivore extinctions. New Phytologist 201:1163-1169.

Glew, J. R. 1991. Miniature gravity corer for recovering short sediment cores. Journal of Paleolimnology 5:285-287.

Goldammer, J. G. 2002. International Forest Fire News: Asia and Oceania Fire Special. United Nations Economic Commission for Europe, Geneva, Switzerland.

Golden Software. 2012. Strater. Golden Software, Colorado.

Good, S. P., and K. K. Caylor. 2011. Climatological determinants of woody cover in Africa. Proc Natl Acad Sci U S A 108:4902-4907.

Goodale, U. M., M. S. Ashton, G. P. Berlyn, T. G. Gregoire, B. M. P. Singhakumara, and K. U. Tennakoon. 2012. Disturbance and tropical pioneer species: Patterns of association across life history stages. Forest Ecology and Management 277:54-66.

GoogleEarth 7.1.5. 2015. 1460000–1520000:716000–734000 (WGS84 UTM48N). Spatial data collected 1/5/2014.

Graham, S. A., M. Diazgranados, and J. C. Barber. 2011. Relationships among the confounding genera Ammannia, Hionanthera, Nesaea and Rotala (Lythraceae). Botanical Journal of the Linnean Society 166:1-19.

Grey-Wilson, C. 1980. Hydrocera triflora, Its Floral Morphology and Relationship with Impatiens: Studies in Balsaminaceae: V. Kew Bulletin 35:213-219.

Gupta, A. K., D. M. Anderson, and J. T. Jonathon. 2003. Abrupt changes in the Asian southwest monsoon during the Holocene and their links to the North Atlantic Ocean. Nature 421:354-357.

Håkanson, L., and M. Jansson. 1983. Principles of lake sedimentology. Springer-Verlag, New York.

Hamilton-Taylor, J., and W. Davison. 1995. Redox-Driven Cycling of Trace Elements in Lakes. Pages 217-264 in A. Lerman, D. M. Imboden, and

J. R. Gat, editors. Physics and Chemistry of Lakes. Springer-Verlag, Berlin, Heidelberg, New York.

Hansen, K. K., and N. Top. 2006. Natural Forest Benefits and Economic Analysis of Natural Forest Conversion in Cambodia. Cambodia Development Resource Institute, Phnom Penh.

Harrison, R. D. 2011. Emptying the Forest: Hunting and the Extirpation of Wildlife from Tropical Nature Reserves. BioScience 61:919-924.

Hayes, F. R., B. L. Reid, and M. L. Cameron. 1958. II. Oxidation-Reduction Relations at The Mud-Water Interface. Limnology and Oceanography 3:303-317.

Heaney, L. R. 1991. A Synopsis of Climatic and Vegetation Change in Southeast Asia. Climatic Change 19:53-91.

Heinimann, A., P. Messerli, D. Schmidt-Vogt, and U. Wiesmann. 2007. The Dynamics of Secondary Forest Landscapes in the Lower Mekong Basin. Mountain Research and Development 27:232-241.

Heiri, O., A. F. Lotter, and G. Lemke. 2001. Loss on ignition as a method for estimating organic and carbonate content in sediments: reproducibility and comparability of results. Journal of Paleolimnology 25:101-110.

Hendrickson, M., Q. Hua, and T. O. Pryce. 2013. Using In-Slag Charcoal as an Indicator of"Terminal" Iron Production Within the Angkorian Period (10th–13th Centuries AD) Center of Preah Khan of Kompong Svay, Cambodia. Radiocarbon 55:31-47.

Hirota, M., M. Holmgren, E. H. Van Nes, and M. Scheffer. 2011. Global resilience of tropical forest and savanna to critical transitions. Science 334:232-235.

Hoffmann, A. A., J.-E. Parry, C. Cuambe, D. Kwesha, and W. Zhakata. 2009. Climate change and wildfires in Mozambique. Pages 227-259 in M. A. Cochrane, editor. Tropical Fire Ecology: Climate Change, Land Use, and Ecosystem Dynamics. Springer and Praxis, Chichester.

Hoffmann, W. A., E. L. Geiger, S. G. Gotsch, D. R. Rossatto, L. C. Silva, O. L. Lau, M. Haridasan, and A. C. Franco. 2012. Ecological thresholds at the savanna-forest boundary: how plant traits, resources and fire govern the distribution of tropical biomes. Ecology Letters 15:759-768.

Holbrook, N. M., J. L. Whitbeck, and H. A. Mooney. 1995. Drought responses of neotropical dry forest trees. Pages 243-276 in S. H. Bullock, H. A. Mooney, and E. Medina, editors. Seasonally Dry Tropical Forests. Cambridge University Press, Cambridge, U.K.

Holdridge, L. R. 1967. Life Zone Ecology. Tropical Science Centre, San Jóse.

Holling, C. S. 1973. Resilience and Stability of Ecological Systems. Annual Review of Ecology and Systematics 4:1-23.

Hong, Y. T., B. Hong, Q. H. Lin, Y. Shibata, M. Hirota, Y. X. Zhu, X. T. Leng, Y. Wang, H. Wang, and L. Yi. 2005. Inverse phase oscillations between the East Asian and Indian Ocean summer monsoons during the last 12000 years and paleo-El Niño. Earth and Planetary Science Letters 231:337-346.

Hor, S., I. Saizen, N. Tsutsumida, T. Watanabe, and S. Kobayashi. 2014. The Impact of Agricultural Expansion on Forest Cover in Ratanakiri Province, Cambodia. Journal of Agricultural Science 6:46-59.

Huang, T. C. 1972. Pollen Flora of Taiwan. National Taiwan University Botany Department Press, Taiwan.

Huntingford, C., P. Zelazowski, D. Galbraith, L. M. Mercado, S. Sitch, R. Fisher, M. Lomas, A. P. Walker, C. D. Jones, B. B. B. Booth, Y. Malhi, D. Hemming, G. Kay, P. Good, S. L. Lewis, O. L. Phillips, O. K. Atkin, J. Lloyd, E. Gloor, J. Zaragoza-Castells, P. Meir, R. Betts, P. P. Harris, C. Nobre, J. Marengo, and P. M. Cox. 2013. Simulated resilience of tropical rainforests to CO2-induced climate change. Nature Geoscience:268–273.

International Organization for Migration. 2009. Mapping Vulnerability to Natural Hazards in Ratanakiri. Phnom Penh.

IPCC. 2013. Summary for Policymakers.in T. F. Stocker, D. Qin, G.-K. Plattner, M. Tignor, S. K. Allen, J. Boschung, A. Nauels, Y. Xia, V. Bex, and P. M. Midgley, editors. Climate Change 2013: The Physical Science Basis. Contribution of Working Group I to the Fifth Assessment Report of the Intergovernmental Panel on Climate Change. Cambridge University Press, Cambridge and New York.

IPCC. 2014. Asia. Climate Change 2014: Impacts, Adaptation and Vulnerability. Contribution of Working Group II to the Fifth Assessment Report of the Intergovernmental Panel on Climate Change. Final Draft. Cambridge University Press, Cambridge and New York.

Ito, E. 2001. Application of stable isotope techniques to inorganic and biogenic carbonates. Pages 351-371 in W. M. Last and J. P. Smol, editors. Tracking Environmental Change Using Lake Sediments. Volume 2: Physical and Geochemical Methods. Kluwer Academic Publishers, Dordrecht, The Netherlands.

Jakovac, C. C., M. Peña-Claros, T. W. Kuyper, and F. Bongers. 2015. Loss of secondary-forest resilience by land-use intensification in the Amazon. Journal of Ecology 103:67-77.

Janzen, D. H. 1988. Management of Habitat Fragments in a Tropical Dry Forest: Growth. Annals of the Missouri Botanical Garden 75:105-116.

Jaramillo, V. J., A. Martínez-Yrízar, and R. L. J. Sanford. 2011. Primary Productivity and Biogeochemistry of Seasonally Dry Tropical Forests. Pages 109-128 in R. Dirzo, H. S. Young, H. A. Mooney, and G. Ceballos, editors. Seasonally Dry Tropical Forests. Island Press, Washington, D.C.

Jentsch, A., J. Kreyling, M. Elmer, E. Gellesch, B. Glaser, K. Grant, R. Hein, M. Lara, H. Mirzae, S. E. Nadler, L. Nagy, D. Otieno, K. Pritsch, U. Rascher, M. Schädler, M. Schloter, B. K. Singh, J. Stadler, J. Walter, C. Wellstein, J. Wöllecke, and C. Beierkuhnlein. 2011. Climate extremes initiate ecosystem-regulating functions while maintaining productivity. Journal of Ecology 99:689-702.

JICA. 2002a. Geology Map of Cambodia (50K). Japan International Cooperation Agency, Tokyo, Japan.

JICA. 2002b. Land Use Map of Cambodia (50K). Japan International Cooperation Agency, Tokyo, Japan.

JICA. 2002c. Hydrology Map of Cambodia (50K). Japan International Cooperation Agency, Tokyo, Japan.

Johnson, C. N. 2009. Ecological consequences of Late Quaternary extinctions of megafauna. Proceedings of the Royal Society B: Biological Sciences 276:2509-2519.

Johnson, L. A., and P. Dearden. 2009. Fire ecology and management of seasonal evergreen forests in mainland Southeast Asia. Pages 289-310 in M. A. Cochrane, editor. Tropical Fire Ecology: Climate Change, Land Use, and Ecosystem Dynamics. Springer and Praxis, Chichester.

Juggins, S. 2012. Package 'rioja': Analysis of Quaternary Science Data. Newcastle University, Newcastle upon Tyne.

Juggins, S. 2014. C2 Data Analysis. Version 1.7.6. University of Newcastle, Newcastle upon Tyne.

Juo, A. S. R., and K. Franzleubbers. 2003. Tropical Soils: Properties and Management for Sustainable Agriculture. Oxford University Press, Oxford.

Kao, D., and S. Iida. 2006. Structural characteristics of logged evergreen forests in Preah Vihear, Cambodia, 3 years after logging. Forest Ecology and Management 225:62-73.

Kealhofer, L. 1996. The human environment during the terminal Pleistocene and Holocene in northeastern Thailand: phytolith evidence from Lake Kumphawapi. Asian Perspectives: the Journal of Archaeology for Asia and the Pacific 35:229-254.

Kealhofer, L., and D. Penny. 1998. A combined pollen and phytolith record for fourteen thousand years of vegetation change in northeastern Thailand. Review of Palaeobotany and Palynology 103:83-93.

Keen, H. F., W. D. Gosling, F. Hanke, C. S. Miller, E. Montoya, B. G. Valencia, and J. J. Williams. 2014. A statistical sub-sampling tool for extracting vegetation community and diversity information from pollen assemblage data. Palaeogeography, Palaeoclimatology, Palaeoecology 408:48-59.

Kelts, K., U. Briegel, K. Ghilardi, and K. Hsu. 1986. The limnogeology-ETH coring system. Swiss Journal of Hydrology 48:104-115.

Kerkhoff, A. J., and B. J. Enquist. 2007. The Implications of Scaling Approaches for Understanding Resilience and Reorganization in Ecosystems. BioScience 57:489-499.

Khin, Z., S. Meffre, C.-K. Lai, C. Burrett, M. Santosh, I. Graham, T. Manaka, A. Salam, T. Kamvong, and P. Cromie. 2014. Tectonics and metallogeny of mainland Southeast Asia — A review and contribution. Gondwana Research 26:5-30.

Khurana, E., R. Sagar, and J. S. Singh. 2006. Seed size: a key trait determining species distribution and diversity of dry tropical forest in northern India. Acta Oecologica 29:196-204.

Kilian, M. R., J. van der Plicht, B. van Geel, and T. Goslar. 2002. Problematic 14C-AMS dates of pollen concentrates from Lake Gosciaz (Poland). Quaternary International 88:21-26.

Knapp, A. K., C. Beier, D. D. Briske, A. T. Classen, Y. Luo, M. Reichstein, M. D. Smith, S. D. Smith, J. E. Bell, P. A. Fay, J. L. Heisler, S. W. Leavitt, R. Sherry, B. Smith, and E. Weng. 2008. Consequences of More Extreme Precipitation Regimes for Terrestrial Ecosystems. BioScience 58:811-821.

Knapp, A. K., M. D. Smith, S. L. Collins, N. Zambatis, M. Peel, S. Emery, J. Wojdak, M. C. Horner-Devine, H. Biggs, J. Kruger, and S. J. Andelman. 2004. Generality in ecology: testing North American grassland rules in South African savannas. Frontiers in Ecology and the Environment 2:483-491.

Knox, R., G. Bisht, J. Wang, and R. Bras. 2011. Precipitation Variability over the Forest-to-Nonforest Transition in Southwestern Amazonia. Journal of Climate 24:2368-2377.

Kodandapani, N., M. A. Cochrane, and R. Sukumar. 2008. A comparative analysis of spatial, temporal, and ecological characteristics of forest fires in seasonally dry tropical ecosystems in the Western Ghats, India. Forest Ecology and Management 256:607-617.

Koinig, K., W. Shotyk, A. Lotter, C. Ohlendorf, and M. Sturm. 2003. 9000 years of geochemical evolution of lithogenic major and trace elements in the sediment of an alpine lake – the role of climate, vegetation, and land-use history. Journal of Paleolimnology 30:307-320.

Kumar, K. K., B. Rajagopalan, and M. A. Cane. 1999. On the Weakening Relationship Between the Indian Monsoon and ENSO. Science 284:2156-2159.

Kylander, M. E., L. Ampel, B. Wohlfarth, and D. Veres. 2011. High-resolution X-ray fluorescence core scanning analysis of Les Echets (France) sedimentary sequence: new insights from chemical proxies. Journal of Quaternary Science 26:109-117.

La Combe, P. 1969. Le Massif basaltique quaternaire à zircons-gemmes de Ratanakiri (Cambodge nord-oriental). Bulletin du Bureau de Recherches Geologiques et Minières 4:31-91.

Lan, C.-Y., S.-L. Chung, T. V. Long, C.-H. Lo, T.-Y. Lee, S. A. Mertzman, and J. J.-S. Shen. 2003. Geochemical and Sr –Nd isotopic constraints from the Kontum massif, central Vietnam on the crustal evolution of the Indochina block. Precambrian Research 122:7-27.

Larcher, W., C. Kainmüller, and J. Wagner. 2010. Survival types of high mountain plants under extreme temperatures. Flora - Morphology, Distribution, Functional Ecology of Plants 205:3-18.

Laumonier, Y. 1997. The Vegetation and Physiography of Sumatra. Kluwer, Dordrecht, The Netherlands.

Lehmann, C. E., T. M. Anderson, M. Sankaran, S. I. Higgins, S. Archibald, W. A. Hoffmann, N. P. Hanan, R. J. Williams, R. J. Fensham, J. Felfili, L. B. Hutley, J. Ratnam, J. San Jose, R. Montes, D. Franklin, J. Russell-Smith, C. M. Ryan, G. Durigan, P. Hiernaux, R. Haidar, D. M. Bowman, and W. J. Bond. 2014. Savanna vegetation-fire-climate relationships differ among continents. Science 343:548-552.

Lehmann, C. E., S. A. Archibald, W. A. Hoffmann, and W. J. Bond. 2011. Deciphering the distribution of the savanna biome. New Phytologist 191:197-209.

Lehmann, C. E. R., J. Ratnam, and L. B. Hutley. 2009. Which of These Continents Is Not Like the Other? Comparisons of Tropical Savanna Systems: Key Questions and Challenges. New Phytologist 181:508-511.

Lewis, S. L. 2006. Tropical forests and the changing earth system. Philosophical Transactions of the Royal Society B: Biological Sciences 361:195-210.

Li, P., Z. Feng, L. Jiang, C. Liao, and J. Zhang. 2014. A Review of Swidden Agriculture in Southeast Asia. Remote Sensing 6:1654-1683.

Linares-Palomino, R., A. T. Oliveira-Filho, and T. Pennington. 2011. Neotropical Seasonally Dry Forests: Diversity, Endemism and Biogeography of Woody Plants. Pages 3-21 in R. Dirzo, H. S. Young, H. A. Mooney, and G. Ceballos, editors. Seasonally Dry Tropical Forests: Ecology and Conservation. Island Press, Washington, D.C.

Linder, H. P., H. M. de Klerk, J. Born, N. D. Burgess, J. Fjeldsa, and C. Rahbek. 2012. The partitioning of Africa: statistically defined biogeographical regions in sub-Saharan Africa. Journal of Biogeography 39:1189-1205.

Lloret, F., A. Escudero, J. M. Iriondo, J. Martínez-Vilalta, and F. Valladares. 2012. Extreme climatic events and vegetation: the role of stabilizing processes. Global Change Biology 18:797-805.

Loarie, S. R., P. B. Duffy, H. Hamilton, G. P. Asner, C. B. Field, and D. D. Ackerly. 2009. The velocity of climate change. Nature 462:1052-1055.

Loucks, C., M. B. Mascia, A. Maxwell, K. Huy, K. Duong, N. Chea, B. Long, N. Cox, and T. Seng. 2009. Wildlife decline in Cambodia, 1953-2005: exploring the legacy of armed conflict. Conservation Letters 2:82-92.

Löwemark, L., H. F. Chen, T. N. Yang, M. Kylander, E. F. Yu, Y. W. Hsu, T. Q. Lee, S. R. Song, and S. Jarvis. 2011. Normalizing XRF-scanner data: A cautionary note on the interpretation of high-resolution records from organic-rich lakes. Journal of Asian Earth Sciences 40:1250-1256.

Maass, J. M. 1995. Conversion of tropical dry forest to pasture and agriculture. Pages 399-422 in S. H. Bullock, H. A. Mooney, and E. Medina, editors. Seasonally Dry Tropical Forests. Cambridge University Press, Cambridge.

Maass, M., and A. Burgos. 2011. Water Dynamics at the Ecosystem Level in Seasonally Dry Tropical Forests. Pages 141-158 in R. Dirzo, H. S. Young, H. A. Mooney, and G. Ceballos, editors. Seasonally Dry Tropical Forests. Island Press, Washington, D.C.

MacKenzie, W. S., and A. E. Adams. 2007. A Colour Atlas of Rocks and Minerals in Thin Section. 9th edition. Mason Publishing, London.

Malhi, Y. 2012. The productivity, metabolism and carbon cycle of tropical forest vegetation. Journal of Ecology 100:65-75.

Maloney, B. 1990. Grass pollen and the origins of rice agriculture in North Sumatra. Modern quaternary research in Southeast Asia 11:135-161

Maloney, B. 1999. A 10,600 year pollen record from Nong Thale Song Hong, Trang Province, south Thailand. Bulletin of the Indo-Pacific Prehistory Association 18:129-138.

Maslin, M. 2004. Ecological Versus Climatic Thresholds. Science 306:2197-2198.

Maxwell, A., and J. A. Cox. 2011. Conservation Planning and Management in Southeast Asia's Seasonally Dry Forest Landscape: Experiences from Cambodia. Pages 365-398 in W. J. McShea, S. J. Davies, and N. Bhumpakphan, editors. The Ecology and Conservation of Seasonally Dry Forests in Asia. Smithsonian Institution Scholarly Press, Washington D.C.

Maxwell, A., and K. B. Liu. 2002. Late Quaternary pollen and associated records from the monsoonal areas of continental South and SE Asia. Pages 189-228 in P. Kershaw, David, B., Tapper, N., Penny, D., and Brown, J., editor. Bridging Wallace's Line: The Environmental and Cultural History and Dynamics of the SE-Asian-Australian Region. Catena Verlag, Reiskirchen.

Maxwell, A. L. 1999. Holocene environmental change in mainland Southeast Asia: pollen and charcoal records from Cambodia. Ph.D. thesis. Louisiana State University, Louisiana.

Maxwell, A. L. 2001. Holocene Monsoon Changes Inferred from Lake Sediment Pollen and Carbonate Records, Northeastern Cambodia. Quaternary Research 56:390-400.

Maxwell, A. L. 2004. Fire regimes in north-eastern Cambodian monsonal forests, with a 9300-year sediment charcoal record. Journal of Biogeography 31:225-239.

Mayle, F. E., R. P. Langstroth, R. A. Fisher, and P. Meir. 2007. Long-term forest-savannah dynamics in the Bolivian Amazon: implications for conservation. Philosophical Transactions of the Royal Society B: Biological Sciences 362:291-307.

McKenny, B., Y. Chea, P. Tola, and T. Evans. 2004. Focusing on Cambodia's High Value Forests: Livlihoods and Management. Cambodia Development Resource Institute and Wildlife Conservation Society, Phnom Penh.

McKillup, S., and M. D. Dyar. 2010. Geostatistics Explained: An Introductory Guide for Earth Scientists. Cambridge University Press, Cambridge.

McShea, W. J., S. J. Davies, and N. Bhumpakphan. 2011. The Ecology and Conservation of Seasonally Dry Forests in Asia. Smithsonian Institution Scholarly Press, Washington D.C.

Meir, P., and R. T. Pennington. 2011. Climate Change and Seasonally Dry Tropical Forests. Pages 279-300 in R. Dirzo, H. S. Young, H. A. Mooney, and G. Ceballos, editors. Seasonally Dry Tropical Forests. Island Press, Washington, D.C.

Menaut, J.-C., M. Legpage, and L. Abbadie. 1995. Savannas, woodlands and dry forests in Africa. Pages 64-92 in S. H. Bullock, H. A. Mooney, and E. Medina, editors. Seasonally Dry Tropical Forests. Cambridge University Press, Cambridge.

Merkt, J., G. Lüttig, and H. Schneekloth. 1971. Vorschlag zur Gliederung and Definition der Limnischen Ledimente. Geologischishes Jahrbuch 89:607-623.

Mertz, O., C. Padoch, J. Fox, R. A. Cramb, S. J. Leisz, N. T. Lam, and T. D. Vien. 2009. Swidden Change in Southeast Asia: Understanding Causes and Consequences. Human Ecology 37:259-264.

Metcalfe, I. 2011. Tectonic framework and Phanerozoic evolution of Sundaland. Gondwana Research 19:3-21.

Metcalfe, I. 2013. Gondwana dispersion and Asian accretion: Tectonic and palaeogeographic evolution of eastern Tethys. Journal of Asian Earth Sciences 66:1-33.

Miles, L., A. C. Newton, R. S. DeFries, C. Ravilious, I. May, S. Blyth, V. Kapos, and J. E. Gordon. 2006. A global overview of the conservation status of tropical dry forests. Journal of Biogeography 33:491-505.

Millennium Ecosystem Assessment. 2005. Ecosystems and Human Well-being: Current State and Trends, Volume 1: Findings of the Condition and Trends Working Group of the Millennium Ecosystem Assessment, Washington, D.C., Covelo, and London.

Mitchard, E. T. A., S. S. Saatchi, F. F. Gerard, S. L. Lewis, and P. Meir. 2009. Measuring Woody Encroachment along a Forest–Savanna Boundary in Central Africa. Earth Interactions 13:1-29.

Mondal, N., and R. Sukumar. 2015. Regeneration of Juvenile Woody Plants after Fire in a Seasonally Dry Tropical Forest of Southern India. Biotropica 47:330-338.

Mooney, H. A., S. H. Bullock, and E. Medina. 1995. Introduction. Pages 1-8 in S. H. Bullock, H. A. Mooney, and E. Medina, editors. Seasonally Dry Tropical Forests. Cambridge University Press, Cambridge.

Moreira, A. G. 2000. Effects of fire protection on savanna structure in Central Brazil. Journal of Biogeography 27:1021-1029.

Morice, C. P., J. J. Kennedy, N. A. Rayner, and P. D. Jones. 2012. Quantifying uncertainties in global and regional temperature change using an ensemble of observational estimates: The HadCRUT4 data set. Journal of Geophysical Research 117:D08101.

Morley, C. G., and J. R. Flenley. 1987. Late Cainozoic Vegetational and Environmental Changes in the Malay Archipelago. Pages 50-59 in T. C. Whitmore, editor. Biogeographical Evolution in the Malay Archipelago. Monographs in Biogeography, Oxford, UK.

Morley, R. J. 2002. Tertiary Vegetational History of Southeast Asia, with Emphasis on the Biogeographical Relationships with Australia. Pages 49-60 in P. Kershaw, B. Daid, N. Tapper, D. Penny, and J. Brown, editors. Bridging Wallace's Line: The Environmental and Cultural Dynamics of the SE-Asian-Australian Region. Catena Verlag, Reiskirchen, Germany.

Motuzova, G. V., and N. Thi Hong Van. 1999. The geochemistry of major and trace elements in the agricultural terrain of South Viet Nam. Journal of Geochemical Exploration 66:407-411.

MRC. 2002. Soils Map of Cambodia (50K). Mekong River Commission, Phnom Penh.

Munsell Colour. 1994. Munsell Soil Colour Charts. Gretag Macbeth, New Windsor, New York.

Murphy, B. P., and D. M. Bowman. 2012. What controls the distribution of tropical forest and savanna? Ecology Letters 15:748-758.

Murphy, B. P., and A. E. Lugo. 1986. Ecology of tropical dry forest. Annual Review of Ecology and Systematics 31:533-536.

Murphy, P. G., and A. E. Lugo. 1995. Dry forests of Central America and the Caribbean. Pages 9-34 in S. H. Bullock, H. A. Mooney, and E. Medina, editors. Seasonally Dry Tropical Forests. Cambridge University Press, Cambridge.

Myers, N., R. A. Mittermeier, C. G. Mittermeier, G. A. B. da Fonseca, and J. Kent. 2000. Biodiversity hotspots for conservation priorities. Nature 403:853-858.

Naeher, S., A. Gilli, R. P. North, Y. Hamann, and C. J. Schubert. 2013. Tracing bottom water oxygenation with sedimentary Mn/Fe ratios in Lake Zurich, Switzerland. Chemical Geology 352:125-133.

Naidoo, R., A. Balmford, R. Costanza, B. Fisher, R. E. Green, B. Lehner, T. R. Malcolm, and T. H. Ricketts. 2008. Global mapping of ecosystem services and conservation priorities. Proc Natl Acad Sci U S A 105:9495-9500.

Nakagawa, T., G. Garfì, M. Reille, and R. Verlaque. 1998. Pollen morphology of Zelkova sicula (Ulmaceae), a recently discovered relic species of the European Tertiary flora: description, chromosomal relevance, and palaeobotanical significance. Review of Palaeobotany and Palynology 100:27-37.

Neal, D. G. 1967. Statistical description of the forests of Thailand. Military Research and Development Center, Bangkok.

Nelson, J. A., K. Licht, C. Yansa, and G. Filippelli. 2009. Climate-related cyclic deposition of carbonate and organic matter in Holocene lacustrine sediment, Lower Michigan, USA. Journal of Paleolimnology 44:1-13.

Nowaczyk, N. R. 2001. Logging of magnetic susceptibility. Pages 155-170 in W. M. Last and J. P. Smol, editors. Tracking Environmental Change Using Lake Sediments Volume 1: Basin Analysis, Coring and Chronological Techniques. Kluwer Academic Publishers, Dordrecht, The Netherlands.

Nüsslein, B., W. Eckert, and R. Conrad. 2003. Stable Isotope Biogeochemistry of Methane Formation in Profundal Sediments of Lake Kinneret (Israel). Limnology and Oceanography 48:1439-1446.

Nuttle, T., T. E. Ristau, A. A. Royo, and F. Gilliam. 2014. Long-term biological legacies of herbivore density in a landscape-scale experiment: forest understoreys reflect past deer density treatments for at least 20 years. Journal of Ecology 102:221-228.

ODC. 2015. Forest Cover (2014). Open Development Cambodia, Phnom Penh.

ODC. 2016a. Geographical Relief Map. Open Development Cambodia, Phnom Penh.

ODC. 2016b. Geological Map. Open Development Cambodia, Phnom Penh.

Ogawa, H., K. Yoda, and T. Kiri. 1961. A Preliminary Survey on the Vegetation of Thailand. Nature and Life in Southeast Asia 1:20-158.

Ohnuki, Y., A. Shimizu, S. Chann, J. Toriyama, C. Kimhean, and M. Araki. 2008. Seasonal change in thick regolith hardness and water content in a dry evergreen forest in Kampong Thom Province, Cambodia. Geoderma 146:94-101.

Oldfield, F., Barbosky, C., Leopold, E.B. and J.P. Smith. 1983. Mineral magnetic studies of lake sediments. Hydrobiologia 103:37-44.

Olson, D. M., and E. Dinerstein. 2002. The Global 200: Priority Ecoregions for Global Conservation. Annals of the Missouri Botanical Garden 89:199-224.

Olson, D. M., E. Dinerstein, E. Wikramanayake, N. D. Burgess, G. V. N. Powell, E. C. Underwood, J. A. D'amico, I. Itoua, H. E. Strand, J. C. Morrison, C. J. Loucks, T. F. Allnutt, T. H. Ricketts, Y. Kura, J. F. Lamoreux, W. W. Wettengal, P. Hedao, and K. R. Kassem. 2001. Terrestrial Ecoregions of the World: A New Map of Life on Earth. BioScience 51:933-938.

Oo, W. P., and F. Koike. 2015. Dry forest community types and their predicted distribution based on a habitat model for the central dry zone of Myanmar. Forest Ecology and Management 358:108-121.

Orwa, C. A. M., R. Kindt, R. Jamnadass, and S. Anthony. 2009. Agroforestree Database: a tree reference and selection guide version 4.0. http://www.worldagroforestry.org/sites/treedbs/treedatabases.asp.

Osman, K. T. 2013. Forest soils : properties and management. Springer, New York.

Owen, R. M., and B. H. Wilkinson. 1983. Mineralogical and biological controls on the Fe/Ca and Mn/Ca ratios of lacustrine carbonate allochems. Chemical Geology 38:175-181.

Pan, Y., R. A. Birdsey, J. Fang, R. Houghton, P. E. Kauppi, W. A. Kurz, O. L. Phillips, A. Shvidenko, S. L. Lewis, J. G. Canadell, P. Ciais, R. B. Jackson, S. W. Pacala, A. D. McGuire, S. Piao, A. Rautiainen, S. Sitch, and D. Hayes. 2011. A large and persistent carbon sink in the world's forests. Science 333:988-993.

Parnell, J. 2003. Pollen of Syzygium (Myrtaceae) from SE Asia, especially Thailand. Blumea – Biodiversity, Evolution and Biogeography of Plants 48:303-317.

Pełechaty, M., A. Pukacz, K. Apolinarska, A. Pełechata, and M. Siepak. 2013. The significance of Chara vegetation in the precipitation of lacustrine calcium carbonate. Sedimentology 60:1017-1035.

Peng, Y., J. Xiao, T. Nakamura, B. Liu, and Y. Inouchi. 2005. Holocene East Asian monsoonal precipitation pattern revealed by grain-size distribution of core sediments of Daihai Lake in Inner Mongolia of north-central China. Earth and Planetary Science Letters 233:467-479.

Pennington, R. T., G. P. Lewis, and J. A. Ratter. 2006. An overview of the plant diversity, biogeography and conservation of Neotropical savannas and seasonally dry forests. Pages 1-29 in R. T. Pennington, G. P. Lewis, and J. A. Ratter, editors. Neotropical savannas and seasonally dry forests: plant diversity, biogeography and conservation. CRC Press, Boca Raton, FL.

Penny, D. 1998. Late Quaternary Palaeoenvironments in the Sakon Nakhon Basin, North-east Thailand. Ph.D. thesis. Monash University, Melbourne.

Penny, D. 1999. Palaeoenvironmental Analysis of the Sakon Nakhon Basin, Northeast Thailand: Palynological Perspectives on Climate Change and Human Occupation. Indo-Pacific Prehistory Assaciation Bulletin 18:139-149.

Penny, D. 2001. A 40,000 year palynological record from north-east Thailand: implications for biogeography and palaeo-environmental reconstruction. Palaeogeography, Palaeoclimatology, Palaeoecology 171:97-128.

Penny, D., and L. Kealhofer. 2005. Microfossil evidence of land-use intensification in north Thailand. Journal of Archaeological Science 32:69-82.

Perrings, C., S. Naeem, F. Ahrestani, D. E. Bunker, P. Burkill, G. Canziani, T. Elmqvist, R. Ferrati, J. Fuhrman, F. Jaksic, Z. Kawabata, A. Kinzig, G. M. Mace, F. Milano, H. Mooney, A. H. Prieur-Richard, J. Tschirhart, and W. Weisser. 2010. Ecosystem Services for 2020. Science 330:323-324.

Phillips, O. L., and A. H. Gentry. 1994. Increasing Turnover Through Time in Tropical Forests. Science 263:954-958.

Prance, G. T. 2006. Tropical savannas and seasonally dry forests: an introduction. Journal of Biogeography 33:385-386.

Prasad Rao, R. S. 2004. Water storage in Terminalia tomentosa. Current Science 87:416-417

Pryce, T. O., M. Hendrickson, K. Phon, S. Chan, M. F. Charlton, S. Leroy, P. Dillmann, and Q. Hua. 2014. The Iron Kuay of Cambodia: tracing the role of peripheral populations in Angkorian to colonial Cambodia via a 1200 year old industrial landscape. Journal of Archaeological Science 47:142-163.

Pulla, S., G. Ramaswami, N. Mondal, R. Chitra-Tarak, H. S. Suresh, H. S. Dattaraja, P. Vivek, N. Parthasarathy, B. R. Ramesh, and R. Sukumar. 2015. Assessing the resilience of global seasonally dry tropical forests. International Forestry Review 17:91-113.

Punt, W., P. P. Hoen, S. Blackmore, S. Nilsson, and A. Le Thomas. 2007. Glossary of pollen and spore terminology. Review of Palaeobotany and Palynology 143:1-81.

Punt, W., A. Marks, and P. P. Hoen. 2003. The Northwest European Pollen Flora, 63: Rhamnaceae. Review of Palaeobotany and Palynology 123:57-66.

Qiang, M., Y. Liu, Y. Jin, L. Song, X. Huang, and F. Chen. 2014. Holocene record of eolian activity from Genggahai Lake, northeastern Qinghai-Tibetan Plateau, China. Geophysical Research Letters 41:589-595.

Quamar, M. F., and M. S. Chauhan. 2011. Pollen analysis of spider webs from Khedla village, Betul District, Madhya Pradesh. Current Science 101:1586-1592.

Quamar, M. F., and M. S. Chauhan. 2014. Signals of Medieval Warm Period and Little Ice Age from southwestern Madhya Pradesh (India): A pollen-inferred Late-Holocene vegetation and climate change. Quaternary International 325:74-82.

Quesada, M., F. Rosas, R. Aguilar, L. Ashworth, V. M. Rosas-Guerrero, R. Sayago, J. A. Lobo, Y. Herrerias-Diego, and G. Sanchez-Montoya. 2011. Human Impacts on Pollination, Reproduction, and Breeding Systems in Tropical Forest Plants.in R. Dirzo, H. S. Young, H. A. Mooney, and G. Ceballos, editors. Seasonally Dry Tropical Forests. Island Press, Washington D.C.

Quesada, M., G. A. Sanchez-Azofeifa, M. Alvarez-Añorve, K. E. Stoner, L. Avila-Cabadilla, J. Calvo-Alvarado, A. Castillo, M. M. Espirito-Santo, M. Fagundes, G. W. Fernandes, J. Gamon, M. Lopezaraiza-Mikel, D. Lawrence, L. P. C. Morellato, J. S. Powers, F. d. S. Neves, V. Rosas-Guerrero, R. Sayago, and G. Sanchez-Montoya. 2009. Succession and management of tropical dry forests in the Americas: Review and new perspectives. Forest Ecology and Management 258:1014-1024.

R Core Team. 2013. R: A language and environment for statistical computing. R Foundation for Statistical Computing, Vienna.

Racey, A. 2009. Mesozoic red bed sequences from SE Asia and the significance of the Khorat Group of NE Thailand. Geological Society, London, Special Publications 315:41-67.

Racey, A., and J. G. S. Goodall. 2009. Palynology and stratigraphy of the Mesozoic Khorat Group red bed sequences from Thailand. Geological Society, London, Special Publications 315:69-83.

Racey, A., M. A. Love, A. C. Canham, J. G. S. Goodall, S. Polachan, and P. D. Jones. 1996. Stratigraphy and Reservoir Potential of the Mesozoic Khorat Group, NE Thailand. Part 1: Stratigraphy and Sedimentary Evolution. Journal of Petroleum Geology 19:5-14.

Ramesh, B. R., P. D. Venugopal, R. Pelissier, S. V. Patil, M. H. Swaminath, and P. Couteron. 2010. Mesoscale Patterns in the Floristic Composition of Forests in the Central Western Ghats of Karnataka, India. Biotropica 42:435-443.

Ratnam, J., W. J. Bond, R. J. Fensham, W. A. Hoffmann, S. Archibald, C. E. R. Lehmann, M. T. Anderson, S. I. Higgins, and M. Sankaran. 2011. When is a 'forest' a savanna, and why does it matter? Global Ecology and Biogeography 20:653-660.

Reimer, P. J., E. Bard, A. Bayliss, J. W. Beck, P. G. Blackwell, C. Bronk Ramsey, C. E. Buck, H. Cheng, R. L. Edwards, M. Friedrich, P. M. Grootes, T. P. Guilderson, H. Haflidason, I. Hajdas, C. Hatté, T. J. Heaton, D. L. Hoffmann, A. G. Hogg, K. A. Hughen, K. F. Kaiser, B. Kromer, S. W. Manning, M. Niu, R. W. Reimer, D. A. Richards, E. M. Scott, J. R. Southon, R. A. Staff, C. S. M. Turney, and J. van der Plicht. 2013. IntCal13 and Marine13 Radiocarbon Age Calibration Curves 0–50,000 Years cal BP. Radiocarbon 55:1869-1887.

Rhodes, A. N. 1998. A method for the preparation and quantification of microscopic charcoal from terrestrial and lacustrine sediment cores. The Holocene 8:113-117.

Riebe, K. 1999. Policy Making for Sustainable Development and the Yeak Laom Commune Protected Area. UNDP/CARERE-Ratanakiri, Ratanakiri.

Robinson, G. S. 2005. Landscape Palaeoecology and Megafaunal Extinction in Souhteastern New York State. Ecological Monographs 75:295-315.

Rollet, B. 1962. Inventaire Forestier de l'Est Mekong. UN FAO, Rome.

Rollet, B. 1972. La Végétation Du Cambodge. Bois et Forèls des Tropiques 146:3-20.

Rothwell, R. G., and I. W. Croudace. 2015. Twenty Years of XRF Core Scanning Marine Sediments: What Do Geochemical Proxies Tell Us? in R. G. Rothwell and I. W. Croudace, editors. Micro-XRF Studies of Sediment Cores: Applications of a non-destructive Tool for the Environmental Sciences. Springer, Dordrecht, Heidelberg, New York, London.

Royer, P. D., N. S. Cobb, M. J. Clifford, C.-Y. Huang, D. D. Breshears, H. D. Adams, and J. C. Villegas. 2011. Extreme climatic event-triggered overstorey vegetation loss increases understorey solar input regionally: primary and secondary ecological implications. Journal of Ecology 99:714-723.

Ruangpanit, N. 1995. Tropical seasonal forests in monsoon Asia: With emphasis on continental southeast Asia. Vegetatio 121:31-40.

Ruiz, L., M. R. R. Varma, M. S. Mohan Kumar, M. Sekhar, J. Maréchal, M. Descloitres, J. Riotte, S. Kumar, C. Kumr, and J. Braun. 2010. Water balance modelling in a tropical watershed under deciduous forest (Mule Hole, India): Regolith matric storage buffers the groundwater recharge process. Journal of Hydrology 380:460-472.

Rule, S., B. W. Brook, S. G. Haberle, C. S. M. Turney, A. P. Kershaw, and C. N. Johnson. 2012. The Aftermath of Megafaunal Extinction: Ecosystem Transformation in Pleistocene Australia. Science 335:1483.

Rull, V. 2003. An Illustrated key for the identification of pollen from Pantepui and the Gran Sabana (Eastern Venezuelan Guayana). Palynology 27:99-133.

Rundel, P., and K. Boonpragob. 1995. Dry forest ecosystems of Thailand. Pages 93-119 in S. H. Bullock, H. A. Mooney, and E. Medina, editors. Seasonally Dry Tropical Forests. Cambridge University Press, Cambridge, U.K.

Russell-Smith, J., P. G. Ryan, and R. Durieu. 1997. A LANDSAT MSS-derived fire history of Kakadu National Park, monsoonal northern Australia, 1980-94: season extent, frequency and patchiness. Journal of Applied Ecology 34:748-766.

Saeki, H., M. Okamoto, J. Azuma, H. Inoue, M. Takiuchi, and H. Tarumi. 1959. Investigations on Cambodian soils. Soil Science and Plant Nutrition 5:16-22.

Saha, K. 2010. Monsoon over Southern Asia (Comprising Pakistan, India, Bangladesh, Myanmar and Countries of Southeastern Asia) and Adjoining Indian Ocean (Region – I). Pages 89-122 Tropical Circulation Systems and Monsoons. Springer, Berlin, Heidelberg.

Saha, S., and H. F. Howe. 2003. Species Composition and Fire in a Dry Deciduous Forest. Ecology 84:3118-3123.

Sampaio, E. V. S. B. 1995. Overview of the Brazilian caatinga. Pages 35-63 in S. H. Bullock, H. A. Mooney, and E. Medina, editors. Seasonally Dry Tropical Forests. Cambridge University Press, Cambridge.

Sánchez-Azofeifa, G. A., and C. Portillo-Quintero. 2011. Extent and Drivers of Change of Neotropical Seasonally Dry Tropical Forests. Pages 45-57 in R. Dirzo, H. S. Young, H. A. Mooney, and G. Ceballos, editors. Seasonally Dry Tropical Forests. Island Press, Washington, D.C.

Sánchez-Azofeifa, G. A., M. Quesada, J. P. Rodríguez, J. M. Nassar, K. E. Stoner, A. Castillo, T. Garvin, E. L. S.-A. Zent, J. C. Calvo-Alvarado, M. E. R. Kalacska, L. Fajardo, J. A. Gamon, and P. Cuevas-Reyes. 2005. Research Priorities for Neotropical Dry Forests. Biotropica 37:477-485.

Sandgren, P., and I. Snowball. 2001. Application of mineral magnetic techniques to paleolimnology. Pages 217-237 in W. M. Last and J. P. Smol, editors. Tracking Environmental Change Using Lake Sediments Volume 2: Physical and Geochemical Methods. Kluwer Academic Publishers, Dordrecht, The Netherlands.

Sankaran, M., N. P. Hanan, R. J. Scholes, J. Ratnam, D. J. Augustine, B. S. Cade, J. Gignoux, S. I. Higgins, X. Le Roux, F. Ludwig, J. Ardo, F. Banyikwa, A. Bronn, G. Bucini, K. K. Caylor, M. B. Coughenour, A. Diouf, W. Ekaya, C. J. Feral, E. C. February, P. G. H. Frost, P. Hiernaux, H. Hrabar, K. L. Metzger, H. H. T. Prins, S. Ringrose, W. Sea, J. Tews, J. Worden, and N. Zambatis. 2005. Determinants of woody cover in African savannas. Nature 438:846-849.

Sano, M., B. M. Buckley, and T. Sweda. 2009. Tree-ring based hydroclimate reconstruction over northern Vietnam from Fokienia hodginsii: eighteenth century mega-drought and tropical Pacific influence. Climate Dynamics 33:331-340.

Sapkota, I. P., M. Tigabu, and P. C. Oden. 2009. Spatial distribution, advanced regeneration and stand structure of Nepalese Sal (Shorea robusta) forests subject to disturbances of different intensities. Forest Ecology and Management 257:1966-1975.

Scheffer, M., J. Bascompte, W. A. Brock, V. Brovkin, S. R. Carpenter, V. Dakos, H. Held, E. H. van Nes, M. Rietkerk, and G. Sugihara. 2009. Early-warning signals for critical transitions. Nature 461:53-59.

Scheffer, M., S. Carpenter, J. A. Foley, C. Folke, and B. Walker. 2001. Catastrophic shifts in ecosystems. Nature 413:591-596.

Scheffer, M., and S. R. Carpenter. 2003. Catastrophic regime shifts in ecosystems: linking theory to observation. TRENDS in Ecology and Evolution 18:648-656.

Scheffer, M., S. R. Carpenter, T. M. Lenton, J. Bascompte, W. Brock, V. Dakos, J. van de Koppel, I. A. van de Leemput, S. A. Levin, E. H. van Nes, M. Pascual, and J. Vandermeer. 2012. Anticipating critical transitions. Science 338:344-348.

Schirrmeister, L., and M. Störr. 1999. The weathering of basaltic rocks in Burundi and Vietnam. Catena 21:243-256.

Schnurrenberger, D., J. Russell, and K. Kelts. 2003. Classification of lacustrine sediments based on sedimentary components. Journal of Paleolimnology 29:141-154.

Scholes, R. J., P. R. Dowty, K. Caylor, D. A. B. Parsons, P. G. H. Frost, and H. H. Shugart. 2002. Trends in Savanna Structure and Composition along an Aridity Gradient in the Kalahari. Journal of Vegetation Science 13:419-428.

Schori, M., and C. A. Furness. 2014. Pollen diversity in Aquifoliales. Botanical Journal of the Linnean Society 175:169-190.

Scott, A. C. 2010. Charcoal recognition, taphonomy and uses in palaeoenvironmental analysis. Palaeogeography, Palaeoclimatology, Palaeoecology 291:11-39.

Scott, A. C., and F. Damblon. 2010. Charcoal: Taphonomy and significance in geology, botany and archaeology. Palaeogeography, Palaeoclimatology, Palaeoecology 291:1-10.

Selvaraj, K., C.-T. Arthur Chen, J.-Y. Lou, and B. S. Kotlia. 2011. Holocene weak summer East Asian monsoon intervals in Taiwan and plausible mechanisms. Quaternary International 229:57-66.

Selvaraj, K., K.-Y. Wei, K.-K. Liu, and S.-J. Kao. 2012. Late Holocene monsoon climate of northeastern Taiwan inferred from elemental (C, N) and isotopic (δ13C, δ15N) data in lake sediments. Quaternary Science Reviews 37:48-60.

Sharma, R. R. 2014. Precipitating Change: Holocene climate change in the Asian monsoon based on sediment archives from tropical lakes. Masters Thesis. The University of Sydney, Sydney.

Shi, F., J. Li, and R. J. Wilson. 2014. A tree-ring reconstruction of the South Asian summer monsoon index over the past millennium. Sci Rep 4:6739.

Shi, Z., T. Xu, and H. Wang. 2016. Sensitivity of Asian climate change to radiative forcing during the last millennium in a multi-model analysis. Global and Planetary Change 139:195-210.

Shokralla, S., J. L. Spall, J. F. Gibson, and M. Hajibabaei. 2012. Next-generation sequencing technologies for environmental DNA research. Mol Ecol 21:1794-1805.

Shukla, A., J. S. Guleria, and R. C. Mehrotra. 2012. A fruit wing of Shorea Roxb. from the Early Miocene sediments of Kachchh, Gujarat and its bearing on palaeoclimatic interpretation. Journal of Earth System Science 121:195-201.

Shuman, B. 2003. Controls on loss-on-ignition variation in cores from two shallow lakes in the northeastern United States. Journal of Paleolimnology 30:371-385.

Shuman, B. N., P. Newby, and J. P. Donnelly. 2009. Abrupt climate change as an important agent of ecological change in the Northeast U.S. throughout the past 15,000 years. Quaternary Science Reviews 28:1693-1709.

Singh, S., R. Kar, and A. Khandelwal. 2010. Impact of modern pollen rain studies from South and Little Andaman Islands, India, to interpret present and past vegetation Current Science 99:1251-1256.

Sinha, A., M. Berkelhammer, L. Stott, M. Mudelsee, H. Cheng, and J. Biswas. 2011a. The leading mode of Indian Summer Monsoon precipitation variability during the last millennium. Geophysical Research Letters 38:L15703.

Sinha, A., K. G. Cannariato, L. D. Stott, H. Cheng, R. L. Edwards, M. G. Yadava, R. Ramesh, and I. B. Singh. 2007. A 900-year (600 to 1500 A.D.) record of the Indian summer monsoon precipitation from the core monsoon zone of India. Geophysical Research Letters 34:L16707.

Sinha, A., L. Stott, M. Berkelhammer, H. Cheng, R. L. Edwards, B. Buckley, M. Aldenderfer, and M. Mudelsee. 2011b. A global context for megadroughts in monsoon Asia during the past millennium. Quaternary Science Reviews 30:47-62.

Smith, M. D. 2011. The ecological role of climate extremes: current understanding and future prospects. Journal of Ecology 99:651-655.

Sodhi, N. S., L. P. Koh, R. Clements, T. C. Wanger, J. K. Hill, K. C. Hamer, Y. Clough, T. Tscharntke, M. R. C. Posa, and T. M. Lee. 2010. Conserving Southeast Asian forest biodiversity in human-modified landscapes. Biological Conservation 143:2375-2384.

Soil Survey Staff. 2010. Keys to Soil Taxonomy. 11th edition. United States Department of Agriculture (USDA), Natural Resources Conservation Service (NRCS), Washington D.C.

Sovu, M. Tigabu, P. Savadogo, P. C. Odén, and L. Xayvongsa. 2009. Recovery of secondary forests on swidden cultivation fallows in Laos. Forest Ecology and Management 258:2666-2675.

Staver, A. C. 2012. Determinants and Dynamics of the global Distribution of Savanna and Forest Biomes. Ph.D Thesis. Princeton University, Princeton, N.J.

Staver, A. C., S. Archibald, and S. A. Levin. 2011a. The global extent and determinants of savanna and forest as alternative biome states. Science 334:230-232.

Staver, C., S. Archibald, and S. Levin. 2011b. Tree cover in sub-Saharan Africa: Rainfall and fire constrain forest and savanna as alternative stable states. Ecology 92:1063-1072.

Sternberg, L. D. S. L. 2001. Savanna-Forest Hysteresis in the Tropics. Global Ecology and Biogeography 10:369-378.

Stevenson, J., and S. Haberle. 2005. Palaeoworks Technical Papers 5: Macro Charcoal Analysis: A modified technique used by the Department of Archaeology and Natural History. Australian National University, http://palaeoworks.anu.edu.au/paltr05.pdf.

Stewart, J., A. J. Parsons, J. Wainwright, G. S. Okin, B. T. Bestelmeyer, E. L. Fredrickson, and W. H. Schlesinger. 2014. Modeling emergent patterns of dynamic desert ecosystems. Ecological Monographs 84:373-410.

Stockmarr, J. 1971. Tablets with Spores used in Absolute Pollen Analysis. Pollen et Spores 13:615-621.

Stoner, K. E., and R. M. Timm. 2011. Seasonally Dry Tropical Forest Mammals: Adaptations and Seasonal Patterns. Pages 85-106 in R. Dirzo, H. S. Young, H. A. Mooney, and G. Ceballos, editors. Seasonally Dry Tropical Forests: Ecology and Conservation. Island Press, Washington, D.C.

Stott, P. A. 1976. Recent Trends in the Classification and Mapping of Dry Deciduous Dipterocarp Forest in Thailand in The classification and mapping of Southeast Asian Ecosystems. University of Hull, Aberdeen.

Stott, P. A. 1984. The savanna forests of mainland southeast Asia: an ecological survey. Progress in Physical Geography 8:315-335.

Stott, P. A. 1986. The spatial pattern of dry season fires in the savanna forests of Thailand. Journal of Biogeography 13:345-258.

Stott, P. A. 1988a. The Forest as Pheonix: Towards a Biogeography of Fire in Mainland South East Asia. The Geographical Journal 154:337-350.

Stott, P. A. 1988b. Savanna forest and seasonal fire in South East Asia. Plants Today November-December 1988:196-200.

Stott, P. A. 1990. Stability and stress in the savanna forests of mainland South-East Asia. Journal of Biogeography 17:373-383.

Stott, P. A., J. G. Goldammer, and W. L. Werner. 1990. The Role of Fire in the Tropical Lowland Deciduous Forest of Asia. Pages 32-43 in J. G. Goldammer, editor. Fire in the Tropical Biota: Ecosystem Processes and Global Challenges. Springer-Verlag, Berlin, Heidelberg.

Sun, K.-Q. 2006. The Cathaysia Flora and the Mixed Late Permian Cathaysian-Angaran Floras in East Asia. Journal of Integrative Plant Biology 48:381-389.

Sunderland, T., D. Apgaua, C. Baldauf, R. Blackie, C. Colfer, A. B. Cunningham, K. Dexter, H. Djoudi, D. Gautier, D. Gumbo, A. Ickowitz, H. Kassa, N. Parthasarathy, R. T. Pennington, F. Paumgarten, S. Pulla, P. Sola, D. Tng, P. Waeber, and L. Wilmé. 2015. Global dry forests: a prologue. International Forestry Review 17:1-9.

Sundstrom, S. M., C. R. Allen, and C. Barichievy. 2012. Species, functional groups, and thresholds in ecological resilience. Conservation Biology 26:305-314.

Sutherland, F. L., P. C. Piilonen, Khin Zaw, S. Meffre, and J. Thompson. 2015. Sapphire within zircon-rich gem deposits, Bo Loei, Ratanakiri Province, Cambodia: trace elements, inclusions, U–Pb dating and genesis. Australian Journal of Earth Sciences 62:761-773.

Swaine, M. D. 1992. Characteristics of dry forest in West Africa and the influence of fire. Journal of Vegetation Science 3:365-374.

Takaya, Y. 1967. Observations on some Pliestocene outcrops in Cambodia. Kyoto University, Kyoto.

Tamuntuan, G., S. Bijaksana, J. King, J. Russell, U. Fauzi, K. Maryunani, N. Aufa, and L. O. Safiuddin. 2015. Variation of magnetic properties in sediments from Lake Towuti, Indonesia, and its paleoclimatic significance. Palaeogeography, Palaeoclimatology, Palaeoecology 420:163-172.

Tanaka, N., T. Kume, N. Yoshifuji, K. Tanaka, H. Takizawa, N. Shiraki, C. Tantasirin, N. Tangtham, and M. Suzuki. 2008. A review of evapotranspiration estimates from tropical forests in Thailand and adjacent regions. Agricultural and Forest Meterology 148:807-819.

Tani, A., E. Ito, M. Kankaki, S. Ohta, S. Khorn, P. Pith, B. Tith, S. Pol, and S. Lim. 2007. Principal Forest Types of Three Regions of Cambodia: Kampong Thom, Kratie, and Mondolkiri. Pages 201-213 in H. Sawada, M. Araki, N. A. Chappell, J. V. LaFrankie, and A. Shimizu, editors. Forest Environments of the Mekong River Basin. Springer, Toyko.

Teegalapalli, K., A. J. Hiremath, and D. Jathanna. 2009. Patterns of seed rain and seedling regeneration in abandoned agricultural clearings in a seasonally dry tropical forest in India. Journal of Tropical Ecology 26:25.

Theilade, I., L. Schmidt, P. Chhang, and J. A. McDonald. 2011. Evergreen swamp forest in Cambodia: floristic composition, ecological characteristics, and conservation status. Nordic Journal of Botany 29:71-80.

Thompson, I., B. Mackey, S. McNulty, and A. Mosseler. 2009. Forest Resilience, Biodiversity and Climate Change: A Synthesis of the Biodiversity/Resilience/Stability Relationship in Forest Ecosystems. Secretariat of the Convention on Biological Diversity, Montreal, Canada.

Thompson, R., R. W. Battarbee, P. E. O'Sullivan, and F. Oldfield. 1975. Magnetic Susceptibility of Lake Sediments. Limnology and Oceanography 20:687-698.

Thompson, R., R. M. Clarke, and G. S. Boulton. 2012. Core Correlation. Pages 415-430 in H. J. B. Birks, A. F. Lotter, S. Juggings, and J. P. Smol, editors. Tracking Environmental Change Using Lake Sediments: Volume 5 - Data Handling and Numerical Techniques. Springer, Dordrecht, Heidelberg, New York, and London.

Thomson, J., I. W. Croudace, and R. G. Rothwell. 2006. A geochemical application of the ITRAX scanner to a sediment core containing eastern

Mediterranean sapropel units. Geological Society, London, Special Publications 267:65-77.

Thomson, J., N. C. Higgs, T. R. S. Wilson, I. W. Croudace, G. J. De Lange, and P. J. M. Van Santvoort. 1995. Redistribution and geochemical behaviour of redox-sensitive elements around S1, the most recent eastern Mediterranean sapropel. Geochimica et Cosmochimica Acta 59:3478-3501.

Timberlake, J., E. Chidumayo, and L. Sawadogo. 2010. Distribution and Characteristics of African Dry Forests and Woodlands.in E. N. Chidumayo and D. J. Gumbo, editors. The Dry Forests and Woodlands of Africa. Earthscan, London and Washington D.C.

Tissot, C., H. Chikhi, and T. S. Nayar. 1994. Pollen of wet evergreen forests of the Western Ghats, India. Institut Français de Pondichéy, Pondicherry.

Tordoff, A. W., R. J. Timmins, A. Maxwell, K. Huy, V. Lic, and E. H. Khou. 2005. Biological Assessment of the Lower Mekong Dry Forests Ecoregion: Final Report. WWF Indochina Programme, Phnom Penh.

Toriyama, J., S. Ohta, M. Araki, M. Kanzaki, S. Khorn, P. Pith, S. Lim, and S. Pol. 2007. Comparison of soil physical properties in evergreen and deciduous forests in central Cambodia. Journal of Forest Research 13:15-24.

Toriyama, J., S. Ohta, M. Araki, K. i. Kosugi, T. Nobuhiro, N. Kabeya, A. Shimizu, K. Tamai, M. Kanzaki, and S. Chann. 2011. Soil pore characteristics of evergreen and deciduous forests of the tropical monsoon region in Cambodia. Hydrological Processes 25:714-726.

Trivedi, A., M. S. Chauhan, and A. Farooqui. 2014. Studies on Pollen Rain vis-a-vis Vegetation Relationship and Thecamoebian Diversity in Bari Tal area, Lucknow District, Uttar Pradesh. Biological Forum 6:68-78.

Uchikawa, J., B. N. Popp, J. E. Schoonmaker, and L. Xu. 2008. Direct application of compound-specific radiocarbon analysis of leaf waxes to establish lacustrine sediment chronology. Journal of Paleolimnology 39:43-60.

van Liere, W., and J. A. McNeely. 2005. Agriculture in the lower Mekong basin: Experience from the Critical Decade of 1966-1976. IUCN, Gland and Cambridge.

Vance, R. E., and A. M. Telka. 1998. Accelerator mass spectrometry radiocarbon dating of 1994 Lake Winnipeg cores. Journal of Paleolimnology 19:329-334.

Vandergoes, M. J., and C. A. Prior. 2003. AMS dating of pollen concentrates - a methological study of late quaternary sediments from South Westland, New Zealand. Radiocarbon 45:479-491.

Vàzquez-Yanes, C. 1998. Trema micrantha (L.) Blume (Ulmaceae): A promising neotropical tree for site amelioration of deforested land. Agroforestry Systems 40:97-104.

Venier, P., M. Cabido, A. Mangeaud, and G. Funes. 2013. Seedlings growth and survival of five Acacia (Fabaceae) species that coexist in neotropical semi-arid forests of Argentina, under different light and water availability conditions. Revista de biologia tropical 61:501-514.

Verschuren, D. 1993. A lightweight extruder for accurate sectioning of soft-bottom lake sediment cores in the field. Limnology and Oceanography 38:1796-1802.

Vysotsky, V. I., R. D. Rodnikova, and M. N. Li. 1994. The Petroleum Geology of Cambodia. Journal of Petroleum Geology 17:195-210.

Walker, B. 2012. Learning how to change in order not to change: Lessons from ecology for an uncertain world. Krebs Lecture 2012, University of Canberra.

Walker, B., C. S. Holling, S. R. Carpenter, and A. Kinzig. 2004. Resilience, Adaptability and Transformability in Social–ecological Systems. Ecology and Society 9:5.

Wan, N.-J., H.-C. Li, Z.-Q. Liu, H.-Y. Yang, D.-X. Yuan, and Y.-H. Chen. 2011. Spatial variations of monsoonal rain in eastern China: Instrumental, historic and speleothem records. Journal of Asian Earth Sciences 40:1139-1150.

Wang, B., S. C. Clemens, and P. Liu. 2003. Contrasting the Indian and East Asian monsoons: implications on geologic timescales. Marine Geology 201:5-21.

Wang, B., and LinHo. 2002. Rainy season of the Asian-Pacific summer monsoon. Journal of Climate 15:386-398.

Wang, R., J. A. Dearing, P. G. Langdon, E. Zhang, X. Yang, V. Dakos, and M. Scheffer. 2012. Flickering gives early warning signals of a critical transition to a eutrophic lake state. Nature 492:419-422.

Wang, Y., H. Cheng, R. L. Edwards, Y. He, X. Kong, Z. An, J. Wu, M. J. Kelly, C. A. Dykoski, and X. Li. 2005a. The Holocene Asian monsoon: links to solar changes and North Atlantic climate. Science 308:854-857.

Wang, Y., H. Cheng, R. Lawrence Edwards, Y. He, X. Kong, Z. An, J. Wu, M. J. Kelly, C. A. Dykoski, and X. Li. 2005b. Dongge Cave Stalagmite High-Resolution Holocene d18O Data. NOAA/NCDC Paleoclimatology Program, Boulder, CO.

Wang, Y. J., H. Cheng, R. L. Edwards, Z. S. An, J. Y. Wu, C. C. Shen, and J. A. Dorale. 2001. A high-resolution absolute-dated late Pleistocene Monsoon record from Hulu Cave, China. Science 294:2345-2348.

Wanthongchai, K., and J. G. Goldammer. 2011. Fire Management in South and Southeast Asia's Seasonally Dry Forests. Pages 97-114 in W. J. McShea, S. J. Davies, and N. Bhumpakphan, editors. The Ecology and Conservation of Seasonally Dry Forests in Asia. Smithsonian Institution Scholarly Press, Washington D.C.

Werneck, F. P., G. C. Costa, G. R. Colli, D. E. Prado, and J. W. Sites Jr. 2011. Revisiting the historical distribution of Seasonally Dry Tropical Forests: new insights based on palaeodistribution modelling and palynological evidence. Global Ecology & Biogeography 20:272-288.

Wharton, C. H. 1966. Man, fire, and wild cattle in north Cambodia. Pages 23-65 in Annual Tall Timbers Fire Ecology Conference. Tall Timbers Research, Tallahassee, FL.

Whitlock, C., and C. Larsen. 2001. Charcoal as fire proxy.in J. P. Smol, H. J. B. Birks, and W. M. Last, editors. Tracking Environmental Change Using Lake Sediments: Volume 3: Terrestrial, Algal, and Siliceous Indicators. Kluwer Academic Publishers, Dordrecht, The Netherlands.

Whitlock, C., and S. H. Millspaugh. 1996. Testing the assumptions of fire-history studies: an examination of modern charcoal accumulation in Yellowstone National Park, USA The Holocene 6:7-15.

Wikramanayaka, E., R. Boonratana, P. Rundel, and N. Aggimarangsee. 2014a. Southeastern Asia: Thailand, Cambodia, Laos, and Vietnam: Ecoregions IM0202. World Wildlife Fund.

Wikramanayaka, E., P. Rundel, R. Boonratana, and N. Aggimarangsee. 2014b. Southeastern Asia: Thailand, Cambodia, Laos, and Vietnam: Ecoregions IM0210. World Wildlife Fund.

Wikramanayake, E., E. Dinerstein, C. J. Loucks, D. M. Olson, J. Morrison, J. Lamoreux, M. McKnight, and P. Hedao. 2002. Terrestrial Ecoregions of the Indo-Pacific, a Conservation Assessment. Island Press, Washington D.C.

Williams, J. W., J. L. Blois, and B. N. Shuman. 2011. Extrinsic and intrinsic forcing of abrupt ecological change: case studies from the late Quaternary. Journal of Ecology 99:664-677.

Williams, L. 1965. Vegetation of Southeast Asia: Studies of Forest Types 1963-1965. Agricultural Research Division, Crops Research Division, Washington D.C.

Williams, R. J., G. A. Duff, D. M. J. S. Bowman, and G. D. Cook. 1996. Variation in the Composition and Structure of Tropical Savannas as a Function of Rainfall and Soil Texture Along a Large-Scale Climatic Gradient in the Northern Territory, Australia. Journal of Biogeography 23:747-756.

Williamson, D., A. Jelinowska, C. Kissel, P. Tucholka, E. Gibert, F. Gasse, M. Massault, M. Taieb, E. Van Campo, and K. Wieckowski. 1998. Mineral-magnetic proxies of erosion/oxidation cycles in tropical maar-lake sediments (Lake Tritrivakely, Madagascar): paleoenvironmental implications. Earth and Planetary Science Letters 155:205-219.

Wohlfarth, B., W. Klubseang, S. Inthongkaew, S. C. Fritz, M. Blaauw, P. J. Reimer, A. Chabangborn, L. Löwemark, and S. Chawchai. 2012. Holocene environmental changes in northeast Thailand as reconstructed from a tropical wetland. Global and Planetary Change 92-93:148-161.

Workman, D. R. 1977. Geology of Laos, Cambodia, South Vietnam and the eastern part of Thailand. Overseas Geology and Mineral Resources 50:1-23.

World Bank Group Climate Change Knowledge Portal. 2016. Climate Change Knowledge Portal For Development Practitioners and Policy Makers. The World Bank Group.

You, R., V. Kleinpeter, and J.-C. Diepart. 2015. Learning for Resilience: Insights from Cambodia's Rural Communities. Pages 147-175 in J.-C. Diepart, editor. Differentiation of swidden agriculture in Northeast Cambodia: Kavet swiddeners, the state and the markets in Kok Lak commune. The Learning Institute, Phnom Penh.

Yuan, D., H. Cheng, R. L. Edwards, C. A. Dykoski, M. J. Kelly, M. Zhang, J. Qing, Y. Lin, Y. Wang, J. Wu, J. A. Dorale, Z. An, and Y. Cai. 2004. Timing, duration, and transitions of the last interglacial Asian monsoon. Science 304:575-578.

Zhang, P., H. Cheng, R. L. Edwards, F. Chen, Y. Wang, X. Yang, J. Liu, M. Tan, B. Wang, J. Lui, C. An, Z. Dai, J. Zhou, D. Zhang, J. Jihong, L. Jin, and K. R. Johnson. 2008. A Test of Climate, Sun, and Culture Relationships from an 1810-Year Chinese Cave Record. Science 322.

Zhang, W., Q. Ming, Z. Shi, G. Chen, J. Niu, G. Lei, F. Chang, and H. Zhang. 2014. Lake sediment records on climate change and human activities in the Xingyun Lake catchment, SW China. PLoS One 9:e102167.

Zimov, S. A., N. S. Zimov, A. N. Tikhonov, and F. S. Chapin. 2012. Mammoth steppe: a high-productivity phenomenon. Quaternary Science Reviews 57:26-45.

Zuidema, P. A., P. J. Baker, P. Groenendijk, P. Schippers, P. van der Sleen, M. Vlam, and F. Sterck. 2013. Tropical forests and global change: filling knowledge gaps. Trends Plant Sci 18:413-419.

A Lake catchment soil analysis

Soil samples taken from each lake catchment area were analysed in order to: 1) characterise the relationship (if any) between site edaphic conditions and forest structure as noted in the literature (Toriyama et al. 2007, Toriyama et al. 2011) and, 2) determine the properties of local soils to aid in fingerprinting terrigenously-sourced lake sediments.

A.1 Field sampling and description

Fifteen soil profiles were described and sampled across the five Ratanakiri crater lake sites in April, 2013. The selection of sample sites was both opportunistic (e.g. where a soil profile was exposed in a path cutting or gully wall) and based on representativeness (where possible, sample sites were taken from opposite sides of the catchment, upslope and downslope, and where there was an apparent lithological change). Mini-trenches were dug using a hoe and shovel until refusal or the C-horizon or water table was encountered. Pre-exposed soil profiles were scraped with the shovel to remove weathered surficial material and accumulated littoral matter. Each sample site was photographed and the total depth of the total profile, each horizon and, where relevant, depth to the water table was measured. The soil profiles were described in the field roughly following the Australian Soils Classification (ASC) system (Isbell 2002).

A total of 13 samples (0.3 to 1 kg) were taken from the A- and B- horizons of soils profiles where adequately-sized samples could be extracted. These included four samples from each Yeak Loam (YLSP2-A1 & YLSP2-B2, YLSP5-A1 & YLSP5-B2) and Yeak Mai (YMSP1-A1 & YMSP1-B2 and YMSP2-A1 & B2/C1), three from Boeng Lumkut (LKSP1-A1, LKSP2-A1 & LKSP2-B2) and two from Yeak Kara (YKSP3-A1 & YKSP3-B2). Given the hardness of ground sampled at Yeak Oam, only three small ($\sim$20 g) samples were taken from this site (YOSP2 A1, A2 and B2). All samples were sealed in air-tight sample bags and transported to the School of Geoscience at the University of Sydney for laboratory analysis of physical and geochemical properties.

A.2 Laboratory analysis

Samples selection for laboratory analysis was based on availability of sample material and the representativeness of the soil profile (relatively deep, non-hydrous soils were favoured). Samples from sites assessed for detailed palaeo-environmental analysis (i.e. Yeak Loam and Yeak Mai) were also

prioritised, particularly for tests useful for fingerprinting lake sediment source.

Field moisture

Approximately 50 to 60 g of the selected soil samples were weighed out to assess field moisture content. Where sample size was large enough, replicate samples were taken. Wet sample weight was then recorded, and the samples oven dried over night at 65 °C. After drying, sample weight was taken and field moisture calculated based on the percentage weight lost between the wet and dry sample. Samples from Yeak Loam (YLSP1-A1 & YLSP1-B2, YLSP2-A1 & YLSP2-B2, and YLSP5-A & YLSP5-B2), Yeak Kara (YKSP3-A1 & YKSP3-B2) and Yeak Mai (YMSP1-A1 & YMSP1-B2 and YMSP2-A1 & B2/C1) were processed for this analysis.

Particle size analysis

Dried soils were gently disaggregated into individual particles using a mortar and pestle. The gravel fraction of each sample was segregated by passing the soil through a 2 mm sieve (Soil Survey Staff 2010). The weight of the gravel fraction was taken and recorded as a percentage of the total sample weight. The <2 mm fraction was then subsampled using a sediment splitter. The quantity of the original sample was progressively reduced by passing half of the previous sample through the splitter approximately eight times. Between 0.5 and 1 g of sample was taken from the final fraction and placed into a 50 ml centrifuge tube for grain size analysis. The remainder of the sample was recombined for analysis of total organic carbon (described below).

The samples prepared for grain size analysis were treated with 5 ml of 35% H_2O_2 and placed into a hot water bath at 65 °C to 80 °C (temperature was dependant on intensity of reaction) for 10 hours. This process was repeated until no reaction was observable. Following digestion, samples were rinsed three times with DI water. Thirty ml of $(NaPO_3)_6$ dispersant was then added to each sample, and the centrifuge tubes were tightly capped and spun for four hours to disaggregate any clumped material. Laser diffraction spectrometry was employed to assess the grain size distribution of each sample using a Malvern Mastersizer 2000 equipped with a hydro G dispersion unit. Three measurements were taken for each sample. Sonication was employed for 20 seconds prior to analysis to break down any remaining grain aggregates. The average distribution of each sample was taken and used to calculate soil texture class based on the USDA system of soil classification (Soil Survey Staff 2010). Samples from Yeak Loam (YLSP1-A1 & YLSP1-B2, YLSP2-A1 & YLSP2-B2, and YLSP5-A & YLSP5-B2), Yeak Kara (YKSP3-A1 & YKSP3-B2), Yeak Mai (YMSP1-A1 & YMSP1-B2 and YMSP2-A1 & B2/C1), and Boeng Lumkut (LKSP1-A1 & LKSP1-B2 and LKSP2-A1, LKSP2-B2 & LKSP2-C1) were processed for textural analysis.

Total organic carbon

Remaining soil samples from grain size analysis preparation were placed into individual, pre-weighed crucibles, and the pre-ignition sample weight was calculated. Where the sample size was too large for the crucibles, the samples were passed through a sediment splitter until an appropriate size was achieved. Samples were then combusted at 550 °C for 4 hours following Heiri et al. (2001). After cooling, post-ignition weight was taken and compared with the pre-ignition weight to estimate the percentage of total organic carbon lost from each sample. Samples from Yeak Loam (YLSP1-A1 & YLSP1-B2 and YLSP5-A & YLSP5-B2), Yeak Kara (YKSP3-A1 & YKSP3-B2), Yeak Mai (YMSP1-A1 & YMSP1-B2 and YMSP2-A1 & B2/C1) and Boeng Lumkut (LKSP1-A1 & LKSP1-B2) were processed for analysis of total organic content.

pH testing

Soil pH was measured using a potentiometric method. Five grams of the selected soil samples in their field condition were weighed out and mixed with $CaCl_2$ using a 1:5 ratio. Samples were spun to mix for 2 hours, and their pH measured with a glass electrode pH sensor that was left in each sample until a consistent reading was obtained (approx. 1 min.). The meter was washed in DI water between sampling. The pH of samples from Yeak Loam (YLSP1-A1 & YLSP1-B2, YLSP2-A1 & YLSP2-B2, and YLSP5-A & YLSP5-B2), Yeak Kara (YKSP3-A1 & YKSP3-B2), Yeak Mai (YMSP1-A1 & YMSP1-B2 and YMSP2-A1 & B2/C1), and Boeng Lumkut (LKSP2-A1, LKSP2-B2 & LKSP2-C1) was measured.

Total nitrogen

Five grams of selected soil samples (field moisture) were placed into a 50 ml centrifuge tube with 40 ml 1 M KCl, and placed on a shaker for an hour. After shaking, the samples were passed through Whatman No. 42 filter paper. The extracts were stored on a Flow Injection Analyser, and subsequently analysed for total nitrogen by University of Sydney Faculty of Agriculture Centre for Carbon, Water and Food. Zero, 5, 10 and 20 ppm NO_3^- and 0, 2.5, 5 and 10 ppm NH_4^+ standards were prepared from standard stock solution. Samples from Yeak Loam (YLSP1-A1 & YLSP1-B2 and YLSP5-A1 & YLSP5-B2), Yeak Mai (YMSP1-A1 & YMSP1-B2 and YMSP2-A1 & YMSP2-B2), and Boeng Lumkut (LKSP2-A1, LKSP2-B2 & LKSP2-B2) were analysed.

Available phosphorous

2.5 grams of select soil samples (field moisture) were placed into a 50 ml Falcon tube and 40 ml of buffered 0.5 M $NaHCO_3$ was added to each. Samples were then shaken on a shaker table for 30 minutes before being filtered through Whatman No. 42 filter paper into a clean Falcon tube. Zero, 1, 2, 5 and 10 ppm P standards were prepared from standard stock solution.

Five ml of each standard were added to clean 50 ml Falcon tubes and 2 drops of p-nitrophenol was added to each sample tube. 6 N HCl drops were added until the yellow colour faded. An extra drop was then added to each and the samples mixed until all bubbles were removed from the solution. Four ml of colour reagent with ascorbic acid was then added to each standard. After 30 minutes, absorbance was measured on a spectrometer at 890 nm. A standard curve was made using absorbance data measured from the standard concentrations. This was used to calculate the concentrations (mg L^{-1}) of available P in the soil samples using:

$$P_{\text{avail.}} = \frac{P_{\text{conc.}} \times V_{\text{NaHCO}_3}}{W_{\text{s}}} \times 100$$

where:

$P_{\text{avail.}}$ = the concentration of available P (mg kg^{-1})

$P_{\text{conc.}}$ = the concentration of P (mg L^{-1})

V_{NaHCO_3} = volume of $NaHCO_3$ (ml)

W_s = dry soil weight (g)

Samples from Yeak Loam (YLSP1-A1 & YLSP1-B2 and YLSP5-A1 & YLSP5-B2), Yeak Mai (YMSP1-A1 & YMSP1-B2 and YMSP2-A1 & YMSP2-B2), and Boeng Lumkut (LKSP2-A1, LKSP2-B2 & LKSP2-B2) were analysed for available P.

Soil mineral magnetics & density

In order to aid source interpretation of both the soil samples and the lacustrine core mineral magnetics (detailed in chapter 4), soil samples were processed for low frequency (χlf) and frequency dependant magnetic ($\chi fd_{\%}$) susceptibility. The former showing the total concentration of ferromagnetic minerals in the soil samples (Dearing 1999) and the latter indicating the presence and proportion of superparamagnetic minerals (diameter <0.03 μm) (Dearing et al. 1996, Dearing 1999).

All of the Yeak Loam and Yeak Mai soil profile units, as well as YOSP2-A1 & YOSP2-B2 were analysed. These soils were selected to correlate with the lake core samples selected for mineral magnetic analysis. Approx 50 g of each sample was dried in a 65 °C oven over night. After drying, samples were disaggregated using a mortar and pestle and placed into preweighed 10 cm^3, cylindrical plastic pots designed for the Bartington MS2B Dual Frequency Magnetic Susceptibility meter. Pots were filled to the rim and very lightly compacted to remove any air gaps. The samples were then weighed, and this was used to determine dry bulk density of the soils. A Bartington MS2B Dual Frequency Magnetic Susceptibility Meter was then used to determine the χlf (0.46 kHz magnetic field), χhf (mass specific high frequency magnetic susceptibility [4.6 kHz magnetic field]) of each sample, and, from this, calculate the percentage frequency dependence ($\chi fd_{\%}$).

Samples were run in triplicates for both frequencies, with 5 second sample measurements and blank (air) measurements taken at the start, end, and between χlf and χhf measurements. Blank sample measurements were made using an empty plastic cylindrical pot. The mean and standard deviation of measurements was calculated for sample replicates. A detailed outline of measurement protocols is provided in (Dearing 1999a).

B SASDTF Forest List

A list of genera and species characteristic of South-east Asian Seasonally Dry Tropical Forest and units within are presented in table B.1.

TABLE B.1: List of flora found within south-east Asian tropical dry forest categorised into representative forest-unit types.
Note: * = regional.

Family	Genus	Species	Auth	Forest Unit	Region	A. Tani et al. (2007)	B. Bunyavejchewin et al. (2011)	C. Maxwell (1999) - including Rollet, (1962)	D. Ruangpanit (1995)	E. Theilade et al. (2011)	F. Gardner et al. (2000)	G. Dy Phon (2000)	H. Yeak Loam	I. Yeak Oam/Yeak Kara	J. Boeng Lumkut	K. Yeak Mai
Achariaceae	*Hydnocarpus*	*anthelmintica*	Pierre ex Laness.	RiF	Cambodia			x								
Achariaceae	*Hydnocarpus*	*anthelminticus*	Pierre ex Laness.	RiF	Cambodia			x								
Anacardiaceae	*Buchanania*	*latifolia*	Roxb.	MDF	Cambodia			x								
Anacardiaceae	*Buchanania*	*reticulata*	Hance	MDF	Cambodia			x								
Anacardiaceae	*Gluta*	*usitata*	(Wall.) Ding Hou	DDF	Thailand		x						x			
Anacardiaceae	*Glycosmis*	*pentaphylla*	Retz.	SeF (BRE)	Cambodia			x								
Anacardiaceae	*Mangifera*	*indicta*	L.	SEDF	Cambodia			x								
Anacardiaceae	*Melanorrhea/ Melanorhea*	*laccifera*	Pierre	MDF	Cambodia			x								
Anacardiaceae	*Spondias*	spp.		MDF/ Intermediate SEDF/MDF	Cambodia			x								
Annonaceae	*Artabotrys*	*siamensis*	Miq.	MDF	Mainland SE-Asia				x							
Annonaceae	*Artabotrys*	sp.		RiF	Cambodia			x								
Annonaceae	*Cananga*	*latifolia*	(Hook.f. & Thomson) Finet & Gagnep	Transition (semi-dense/mixed dry)	Cambodia			x								
Annonaceae	*Miliusa*	sp.		SEDF (BRE)	Cambodia			x								
Annonaceae	*Mitrephora*	*thorelii*	Pierre	SEDF (BRE)	Cambodia			x		x						
Annonaceae	*Saccopetalum*	*lineatum*	Craib	SEDF	Thailand		x									
Aparagaceae	*Dracaena*	*gracilis*	Wall.	SwF	Cambodia											
Apocynaceae	*Wrightia*	sp.		SeF (BRE)	Cambodia			x								
Apocynaceae	*Wrightia*	*annamensis*	Eberh. & Dubard	SEDF	Cambodia							x				

Continued...

Family	Genus	Species	Auth	Forest Unit	Region	A.	B.	C.	D.	E.	F.	G.	H.	I.	J.	K.
Apocynaceae	*Wrightia*	*arborea/ tomentosa*	(Dennst.) Mabb.	MDF/SEDF	Cambodia							x				
Apocynaceae	*Wrightia*	*pubescens*	R. Br.	SEDF	Cambodia							x				
Apocynaceae	*Wrightia*	*religiosa*	(Teijsm. & Binn.) Benth.	SeF	Cambodia							x				
Apocynaceae) Asclepiadaceae	*Telectadium*	*dongnaiensis*	Pierre.ex Cost	RiF	Cambodia			x								
Aquifoliceae	*Ilex*	*thorelii*	Pierre	SEDF (BRE)	Cambodia			x		x						x
Arecaceae (Palmae)	*Areca*	sp.		SwF	Cambodia					x						x
Arecaceae (Palmae)	*Calamus*	sp.		SwF, MDF	Cambodia, Mainland SE-Asia				x							
Arecaceae (Palmae)	*Corypha*	*lecomtei*	Becc. ex Lecomte	DDF	Cambodia			x		x						
Arecaceae (Palmae)	*Licuala*	sp.		SwF	Cambodia					x						
Arecaceae (Palmae)	*Livistona*	*cochinchinensis (saribus)*	Merr. ex A.Chev. Syn. L. (Mart.)	SwF, DDF	Cambodia			x								
Arecaceae (Palmae)	*Phoenix*	*acaulis*	Roxb.	DDF. MDF	Cambodia, Mainland SE-Asia			x	x							
Arecaceae (Palmae)	*Phoenix*	*humilis*	Royle ex Becc.	MDF	Cambodia, Mainland SE-Asia			x	x					x	x	
Aristolochiaceae	*Aristolochia*			MDF	Mainland SE-Asia				x							
Asteraceae	*Chromolaena*	*odorata*	(L.) King & H.E. Robins.		Cambodia											
Bignoniaceae	*Oroxylum*	*indicum*	(L.) Benth. ex Kurz	SeF (SEDF), Intermediate SEDF/MDF, MDF	Cambodia			x								
Bignoniaceae	*Stereospermum*	*chelonoides*	(L.f.) DC.	Intermediate SEDF/MDF	Cambodia			x								
Bixaceae	*Cochlospermum*	*gossypium*	(Linn.) DC.	Intermediate SEDF/MDF	Cambodia			x						x	x	x
Blechnaceae	*Stenochlaena*	*palustris*	(Burm. f.) Bedd.)	SwF	Cambodia			x								
Boraginaceae	*Cordia*	*obliqua*	Willd.	RiF	Cambodia			x								
Burseraceae	*Canarium*	*subulatum*	Guillaumin	Intermediate SEDF/MDF/MDF	Cambodia			x		x						
Burseraceae	*Garuga*	*pinnata*	Roxb.	MDF	Thailand		x									

Continued...

Family	Genus	Species	Auth	Forest Unit	Region	A.	B.	C.	D.	E.	F.	G.	H.	I.	J.	K.
Calophyllaceae (Clusiaceae)	*Calophyllum*	*spectabile*	Willd.	SwF	Cambodia					x						
Calophyllaceae (Clusiaceae)	*Calophyllum*	*tetrapetalum*	Roxb.	SwF	Cambodia					x						
Cannabaceae	*Celtis*	sp.		SEDF, MDF	Cambodia											
Capparidaceae	*Capparis*	*micrantha*	DC.	SwF	Cambodia											
Capparidaceae	*Crateva*	*magna*	(Lour.) DC.	RiF	Cambodia			x		x						
Celastraceae	*Euonymus*	*glaber*	Roxb.	SwF	Cambodia					x						
Chrysobalanaceae	*Parinarium*	*annamensis*	(Hance) J. E.Vidal	MDF, SeF (SEDF & BRE), SEDF (BRE), SwF	Cambodia					x						
Clusiaceae	*Garcinia*	*benthamii*	Pierre	BRE (SEDF)	Cambodia			x								
Clusiaceae	*Garcinia*	*schomburgkiana*	Pierre	BRE (SEDF)	Cambodia											
Clusiaceae	*Garcinia*	*speciosa*	Wall.	SEDF	Thailand		x									
Clusiaceae	*Garcinia*	*xanthochymus*	Hook.f.	SwF	Cambodia											
Combretaceae	*Anogeissus*	*acuminata*	Wall.	MDF, RiF	Thailand			x								
Combretaceae	*Anogeissus*	*rivularis*	(Gagnep.) O.Lecompte	RiF	Cambodia			x								
Combretaceae	*Combretum*	*pilosum*	Roxb.	SeF (BRE)	Cambodia			x								
Combretaceae	*Combretum*	*quadangulare*	Kurz	SeF (SEDF), Intermediate SEDF/MDF, RiF	Cambodia			x								
Combretaceae	*Combretum*	*trifoliatum*	Vent.	RiF	Cambodia			x								
Combretaceae	*Quisqualis*	*indicta*	L.	SEDF (BRE)	Cambodia			x	x						x	x
Combretaceae	*Terminalia*	*alata/ tomentosa/ elliptica*	Heyne ex. Roth	DDF, MDF	Cambodia, Thailand, Mainland SE-Asia		x	x	x							
Combretaceae	*Terminalia*	*bellirica*	(Gaertn.) Roxb.	MDF, SeF (BRE)	Mainland SE-Asia				x							
Combretaceae	*Terminalia*	*bialata*	(Roxb.) Steud.	SEDF (BRE), Intermediate SEDF/MDF, RiF	Cambodia			x								
Combretaceae	*Terminalia*	*chebula*	Retz.	MDF	Cambodia			x								
Combretaceae	*Terminalia*	*mucronata/ corticosca*	Craib & Hutch./ Pierre ex Lanessan	DDF, MDF	Cambodia, Thailand		x	x								
Combretaceae	*Terminalia*	*nigrovenulosa*	Pierre	SeF (SEDF)	Cambodia, Mainland SE-Asia			x	x						x	x
Combretaceae	*Terminalia*	spp.		DDF	Thailand		x									

Continued...

Family	Genus	Species	Auth	Forest Unit	Region	A.	B.	C.	D.	E.	F.	G.	H.	I.	J.	K.
Connaraceae	*Connarus*	*cochinchinensis*	(Baill.) Pierre	SeF (SEDF)	Cambodia			x								
Cornaceae	*Alangium*	sp.		RiF	Cambodia			x		x						
Cornaceae	*Mastixia*	*pentandra*	Bl. spp. chinensis (Merr.) Matt.	SwF	Cambodia									x		
Costaceae	*Costus*	spp.		MDF	Cambodia		x								x	x
Cycadaceae	*Cycas*	*siamensis*	Miq.	DDF, MDF	Cambodia, Thailand		x	x		x						
Cyperaceae	*Carex*			MDF	Mainland SE-Asia				x							
Cyperaceae	*Cyperus*			MDF	Mainland SE-Asia				x							
Dicksoniaceae	*Cibotium*	*barometz*	(L.) J.Sm.	SwF	Cambodia											
Dilleniaceae	*Dillenia*	*aurea*	Sm. var. kurzii Pierre		Mainland SE-Asia				x							
Dilleniaceae	*Dillenia*	*ovata*	Wall. ex Hook.f. & Thomson	MDF	Cambodia			x								
Dilleniaceae	*Dillenia*	*pentagyna*	Roxb.	MDF	Cambodia			x	x							
Dipterocarpaceae	*Anisoptera*	*cochinchinensis (costata)*	Kort.	SeF (BRE), Intermediate SEDF/MDF	Cambodia			x								
Dipterocarpaceae	*Dipterocarpus*	*turbinatus*	C.F.Gaertn.	SEDF, SEDF (BRE)	Cambodia, Thailand		x	x								
Dipterocarpaceae	*Dipterocarpus*	*alatus*	Roxb.	SEDF, SEDF (BRE), RiF	Cambodia			x					x			
Dipterocarpaceae	*Dipterocarpus*	*costatus*	C.F.Gaertn.	SEDF, SEDF (BRE)	Cambodia, Thailand		x	x								
Dipterocarpaceae	*Dipterocarpus*	*dyeri*	Pierre	SEDF, Intermediate SEDF/MDF, SeF (BRE)	Cambodia			x								
Dipterocarpaceae	*Dipterocarpus*	*intricatus*	Dyer	DDF, MDF, SeF (SEDF)	Cambodia			x						x		
Dipterocarpaceae	*Dipterocarpus*	*obtusifolius/ vestitus/ punctulatus*	Teijsm. ex Miq. / Wall. Ex Dyer/ Pierre	DDF	Cambodia, Thailand	x	x								x	x
Dipterocarpaceae	*Dipterocarpus*	*tuberculatus*	Roxb.	DDF, MDF	Cambodia, Thailand	x	x	x							x	x
Dipterocarpaceae	*Hopea*	*ferrea*	Laness.),	SEDF	Cambodia			x								
Dipterocarpaceae	*Hopea*	*odorata*	Roxb.	SEDF, SEDF (BRE), RiF	Cambodia		x	x								
Dipterocarpaceae	*Hopea*	*pierrei*	(Hance) Pierre	SEDF	Cambodia								x			
Dipterocarpaceae	*Hopea*	*recopei*	Pierre ex Laness.	SeF (SEDF)	Cambodia			x								

Continued...

Family	Genus	Species	Auth	Forest Unit	Region	A.	B.	C.	D.	E.	F.	G.	H.	I.	J.	K.
Dipterocarpaceae	*Shorea*	*cochinchinensis*	H. Baill	MDF	Cambodia			x								
Dipterocarpaceae	*Shorea*	*guiso*	(Blanco) Bl.	SwF	Cambodia					x						
Dipterocarpaceae	*Shorea*	*henryana*	Pierre	SEDF	Thailand		x									
Dipterocarpaceae	*Shorea*	*hypochra*	Hance	SeF (BRE)	Cambodia			x					x		x	x
Dipterocarpaceae	*Shorea*	*obtusa*	Wall	DDF, Intermediate MDF/SEDF	Cambodia, Thailand	x	x	x								
Dipterocarpaceae	*Shorea*	*roxburghii*	G.Don	SeF (SEDF), Intermediate SEDF/MDF	Cambodia			x							x	x
Dipterocarpaceae	*Shorea*	*siamensis*	Miq.	DDF, Intermediate SEDF/MDF	Cambodia, Thailand	x	x	x								
Dipterocarpaceae	*Shorea*	*talura/ laccifera(??)/ laurifolia(??)/ roxburghii(??)*	Roxb.	MDF	Cambodia			x		x			x			
Dipterocarpaceae	*Shorea*	*thorelii*	Pierre ex Laness.	SEDF	Thailand		x									
Dipterocarpaceae	*Vatica*	sp.		SeF (SEDF)	Cambodia			x								
Dipterocarpaceae	*Vatica*	*astrotricha*	Hance	SeF (SEDF)	Cambodia			x								
Ebenaceae	*Diospyros*	*bejaudii*	Lecomte	SeF (BRE), Intermediate SEDF/MDF	Cambodia			x								
Ebenaceae	*Diospyros*	*decandra*	Lour.	Intermediate SEDF/MDF	Cambodia			x								
Ebenaceae	*Diospyros*	*filipendula*	Pierre ex Lecomte	SeF (SEDF)	Cambodia			x								
Ebenaceae	*Diospyros*	*hasseltii*	Zoll.	Intermediate SEDF/MDF	Cambodia			x								
Ebenaceae	*Diospyros*	*helferi/pilosanthera*	C.B.Clarke/Blanco	MDF, RiF	Cambodia			x								
Ebenaceae	*Diospyros*	*hermaphroditica*	Zoll.	SeF (SEDF)	Cambodia			x								
Ebenaceae	*Diospyros*	*mollis*	Griff.	MDF	Mainland SE-Asia				x							
Ebenaceae	*Diospyros*	*montana*	Roxb.	MDF	Mainland SE-Asia				x							
Ebenaceae	*Diospyros*	*nitida*	Merrill	Intermediate SEDF/MDF	Cambodia			x								
Ebenaceae	*Diospyros*	*pemdula*	Hasselt ex Hassk.	MDF	Thailand		x									
Ebenaceae	*Diospyros*	spp.		MDF	Cambodia			x		x						
Elaeocarpaceae	*Elaeocarpus*	spp.		SwF, SeF (SEDF), SEDF	Cambodia			x								
Euphorbiaceae	*Antidesma*	*acidum*	Retz.	MDF	Thailand		x									
Euphorbiaceae	*Antidesma*	*cambodianum*	Gagnep.	SwF	Cambodia											
Euphorbiaceae	*Antidesma*	*ghaesembilla*	Gaertn.	MDF, SeF (SEDF)	Cambodia			x								
Euphorbiaceae	*Antidesma*	*montanum*	Bl. var. montanum	SwF	Cambodia					x						
Euphorbiaceae	*Aporusa*	*octandra*	(Buch.-Ham. ex D. Don)	DDF	Cambodia											

Continued...

Family	Genus	Species	Auth	Forest Unit	Region	A.	B.	C.	D.	E.	F.	G.	H.	I.	J.	K.
Euphorbiaceae	*Aporusa*	sp.		SeF (SEDF), SeF (BRE)	Cambodia			x		x						
Euphorbiaceae	*Aporusa*	*villosa/ glabrifolia/ sphaerosperma*	(Lindl.) Baill	DDF	Cambodia			x								
Euphorbiaceae	*Baccaurea*	*brateata*	M. A.	SwF	Cambodia											
Euphorbiaceae	*Baccaurea*	sp.		SEDF (SRE)	Cambodia			x								
Euphorbiaceae	*Croton*	*oblongifolius*	Roxb.	SeF (MDF)	Mainland SE-Asia				x							
Euphorbiaceae	*Croton*	sp.		SwF, MDF, SeF (SEDF)	Cambodia, Mainland SE-Asia			x	x	x						
Euphorbiaceae	*Glochidion*	*fagifolium*	(Müll.Arg.) Miq. ex Bedd	SeF (BRE)	Cambodia			x						x	x	
Euphorbiaceae	*Macaranga*	sp.			Cambodia					x						
Euphorbiaceae	*Macaranga*	*triloba*	(Reinw. ex Blume) Müll.Arg.	SwF	Cambodia											
Euphorbiaceae	*Mallotus*	*cochinchinensis*	Lour.	SeF (SEDF), Intermediate SEDF/MDF	Cambodia			x								
Euphorbiaceae	*Mallotus*	*macrostachys*	(Miq.) Müll.Arg.	SeF (MDF)	Mainland SE-Asia				x							
Euphorbiaceae	*Mallotus*	*philippensis*	(Lam.)	MDF	Mainland SE-Asia				x							
Euphorbiaceae	*Mallotus*	spp.		RiF	Cambodia			x		x						
Euphorbiaceae	*Suregada*			SeF (BRE)	Cambodia			x					x			
Euphorbiaceae (Phyllanthaceae)	*Cleistanthus*	*tomentosus*	Hance	SwF	Cambodia											
Euphorbiaceae (Phyllanthaceae)	*Phyllanthus*	*emblica*	L.	MDF	Cambodia		x									
Fabaceae	*Albizia*	*lebbek*	(L.) Benth	MDF, Intermediate SEDF/MDF	Cambodia, Mainland SE-Asia			x	x							
Fabaceae	*Butea*	*superba*	Roxb.	MDF	Mainland SE-Asia				x							

Continued...

Family	Genus	Species	Auth	Forest Unit	Region	A.	B.	C.	D.	E.	F.	G.	H.	I.	J.	K.
Fabaceae (Caesalpinioideae)	*Afzelia*	*xylocarpa (cochinchinensis)*	(Kurz.) Craib	SEDF (BRE), Intermediate SEDF/MDF, MDF	Cambodia, Thailand, Mainland SE-Asia		x	x	x							
Fabaceae (Caesalpinioideae)	*Bauhinia*	*malabarica*	Roxb.	MDF	Cambodia				x							
Fabaceae (Caesalpinioideae)	*Bauhinia*	*racemosa*	(Lam.)	MDF	Cambodia				x							
Fabaceae (Caesalpinioideae)	*Bauhinia*	sp.		SeF (SEDF), SeF (BRE)	Cambodia			x								
Fabaceae (Caesalpinioideae)	*Cassia*	*garretiana*	Craib	Intermediate SEDF/MDF	Cambodia			x							x	
Fabaceae (Caesalpinioideae)	*Cassia*	*javanica*	L.	SeF (BRE)	Cambodia			x					x			
Fabaceae (Caesalpinioideae)	*Cassia*	*siamensis*	Lam.	SEDF (BRE)	Cambodia			x	x							
Fabaceae (Caesalpinioideae)	*Crudia*	*chrysantha*	(Pierre) K.Schum	RiF	Cambodia			x								
Fabaceae (Caesalpinioideae)	*Cynometra*	*dongnaiensis*	Pierre	RiF	Cambodia			x					x			
Fabaceae (Caesalpinioideae)	*Peltophorum*	*pedatus*	(DC.) K. Heyne	SEDF (BRE), SeF (SEDF), Intermediate MDF/SEDF	Cambodia			x								
Fabaceae (Caesalpinioideae)	*Peltophorum*	*dasyrachis*	Kurz ex Baker	MDF	Mainland SE-Asia				x							
Fabaceae (Caesalpinioideae)	*Peltophorum*	*ferrugineum*	Benth	Intermediate SEDF/MDF, SeF (SEDF)	Cambodia			x								
Fabaceae (Caesalpinioideae)	*Sindora*	*cochinchinensis*	H. Baill	MDF, SEDF, Intermediate SEDF/MDF, SeF (SEDF)	Cambodia			x								
Fabaceae (Faboideae)	*Butea*	*monosperma*	(Lam.) Taub.	SeF (SEDF)	Cambodia			x		x						
Fabaceae (Faboideae)	*Dalbergia*	*cultrata*	Benth.	DDF, MDF	Thailand, Mainland SE-Asia		x		x				x			
Fabaceae (Faboideae)	*Dalbergia*	*nigrescens*	Pierre	MDF, Intermediate SEDF/MDF	Cambodia											

Continued...

Family	Genus	Species	Auth	Forest Unit	Region	A.	B.	C.	D.	E.	F.	G.	H.	I.	J.	K.
Fabaceae (Faboideae)	*Dalbergia*	*oliveri/ dongnaiense/ bariensis*	Gamble ex Prain	MDF, Intermediate SEDF/MDF	Cambodia, Thailand, Mainland SE-Asia		x	x	x							
Fabaceae (Faboideae)	*Dalbergia*	*ovata*	Benth.	MDF	Mainland SE-Asia				x							
Fabaceae (Faboideae)	*Dalbergia*	*rimosa*	Roxb.	MDF	Mainland SE-Asia				x							
Fabaceae (Faboideae)	*Dalbergia*	spp.		MDF	Cambodia	x				x						
Fabaceae (Faboideae)	*Derris*	*polyphylla*	Baker	SeF (BRE)	Cambodia			x								
Fabaceae (Faboideae)	*Desmodium*	spp.		MDF	Mainland SE-Asia				x							
Fabaceae (Faboideae)	*Millettia*	*brandisiana*	Kurz	MDF	Mainland SE-Asia				x							
Fabaceae (Faboideae)	*Millettia*	*erythrocalyx*	Gagnep.	Intermediate SEDF/MDF	Cambodia			x						x		
Fabaceae (Faboideae)	*Pterocarpus*	*macrocarpus (pedatus)*	Kurz	DDF, MDF, Intermediate SEDF/MDF, SEDF (BRE)	Thailand, Cambodia, Mainland SE-Asia		x		x							
Fabaceae (Mimosoideae)	*Acacia*	*harmandiana*	(Pierre) Gagnep.	RiF	Cambodia			x						x		
Fabaceae (Mimosoideae)	*Acacia*	*leucophloea*	(Roxb.)Willd.	MDF	Mainland SE-Asia				x							
Fabaceae (Mimosoideae)	*Adenanthera*	*pavonina/gersenii*	L./Scheffer	SEDF (BRE), Intermediate MDF/SEDF, MDF	Cambodia			x								
Fabaceae (Mimosoideae)	*Albizia*	*lucida*	(Roxb.) Benth.	MDF	Mainland SE-Asia				x							
Fabaceae (Mimosoideae)	*Albizia*	*procera*	(Roxb.) Benth.	Intermediate SEDF/MDF	Cambodia											
Fabaceae (Mimosoideae)	*Albizia*	sp.		SeF (SEDF)	Cambodia											
Fabaceae (Mimosoideae)	*Archidendron*	*clypearia*	F.Muell.	SwF	Cambodia											

Continued...

Family	Genus	Species	Auth	Forest Unit	Region	A.	B.	C.	D.	E.	F.	G.	H.	I.	J.	K.
Fabaceae (Mimosoideae)	*Dialium*	*cochinchinense*	Pierre	SEDF	Thailand		x									
Fabaceae (Mimosoideae)	*Xylia*	*dolabriformis/ xylocarpa/ kerrii*	Benth./Roxb.	DDF, MDF, Intermediate SEDF/MDF, SeF (SEDF)	Thailand, Cambodia	x	x	x								
Fagaceae	*Lithocarpus*	*dealbatus*	(Hook.f. and Thomson). Rehder	MDF	Thailand		x									
Fagaceae	*Quercus*	*kerrii*	Craib	MDF	Thailand		x									
Gentianaceae	*Fagraea*	*racemosa*	Jack ex Wall.	SwF	Cambodia					x						
Guttiferae	*Cratoxylum*	*formosum*	(Jack) Dyer	MDF, SeF (BRE), SeF (SEDF), Intermediate SEDF/MDF	Cambodia			x	x							
Guttiferae	*Cratoxylum*	*spp.*		SeF (SEDF)	Cambodia			x								
Guttiferae	*Mesua*	*ferrea*	L.	SEDF	Cambodia			x								
Irvingiaceae	*Irvingia*	*malayana/ harmandiana(?)/oliveri*	Oliv. ex A.W. Benn./van Tiegh. Pierre	MDF, SwF, SeF (BRE), Intermediate MDF/SEDF	Cambodia, Thailand		x	x		x			x			
Lamiaceae	*Congea*	*tomentosa*	Roxb.	MDF	Mainland SE-Asia				x							
Lamiaceae	*Hymenopyramis*	*brachiata*	Wall. ex Griff.	MDF	Mainland SE-Asia				x							
Lauraceae	*Cinnamomum*	*cambodianum*	Lecomte	SwF	Cambodia			x								
Lauraceae	*Cinnamomum*	*cassia*	(Nees & T.Nees) J.Presl	BRE (SEDF)	Cambodia			x								
Lauraceae	*Dehaasia*	*cuneata*	Blume	SEDF	Cambodia			x								
Lauraceae	*Dehaasia*	*cuneata*		SeF (SEDF)	Cambodia			x								
Lauraceae	*Litsea*	spp.		SwF	Cambodia					x						
Lauraceae	*Litsea*	*vang*	Lecomte	SEDF, BRE (SEDF)	Cambodia			x								
Lauraceae	*Phoebe*	*cuneata*		SeF (SEDF)	Cambodia			x								
Lecythidaceae	*Barringtonia*	*acutangula*	(L.) Gaertn.	RF	Cambodia			x								
Lecythidaceae	*Barringtonia*	*longipes/pauciflora*	Gagnep./King.	BRE (SEDF), Intermediate SEDF/BRE	Cambodia			x								
Lecythidaceae	*Barringtonia*	*racemosa*	(L.) Spreng.	MDF	Mainland SE-Asia				x							
Lecythidaceae	*Careya*	*sphaerica/ arborea*	Roxb.	MDF, SeF (SEDF)	Cambodia, Mainland SE-Asia			x	x					x*		x
Loganiaceae	*Strychnos*	sp.		RiF	Cambodia			x								
Lythraceae	*Lagerstroemia*	*angustifolia*	Pierre ex Laness.	Intermediate SEDF/MDF, SeF (BRE)	Cambodia			x								

Continued...

Family	Genus	Species	Auth	Forest Unit	Region	A.	B.	C.	D.	E.	F.	G.	H.	I.	J.	K.
Lythraceae	*Lagerstroemia*	*balansae*	Koehne	MDF	Thailand		x									
Lythraceae	*Lagerstroemia*	*calyculata*	Kurz	MDF, SEDF	Thailand		x									
Lythraceae	*Lagerstroemia*	*duperreana*	Pierre ex Gagnep.	MDF	Cambodia			x								
Lythraceae	*Lagerstroemia*	sp.			Cambodia								x	x	x	x
Lythraceae	*Lagerstroemia*	*speciosa*	(L.) Pers.	Intermediate SEDF/MDF, MDF	Cambodia, Mainland SE-Asia			x	x							
Lythraceae	*Lagerstroemia*	*tomentosa*	C.Presl	MDF	Mainland SE-Asia				x							
Lythraceae	*Lagerstromia*	*floribunda*	Jack	MDF	Mainland SE-Asia				x							
Lythraceae	*Lagerstromia*	spp.		MDF	Cambodia	x										
Lythraceae	*Lagerstromia*	*thorelli*	L.	SeF (BRE), MDF, Intermediate SEDF/MDF				x								
Lythraceae	*Lagerstromia*	*villosa*	Wall. ex Kurz	MDF	Mainland SE-Asia				x							
Malvaceae	*Hibiscus*			MDF	Mainland SE-Asia				x							
Malvaceae	*Hibisus*	*macrophyllus*	Roxb. ex Hornem.	BRE (SEDF)	Cambodia			x								
Malvaceae	*Sterculia*	*foetida*	L.	RF	Cambodia			x								
Malvaceae (Bombacaceae)	*Bombax*	*ceiba*	L.	MDF	Cambodia			x								
Malvaceae (Bombacaceae)	*Bombax*	*insigne*	Wall.	MDF	Cambodia, Thailand, Mainland SE-Asia		x	x	x				x		x	
Malvaceae (Sterculiaceae)	*Pterocymbium*	*campanulata*	Pierre	Intermediate SEDF/MDF, SeF SEDF/MDF	Cambodia			x								
Malvaceae (Sterculiaceae)	*Pterospermum*	*acerifolium*	(L.) Willd.	SeF (BRE)	Cambodia			x								
Malvaceae (Sterculiaceae)	*Pterospermum*	*diversifolium*	Blume	RiF	Cambodia			x								
Malvaceae (Sterculiaceae)	*Pterospermum*	*grewiaefolium*	Pierre	BRE (SEDF), Intermediate SEDF/BRE	Cambodia			x								
Malvaceae (Sterculiaceae)	*Sterculia*	*colorata*	(Roxb.) Burk.	Intermediate SEDF/MDF	Cambodia			x								

Continued...

Family	Genus	Species	Auth	Forest Unit	Region	A.	B.	C.	D.	E.	F.	G.	H.	I.	J.	K.
Malvaceae (Sterculiaceae)	*Sterculia*	*foetida*	L.	SwF	Cambodia			x								
Malvaceae (Sterculiaceae)	*Strychnos*	*nux-blanda*	A.W. Hill	DDF	Thailand		x									
Malvaceae (Sterculiaceae)	*Strychnos*	sp.		SeF (BRE), SeF (SEDF)	Cambodia			x								
Malvaceae (Tiliacea)	*Brownlowia*	*tabularis*	Pierre	BRE (SEDF), Intermediate SEDF/MDF	Cambodia			x								
Malvaceae (Tiliacea)	*Colona/Columbia*	*auriculata*	(Desf.) Craib	MDF, SeF (SEDF)	Cambodia			x								
Malvaceae (Tiliacea)	*Grewia*	*tomentosa*	Juss.	SeF (SEDF)	Cambodia			x								
Malvaceae (Tiliacea)	*Grewia/Microcos*	*paniculata/ tomentosa*	DC./Sm.	BRE (SEDF)	Cambodia			x								
Melastomataceae	*Melastoma*	*polyanthum*	Blume	SeF (SEDF)	Cambodia			x								
Melastomataceae	*Memecylon*	*edule*	Roxb.	MDF, SeF (SEDF)	Cambodia			x								
Melastomataceae	*Memecylon*	*laevigatum/ lilacinum*	Blume/ Zoll. & Moritzi	BRE (SEDF), Intermediate SEDF/MDF	Cambodia			x								
Melastomataceae	*Memecylon*	*laevigatum/ lilacinum*	Blume/ Zoll. & Moritzi	Intermediate SEDF/MDF	Cambodia			x								
Melastomataceae	*Memecylon*	*umbellatum*	Burm.f.	SwF	Cambodia					x						
Melastomataceae	*Pternandra*	*caerulescens*	Jack ex Wall.	SwF	Cambodia					x						
Meliaceae	*Aglaia*	*gigantea*	Pierre Pellegr.	SEDF (BRE)	Cambodia			x								
Meliaceae	*Aglaia*	sp.		SwF	Cambodia					x						
Meliaceae	*Azadirachta*	*indicta*	A. Juss	Intermediate SEDF/MDF	Cambodia			x								
Meliaceae	*Melia*	*azedarach*	L.	SeF (BRE)	Cambodia			x								
Meliaceae	*Toona*	*sureni (febrifuga)*	(Blume) M. Roem	Intermediate SEDF/MDF, BRE (SEDF)	Cambodia			x								
Moraceae	*Antiaris*	*toxicaria*	Lesch.	BRE (SEDF)	Cambodia			x								
Moraceae	*Artocarpus*	*sampor*	Gagnep. / Merr	MDF, BRE (SEDF)	Cambodia			x								
Moraceae	*Ficus*	*geniculata*	Kurz	MDF	Thailand		x									
Moraceae	*Ficus*	spp.		BRE (SEDF), Intermendiate SEDF/MDF, RiF	Cambodia			x								
Moraceae	*Streblus*	*asper*	Lour.	Intermediate SEDF/MDF, SeF (SEDF), MDF	Cambodia			x								
Musaceae	*Musa*	sp.			Cambodia				x					x		

Continued...

Family	Genus	Species	Auth	Forest Unit	Region	A.	B.	C.	D.	E.	F.	G.	H.	I.	J.	K.
Musaceae	*Musa*	*sylvestris*	(Lour.) Colla	SeF (BRE)	Cambodia			x								
Myristicaceae	*Horsfieldia*	*glabra*		BRE (SEDF)	Cambodia			x								
Myristicaceae	*Myristica*	*iners*	Blume	SwF	Cambodia					x						
Myrtaceae	*Eugenia*	*cambodiana*	Gagnep.	RiF	Cambodia			x								
Myrtaceae	*Eugenia*	spp		SwF, MDF, SeF (SEDF)	Cambodia			x		x						
Myrtaceae	*Rhodamnia*	*rubescens*	(Benth.) Miq.	SeF (SEDF)	Cambodia			x								
Myrtaceae	*Streblus*	sp.		SeF (SEDF)	Cambodia			x								
Myrtaceae	*Syzygium*	*claviflorum*	(Roxb.) Wall. ex Steud.	MDF	Mainland SE-Asia				x							
Myrtaceae	*Syzygium*	*cuminii*	(L.) Skeels.	MDF	Thailand, Cambodia		x						x			x
Oleaceae	*Schrebera*	sp.		Intermediate SEDF/MDF	Cambodia											
Orchidaceae	*Habernaria*			MDF	Mainland SE-Asia				x							
Pinaceae	*Pinus*	*kesiya*	Royle ex Gordon	PF	Thailand		x									
Pinaceae	*Pinus*	*merkusii*	Jungh. & de Vriese	PF	Thailand		x									
Poaceae	*Andropogon*			MDF	Mainland SE-Asia				x							
Poaceae	*Bambusa*	*arundinacea*		MDF/DDF transition	Mainland SE-Asia				x							
Poaceae	*Bambusa*	*tuida*	Roxb.	MDF	Mainland SE-Asia				x							
Poaceae	*Cephalostachyum*	*pergracile*	Munro	mdF	Mainland SE-Asia				x							
Poaceae	*Dendrocalamus*	*membranaceus*	Munro	MDF	Mainland SE-Asia				x							
Poaceae	*Dendrocalamus*	*strictus*	(Roxb.) Nees	SeF (MDF), MDF	Mainland SE-Asia				x							
Poaceae	*Eragrostis*			MDF	Mainland SE-Asia				x							
Poaceae	*Gigantochloa*	*albociliata*	(Munro) Kurz	MDF, SeF (MDF)	Mainland SE-Asia				x							
Poaceae	*Imperata*	*cylindrica*	(L.) P.Beauv.	Grassland	Cambodia			x								
Poaceae	*Imperata*			MDF	Mainland SE-Asia				x							

Continued...

Family	Genus	Species	Auth	Forest Unit	Region	A.	B.	C.	D.	E.	F.	G.	H.	I.	J.	K.
Poaceae	*Saccharum*			MDF	Mainland SE-Asia				x							
Poaceae	*Themeda*			MDF	Mainland SE-Asia				x							
Poaceae	*Thyrosostachys*	*siamensis*		MDF/DDF transition	Mainland SE-Asia				x							
Rhamnaceae	*Ziziphus*	*cambodiana*	Pierre	SeF (SEDF)	Cambodia			x								
Rhamnaceae	*Zizyphus*	*cambodiana*	Pierre	SeF (SEDF)	Cambodia			x								
Rhizophoraceae	*Carallia*	*brachiata*	Merr.	SwF	Cambodia			x								
Rhizophoraceae	*Carallia*	*lucida/brachiata*	Roxb./(Lour.) Merr.	Intermediate SEDF/SEDF	Cambodia			x						x		
Rubiaceae	*Adina (Neonauclea)*	*sessilifolia*	(Roxb.) Hook.f. ex Brandis/ (Roxb.) Merr.	MDF	Cambodia			x								
Rubiaceae	*Gardenia*	*angkoriensis*	Pit.	Intermediate SEDF/MDF	Cambodia			x								
Rubiaceae	*Gardenia*	*coronaria*	Buch.-Ham.	MDF	Mainland SE-Asia				x							
Rubiaceae	*Gardenia*	*philastrei*	Pierre ex Pit.	MDF, SeF (SEDF)	Cambodia			x								
Rubiaceae	*Haldina (Adina)*	*cordifolia*	(Roxb.) Ridsdale	MDF	Cambodia, Mainland SE-Asia			x	x							
Rubiaceae	*Hymenodictyon*	*excelsum*	(Roxb.) Wall.	Intermediate SEDF/MDF	Cambodia			x								
Rubiaceae	*Ixora*	sp.		DDF/MDF	Cambodia											x
Rubiaceae	*Morinda*	*persicaefolia*		RiF	Cambodia			x								
Rubiaceae	*Morinda*	spp.		MDF	Cambodia			x								
Rubiaceae	*Nauclea*	*officinalis*	(Pierre ex Pit.) Merr. & Chun	SF	Cambodia							x				
Rubiaceae	*Nauclea*	*orientalis*	(L.) L.	RiF, SF	Cambodia			x								
Rubiaceae	*Randia*	*tomentosa*	Wight & Arn.	MDF	Cambodia			x								
Rubiaceae	*Uncaria*	*homomalla*	Miq.	SEDF, RiF	Cambodia							x				
Salicaceae	*Homalium*	*tomentosum*	(Vent.) Benth.	MDF	Mainland SE-Asia				x							
Sapindaceae	*Dimocarpus*	*longan*	Lour.	SEDF	Thailand		x									
Sapindaceae	*Lepisanthes*	sp.		SeF (SEDF)	Cambodia			x								
Sapindaceae	*Nephelium*	*chryseum*	L.	BRE (SEDF), Intermediate SEDF/MDF, SeF (SEDF)	Cambodia			x								
Sapindaceae	*Schleichera*	*oleosa*	Lour.	BRE (SEDF), SeF (BRE), Intermediate SEDF/MDF, MDF	Cambodia, Thailand		x	x								

Continued...

Family	Genus	Species	Auth	Forest Unit	Region	A.	B.	C.	D.	E.	F.	G.	H.	I.	J.	K.
Sapindaceae	*Xerospermum*	*noronhianum*	Blume	SwF	Cambodia					x						
Sapotaceae	*Madhuca (Payena)*	*elliptica*	(Pierre ex Dubard) H.J.Lam.	SeF (SEDF)	Cambodia			x								
Simaroubaceae	*Brucea*	*javanica*	(L.) Merr	SeF (BRE)	Cambodia			x								
Simaroubaceae	*Samandura*	*harmandiana*	Pierre	RiF	Cambodia			x								
Tetrameleaceae	*Tetrameles*	*nudiflora*	R. Br.	SEDF (BRE), Intermediate SEDF/MDF	Cambodia			x				x	x	x		
Ulmaceae	*Aphananthe*	*cuspidata*	(Bl.) Planch	SEDF	South-east Asia											
Ulmaceae	*Holoptelea*	*integrifolia*	Roxb.	MDF	Thailand						x					
Ulmaceae/ Cannabaceae [reclassified]	*Trema*	*angustifolia*	(Planch.) Blume	SeF (BRE), SeF (MDF)	Cambodia			x	x							
Ulmaceae/ Cannabaceae [reclassified]	*Trema*	*velutina/tomentosa*	Blume/ (Roxb) Hara	SEDF, MDF	Cambodia			x				x				
Urticaceae	*Laportea*	sp.		BRE (SEDF)	Cambodia			x								
Verbenaceae	*Gmelina*	*arborea*	Roxb.	MDF	Mainland SE-Asia			x								
Verbenaceae	*Gmelina*	*asiatica*	L.	RiF	Cambodia			x								
Verbenaceae	*Vitex*	*canescens*	Kurz	MDF	Mainland SE-Asia				x							
Verbenaceae	*Vitex*	*limonifolia*	Wall. ex C.B.Clarke	MDF	Thailand		x									
Verbenaceae	*Vitex*	*peduncularis*	Wallich ex Schauer	DDF	Thailand		x									
Verbenaceae	*Vitex*	*pinnata/ pubescens*	L./Vahl	MDF, Intermediate SEDF/MDF, MDF	Cambodia, Mainland SE-Asia		x	x	x							
Verbenaceae	*Vitex*	sp.		SeF (SEDF)	Cambodia			x								
Xanthophyllaceae	*Xanthophyllum*	*glaucum*	Wall.	RiF	Cambodia			x								
Zingiberaceae	*Boesenbergia*			MDF	Mainland SE-Asia				x							
Zingiberaceae	*Curcuma*	*longa*		SeF (SEDF)	Cambodia			x								
Zingiberaceae	*Curcuma*			MDF	Mainland SE-Asia				x							
Zingiberaceae	*Zingiber*	spp.		MDF	Cambodia		x									x

C Radiocarbon Dating

The following technique was applied in attempt to extract a terrestrial signal from core sediments for radiocarbon dating.

C.1 Methods

C.1.1 Concentration of pollen from lacustrine sediments using heavy liquid separation — after Vandergoes and Prior (2003)

Chemical treatment

Removal of carbonates

1. Place each sediment sample (2.5-4 g dry weight) into individual, clean and appropriately labelled 50 ml centrifuge tubes.
2. Add 20 ml 10% HCL to each sample and mix with a vortex mixer.
3. Place samples into a hot water bath at 80 °C for 10 minutes.
4. Remove from bath and fill each sample tube with DI water.
5. Centrifuge for 5 minutes at 3 000 rpm. Decant supernatant.

Removal of silicates

6. Wearing appropriate safety equipment, add 10 ml 40-55% HF to each sample. Cap tightly and mix with a vortex mixer.
7. Loosen caps slightly, and place samples into a near boiling hot water bath for 60 minutes, mixing every 5-10 minutes.
8. Carefully remove samples from bath and fill sample tubes with DI water.
9. Centrifuge for 5 minutes at 3 000 rpm. Decant supernatant into appropriate HF disposal unit.
10. Repeat steps 8 and 9 three times to clean samples of HF residue.

Removal of organic residue

11. Add 20 ml of 10% nitric acid to each sample, mix with a vortex mixer and allow to stand for 2 minutes.
12. Fill each sample tube with DI water.
13. Centrifuge for 5 minutes at 3 000 rpm. Decant supernatant.

Removal of unsaturated humic colloids

14. Add 25 ml of 10% KOH to each sample and mix with a vortex mixer.
15. Place samples into a hot water bath at 80°C for 10-20 minutes.
16. Remove from bath and fill each sample tube with DI water.
17. Centrifuge for 5 minutes at 3000 rpm. Decant supernatant.

Sieving

18. Pass each sample through a thoroughly cleaned 105 μm mesh sieve using DI water. Place the <105 μ fraction back into the appropriate centrifuge tube.
19. Centrifuge samples for 5 minutes at 3 000 rpm. Decant supernatant.

Density (heavy liquid) separation

20. Add 30 ml LST (2.1 sg) to the <105 μm sample fraction. Mix well. Centrifuge at 3 500 rpm for 5 minutes.
21. Decant supernatant into a separate, labelled and clean centrifuge tube — allow to stand (light fraction), leaving the concreted precipitate in the original sample tube (heavy fraction).

Heavy fraction

22. Fill the heavy fraction sample tube with DI water, mix using the vortex mixer and centrifuge sample for 5 minutes at 3 000 rpm. Decant supernatant.
23. Use a glass pipette to place precipitate into a microvial labelled with the depth and density of the LST used. Cap and set aside.
24. Clean 50 ml sample tube using DI water.

Light fraction

25. Once the floating organic matter is sitting on top of LST in the light fraction centrifuge tube, pour the organic "float" off into the original, cleaned sample tube for that depth. Try to minimise amount of LST poured out with sample. Once floating organics have been separated, decant remnant LST into a clean, large bottle so that it can be recycled.
26. Dilute heavy liquid fraction by filling tube with DI water.
27. Centrifuge at 3 500 rpm for 5 minutes.
28. Once organics have settled, decant dilute LST into the recycle bottle.
29. Repeat steps 20-28 seven times using the settled "light fraction" from the previous separation (i.e. the precipitate retained at the end of step 28), decreasing the density of the LST used to the following sg values — 1.6, 1.4, 1.3, 1.25, 1.2, 1.15, 1.1

Microscopic analysis

30. Place an aliquot of each sample onto a clean glass slide and visually estimate the percentage of pollen:organic residue retained in the extracted pollen sample.

C.1.2 Laboratory treatment of macro-charcoal samples

Extraction: Batch 1

Sieving

1. Pass each sediment sample through a thoroughly cleaned 250μm mesh sieve using DI water. Retain the <250 μm fraction and place into clean, labelled 50 ml centrifuge tubes.
2. Centrifuge samples for 5 minutes at 3 000 rpm. Decant excess water.

Removal of silicates

3. Wearing appropriate safety equipment, add 10 ml 50% HF to each sample. Cap tightly and mix with a vortex mixer.
4. Loosen caps slightly, and place samples into a 60 °C hot bath for 40 minutes.
5. Carefully remove samples from bath and fill sample tubes with DI water.
6. Centrifuge for 5 minutes at 3 000 rpm. Decant supernatant into appropriate HF disposal unit.
7. Rinse with DI water three times to clean samples of HF residue.

Sample consolidation

8. Label clean 1.5 ml micro-centrifuge tube vials with appropriate sample depths and fraction sizes.
9. Using a disposable glass pipette, collect the material from the 50 ml centrifuge tubes and place into the 1.5 ml tubes.
10. Cap the micro-tube and centrifuge at 1500 rpm for 3 minutes. Decant using disposable glass pipette.

Extraction: Batch 2

Sieving

11. Pass each sediment sample through a thoroughly cleaned, stacked 250 μm and 105 μm mesh sieves using DI water. Retain the <250 μm and 105-250 μm fractions and place into clean, labelled 50 ml centrifuge tubes.
12. Centrifuge samples for 5 minutes at 3 000 rpm. Decant excess water.

Removal of unsaturated humic colloids

13. Add 10 ml of 10% KOH to each sample and mix with a vortex mixer.
14. Place samples into a hot water bath at 80 °C for 30 minutes.
15. Remove from bath and fill each sample tube with DI water.
16. Centrifuge for 5 minutes at 3 000 rpm. Decant supernatant.

Oxidation of organics

17. Add 5 ml of 6% NaClO to each sample tube and mix with a vortex mixer.
18. Leave sample to stand for 10 minutes.
19. Fill sample tubes with DI water.
20. Centrifuge for 5 minutes at 3 000 rpm. Decant supernatant.

Removal of silicates

21. Wearing appropriate safety equipment, add 10 ml 50% HF to each sample. Cap tightly and mix with a vortex mixer.
22. Loosen caps slightly, and place samples into a 60 °C hot bath for 40 minutes.
23. Carefully remove samples from bath and fill sample tubes with DI water.
24. Centrifuge for 5 minutes at 3 000 rpm. Decant supernatant into appropriate HF disposal unit.
25. Rinse with DI water three times to clean samples of HF residue.

Sample consolidation

26. Label clean 1.5 ml micro-centrifuge tube vials with appropriate sample depths and fraction sizes.
27. Using a disposable glass pipette, collect the material from the 50 ml centrifuge tubes and place into the 1.5 ml tubes.
28. Cap the micro-tube and centrifuge at 1500 rpm for 3 minutes. Decant using disposable glass pipette.

C.1.3 Extraction of plant lipids (*n*-alkanes) from sediment via sonication

Standard

Mix 50 μL squalane with DCM to a total volume of 10 ml.

Procedure

Glassware preparation

1. Soak all glassware in detergent bath (alkaline cleaning agent) for 3 hours. Wash well, rinse with DI water, rinse with hexane.
2. Place all glassware in furnace.
3. Heat to 550 °C and anneal all glassware (beakers, flasks, pipettes and vials) at full temperature for an hour. Allow to cool to room temperature (approx. 4 hours).

Preparation of sediment sample for sonication

4. Weigh annealed sample vessel (glass beaker or 100 ml glass centrifuge tube).
5. Place an aliquot of sediment (approx. equivalent 2 g dry weight) into vessel.
6. Freeze overnight.
7. Freeze-dry sample until moisture has been removed from sample (approx. 6 hours).
8. Weigh dry sample and remove any excess as necessary.

Sonication of Sample

9. Prepare squalane standard by diluting 50 μL squalane with 10 ml DCM.
10. Add 2 μl internal standard to sample jar.
11. Add 50 ml of DCM:MeOH (9:1). Cover with aluminium foil.
12. Place sample in sonication bath and sonicate for 15 minutes.
13. Separate lipid extract by centrifuging.
14. Sonicate a grade 1 filter paper in DCM:MeOH (9:1) for 15 minutes. Allow to dry.
15. Decant lipid extract through prepared filter paper into a round bottom flask.
16. Repeat steps 11-15 five times.

Concentration of lipid extract

17. Prepare rotary evaporator by cleaning in solvent and annealing glass adaptors.
18. Set up according to safety instruction for model.
19. Place sample into rotary evaporator to evaporate solvent under reduced pressure until 1-2 ml remains.
20. Transfer remaining total lipid extract into a glass microvial using annealed Pasteur pipette.
21. Wrap vials in foil and loosely cover samples with foil. Place in to dry.
22. Weigh samples.
23. Prepare a short silica column in a Pasteur pipette. Recommended specs: 0.063-0.200 mm granule size with a 70-230 mesh ASTM from MERCK (107734).
24. Rinse column with hexane.
25. Add 2 ml of hexane to total lipid extract using Pastuer pipette. Mix.
26. Label and weigh empty vial with lid. Record weight.

27. Pass the hexane/lipid extract mix through the silica column and collect in pre-weighed vial. Repeat 5 times.
28. Wash 2 ml hexane through the column into vial to elute remaining *n*-alkanes.
29. Evaporate hexane from sample under stream of N_2 gas (or cover with foil and leave to evaporate).
30. Once dry, cap sample and record weight.

Preparation of Blanks

31. Prepare one solvent blank (using internal standard passed through a sonicated filter paper) and one sonicated filter paper blank per extraction.

C.2 Results

C.2.1 Concentration of pollen from lacustrine sediments using heavy liquid separation

Results of the microscopic component based analysis for the plant microfossil heavy liquid separations attempted for selected YL1211B and YM0413B samples are shown on table C.1. Amorphous algae (sapropel) and other structured organics were the dominant materials found in all samples assessed across all density classes. Pollen and spore percentages across all samples account for a maximum of 10% of sample materials, with slightly higher concentrations found in samples extracted at 1.2 to 1.4 s.g.

TABLE C.1: Results of microscopic component analysis of radiocarbon dating plant microfossil samples processed using heavy lipid separation. The relative proportion of materials is estimated for the eight density separates produced for each sample

Core	sample depth (cm)	s.g.	amorphous algae	structured organics	silica (%)	spone spicules (%)	charcoal (%)	pollen (%)	fungal matter (%)
YM0413B	521 to 522	2.02	45	0	45	3	5	0	2
		1.6	80	0	0	0	15	0	5
		1.4	90	0	0	0	5 to 10	<1	2
		1.3	60	25	0	0	5 to 10	5 to 10	2
		1.25	55	35	0	0	5	<5	2
		1.2	50	0	20	0	15	10	0
		1.15	50	40	0	0	5	<1	0
		1.1	55	40	0	0	0	5	0
	100 to 101	2.02	65	20	10	<1	5	<2	<2
		1.6	80	10	0	<1	10	0	<2
		1.4	45	40	0	0	5	<1	5
		1.3	40	50	0	0	5	<1	5

Continued...

Core	sample depth (cm)	s.g.	amorphous algae	structured organics	silica (%)	spone spicules (%)	charcoal (%)	pollen (%)	fungal matter (%)
		1.25	40	50	0	0	5	<1	5
		1.2	15	80	0	0	<5	<1	<1
		1.15	85	10	0	0	5	0	0
		1.1	insufficient sample size						
YL1211B	35.5 to 36.5	2.02	65	10	<5	0	20	2	<2
		1.6	65	15	0	0	15	0	5 to 10
		1.4	75	15	0	0	5	0	<2
		1.3	90	5	0	0	<5	<2	0
		1.25	100	0	0	0	0	0	0
		1.2	90	0	0	0	1 to 2	1 to 2	0
		1.15	95	5	0	0	0	0	0
		1.1	insufficient sample size						
	101.0 to 102.0	2.02	40	40	<5	0	15	<2	<2
		1.6	40	40	0	0	20	2	0
		1.4	85	10	0	0	5	0	<2
		1.3	85	10	0	0	<5	2	0
		1.25	90	0	0	0	<4	3	0
		1.2	95	0	0		<2	3	0
		1.15	82	15	0	0	0	2 to 3	0
		1.1	85	15	1	1	1	<1	0
	146 to 147	2.02	40	40	0	0	15	<1	<2
		1.6	40	40	0	0	15	0	5
		1.4	60	30	0	0	5	<1	2
		1.3	95	5	0	0	<1	<1	0
		1.25	90	5	0	0	<1	3	0
		1.2	95	3	0	0	<1	1	0
		1.15	90	5	0	0	<1	<1	0
		1.1	85	10	0	0	<1	<1	0
	188 to 189	2.02	55	30	<2	0	15	<1	<3
		1.6	65	25	0	0	15	<1	<3
		1.4	90	5	0	0	<5	1	<1
		1.3	95	<5	0	0	<2	<1	<1
		1.25	80	10	0	0	3	5	<1
		1.2	85	10	0	0	<1	3	<1
		1.15	100	<1	0	0	<1	<1	<1
		1.1	100	<1	0	0	<1	<1	<1
	202.5 to 203.5	2.02	70	10	5	5	10	0	0
		1.6	50	40	0	0	10	<1	2
		1.4	45	45	0	0	5	2	0
		1.3	55	30	0	0	5	15	<1
		1.25	70	20	0	0	<5	3 to 5	<1
		1.2	75	20	0	0	2	2	<1
		1.15	80	20	<1	<1	<1	<1	<1
		1.1	insufficient sample size						

A photograph of the most concentrated pollen and spore sample encountered from this procedure is shown in figure C.1. Due to the low percentage of plant microfossils within the samples, none were used for radiocarbon dating.

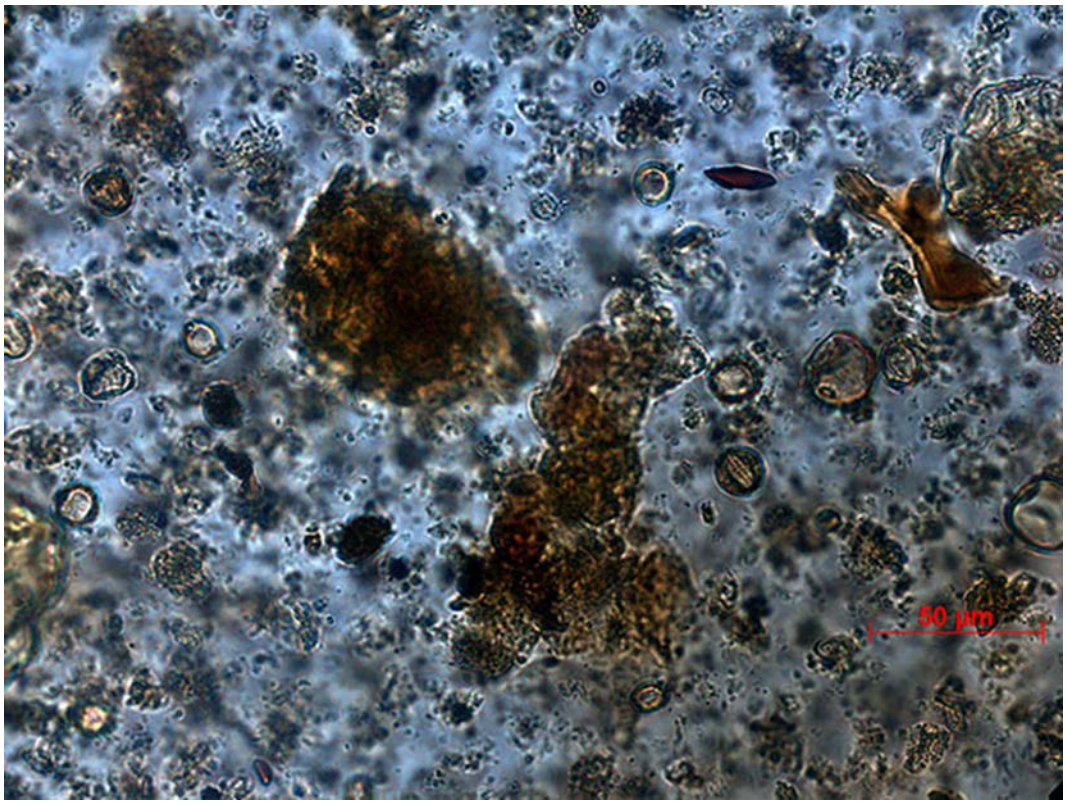

FIGURE C.1: Photograph of pollen and spore concentrate from YL1211B sediments at 202.5 to 203.5cm depth extracted using heavy liquid separation techniques (1.3 s.g.). This sample represents the highest pollen and spore concentrate of all the samples processed for extraction

C.2.2 Extraction of plant lipids from sediment

The low extract yield from all samples processed for lipid extraction complicated by technical issues associated with the equipment needed for further analysis of the samples meant that none of the extracts were processed for radiocarbon dating. The final mass of extracted lipid extracts and internal standards is shown on table C.2.

TABLE C.2: Extract mass for samples and blanks processed for plant lipid extraction.

Sample	sample depth (cm)	sample dry mass (g)	pre-hexane extract mass (mg)	post-hexane extract mass (mg)
Solvent Blank			0	0.1
Filter Paper Blank			0	0.9
YL1211B	65.5	1.1207	349.2	4.4
YL1211B	123.5	1.6644	566	2.3
YL1211B	200.5	1.007	318.8	1.7
YM0413B	536	1.5955	119.5	2.0

D Environmental Magnetism

D.1 Mass Specific Magnetic Susceptibility Volumetric Experiment

D.1.1 Methods

Two dried and crushed sediment samples from YL1211A and YO0712B were processed to characterise the significance of using a lower than recommended sample volume for assessment of YL1211B χlf and χfd$_{\%}$. These samples were selected both opportunistically (they were left over from processing for chronological analysis), and due to the fact that they were presumed to be similar to those assessed from YL1211B in terms of grain size, magnetism and sedimentary make-up. The selected samples include YO0712C (100 to 101 cm) termed **YOC 100** and YL1211A (15.5 to 17.5 cm) termed **YLA 15.5**.

Where necessary, sample sediments were disaggregated into individual particle sizes using a mortar and pestle and placed into pre-weighed, appropriately labelled 10 cm^3, cylindrical plastic pots designed for the Bartington MS2B Dual Frequency Magnetic Susceptibility Meter (Dearing 1999). The sediments were very lightly compacted to remove any air gaps and the sediment weight and volume recorded. YOC 100 was assessed at volumes of a) 10 cm^3; b) 6.1 cm^3; c) 5.1 cm^3; d) 4.1 cm^3; and, e) 2.9 cm^3, and YLA 15.5 was tested at volumes of a) 6.1 cm^3 and b) 3.9 cm^3. A Bartington MS2B Dual Frequency Magnetic Susceptibility Meter was then used to determine the χlf (0.46 kHz magnetic field) and χhf (mass specific high frequency magnetic susceptibility [4.6 kHz magnetic field]) for each sample volume size. From these calculations, the percentage frequency dependence (χfd$_{\%}$) was calculated for each sample measurement using Barsoft software, which automatically divides the change in susceptibility per decade frequency by the χlf measurement.

Samples were set to run in triplicates for both frequencies, with 5 second sample measurements and blank (air) measurements taken at the start, end, and between χlf and χhf measurements. This processes was repeated between 2 and 4 times for YOB 100 samples (n=6-12). No repeat measurements were taken for the two YLA 15.5 sample volumes as results fell outside of the maximum resolution of the MS2B Dual Frequency Meter (2 x 10^{-6} SI).

Sample Analysis

The mean χlf χhf and χfd$_{\%}$ values returned from each sample volume were plotted as a scatter graph fitted with a trend line to determine the relationship between volume and χlf SI (and hence χfd$_{\%}$) for each sediment sample. A student's t-test was then used to assess the significance of changing volume fractions onχlf andχfd$_{\%}$ for each sediment sample.

D.1.2 Results

Relationship between volume and χlf and χfd$_{\%}$ values

The results of mass-specific magnetic susceptibility tests applied to YOC 100 and YLA 15.5 samples are presented in figure D.1 and table D.1. Tests conducted on both samples indicate that as sample volume size decreases, χlf SI declines and χfd$_{\%}$ increases linearly. This confirms the assertion made by Dearing (1999) that the χlf of small-volume samples will be underestimated, thereby overestimating χfd$_{\%}$. While the mean of YOB 100 measurements taken at 6.1 cm^3 and 4.1 cm^3 show a minor reversal in this trend (probably due to experimental error), the χlf and χfd$_{\%}$ measurements appear to display a linear trend with reducing volume size (R^2= 0.86 and 0.90 respectively). Specifically, χlf SI decreases at a rate of approximately 11% per cubic centimeter, while χfd$_{\%}$ increased by 2.11% per cubic centimeter. The rate of change calculated from the two volume-points measured for YLA 15.5 was much greater, with χfd$_{\%}$ found to increase at a rate of 15.5%, and χlf SI decreasing by 20% per cubic centimeter. These results indicate that rate of change across volume size may be reliant on sample type or magnetism. However, there may be a large degree of experimental error associated with these findings, particularly with respect to the YLA 15.5 sample, due to the fact that 1) a small experimental sample size was used in this experiment, and 2) the χlf SI values measured from YLA 15.5 falls outside of the maximum resolution of the MS2B Dual Frequency Meter (2 x 10^{-6} SI).

Significance of volume-size on χlf and χfd$_{\%}$ values

A minimum of 9 χlf, and χfd$_{\%}$ measurements from each YOB 100 volume size (10 cm^3, 6.1 cm^3, 4.1 cm^3 and 2.9 cm^3) were compared using a two-tailed student's t-test. Three samples at 6.1 cm^3 and 3.1 cm^3 were compared from YLA 15.5. Results of this analysis are presented in table D.2, and demonstrate that the χlf, and χfd$_{\%}$ values returned for all volume sizes are all significantly different from each other. This includes comparison of 6.1 cm^3 vs. 10 cm^3 χlf, and χfd$_{\%}$ values from YOB 100, suggesting that, in the context of the crater lake sediments, taking 5.7 cm^3 as a minimum volume threshold value for mass specific magnetic susceptibility (as suggested by Dearing (1999)), must be approached with caution.

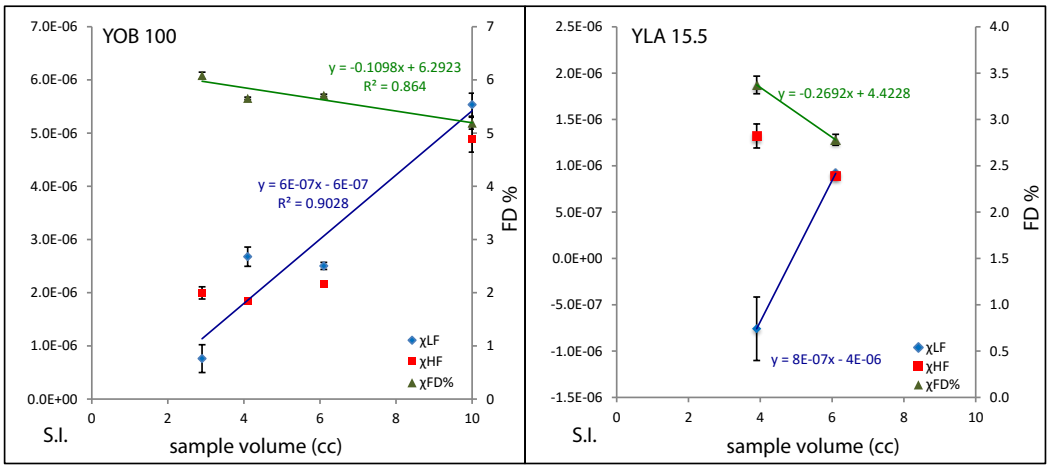

FIGURE D.1: Plots showing impact of changing volume size on χlf, χhf and χfd$_{\%}$ measurements for samples YOB 100 and YLA 15.5.

TABLE D.1: Summary of mass-specific magnetic susceptibility results showing the mean and standard deviation for χlf, χhf and χfd$_{\%}$ measurements taken for each sample volume size.

sample ID	sample volume (cm^3)	n	χlf	χhf	χfd$_{\%}$
YOB 100	10	4 (×3)*	$5.53 \times 10^{-6} \pm 2.16 \times 10^{-7}$	$4.88 \times 10^{-6} \pm 2.4 \times 10^{-7}$	5.19 ± 0.11
YOB 100	6.1	4 (×3)	$2.5 \times 10^{-6} \pm 6.7 \times 10^{-8}$	$2.17 \times 10^{-6} \pm 2.0 \times 10^{-8}$	5.71 ± 0.2
YOB 100	4.1	2 (×3)	$2.7 \times 10^{-6} \pm 1.8 \times 10^{-7}$	$1.84 \times 10^{-6} \pm 3.8 \times 10^{-9}$	5.65 ± 0.02
YOB 100	2.9	2 (×3)	$7.61 \times 10^{-7} \pm 2.9 \times 10^{-7}$	$1.99 \times 10^{-6} \pm 1.2 \times 10^{-7}$	6.08 ± 0.06
YLA 15.5	6.1	1 (×3)	$9.17 \times 10^{-7} \pm 2.5 \times 10^{-9}$	$8.9 \times 10^{-7} \pm 1.1 \times 10^{-9}$	2.78 ± 0.06
YLA 15.5	3.9	1 (×3)	$-7.59 \times 10^{-7} \pm 3.4 \times 10^{-7}$	$1.32 \times 10^{-6} \pm 1.3 \times 10^{-7}$	3.37 ± 0.1

* (×3) represents the triplicate measurements taken from each sample run

TABLE D.2: Results of two-tailed student's t-test comparing χlf, and χfd$_{\%}$ results for different volume sizes (95% C.I.).

		χlf					χfd$_{\%}$				
		10 cm^3	6.1 cm^3	4.1 cm^3	3.9 cm^3	2.9 cm^3	10 cm^3	6.1 cm^3	4.1 cm^3	3.9 cm^3	2.9 cm^3
6.1 cm^3	**sample**	YOB 100	n/a	YOB 100	YLA 15.5	YOB 100	YOB 100	n/a	YOB 100	YLA 15.5	YOB 100
	df	11		9	2	9	11		9	2	9
	t Stat	-10.8		-3.2	4.2	8.0	-6.0		-0.4	-3.8	-11.5
	t Critical two-tail	2.2		2.3	4.3	2.3	2.2		2.3	4.3	2.3
4.1 cm^3	**sample**	YOB 100	YOB 100	n/a	n/a	YOB 100	YOB 100	YOB 100	n/a	n/a	YOB 100
	df	8	9			8	8	9			8
	t Stat	8.0	-3.2			8.0	-3.2	-0.4			-18.6
	t Critical two-tail	2.3	2.3			2.3	2.3	2.3			2.3
3.9 cm^3	**sample**	n/a	YLA 15.5	n/a	n/a	n/a	n/a	YLA 15.5	n/a	n/a	n/a
	df		2					2			
	t Stat		4.2					-3.8			
	t Critical two-tail		4.3					4.3			
2.9 cm^3	**sample**	YOB 100	YOB 100	YOB 100	n/a	n/a	YOB 100	YOB 100	YOB 100	n/a	n/a
	df	8	9	9			8	9	9		
	t Stat	12.8	12.5	8.0			-21.4	-11.5	-18.6		
	t Critical two-tail	2.3	2.3	2.3			2.3	2.3	2.3		

D.2 Correlation of Yeak Loam and Yeak Oam master and replicate core κSI records

D.2.1 Methods

Relative peaks and troughs in the κSI records for each master core were matched to those found in their respective replicate cores in order to provide depth-matching (tie-point) constraints for CPL slotting (which otherwise assumes that the records are a similar length). Eight points (a to h) were tied in the YL1211A-YL1211B record pair shown in table D.3. Due to the number of "no core" gaps in the YO0712B record, and the large difference in the magnitude of the κSI values obtained for the master and replicate record, it was more challenging to visually identify tie-points in the Yeak Oam records. However, nine tentative points were selected as potential constraints (a to i) shown in table D.3.

TABLE D.3: Results of CPL slot correlation using selected tie points whereby κSI data was matched between Yeak Loam and Yeak Oam master and and replicate cores.

Tie point	Sequence A (YL1211B)	Sequence B (YL1211A)	Sequence A (YO0712B)	Sequence B (YO0712C)
a	14.25	7.75	1	25.5
b	36.25	27.75	2.5	29.5
c	48.75	42.25	21	37
d	83.25	71.25	54	49.5
e	89.75	76.75	56.5	50
f	153.75	132.75	85	61.5
g	174.75	158.75	98.5	70.5
h	200.75	179.25	137.5	84.5
i			151	94

The master core and replicate core κSI records for each lake site were then imported into CPLSLOT as two, 1-variable, scalar sequences. Replicate core data (sequence B) were slotted into master core data (sequence A). The visually identified tie-points were selectively added into the model as ABN constraints until the highest correlation (Pearson's) between the core sequences was achieved (ABN function assumes that these points in the record are near-neighbours), using a Euclidean distance measure and the Z-score to normalise the data.

D.2.2 Results

Results of the CPL slot core correlation are summarized in table D.4, which shows the correlation coefficient (Pearson's r) for the different tie-point combinations applied to the model. The most significant correlation found between the YO0712B master and replicate record was found where none of the tentatively identified tie-points were used in the model (r = 0.72). This suggests that the total length of each sediment record is approximately the

same. Incorporation of tie-points a, b, c and h into the YL model yielded the highest correlation (r = 0.89) between the master and replicate core records.

TABLE D.4: Results of CPL slot correlation using selected tie points whereby κSI data was matched between Yeak Loam and Yeak Oam master and and replicate cores.

core pairs	Constraints	Pearson's r	sum-squared difference of ranks
Yeak Loam	a to h	0.467	1852750
Yeak Loam	a, b, c, g & h	0.881	801206
Yeak Loam	a, b, c & h	0.888	767023
Yeak Loam	a & h	0.848	932317
Yeak Loam	none	0.842	1403839
Yeak Oam	i to h	0.309	1989458
Yeak Oam	d to i	0.592	1662946
Yeak Oam	none	0.715	1057650

E Sedimentology correlation matrices for YM0413B

Pearson's correlation matrices showing associations between different geochemical and sedimentological properties of the YM0413B and YL1211B cores sediments are shown on E.1 — YM0413B whole core correlations; E.2 — YM0413B sedimentary unit I correlations; E.3 — YM0413B sedimentary unit II correlations; E.4 —YM0413B sedimentary unit III correlations; E.5 — YM0413B sedimentary unit IV correlations; and E.6 —YL1211B whole core correlations.

TABLE E.1: Pearson's correlation matrix for YM0413B XRF geochemical and sedimentological data (whole core). Significant correlations are underlined (p<0.05).

	Al	*Si*	*K*	*Ca*	*Ti*	*Cr*	*Mn*	*Fe*	*Ni*	*Cu*	*Zn*	*Rb*	*Sr*	*Y*	*Zr*	*Ba*	*Pb*	*Mn/Ti*	*Cu/Ti*	*Fe/Ti*	*Fe/Si*	*Mn/Ca*	*Zr/Rb*	*κSI*	*TOC*	*wc%*	*mean*	*sort*	*skew*	*kurt*	*clay*	*silt*	*sand*	*ρ(dry)*
Al	1.0	0.4	0.3	0.4	0.4	0.3	0.2	0.3	-0.2	0.2	0.0	0.2	0.2	0.1	0.1	0.2	0.1	0.0	-0.3	-0.2	-0.3	0.1	0.0	0.1	-0.1	-0.2	0.0	0.1	-0.2	0.0	0.0	-0.1	0.1	0.1
Si		1.0	0.9	0.9	1.0	0.9	0.5	0.8	-0.1	0.6	0.5	0.9	0.9	0.7	0.8	0.8	0.3	0.1	-0.8	-0.4	-0.5	0.4	-0.4	0.5	-0.7	-0.9	-0.1	-0.1	-0.5	-0.2	0.0	0.1	-0.3	0.3
K			1.0	0.9	0.9	1.0	0.6	0.9	-0.1	0.5	0.4	1.0	0.9	0.6	0.8	0.8	0.3	0.2	-0.8	-0.3	-0.3	0.5	-0.6	0.7	-0.8	-0.9	-0.2	-0.2	-0.5	-0.2	0.1	0.2	-0.4	0.4
Ca				1.0	0.9	0.9	0.6	0.8	-0.3	0.5	0.3	0.8	0.7	0.6	0.7	0.8	0.3	0.2	-0.8	-0.3	-0.3	0.4	-0.4	0.6	-0.6	-0.8	-0.1	0.0	-0.4	-0.1	0.0	0.1	-0.2	0.4
Ti					1.0	0.9	0.5	0.8	0.0	0.7	0.5	0.9	0.9	0.7	0.8	0.9	0.4	0.1	-0.8	-0.4	-0.4	0.4	-0.5	0.5	-0.7	-0.9	-0.2	-0.1	-0.4	-0.2	0.1	0.1	-0.3	0.4
Cr						1.0	0.6	0.9	-0.1	0.5	0.4	0.9	0.9	0.6	0.8	0.8	0.3	0.3	-0.8	-0.2	-0.2	0.5	-0.5	0.7	-0.8	-0.9	-0.2	-0.2	-0.5	-0.1	0.0	0.2	-0.3	0.4
Mn							1.0	0.9	-0.2	-0.1	0.0	0.6	0.3	0.0	0.3	0.4	0.1	0.9	-0.5	0.4	0.3	1.0	-0.5	0.6	-0.4	-0.5	-0.2	-0.1	-0.3	-0.2	0.1	0.0	-0.3	0.3
Fe								1.0	-0.2	0.2	0.2	0.9	0.7	0.3	0.6	0.7	0.3	0.6	-0.7	0.1	0.1	0.8	-0.6	0.7	-0.6	-0.8	-0.2	-0.1	-0.4	-0.2	0.1	0.1	-0.3	0.4
Ni									1.0	0.5	0.7	-0.1	0.1	0.0	0.1	0.0	0.5	-0.3	0.3	-0.3	-0.1	-0.2	0.0	-0.3	-0.1	0.0	0.1	-0.2	0.1	0.1	-0.2	0.3	0.0	-0.1
Cu										1.0	0.8	0.4	0.6	0.7	0.5	0.6	0.6	-0.5	-0.4	-0.8	-0.6	-0.2	-0.2	0.0	-0.4	-0.5	0.0	-0.1	-0.2	-0.1	-0.1	0.1	0.0	0.0
Zn											1.0	0.4	0.5	0.6	0.5	0.4	0.6	-0.3	-0.3	-0.5	-0.4	0.0	-0.2	0.0	-0.5	-0.5	-0.1	-0.2	-0.2	-0.2	0.0	0.1	-0.2	0.0
Rb												1.0	0.9	0.6	0.8	0.8	0.2	0.3	-0.8	-0.2	-0.2	0.6	-0.6	0.7	-0.9	-0.9	-0.3	-0.2	-0.5	-0.2	0.1	0.2	-0.5	0.4
Sr													1.0	0.8	1.0	0.7	0.2	0.0	-0.7	-0.4	-0.4	0.3	-0.4	0.6	-0.9	-0.9	-0.1	-0.2	-0.4	-0.1	-0.1	0.3	-0.3	0.4
Y														1.0	0.8	0.6	0.2	-0.3	-0.6	-0.6	-0.6	-0.1	-0.3	0.2	-0.6	-0.7	-0.1	-0.2	-0.4	-0.2	0.1	0.1	-0.2	0.2
Zr															1.0	0.6	0.2	-0.1	-0.7	-0.4	-0.4	0.2	-0.2	0.5	-0.8	-0.8	0.0	-0.2	-0.4	-0.1	-0.1	0.3	-0.3	0.4
Ba																1.0	0.5	0.0	-0.7	-0.4	-0.3	0.3	-0.5	0.5	-0.7	-0.8	-0.2	-0.1	-0.4	-0.1	0.0	0.1	-0.2	0.2
Pb																	1.0	-0.1	-0.2	-0.4	-0.2	0.1	-0.2	0.0	-0.2	-0.3	0.0	-0.1	-0.1	0.0	-0.2	0.1	0.1	-0.1
Mn/Ti																		1.0	-0.2	0.8	0.7	0.9	-0.3	0.5	-0.1	-0.2	-0.2	0.0	-0.1	-0.1	0.2	-0.1	-0.2	0.2
Cu/Ti																			1.0	0.3	0.2	-0.4	0.3	-0.6	0.6	0.8	0.1	0.1	0.3	0.3	-0.1	0.0	0.2	-0.4
Fe/Ti																				1.0	0.9	0.6	-0.1	0.2	0.3	0.3	-0.1	0.0	0.1	0.0	0.2	-0.1	-0.1	0.0
Fe/Si																					1.0	0.5	-0.1	0.1	0.2	0.3	-0.1	0.0	0.2	0.0	0.2	-0.1	-0.2	0.0
Mn/Ca																						1.0	-0.5	0.6	-0.3	-0.5	-0.2	-0.1	-0.3	-0.2	0.2	0.0	-0.3	0.3
Zr/Rb																							1.0	-0.4	0.5	0.5	0.5	0.2	0.3	0.2	-0.3	0.0	0.5	-0.2
κSI																								1.0	-0.6	-0.7	-0.1	-0.2	-0.3	-0.1	-0.1	0.3	-0.3	0.4
TOC																									1.0	0.9	0.3	0.4	0.3	0.2	-0.3	-0.1	0.6	-0.5
wc%																										1.0	0.2	0.2	0.4	0.2	0.0	-0.2	0.3	-0.4
mean																											1.0	0.2	0.2	0.3	-0.7	0.3	0.7	-0.3
sort																												1.0	0.1	-0.2	0.1	-0.5	0.6	-0.2
skew																													1.0	0.1	0.2	-0.4	0.2	-0.4
kurt																														1.0	-0.5	0.4	0.2	-0.2
clay																															1.0	-0.8	-0.4	0.3
silt																																1.0	-0.2	0.0
sand																																	1.0	-0.4
ρ(dry)																																		1.0

TABLE E.2: Pearson's correlation matrix for YM0413B XRF geochemical and sedimentological data from sedimentary unit I. Significant correlations are underlined (p<0.05).

	Al	*Si*	*K*	*Ca*	*Ti*	*Cr*	*Mn*	*Fe*	*Ni*	*Cu*	*Zn*	*Rb*	*Sr*	*Y*	*Zr*	*Ba*	*Pb*	*Mn/Ti*	*Cu/Ti*	*Fe/Ti*	*Fe/Si*	*Mn/Ca*	*Zr/Rb*	*κSI*	*TOC*	*wc%*	*mean*	*sort*	*skew*	*kurt*	*clay*	*silt*	*sand*	*ρ(dry)*
Al	1.0	0.0	-0.1	0.0	0.0	0.0	0.2	0.1	-0.4	-0.2	-0.3	0.0	-0.1	-0.1	-0.1	-0.1	-0.3	0.1	-0.1	0.1	0.0	0.1	-0.1	-0.1	0.3	0.0	0.5	0.3	-0.1	0.3	-0.4	-0.3	0.5	-0.4
Si		1.0	0.9	0.9	0.9	0.9	0.0	0.3	0.1	0.7	-0.1	0.8	0.9	0.7	0.9	0.8	0.0	-0.6	-0.8	-0.8	-0.8	-0.4	0.5	0.7	-0.8	-0.9	0.2	-0.3	-0.3	0.3	-0.3	0.3	0.1	0.8
K			1.0	0.8	0.9	0.9	0.1	0.5	0.1	0.7	0.0	1.0	0.9	0.6	0.9	0.8	0.0	-0.5	-0.9	-0.7	-0.6	-0.2	0.2	0.8	-0.9	-0.9	0.1	-0.3	-0.1	0.1	-0.1	0.1	0.0	0.8
Ca				1.0	0.9	0.9	0.1	0.2	-0.2	0.7	-0.4	0.7	0.9	0.7	0.9	0.8	-0.2	-0.5	-0.8	-0.8	-0.7	-0.3	0.6	0.7	-0.8	-0.9	0.0	-0.3	-0.3	0.1	-0.2	0.4	-0.1	0.8
Ti					1.0	1.0	0.1	0.4	-0.1	0.7	-0.3	0.9	0.9	0.7	0.9	0.9	-0.2	-0.5	-0.9	-0.8	-0.6	-0.3	0.5	0.8	-0.8	-0.9	-0.1	-0.5	-0.2	0.0	0.0	0.3	-0.2	0.8
Cr						1.0	0.2	0.5	0.0	0.8	-0.1	0.9	0.9	0.7	0.9	0.9	-0.1	-0.4	-0.9	-0.7	-0.6	-0.2	0.4	0.8	-0.8	-0.9	0.1	-0.3	-0.2	0.1	-0.1	0.3	0.0	0.7
Mn							1.0	0.8	-0.5	-0.2	-0.2	0.1	-0.2	-0.2	0.0	0.0	-0.1	0.8	-0.2	0.5	0.5	0.9	-0.3	-0.2	0.0	0.1	0.3	0.3	0.1	0.1	-0.1	-0.4	0.3	-0.3
Fe								1.0	-0.2	0.0	0.0	0.5	0.1	-0.1	0.2	0.3	0.1	0.5	-0.5	0.3	0.3	0.7	-0.3	0.1	-0.3	-0.2	0.3	0.3	0.3	0.2	-0.1	-0.5	0.4	0.0
Ni									1.0	0.4	0.8	0.1	0.1	0.0	0.0	0.1	0.8	-0.4	0.2	-0.1	-0.2	-0.4	0.0	0.1	-0.3	0.0	0.2	0.0	0.0	0.2	-0.2	-0.1	0.2	0.5
Cu										1.0	0.2	0.6	0.8	0.6	0.8	0.8	0.2	-0.6	-0.5	-0.7	-0.6	-0.5	0.6	0.6	-0.9	-0.7	0.0	-0.3	-0.2	0.1	-0.1	0.3	-0.1	0.9
Zn											1.0	-0.1	-0.2	-0.2	-0.2	-0.1	0.8	0.0	0.3	0.2	0.2	0.0	-0.2	-0.2	0.1	0.2	0.1	0.3	0.4	0.1	0.0	-0.4	0.2	0.0
Rb												1.0	0.8	0.6	0.8	0.8	-0.1	-0.5	-0.9	-0.6	-0.5	-0.2	0.1	0.8	-0.9	-0.8	0.0	-0.4	-0.1	0.0	0.0	0.1	-0.1	0.7
Sr													1.0	0.8	1.0	0.9	-0.1	-0.7	-0.8	-0.9	-0.8	-0.5	0.6	0.8	-0.9	-0.9	0.0	-0.6	-0.4	0.1	-0.1	0.5	-0.2	0.9
Y														1.0	0.8	0.7	-0.3	-0.6	-0.6	-0.8	-0.8	-0.5	0.5	0.6	-0.8	-0.7	-0.2	-0.7	-0.4	0.0	0.1	0.5	-0.4	0.8
Zr															1.0	0.9	-0.1	-0.6	-0.8	-0.8	-0.8	-0.4	0.6	0.8	-1.0	-0.9	-0.1	-0.6	-0.3	0.0	0.0	0.3	-0.2	0.9
Ba																1.0	-0.2	-0.5	-0.8	-0.8	-0.6	-0.3	0.3	0.7	-0.9	-0.8	-0.1	-0.6	-0.4	0.0	0.0	0.4	-0.3	0.8
Pb																	1.0	0.0	0.3	0.2	0.1	0.0	-0.1	-0.1	0.0	0.1	0.5	0.5	0.1	0.4	-0.5	-0.3	0.6	0.1
Mn/Ti																		1.0	0.4	0.9	0.8	0.9	-0.4	-0.7	0.7	0.6	0.3	0.6	0.2	0.2	-0.2	-0.5	0.4	-0.8
Cu/Ti																			1.0	0.7	0.5	0.2	-0.2	-0.8	0.8	0.8	0.1	0.4	0.0	0.0	-0.1	-0.2	0.2	-0.7
Fe/Ti																				1.0	0.9	0.8	-0.6	-0.8	0.9	0.8	0.3	0.7	0.4	0.1	-0.1	-0.6	0.5	-0.9
Fe/Si																					1.0	0.8	-0.6	-0.7	0.8	0.7	0.0	0.5	0.6	-0.2	0.3	-0.7	0.2	-1.0
Mn/Ca																						1.0	-0.5	-0.5	0.4	0.4	0.3	0.5	0.3	0.1	-0.1	-0.5	0.4	-0.7
Zr/Rb																							1.0	0.3	-0.9	-0.4	-0.2	-0.6	-0.4	0.0	0.0	0.6	-0.4	1.0
κSI																								1.0	-0.9	-0.9	-0.1	-0.6	-0.2	0.0	0.1	0.3	-0.3	0.8
TOC																									1.0	1.0	0.5	0.9	0.4	0.4	-0.3	-0.7	0.7	-0.9
wc%																										1.0	-0.1	0.4	0.4	-0.2	0.2	-0.4	0.1	-0.9
mean																											1.0	0.5	-0.4	0.9	-0.9	-0.2	0.9	-0.5
sort																												1.0	0.2	0.3	-0.5	-0.5	0.8	-0.8
skew																													1.0	-0.5	0.7	-0.8	-0.1	-0.8
kurt																														1.0	-0.9	0.1	0.7	-0.1
clay																															1.0	-0.2	-0.8	0.2
silt																																1.0	-0.5	1.0
sand																																	1.0	-0.7
ρ(dry)																																		1.0

TABLE E.3: Pearson's correlation matrix for YM0413B XRF geochemical and sedimentological data from sedimentary unit II. Significant correlations are underlined (p<0.05).

	Al	*Si*	*K*	*Ca*	*Ti*	*Cr*	*Mn*	*Fe*	*Ni*	*Cu*	*Zn*	*Rb*	*Sr*	*Y*	*Zr*	*Ba*	*Pb*	*Mn/Ti*	*Cu/Ti*	*Fe/Ti*	*Fe/Si*	*Mn/Ca*	*Zr/Rb*	*κSI*	*TOC*	*wc%*	*mean*	*sort*	*skew*	*kurt*	*clay*	*silt*	*sand*	*ρ(dry)*
Al	1.0	0.3	0.2	0.4	0.2	0.2	0.1	0.1	0.0	0.2	0.0	0.0	0.0	-0.1	0.0	0.2	0.2	-0.1	-0.1	-0.2	-0.3	-0.1	0.0	-0.2	0.1	0.0	0.2	-0.2	-0.1	0.2	-0.2	0.2	0.1	0.0
Si		1.0	0.9	0.9	1.0	0.9	0.5	0.8	0.2	0.5	0.5	0.8	0.8	0.5	0.7	0.7	0.2	0.3	-0.8	0.0	0.0	0.5	-0.3	0.4	-0.6	-0.7	-0.2	-0.4	-0.5	0.0	0.0	0.4	-0.4	0.5
K			1.0	0.8	1.0	0.9	0.6	0.9	0.2	0.4	0.5	0.9	0.8	0.5	0.7	0.7	0.1	0.5	-0.9	0.2	0.2	0.6	-0.5	0.5	-0.7	-0.8	-0.4	-0.4	-0.5	-0.1	0.2	0.3	-0.6	0.6
Ca				1.0	0.8	0.8	0.6	0.7	0.0	0.4	0.2	0.6	0.5	0.1	0.4	0.8	0.4	0.4	-0.6	0.0	0.0	0.4	-0.3	0.3	-0.3	-0.5	-0.2	-0.2	-0.4	0.1	0.0	0.3	-0.3	0.3
Ti					1.0	1.0	0.5	0.8	0.2	0.5	0.5	0.9	0.8	0.5	0.8	0.8	0.2	0.3	-0.9	0.0	0.1	0.5	-0.4	0.5	-0.7	-0.7	-0.3	-0.3	-0.5	0.0	0.1	0.4	-0.5	0.5
Cr						1.0	0.6	0.9	0.2	0.4	0.5	0.9	0.8	0.5	0.8	0.7	0.1	0.5	-0.8	0.2	0.2	0.6	-0.3	0.6	-0.7	-0.8	-0.3	-0.4	-0.6	-0.1	0.1	0.3	-0.5	0.5
Mn							1.0	0.9	0.1	-0.1	0.3	0.6	0.4	0.0	0.3	0.4	0.1	0.9	-0.5	0.7	0.7	1.0	-0.5	0.6	-0.4	-0.6	-0.3	-0.3	-0.4	-0.3	0.3	0.0	-0.5	0.4
Fe								1.0	0.2	0.1	0.5	0.5	0.7	0.3	0.6	0.5	0.1	0.8	-0.8	0.6	0.6	0.9	-0.5	0.7	-0.6	-0.8	-0.4	-0.4	-0.5	-0.3	0.3	0.1	-0.6	0.6
Ni									1.0	0.5	0.8	0.2	0.3	0.3	0.2	0.1	0.3	0.0	0.0	0.1	0.1	0.2	-0.1	0.2	-0.2	-0.2	0.0	0.0	-0.2	0.0	0.0	0.1	-0.1	0.2
Cu										1.0	0.5	0.2	0.4	0.4	0.4	0.5	0.5	-0.3	-0.1	-0.5	-0.4	-0.2	0.0	0.0	-0.1	-0.2	0.1	-0.1	-0.3	0.3	-0.4	0.5	0.1	0.0
Zn											1.0	0.5	0.6	0.5	0.6	0.2	0.1	0.1	-0.4	0.1	0.2	0.3	-0.1	0.4	-0.5	-0.5	-0.2	-0.2	-0.4	-0.1	0.1	0.2	-0.3	0.4
Rb												1.0	0.9	0.6	0.8	0.6	0.0	0.5	-0.9	0.3	0.4	0.7	-0.6	0.7	-0.8	-0.9	-0.5	-0.4	-0.6	-0.3	0.3	0.2	-0.7	0.6
Sr													1.0	0.8	1.0	0.5	-0.1	0.3	-0.7	0.1	0.2	0.4	-0.2	0.7	-0.8	-0.8	-0.2	-0.4	-0.7	-0.1	0.0	0.4	-0.4	0.5
Y														1.0	0.8	0.3	-0.2	-0.1	-0.5	-0.2	0.0	0.1	0.0	0.4	-0.5	-0.6	-0.1	-0.3	-0.5	-0.1	-0.1	0.4	-0.3	0.3
Zr															1.0	0.4	-0.2	0.2	-0.7	0.0	0.1	0.3	0.0	0.6	-0.7	-0.8	-0.1	-0.4	-0.6	-0.1	0.0	0.3	-0.4	0.5
Ba																1.0	0.4	0.2	-0.6	-0.2	0.0	0.3	-0.5	0.2	-0.4	-0.5	-0.2	-0.2	-0.4	0.1	0.0	0.3	-0.2	0.2
Pb																	1.0	0.0	0.1	-0.1	-0.1	0.0	-0.2	-0.1	0.2	0.0	0.1	-0.1	-0.1	0.3	-0.2	0.3	0.1	-0.1
Mn/Ti																		1.0	-0.4	0.9	0.8	1.0	-0.5	0.6	-0.4	-0.5	-0.3	-0.3	-0.3	-0.4	0.4	-0.2	-0.5	0.4
Cu/Ti																			1.0	-0.2	-0.3	-0.5	0.4	-0.6	0.7	0.7	0.5	0.3	0.4	0.3	-0.4	-0.1	0.7	-0.5
Fe/Ti																				1.0	0.9	0.8	-0.3	0.6	-0.3	-0.3	-0.3	-0.2	-0.1	-0.5	0.5	-0.3	-0.4	0.4
Fe/Si																					1.0	0.8	-0.5	0.6	-0.4	-0.4	-0.4	-0.2	-0.2	-0.6	0.6	-0.4	-0.5	0.4
Mn/Ca																						1.0	-0.5	0.7	-0.5	-0.6	-0.4	-0.3	-0.4	-0.4	0.4	-0.1	-0.5	0.5
Zr/Rb																							1.0	-0.3	0.3	0.4	0.6	0.0	0.1	0.3	-0.4	0.1	0.5	-0.3
κSI																								1.0	-0.7	-0.8	-0.3	-0.3	-0.6	-0.3	0.2	0.2	-0.5	0.6
TOC																									1.0	0.9	0.4	0.2	0.3	0.5	-0.4	0.1	0.6	-0.7
wc%																										1.0	0.3	0.4	0.5	0.2	-0.1	-0.2	0.5	-0.6
mean																											1.0	-0.2	-0.1	0.6	-0.8	0.4	0.9	-0.4
sort																												1.0	0.3	-0.1	0.1	-0.3	0.2	0.0
skew																													1.0	-0.1	0.4	-0.7	0.1	-0.1
kurt																														1.0	-0.8	0.6	0.6	-0.4
clay																															1.0	-0.8	-0.7	0.4
silt																																1.0	0.2	-0.2
sand																																	1.0	-0.4
ρ(dry)																																		1.0

TABLE E.4: Pearson's correlation matrix for YM0413B XRF geochemical and sedimentological data from sedimentary unit III. Significant correlations are underlined (p<0.05).

	Al	*Si*	*K*	*Ca*	*Ti*	*Cr*	*Mn*	*Fe*	*Ni*	*Cu*	*Zn*	*Rb*	*Sr*	*Y*	*Zr*	*Ba*	*Pb*	*Mn/Ti*	*Cu/Ti*	*Fe/Ti*	*Fe/Si*	*Mn/Ca*	*Zr/Rb*	*κSI*	*TOC*	*wc%*	*mean*	*sort*	*skew*	*kurt*	*clay*	*silt*	*sand*	*ρ(dry)*
Al	1.0	0.5	0.3	0.6	0.5	0.5	0.3	0.3	0.0	0.0	0.0	0.1	-0.1	-0.4	-0.1	0.3	0.4	0.2	-0.4	0.2	0.2	0.2	0.0	0.4	0.3	-0.1	0.4	-0.3	-0.2	0.3	-0.4	0.4	0.2	0.0
Si		1.0	0.5	0.9	0.9	0.6	0.0	0.2	0.4	0.3	0.3	0.0	0.3	-0.2	0.3	0.7	0.2	-0.1	-0.3	-0.2	-0.2	-0.1	0.2	0.3	-0.1	0.0	0.3	-0.3	0.0	0.0	-0.2	0.2	0.1	-0.1
K			1.0	0.5	0.5	0.7	0.6	0.7	-0.3	-0.4	0.0	0.8	-0.3	-0.6	-0.4	0.3	0.7	0.5	-0.7	0.5	0.5	0.6	-0.6	0.5	-0.1	-0.5	-0.4	0.0	-0.3	0.0	0.3	-0.1	-0.4	0.3
Ca				1.0	1.0	0.8	0.3	0.4	0.2	0.1	0.0	0.1	0.1	-0.5	0.1	0.5	0.5	0.2	-0.5	0.1	0.1	0.2	0.1	0.4	0.1	0.0	0.2	-0.2	-0.2	-0.1	-0.1	0.1	0.1	0.0
Ti					1.0	0.8	0.2	0.3	0.3	0.2	0.2	0.1	0.2	-0.4	0.3	0.6	0.4	0.0	-0.4	0.0	0.0	0.0	0.1	0.4	-0.1	0.0	0.2	-0.2	-0.2	0.0	-0.1	0.1	0.1	0.1
Cr						1.0	0.7	0.8	-0.2	-0.3	-0.2	0.4	-0.3	-0.7	-0.3	0.4	0.7	0.6	-0.8	0.5	0.5	0.6	-0.3	0.6	0.1	-0.3	-0.1	-0.1	-0.5	0.0	0.0	0.1	-0.2	0.3
Mn							1.0	1.0	-0.8	-0.8	-0.7	0.7	-0.8	-0.9	-0.8	-0.2	0.9	1.0	-0.9	1.0	1.0	1.0	-0.8	0.6	0.3	-0.5	-0.4	0.2	-0.5	-0.2	0.4	-0.2	-0.3	0.4
Fe								1.0	-0.7	-0.8	-0.6	0.7	-0.7	-0.9	-0.7	-0.1	0.9	0.9	-0.9	0.9	0.9	0.9	-0.8	0.6	0.3	-0.5	-0.4	0.1	-0.5	-0.2	0.3	-0.2	-0.3	0.4
Ni									1.0	0.9	0.7	-0.5	0.8	0.6	0.8	0.5	-0.6	-0.9	0.6	-0.9	-0.9	-0.9	0.8	-0.3	-0.4	0.4	0.4	-0.2	0.3	0.1	-0.3	0.2	0.3	-0.2
Cu										1.0	0.7	-0.6	0.8	0.7	0.9	0.5	-0.6	-0.9	0.8	-0.9	-0.9	-0.9	0.8	-0.4	-0.3	0.4	0.5	-0.4	0.3	0.2	-0.5	0.4	0.3	-0.3
Zn											1.0	-0.2	0.7	0.5	0.7	0.5	-0.5	-0.7	0.5	-0.7	-0.7	-0.7	0.4	0.0	-0.4	0.1	0.1	-0.2	0.3	0.0	-0.1	0.1	0.0	0.2
Rb												1.0	-0.5	-0.6	-0.6	-0.1	0.7	0.7	-0.6	0.7	0.7	0.7	-0.9	0.4	0.0	-0.5	-0.6	0.3	-0.3	-0.2	0.5	-0.4	-0.5	0.4
Sr													1.0	0.7	0.9	0.5	-0.5	-0.8	0.6	-0.8	-0.8	-0.8	0.7	-0.4	-0.7	0.3	0.4	0.0	0.6	0.2	-0.3	0.2	0.3	-0.2
Y														1.0	0.7	0.1	-0.8	-0.9	0.9	-0.8	-0.8	-0.8	0.7	-0.7	-0.4	0.4	0.3	-0.1	0.5	0.2	-0.3	0.2	0.3	-0.4
Zr															1.0	0.5	-0.6	-0.9	0.7	-0.9	-0.9	-0.9	0.9	-0.4	-0.5	0.4	0.5	-0.1	0.5	0.2	-0.4	0.3	0.4	-0.2
Ba																1.0	0.0	-0.3	0.0	-0.3	-0.3	-0.3	0.3	0.1	-0.2	0.0	0.1	-0.1	0.2	0.2	-0.2	0.3	-0.1	0.1
Pb																	1.0	0.8	-0.8	0.8	0.8	0.8	-0.7	0.6	0.3	-0.4	-0.3	0.3	-0.5	-0.1	0.3	-0.2	-0.2	0.3
Mn/Ti																		1.0	-0.8	1.0	1.0	1.0	-0.8	0.6	0.3	-0.5	-0.4	0.2	-0.5	-0.1	0.3	-0.2	-0.4	0.3
Cu/Ti																			1.0	-0.8	-0.8	-0.8	0.7	-0.7	-0.2	0.4	0.3	-0.1	0.4	0.2	-0.3	0.3	0.2	-0.3
Fe/Ti																				1.0	1.0	1.0	-0.9	0.5	0.3	-0.5	-0.5	0.2	-0.5	-0.1	0.4	-0.2	-0.4	0.3
Fe/Si																					1.0	1.0	-0.8	0.5	0.3	-0.5	-0.5	0.2	-0.5	-0.1	0.4	-0.2	-0.4	0.4
Mn/Ca																						1.0	-0.8	0.6	0.3	-0.5	-0.5	0.2	-0.5	-0.1	0.4	-0.2	-0.4	0.3
Zr/Rb																							1.0	-0.5	-0.2	0.5	0.7	-0.3	0.5	0.2	-0.6	0.3	0.6	-0.4
κSI																								1.0	0.1	-0.5	-0.4	0.0	-0.5	-0.5	0.5	-0.4	-0.4	0.6
TOC																									1.0	0.3	0.5	-0.6	-0.2	0.7	-0.8	0.8	0.1	-0.3
wc%																										1.0	0.7	-0.4	0.4	0.0	-0.5	0.3	0.4	-0.6
mean																											1.0	-0.5	0.5	0.5	-0.9	0.6	0.8	-0.7
sort																												1.0	0.0	-0.2	0.4	-0.6	0.1	0.2
skew																													1.0	0.3	-0.4	0.1	0.6	-0.6
kurt																														1.0	-0.8	0.8	0.5	-0.5
clay																															1.0	-0.9	-0.7	0.6
silt																																1.0	0.2	-0.4
sand																																	1.0	-0.5
ρ(dry)																																		1.0

TABLE E.5: Pearson's correlation matrix for YM0413B XRF geochemical and sedimentological data from sedimentary unit IV. Significant correlations are underlined (p<0.05).

	Al	*Si*	*K*	*Ca*	*Ti*	*Cr*	*Mn*	*Fe*	*Ni*	*Cu*	*Zn*	*Rb*	*Sr*	*Y*	*Zr*	*Ba*	*Pb*	*Mn/Ti*	*Cu/Ti*	*Fe/Ti*	*Fe/Si*	*Mn/Ca*	*Zr/Rb*	*κSI*	*TOC*	*wc%*	*mean*	*sort*	*skew*	*kurt*	*clay*	*silt*	*sand*	*ρ(dry)*
Al	1.0	0.1	-0.3	0.1	-0.2	-0.2	0.0	-0.2	-0.3	-0.3	-0.4	-0.4	-0.3	-0.3	-0.2	-0.4	-0.4	0.1	-0.1	0.0	-0.3	0.0	0.4	-0.4	0.3	0.3	0.0	0.3	-0.1	-0.1	0.2	-0.3	0.3	0.1
Si		1.0	0.8	0.6	0.9	0.8	0.3	0.7	0.2	0.4	0.4	0.7	0.6	0.4	0.7	0.5	0.5	-0.4	-0.6	-0.5	-0.4	0.0	0.1	0.5	-0.5	-0.7	0.2	-0.3	0.1	0.1	-0.5	0.5	-0.1	0.1
K			1.0	0.5	0.9	0.9	0.3	0.8	0.5	0.7	0.6	0.9	0.9	0.5	0.8	0.8	0.7	-0.4	-0.5	-0.5	-0.1	0.0	-0.3	0.7	-0.8	-0.9	0.2	-0.4	0.1	0.2	-0.5	0.6	-0.3	0.1
Ca				1.0	0.6	0.6	0.6	0.6	-0.1	0.1	0.0	0.3	0.2	0.1	0.5	0.3	0.1	0.0	-0.7	-0.2	0.0	0.1	0.3	0.3	-0.1	-0.3	0.4	0.2	0.3	0.1	-0.2	0.1	0.2	0.6
Ti					1.0	0.9	0.3	0.9	0.4	0.6	0.6	0.8	0.8	0.4	0.9	0.7	0.7	-0.4	-0.7	-0.6	-0.1	0.1	0.0	0.8	-0.7	-0.8	0.3	-0.3	0.2	0.1	-0.5	0.5	-0.1	0.1
Cr						1.0	0.4	0.9	0.5	0.7	0.6	0.7	0.8	0.3	0.8	0.7	0.7	-0.4	-0.6	-0.5	0.0	0.1	0.0	0.8	-0.7	-0.8	0.3	-0.3	0.2	0.2	-0.5	0.5	-0.1	0.2
Mn							1.0	0.7	-0.3	-0.2	-0.2	0.1	-0.1	0.1	0.1	0.0	-0.1	0.6	-0.6	0.4	0.5	0.9	0.0	0.1	0.2	0.0	0.1	0.0	0.2	-0.1	0.1	-0.1	0.0	0.1
Fe								1.0	0.3	0.4	0.5	0.7	0.6	0.3	0.7	0.6	0.5	0.0	-0.7	-0.1	0.3	0.4	-0.1	0.7	-0.5	-0.7	0.2	-0.3	0.2	0.1	-0.3	0.4	-0.2	0.2
Ni									1.0	0.9	0.9	0.5	0.7	0.1	0.5	0.6	0.8	-0.6	0.2	-0.4	-0.1	-0.3	-0.2	0.6	-0.8	-0.6	0.1	-0.4	-0.1	0.3	-0.5	0.6	-0.3	-0.1
Cu										1.0	0.9	0.7	0.8	0.2	0.7	0.7	0.8	-0.7	0.1	-0.6	-0.1	-0.3	-0.2	0.7	-0.9	-0.7	0.1	-0.4	0.0	0.3	-0.5	0.6	-0.2	0.0
Zn											1.0	0.7	0.8	0.3	0.7	0.7	0.9	-0.6	0.0	-0.5	-0.1	-0.2	-0.2	0.8	-0.8	-0.8	0.1	-0.5	-0.1	0.2	-0.5	0.7	-0.3	-0.1
Rb												1.0	0.9	0.6	0.8	0.8	0.7	-0.5	-0.3	-0.5	-0.1	-0.1	-0.5	0.7	-0.9	-0.9	0.1	-0.4	0.1	0.2	-0.4	0.6	-0.4	0.1
Sr													1.0	0.5	0.9	0.8	0.8	-0.7	-0.2	-0.6	-0.2	-0.3	-0.2	0.8	-0.9	-0.9	0.2	-0.4	0.1	0.2	-0.5	0.6	-0.3	0.0
Y														1.0	0.4	0.4	0.3	-0.2	-0.2	-0.2	-0.1	0.0	-0.4	0.4	-0.4	-0.5	-0.2	-0.4	0.0	0.0	-0.1	0.3	-0.4	-0.2
Zr															1.0	0.7	0.8	-0.6	-0.5	-0.7	-0.2	-0.2	0.1	0.9	-0.8	-0.9	0.4	-0.2	0.2	0.1	-0.5	0.6	0.0	0.2
Ba																1.0	0.7	-0.5	-0.2	-0.5	-0.1	-0.2	-0.3	0.6	-0.9	-0.8	0.0	-0.4	0.0	0.3	-0.3	0.5	-0.4	0.0
Pb																	1.0	-0.5	-0.1	-0.5	0.0	-0.2	-0.1	0.9	-0.8	-0.8	0.1	-0.4	0.0	0.1	-0.5	0.6	-0.2	0.0
Mn/Ti																		1.0	-0.1	0.9	0.6	0.8	0.0	-0.4	0.6	0.6	-0.2	0.1	0.1	-0.1	0.4	-0.5	0.1	-0.1
Cu/Ti																			1.0	0.1	-0.1	-0.4	-0.3	-0.4	0.1	0.3	-0.3	0.0	-0.2	0.0	0.2	-0.1	-0.1	-0.2
Fe/Ti																				1.0	0.7	0.6	-0.2	-0.5	0.5	0.6	-0.2	0.0	0.0	-0.1	0.5	-0.4	-0.1	-0.1
Fe/Si																					1.0	0.6	-0.2	0.1	0.0	0.1	-0.1	0.0	0.2	0.0	0.4	-0.3	-0.1	0.0
Mn/Ca																						1.0	0.0	0.0	0.2	0.1	-0.1	-0.1	0.0	-0.1	0.2	-0.2	-0.1	-0.1
Zr/Rb																							1.0	0.0	0.5	0.2	0.3	0.5	0.1	-0.1	-0.1	-0.2	0.6	0.2
κSI																								1.0	-0.8	-0.9	0.3	-0.3	0.2	0.0	-0.4	0.5	-0.2	-0.1
TOC																									1.0	0.9	0.1	0.3	-0.5	-0.5	0.3	-0.5	0.3	0.0
wc%																										1.0	-0.2	0.4	-0.1	-0.1	0.5	-0.6	0.3	0.1
mean																											1.0	0.4	0.3	0.0	-0.5	0.2	0.7	0.2
sort																												1.0	0.0	-0.2	0.1	-0.5	0.8	-0.3
skew																													1.0	0.1	0.2	-0.3	0.2	-0.1
kurt																														1.0	-0.1	0.2	-0.1	0.4
clay																															1.0	-0.9	-0.2	-0.2
silt																																1.0	-0.3	0.3
sand																																	1.0	-0.1
ρ(dry)																																		1.0

TABLE E.6: Pearson's correlation matrix for YL1211B XRF geochemical and sedimentological data (whole core). Significant correlations are underlined (p<0.05).

	Si	*K*	*Ca*	*Ti*	*Mn*	*Fe*	*Zn*	*Rb*	*Sr*	*Zr*	*Pb*	*Mn/Ti*	*Fe/Ti*	*Mn/Fe*	*Mn/Ca*	*Zr/Rb*	*TOC*	*clay*	*silt*	*sand*	*κSI*	*wc%*	*ρ(dry)*	*χfd%*	*χlf*
Si	1.0	0.9	0.5	0.7	0.0	0.2	0.4	0.1	0.1	0.2	0.2	-0.2	-0.3	-0.1	-0.2	-0.3	0.2	0.0	0.0	0.0	0.0	-0.1	0.0	-0.1	-0.2
K		1.0	0.6	0.9	0.0	0.2	0.6	0.1	0.1	0.3	0.2	-0.3	-0.5	-0.1	-0.3	-0.3	0.2	-0.1	0.0	0.1	0.1	0.0	0.0	-0.1	-0.1
Ca			1.0	0.5	0.1	-0.1	0.6	-0.2	0.0	0.2	0.0	-0.1	-0.4	0.2	-0.3	0.0	0.3	0.0	-0.4	0.5	0.2	0.0	0.1	-0.1	-0.2
Ti				1.0	0.3	0.5	0.4	0.4	0.3	0.6	0.4	0.0	-0.3	0.1	0.1	-0.5	0.2	0.1	-0.2	0.2	0.1	-0.2	0.0	-0.1	-0.1
Mn					1.0	0.5	-0.1	0.5	0.3	0.2	0.3	0.9	0.3	0.8	0.9	-0.4	0.0	0.1	-0.1	0.1	0.1	-0.4	0.0	0.2	0.0
Fe						1.0	-0.4	1.0	0.2	0.5	0.9	0.3	0.7	-0.1	0.5	-0.9	0.4	0.2	-0.3	0.2	0.2	-0.4	-0.1	-0.1	0.1
Zn							1.0	-0.5	-0.2	0.0	-0.3	-0.3	-0.7	0.1	-0.4	0.2	-0.1	-0.2	0.1	0.0	0.0	0.3	0.1	-0.1	-0.1
Rb								1.0	0.2	0.4	0.9	0.3	0.8	-0.1	0.5	-0.9	0.4	0.2	-0.2	0.2	0.2	-0.4	-0.1	-0.1	0.1
Sr									1.0	0.3	0.0	0.2	-0.1	0.3	0.3	-0.1	-0.1	0.1	-0.1	0.1	0.0	-0.3	0.0	0.1	0.0
Zr										1.0	0.5	-0.1	0.1	-0.1	0.1	-0.3	0.5	0.3	-0.4	0.2	-0.1	-0.4	0.1	-0.1	0.0
Pb											1.0	0.2	0.6	-0.2	0.3	-0.8	0.5	0.2	-0.3	0.2	0.2	-0.4	0.0	-0.2	0.1
Mn/Ti												1.0	-0.3	0.8	0.9	-0.2	-0.1	0.1	-0.1	0.0	0.1	-0.3	0.0	0.2	0.0
Fe/Ti													1.0	-0.2	0.5	-0.6	0.3	0.1	-0.1	0.1	0.1	-0.2	-0.2	-0.1	0.1
Mn/Fe														1.0	0.8	0.1	-0.3	0.0	0.0	0.0	0.1	-0.1	0.0	0.3	0.0
Mn/Ca															1.0	-0.3	-0.1	0.1	0.0	-0.1	0.0	-0.4	0.0	0.2	0.1
Zr/Rb																1.0	-0.3	0.0	0.1	-0.1	-0.3	0.2	0.2	0.1	-0.1
TOC																	1.0	0.3	-0.6	0.5	0.1	-0.3	0.2	-0.3	0.0
clay																		1.0	-0.6	-0.1	-0.1	-0.3	0.0	0.0	0.0
silt																			1.0	-0.7	-0.1	0.4	0.0	0.1	0.1
sand																				1.0	0.2	-0.2	0.0	-0.1	0.0
κSI																					1.0	0.0	-0.1	-0.1	0.0
wc%																						1.0	0.0	0.0	-0.1
ρ(dry)																							1.0	0.0	0.0
χfd%																								1.0	-0.6
χlf																									1.0

F Plant microfossil and micro-charcoal extraction techniques

F.1 Procedure for pollen extraction from field reference samples (flowers) (after Faegri and Iversen (1989))

Removal of unsaturated humic colloids

1. Label clean, 50 ml centrifuge tubes with appropriate sample codes, and place the individual pollen samples (flowers) into their relevant tubes.
2. In a fume hood, add 20 ml 10% KOH to each sample and mix with a vortex mixer.
3. Place samples tubes into a near-boiling (80 °C) hot water bath for 20 minutes.
4. Remove samples from bath, fill with distilled water, centrifuge at 3 000 rpm for 5 minutes and decant the supernatant.
5. Fill samples tubes with distilled water, centrifuge at 300 rpm for 5 minutes and decant the supernatant.

Sieving

6. Wash samples through a 105 μm sieve into a collecting basin.
7. Place the <105 μm fraction back into the sample tubes and centrifuge at 3 000 rpm for 5 minutes.
8. Decant supernatant.

Removal of cellulose (Acetolysis)

9. Add 10 ml glacial acetic acid to each sample, mix with the vortex mixer, centrifuge samples at 3 000 rpm for 5 minutes and decant the supernatant.
10. Repeat above step.
11. Prepare acetolysis mixture (9:1 ratio of anhydride to concentrated sulphuric acid). Add 10 ml of this mixture to each sample.
12. Cap loosely and place the samples tubes in a near-boiling (80 °C) hot water bath for 5 minutes.
13. Tighten caps and centrifuge at 3 000 rpm for 5 minutes and decant supernatant.
14. Add 10 ml glacial acetic acid to each sample, mix with the vortex mixer, centrifuge at 3 000 rpm for 5 minutes, and decant the supernatant.

15. Add 30 ml distilled water to samples and mix with the vortex mixer, centrifuge at 3 000 rpm for 5 minutes and decant the supernatant.
16. Repeat above step twice.

Preparation for mounting

17. Label clean, 1.5 ml micro-centrifuge tube vials with relevant samples codes.
18. Using a new glass pipette for each sample, collect the remaining material and place into the appropriate vials.
19. Cap vials and centrifuge at 3 000 rpm for 5 minutes and pipette off the supernatant.
20. Add sufficient glycerol to bring the total sample volume to 1.5 ml

Mounting

21. Warm a beaker of paraffin wax on a hotplate set to 50 °C.
22. Using a micro-pipette, stir sample and place a single drop onto a glass microscope slide. Put slide on hotplate.
23. Using the melted paraffin wax, seal the sample with a coverslip.
24. Take slide off plate and let wax set.

F.2 Procedure for plant microfossil and micro-charcoal extraction from core samples (after Faegri and Iversen (1989))

Sampling, weighing and addition of exotic markers

1. Label a clean, 15 ml centrifuge tube with an appropriate sample code.
2. Measure out 1 cm^3 (field moisture condition) of core sediment sample and place into tube.
3. Add one *Lycopodium clavatum* spore tablet into each sample tube.

Removal of unsaturated humic colloids

4. In a fume hood, add 7-10 ml 10% KOH to each sample and mix with a vortex mixer.
5. Place sample tubes into a near-boiling (80 °C) hot water bath for 20 minutes.
6. Remove samples from bath, fill with distilled water and centrifuge at 3 000 rpm for 5 minutes and decant the supernatant.
7. Fill sample tubes with distilled water, mix well with the vortex mixer, centrifuge at 3 000 rpm for 5 minutes and decant the supernatant.

Sieving

8. Add 5 ml of distilled water to the centrifuge tubes and mix with a vortex mixer.
9. Wash samples (using distilled water) through a 105 μm sieve into a clean collecting basin.
10. Place the <105 μm fraction back into the sample tube and centrifuge at 3 000 rpm for 5 minutes.
11. Decant the supernatant.

Removal of silicates

12. Wearing appropriate safety equipment and working in a fume hood, add 5 ml HF (50%) to each sample, cap tightly and mix with a vortex mixer.
13. Place samples into a near-boiling (80 °C) hot water bath for 60 minutes.
14. Carefully remove samples from bath, fill sample tubes with distilled water and mix with the vortex mixer.
15. Centrifuge at 3 000 rpm for 5 minutes, and decant the supernatant into a HF waste receptacle.
16. Fill each sample tube with distilled water, mix with the vortex mixer, centrifuge at 3 000 rpm for 5 minutes and decant the supernatant.
17. Repeat the above step twice.

Removal of cellulose (Acetolysis)

18. Add 7 ml glacial acetic acid to each sample, cap and mix with the vortex mixer, centrifuge samples at 3 000 rpm for 5 minutes and decant the supernatant.
19. Repeat above step.
20. Prepare acetolysis mixture (9:1 ratio of anhydride to concentrated sulphuric acid). Add 7 ml of this mixture to each sample.
21. Place the samples tubes in a near-boiling (80 °C) hot water bath for 5 minutes.
22. Tighten caps and centrifuge at 3 000 rpm for 5 minutes and decant supernatant.
23. Add 5-7 ml glacial acetic acid to each sample, mix with the vortex mixer, centrifuge at 3 000 rpm for 5 minutes, and decant the supernatant.
24. Fill each sample tube with distilled water, mix with the vortex mixer, centrifuge at 3 000 rpm for 5 minutes and decant the supernatant.
25. Repeat above step twice.

Preparation for mounting

26. Label clean, 1.5 ml micro-centrifuge tube vials with relevant samples codes.
27. Using a new glass pipette for each sample, collect the remaining material and place into the appropriate vials.
28. Cap vials and centrifuge at 3 000 rpm for 5 minutes and pipette off the supernatant.

29. Add sufficient glycerol to bring the total sample volume to 1.5 ml

Mounting

30. Warm a beaker of paraffin wax on a hotplate set to 50 °C.
31. Using a clean micro-pipette for each sample, stir the sample and place a single drop onto a glass microscope slide. Put slide on hotplate.
32. Using the melted paraffin wax, seal the sample with a coverslip.
33. Take slide off plate and let wax set.

G Plant microfossil reference collection

The plant microfossil reference material collected for this project are listed in table G.1. The sample numbers referred to in this table correspond to photographs presented in G.1 and G.2.

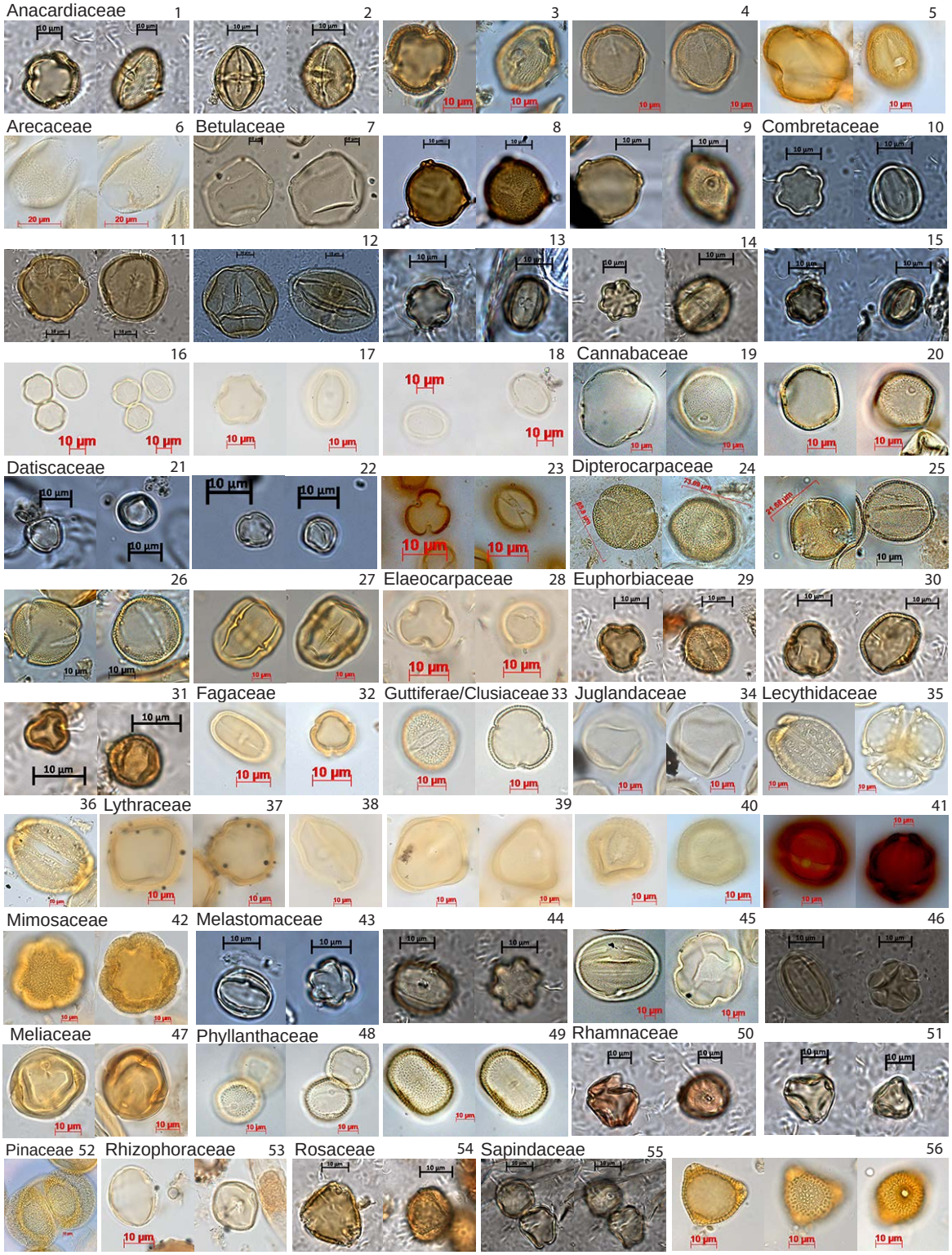

FIGURE G.1: Photomicrographs taken of microfossil reference samples (plate 1).

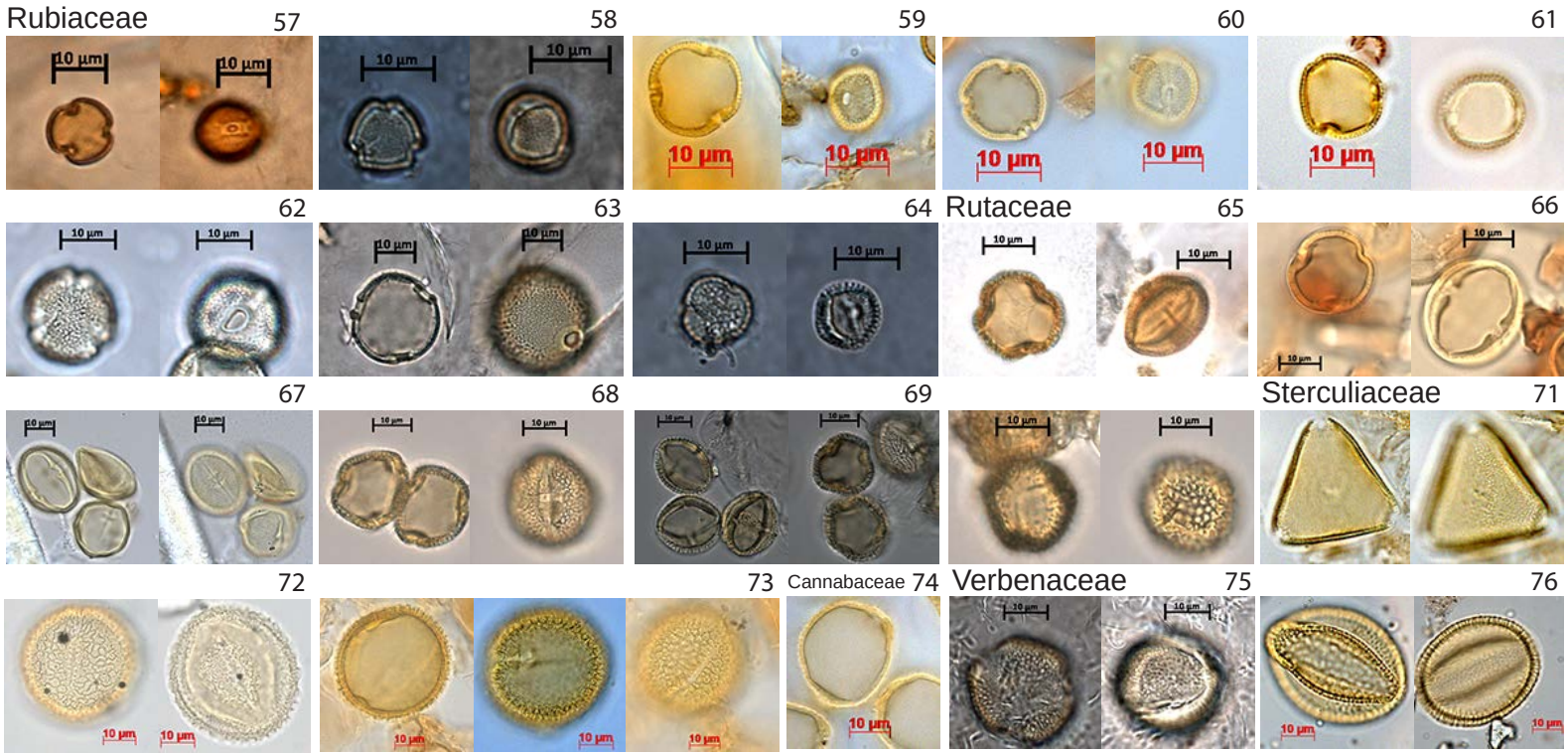

FIGURE G.2: Photomicrographs taken of microfossil reference samples (plate 2).

TABLE G.1: List of described and photographed reference material. Lied = Leiden collection; APSA = Australian Pollen and Spore Atlas Collection.

Sample Number	Family	Genus	Species	Collection	Reference Code	mean P (μm)	mean E (μm)	E-shape
1	Anacardiaceae	*Buchanania*	*arborescens*	ANU APSA	155 4 2a	23.0	14.9	prolate
2	Anacardiaceae	*Buchanania*	*heterophylla*	ANU APSA	155 4 7	22.2	17.2	sub-prolate
3	Anarcardiaceae	*Gluta*	*renghas*	Leiden	245	35.0	21.0	prolate
4	Anarcardiaceae	*Mangifera*	*gedebe*	Leiden	318	22.0	23.0	oblate-spheroidal
5	Anarcardiaceae	*Spondias*	*pinnata*	Leiden	582	34.0	26.0	sub-prolate

Continued...

Sample Number	Family	Genus	Species	Collection	Reference Code	mean P (μm)	mean E (μm)	E-shape
6	Arecaceae	*Calamus*	*sp.*	Leiden	240	29.0	31.0	oblate-spheroidal
7	Betulaceae	*Carpinus*	*betulus*	ANU APSA	58 51 3	-	34.8	-
8	Betulaceae	*Carpinus*	*orientalis*	ANU APSA	58 5 2	-	27.6	-
9	Betulaceae	*Ostrya*	*carpinifolia*	ANU APSA	58 3 49	16.1	20.8	sub-oblate
10	Combretaceae	*Anogeissus*	*acuminata*	ANU APSA	224 6 1	15.7	14.5	prolate spheroidal
11	Combretaceae	*Calycoperis*	*floribunda*	ANU APSA	224 8 1	32.5	31.8	prolate spheroidal
12	Combretaceae	*Quisqualis*	*indica*	ANU APSA	224 7 1	36.2	47.9	prolate spheroidal
13	Combretaceae	*Terminalia*	*belerica*	ANU APSA	224 4 13	15.9	12.8	sub-prolate
14	Combretaceae	*Terminalia*	*catappa*	ANU APSA	224 4 5	12.2	9.6	sub-prolate
15	Combretaceae	*Terminalia*	*tomentosa*	ANU APSA	224 4 14	13.9	11.7	sub-prolate
16	Combretaceae	*Terminalia*	*alata*	Leiden	326	25.8	17.7	prolate
17	Combretaceae	*Terminalia*	*chebula*	Leiden	323	23.3	16.5	prolate
18	Combretaceae	*Terminalia*	*mucronata*	Leiden	325	25.8	25.5	prolate spheroidal
19	Cannabaceae	*Celtis*	*tetrandra*	Leiden	272	-	-	-
20	Cannabaceae	*Celtis*	*timorensis*	Leiden	273	-	-	-
21	Datiscaceae	*Octomeles*	*sumatranum*	ANU APSA	208 2 1a	11.1	12.8	sub-oblate
22	Datiscaceae	*Tetrameles*	*nudiflora*	ANU APSA	208 3 1	10.1	8.9	prolate spheroidal
23	Datiscaceae	*Tetrameles*	*nudiflora*	catchment	Yeak Loam	13.8	12.6	prolate spheroidal
24	Dipterocarpaceae	*Dipterocarpus*	*obtusifolius*	Leiden	41, 42 & 43	84.6	74.7	prolate spheroidal
25	Dipterocarpaceae	*Hopea*	*odorata*	Leiden	45	21.7	21.2	prolate spheroidal
26	Dipterocarpaceae	*Shorea*	*siamensis*	Leiden	46 & 47	29.8	29.3	prolate spheroidal
27	Dipterocarpaceae	*Vatica*	*russak*	Leiden	52	43.0	32.4	sub-prolate
28	Elaeocarpaceae	*Elaeocarpus*	*macrocerus*	Leiden	55	13.9	14.4	oblate-spheroidal
29	Euphorbiaceae	*Baccaurea*	*obtusa*	ANU APSA	149 3 2	17.4	14.8	sub-prolate
30	Euphorbiaceae	*Baccaurea*	*stylaris*	ANU APSA	149 3 5	20.7	16.9	sub-prolate
31	Euphorbiaceae	*Macaranga*	*trilobata*	ANU APSA	149 19 1	10.6	10.1	prolate spheroidal
32	Fagaceae	*Lithocarpus*	*curtisii*	Leiden	68	20.5	11.9	prolate
33	Guttiferaea / Clusiaceae	*Cratoxylum*	*glaucum*	Leiden	84	21.8	24.2	oblate-spheroidal
34	Juglandaceae	*Engelhardtia*	*spicata*	Leiden	300	29.5	27.5	prolate spheroidal
35	Lecythidaceae	*Barringtonia*	*acutanglia*	Leiden	236	48.0	37.0	sub-prolate
36	Lecythidaceae	*Barringtonia*	*augusta*	Leiden	237	59.0	43.5	prolate
37	Lythraceae	*Lagerstroemia*	*floribunda*	Leiden	263	31.4	30.0	prolate spheroidal
38	Lythraceae	*Lagerstroemia*	*indica*	Leiden	264	50.0	38.0	sub-prolate
39	Lythraceae	*Lagerstroemia*	*macrocarpa*	Leiden	267	46.0	39.0	sub-prolate
40	Lythraceae	*Lagerstroemia*	*tomentosa*	Leiden	268	32.0	29.0	prolate spheroidal
41	Lythraceae	*Lagerstroemia*	sp.	catchment	Boeng Lumkut	39.1	35.7	prolate spheroidal
42	Mimosacaceae	*Sindora*	*cochinchinensis*	Leiden	105	-	-	-

Continued...

Sample Number	Family	Genus	Species	Collection	Reference Code	mean P (μm)	mean E (μm)	E-shape
43	Melastomaceae	*Melastoma*	*affine*	ANU APSA	226 4 9	15.4	14.3	prolate spheroidal
44	Melastomaceae	*Melastoma*	*polyanthum*	ANU APSA	226 4 4	21.9	18.0	sub-prolate
45	Melastomaceae	*Memecycon*	*normale*	Leiden	297	77.0	62.0	sub-prolate
46	Melastomaceae	*Memecyclon*	*umbellatum*	ANU APSA	226 19 1	22.6	16.4	prolate
47	Meliaceae	*Aglaia*	*rubiginosa*	Leiden	112	-	-	-
48	Phyllanthaceae	*Phyllanthus*	*collumnaris*	Leiden	316	-	-	-
49	Phyllanthaceae	*Phyllanthus*	*roseus*	Leiden	321	-	-	-
50	Rhamnaceae	*Zizyphus*	*jujuba*	ANU APSA	172 14 1	21.8	24.5	oblate-spheroidal
51	Rhamnaceae	*Zizyphus*	*maurita*	ANU APSA	172 14 2	12.8	17.2	oblate
52	Pinaceae	*Pinus*	*merkusii*	Leiden	237	62.0	69.4	oblate-spheroidal
53	Rhizophoraceae	*Carallia*	*brachiata*	Leiden	234	16.6	20.0	sub-oblate
54	Rosaceae / Chrysobalanaceae	*Parinari*	*anamensis*	ANU APSA	127 16 4	16.6	21.1	sub-oblate
55	Sapindaceae	*Nephelium*	*hypoleucum*	ANU ASPA	168 42 2	15.9	17.0	oblate-spheroidal
56	Sapindaceae	*Nephelium*	*cuspidatum*	Leiden	201	-	17.0	-
57	Rubiaceae	*Adina*	*fagifolia*	ANU APSA	275 58 2	14.9	13.7	prolate spheroidal
58	Rubiaceae	*Adina*	*rubescens*	ANU APSA	275 58 1	11.4	11.1	prolate spheroidal
59	Rubiaceae	*Nauclea*	*bartingii*	Leiden	154	14.7	14.3	prolate spheroidal
60	Rubiaceae	*Neonauclea*	*borneensis*	Leiden	155	13.9	12.5	prolate spheroidal
61	Rubiaceae	*Neonauclea*	*excelsa*	Leiden	163	12.8	14.2	oblate-spheroidal
62	Rubiaceae	*Nauclea*	*orientalis*	ANU APSA	275 35 1	19.6	18.4	prolate spheroidal
63	Rubiaceae	*Randia*	*sinensis*	ANU APSA	275 34 10	28.5	26.3	prolate spheroidal
64	Rubiaceae	*Wendlandia*	*glabrata*	ANU APSA	275 13 7	12.6	11.8	prolate spheroidal
65	Rutaceae	*Clausena*	*anisumolens*	ANU APSA	139 20 1 3	20.1	16.7	sub-prolate
66	Rutaceae	*Glycosmis*	*arborea*	ANU APSA	139 15 2	22.5	21.2	prolate spheroidal
67	Rutaceae	*Glycosmis*	*pentaphylla*	ANU APSA	139 15 1a	26.4	22.1	sub-prolate
68	Rutaceae	*Zanthoxylum*	*megistophyllum*	ANU APSA	139 17 3	23.2	21.0	prolate spheroidal
69	Rutaceae	*Zanthoxylum*	*ovalifolium*	ANU APSA	139 17 5	21.5	18.5	sub-prolate
70	Rutaceae	*Zanthoxylum*	*pluviatile*	ANU APSA	139 17 2	20.9	18.8	prolate spheroidal
71	Sterculiaceae	*Kleinhovia*	*hospita*	Leiden	209	-	-	-
72	Sterculiaceae	*Sterculia*	*ornata*	Leiden	280	-	-	-
73	Sterculiaceae	*Pterocymbium*	*tinctorium*	Leiden	210	-	-	-
74	Cannabaceae (formerly Ulmaceae)	*Trema*	*orientalis*	Leiden	274	23.0	27.7	sub-oblate
75	Verbenaceae	*Vitex*	*pubescens*	ANU APSA	258 14 9	28.0	25.0	prolate spheroidal
76	Verbenaceae	*Vitex*	*pinnata*	Leiden	313	-	-	-

H Key microfossil taxa from lake surface and core sediments

Microfossil taxa that make up greater than 0.5% of the surface core counts, and greater than 0.1% of the lake sediment core counts are identified to various degrees of certainty in table H.1.

Sources used to identify each taxon are included on this table. Identification of pteridophyte spores was refined though a species list of ferns provided in Lee et al. (2014). Photographs of specimens associated with the pollen and spores described in table H.1 is provided in figures H.1, H.2, H.3, and H.4.

TABLE H.1: List of plant microfossil taxa identified from analysis of crater lake surface samples and sediment cores. Note: PRC = Project reference collection. Numbers match those on table G.1; APSA = Australasian Pollen and Spore Atlas ♠ - This group is split for YM0413B and YL1211B samples based on pore size ; i) C0P3 pores <1 μm C0P2, ii) C0P3 pores >1.5 μm, iii) C0P2 pores <1 μm (excluding *Ficus*), iv) C0P2 pores >1.5 μm.

Family	Sample Name	Taxonomy Reference	YO0712A	YL0413A	YM0413A	LK0712A	YM0413B	YL1211B	Photograph code/s
Poaceae	Poaceae		5.8	15.3	45.4	20.7	45.4	11.3	p1
Cyperaceae	Cyperaceae		1.2	0.0	9.3	2.4	6.6	1.5	p2
Cannabaceae	*Trema*	PRC #74	5.3	3.5	7.2	6.1	5.0	40.4	p3i & ii
Cannabaceae	*Aphananthe* cf	Huang (1972) pl154; APSA 60-4-1	0.0	17.6	1.0	0.0	0.3	0.7	p4
Cannabaceae	*Celtis* type	PRC #19 & #20; Huang (1972) pl154	1.8	4.7	0.0	2.4	0.6	0.3	p5i & ii
Ulmaceae / Apocynaceae	*Holoptelea / Wrightia* sf C0P4	quamar and Chauhan (2011) / APSA 251-20-6	0.0	0.0	0.0	0.0	0.1	0.5	p6
Ulmaceae	*Holoptelea* C0P5 cf	quamar and Chauhan (2011)	0.0	0.0	0.0	0.0	<0.1	0.1	p7
Ulmaceae	*Holoptelea* C0P6 sf	quamar and Chauhan (2011)	0.0	0.0	0.0	0.0	<0.1	0.1	p8
Ulmaceae	*Zelkova*	Huang (1972) pl154; Nakagawa et al (1998)	0.0	0.0	0.0	0.0	<0.1	0.1	p9
Combretaceae	*Terminalia*	PRC #15	0.0	0.0	3.1	7.3	2.9	0.4	p10
Combretaceae / Melastomataceae	Combretaceae / Melastomataceae undiff.	Huang (1972) pl106, pl48	2.3	0.0	0.0	2.4	0.6	0.1	p11i, ii & iii
Combretaceae / Melastomataceae	*Anogeissus / Memecyclon* cf	PRC #10 & #43	1.2	1.2	0.0	3.7	0.7	1.1	p12
Myrtaceae	Myrtaceae <17 μm	Parnell (2003)	4.7	0.0	0.0	17.1	3.4	5.1	p13
Myrtaceae	Myrtaceae >17 μm	Parnell (2003)	2.3	5.9	0.0	6.1	0.1	0.2	p14
Urticaceae / Moraceae	Urticaceae / Moraceae type	Huang (1972) pl157, pl108	23.4	4.7	2.1	2.4	2.4	8.1	p15i, 15ii, 15iii & 15iv ♠
Moraceae	*Ficus*		8.8	2.4	0.0	0.0	0.4	1.1	p16
Fagaceae	*Lithocarpus / Castanopsis* type	PRC #32	0.0	0.0	2.1	0.0	1.7	3.5	p17
Fagaceae	*Quercus*		2.3	1.2	1.0	0.0	2.4	1.4	p18i & 18ii
Betulaceae	*Carpinus / Ostrya* sf	PRC #9	0.0	0.0	0.0	0.0	1.2	1.8	p19
Betulaceae	*Betula* sf	APSA 58-1-6a	0.0	0.0	0.0	0.0	0.3	0.3	p20
Myricaceae	*Myrica* cf	APSA 52-1-6	0.0	2.4	0.0	1.2	0.1	0.3	p21
Juglandaceae	*Engelhardtia* cf	APSA 55-4-2	0.0	0.0	0.0	0.0	<0.1	0.4	p22
Dipterocarpaceae	*Hopea/Shorea* type	PRC #25 & #26	1.8	1.2	1.0	0.0	1.1	1.2	p23i (*Shorea*-type) & 23ii (*Hopea*-type)

Continued...

Family	Sample Name	Taxonomy Reference	YO0712A	YL0413A	YM0413A	LK0712A	YM0413B count %	YL1211B count %	Photograph code/s
Dipterocarpaceae	*Dipterocarpaceae obtusifolia/ D. tuberculatus*	PRC #24	0.0	1.2	0.0	2.4	0.3	<0.1	p24
Dipterocarpaceae	*Dipterocarpus* undiff grouped	PRC #24, #25 & #26	0.0	2.4	1.0	2.4	0.9	<0.1	p25
Datiscaceae	*Tetrameles*	PRC #22 & #23	13.5	3.5	1.0	1.2	1.1	1.0	p26i & ii
Datiscaceae	*Tetrameles* sf	PRC #22 & #23	0.0	0.0	0.0	0.0	0.3	0.5	p27i, p27ii & p27iii
Primulaceae (formerly Myrisinaceae)	*Ardisia* cf	Huang (1972) pl109	0.0	0.0	0.0	0.0	<0.1	0.1	p28
Elaeocarpaceae	*Elaeocarpus* cf	PRC #28	0.6	0.0	0.0	0.0	0.1	0.9	p29
Unknown	Unknown pollen B391		0.0	0.0	0.0	0.0	0.2	<0.1	p30
Euphorbiaceae	*Mallotus*	Huang (1972) pl68	2.9	2.4	2.1	0.0	1.0	5.1	p31
Euphorbiaceae	*Macaranga*	PRC #31; APSA 149-19	0.6	0.0	0.0	1.2	0.6	0.8	p32
Euphorbiaceae	*Aporusa / Antidesma* cf	APSA 149-61-1; PRC #29 & #30	0.0	1.2	0.0	2.4	1.5	1.9	p33
Phyllanthaceae	*Phyllanthus*	Huang (1972) pl69; PRC #48	0.0	0.0	0.0	0.0	0.2	<0.1	p34
Phyllanthaceae	*Glochidion*	Huang (1972) pl68; Penny (1998) p209:35	0.0	0.0	0.0	0.0	0.1	<0.1	p35
Lythraceae	*Lagerstroemia*	PRC #37-#41	3.5	3.5	4.1	9.8	0.7	0.6	p36
Lythraceae	*Rotala*	Huang (1972) pl101; PRC #37-#41	0.6	0.0	0.0	0.0	0.2	<0.1	p37
Lythraceae	Lythraceae cf	PRC #37-#41	0.0	0.0	0.0	0.0	0.1	0.2	p38
Sapotaceae	Madhuca cf	Trivedi et al. (2014)	0.0	0.0	0.0	0.0	<0.1	<0.1	p39i & p39ii
Lauraceae	*Litsea* cf	APSA 101-6-10	0.0	1.0	0.0	0.0	<0.1	0.1	p40
Rubiaceae	*Adina / Nauclea* types	PRC #57-#60	1.2	1.2	2.1	0.0	0.0	0.4	p41i & p41ii
Rubiaceae	*Uncaria / Wendania*	PRC #64	0.0	0.0	0.0	0.0	0.2	0.3	p42
Rubiaceae	*Rubia* cf	Huang (1972) pl135	0.0	0.0	0.0	0.0	0.1	<0.1	p43
Rubiaceae	*Timonius* sf	Huang (1972) pl135	0.6	0.0	0.0	0.0	<0.1	<0.1	p44
Rubiaceae	Rubiaceae sf type 1		1.2	0.0	0.0	0.0	<0.1	<0.1	p45
Rubiaceae	Rubiaceae other grouped		0.0	1.2	0.0	1.2	0.2	0.3	n/a
Sapindaceae / Rubiaceae	Sapindaceae / Rubiaceae type 1 & type 2		0.6	0.0	0.0	0.0	0.5	0.2	p46i & p46ii
Sapindaceae	*Schleichera oleosa / Cupaniopsis*	APSA 168-7-4 & APSA 168-34-1	12.9	0.0	3.1	2.4	0.2	<0.1	p47
Rhamnaceae	*Rhamnus / Sageretia*	Huang (1972) pl126, Punt et al. (2003)	0.0	0.0	0.0	0.0	0.2	0.2	p48
Rhamnaceae / Sapindaceae	*Zizyphus / Nephelium* sf	PRC #50, #51 & #55; Punt et al. (2003)	0.0	0.0	0.0	0.0	0.2	0.1	p49
Irvingiaceae	*Irvingia malayana*	APSA 140-12-1	0.6	0.0	0.0	1.2	0.2	0.2	p50

Continued...

Family	Sample Name	Taxonomy Reference	YO0712A	YL0413A	YM0413A	LK0712A	YM0413B count %	YL1211B count %	Photograph code/s
Rutaceae	*Zanthoxylum* cf	PRC #69 & #70; Huang (1972) pl137	0.0	0.0	0.0	0.0	0.1	0.5	p51
Ebenaceae	*Diospyros* cf	APSA 245-1	0.6	0.0	0.0	0.0	0.1	<0.1	p52
Stemonuraceae / Proteaceae	*Gomphandra* /Roupala / Helicia sf	Schori and Furness (2014); Rull (2003)	0.0	0.0	0.0	0.0	<0.1	0.2	p53
Rhamnaceae (?)	Unknown — *Alphitonia* sf (?)		3.5	0.0	0.0	0.0	<0.1	0.2	p54
Burseraceae	*Canarium* cf	Maxwell (1999) pl4	0.0	0.0	0.0	0.0	<0.1	0.1	p55
Meliaceae	*Toona* cf	Tissot (1994) pl46	0.6	0.0	0.0	0.0	<0.1	0.1	p56
Aquifoliaceae	*Ilex*	APSA 59-1	1.2	0.0	0.0	0.0	<0.1	0.1	p57
Fabaceae - Mimosoideae	*Adenanthera* cf	Huang (1972) pl85	0.6	2.4	0.0	0.0	<0.1	<0.1	p58
Fabaceae - Mimosoideae	*Acacia / Albizzia*	Huang (1972) pl84	0.0	0.0	0.0	0.0	<0.1	0.2	p59
Fabaceae - Caesalpinioideae	*Intsia*	Banks (2007)	0.0	0.0	0.0	0.0	<0.1	<0.1	p60
Fabaceae	Legume		0.0	0.0	0.0	0.0	<0.1	0.1	p61
Bombacaceae	Bombax cf type 1	Huang (1972) pl26	0.0	1.2	0.0	0.0	<0.1	<0.1	p62
Bombacaceae	Bombax type 2	Huang (1972) pl26	0.0	0.0	1.0	0.0	<0.1	<0.1	p63
Pinaceae	*Pinus*	Huang (1972) pl2	0.0	0.0	0.0	0.0	0.8	0.3	p64
Podocarpaceae	*Dacrycarpus*	APSA 305-2	0.0	0.0	0.0	0.0	<0.1	<0.1	p65
Podocarpaceae	Podocarpaceae	Huang (1972) pl2	0.0	0.0	1.0	0.0	<0.1	<0.1	p66
Chenopodiaceae	Chenopodiaceae sf e>10 μm	Huang (1972) pl38	0.0	0.0	0.0	0.0	0.1	<0.1	p67
Chenopodiaceae	Chenopodiaceae	Huang (1972) pl38	0.0	0.0	0.0	0.0	0.1	<0.1	p68
Caryophyllaceae	Caryophyllaceae	Huang (1972) pl5 & 36	0.0	0.0	0.0	0.0	<0.1	<0.1	p69
Asteraceae	other Asteraceae grouped		0.0	0.0	0.0	0.0	0.3	0.3	p70i to p70v
Arecaceae	Arecaceae cf		0.0	0.0	0.0	0.0	0.3	0.3	p71
Polygonaceae	*Persicaria* cf	APSA 75-15	0.0	0.0	0.0	0.0	<0.1	<0.1	p72i, p72ii
Amaranthaceae	Amaranthaceae sf	Huang (1972) pl11	0.0	0.0	0.0	0.0	0.8	<0.1	p73
Unknown	Unknown pollen type 1		0.0	0.0	0.0	0.0	0.2	<0.1	p74
Unknown	Unknown pollen type 2		1.2	0.0	0.0	0.0	0.1	<0.1	p75
Unknown	Unknown pollen type 3		0.0	0.0	0.0	0.0	0.1	<0.1	p76
Euphorbiaceae (?)	Unknown pollen type 4		0.0	0.0	0.0	0.0	<0.1	0.2	p77
Potamogetonaceae (?)	Unknown pollen type 5		0.0	0.0	0.0	0.0	<0.1	0.1	p78
Unknown	Unknown pollen type 6		0.0	0.0	0.0	0.0	<0.1	0.1	p79
Balsaminaceae	*Hydrocera triflora*	Penny (1998) p207:5, Janssens et al. (2005)	0.0	0.0	0.0	0.0	3.3	<0.1	p80
Hydrocharitaceae	*Blyxa* cf	APSA 10-4-1	0.0	0.0	2.4	0.0	0.7	0.0	p81
Blechnaceae	*Stenochlaena palustris*	APSA 407-25-3-2	0.0	11.8	6.2	1.2	1.3	0.4	p82
Aspleniaceae	*Asplenium* cf	APSA 407-21	0.0	0.0	0.0	0.0	0.1	<0.1	p83
Gleicheniaceae	*Gleichenia* cf		0.0	0.0	0.0	0.0	0.1	<0.1	p84
Nephrolepidaceae	*Nephrolepis* cf	407-14-1-5a	0.0	1.2	2.1	0.0	0.2	0.4	p85

Continued...

Family	Sample Name	Taxonomy Reference	YO0712A	YL0413A	YM0413A	LK0712A	YM0413B count %	YL1211B count %	Photograph code/s
Davalliaceae	Davalliaceae cf	Demske et al. (2013)	0.0	1.0	0.0	0.0	0.1	0.2	p86
Unknown	Unknown spore type 1		0.0	0.0	0.0	0.0	<0.1	0.5	p87
Pandanaceae (?)	Unknown spore type 2		0.0	0.0	0.0	0.0	<0.1	0.3	p88

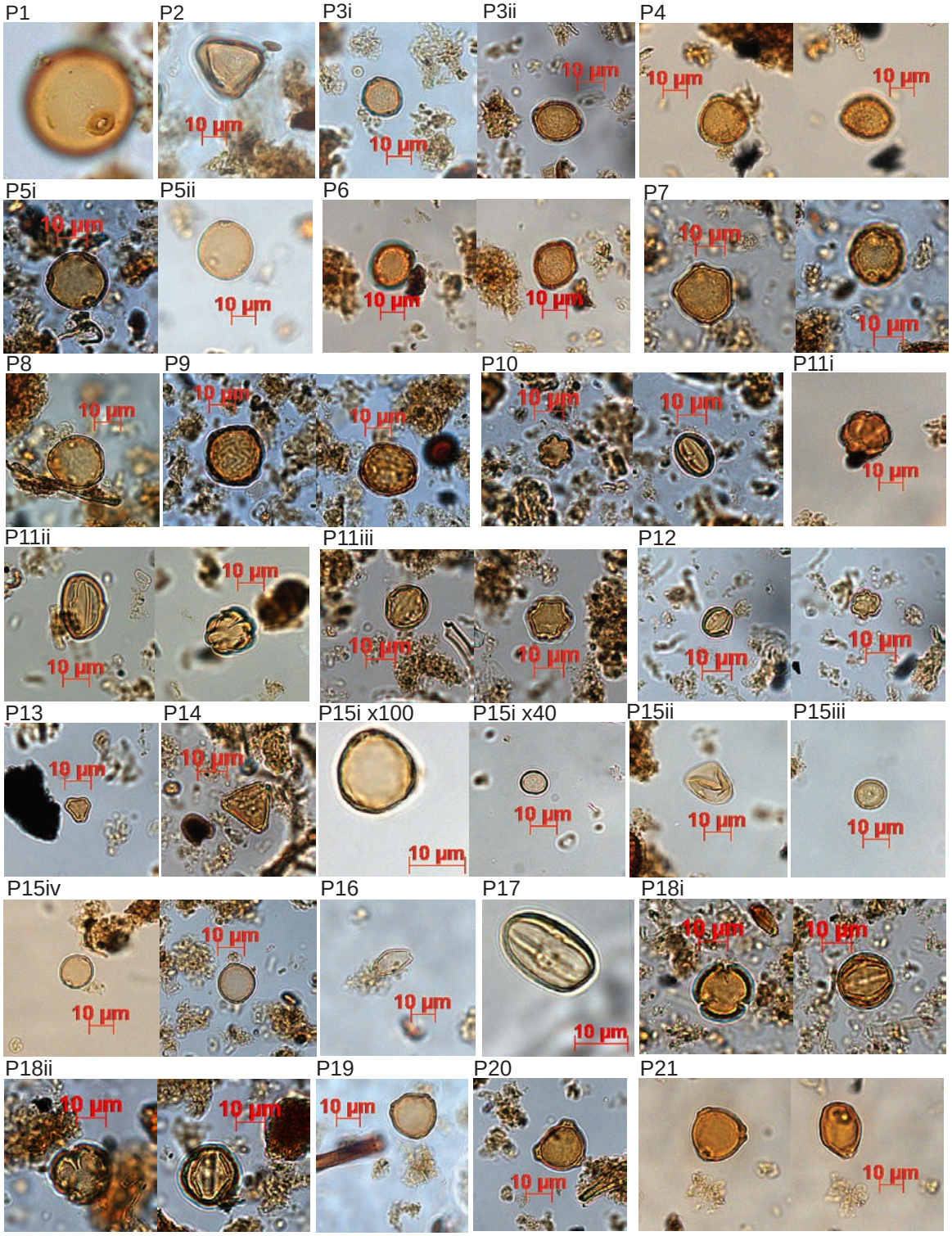

FIGURE H.1: Photomicrographs taken of key pollen and spore types encountered in lake surface and long cores (plate 1).

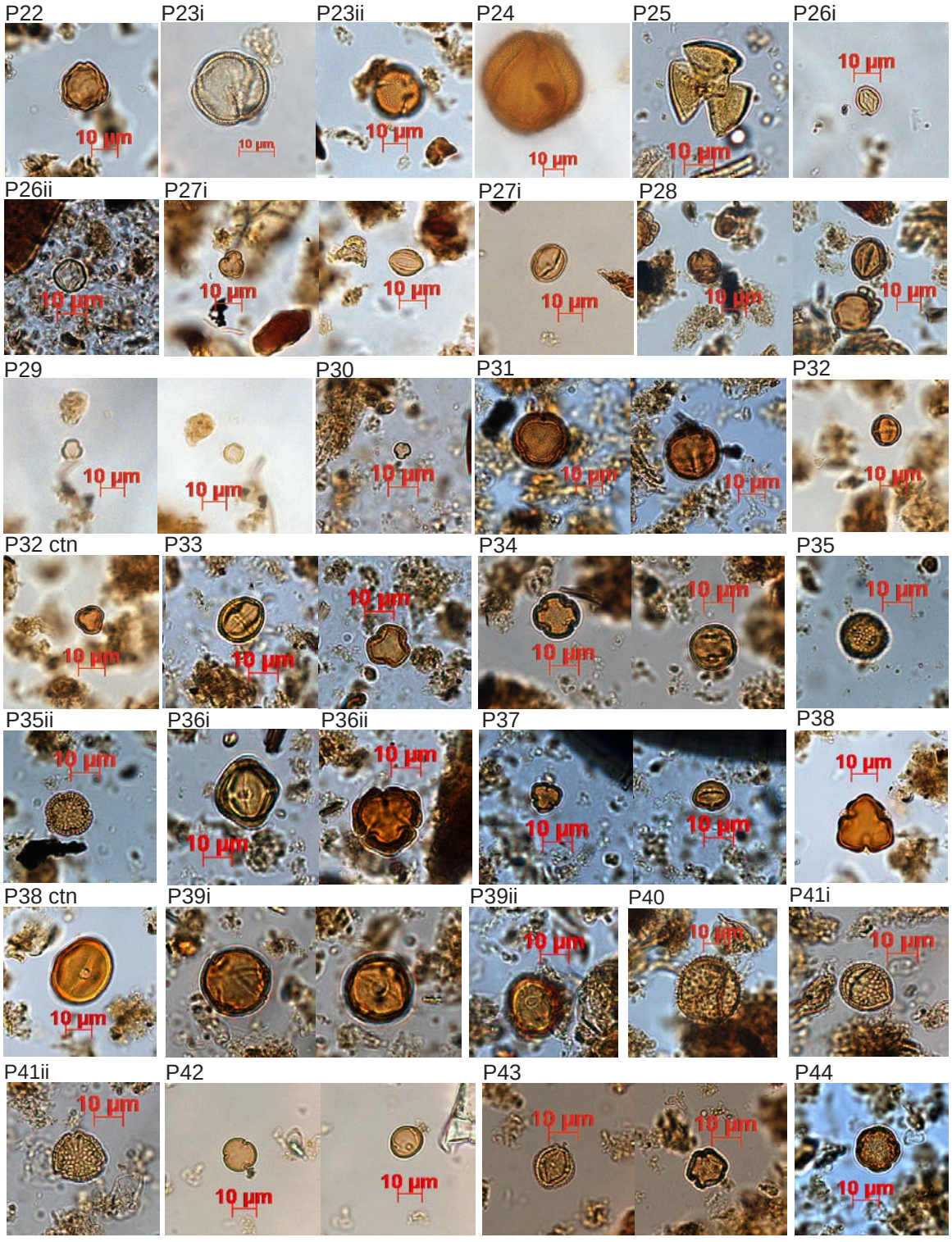

FIGURE H.2: Photomicrographs taken of key pollen and spore types encountered in lake surface and long cores (plate 2).

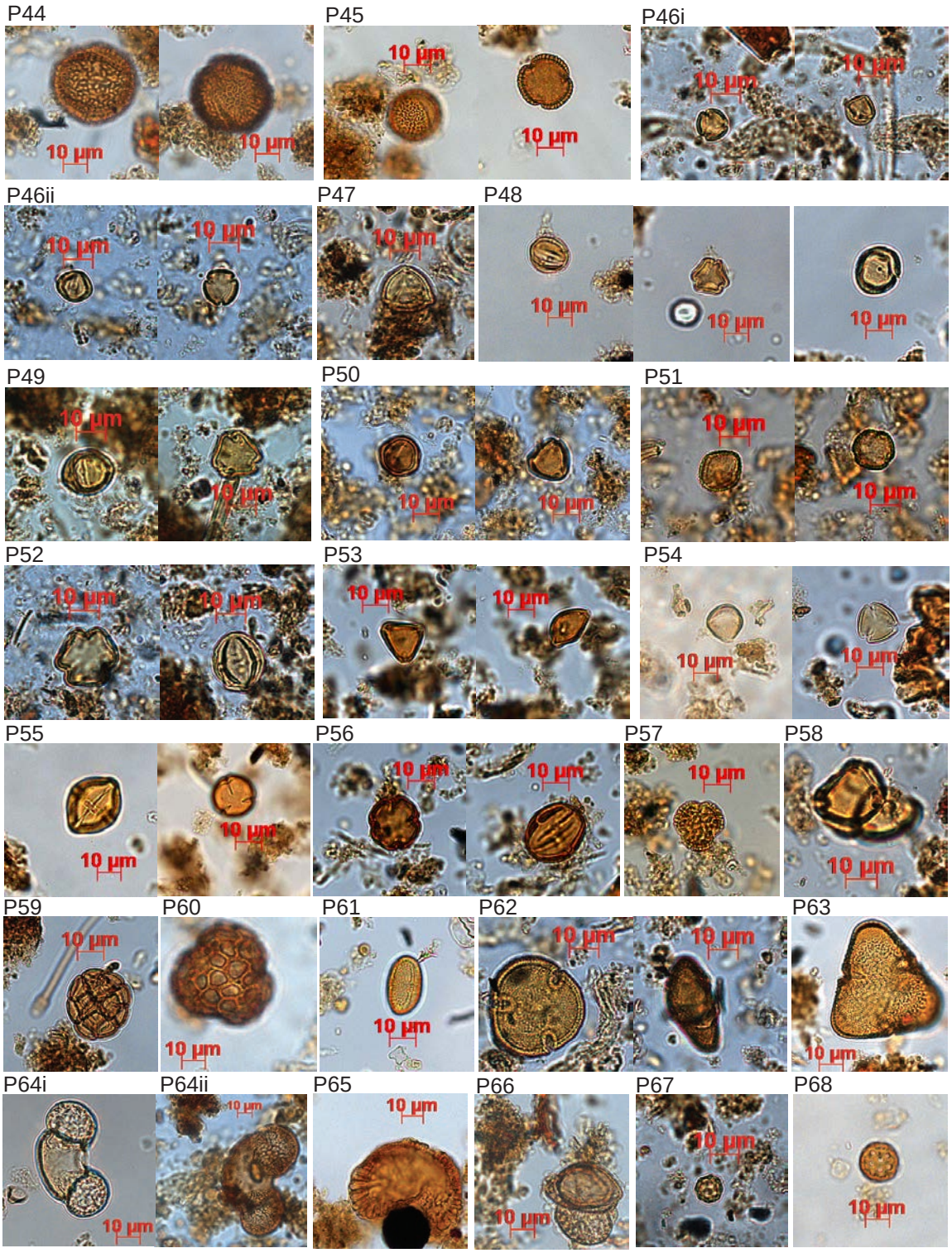

FIGURE H.3: Photomicrographs taken of key pollen and spore types encountered in lake surface and long cores (plate 3).

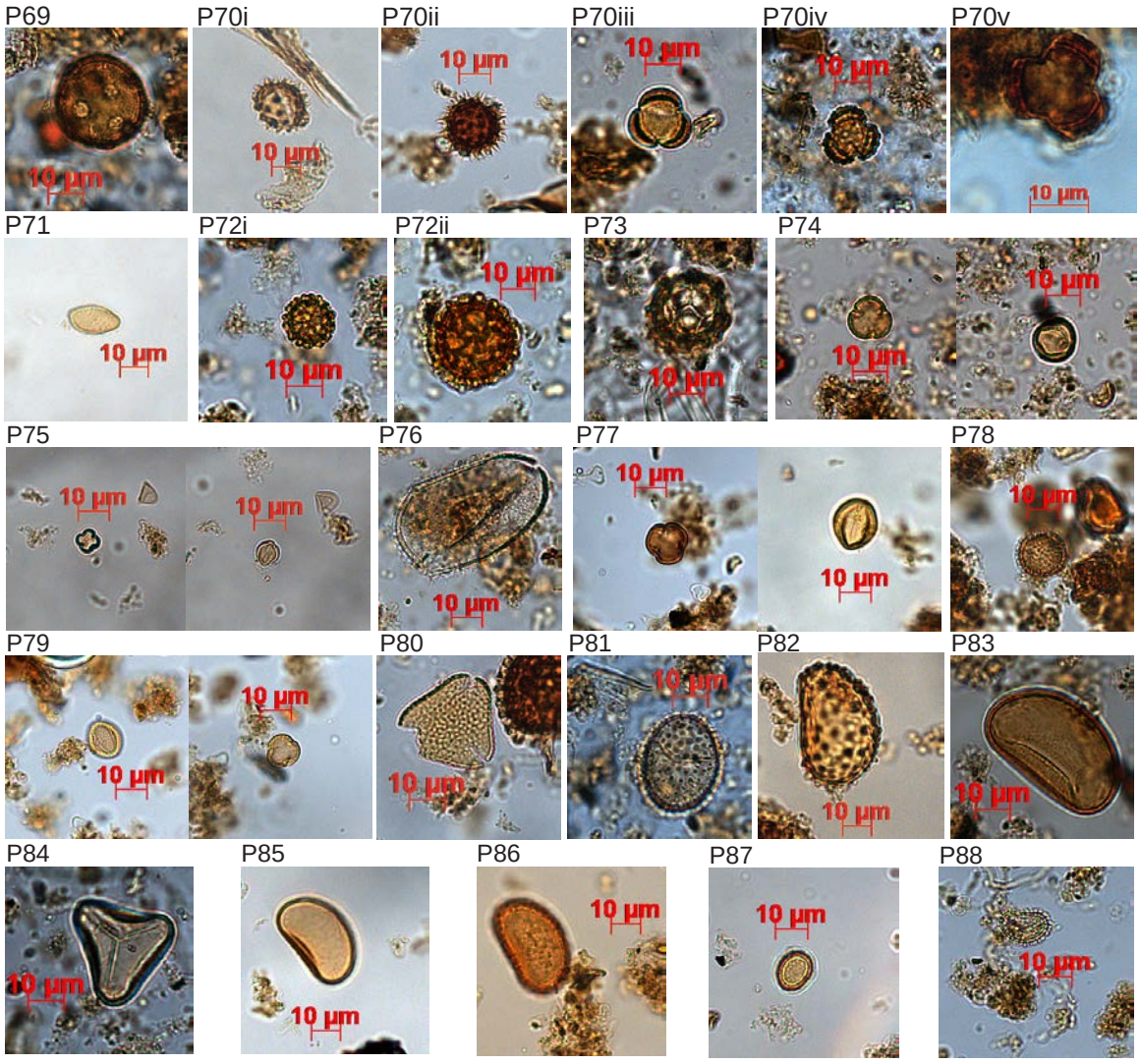

FIGURE H.4: Photomicrographs taken of key pollen and spore types encountered in lake surface and long cores (plate 4).

I References

Banks, H. 1997. The Pollen of Delonix (Leguminosae: Caesalpinioideae: Caesalpinieae). Kew Bulletin 52:417-434

Bunyavejchewin, S., P. J. Baker, and S. J. Davies. 2011. Seasonally Dry Tropical Forests in Continental Southeast Asia: Structure, Composition, and Dynamics. Pages 9-35 in W. J. McShea, S. J. Davies, and N. Bhumpakphan, editors. The Ecology and Conservation of Seasonally Dry Forests in Asia. Smithsonian Institution Scholarly Press, Washington D.C.

Dearing, J. 1999. Environmental Magnetic Susceptibility: Using the Bartington MS2 System. 2nd edition. British Library Catalogue, West Yorkshire.

Dearing, J. A., R. J. L. Dann, K. Hay, J. A. Lees, P. J. Loveland, B. A. Maher, and K. O'Grady. 1996. Frequency-dependent susceptibility measurements of environmental materials. Geophysical Journal International 124:228-240.

Demske, D., P. E. Tarasov, and T. Nakagawa. 2013. Atlas of pollen, spores and further non-pollen palynomorphs recorded in the glacial-interglacial late Quaternary sediments of Lake Suigetsu, central Japan. Quaternary International 290-291:164-238.

Dy Phon, P. 2000. Dictionary of Plants used in Cambodia. 1st edition. Imprimerie Olympic, Phnom Penh.

Faegri, K., and J. Iversen. 1989. Textbook of pollen analysis. 4th edition. John Wiley & Sons, Chichester.

Gardner, S., P. Sidisunthorn, and V. Anusarnsunthorn. 2000. A Field Guide to the Forest Trees of Northern Thailand. Kobfai Publishing Project, Bangkok.

Heiri, O., A. F. Lotter, and G. Lemke. 2001. Loss on ignition as a method for estimating organic and carbonate content in sediments: reproducibility and comparability of results. Journal of Paleolimnology 25:101-110.

Huang, T. C. 1972. Pollen Flora of Taiwan. National Taiwan University Botany Department Press, Taiwan.

Isbell, R. F. 2002. The Australian Soil Classification. 2nd edition. CSIRO, Clayton.

Janssens, S., F. Lens, S. Dressler, K. Geuten, E. Smets, and S. Vinckier. 2005. Palynological variation in Balsaminoid Ericales. II. Balsaminaceae, Tetrameristaceae, Pellicieraceae and general conclusions. Ann Bot 96:1061-1073.

Lee, C.-Y., C.-L. Chang, P.-M. Liew, T.-Q. Lee, and S.-R. Song. 2014. Climate change, vegetation history, and agricultural activity of Lake Li-yu Tan, central Taiwan, during the last 2.6 ka BP. Quaternary International 325:105-110.

Maxwell, A. L. 1999. Holocene environmental change in mainland Southeast Asia: pollen and charcoal records from Cambodia. Ph.D Thesis. Louisiana State University, Louisiana.

Nakagawa, T., G. Garfì, M. Reille, and R. Verlaque. 1998. Pollen morphology of Zelkova sicula (Ulmaceae), a recently discovered relic species of the European Tertiary flora: description, chromosomal relevance, and palaeobotanical significance. Review of Palaeobotany and Palynology 100:27-37.

Parnell, J. 2003. Pollen of Syzygium (Myrtaceae) from SE Asia, especially Thailand. Blumea - Biodiversity, Evolution and Biogeography of Plants 48:303-317.

Penny, D. 1998. Late Quaternary Palaeoenvironments in the Sakon Nakhon Basin, North-east Thailand. Ph.D Thesis. Monash University, Melbourne.

Punt, W., A. Marks, and P. P. Hoen. 2003. The Northwest European Pollen Flora, 63: Rhamnaceae. Review of Palaeobotany and Palynology 123:57-66.

Quamar, M. F., and M. S. Chauhan. 2011. Pollen analysis of spider webs from Khedla village, Betul District, Madhya Pradesh. Current Science 101:1586-1592.

Rollet, B. 1962. Inventaire Forestier de l'Est Mekong. UN FAO, Rome.

Ruangpanit, N. 1995. Tropical seasonal forests in monsoon Asia: With emphasis on continental southeast Asia. Vegetatio 121:31-40.

Rull, V. 2003. An Illustrated key for the identification of pollen from Pantepui and the Gran Sabana (Eastern Venezuelan Guayana). Palynology 27:99-133.

Schori, M., and C. A. Furness. 2014. Pollen diversity in Aquifoliales. Botanical Journal of the Linnean Society 175:169-190.

Soil Survey Staff. 2010. Keys to Soil Taxonomy. 11th edition. United States Department of Agriculture (USDA), Natural Resources Conservation Service (NRCS), Washington D.C.

Tani, A., E. Ito, M. Kankaki, S. Ohta, S. Khorn, P. Pith, B. Tith, S. Pol, and S. Lim. 2007. Principal Forest Types of Three Regions of Cambodia: Kampong Thom, Kratie, and Mondolkiri. Pages 201-213 in H. Sawada, M. Araki, N. A. Chappell, J. V. LaFrankie, and A. Shimizu, editors. Forest Environments of the Mekong River Basin. Springer, Toyko.

Theilade, I., L. Schmidt, P. Chhang, and J. A. McDonald. 2011. Evergreen swamp forest in Cambodia: floristic composition, ecological characteristics, and conservation status. Nordic Journal of Botany 29:71-80.

Tissot, C., H. Chikhi, and T. S. Nayar. 1994. Pollen of wet evergreen forests of the Western Ghats, India. Institut Francais de Pondichéy, Pondicherry.

Toriyama, J., S. Ohta, M. Araki, M. Kanzaki, S. Khorn, P. Pith, S. Lim, and S. Pol. 2007. Comparison of soil physical properties in evergreen and deciduous forests in central Cambodia. Journal of Forest Research 13:15-24.

Toriyama, J., S. Ohta, M. Araki, K. i. Kosugi, T. Nobuhiro, N. Kabeya, A. Shimizu, K. Tamai, M. Kanzaki, and S. Chann. 2011. Soil pore characteristics of evergreen and deciduous forests of the tropical monsoon region in Cambodia. Hydrological Processes 25:714-726.

Trivedi, A., M. S. Chauhan, and A. Farooqui. 2014. Studies on Pollen Rain vis-a-vis Vegetation Relationship and Thecamoebian Diversity in Bari Tal area, Lucknow District, Uttar Pradesh. Biological Forum 6:68-78.

Vandergoes, M. J., and C. A. Prior. 2003. AMS dating of pollen concentrates – a methological study of late quaternary sediments from South Westland, New Zealand. Radiocarbon 45:479-491.